WestVirginiaUniversity
THE RESEARCH REPOSITORY @ WVU

Graduate Theses, Dissertations, and Problem Reports

2013

# Effect of Thermal Loading on the Performance of Horizontally Curved I-Girder Bridges

Kevyn C. McBride
*West Virginia University*

Follow this and additional works at: https://researchrepository.wvu.edu/etd

## Recommended Citation

McBride, Kevyn C., "Effect of Thermal Loading on the Performance of Horizontally Curved I-Girder Bridges" (2013). *Graduate Theses, Dissertations, and Problem Reports*. 325.
https://researchrepository.wvu.edu/etd/325

This Dissertation is protected by copyright and/or related rights. It has been brought to you by the The Research Repository @ WVU with permission from the rights-holder(s). You are free to use this Dissertation in any way that is permitted by the copyright and related rights legislation that applies to your use. For other uses you must obtain permission from the rights-holder(s) directly, unless additional rights are indicated by a Creative Commons license in the record and/ or on the work itself. This Dissertation has been accepted for inclusion in WVU Graduate Theses, Dissertations, and Problem Reports collection by an authorized administrator of The Research Repository @ WVU. For more information, please contact researchrepository@mail.wvu.edu.

# Effect of Thermal Loading on the Performance of Horizontally Curved I-Girder Bridges

**Kevyn C. McBride**

**Dissertation Submitted to the**
**Benjamin M. Statler College of Engineering and Mineral Resources**
**at West Virginia University**
**in partial fulfillment of the requirements**
**for the degree of**

**Doctor of Philosophy**
**in**
**Mechanical Engineering**

**Dr. Samir N. Shoukry, Ph.D., Chair**
**Dr. Gergis W. William, Ph.D., Co-Chair**
**Dr. Mourad Y. Riad, Ph.D.**
**Dr. Jacky C. Prucz, Ph.D.**
**Dr. Kenneth N. Means, Ph.D.**

**Department of Mechanical and Aerospace Engineering**

**Morgantown, West Virginia**
**2013**

**Keywords: Finite Element Modeling; Curved Steel I-Girder Bridges; Thermal Loading; Web Buckling**

**ABSTRACT**

**Effect of Thermal Loading on the Performance of Horizontally Curved I-Girder Bridges**

**Kevyn C. McBride**

As the amount of infrastructure in the United States continues to grow and older infrastructure is replaced or updated, bridge designers are faced with increasing space and geometrical limitations. Curved bridges have become a popular design alternative to the traditional straight girder or chorded bridges as they can provide the designer a more cost effective solution to complicated geometrical limitations or site irregularities. However, the volume of research and knowledge on the behavior of curved bridges is lacking compared to straight and chorded bridges, especially in terms of their response to changing thermal conditions. In most cases, it is assumed that bearing design allows expansion and contraction of the superstructure that relieves thermal stresses, but in reality this is rarely true. Bridge curvature complicates the structures response to thermal loading as the bearing configuration must handle a larger degree of expansion and contraction in the transverse, or radial, direction. Failure to properly design bridge bearings to accommodate thermal loads will lead to unaccounted for deformations and stresses in the superstructure.

This research begins with two small scale parametric studies, performed using finite element modeling, that investigate how uniform thermal loading effects web deformations and web and flange stresses of a single curved steel I-girder and also of a section consisting of two curved steel I-girders connected with cross frames. The major focus of this research is a case study on the response of the Buffalo Creek Bridge, located in Logan County, West Virginia, to changing thermal conditions prior to any in-service loading. Two detailed 3D finite element models of the bridge were created, one modeling the piers as rigid members and one modeling the piers as flexible members, and both models were subjected to uniform temperature increase and decrease.

Results indicate that uniform thermal loading leads to global and local buckling along the I-girder web centerlines, lateral distortional buckling in the web cross section, and thermal stresses in the I-girder webs. Although pier flexibility is shown to reduce the magnitude of thermally induced local and lateral distortional buckling and thermal stresses, I-girders experience larger global buckling when the piers are flexible. The results indicate that the introduction of pier flexibility did not relieve all the thermal stresses in the I-girder webs. At some locations, when the piers are rigid, the I-girder stresses exceed the AASHTO web bend-buckling capacity as well as the overall stress capacity of the section.

This study shows that uniform thermal loading will lead to increased out-of-plane web deformations and increased web stress levels, which will both combine to decrease the load carrying capacity of the bridge when subject to subsequent live-loading conditions. This dissertation outlines a methodology that should be utilized by bridge designers and/or owners

to validate the integrity of traditional bridge designs, especially in the case of more complicated bridge structures.

**ACKNLOWLEDGEMENTS**

First, I would like to thank my research advisor, Dr. Samir Shoukry, for providing me with the opportunity to work with his exceptional research team during my years of graduate study at West Virginia University.

I would like to extend a special thank you to Dr. Gergis William for the countless advice and support offered to me throughout my graduate studies. I will be forever grateful to you for your willingness to mentor me throughout my years at West Virginia University. I'm lucky to be able to count you as a colleague and a friend.

Thank you to my Phillips Machine Service family for being supportive over the past five years as I have worked to complete this research project. In particular, Jack Phillips, Jim Phillips, Tom Cushman, C.R. Allen, and Bruce Dickerson, without your understanding and encouragement, realizing the completion of this research study would have been impossible.

Most importantly, I would like to offer my most overwhelming thank you to my family. Mom, Dad, Jordan, and Kent, thank you for your encouragement, support, guidance, and love throughout these studies and throughout my life. I'm thankful beyond words for each of you, and in particular, thankful for the unwavering support you've given me during studies.

# TABLE OF CONTENTS

## LIST OF FIGURES

# LIST OF TABLES

# CHAPTER ONE

# INTRODUCTION

## 1.1 Background

As the amount of infrastructure in the United States continues to grow, especially in urban areas, engineers are forced to more often deal with space and geometrical limitations. To this end, the number of curved bridge structures constructed in the United States has steadily risen over the past several decades to the point that, as of 2004, over one-third of all steel superstructure bridges constructed were curved (Davidson et al., 2004). Curved bridge popularity experienced a boom partially due to the fact that a curved bridge can offer the designer solutions to complicated geometrical limitations or site irregularities as compared to traditional straight bridges. Additionally, as the use of high performance steel has become more prevalent, engineers have become able to design more complicated structures as the girder can handle greater loads. A previous alternative to constructing a bridge using a curved girder section was to use a chorded structure composed of a series of straight girder sections oriented in a curve to produce a curved bridge. However, using curved girder sections provides aesthetic as well as cost benefits over these traditional chorded structures.

Studies have been conducted for quite some time on the behavior of curved beams, but research on the analysis and design of horizontally curved bridges in the United States began in 1969 when the FHWA formed the Consortium of University Research Teams (CURT) whose work resulted in the initial development of working stress design criteria and tentative design specifications. This work, along with most of the research conducted prior to 1976, was gathered by The American Society of Civil Engineers and the American Association of State Highway and Transportation Officials and compiled into recommendations for the design of curved I-girder bridges (ASCE-AASHTO Committee on Curved Girders, 1977). Later, Load Factor Design criteria was developed

(AASHTO, 1980) out of the work of Stegmann and Galmabos (1976) and Galambos (1978) as well as the working stress design criteria in the first set of Guide Specifications for Horizontally Curved Highway Bridges (AASHTO, 1987). In 1992, the Federal Highway Administration (FHWA) initiated the Curved Steel Bridge Research Project (CSBRP) as a large scale experimental and analytical program aimed at developing new, rational guidelines for horizontally curved steel bridges. This work resulted in the newest set of Guide Specifications for Horizontally Curved Highway Bridge (AASHTO, 2003). Although there has been substantial continuing research in the areas of curved beam behavior and the behavior of curved bridges, the volume of information on these structures pales in comparison to that of straight structures. This is to be expected as the use of curved members in bridge construction is a fairly novel concept when compared to the use of straight sections.

## 1.2 Problem Statement

The use of curved girders adds complexities in the bridge design, construction, and analysis that are not present when straight members are used. I-beams are designed to primarily carry vertical bending loads and do not perform well when lateral loading or torsion is placed on the member. However, curved bridges will experience torsion and lateral forces under normal loading conditions which will affect the stability of the I-girders. Additionally, much more care must be taken in designing the erection procedures for a curved I-girder bridge because curved steel members will experience lateral deflections in addition to vertical deflections under gravity loading. Most problems that have occurred with curved girder bridges have been related to fabrication and assembly procedures or unanticipated or unaccounted for deformations that occur during construction (Grubb et al., 1996). In the curved I-girder bridge system, nonuniform torsion results in warping normal stresses in the flanges. Also, because of torsion, the diaphragms or cross frames, or both, become primary load-carrying members (Davidson and Yoo, 2003). Where cross frames are secondary members in

straight girder systems, they are designed as main members on curved bridges because they function to stabilize the girders and redistribute the loads. In general, the simple addition of curvature to a bridge system leads to structural intricacies that do not exist in straight bridges.

Presently, curved I-girder bridge design procedures treat thermal loading as a secondary loading condition. *AASHTO Guide Specifications* (2003) specify that thermal loading effects in a curved bridge superstructure shall be determined for uniform temperature changes as specified in *AASHTO Guide Specifications* (2002) Article 3.16, which states that for metal structures a range of temperatures from 0 to 120° F (-17.8 to 48.9° C) should be considered, which is also adopted by the AASHTO LRFD Specifications (2004, 2007 and 2010). In addition, *AASHTO Guide Specifications* (2003) state that the load effects due to a temperature differential of 25° F (-3.9° C) between the deck and the girders shall be added to the uniform temperature effects when the width of the deck is less than one-fifth the longest span. *AASHTO Guide Specifications* (2003) acknowledges that although temperature changes in a bridge do not occur uniformly, bridges are usually designed for an assumed uniform temperature change. An assumption that is often made is that the bearing orientation on a curved bridge is such that as thermal expansion and contraction occurs, the bridge is allowed to move freely along rays emanating from a fixed point, causing the thermal forces to be minimal. This presumes that the conditions at the bearings act precisely as designed, that the temperature change is in fact uniform, and the constraints of the concrete deck have no effect on the expansion and contraction of the girders.

Consequently, the concept of thermal loading on horizontally curved I-girder bridges is a topic which has received very little attention by researchers. In contrast to traditional straight bridges, thermal effects will be greater on curved structures because the thermal expansion and contraction will invoke both longitudinal and transverse responses, as compared to the primarily longitudinal response for straight bridges. The

simple addition of curvature will likely cause temperature conditions to have an impact on phenomenon such as cross member forces, cross section buckling, girder load carrying capacity, and cross member fitting, just to name a few. It is evident investigations must be performed to study the impact, if any, changing environmental conditions will have on the behavior and performance of curved I-girder bridges.

## 1.3 Research Objectives

The aim of this study is to investigate the influence that thermal loading has on curved I-girders in terms of various displacements and stresses. The first part of the research focuses on small scale single and paired curved I-girder sections and their response to the introduction of uniform temperature changes. The major focus of this research is a full scale case study performed on an existing bridge to determine the impact changing thermal conditions will have prior to the bridge being placed in service. The scope of the research can be broken down into the following more specific objectives:

- Determine if uniform thermal loading will have an effect on a simple curved I-girders section. A parametric study performed by previous researchers (Davidson et al., 1999a) will be reproduced and extended to study the effect of thermal loads on the curved I-girder section. In particular, web out-of-plane deformation, web longitudinal stress, and flange longitudinal stress as a result of temperature loading will be investigated and these results will be correlated with those from Davidson et al. (1999a) to produce conclusions as to what impact the thermal loads have on the performance of the curved I-girder section.

- Examine how varying the radii of curvature of a small I-girder test section consisting of two I-girders connected with cross frames influences the response to changing thermal conditions. The test section is modeled as a copy of The Horizontally Curved Steel I-Girder Design Example in the *AASHTO Guide*

*Specifications* (2003), which only considers self-weight and wind loading. The purpose is to determine how thermal loading influence lateral web buckling, torsional buckling, and flanges stresses as the degree of curvature changes and how might these effects translate to a full-scale curved I-girder bridge.

- The main focus of this research is to develop a full scale 3D finite element model of an existing curved I-girder bridge which accurately replicates the behavior of the structure and employ it to study the following phenomenon:
    - The influence that uniform thermal loading has on I-girder web distortions, both longitudinally and through the web depth, at the stage just after the completion of construction but before any live loading is placed on the bridge and how these thermal deformations might impact the performance of the curved I-girder bridge.
    - Investigate what effect uniform thermal loading has on the state of stress in curved I-girder webs prior to the introduction of in-service loading and how these additional stresses might impact bridge capacity.
    - In both the study of deformations and stresses, compare results when bridge piers are rigid and when they are flexible to determine what impact pier movement has on the response of the structure to changing temperature conditions.

## 1.4 Dissertation Outline

Chapter Two presents a literature review on various topics related to curved I-beams and curved I-girder bridges. Since little information was obtained pertaining to studies related to thermal loading on curved I-girder bridges, the emphasis of this chapter was to gather as much information as possible regarding all areas of curved I-girder bridge research to identify the state-of-the-art in analysis and design of curved bridges.

Chapter Three describes two preliminary finite element investigations into the effect of temperature loading on curved members. The first study of a simple curved I-girder section examines the effect that varying certain girder parameters has on the deformations and stresses at the mid-span of the section. The second study uses finite element modeling to examine a section consisting of two braced curved I-girders under gravity and thermal loading. Results from each of these studies indicate that thermal loading applied to curved I-girder sections results in a significant response which requires further investigation.

Chapter Four presents a detailed description of the finite element model of the Buffalo Creek Bridge created as the case study for this research study. Two distinct models are used for this investigation: one with rigid bridge piers and one with flexible bridge piers.

Chapter Five details results validating the finite element model of the Buffalo Creek Bridge. Validation is performed by loading the finite element model with self weight loading in two stages, first the weight of the steel superstructure followed by the weight of the concrete deck. The vertical girder deflections at both of these stages of loading along the length of each girder are checked against the camber values given in the design sheets for validation of the results. Since the camber values do not consider pier flexibility, the finite element model validation was performed using the Buffalo Creek Bridge model with rigid piers.

Chapter Six investigates how gravity loading and gravity loading followed by a uniform temperature load impact the lateral displacements of the I-girder webs and comparisons are made between the rigid and flexible pier cases. Global lateral displacement and out-of-plane web lateral displacement profiles along the centerline of each girder web for each load state are presented. Web cross-section displacement profiles at critical locations at girder mid-spans and at and near the piers under each

type of load are also plotted and studied. Data presented in this chapter confirms that curved bridge I-girders experience global, local, and lateral distortional web buckling when only gravity loading is applied, and these buckling values are only exaggerated with the addition of thermal loads. Pier flexibility leads to larger global buckling values along the web centerline, while rigid piers result in larger local and lateral distortional web buckling. This bucking of the I-girder webs prior to any live loading on the structure will decrease the load carrying capacity of the respective I-girders, and thus the entire bridge structure.

Chapter Seven explores the effect that gravity and thermal loading has on the state of stress in the I-girder webs and how the additional thermal stresses might impact bridge capacity. At the same critical cross sections studied in Chapter Six, this portion of the research investigates the magnitude of effective and longitudinal stress through the web profile. The longitudinal stress profile is further decomposed into axial and bending stress components in an attempt to better isolate the effects of temperature loading. Although it is postulated that pier flexibility minimizes the impact that uniform temperature loading has on the state of web stresses, both types of modeling reveal that stresses arise in the web cross sections as a result of thermal loading, indicating that the superstructure is not free to expand and contract under as the temperature changes. In fact, after gravity and +45°F thermal loading only, some locations fail the AASHTO (2007) web bend-buckling criteria and some web cross section stress profiles indicate the web stresses have exceeded their capacity. These conclusions are drawn without any influence of the design or live loading being applied.

Chapter Eight presents a concise summary of the conclusions drawn throughout the study and makes suggestions for future work that should be performed to further solidify this body of research.

Appendix A contains plots of girder deformations due only to gravity loading. For each span of each girder, comparisons are made between the flexible and rigid pier cases for global lateral deformation along the web centerline, out-of-plane (local) deformation along the web centerline, and cross-sectional web displacement at critical mid-span and pier locations.

Appendix B contains plots of the same displacements as were plotted in Appendix A, only with the addition of results for either -45°F or +45°F uniform thermal loading.

Appendix C is composed of plots of web stress profiles at critical mid-span and pier locations. Von Mises and longitudinal stresses are compared between the rigid and flexible pier cases at each location when the bridge is subject to gravity loading only, gravity loading followed by -45°F uniform thermal loading, and gravity loading followed by +45°F thermal loading.

# CHAPTER TWO

# LITERATURE REVIEW

## 2.1 Introduction

The percentage of highway bridges in the United States constructed using horizontally curved girders has steadily increased over the past several decades. In fact, according to Davidson et al. (2004), over one-third of all steel superstructure bridges constructed today are curved. Curved bridges have gained popularity because they can often provide geometrical solutions to complicated geographical limitations or irregularities faced by designers. Moreover, horizontally curved steel bridges also offer aesthetic and cost benefits over more traditional chorded structures that make their selection attractive even when site restrictions are not an issue (Linzell et al., 2004a).

It is widely acknowledged that due to the continued decrease in available land for new and replacement structures, the need for horizontally curved bridges will continue to grow because of the benefits they provide under these situations. With these advantages, curved bridges provide some added complexities in their analysis, design, and construction when compared to straight girder bridges. The presence of curvature adds a torsional component to the overall system response that can have a significant effect on structural behavior. Although the design and construction process of curved bridge systems is immensely more complicated than straight bridge systems, the curved bridge design specifications are far less detailed and less complete than the straight girder specifications.

## 2.2 Development of Curved Bridge Design Guidelines

The first set of guidelines governing the design of horizontally curved bridges was published in 1980 as the *AASHTO Guide Specifications for Horizontally Curved Highway Bridges* (*Guide Specifications*). These guidelines were a result of the allowable stress design (ASD) specifications developed as a part of the Consortium of University Research Teams (CURT) project sponsored in the late 1960's and early 1970's by the Federal Highway Administration (FHWA) and 25 participating state highway departments along with load factor design (LFD) specifications funded by the American Iron and Steel Institute during the mid-1970's (Stegmann and Galambos, 1976). The CURT research team was comprised of Carnegie Mellon University, the University of Pennsylvania, the University of Rhode Island, and Syracuse University.

An updated version of the *Guide Specifications* was published in 1993 that was written in both ASD and LFD format. Advances were made from the previous edition in recognizing the need to directly interrelate lateral flange bending stress with vertical bending stress and the need for additional shear studs in the composite region due to the radial component of shear between the deck and the girders. However, these guidelines did not reflect any of the important research on curved girder bridges conducted since 1980.

In 1992, the FHWA initiated the Curved Steel Bridge Research Project (CSBRP) based in part on the research needs identified by NCHRP Project 12-38. NCHRP Project 12-38 resulted in updated *Guide Specifications* (2003) using the state of the art in curved bridge research and written in the LFD format. It was expected that the results from the CSBRP would be used by NCHRP Project 12-52 to further develop work done by NCHRP Project 12-38 into LRFD based design and construction guidelines for horizontally curved bridges. New straight girder provisions from NCHRP Project 12-52 were published in the third edition of the *AASHTO LRFD Bridge Design Specifications* (2004) (*LRFD*

*Specifications*). The 2006 interim to the *AASHTO LRFD Bridge Design Specifications* were published containing the curved girder provisions and unified the specifications for straight and curved bridges.

## 2.3 Consortium of University Research Teams Project (CURT)

As of 1969, there was no set of uniform specifications available that governed the design of horizontally curved bridges. To remedy this, the FHWA, along with 25 participating states, created the Consortium of University Research Teams (CURT) to study the behavior of curved girder bridges and to develop design requirements. The described goals of this research were: 1) perform a thorough review of all information on the subject of curved bridges, 2) conduct analytical and experimental studies on curved girders as an addition to the reviewed studies, 3) develop simplified analysis and design methods along with supporting computer programs and design aids, and 4) correlate the developed analysis and design methods with analytical and experimental data. To accomplish these goals, a number of single and double girder systems were examined to study the behavior and interaction of the members under various loading conditions. The culmination of this research was the development of the *AASHTO Guide Specifications for Horizontally Curved Highway Bridges* (1980), the first set of design guidelines for horizontally curved bridges.

### 2.3.1 Developing Analysis Techniques

Heins and Spates (1970) described the behavior of a single curved girder subjected to various loading and boundary conditions. The study aims at describing the response of any curved open cross section member under various loads. A general set of differential equations were developed for a curved girder section and were solved using a computer program developed by the authors. Also, an experimental girder test was set up that

was subjected to concentrated load and torsional moments to be used in verifying the analytical technique. The results from the experimental tests correlated well with the computer program results showing the versatility and accuracy of the computer program in evaluating internal forces and external deflections and rotations for various beams and load cases. This technique could now be used to provide a means for developing design equations for curved girder systems along with analyzing single girders.

### 2.3.2 Compression Flange Buckling

Culver and Frampton (1970) performed a study on flange local buckling of curved I-girders in the elastic range and compared this behavior to that of comparable straight girders. A theory of elasticity approach was used to determine the prebuckling longitudinal and radial normal and shearing stresses by treating each half of the flange as a separate plane stress problem. Also, the governing differential equations for the flange halves were derived and solved using the finite-differences method. Using these approaches, the plate bucking coefficients (*k*) were obtained for several combinations of bending stress and warping normal stress. These buckling coefficients can be used in the equation

$$\frac{b_f}{t_f} \leq 26.99\sqrt{k} \qquad (2.1)$$

to obtain the value of flange width-to-thickness ratio to prevent buckling in the elastic range. The study found, among other conclusions, that as girder curvature increases, the prebuckling radial flange stresses will increase, and that the difference in the buckling behavior of curved plates and rectangular plates within the elastic range is primarily due to the curvature of the plates.

Culver and Nasir (1971) continued Culver and Frampton's research of investigating the buckling behavior of curved I-girder flanges by studying the effects of the residual flange stresses due to curved I-girder fabrication processes. This study considered buckling in both the elastic and inelastic ranges. The fabrication methods investigated are flame cutting flanges from rectangular plates, cold bending a straight girder or roller beam, and fabricating a straight girder and then heat curving. The flanges were modeled similarly to the flanges in Culver and Frampton (1970) and the equations were once again solved using the finite-differences method.

The study found that an increase in web thickness results in increasing the minimum buckling coefficient value. Additionally, researchers concluded that the degree of yielding across the flange width had a significant effect on both the minimum buckling coefficient and the associated buckled wave length of the section. The efficient use of diaphragms and a composite deck slab limited the warping normal stresses in curved girders due to a nonuniform torsion. Presence of residual stresses in fabricated girders caused portions of the compression flange to yield even though the applied moment was less than the yield moment in a residual stress free girder. For flame cutting and cold rolling fabrication, the combination of residual stresses with a small flange bending moment reduced the factor of safety against local buckling provided by existing flange width-to-thickness limitations for straight girders. For heat curved fabrication, the tensile residual stresses are beneficial and resulted in an increase in the factor of safety for yielding moment under bending alone.

### 2.3.3 Web Panel Behavior

Culver et al. (1972) conducted a theoretical investigation into the bending behavior of cylindrical web panels of transversely stiffened curved I-girders. A simple physical model was derived numerically to perform the investigation. This model provided results pertaining to the magnitude of web bending stresses along with the reduction in

yield moment due to curvature effects. The researchers presented an equation for the limiting value of web slenderness for a transversely stiffened curved section:

$$\frac{d}{t_w} \le \frac{35000}{\sqrt{F_y}}\left[1 - 8.6\left(\frac{2a}{R}\right) + 34\left(\frac{2a}{R}\right)^2\right] \qquad (2.2)$$

where $F_y$ is the girder yield strength, $2a$ is the girder span length, and $R$ is the radius of curvature. Although equations are presented for the reduction in girder yield moment due to curvature, the reduction in moment is negligible within the limits for girder yield ratio presented in Equation 2.2. Finally, the research concluded that the existing transverse stiffener requirements for straight girders are applicable for curved girders as well.

Mariani et al. (1973) investigated a curved panel with transverse stiffeners representative of a stiffened web of a curved I-girder to determine the optimal design rigidity of transverse stiffeners to prevent web buckling. The model was quite simple having all sides simply supported and neglecting bending as well as the restraint provided by the flanges. The numerical analysis implored the system equilibrium equations solved using Galerkin's variational method. Because curved web panels have a higher elastic buckling strength than straight panels, it was recommended that existing AASHTO formula for transverse spacing of stiffeners be used for curved girders. The required stiffener rigidity can be obtained by multiplying the AASHTO stiffener rigidity for straight girders by a factor, $\gamma_c^o/\gamma_s^o$, to account for curvature. Although for an aspect ratio less than 0.78, the required stiffener rigidity of a curved panel was found to be less than that of a straight panel, it was decided that the rigidity requirements for curved girders should not be less than those for straight girders. For an aspect ratio between 0.78 and 1.0, the required stiffener rigidity increases nonlinearly with curvature. The optimal design rigidity of transverse stiffeners to prevent premature failure due to shear buckling is given as:

$$\frac{a}{d} \le 0.78, \qquad \frac{\gamma_c^o}{\gamma_s^o} = 1.0 \tag{2.3}$$

$$0.78 < \frac{a}{d} \le 1.0, \qquad \frac{\gamma_c^o}{\lambda_s^o} = 1.0 + \frac{\left(\frac{a}{d} - 0.78\right) Z^4}{1{,}775} \tag{2.4}$$

where *a* is transverse stiffener spacing, *d* is web depth, and *Z* is a panel curvature parameter defined as:

$$\frac{a}{d} > 1.0, \qquad Z = \frac{d^2}{Rt_w}\sqrt{1-\nu^2} \tag{2.5}$$

$$\frac{a}{d} \le 1.0, \qquad Z = \frac{a^2}{Rt_w}\sqrt{1-\nu^2} \tag{2.6}$$

Culver et al. (1973) continued the study on curved web panels by investigating the effect of the addition of longitudinal stiffeners on web response. Instead of idealizing the web as a small cylindrical strip as was done in Culver et al. (1972), a model of the entire web panel was developed numerically. The study yielded a web slenderness ratio for curved girders with longitudinal stiffeners required to limit the web bending stresses in a curved panel to the web bending stress level in a straight panel as:

$$\frac{d}{t_w} = 330\left[1 - 2.9\sqrt{\frac{2a}{R}} + 2.2\left(\frac{2a}{R}\right)\right] \tag{2.7}$$

If adequate longitudinal stiffeners are provided in both the tension and compression regions, Equation 2.7 need not be used because no reduction in $d/t_w$ is required. Additionally, the authors present tentative design recommendations for longitudinal stiffener design in the form of rigidity (Equation 2.8), radius of gyration (Equation 2.9), and width-to-thickness ratio (Equation 2.10).

$$I = dt_w^3\left[2.4\left(\frac{2a}{d}\right) - 0.13\right] \quad (2.8)$$

$$r \geq \frac{2a\sqrt{F_y}}{23{,}000} \quad (2.9)$$

$$\frac{b}{t} \leq \frac{2600}{\sqrt{F_y}} \quad (2.10)$$

## 2.4 Curved I-Girder Compression Flange Behavior

Kang and Yoo (1990) presented an analytical study to examine the allowable flexural stresses permitted by AASHTO Specifications (1980) for curved I-girder members. MSC/NASTRAN was used to produce a simple curved I-girder finite element model for the analysis. Results indicated that the effect of warping on girder lateral buckling strength is negligibly small for a wide range of parameters and initial (small) curvature actually slightly increases buckling strength. Study results concluded that the local buckling strength is not only affected by the compression flange width-thickness ratio but also substantially affected by the initial curvature and warping normal stresses. Finally, numerical analyses presented in this paper based on MSC/NASTRAN models showed considerable differences in dealing with curved bridge girders as compared to the 1980 AASHTO Guide Specifications.

Madhavan and Davidson (2003) studied the effect of curvature on the elastic local buckling behavior of the compression flange of curved I-girders. The analysis simplified a curved flange as a straight flange subjected to lateral forces which are in the form of linearly varying edge loads simulating the combined effects of bending and torsion. Three analytical approaches were used: 1) Bucking solutions were obtained for the inner and outer flange half separately using the energy method. The conditions at the flange-web juncture are taken as simply supported and fixed, 2) the Galerkin method

was used to derive and solve system differential equations for a full flange with the flange-web juncture modeled as simply supported, and 3) the FE program MSC/PASTRAN version 2000 was used to create models of the full flange and the results were compared to those from the first two approaches. Boundary conditions at the flange-web juncture were varied to represent all the conditions in the previous two analyses.

The researchers found that the full flange model demonstrates a greater load carrying capacity than the half flange models due to the stiffness provided by the inner flange; thus, design criteria cannot be based upon buckling behavior of the isolated half flange solutions. Also, even in the case of maximum load variation without causing tension in the inner flange, the decrease in buckling capacity compared to uniform compression was only around 2 percent, indicating that the effect of load variation (girder curvature) was insignificant when a full flange was considered.

Davidson and Madhaven (2005) conducted a study to improve the understanding of curvature effects on the buckling resistance provided by the flanges and to improve the definition of slenderness limits for horizontally curved bridge I-girders. The authors developed slenderness limits for non-compact, compact, and compact-flange sections. To define the non-compact section limit, the theoretical model created by Madhavan and Davidson (2005) in which the curved flange section was modeled using a straight plate section subjected to compressive stress gradient with the loaded edges simply supported and the non-loaded edges free and rotationally stiffened along the centerline was used. A Galerkin series was used to solve the flange plate and to define the non-compact limit ($\lambda_r$).

$$\left(\lambda_r\right)_{cv} = \left(\lambda_r\right)_{st}\sqrt{\varphi} \tag{2.11}$$

$$\varphi = \frac{10}{10 + \frac{f_l}{f_b}} \tag{2.12}$$

Where $f_l$ is the total factored flange bending stress at the section under consideration and $f_b$ is the factored average flange stress at the section under consideration. The slenderness limit for curved compact sections ($\lambda_p$) can be taken as the same as that of a straight section.

$$\lambda_p \leq 0.382\sqrt{\frac{E}{F_y}} \tag{2.13}$$

Where $F_y$ is the yield stress. The slenderness limit for a compact-flange section ($\lambda_{cf}$) was derived using a modified form of Lay's model (1965).

$$\lambda_{cf} = \left[\frac{2}{\sqrt{4-\alpha}}\right]\lambda_p \tag{2.14}$$

Where $\alpha$ is the ratio of lateral bending to vertical bending stress. Also, based on the compactness limits developed, nominal flexural resistance equations for flange local buckling of curved I-girders were proposed. Finally, the authors stated that design criteria cannot be based upon buckling behavior of isolated half flanges for load situations that result in a stress gradient across the flanges.

Madhavan and Davidson (2007) evaluated the elastic buckling capacity of the flanges of I-shaped beam members subjected to a stress gradient considering three sets of support conditions. The objective was to define the effect of stress gradient on the elastic local buckling behavior of flange plates and to develop equations based upon this for design use. This phenomenon is important for curved girders because beam curvature causes stress gradients in flanges under normal loading conditions. To accomplish this, the researchers evaluated an isolated plate system with web interaction idealized as a centerline boundary condition. Three sets of boundary conditions were used: 1) The half flange was considered and a simple support condition was applied at the

web/flange boundary. 2) Similar to condition 1, but this condition considers a clamped boundary at the web line. 3) A Galerkin series was adopted for analyzing the full width of a flange plate with a variable rotational stiffness at the web line.

The conclusion of the study presented a series of equations that reflect the influence of the stress gradient and web plate rigidity on elastic flange buckling. Researchers also found that the effect of stress gradient is coupled with the rotational resistance provided by the web, and therefore the two sides cannot be isolated in evaluating the buckling resistance of the flange plate system when a stress gradient is present. An approach for incorporating the effect of a stress gradient into flange slenderness design requirements was illustrated. Most notably, a flange slenderness parameter is presented which incorporates the effect of stress gradients on the slenderness requirements.

$$\lambda_f = 1.35\sqrt{\frac{E}{F_{yf}/k_c\varphi}} \qquad (2.15)$$

In Equation 2.15, $\varphi$ is a parameter that reflects the reduction in buckling capacity due to the stress gradient coupled with the rotational resistance of the web. Values for this parameter are given in the paper, but they are omitted here to maintain brevity. The symbol $k_c$ is the buckling coefficient incorporating the effect of web restraint.

## 2.5 Curved I-Girder Web Panel Behavior

Abdel-Sayed (1973) used the theory of linear shells to study the prebuckling behavior of curved web panels subjected to loading in the form of pure shear, pure normal stresses, and combined shear and normal stresses. The web panel was simply supported on all sides with the flanges providing no torsional rigidity. The flanges and web stiffeners were assumed to have a rigidity great enough in their direction that no strains

developed along the edges of the panel. The lower bound of the critical load was investigated which resulted from allowing the vertical edges to move freely in the direction of the panel rather than restraining them to remain straight. In allowing the vertical edges to move freely, the normal forces were assumed to be linearly distributed over the height of the web. The Galerkin method was used to solve a series of differential equations from which the minimum eigenvalues were computed corresponding to the minimum critical loads under each loading condition. Approximate formulas were given to determine the critical load limit under shear, normal, and combined loading and it was found that, in each case, the critical loading increases as the panel curvature increases from zero curvature.

Web panels of horizontally curved I-girders subjected to pure bending and combined bending and shear were also analyzed by Mikami and Furunshi (1984). A set of nonlinear differential equations were developed based upon Washizu's (1975) nonlinear theory of shells and were then solved using the finite differences method. The equations were developed for a panel subjected to pure bending and shear with boundary conditions of simple supports along the curved edges and both simple supports and fixed along the straight edges. The researchers examined cylindrical panels with various aspect ratios and curvatures. The numerical analysis came to the conclusions that the circumferential membrane stresses in the panel decrease with the increase in girder curvature, the panel under combined loading exhibits a lower level of membrane stress than the panel under pure bending, and the bending stresses under combined loading are larger than those under pure bending.

## 2.6 Bending Moment Interactions

Schilling (1996) investigated the interaction between vertical and lateral bending moments in curved girder sections. At the time of the study, AASHTO Guide Specifications (1993) permitted the vertical bending stress in the tension flange of a

compact section to equal the yield stress regardless of the magnitude of the lateral moment. However, curved I-girders must sustain lateral moments in addition to the vertical moment sustained by straight girders. A set of yield-interaction equations for compact, noncompact, and compact-flange sections were developed in this study which can be accurately used to account for the effect of lateral moments in reducing the vertical bending strength of curved I-girders. The most convenient of these relationships are equations defining the reduced flange widths as a function of the lateral moment. For a compact section, the reduced flange width ratio is defined as

$$\frac{b_y}{b} = \sqrt{1 - \frac{2M_L}{3M_{yL}}} \tag{2.16}$$

and for compact-flange sections

$$0 \le \frac{M_L}{M_{yL}} \le 1.0\,; \qquad \frac{b_y}{b} = 1 - \frac{M_L}{2M_{yL}} \tag{2.17}$$

$$1.0 \le \frac{M_L}{M_{yL}} \le 1.5\,; \qquad \frac{b_y}{b} = \sqrt{0.75 - \frac{M_L}{2M_{yL}}} \tag{2.18}$$

and for noncompact sections

$$\frac{b_y}{b} = 1 - \frac{M_L}{M_{yL}} \tag{2.19}$$

Where $b_y$ is the reduced flange width, $b$ is the full flange width, $M_L$ is the lateral moment in the flange, and $M_{yL}$ is the lateral yield moment of the flange. Reduced flange width is the flange width available to carry the vertical moment because of the addition of the lateral moment. The vertical bending strength can be calculated based on the reduced section.

## 2.7 Dynamic Analyses

Tan and Shore (1968) studied the effects of radius of curvature, rigidity ratio, vehicle speed, bridge damping, and girder warping on the dynamic response of a horizontally curved bridge when traversed by a constant moving force. The bridge is idealized as a simple prismatic beam with curvature in the horizontal plane, and differential equations representing the out of plane vibrational motion are derived. This study concluded that the two most significant parameters describing the dynamic behavior of a horizontally curved bridge are the radius of curvature and the rigidity ratio. A change in either of these parameters will result in a change in the fundamental frequency of the bridge system. As either value increases, the fundamental natural frequency of the curved bridge will approach that of an equivalent straight bridge.

A curved bridge with four I-girders is subjected to live load static and dynamic testing using a test vehicle simulating AASHTO HS20-44 design loading by Armstrong (1972). Two sets of tests were performed: the first determined the neutral axis location and load distribution and the second examined the response of the bottom flange and the cross-frames of the bridge. The study found that under both testing conditions, the maximum bending stress occurred on the inside beam, but the stress effects from combined loading did not exceed 63% of the allowable working stress. In the two outside sections, the use of lateral bracing caused the girder pairs to behave as closed box girder sections. As the truck loading moved from the outside towards the inside beam, the bottom flange warping stresses reversed. Under dynamic loads, greater vibration amplitudes were experienced on the longer outside beams than on the shorter inside beams and the maximum stress amplification was excited on the two outside girders at a truck speed of 20 m/hr.

## 2.8 Curved Bridge Load Rating

Currently used load rating analysis methods roughly estimate the effects of curvature and conservative assumptions are typically made concerning these structures. Research conducted by Krzmarzick and Hajjar (2006) was an effort to improve the accuracy of load ratings for horizontally curved composite steel I-girder bridges. To perform this research, Mn/DOT Bridge No. 69824, a horizontally curved steel I-girder bridge, was experimentally load tested and used to calibrate a computational grillage model of the bridge. The results from two other experimentally studied bridges, Mn/DOT Bridge No. 27988 and the Curved Steel Bridge Research Project test bridge (presented in later section), were also used in the sensitivity study. The grillage method was used as the analytical method because of its ease of application and availability in commercial programs. A computer program utilizing the grillage method (UMN Program) written at the University of Minnesota was used along with the commercial program MDX (2004) for comparative purposes. Experimental and analytical loading came in the form of 43 static and 13 dynamic loading configurations.

In general, the research project outlined methods that can be used to provide more accurate load ratings of horizontally curved composite steel I-girder bridges. Results show that grillage analysis can be used as the primary tool to provide accurate and efficient load rating of horizontally curved composite steel I-girder bridges, thus reducing the need for load testing on most of these structures. Moreover, since the grillage method is capable of many levels of reinforcement, the authors present recommendations to guide bridge rating evaluators toward more accurate analysis. Finally, the authors recommend that load testing should only be conducted when pretest evaluations of the bridge indicate that load testing will likely provide an improved rating for the bridge.

## 2.9 Evaluation and Development of Various Design Criteria

### 2.9.1 Distribution Factors

The study performed by Heins and Jin (1984) focused on examining the response of single and continuous curved composite steel girder bridges and developing equations for the live load distribution factor as a function of various structural configurations. The analysis was performed by modeling the structures as 3D space frame elements with the top longitudinal space frame members having the properties of the girder top flange combined with the composite deck. Bottom longitudinal members had the properties of the girder bottom flange and were connected to the top longitudinal member using vertical and diagonal web elements. AASHTO (1977) design truck or lane loading was applied, depending on the bridge length, and the model results were calibrated and verified against static calculations. Distribution factor equations developed by Heins and Jin (1982) are presented that can be used for preliminary design of curved composite I-girders. Live loads applied to isolate straight girders are multiplied by these distribution factors to account for system interaction. Additionally, a set of distribution factors was given that can be applied to stresses from the grid analysis to account for load redistribution for curved systems with bottom lateral bracing in each bay or in every other bay. The study found that, as expected, as lateral bracing in the form of bottom flange wind bracing is added to the structure, the distribution factor decreases.

The study by Schelling et al. (1989) was a continuation of the work performed by Heins and Jin (1984) by considering dead-loading that the structure will incur during construction. The study investigated the response of single and continuous span, horizontally curved, steel I-girder bridges, with and without a top lateral bracing system subjected to girder self-weight and concrete deck weight. The study presented dead

load distribution factors for varied combinations of bracing systems and system configurations.

A three-dimensional space frame model similar to the one used in the initial phase of the study was once again used. Results show that dead load was distributed more evenly among girders that are laterally braced, which results in decreasing the load to the critical outer girder. During the construction phase, the top and bottom lateral bracing acted together to reduce the dead load stresses by creating a pseudo-box girder which had higher torsional rigidity. The equations developed in this study could be used to determine the effect that a lateral bracing system has on the bridge system during construction. This analysis also indicated that results from simple spans can be conservatively applied to continuous span bridges as long as the span ratios between the single and the continuous spans do not differ greatly from unity and the supports are not skewed.

Brockenbrough (1986) conducted a series of finite element analyses to determine rational factors for the lateral distribution of live loads on typical composite curved I-girder bridges. The aim of this study was to determine the factors for typical bridge geometries as well as explore the effect of cross-frame spacing, radius of curvature, girder stiffness, and span length. The bridges investigated were two-span, continuous, four girder bridges of varying widths with simple radial end supports and fixed interior supports. Several load cases were explored for unit loads located at various transverse locations and loads located longitudinally at intervals causing maximum positive and negative longitudinal bending moments. Results from two- and three-dimensional FE models were compared to calculate the distribution factors. The 3D-FE model idealized the concrete deck and girder web as shell elements and the girder flanges, cross frames, and flange/girder connection as beam elements and the 2D-FE model exhibited the same idealization except the deck was modeled using an equivalent beam element. The FE analysis of typical bridges showed that variations in girder stiffness and cross-frame spacing had relatively small effects on live-load distribution factors, but the central

angle per span, which includes the combined effect of curvature and span length, had the largest effect on live-load distribution factor. Also, reasonable values for live-load factors can be obtained from a V-load modification of the AASHTO (1983) factors for straight girders bridges, which agreed with the FE results for exterior girders but are conservative for interior girders.

McElwain and Laman (2000) conducted a study that determined the behavior of three different in-service, curved, steel I-girder bridges when subjected to a test truck and normal truck traffic by gathering response data from instrumentation placed on the bridges. Each bridge was instrumented to measure various strains and deflections at or very close to the maximum bending moment location. In addition, SAP2000 was used to create a numerical grillage model of each bridge consisting of three-dimensional frame elements for comparison with the experimental results. The purpose of this study was to determine the dynamic load allowance values, moment-distribution factors, and the effectiveness of the grillage method.

The study showed a good agreement between the experimental and grillage method values and recommended that the grillage method be used to predict the transverse load distribution in curved girder bridges. The results also showed that AASHTO (1998) bending girder distribution factors (GDF) for single truck loading match the experimental results well while AASHTO (1993) bending GDF's under the same conditions are conservative. On the other hand, AASHTO (1993) bending GDF's for two trucks are a better approximation than then slightly conservative AASHTO (1998). The researchers found that bending dynamic load allowance (DLA) values decreased to a limiting value with increasing strain and the largest DLA values occurred at an interior girder near the centerline of the bridge, contrary to straight girder bridges where exterior girders exhibit the largest DLA.

Research reported by DePolo and Linzell (2005) evaluated the accuracy of the lateral bending distribution factors (LBDF's) presented in the 1993 AASHTO Guide

Specifications by examining calibrated numerical data. The study examined experimentally the behavior of a three-span, continuous, five I-girder, curved steel bridge using instrumentation placed upon the bridge and truck loading tests along with a finite element model created using ABAQUS (2002). Instrumentation was placed at locations of maximum positive and negative bending moment, as determined by Linzell et al. (2002). The finite element model used to numerically determine LBDF values idealized the deck and girders as shell elements, the cross-frames as beam elements, and the deck-girder connection using frame elements.

The research found that the 1993 AASHTO LBDF equation conservatively predicts the LBDF's with a level of conservatism between 20-30%. The modified AASHTO procedure, outlined in the paper, also produced conservative results near the center of gravity of the test truck, but the level of conservativeness was insignificant. Finally, it was stated that the LBDF equation in AASHTO (1993) can be used in the preliminary design analysis and initial sizing of the girder flanges, but further studies need to be done to possibly reduce the conservatism of the AASHTO equations which would reduce the size of the girder flanges.

Zhang et al. (2005) presented a study which set out to develop new formulas for live load moment and shear distribution in horizontally curved steel I-girder bridges designed for one-lane and/or multiple-lane loading. The bridges modeled in this study are done so using the grillage method with vertical and lateral translations restricted at the supports. A detailed 3DFE model idealizing the slab as a solid, the girders as plate elements, and the cross frames as trusses was created as a means to verify the grillage method. A hypothetical three-span continuous bridge structure model was created based upon mean values of bridge dimensions obtained from 111 bridges with radii of curvature less than 1500 ft. AASHTO HL93 truck loading was placed on the structures to produce maximum moment and was moved transversely across the structure in small increments.

A parametric study revealed that some key parameters for live load distribution were radius of curvature, girder spacing, span length, overhang, number of girders, ratio of girder stiffness to overall bridge stiffness, slab thickness, and girder longitudinal bending inertia. The study also found that the effects of cross frame spacing and girder torsional inertia can be neglected when concerning live load distribution. Researchers developed simplified formulas for positive moment, negative moment, and shear distribution factors for inside and outside exterior girders due to one-lane and multiple-lane loading. Comparison with FEM and grillage analysis showed that these proposed formulas have more accurate results than those presented in various AASHTO specifications.

Kim et al. (2007a) conducted a study to determine the effect of major parameters on maximum total bending moments of curved girders, establish the relationship between key parameters and girder distribution factors (GDF's), and develop new approximate distribution factor equations. The bridge investigated to perform this study was a simply supported, four curved I-girder steel bridge with a concrete deck. A preliminary study showed that the key parameters on the radial live load distribution were bridge radius, girder spacing, bridge span length, and cross frame spacing. A group of 81 bridges were designed by varying these parameters using the commercially available software program DESCUS. Standard HL-93 truck loading was used in conjunction with *AASHTO LRFD* (2006) multiple presence factors to induce the maximum girder response accounting for bending and warping normal stress in the flange of the outside girder.

Results showed that the bending effect on the GDF increases as span length increases while the warping effect on the GDF increases as the radius decreases. The most influential parameter on the total bending GDF was found to be span length. The authors proposed a GDF equation that is accurate and simple to apply for preliminary design purposes.

### 2.9.2 Stiffener Design Criteria

Kim et al. (2007b) used finite element analysis to study the behavior of one- and two-sided transverse stiffeners in straight and horizontally curved steel I-girders, mainly focusing on the influence of size and geometry of transverse stiffeners on the maximum shear strength for a range of girder geometries. The web slenderness, web panel aspect ratios, horizontal curvature, stiffener width-to-thickness ratio, and yield strength were varied during the tests.

The study developed united recommendations for the design of transverse stiffeners based on the results from the FE studies and the results from a number of prior research studies. The researchers showed that providing adequate transverse stiffener bending stiffness and strength is a more important consideration in developing shear postbuckling resistance than the satisfaction of an area of axial force requirement, so the proposed design equations were based on these considerations.

### 2.9.3 Cross Frame Spacing Design

Yoo and Littrell (1986) developed full-scale three-dimensional finite element models of various curved bridge configurations using the commercial software SAP (1977) to perform a parametric study as a means to develop empirical design equations. The variables for the parametric study were bridge length, radius of curvature, and number of unbraced intervals. The section consisted of 5 girders, a concrete deck, and cross members and was modeled using 8 node brick elements for the girders and deck and truss elements for the cross members. Boundary conditions were in the form of pinned-roller bearings at the girder ends. Dead loads were imposed in the form of gravity loading as well as dead loading corresponding to a lightweight traffic railing over the

slab edges. Live loads came in the form HS 20-44 truck loads located to produce maximum torsional loads.

The results from the FE modeling were analyzed by linear and nonlinear regression techniques to produce empirical design equations. An equation was developed, based on dead and live loads, which provided a guideline for maximum cross-member spacing.

$$\frac{L}{N} = L\left[\ln\left(\frac{F_{ws}R}{18.890L}\right)\right]^{-1.3364} \qquad (2.20)$$

where *L/N* is the cross-member spacing, $F_{ws}$ is the ratio of maximum warping stress in a curved bridge to maximum bending stress in a straight girder bridge, *L* is span length, and *R* is radius of curvature.

Some conclusions formed from this study are that the girder cross section will warp considerably under dead and live loads if not laterally braced, but the addition of cross bracing past a two-bay installation does not significantly affect the normal bending stress or maximum deck deflection.

### 2.9.4 Response of Curved Compared to Straight I-Girders

The previously discussed study by Yoo and Littrell (1986) also investigates a group of curved I-girder responses and compares them to the similar responses encountered in a straight girder system under identical loading conditions. The testing procedure for this study has been previously discussed in Section 2.9.3. Once again, finite element results analyzed using linear and nonlinear regression produced a set of design equations. Along with a maximum cross-member spacing equation, equations predicting the ratio between curved and straight girder maximum bending stress, maximum warping stress, and maximum deck deflection under dead and live loading were developed. The study

also showed that, in curved I-girders, cross-sectional deformation leads to high warping stresses that may exceed the magnitude of longitudinal bending stresses.

A study by DeSantiago et al. (2005) used a simple three-dimensional finite element analysis on a series of single span horizontally curved bridges to investigate the significance of curvature in increasing bending moment and causing torsion in curved girder systems compared to straight girder systems. A bridge consisting of seven parallel I-girders was studied with varying curvatures of 10, 15, 20, 25, and 30 degrees, varying lateral bracing configurations ranging from no lateral bracing to bracing at 1/30 of the span length, varying unsupported girder lengths, and with and without a compositely attached concrete deck. Finite element modeling idealized the slab and girder webs as shells and the flanges, cross-bracing, and shear studs as beam elements. Loading came in the form of dead weight loading and AASHTO recommended truck loads placed at various locations.

The results showed that the largest bending moment and vertical deflection is found in the outside girder and the location of the maximum torisonal moment varied with the most severe cases in the middle girders closer to the inner girders. Considering the most extreme curvature (30 degrees), the vertical deflection of the curved bridge was about 80% higher than that of a straight bridge. It was noted that vertical deflection increased as the distance between lateral supports increases, curved bridges experienced about 23.5% higher bending moment than straight bridges, and a sizable amount of torsional moment was introduced.

## 2.10 Curved Steel Bridge Research Project (CSBRP)

In 1992, the Federal Highway Administration (FHWA) initiated the Curved Steel Bridge Research Project (CSBRP) as a large scale experimental and analytical program aimed at developing new, rational guidelines for horizontally curved steel bridges. This project

was divided into six major tasks: 1) synthesis of previous research, reported in Zureick (1994) and Zureick et al. (2000) 2) investigation of construction issues, 3) determination of nominal bending and shear strengths, 4) study of connection details, 5) serviceability considerations, and 6) determination of the levels of analysis required for horizontally curved girders (Zureick et al., 2000). The information from this study was recounted through a number of papers, thesis, dissertations, and reports.

Because all previous research on curved bridges had been performed on either small scale systems or on medium scale single girder systems with idealized loading and boundary conditions, a test frame bridge was constructed at the FWHA Turner-Fairbanks Research Center consisting of three concentric girders with a center span length of 90 ft. For the initial testing, six I-girder compact specimens were spliced into the center of the outside girder to investigate the response of different I-sections under a myriad of loading conditions. A major analytical and experimental effort in the first part of this study was dedicated to establishing the size of the cross frame members (Linzell et al., 2003), but was omitted here because it is not relevant to the present study. An elaborate instrumentation system consisting of nearly 800 data channels was installed on the test frame prior to construction. The vast instrumentation system consisted of load cells, displacement transducers, inclinometers, and resistance and vibrating wire strain gages. This test section was used for a majority of the experimental analyses performed for this study, which were combined with theoretical and analytical analyses to meet the research goals.

### 2.10.1 Connection Details

The thesis by Keller (1994), also detailed in Davidson et al. (1996), developed a series of FE models of curved steel I-girder bridges using ABAQUS (1988) to study the effect of a number of parameters on a curved bridge system response compared to an equivalent straight bridge system response. The modeling technique idealized girder webs and

bridge deck as shell elements, flanges as beam elements, and cross-frames as beams and trusses. The deck-girder shear connection was modeled using beam elements designed with low bending stiffness. For composite loading, the deck was assumed fully cured with live loading in the form of HS 20-44 AASHTO (1992) truck loading, but for noncomposite loading, the weight of the uncured deck as well as the girders was applied as a distributed load.

The bridge parameters investigated included cross-frame spacing, span length, girder depth, number of girders, flange width, girder spacing, and degree of curvature. Based upon the finite element analysis, the studies concluded that span length, radius of curvature, flange width, and cross-frame spacing have the greatest effect on bending-to-warping stress ratio of curved systems in comparison to straight systems. The study also concludes that design equations for cross-frame spacing presented by Yoo and Littrell (1986) consistently give values that are unconservative with respect to values used in actual design. Three dimensional FE analysis on a large number of hypothetical curved I-bridges was used to produce the following equation for the required cross frame spacing ($l$) needed to limit lateral flange bending in curved I girders:

$$l = L\left\{-\ln\left[\frac{(F_{ws})Rb_f}{6.108L^2}\right]\right\}^{-1.52} \tag{2.21}$$

where, $F_{ws}$ is the warping-to-bending stress ratio, $R$ is the radius of curvature of the exterior girder, $L$ is the girder span length, and $b_f$ is the flange width. Another design equation for cross-frame spacing derived from a simple static analysis using the V-load method was given as:

$$l = \sqrt{\frac{5}{3}F_{ws}Rb_f} \tag{2.22}$$

Equation 2.22 was shown to give more favorable, or conservative values, for cross-frame spacing than Yoo and Littrell's. AASHTO *Guide Specifications* (2003) instruct use of Equation 2.22 as a preliminary guide for intermediate cross frame spacing with a maximum value of 0.3 used for $F_{ws}$.

The work by Keller continued by studying the effectiveness of the United States Steel Corporation's (1984) V-load method in determining the cross member forces in a curved structure. The finite element results and V-load results for cross member forces exhibited a good correlation indicating that the V-load method translates well to design and no improvement in accuracy or simplicity can be expected to be made. Also, Keller studies the effect of lateral bracing in the plane of the top and bottom flange. Results showed that the addition of lateral bracing significantly increases the torsional rigidity of a curved I-girder system by causing the system to behave more like a box-girder system. However, because the warping to bending stress ratio remained nearly the same as that of an unbraced section, the previously derived equations are still valid when lateral bracing is present in the plane of the flanges.

### 2.10.2 Curved I-Girder Strength

Yoo et al. (1996) derived elastic stiffness and geometric stiffness matrices for a curved beam element and verified the rigor and validity of the derivation by a series of numerical examples. A strength predictor equation was developed correlating the critical moment for straight and curved beams:

$$y = \left(1 - 0.1058x^{2.129}\right)^{2.152} \qquad (2.23)$$

where $y$ is the critical moment ratio ($M_{buckling}$ /$M_{straight}$) and $x$ is subtended angle.

The elastic buckling behavior of the compression flange of horizontally curved I-girders was studied by Davidson and Yoo (1996) through the solving of the system differential equations and finite element modeling. First of all, through a finite element load buckling investigation, the study showed that as girder curvature increases (radius of curvature decreases) the normal bending stress and warping-to-bending stress ratio of a curved girder system increases.

The governing differential equations were developed in polar coordinates using a classical approach for a curved plate segment subjected to forces at the middle of the plate, solved using the finite differences method, then developed into a computer program to produce numerical results. The flange plate was modeled in various ways such as the inside half alone, the outside half alone, and the entire plate as one with the web modeled as a set of both simply supported and fixed boundary conditions. Loading came in the form of stress gradients representing the warping stress. These finite difference models produced an equation for the elastic buckling stress of a plate with results that agree with Culver and Frampton (1970) that curvature has no significant effect on the elastic buckling behavior of curved compression flanges at aspect ratios greater than four.

Finite element models were created using MSC/NASTRAN (1994) utilizing four node shell elements with distributed loading applied to the top flange and boundary conditions chosen to simulate the central section of a full curved bridge girder. A number of sections of varying cross section and length were investigated to determine which parameters effected flange buckling. Lastly, a FE model of just the compression flange was created with the web represented by boundary conditions at flange midline allowing either fixation or rotational freedom about the longitudinal direction with a distributed load placed along the flange midline.

This study concluded that the presence of the stress gradient, not the girder curvature, affects local flange buckling. Two major parameters contributing to the effect of curvature on compression flange buckling are the stress gradient at the top flange and the relative torsional restraint provided between the flange and the web. Also, the study found a complex interaction between the web and the compression flange that cannot be accurately modeled by assuming boundary conditions for the web, indicating that solving the system using differential equations and the finite difference approach is flawed. An equation is presented to be used for the reduction in buckling strength of a curved compression flange which was found to be conservative compared to the AASHTO (1993) guidelines but not as conservative as the Haushin guidelines (1988).

$$\varphi = 1.05 - \frac{l^2}{4Rb_f} \tag{2.24}$$

where ϕ is the reduction in buckling strength due to curvature, *l* is the length between cross-members, *R* is the girder radius of curvature, and $b_f$ is the flange width. This reduction in buckling strength can be applied to the straight compression flange width/thickness design equation for preventing local buckling, resulting in the equation for required curved compression flange width/thickness ratio to prevent local buckling

$$\left(\frac{b}{t}\right)_{cv} = \left(\frac{b}{t}\right)_{st} \sqrt{\varphi} \tag{2.25}$$

where *b/t* is the compression flange width-to-thickness ratio.

Yield-interaction equations proposed by Schilling (1996) did not include the unbraced girder length as a parameter, and Yoo and Davidson (1997) stated that any strength equation for the design of curved girders without this parameter cannot be very useful. Therefore, Yoo and Davidson took unbraced length into account when developing

interaction equations for determining the combination of vertical and lateral moments that could be sustained by compact, compact-flange, and noncompact sections of horizontally curved composite and noncomposite steel I-girders.

The overall study examined 18 bridges with six having a single span and 12 having three spans. Half of the bridges had three girders while the other half had four girders. Bridge bearings were assumed as pin-roller connections. A uniformly distributed dead load corresponding to the weight of the girders, deck, and cross frames was applied to the girders. The method of finite-differences was used for analysis by implementing the software CURSYS developed by Yoo and Heins (1973).

Comparing the results of the strength predictors given in this study to previously formed ultimate strength tests as well as results obtained from the predictor equations of others yielded what appeared to be an excellent agreement. The equations are not presented here and readers are referred to the work for more detailed explanation. Yoo and Davidson's formulations are theoretically pure and solely based on the static equilibrium of the cross sections. They offer a theoretically pure starting point for defining the strength of current composite sections and offer advantages over previous works.

Davidson et al. (1999a) reported on the theoretical portion of the study which developed predictor equations that can be used to approximate the linear behavior of the system and also used the finite element method to verify the validity of the theoretical equations. The FE program MSC/NASTRAN (1994) was employed to create a number web panel models with varying girder dimensions. Boundary conditions were modeled as both simple and fixed at the panel ends and top and bottom along with an additional boundary condition on the top and bottom in which beam elements are used to simulate top and bottom flange rigidity. Loading was applied to the panel ends to simulate bending moments.

A lateral pressure analogy was used to develop equations to predict the maximum curved web transverse, or "bulging", displacement ($\delta_{max}$) as:

$$\delta_{\max} = \frac{\alpha h_c \sigma_m 12\left(1-\upsilon^2\right)}{E t_w^2 R} \tag{2.26}$$

and also the resulting maximum plate bending stress at the flange/web junction ($M_{b\vartheta}$) as:

$$M_{b\theta} = \frac{\beta h_c^2 t_w \sigma_m}{R} \tag{2.27}$$

with $\alpha$ and $\beta$ being constants depending on the location of the displacement or moment, $h_c$ the height of the web panel in compression, $\sigma_m$ the stress at the flange/web line resulting from vertical bending moment, $t_w$ the web panel thickness, and $\upsilon$ and $E$ the Poisson's ratio and Young's Modulus of the material, respectively. Comparison of results of these equations with finite element values confirmed the use of these equations for conservative analysis. Davidson et al. (1999a) also concluded that as web curvature and panel slenderness increases, the membrane stress distribution becomes increasingly nonlinear through the section depth, a curved section would be unable to carry as much of a vertical moment as a straight section before yielding, and elastic buckling critical stresses are higher for curved panels compared to flat panels.

A subsequent paper by Davidson et al. (1999b) continues on the aforementioned research by developing equations representing the decrease in nominal strength of the curved I-girder due to curvature. To accomplish these goals, previously mentioned theoretical equations and finite element models were used to investigate the elastic buckling and geometrically nonlinear behavior of the curved web panels.

The researchers computed reduction factors on the girder web slenderness due to curvature based upon the maximum transverse displacement ($R_d$):

$$R_d = 0.185\sqrt{\frac{R}{D}} \leq 1.0 \tag{2.28}$$

and based upon the maximum stress of the curved web panels ($R_s$):

$$R_s = \sqrt{\frac{1}{\varphi_w}} \tag{2.29}$$

$$\varphi_w = \sqrt{1 + 0.161\left(\frac{h_c}{t_w}\right)\left(\frac{h_c}{R}\right) + 0.128\left(\frac{h_c}{t_w}\right)^2\left(\frac{h_c}{R}\right)^2\left(1 + 1.5\sqrt{\frac{h_c}{R}}\right)} \tag{2.30}$$

where $D$ is the web depth and $\varphi_w$ is the factor representing the curvature effects on the maximum stresses in the web panel due to vertical bending moment. These factors indicate the reduction in moment carrying capacity of curved girders due to bulging displacement. It should be noted that at this point, experimental verification still needed to be performed before adopting these criteria. However, it was found that the factors based on maximum stress from this study match favorably with those developed by Nakai (1986) and Daniels (1980) and also show that results from Culver (1972) are ultraconservative (just as Daniels concluded). Comparisons in this investigation showed that the stress criteria will always govern the design of curved I-girders.

The next phase of the study, reported by Davidson and Yoo (2000), consisted of creating a finite element model of the three-girder test frame constructed as part of the CSBRP. Analysis using this FE model was used to further evaluate the applicability of the previously discussed strength predictor equations along with equations developed by other researchers. The FE model dimensions were based on the dimensions of the

CSBRP test frame and the model was created using MSC/NASTRAN (1994). As in the experimental tests, specimen of varying dimensions were placed at the center span of the outside girder and analyzed.

The FE study revealed an excellent agreement between FE results and predictor equations for the ultimate strength and yield moment presented by Yoo and Davidson (1997) for doubly symmetric sections. However, the yield interaction equations are less accurate for singly symmetric sections. Also, a generally good correlation was observed between FE results and predictor equations given in Davidson et al. (1999a,b) for both maximum bulging lateral displacement and maximum stress while showing that all cases are conservative with respect to design. Finite element results also confirmed that critical stresses for curved panels are slightly higher than those for straight panels. Generally, the predictor equations developed in previous research by the authors exhibited a good correlation with the FE analysis that was found to be conservative for design use. The only exception appeared to be the yield interaction equations when used for prediction on singly symmetric sections with smaller compression flanges. It is of note that this research did not include a concrete deck, and the authors state that further research is needed on a composite section.

Davidson et al. (2000a) continued the study on curved I-girder webs by investigating the curved web panels under combined bending and shear to determine if the addition of shear loading decreases the girder strength. Namely, the research investigated if the previously mentioned predictor equations are still applicable under bending and shear.

The previously discussed curved girder FE model was once again used with incremental bending and shear loading applied beyond the critical load of combined bending and shear. Results showed an increase in transverse displacement when applied shear is combined with applied bending, but the magnitude of the displacement increase decreases as the curvature becomes greater. There was only a small decrease in

moment carrying capacity observed and it was determined that the previously calculated predictor equations were still conservative. Therefore, it is reasonable to neglect a decrease in vertical bending strength with combined shear up to one-sixth the maximum shear strength.

The next step was performed by Davidson et al. (2000b) using the same techniques as the previous studies to formulate strength reduction equations for curved plate girders with longitudinal stiffeners. Two stiffener cases are considered, one stiffener in the compression region only and one stiffener in each the compression and tension region of the web. FE buckling analysis has showed that elastic buckling behavior of curved panels with longitudinal stiffeners is basically the same as that of straight girders, so the stiffeners are placed at the same locations specified in design for straight girders. Equations are developed defining values that can be used in Equation 2.29 to obtain a slenderness reduction factor based on stresses.

$$\varphi_{w-t} = \sqrt{1 + 0.161\left(\frac{h-h_c}{t_w}\right)\left(\frac{h-h_c}{R}\right) + 0.128\left(\frac{h-h_c}{t_w}\right)^2\left(\frac{h-h_c}{R}\right)^2} \qquad (2.31)$$

$$\varphi_{w-c} = \sqrt{1 + 0.0384\left(\frac{h_c}{t_w}\right)\left(\frac{h_c}{R}\right) + 0.00728\left(\frac{h_c}{t_w}\right)^2\left(\frac{h_c}{R}\right)^2} \qquad (2.32)$$

Values from Equations 2.31 and 2.32 are input into Equation 2.29 in place of $\varphi_w$. If one stiffener is present in the compression region, the greater of Equation 2.31 and 2.32 should be used, but if there is a single stiffener in the compression and tension region, Equation 2.32 is to be used. The study demonstrated the superiority of the developed equations to design equations in both the American and Japanese design codes. However, although these equations improved understanding of behavior, at this point experimental verification was still needed.

### 2.10.3 Curved Bridge Behavior During Construction

In general, the construction of horizontally curved steel bridges is far more complex compared to the construction of equivalent straight bridges. However, once curved girder bridges are constructed they generally perform as they were intended. Most problems that have occurred with curved girder bridges have been related to fabrication and assembly procedures or unanticipated or unaccounted for deformations that occur during construction (Grubb et al., 1996). Therefore, for a curved structure to perform properly, or as designed, construction issues become very important and any irregularities must be resolved. Although there were no specific solutions presented to construction problems, Grubb et al. (1996) identified and provided some in depth information on some important issues related to fabrication, erection, and concrete deck placement of curved steel bridges which helped serve as an initial step of the CSBRP program in investigating the behavior or curved steel bridges during construction.

The dissertation by Linzell (1999) detailed various aspects of the analytical and experimental work performed for the CSBRP. In particular, Linzell described in detail the experimental test frame including all geometrical and material properties, erection sequence, and problems encountered, documented the instrumentation used in the study, discussed and examined the cross frame component tests completed during the instrument planning phase, documented nine erection study tests completed during the construction of the test frame, performed FE studies of the erection sequence for comparisons with experimental work, and compared V-load method calculations with experimental and FE values.

The FE model was solved using ABAQUS and idealized all of the web panels as shell elements. The flanges of the inside and center girders were modeled as equivalent

beam elements, but the flanges of the outside girder were modeled as shell elements. Beam elements were also used to represent the cross frame and lateral bracing members. The boundary conditions were created to simulate the actual support conditions on the structure. Spherical bearings allowing movement in all directions except vertical displacements were modeled on the inside and outside girders and guided bearings were modeled on the center girder. Guided bearings are similar to spherical bearings but constrain radial translation. Intermediate shoring points utilized during erection studies were accounted for by constraining corresponding nodes on the bottom flanges. Loads representing the self-weight were implemented in the study.

Linzell showed that the detailed ABAQUS finite element model created for this study provided acceptable predictions of erection behavior. Interestingly, results showed that using measured geometric and material properties instead of nominal properties did not significantly improve analytical results. From comparisons with one erection sequence, the V-load method was shown to give conservative estimates of mid-span moment for the exterior girder and cross frame axial forces, but a nonconservative estimate of the interior girder mid-span moment.

Linzell et al. (2004b) reported on a series of experimental studies conducted on the aforementioned CSBRP curved girder test section during erection. The main purpose of this study was to assess the capability of analytical tools in predicting girder response during construction, namely the finite element and V-load method. A three girder, simply supported test frame was equipped with a vast instrumentation system prior to construction which measured girder support reactions, girder, cross-frame, and lateral bracing strains, and numerous girder displacements. The FE model of the test section was created using ABAQUS.

One, two, and three girder tests with varying cross bracing arrangements were performed on the test frame by removing the shoring and measuring the test frame

response. Results from the tests demonstrated the beneficial effects of providing minimal radial restraint for curved I-girder during construction and also the effects of nonuniform shoring removal on system response. The analysis also showed that the finite element method was a good predictor of the erection behavior and that replacing nominal geometric and material properties with measured properties in the FE model, once again, did not significantly improve the analytical results. Use of the V-load method provided conservative force estimates for the outside girder and nonconservative estimates for the inside girder as well as conservative predictions of cross-frame axial forces.

### 2.10.4 Reliability of Modeling Techniques for Design Use

Zureick and Naqib (1999) complimented previously published reviews by presenting an updated survey of the analytical work conducted on horizontally curved steel I-girder bridges. Based on the review of published literature, the authors made conclusions concerning the usefulness of various analysis methods. Mainly because of underlying assumptions made during their application, the plane grid, space frame, and the V-load methods are recommended only for preliminary design use. Although the finite element method is the most involved and time consuming of the analysis methods, it was still found to be the most general and comprehensive technique available. The other refined methods (finite-strip method, finite-difference method, analytical solutions to differential equations, and the slope deflection method) proved to be as good as the finite element method, but are limited to certain configurations and boundary conditions and are generally more cumbersome to use.

Chang et al. (2005) investigated the qualities and limitations of using a number of different modeling strategies for the design analysis of curved I-girder bridge systems. These modeling strategies include a modified line girder analysis using the V-load method, the grillage method, and finite element methods. This study was performed as

a part of the CSBRP and the experimental results from the study were used for the assessment of the different approaches. The study found that a finite element model using shell elements to model the slab and beam and shell elements to model the I-girders provided the most accurate representation of the structural responses. Another FE method was investigated that used shell elements for the slab and open walled section beam elements for the girders. This method gives accurate to somewhat conservative results as long as rotational release is provided between the slab and the open walled section beam elements at the top flange of the I-girder. A 3D-grillage method also gives accurate to conservative results as long as the contribution of the slab to the St. Venant torsional constant is neglected. The other more simplified methods predict some responses well, but are inaccurate for other responses indicating that they are less useful in design analysis than the aforementioned methods.

### 2.10.5 Dynamic Testing

In a separate study by the FHWA and the Virginia Transportation Research Council (VTRC), Tilley et al. (2006) attempted to develop a FE model using SAP2000 that could be used for predicting and evaluating the dynamic response of a curved girder bridge. The curved girder test bridge erected for the CSBRP was once again employed for this study. Dynamic testing using a mass shaker was performed on the full scale bridge in the Turner-Fairbanks Structures Laboratory before and after the deck was placed. The validation of the SAP2000 model was performed by comparing response information with data from computer models created in ANSYS and ABAQUS and also with experimental data. The SAP2000 model in question consisted of shell elements representing the flanges and web, beam elements modeling the cross frames, and shell elements rigidly connected to the girders idealizing the deck. Research showed that the more detailed ANSYS and ABAQUS models provided response data the matched more favorably with experimental data. However, the SAP2000 model more accurately represented the lower modes and frequencies of the bridge.

The work by Maneetes and Linzell (2003) examined the response of the CSBRP test bridge to free vibration using finite element analysis. The experimental models were used in comparison with the experimental test results from the VTRC (Tilley, 2006). Maneetes and Linzell focused on parametric studies to investigate the effects of cross frames and lateral bracing on the bridge free vibration response. The FE model used in this study was a slight variation of the model presented by Linzell (1999). The model was calibrated by comparing VTRC experimental fundamental mode natural frequencies against fundamental frequencies from the analytical model and then the boundary conditions, geometric properties, material properties, and mass distribution were modified to satisfy the calibration.

The parametric study provided several conclusions about the influence of cross frames and lateral bracing on the bridge dynamic response. The difference between the response of the system with K-type bracing and X-type bracing is negligible. Addition of lateral bracing does not have a significant effect on the vertical girder displacement but does lead to a reduction in lateral displacement. When the dynamic response is a concern, the use of upper lateral bracing appeared to have the most benefit for this structure but lateral bracing had a negligible effect on the vertical bending stress in the structure caused by self weight. Finally, bracing in the exterior bays led to a reduction in dynamic stresses and was more effective than an unbraced system, but the addition of bracing in all bays did not significantly further reduce dynamic stresses.

### 2.10.6 Utah Bridge Study

Upon discovering that a curved steel I-girder bridge in Salt Lake City, Utah was scheduled for demolition, it was decided that this bridge should be tested as a companion project to the CSBRP. The primary objective of this study was to provide bridge behavior data to be used in validating a computer model of the bridge with the

secondary objective to examine the potential for using dynamic testing as a nondestructive evaluation technique.

Womack et al. (2001) performed static and dynamic tests on a three span continuous curved steel I-girder bridge in Salt Lake City to study the behavior of curved steel I-girders under dead load, investigate the ability of modal analysis to determine the changes in boundary conditions or structural damage, and to provide field test data for the verification of a finite element model. The dynamic testing came in the form of sinusoidal forcing and impact testing while the static loading was performed by slowly driving one or two weighted trucks along one of three predetermined paths. Researchers were permitted to alter the boundary conditions of a formerly in-service bridge and perform tests on the bridge scheduled for demolition. Three boundary condition states were studied: 1) The as-is condition in which the bridge is supported on bronze rocker bearings at abutments and piers. A number of these rocker bearings had been welded at the piers which restrained movement and the bearings at the abutments had ceased to function. The deck was also found to be integral with the approach slab for nearly 30 ft. at each end. This condition was used as the baseline test condition. 2) The boundary conditions were similar to state 1 but the integral approach slab was severed. 3) The abutment bearings were replaced and the welds were removed from the pier bearings and the bearings were greased, reducing the translational and rotational stiffness at the bearing points. For dynamic testing, the structure was instrumented with 36 velocity transducers and 8 accelerometers and for static analysis the bridge was fit with a set of 44 strain gages placed at varying locations. A linear finite element model was also created using SAP2000 which uses four node shell elements to model the girders, stiffeners, diaphragms, and deck and eight node shell elements to model the parapets. The deck to girder connection is modeled using two node beam elements with a very high axial stiffness and a flexural stiffness allowing differential movement between girders and deck.

The study discovered that, at the abutments, the interior girders and deck behaved in a non-composite fashion but at the centerline of each span they behaved in a more composite fashion. Under wheel loading, the upper girder flanges experienced significant local deformations and significant lateral bending occurred in the girders. When the deck was cut for boundary state 2, more of a pinned support behavior appeared in the exterior girders. The computer analysis showed an increase in stress of up to 9% in the bottom flanges and a shift in maximum bending stress from the exterior of the bridge to the center girder when the diaphragms were removed. The dynamic testing supports the premise that modal analysis can be used as a non-destructive evaluation technique for determining the location and type of damage a structure has experienced due to a catastrophic event.

Womack and Crookston (2003) continued the study by investigating different analysis strategies for curved, steel I-girder bridges. Although the previously mentioned SAP2000 models predicted results well, it was desirable to find other analysis methods, or FE models, that are less complicated but still give accurate results for use in analysis and design. The study basically came down to a comparison between the V-load method and various levels of FE models with the baseline information for comparison coming from the field test data collected from the Salt Lake City Bridge. The FE models were constructed with several levels of sophistication, from a flattened model using beams for the girders and shell elements for the deck to an extremely complicated model with shell elements modeling all major structural components, vertical beams modeling semi-composite behavior, springs simulating boundary conditions, and super elevation and curvature maintained. The basic comparison parameters were percent error in strain, influence diagrams created for strain, and girder deflections.

Researchers found that the use of the strain influence data is the best method for comparison between the analytical and field tested data. The analytical displacements were very sensitive to FE model changes, but the strains predicted by the various

analytical methods were quite accurate. The V-load method proved to be the most conservative analytical approach, often to extremes which will lead to significant over design of bridges. The most accurate analysis method was, as expected, the most complicated and detailed FE model. However, the FE models using beam elements for the girders and shell elements for the deck are recommended for use in design because they exhibit good, conservative accuracy, have simple implementation, are solved quickly, and provide the best combination of efficiency and result accuracy.

Mertlich et al. (2007) expanded on the research by Womack et al. (2001) to determine the load carrying capacity of the bridge under three boundary condition states. The loading and boundary conditions for the study were identical to the ones used by the previous researchers.

In general, the report concluded that changing the boundary conditions increased the maximum moments by only 5%, but the modal frequencies were changed by up to 34%. This conclusion is a further encouraging indication of the feasibility of structural health monitoring using dynamic techniques. Additionally, a reduction in the restraint stiffness resulted in a change in the order of modes for each of the testing boundary condition states. A few of the recorded modes increased in natural frequency between boundary condition states. The study also discovered that impact testing may not be suitable for testing certain types of structures because it cannot provide enough energy or time for resonance to promote the formation of contact points.

Barr et al. (2007) also presented a study on the same structure which focused on determining the bridge live-load response on the three aforementioned boundary condition states. Strain gages were placed at various predetermined critical bridge girder locations and also on a few diaphragms. Live-loading came in the form of driving two dump trucks of known weight across the structure along predetermined paths. Along with experimental results, a finite element model was created using SAP2000 as

another means of evaluating the bridge response. The model idealized the girders, deck, and diaphragms as shell elements while the concrete parapets were modeled as solid elements. Vertical frame elements were used to connect the girders and the deck and were modeled such that the properties could be varied to investigate the effect composite action had on the behavior of the bridge. The boundary conditions were varied to replicate the original and modified boundary conditions states of the test bridge. The bridge and model were subjected to live-loading under the three boundary conditions states.

Comparison of the results from field testing and the FE analysis revealed that the FE model predicted girder strains under live loading with good accuracy. Analyses found that changing the boundary conditions resulted in a change in strain that can be neglected in design. In comparing results using the V-Load Method (1984), the study shows that the overall positive moments using the V-load method were slightly unconservative for the exterior girders and slightly conservative for the interior girders when compared to the FE results. Additionally, the difference between the calculated V-load and FE negative moment was, in general, larger than the difference for the positive moment comparison. Lastly, the AASHTO (2002) distribution factors were found to be conservative for interior girders, but the FE results agreed more closely with AASHTO distribution factors for exterior girders.

## 2.11 Investigation of Construction Issues

### 2.11.1 Ford City Bridge Study

A research study was performed on the Ford City Bridge, a three span continuous partially curved I-girder bridge with four girders located just north of Pittsburgh, Pennsylvania, directed towards analyzing and promoting awareness of construction

stability issues for horizontally curved steel I-girder bridges by monitoring critical girder response parameters through nonlinear finite element modeling of the bridge. A nonlinear FE model of the bridge was created using ABAQUS idealizing the curved girder sections as QUAD4 shell elements, the cross frames as B32 beam elements, the straight girder sections as B32 beam elements connected to the neutral axis of the shell girder elements, and with the prescribed boundary conditions applied with girder uplift permitted at the supports. Since only a small amount of field data was obtained during bridge construction, another method of verification was required for the FE model. The modeling technique was verified using the experimental data from the CSBRP erection study presented by Linzell (1999). The CSBRP erection sequence was recreated using the Ford City Bridge modeling technique and the comparison of results from the experimental and analytical analyses served to validate the modeling techniques used in the Ford City Bridge study (Chavel and Earls, 2002a).

Chavel and Earls (2002a) briefly described difficulties that often occur during construction of horizontally curved steel I-girder bridges. The difficulties can come in several forms including excessive out-of-plane displacements, girders "lifting-off" of supports during construction, and inconsistent detailing of the girder cross members leading to fit-up problems. The study states that it is necessary to pay close attention to displacements during the construction of curved bridges.

Chavel and Earls (2003, 2002b), studying the erection sequence of the Ford City Bridge, revealed that displacements and stresses are very minor and support reactions follow a typical load distribution path during the construction sequence when consistent detailing is followed. However, problems were encountered in the field with girder and cross frame misalignment due to inconsistent detailing. Comparing girder deflections at one location using the FE model, field surveying, and design values showed an agreement between the FE and surveyed values which are different than design predicted values. This can be attributed to the fact that the cross-frames in the actual

structure are detailed inconsistently. This inconsistent detailing can lead to cross-frame diagonal members being of incorrect size, which will in turn lead to locked-in girder and cross-frame stresses because of external forces applied to bring components into alignment. This research showed that considerable attention must be given to construction issues related to the erection of horizontally curved I-girder bridges.

### 2.11.2 Additional Construction Studies

Hilton (1984) instrumented a simply supported, four I-girder, curved bridge span during construction to check the girder camber loss. This was of importance because the current AASHTO specifications for highway bridges required that, for heat curved I-girders, an additional amount of camber be included in them during fabrication to compensate for possible losses during service as residual stresses dissipate. Thermal gradients were documented through the thickness of the girders at various construction stages and were shown to induce bending moments in the girders causing deflections. However, this phenomenon was not of paramount concern in this study. The thermal deflections were only of interest so that they could be removed from deflection measurements in order to get true deflections due to structure weight alone. The results showed that the amount of camber loss from construction loading incurred after deck placement was only 24% of that determined from the AASHTO equation used to predict camber loss under construction loading. Additionally, no further camber losses were caused by service loading for 6 ½ months after the completion of construction. The results suggest that the AASHTO equation may not be applicable to girder having a radius of curvature of 500 to 800 feet and the radius of curvature might be a variable that should be considered in determining camber loss.

Hajjar et al. (1999) and Galambos et al. (2000) performed a study investigating the behavior of a curved I-girder bridge system during construction to determine whether the stresses in the system were accurately predicted by linear elastic analysis software

developed in this study as well as by software typically used in design. Sixty strain gages were mounted at various locations on the girders of a two-span curved structure with four girders of varying depth and with two spans divided into three sections. The spans are continuous over the central support and have cross frames consisting of a bottom chord, top angle chord, and X-brace diagonals.

The Grillage Method was used to model the structure and the girders were idealized as curved beam elements, the cross frames as truss elements, and the concrete slab as transverse beam elements. No shear studs were present on the girders in the negative moment regions, but the FE models investigated both the cases of full- and non-composite action in the negative moment regions. The boundary conditions included pins at the center support and rollers at the abutments.

Strains were measured at all construction stages of the structure as well as during field tests conducted using up to nine trucks with known weight and axel configurations. Through the field measurements and FE modeling, the researchers concluded that design was controlled by stiffness and not strength as the stresses were well below yield stress levels during construction. The FE models generally performed well in predicting bridge behavior and the main difference between measured and computed results was due to the warping restraint and minor axis bending in the measured results and to the less predictable behavior seen in the measured results of the cross-frames. The correlation between the measured and computed results increased greatly for the cases considering composite action in the negative moment regions which shows that some degree of composite action was actually present in the structure due to friction and adhesion.

A large research study reported in Domalik et al. (2005) and Shura and Linzell (2006) conducted field and numerical studies on a two-span, horizontally curved, steel plate girder bridge in Port Matilda, Pennsylvania during erection and deck placement to

provide some insight into bridge behavior during construction as well as aid in the development of better construction procedures. The field studies came in the form of an instrumentation system placed on the structure that recorded structural response throughout the construction sequence. SAP2000 was employed to create what the authors referred to as a modified grillage model, which consisted of a conventional two-dimensional grillage model of the substructure rigidly connected to shell elements representing the concrete deck. The finite element modeling technique was also used by the authors to determine the locations on the superstructure where the instrumentation was placed.

The objectives of the study were the following: 1) Evaluate the effects of curvature on warping stresses and vertical and radial deformations during all phases of construction. 2) Determine if a grillage model can accurately predict the effect of curvature on vertical bending stresses, warping stresses, and deformations during construction of the study bridge. 3) To explore the basis of the limits set forth in AASHTO (1998) Table 4.6.1.2.1-1 and determine if these limits are appropriate for the study bridge.

Research by Domalik et al. (2005) determined that curvature had a measurable effect on the vertical bending of the girders. Additionally, the SAP2000 grillage model predicted vertical bending stresses throughout the girder erection sequence and deck placement reasonably well. Although the vertical deflection comparison showed reasonable agreement, the grillage model predictors were consistently nonconservative when compared to the deflections measured in the field using full scale photogrammerty scans. Finally, the researchers suggest that the additional lateral flange bending moments generated by the out-of-plumb nature of curved girders should be considered during design.

In the report by Shura and Linzell (2006), the researchers made several conclusions based on the comparison of the field and numerical studies. First, curvature effects

were not critical when considered alone, but when combined with the construction procedures, the curvature had a significant impact on the dead load stress. Also, the effect of construction procedures on flange stresses and girder deformations should be considered when developing superstructure erection procedures for bridges of large radii. The modified grillage method did not accurately predict vertical bending and warping stress during superstructure erection, but the model accuracy improved significantly during deck placement. Additionally, researchers found that exterior-to-interior construction sequence results in lower dead load stresses and deflections than interior-to-exterior construction sequence.

Howell and Earls (2007) used detailed finite element modeling to investigate the effects that web out-of-plumbness has on flange tip stresses, vertical and lateral deflections, cross sectional distortion, and cross-frame demands, particularly during the construction process. A FE model of a three-span continuous curved steel I-girder bridge with six cocentric girders was created using ADINA (2003). The model idealizes the girders, connector plates, and transverse stiffeners as shells while modeling the cross-frames as Hermetian beam elements. The cross frames are connected to the girders using constraint equations and the boundary conditions at the piers consisted of tangentially and transversely guided bearings along with nondimensional bearing pads. Since the construction state of the girders is of concern, gravity loading is applied to the model in the form of a body force.

The results show that web plumbness has an important influence over flange tip stresses, with stress changes on the order of 20% over what normally would be computed by designers. Research also shows that increasing web out of plumbness increases vertical and lateral deflections with the outermost girders showing the greatest amplification of deflections. The vertical deflections exhibit very little sensitivity to web plumbness while the lateral deflections are considerably more sensitive. It is also observed that the cross-sectional distortion of the individual girder

sections is pronounced and likely of importance when determining the validity of applying various engineering theories of the calculation of internal cross-section stresses. Finally, the forces in the cross-frames show considerable sensitivity to increasing out-of-plumbness.

A horizontally curved, six-span steel I-girder bridge which experienced severe geometric misalignments and fit-up problems during steel erection was studied by Bell and Linzell (2007) to better understand the behavior of curved girders under construction. The complete structure consisted of two, three span continuous sections, but only one of these sections was studied. Field data in the form of girder strains and vertical and radial displacements was collected during the realignment of two previously erected spans and the completion of the final two constructed spans. A finite element model was created to study girder response during a series of different erection schemes imposed on the span. The model was created using SAP2000 with quadrilateral shell elements representing the girder flanges and webs and frame elements representing the stiffeners, cross-frames, and bracing members.

Results from the study indicated that constructing girders singly from outside-to-inside girder resulted in smaller overall deformations than constructing from inner-to-outer girder. The deformations were further reduced when constructing the girders in pairs, with the sequence placing the pairs with smaller radii first yielding the smaller deformations. By adding shoring towers and/or upper lateral bracing to the construction sequence, deformations during construction were lowered. In general, the study shows that taking steps to stiffen the overall system during construction will reduce the final overall deformations, which should result in lower induced and locked-in stresses and improved fit-up between superstructure elements.

## 2.12 Curved Girder Capacity

Shanmugam et al. (1995) determined the ultimate load carrying capacity of curved I-beams with intermediate lateral restraint and examined the effects of curvature on the behavior of these beams under bending loads. A group of experimental tests were performed on sets of hot rolled and welded I-girders with varying radii of curvature. The I-beams were simply supported at each end, but also restrained from twisting at the ends and at the location of the lateral restraint. Concentrated loading was applied at the intermediate sections where the section was laterally restrained and numerous strains and deflections were measured. A finite element analysis was performed using the software ABAQUS with triangular and quadrilateral shell elements used for idealization, material nonlinearity modeled, and boundary conditions representing the experimental set-up. The testing results indicated that the ultimate capacity of the I-beams decreases significantly with a decrease in the radius of curvature/span length ratio. Also, tests showed that cold bending of the curved sections offers a certain degree of strain hardening, which tends to give rise to a higher material strength. Comparison of the experimental and analytical results showed that the ABAQUS model was capable of predicting the ultimate load with reasonable accuracy.

The Masters thesis by Cullen (2007) used a three dimensional nonlinear FE analysis to determine the capacity of the CSBRP composite test bridge and noncomposite bending component specimens, and to compare this to the *2003 Guide Specifications* and *2004 LRFD Specifications*. The finite element models created using ABAQUS (2002) modeled the girders and deck as shell elements, the cross frames as beam elements, and used nonlinear material modeling throughout. Comparison of the bending components of the specimen B4 and B6 showed a good agreement between the FEA results and the experimental results from the previously described noncomposite test frame. A study of the maximum moment capacity showed that *2004 LRFD Specifications* was an accurate but conservative predictor and *2003 Guide Specifications* gave less accurate

predictions. *2004 LRFD Specifications* were used to calculate the capability of the test bridge at various load levels, revealing capacities all within acceptable levels. Although the *2004 LRFD Specifications* limit horizontally curved I-girder bridges to noncompact section-type requirements at the moment of first yield, this study determined that the capacity of the system at the strength limit state using the 1/3-rule equation exceeded the plastic moment capacity. The author recommended that the noncompact section-type limitations of horizontally curved I-girder bridges be removed from the *2003 Guide Specifications* and the compact section-type requirements be extended to those structures.

## 2.13 Accuracy of Curved Bridge Analysis Methods

The investigation by Nevling et al. (2006) took aim at determining the accuracy of different analysis methods in predicting horizontally curved steel I-girder bridge response. They study compared responses from the analysis methods and monitoring of an in-service horizontally curved steel I-girder bridge in the form of vertical and bottom flange lateral bending moments induced by various truck loading configurations. The analysis methods were divided into three levels with level 1 being two manual calculation methods (line girder analysis from AASHTO (1993) and the V-load method (NSBA 1996)), level 2 consisting of grillage models created using SAP2000, MDX, and DESCUS, and level 3 being three-dimensional finite element models created using SAP2000 and the BSDI 3D (2000) system.

The two manual calculation methods determined girder bending moments by analyzing the girders as equivalent straight girders and then multiplying the resulting straight girder moments by the distribution factors. The 2D methods idealized the girders as small straight frame elements, the cross frames as frame elements, and considered composite action between the flange and the deck slab only in the positive moment regions. The 3D FE models represented the top flanges, bottom flanges and cross

frames as frame elements, the webs and deck as shell elements, the parapets by increasing the stiffness of the shells at the parapet locations, and the girder/deck connection as rigid links. The support conditions were modeled to match the structure support conditions.

In general, the researchers concluded that the level 2 and 3 analyses produce girder vertical bending moments that correlate well with the field measurements. On the other hand, neither level 1 or 3 analyses accurately predicted lateral bending moments very well within the tested structure. Although level 2 and 3 analyses both produce good correlations for vertical bending moments, level 3 does not provide a considerable increase in accuracy, so the level 2 analyses were recommended as the approach when vertical bending moment predictions are required for a horizontally curved steel I-girder bridge.

## 2.14 Thermal Effects on Horizontally Curved I-Girder Bridges

Roeder and Moorty (1990) present a small summary of experimental results and field observations of thermal bridge movements for straight, skewed, and curved bridges as well as case studies of bridges damaged by thermal movements. The Sutton Creek Bridge in Montana was an example of a curved I-girder bridge that experienced problems related to thermal movements. Rocker bearings over the more slender piers were not frozen, but there appeared to be very little movement at these locations. It was hypothesized that the bridge movement was accommodated by bending of the piers. Also, inspectors noticed some of the bearing had lifted approximately 0.25 in. (6 mm) above the piers on a very hot day shortly after construction. For a curved I-girder bridge, preliminary results showed that radial bridge movements are comparable to tangential movements (which is not how the bridge is designed) and that flexibility at the bridge piers is an important factor in observed movements.

A following paper by Moorty and Roeder (1992) studies the response of straight, skewed, and curved I-girder bridges exposed to thermal environment conditions. Additionally, analytical methods are developed to obtain temperature distributions and the maximum bridge temperature ranges for steel and concrete bridges. Of interest for this investigation, is the thermal structural analysis that was performed to determine the effect of various geometrical parameters, orientation of the bearings, and the stiffness and resistance of the substructure on the thermal response of horizontally curved I-girder bridges. The temperature distribution investigated consisted of a uniform temperature in the girders with a nonlinear temperature gradient through the deck and the results presented are the overall movements of the bridge under the thermal loading conditions. The authors conclude that bearing orientation along the chord from the fixed point is a better choice when the fixed point is at a rigid support, because if the fixed point is at a pier, the pier deflection complicates the bridge movement. Also, bearings with unguided sliding surfaces that allow movement in the longitudinal and transverse directions are often a better choice for curved girders. Movements in curved bridges are sensitive to the relative stiffness of the bridge, the bearings, and the substructure. Results conclude that integral construction would require greater caution in complex bridge structures and curved structures would require more frequent maintenance to ensure satisfactory performance at the bearings and expansion joints.

Although these studies present invaluable information on the effect that changing environmental conditions have on curved I-girder bridges, they only investigate the response of the bridges in the form of the global deformations of the structure. While this information is very useful, it is of interest to know how the thermal loading will affect the stresses in the structure, particularly stresses at critical girder and deck locations. In addition, the local deformations of the girders need be considered to determine if the girder deflections due to thermal loading may reach a critical level.

Thanasattayawibul (2006) performed a dissertation study on a series of horizontally curved steel I-girder integral abutment bridges (IAB's) with degrees of curvature ranging from 0° to 172° based on a 1200 ft. bridge length. A detailed 3D finite element model idealizing the slabs, girders, and piles as shell elements, cross bracings as beam elements, abutments as solid elements, and soil as nonlinear springs was created in ANSYS to perform a parametric study to investigate the effect of different parameters (bridge length, temperature, soil profile type, span length, radius, and pile type) on the behavior of curved steel I-girder IAB's. The behavior studied included the stress intensity in the piles and the lateral displacement of the bridge superstructure.

A large focus of this study concentrated on the behavior and response of the abutment piles, but it was concluded that as temperature increased, the curved IAB's with smaller radii experience a larger lateral displacement increase than those with larger radii. Additionally, curved IAB's with 50 ft. spans have a lateral displacement increase greater than curved IAB's with 100 ft. spans. This study only examines the global deflections of the structure under thermal loading. The majority of the focus was directed toward the behavior of the integral abutments and no effort was given to the stresses and local deformations in the bridge superstructure.

## 2.15 Conclusions

As stated previously, the number of curved bridges constructed in the United States continues to rise because they can offer designers unique solutions to geometrical and geographical limitations unavailable using straight bridges. Additionally, curved structures sometimes offer aesthetic and cost advantages over their straight counterparts. This increase in curved bridge construction has resulted in an increase in the research performed on these structures. Research conducted on curved panels, curved I-girders, and curved I-girder bridges has ultimately resulted in a set of guidelines

for the construction of horizontally curved steel girder highway bridges (AASHTO, 2003) as well as the following pertinent conclusions:

- Although the critical vertical bending load for a curved web panel increases with increasing curvature, the membrane stress distribution becomes increasingly nonlinear through the section depth. As a result, a curved I-girder section would be unable to carry as much of a vertical moment as straight girders before yielding because the flanges are forced to carry more of the load.
- Curved I-girders must be designed to sustain lateral moments in addition to the vertical moments sustained by straight girders.
- Simply adding curvature to a bridge increases the complexities in the analysis and design of the structure. Under normal curved bridge conditions torsional behavior, which is not a major concern for straight bridges, is unavoidable and must be accounted for during design, construction, and analysis. The addition of torsion and out-of-plane displacement greatly complicates the behavior of curved girder bridge systems.
- For curved I-girder bridges, dead loads were distributed more evenly about laterally braced girders; thus, decreasing the load to the critical outside girder.
- The girder cross section will warp considerable under dead and live loads if not laterally braced. Lateral bracing significantly increases the torsional rigidity of a curved I-girder system by causing the system to behave more like a box girder system.
- While the finite element method can be an expensive and time consuming analysis method, it was found to be the most general and comprehensive method available for curved I-girder bridge analysis.
- When dynamic response is of concern, the use of upper lateral bracing appeared to have the most benefit for the structure and lateral bracing is the exterior bays led to a reduction in dynamic stresses, but the addition of lateral bracing in all bays did not significantly further reduce dynamic stresses.

- Difficulties during curved bridge erection can come in several forms including excessive out-of-plane displacements, girders "lifting-off" supports during construction, and inconsistent detailing of girder cross members. Inconsistent detailing can lead to cross-frame diagonal members being of incorrect size, which will in turn lead to locked-in girder and cross-frame stresses because of external forces that must be applied to the system to bring components into alignment.
- Results indicate that constructing girders singly from the outside-to-inside resulted in smaller overall deformations and deal load stress. However, constructing girders in pairs will further reduced deformations and stresses, but girder pairs should be constructed by placing the pairs with smaller radii of curvature first.
- Adding shoring towers and/or upper lateral bracing to the construction sequence lowers deformations during construction. In general, taking steps to stiffen the overall system during construction will reduce the final overall deformations, which should result in lower induced and locked-in stresses and improved fit-up between superstructure elements.
- Thermal movements in horizontally curved I-girder bridges are sensitive to the relative stiffness of the bridge, the bearings, and the substructure.

However, although knowledge on the behavior of curved bridge structures has advanced greatly over the last few decades, there is still much more to be understood when compared to the knowledge of straight bridge behavior. Some important aspects of curved I-girder bridge behavior that have not, in the author's estimation, that require further investigation include:

- How changing environmental conditions (temperature) will impact the deformations and state of stress of curved I-girder bridges when applied to the structure in conjunction with already considered design loading. In particular,

the effect thermal loads will have on the out-of-plane displacement and buckling behavior of the curved I-girders as well as the stress state related to concrete cracking in bridge decks.

- The impact thermal loading will have on the deformation of curved I-girders during the erection procedure. *AASHTO Guide Specifications* (2003) do not require the designer to consider temperature loads when developing the construction sequence for curved I-girder bridges. If thermal loading during construction leads to additional girder displacements, additional girder fit up problems may occur leading to a higher level of stresses that are locked into the curved I-girder bridges.
- The significance of bearing configuration design in the relief of thermal stresses in horizontally curved I-girder bridges. *AASHTO Guide Specifications* (2003) state the orienting bearing guides towards a "fixed point" and allowing the bridge to move freely along rays emanating from the fixed point causes thermal forces to be zero if the structure changes temperature uniformly. Even under uniform temperature loading, it is not likely that thermal stresses will be totally relieved in the structure. This possibility needs to be studied along with an investigation into the ideal bearing configuration with regard to thermal loading for horizontally curved I-girder bridges.
- *AASHTO Guide Specifications* (2003) mainly specify the temperature to be considered during bridge design to be uniform temperature, but a uniform temperature difference between the deck and girders of 25°F (-3.9°C) is given for consideration in Article 3.6. However, in practice, temperature loading on the bridge will be nonuniform in nature, both through the depth and across the width of the superstructure. Nonuniform temperature on a horizontally curved I-girder bridge, especially a large structure, could have significant consequences on the response of the structure and needs to be explored in detail.

To this end, the work considered as part of this dissertation research will attempt to correct some or all of the deficiencies in the research presented here.

# CHAPTER THREE

# PRELIMINARY INVESTIGATIONS

## 3.1 Introduction

The design of a curved girder bridge differs from the design of a comparable straight girder bridge because simply adding curvature to the structure greatly complicates the structural behavior. The introduction of curvature to a bridge causes temperature changes to invoke structural responses in both the radial and tangential directions, making the thermal response phenomenon far more complicated compared to a straight section. Furthermore, there are no provisions in the design guidelines that call for the designer to consider possible I-girder thermal deformations during erection of the steel superstructure. Therefore, it is important to investigate the effect, if any, that changing temperature conditions will have on curved I-girders, and, in particular, on curved I-girder bridge systems.

This Chapter presents two preliminary finite element investigations into the effect of temperature loading on curved members. The first study of a simple curved I-girder section examines the effect that varying certain girder parameters has on the deformations and stresses at the mid-span of the section. The second study uses finite element modeling to examine a section consisting of two braced curved I-girders under gravity and thermal loading. Results from each of these studies indicate that thermal loading applied to curved I-girder sections results in a significant response which requires further investigation.

## 3.2 Single Span Parametric Study

Web panels of I-shaped plate girders are normally designed to be as slender as possible while still maintaining the relative distance between the top and bottom flanges. Efficient design of an I-girder results in the flange plates carrying the majority of the bending moment and web buckling occurring prior to reaching the nominal moment strength of the girder. However, the introduction of curvature greatly complicates the behavior of an I-girder by introducing torsion to the structural response that will not be present under normal service conditions in a straight bridge system. According to Davidson et al. (1999b), curvature induces both warping of the cross section and, more importantly for web considerations, transverse displacement of the web.

Previous research (outlined in the Literature Review) has stated that nonlinear web stresses and out-of-plane web deformations can have a significant impact on the behavior of curved I-beams. Studies have been performed using a myriad of techniques to investigate the effect that varying parameters such as aspect ratio, curvature, cross section dimension (web slenderness), and boundary conditions has on I-beam responses, in particular web panel response. Some conclusions derived from these studies are that as web panel curvature increases (radius of curvature decreases) out-of-plane web displacements increase while the degree of nonlinearity in the displacement profile decreases, membrane stresses in the circumferential direction decrease but the stress distribution becomes increasingly nonlinear through the section depth, panel critical loads increase, bifurcation type instability becomes less likely and deflection amplitude behavior begins to control, the buckling mode shape changes from an S shape to an M shape, and bending stress is remarkably reduced in the compression zone. Additionally, as the web panel slenderness increases, the critical web panel stresses decrease while the membrane stress distribution becomes increasingly nonlinear through the depth of the section. The aspect ratio was found to have a negligible effect on the out-of-plane deflection and stresses when within AASHTO

prescribed limits. Finally, for a single curved I-girder, pinned end conditions were found to effect the critical stress ratio (ratio between critical stress of a curved section versus critical stress of a straight section) very little while fixed end conditions on the span caused the critical stress ratio to increase.

The addition of curvature to girder design will introduce out-of-plane displacement to the girder behavior under all normal loading conditions. With this increased displacement comes an increase in web panel stresses as well as web panel bending stresses in the vertical and circumferential direction that would not exist in straight panels. According to Davidson et al. (1999a), the increased nonlinearity of web stress distribution and reduction in overall web stress from increasing girder curvature and/or web slenderness will lead to reduced I-girder vertical moment carrying capacity of curved sections as compared to a straight section because the flanges are forced to carry more of the load. Therefore, according to Davidson et al. (1999a), although the critical bending moment load of a curved web panel is higher than that of a straight panel, a curved I-beam section can accommodate a smaller vertical bending moment than a comparable straight section before yielding occurs in the flanges.

An initial step in this investigation involves using finite element analysis to perform a small parametric study on a simple curved I-beam in an effort to examine the validity of the aforementioned conclusions when the girder is subjected to uniform temperature changes. The parametric study focuses on the circumferential stresses in the web panel and top and bottom flanges along with the out-of-plane web displacement. The variables considered were web slenderness ratio (height/thickness), radius of curvature, changing thermal conditions, and girder boundary conditions.

A finite element model similar to the one created as part of the Curved Steel Bridge Research Project and described by Davidson et al. (1999a) has been developed using the software package ADINA (2003) and is used as the baseline model for this study. The

model used in this study has a few differences from the CSBRP model including: transverse stiffeners are included at the I-beam ends, the top and bottom flanges are included as shell elements in the model, and loading is applied as gravity loading followed by a uniform pressure load on the top flange corresponding to the weight of a 10 ft. x 8 in. deck section placed on the top flange of the girder. Figure 3.1 shows the baseline FE model and describes the section dimensions and steel material properties used. All of the surfaces were modeled as MITC4 4-node shell elements and the boundary conditions at the girder ends were modeled as fixed. Because of the simplicity of the models, the use of the default sparse solver in ADINA yields sufficiently accurate results.

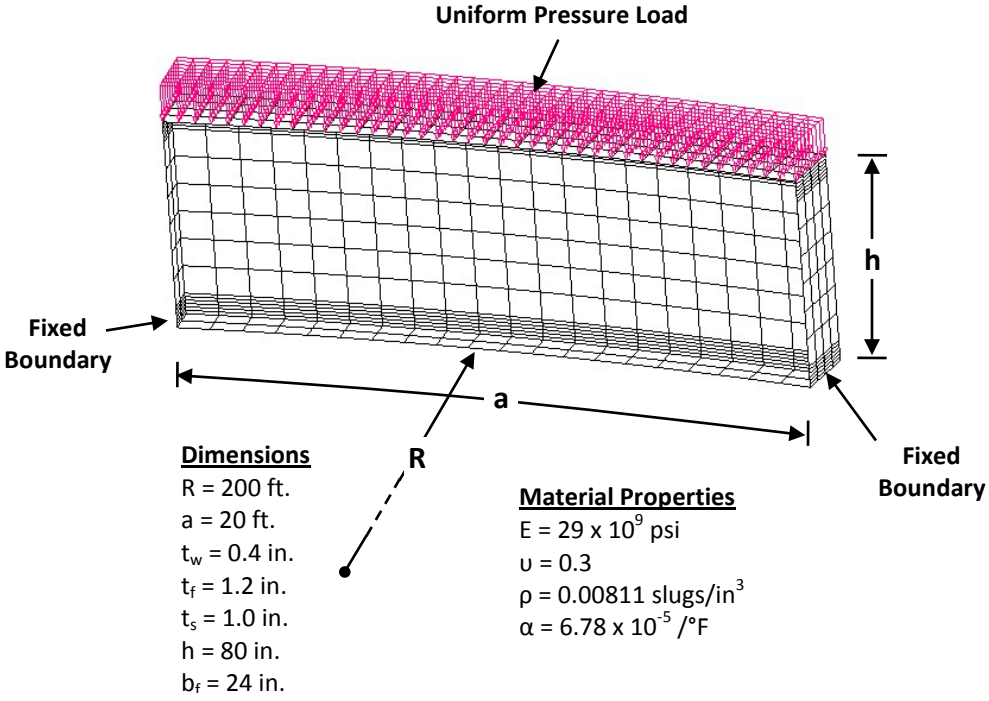


**Figure 3.1. FE Model Used for Simple Span Parametric Study**

### 3.2.1 Web Slenderness Variation

The previously mentioned FE model is employed to study the effect that changing the web slenderness ($h/t_w$) of a curved I-girder will have on the longitudinal stresses in the web and flanges as well as the out-of-plane web deformations. Web slenderness values of 800, 400, 200, 133.3, and 100 are used in the FE model with loading applied as gravity loading followed by a pressure load applied to the flange. Figures 3.2 – 3.5 plot the results obtained from the web slenderness study. All of the values are taken at the middle cross section of the FE model.

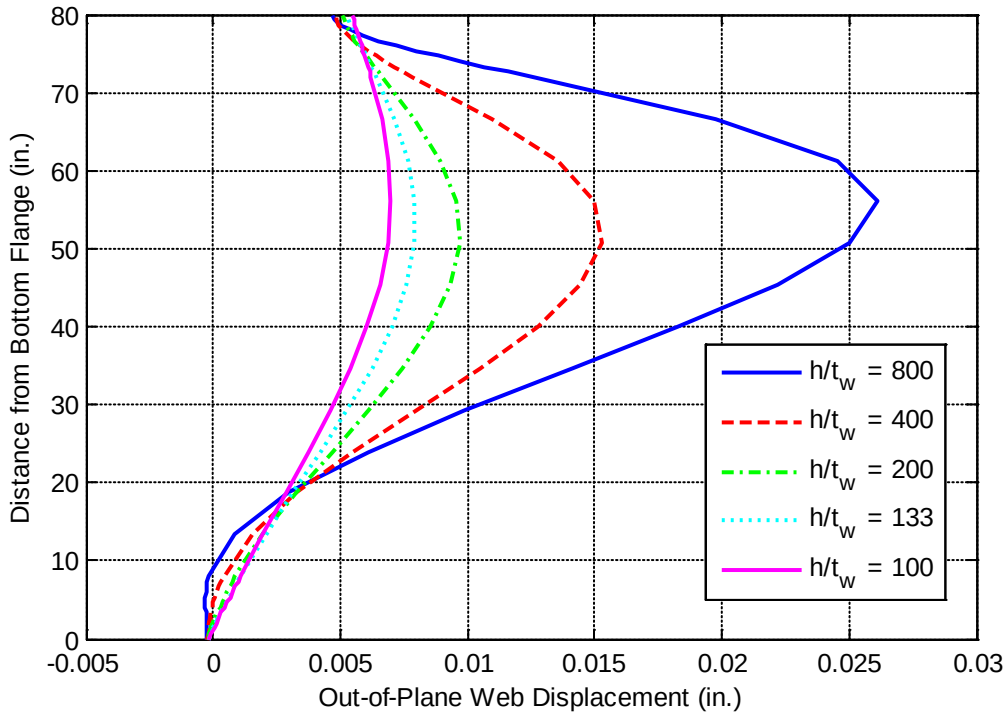


**Figure 3.2. Out-of-Plane Deformation of Curved I-Girder Webs with Varying Web Slenderness**

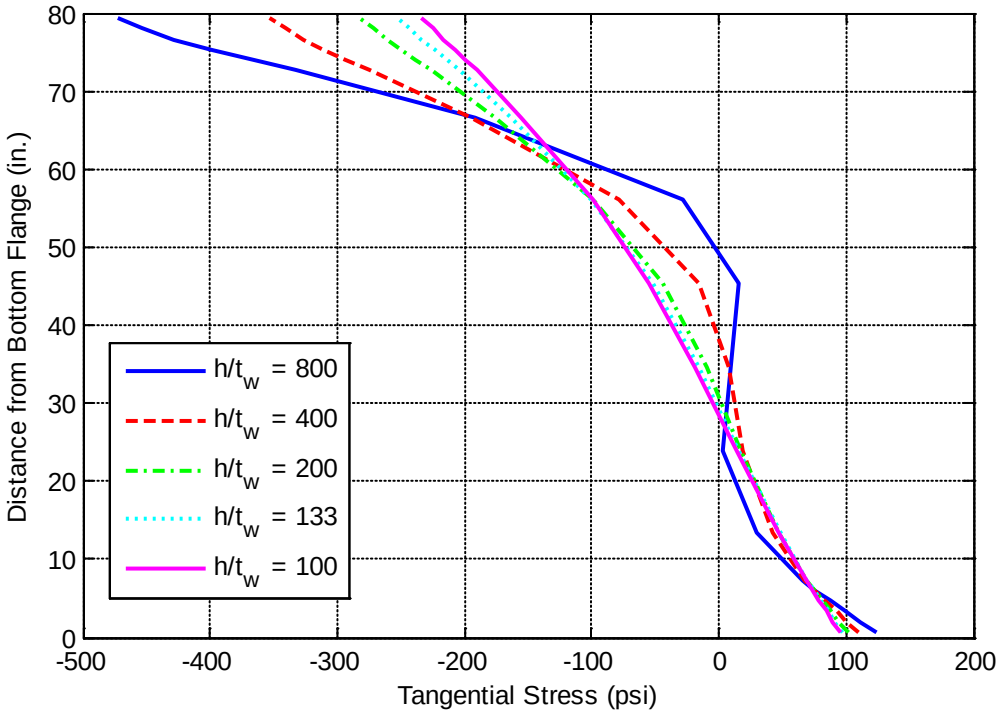


**Figure 3.3. Tangential Web Stress of Curved I-Girder Webs with Varying Web Slenderness**

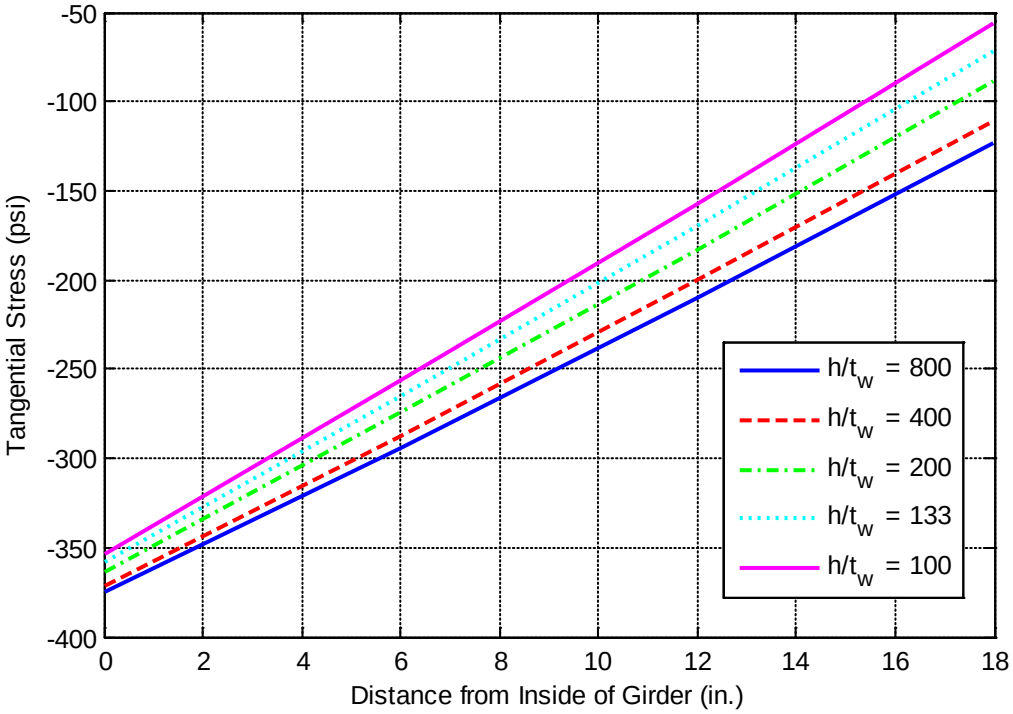


**Figure 3.4. Top Flange Tangential Stresses for Curved I-Girders with Varying Web Slenderness**

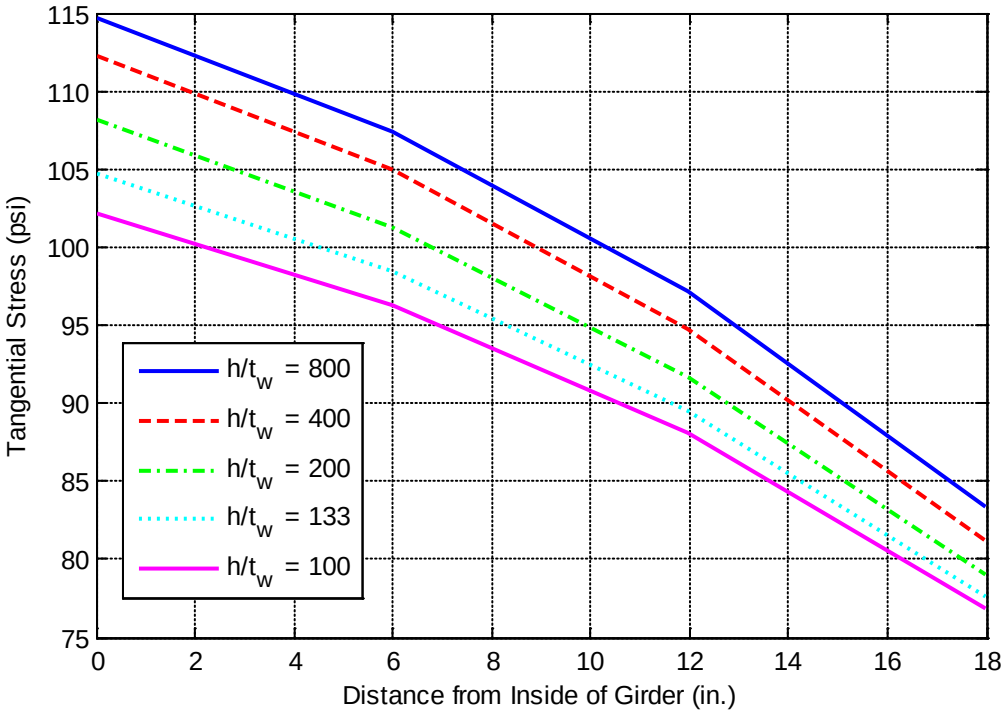


**Figure 3.5. Bottom Flange Tangential Stresses for Curved I-Girders with Varying Web Slenderness**

Conclusions can be drawn from this portion of the parametric study that match conclusions drawn by previous researchers. Namely, Figure 3.3 confirms that as the web panel slenderness increases, the membrane stress distribution becomes increasingly nonlinear through the depth of the section. Results also indicate that as web slenderness increases, the nonlinearity and magnitude of out-of-plane web deformation increases, compressive stress in the top flange increases, and tensile stress in the bottom flange increases. Greater stresses in the flanges support the hypothesis by Davidson et al. (1999a) that as the web slenderness increases, the out-of-plane deformation of the web causes the flanges to carry more of the bending moment load; thus, reducing the moment carrying capacity of the I-girder section. Hence, as web slenderness increases the moment carrying capacity of a curved I-beam section decreases.

### 3.2.2 Radius of Curvature Variation

The effect that varying I-girder curvature will have on the tangential stresses and out-of-plane deformations of a simple I-girder is briefly studied. The model in Figure 3.1 is constructed with radii of curvature (*R*) of infinity (straight), 100, 200, 500, and 1000 ft and solved under the same loading conditions mentioned in Section 3.2.1. Results are presented in Figures 3.6 – 3.9.

Once again, some results from this portion of the parametric study produce conclusions that are agreeable with conclusions derived from previous studies of curved I-sections subjected to mechanical loading. For example, Figure 3.6 shows that as curvature increases (radius of curvature decreases), the degree of out-of-plane web displacement increases but the nonlinearity of the profile seems to decrease. Additionally, Figure 3.7 indicates that increasing curvature leads to an increase in the nonlinearity of tangential web stress distribution but a slight decrease in the overall tangential web stresses. The increase in web-out-of-plane deformation and web membrane stress nonlinearity as curvature increases indicates that as I-beam curvature increases the vertical moment carrying capacity decreases.

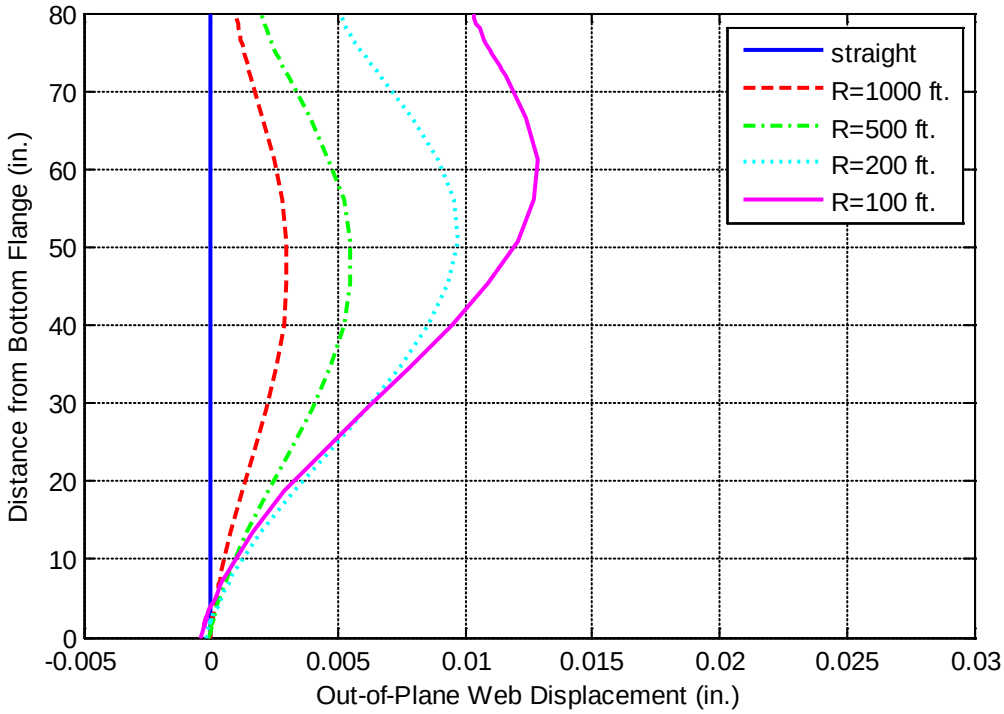


**Figure 3.6. Out-of-Plane Deformation of Curved I-Girder Webs with Varying Radii of Curvature**

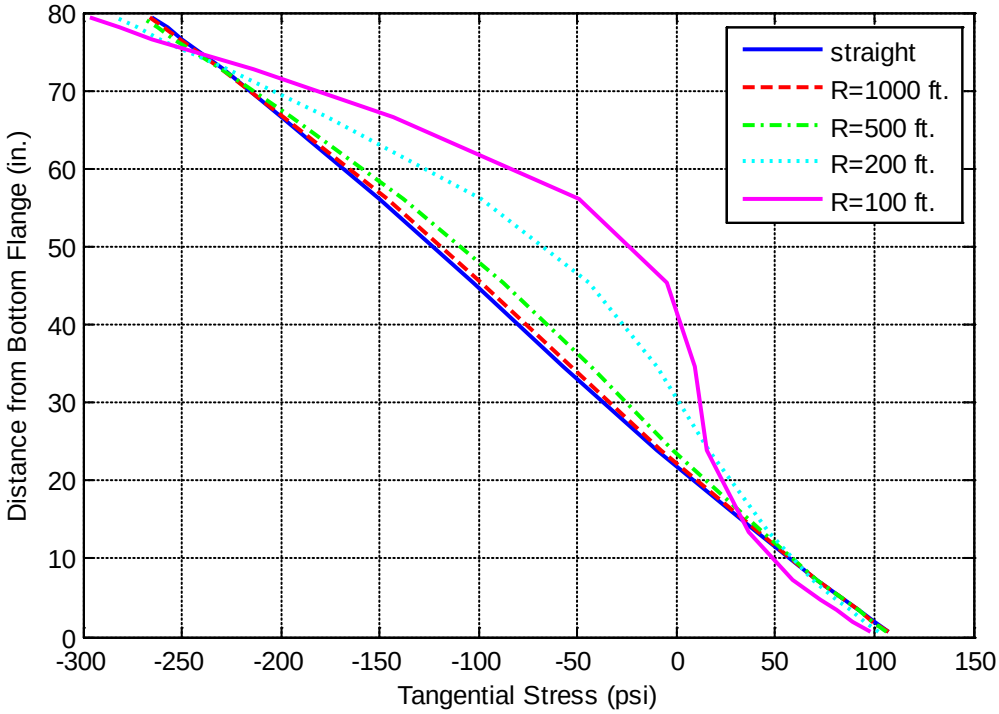


**Figure 3.7. Tangential Web Stress of Curved I-Girder Webs with Varying Radii of Curvature**

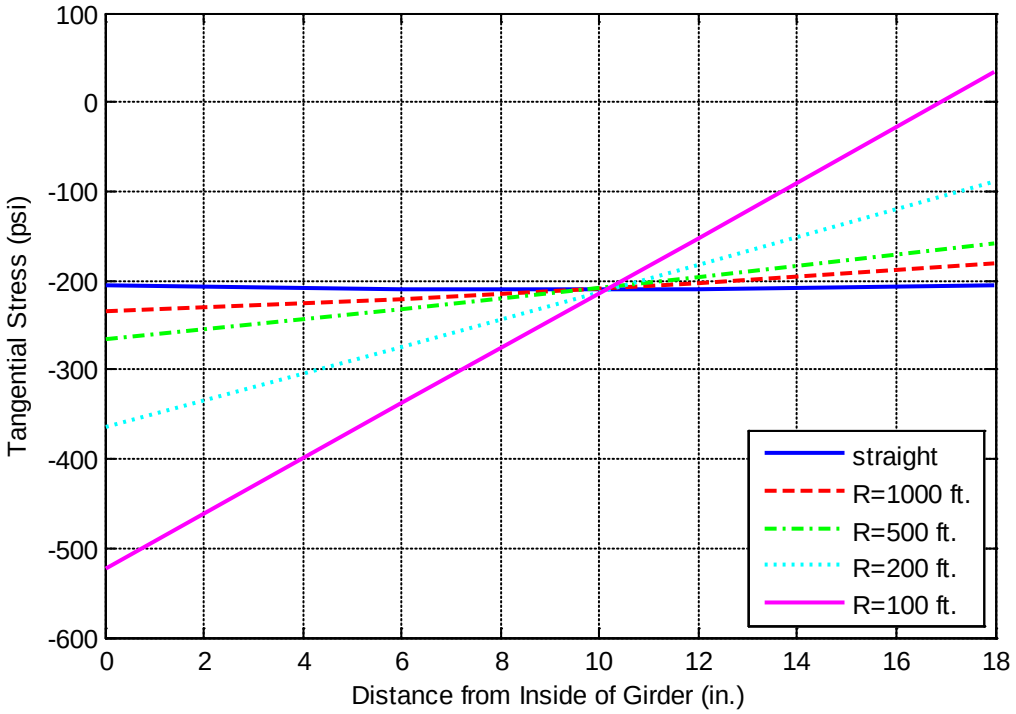


**Figure 3.8. Tangential Stress of Curved I-Girder Top Flange with Varying Radii of Curvature**

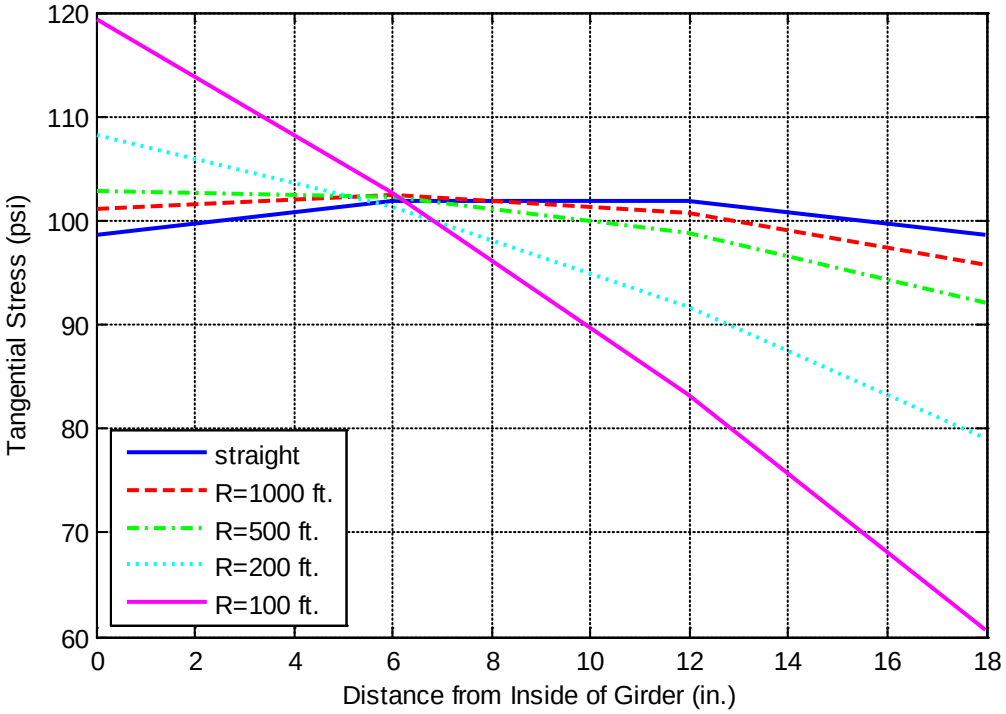


**Figure 3.9. Tangential Stress of Curved I-Girder Bottom Flange with Varying Radii of Curvature**

While the tangential stresses across the width of the top flange are uniform for a straight girder, the stresses vary linearly across the flange width for curved I-sections as depicted in Figures 3.8 and 3.9. This stress variation across the flange width is an indication of a lateral bending moment in the flange. Lateral bending moments in the top flange increase as curvature increases with the maximum tangential stress occurring at the inside flange edge (flange edge closest to the center of curvature). Tangential stresses also vary across the width of the bottom flange, but the gradient does not appear to be linear. In both cases, the maximum longitudinal stresses in the flanges increase as curvature increases. In addition, the increasing stress variation across the girder width is evidence that increasing curvature leads to increasingly large lateral bending moments in the flanges. This is further evidence that an increase in curvature results in a decrease in moment carry capacity because the greater curvature causes the flanges to carry more of the load.

### 3.2.3 Thermal Loading Investigation

The parameters investigated as part of this brief parametric study have been studied by other researchers. To this point, results obtained from the present study yield conclusions agreeing with those of previous researchers. As a result, it appears that the current modeling procedure is adequate in predicting simple curved I-beam behavior. The next step was to use this model to determine how thermal loads will affect web out-of-plane deformation and girder longitudinal stresses as an initial step in investigating how thermal loading affects curved I-girder bridges. Loading is applied to the models as a gravity load followed by a uniform temperature load applied in ±9°F increments up to a total temperature load of ±45°F. Results from these analyses are given in Figures 3.10-3.17 for a case of radius of curvature of 200 ft.

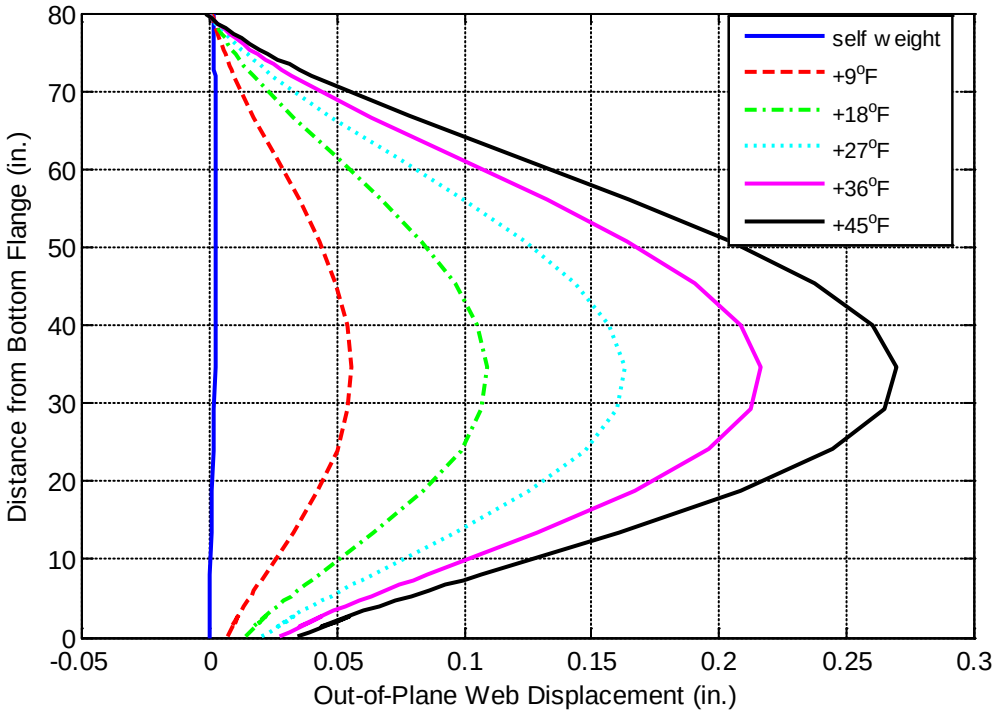


**Figure 3.10. Out-of-Plane Web Deformation of Curved I-Girder Webs Subjected to Increasing Thermal Loads**

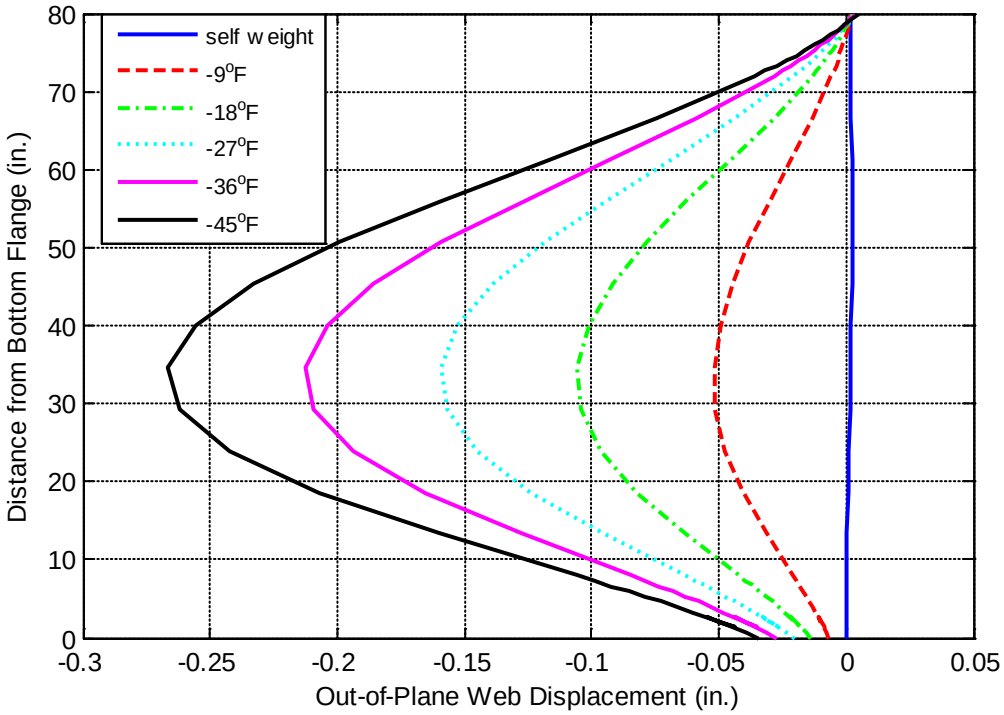


**Figure 3.11. Out-of-Plane Web Deformation of Curved I-Girder Webs Subjected to Decreasing Thermal Loads**

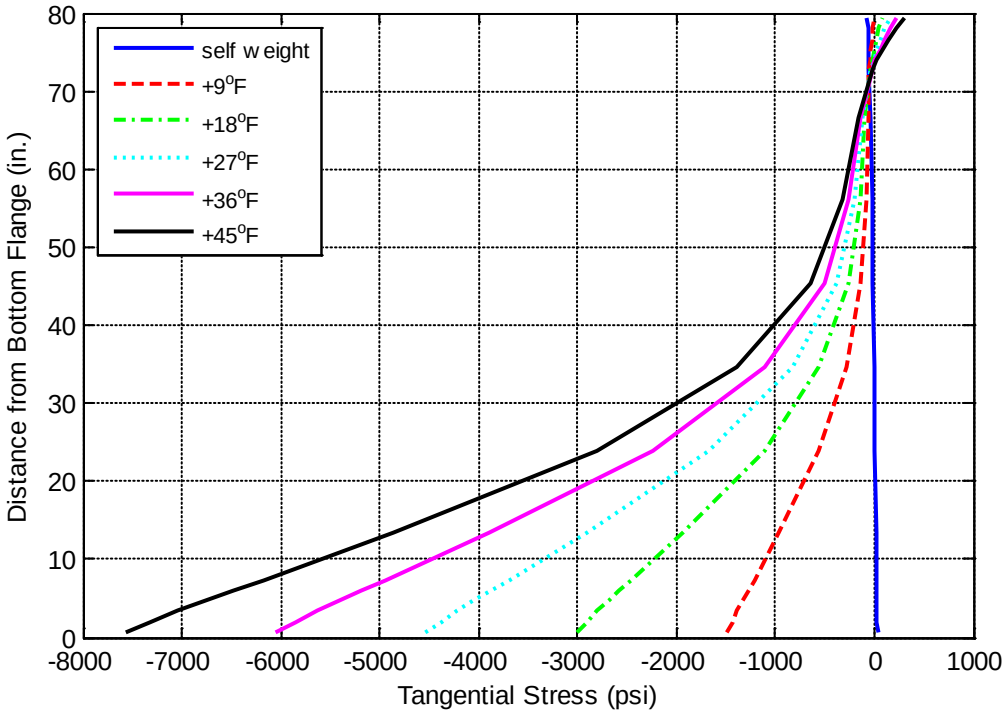


**Figure 3.12. Tangential Stress of Curved I-Girder Web Subjected to Increasing Thermal Loads**

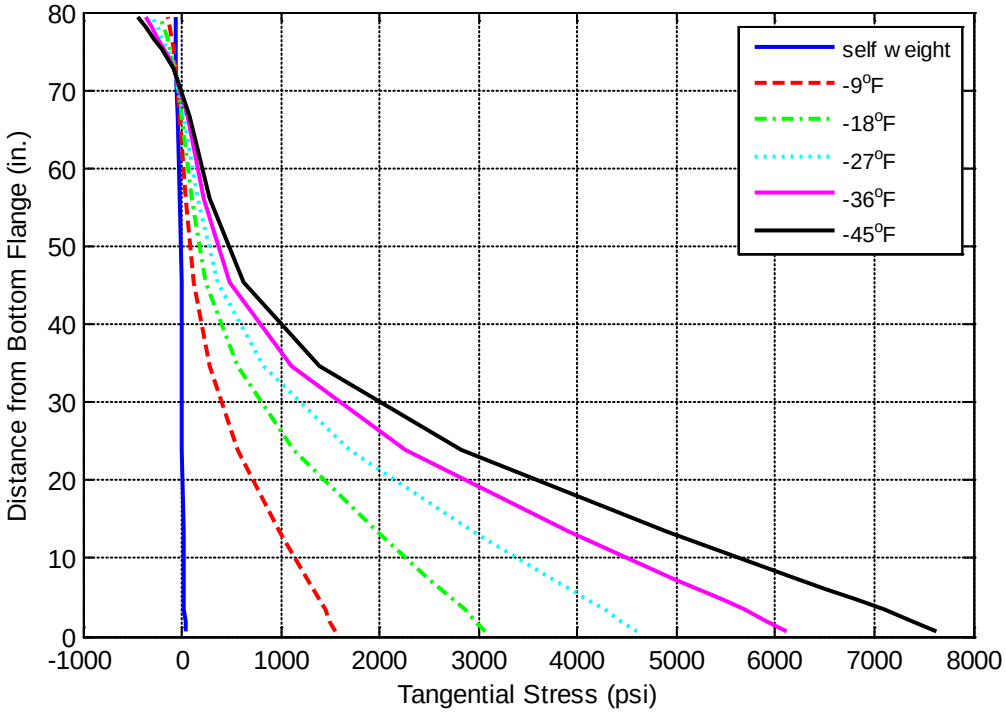


**Figure 3.13. Tangential Stress of Curved I-Girder Web Subjected to Decreasing Thermal Loads**

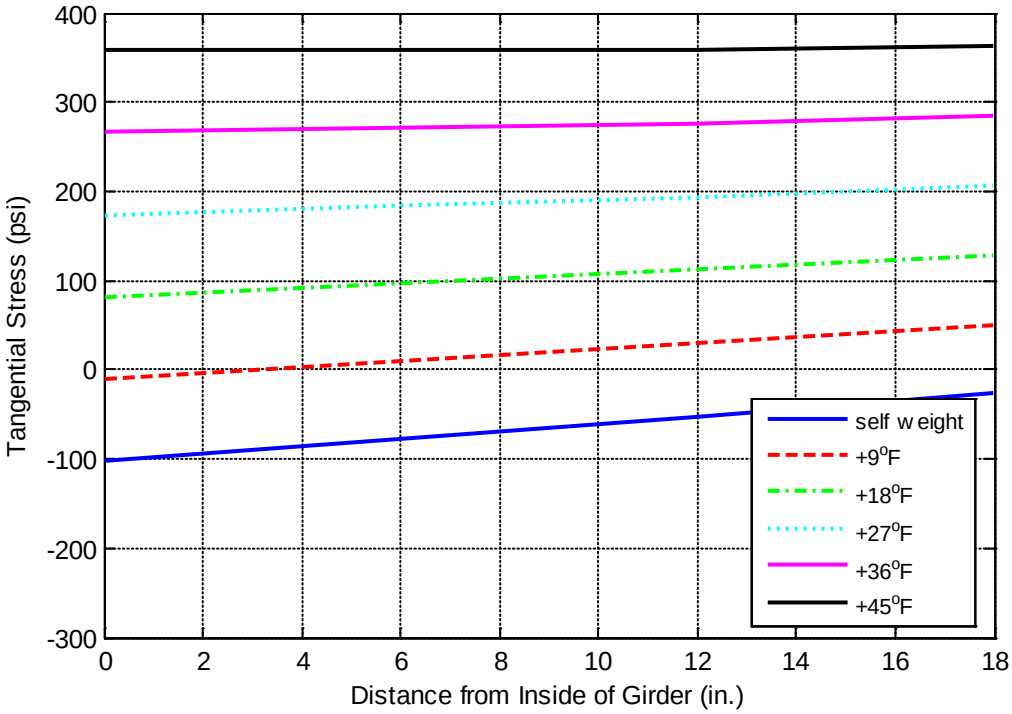


**Figure 3.14. Top Flange Tangential Stresses for Curved I-Girders with Increasing Thermal Loads**

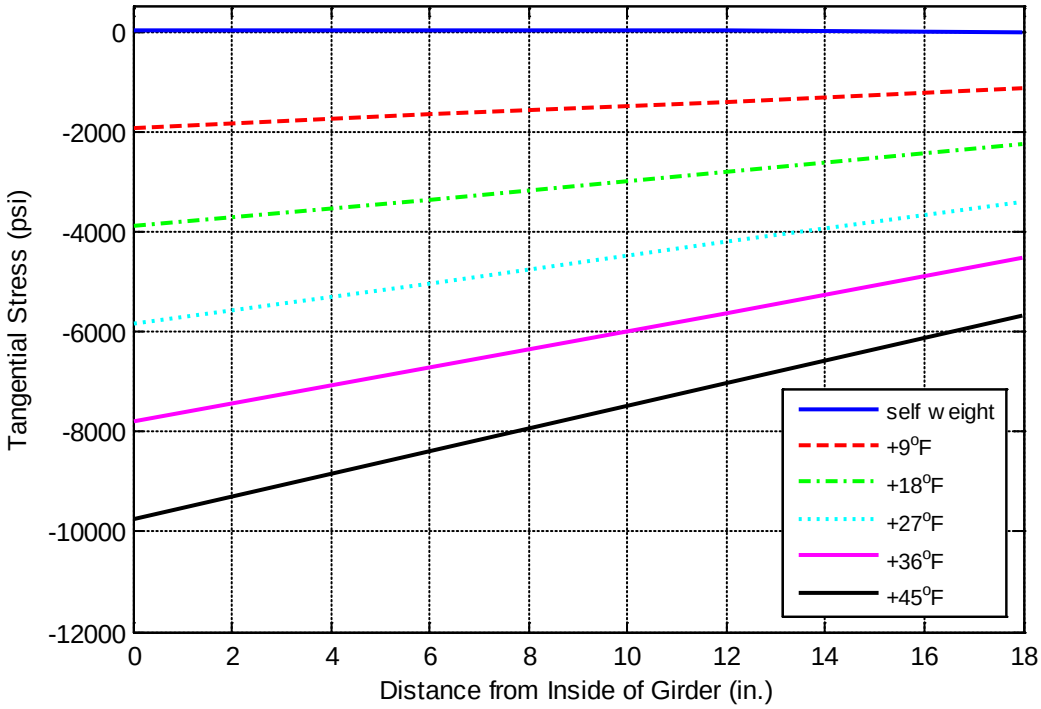


**Figure 3.15. Bottom Flange Tangential Stresses for Curved I-Girders with Increasing Thermal Loads**

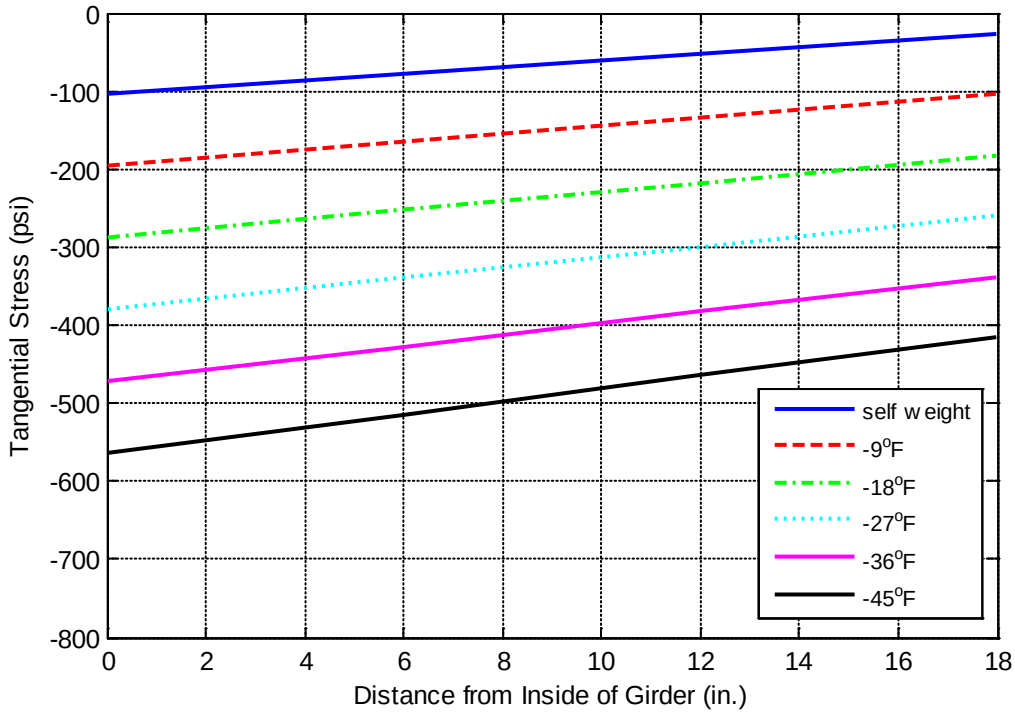


**Figure 3.16. Top Flange Tangential Stresses for Curved I-Girders with Decreasing Thermal Loads**

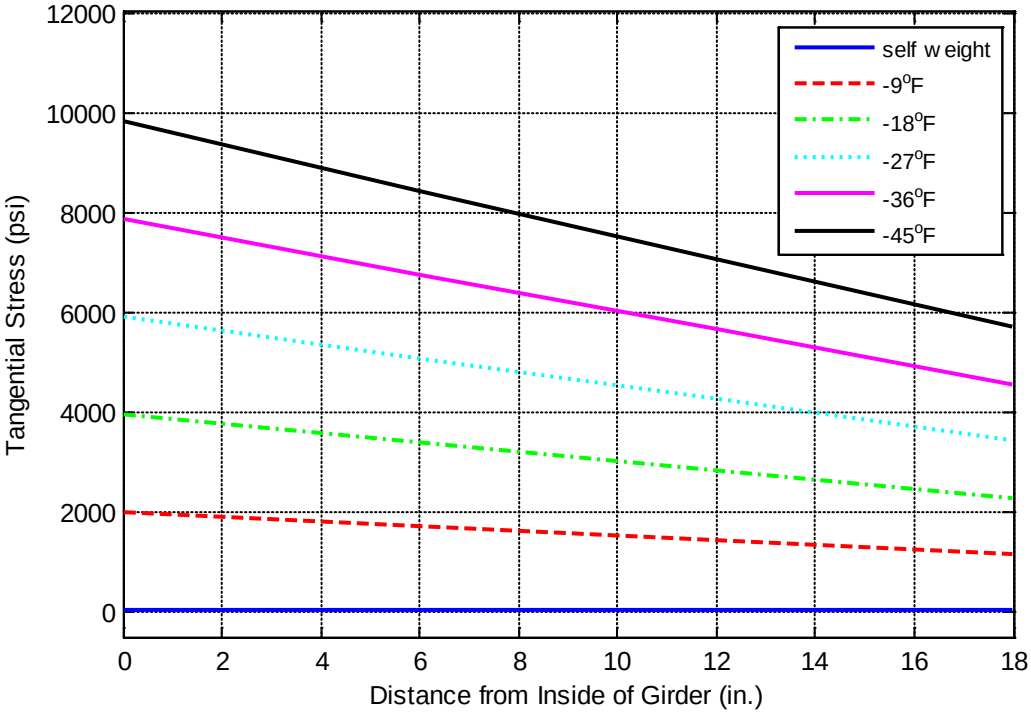


**Figure 3.17. Bottom Flange Tangential Stresses for Curved I-Girders with Decreasing Thermal Loads**

Figures 3.10 and 3.11 indicate that, for a curved girder section, as the magnitude of thermal loading increases the out-of-plane deformation of the web increases. For a temperature increase, the web deforms outward (away from the center of curvature) while the web deforms inward (towards the center of curvature) for a temperature decrease. Also, Figures 3.12 and 3.13 show that the nonlinearity of the web longitudinal stress profile increases as the magnitude of thermal loading increases. Although tangential stresses at the juncture of the top flange and the web are largely unaffected by changing thermal conditions, the stress at the web bottom shows significant sensitivity to temperature changes.

Stresses in the flanges of the curved section are significantly affected as thermal loading is added. As temperature increases, the top flange stresses go from slight compression to tension and the stress distribution across the flange width becomes increasingly more uniform as the temperature increases. On the other hand, the bottom flange goes from a state of slight tension to compression with the slope of the lateral flange stress profile increasing with temperature. With temperature decrease, the tensile stresses in the top flange and the compressive stresses in the bottom flange increase with the bottom flange stresses becoming increasingly varying across the flange width as the temperature load decreases. For each case, maximum stresses, whether they be tensile or compressive, occur at the inside edge of the bottom flange and bottom flange lateral bending stresses increase as temperature magnitude increases.

Naturally, the boundary conditions on the section will have a significant impact on the magnitude and type of longitudinal stresses that occur in the section. For the fixed-fixed case investigated here, a temperature decrease appears to produce the highest level of stress in the top flange while all other stresses and deformation are equal in magnitude but opposite in direction for increasing and decreasing thermal loading. As with earlier analyses, the increasing out-of-plane web deformation and membrane stress nonlinearity as temperature loading increases indicates that a thermal load on a curved

I-girder section will decrease the sections load carrying capacity by increasing the stress magnitude in the flanges; thus, decreasing the flange capacity to carry further loading.

### 3.2.4 Boundary Condition Variation

As temperature changes, the thermal stresses that arise in a curved I-girder section largely depend on the types of constraints that are present on the section. The previous investigations presented as part of this parametric study all employed fixed end boundary conditions which will result in the most critical stresses and deformations. This portion of the parametric study was devoted to investigating the effect that changing boundary conditions on the simple section have on the section response to thermal loading. Boundary conditions investigated included fixed - fixed, fixed – pinned, fixed – guided, fixed – non-guided, pinned – pinned, pinned – guided, pinned – non-guided, guided – guided, and guided – non-guided. However, during the analysis it was found that these boundary conditions can be put into two groups that elicit similar responses under thermal loading: 1) both ends either fixed or pinned and 2) at least one end guided or non-guided. Therefore, results presented in Figures 3.18-3.21 are only for the boundary condition states fixed – fixed and fixed – guided.

Figures 3.18-3.21 show that thermal loading has a negligible effect on the girder tangential stresses and web deformations of a single curved I-beam section when boundary conditions allow movement at one end of the section. The guided bearing at the end of the beam allows the girder to expand and contract as temperature changes; thus, relieving most of the thermal stresses that would arise. This would tend to indicate that bridge bearings could be designed to allow the bridge girders to expand and contract in such a manner that no thermal stresses would be present in the structure. The belief of the author is that, in reality, this is not practical. Many factors within a bridge structure will inhibit full thermal movements of the bridge girders

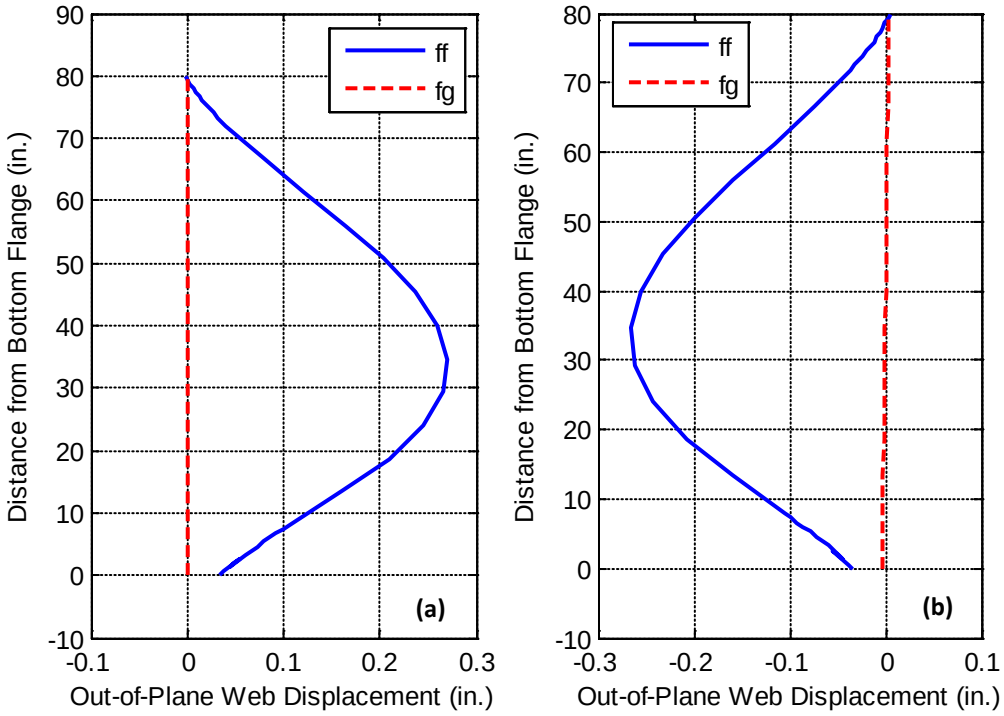


**Figure 3.18. Out-of-Plane Deformation of Curved I-Girder Webs with Varying Boundary Conditions Under Self-Weight and (a) +45°F or (b) -45°F loading**

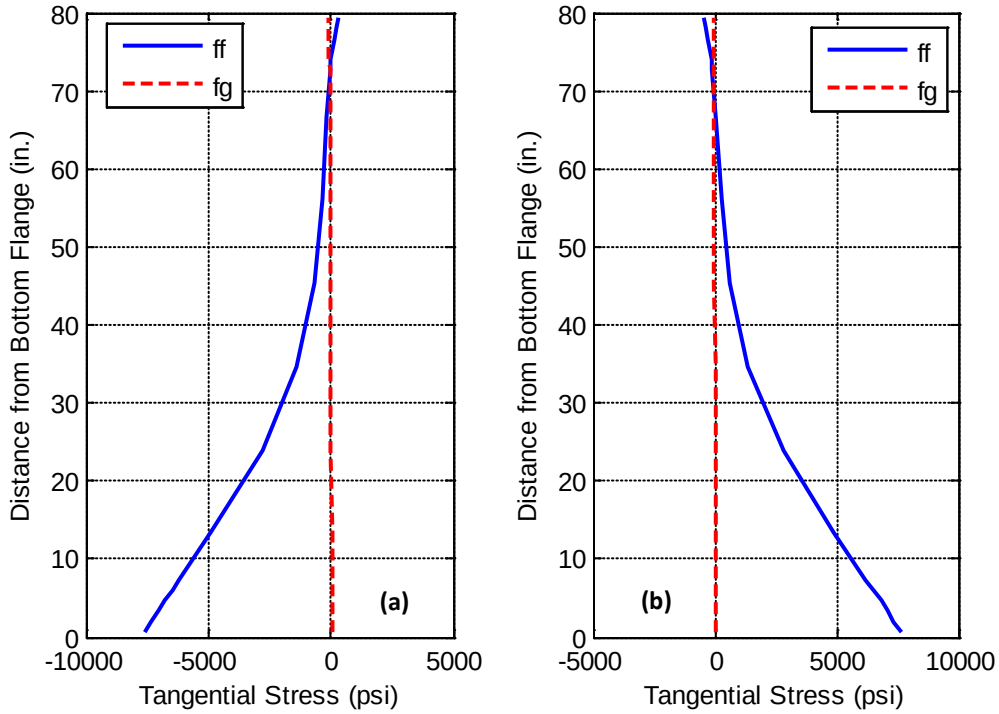


**Figure 3.19. Tangential I-Girder Web Stresses with Varying Boundary Conditions Under Self-Weight and (a) +45°F or (b) -45°F Loading**

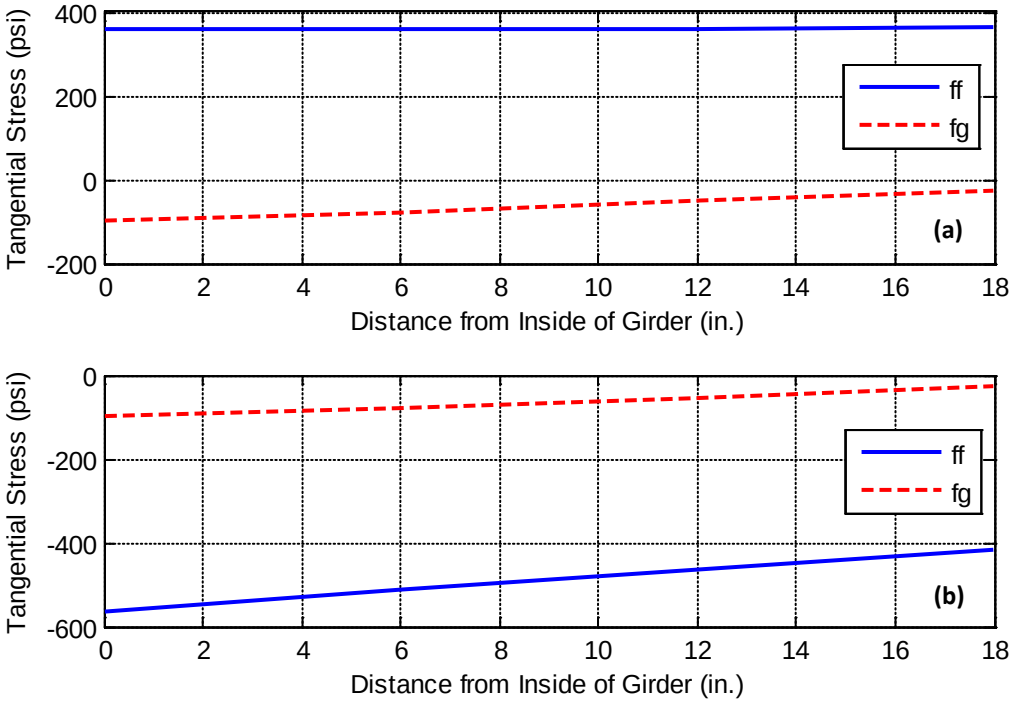


**Figure 3.20. Top Flange Tangential Stresses in Curved I-Girders with Varying Boundary Conditions Under Self-Weight and (a) +45°F or (b) -45°F Loading**

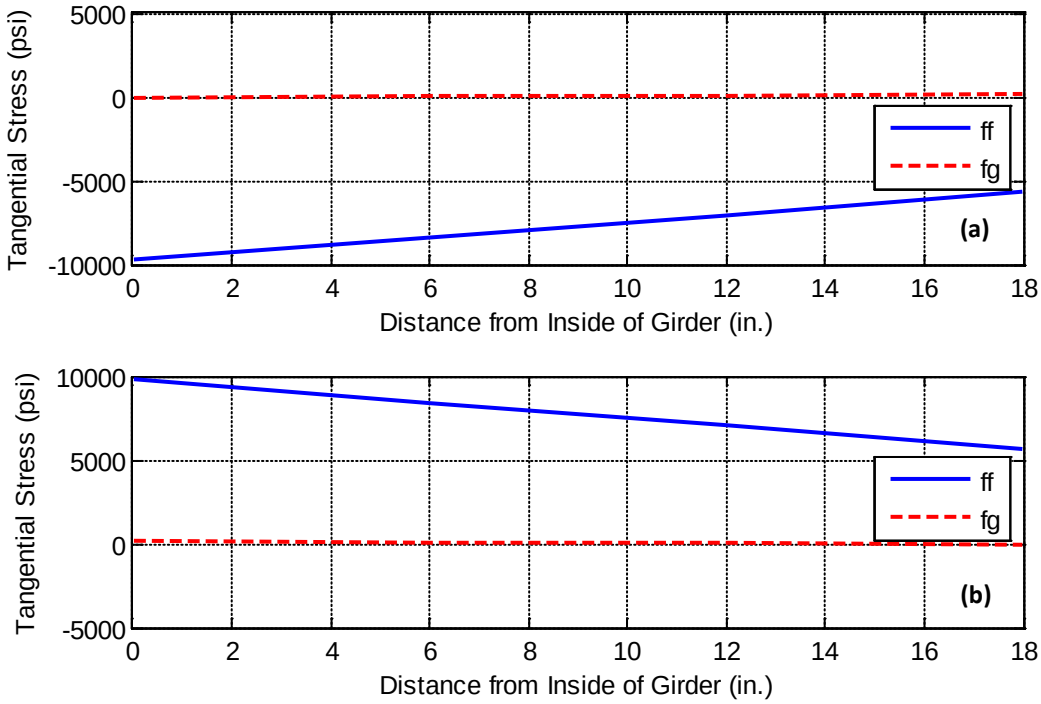


**Figure 3.21. Bottom Flange Tangential Stresses in Curved I-Girders with Varying Boundary Conditions Under Self-Weight and (a) +45°F or (b) -45°F Loading**

including, but not limited to, the cross bracings constricting thermal movements, the bridge deck providing fixation at the girder top flange, and bridge bearings not performing exactly as designed. Further research is required to determine the effect that thermal loads have on an actual curved I-girder bridge.

## 3.3 Braced Girder Pair Thermal Study

A major concern in the design of curved I-girder bridges is the construction sequence and the deformations during construction. Chavel and Earls (2002a) state that generally, problems with curved steel I-girder bridges result from unwanted displacements and rotations that occur during bridge erection, which are typically unaccounted for by the designers. AASHTO (2003) requires that vertical and lateral deflections shall be evaluated through the construction sequence to ensure that the final position of the steel will correspond to deflections computed during design. Additionally, factored stresses due to self-weight of the steel and wind at each stage of erection shall satisfy provisions of Division I, Article 2.5.2 and AASHTO Division II, Article 11.6.4.2, as applicable.

Typically, curved I-girders are fabricated to fit together under the zero-stress conditions and the girders are combined to account for the dead-load deflection from the zero stress state. Curved bridges also normally require more temporary support during construction compared to straight bridges to minimize deflections. Often, sets of girders (typically sets of two) are connected with cross frames prior to placement while they are in a zero-stress state and the girders are then erected in pairs. Erecting girders in pairs also serves to minimize girder deflections during construction.

Although precautions are taken to reduce and control the level of deformations during the construction of a curved I-girder bridge, displacements will inevitably arise that could cause problems with the structure. Out-of-plane deformations can lead to cross

frame fit-up problems, resulting in additional stresses being placed on the girders as they are forced into position in order to properly attach the cross frames. Also, when the girders are twisted, the vertical loads are not applied through the shear center of the girder which will intensify the effects of twist in the members beyond what would generally be computed from a simple first order analysis. Within the Horizontally Curved Steel I-Girder Design Example, *AASHTO Guide Specifications* (2003) states that the inherent torsion must be resisted or else the girder will not stand, i.e., it will not meet the requirements of static equilibrium. Obviously, the problem of girder deformations during the erection sequence is a critical one for curved I-girder bridges.

The Horizontally Curved Steel I-Girder Design Example in the *AASHTO Guide Specifications* (2003) lays out an example of the procedure used to design a three-span horizontally curved steel I-girder bridge with four girders in the cross section. During the analysis of the construction sequence, the response of the structure is investigated under self-weight and wind loading. However, in neither the specifications nor the design example is thermal loading considered during the construction process. Section 3.2 reveals that changing temperature conditions can elicit an out-of-plane response for curved I-girders which will lead to problems during erection. Consequently, a brief investigation is performed to determine if changing thermal conditions during the erection of a curved I-girder bridge could have significant effects.

### 3.3.1 FE Model Description

The AASHTO Design Example specifies that the I-girders are to be erected in sets of girder pairs already connected with cross-frames and then those pairs are fit up together to obtain the final steel superstructure. Since this practice of erecting girders in pairs is commonplace, the analysis herein will simply focus on a set of two girders connected by cross frame members. The two girders and cross frames chosen for analysis roughly resemble the middle span of Girders 1 and 2 in the Design Example. A

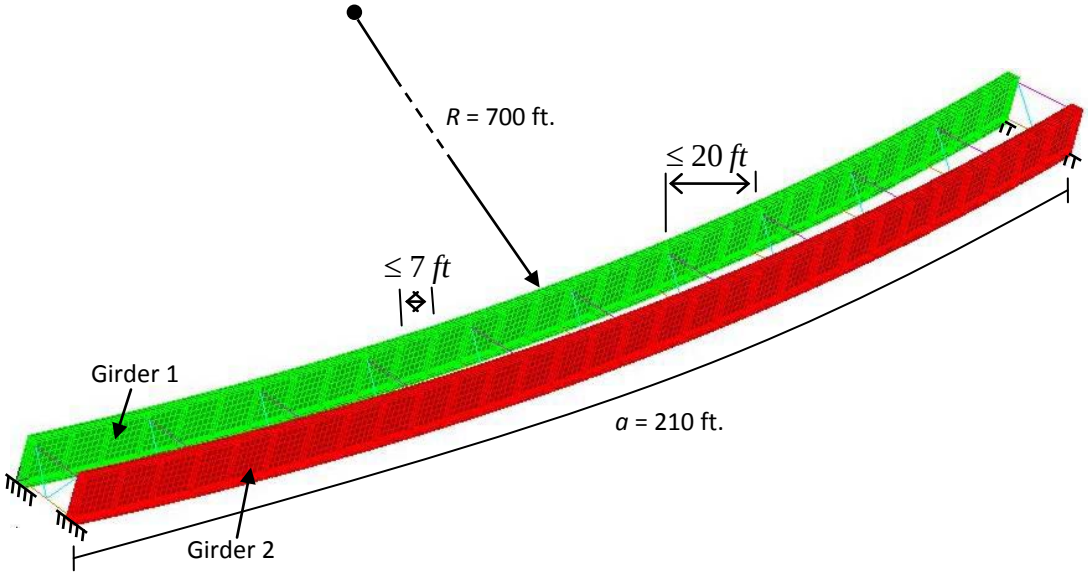


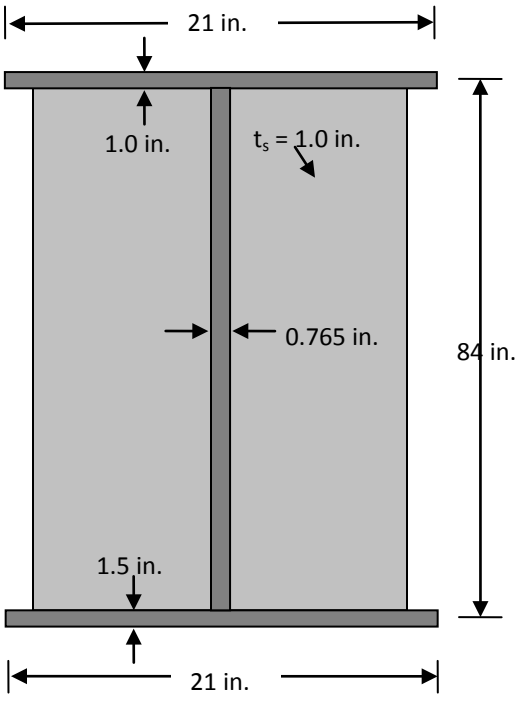


**Steel Properties**

$E = 29 \times 10^9$ psi

$\upsilon = 0.3$

$\rho = 0.00881$ slugs/in$^3$

$\alpha = 6.78 \times 10^{-5}$ /°F

**Cross Member Properties**

$A_{c.s.} = 5.0$ in.$^2$

$I_y = I_z = 4.417$ in.$^4$

$J = 8.834$ in.$^4$

**Figure 3.22. Description of Two Girder FE Model**

set of finite element models with varying radii of curvature (R) were created in ADINA (2003) and subjected to gravity and thermal loads. The baseline FE model (*R* = 700 ft.) is shown and the properties of the model are given in Figure 3.22.

Along with the model in Figure 3.22, models with radii of curvature of 200, 500, 1000, and 1500 ft. were created and solved under gravity and thermal loading. The purpose of this analysis was to determine if the degree of curvature of a section will affect the response to thermal loading. As the radius of curvature changes, some girder parameters must be checked against *AASHTO Guide Specifications* (2003). Namely, intermediate cross frame spacing, transverse stiffener spacing, transverse stiffener thickness, and web slenderness values are a function of the radius of curvature and their values are adjusted so that the section geometry meets specifications for each radius of curvature.

### 3.3.2 Out-of-Plane Web Displacement

The model created for this analysis is solved under extreme conditions so that the thermal effects are more recognizable. Most likely, construction of a 210 ft. curved span would involve using temporary supports along the span, which are not implemented in the model. However, if temporary supports used during construction only support the girders in the vertical direction, they will likely not restrict any lateral motion of the girders caused by changing thermal conditions. Figures 3.23-3.27 present the measured lateral deflection of the outside girder web at the middle of the span under self-weight loading (SW), self-weight plus -54°F loading (SW/-54°F), and self-weight plus 54°F loading (SW/+54°F) for spans with radii of curvature of 200, 500, 700, 1000, and 1500 ft., respectively. Results are investigated for the outside of the two girders because this girder will experience the most extreme deflections during the erection process.

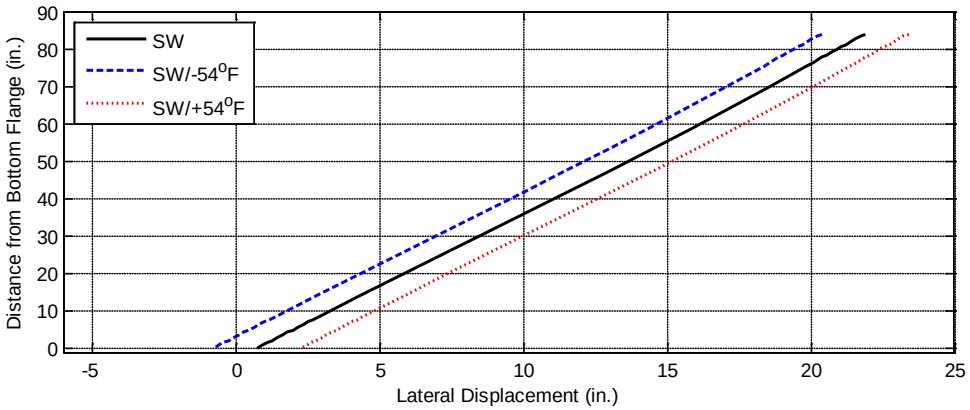


**Figure 3.23. Lateral Web Displacement at Mid-Span for Girders with R=200 ft.**

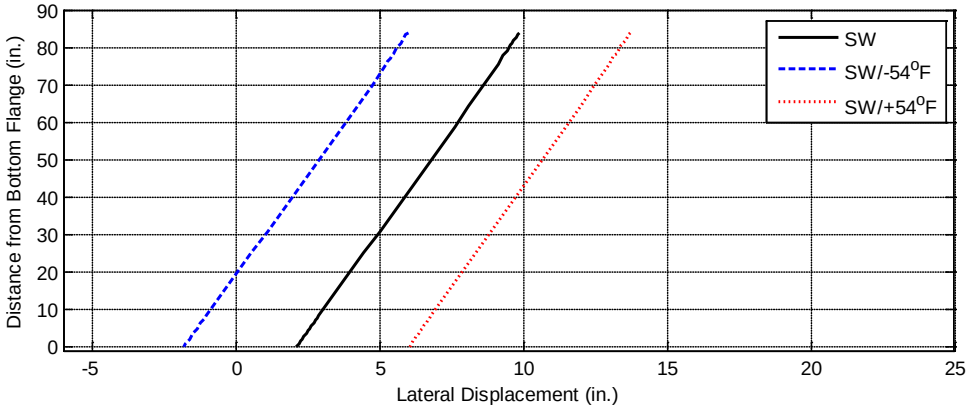


**Figure 3.24. Lateral Web Displacement at Mid-Span for Girders with R=500 ft.**

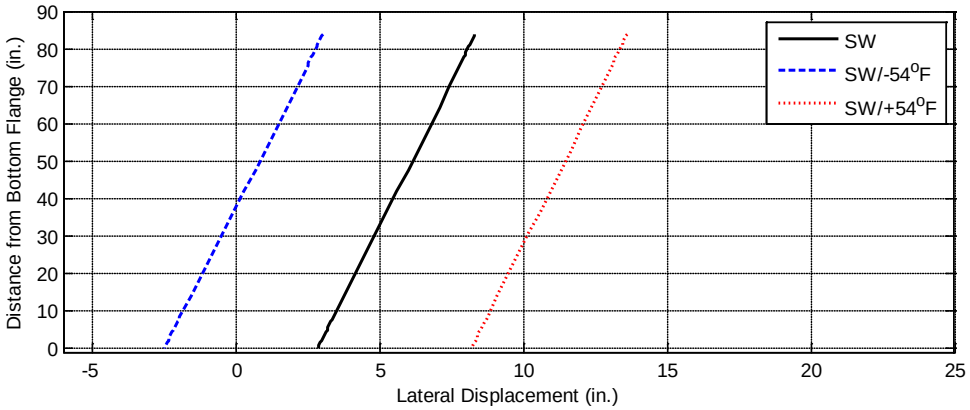


**Figure 3.25. Lateral Web Displacement at Mid-Span for Girders with R=700 ft.**

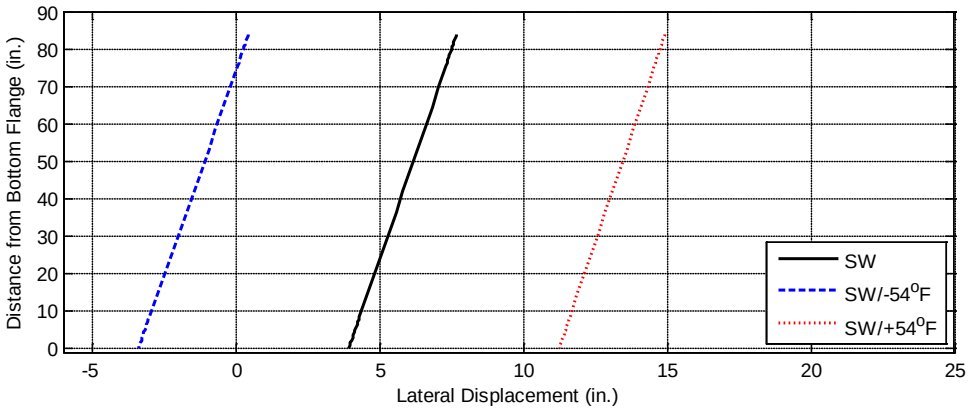


**Figure 3.26. Lateral Web Displacement at Mid-Span for Girders with R=1000 ft.**

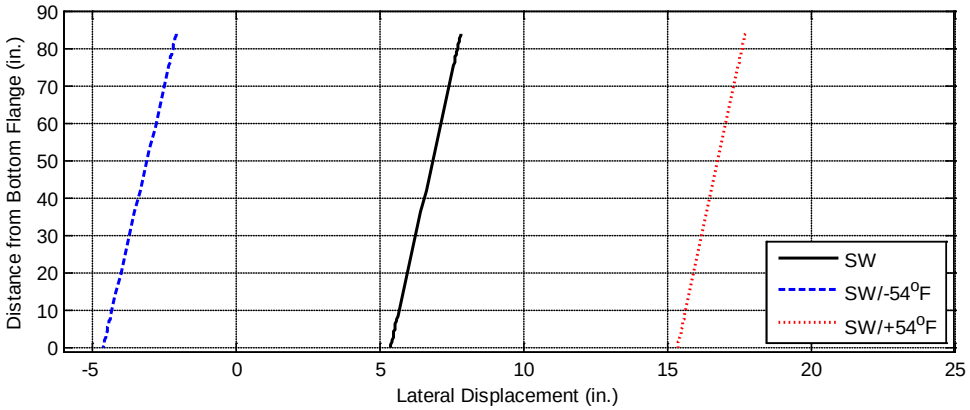


**Figure 3.27. Lateral Web Displacement at Mid-Span for Girders with R=1500 ft.**

Figures 3.23 – 3.27 reveal that the majority of the torsion in the I-girder webs in this portion of the study is a result of gravity loading. The smaller the radius of curvature of the two I-girder section, the larger the magnitude of web torsional deformation gravity loading will cause. As the girders twist under their self weight, the profile of the I-girder rotates, resulting in a deformed section with increased stiffness in the radial direction. The effect of changing temperature conditions on this model will manifest itself in the girders in the radial direction because of the fixation at the ends of the spans. As boundary conditions resist thermal expansion and contractions, girders will displace laterally in an attempt to accommodate thermal movements, which is portrayed in the web deformation plots. As results in the plots in Figures 3.23 – 3.27 show, as gravity

induced torsional displacements stiffen the sections in the radial direction, the effect of thermal loading on web displacements decreases as the degree of curvature increases (R decreases).

### 3.3.3 Girder Torsion

Bridges constructed of curved I-girders will inevitably experience some torsional response under normal in-service loading conditions that would not be present in a bridge constructed of straight I-girders. Loading on curved structures is never applied in the same plane as the center of gravity of the members which will lead to warping and torsion in the members. One way that torsion about the tangential axis of I-girders can be observed is through the twisting of the girder cross section. As previously mentioned, twisting of the girders causes vertical loads (deck weight, vehicle loads, ect.) to not be applied through the shear center of the girder which will further intensify the effects of twist in the girder. This twisting can lead to a number of problems including decreasing structural load capacity, cross frame misalignment, and errors in roadway alignment just to name a few.

Ideally, the twisting of the girder cross sections under self weight is accounted for during design by adjusting the camber of the girder as well as using temporary supports and/or cranes when erecting the girders. However, *AASHTO Guide Specifications* (2003) do not require designers to consider thermal loading on the I-girders during construction; thus, any additional twist in the girders due to thermal loading would likely be unaccounted for when formulating girder erection procedures. Additional twisting in the girders could likely lead to miscalculation of cross member sizing, requiring the contractor to adjust the position of the girders to fit the cross frames, possibly creating additional stresses that would be locked into the girders once the cross frames are secured.

For this analysis, cross section twist is quantified as the difference between the top flange and bottom flange centerline lateral deflections as demonstrated in Figure 3.28. A positive value for girder twist indicates the top flange displaces further away from the center of curvature than the bottom flange and vice versa for negative twist. Figures 3.29-3.33 plot comparisons of the additional twist that temperature change induces along the lengths of girders 1 and 2 after self-weight is applied. The units of the x-axis of the plots are given as the percentage of the total length of the span because each of the spans is of slightly different length and plotting using this parameter allows the tangential positions along each girder to be aligned.

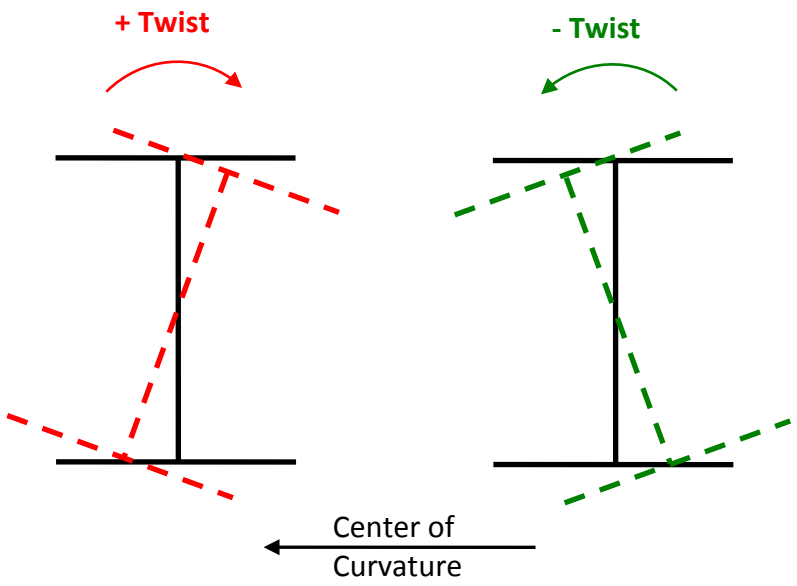


**Figure 3.28. Girder Twist Plot Conventions**

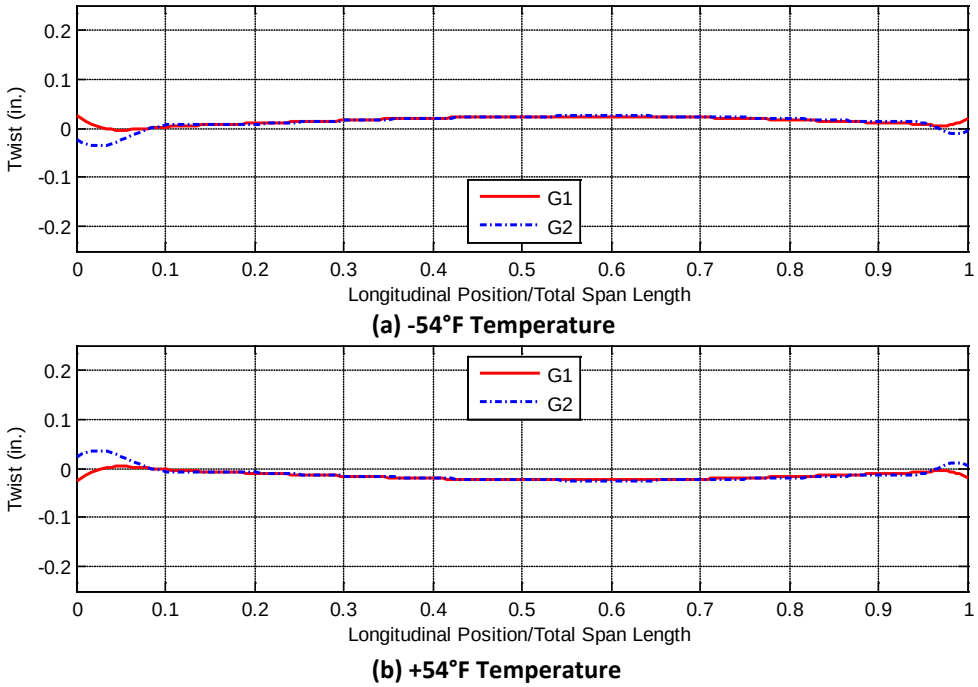


**Figure 3.29. Thermal Loading Induced Twist Comparison for Girders with R = 200 ft.**

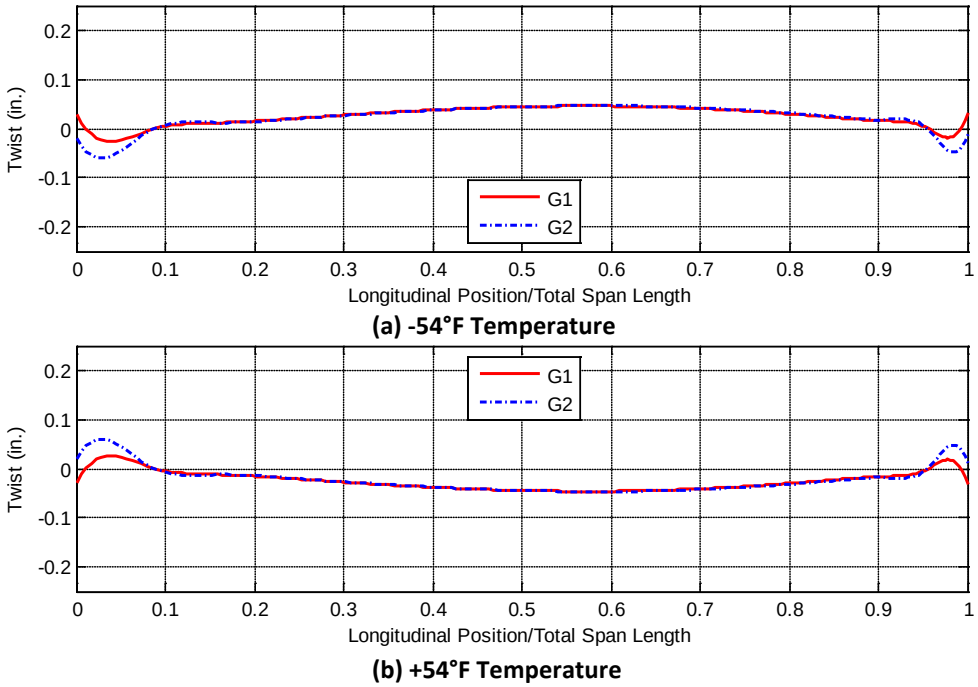


**Figure 3.30. Thermal Loading Induced Twist Comparison for Girders with R = 500 ft.**

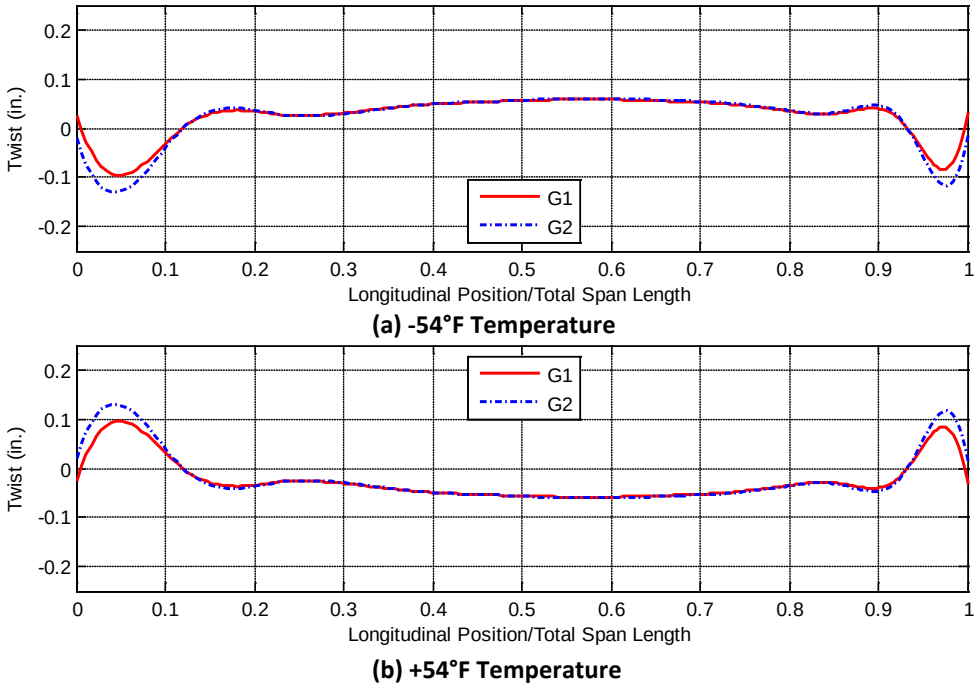


**Figure 3.31. Thermal Loading Induced Twist Comparison for Girders with R = 700 ft.**

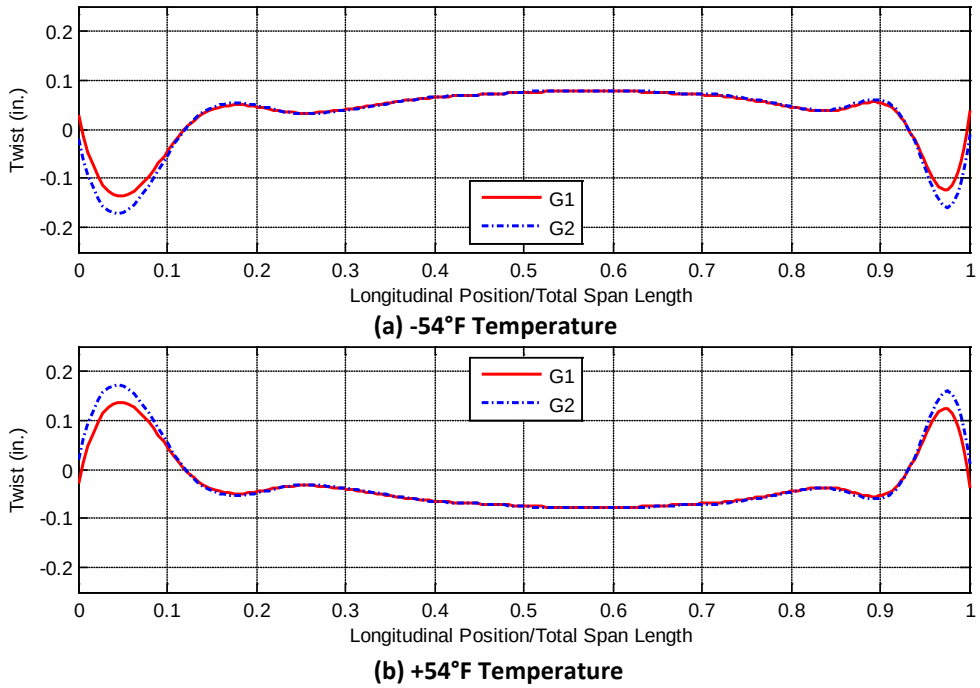


**Figure 3.32. Thermal Loading Induced Twist Comparison for Girders with R = 1000 ft.**

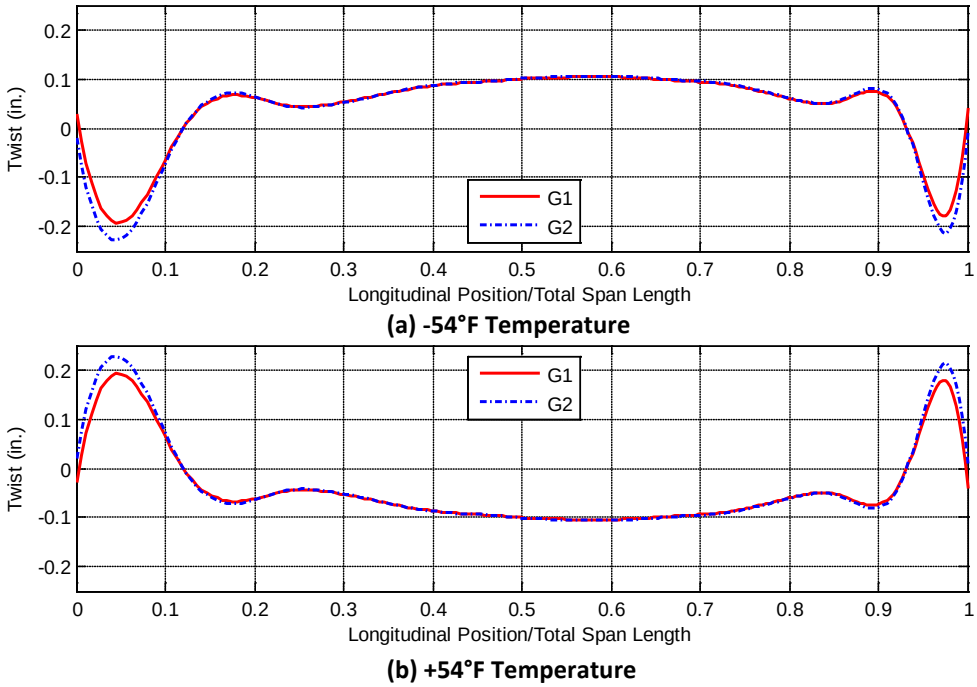


**Figure 3.33. Thermal Loading Induced Twist Comparison for Girders with R = 1500 ft.**

Results in Figures 3.29-3.33 reveal that the addition of thermal loading, either positive or negative, induces twisting in the girder cross section. The magnitude of girder twist is greater for those sections with a larger radius of curvature. Although the overall magnitude of torsional web deformation decreases as the radius of curvature increases, web twist from gravity loads leads to smaller radius of curvature sections becoming more stiff in the radial direction prior to the introduction of thermal loading. This increased stiffness leads to decreased thermally induced twisting of the I-girders. As stated previously, twisting of the girder cross section can have several negative effects on structural behavior, but the amount of twisting caused by thermal loads is very small compared to the twist from gravity loading. It is also of interest to note that, along the majority of the span, the girder twist of the inside and outside girder appears to be similar, but near the end supports the girders twist in the opposite direction of the middle of the span and the magnitude of twist is not the same for both girders. The differential twist at the girder ends would likely become a problem during erection of

the girders. As the pairs of girders are erected adjacent to each other and the temperature conditions change, if the inside and outside girders experience similar amounts of twist, then the cross frames are likely to still fit up properly because the distance between pairs will remain unchanged. However, if at some locations along the two girder section (i.e. at the supports in Figures 3.29-3.33), each girder twists a different amount, then the distance between the outside section of one girder and the inside section of the adjacent girder will change from the distance computed by the designer. Since designers do not account for changing temperature when designing the steel superstructure erection procedures, these deformations would likely lead to difficulties for the contractor in fitting the various sections of girder together once they are placed on their supports. In addition, the additional twist caused by thermal loads may lead to further problems as the bridge deck is constructed and in-service loads are applied as additional vertical loading will only increase the girder twisting.

### 3.3.4 Girder Stresses

A brief investigation of the longitudinal stresses induced by changing thermal conditions on the outside girder of the two-girder section was performed. The main objective of this narrow investigation was to determine if thermal loading on the section may affect the girder load carrying capacity. For this initial stage of the investigation, the focus is only on the longitudinal stresses in the flanges and web. Study of the longitudinal membrane stresses in the girder web showed that adding thermal loading to gravity loads did not significantly affect the state of web stress. Additionally, the stress distribution through the depth of the web is linear, indicating that the transverse stiffeners and cross frames are functioning to minimize nonlinear stress distribution in the web. On the other hand, the introduction of thermal loading does affect the tangential stresses across the width of the girder top and bottom flanges. Tangential stress distributions across the width of the top and bottom flanges are visually represented in Figures 3.34-3.38.

Stress distributions in Figures 3.34-3.38 are evidence that the additions of thermal loading to a curved section will change the longitudinal stresses in the girder flanges. Changing temperature has a larger effect on both the top and bottom flange longitudinal stress distribution as the radius of curvature of the section increases. In the top flanges, a decrease in temperature results in an overall decrease in tangential stress across the flange and a decrease in the difference between inside and outside flange flanges. A decrease in flange tip stress differential indicates a decrease in the flange lateral bending moment. The opposite is true as thermal loading increases, overall longitudinal stress increases as does the lateral bending moment in the top flange. However, for a curvature of 1500 ft. a temperature increase causes the lateral flange bending moment to change directions from gravity induced bending moment. In the case of the bottom flanges, temperature drop increases tangential stress at the inside flange tip and decreases the stress at the outside flange tip, which reverses the sign of girder lateral bending moment from the lateral bending moment present due to gravity loading. As expected, the opposite is true for a temperature increase. Inside edge stresses decrease while outside edge stresses increase, increasing the magnitude of the lateral flange bending moment. Positive thermal loads introduce additional lateral flange bending that leads to the largest maximum magnitude of longitudinal stress in the top and bottom flanges. This magnitude increases as the radius of curvature increases.

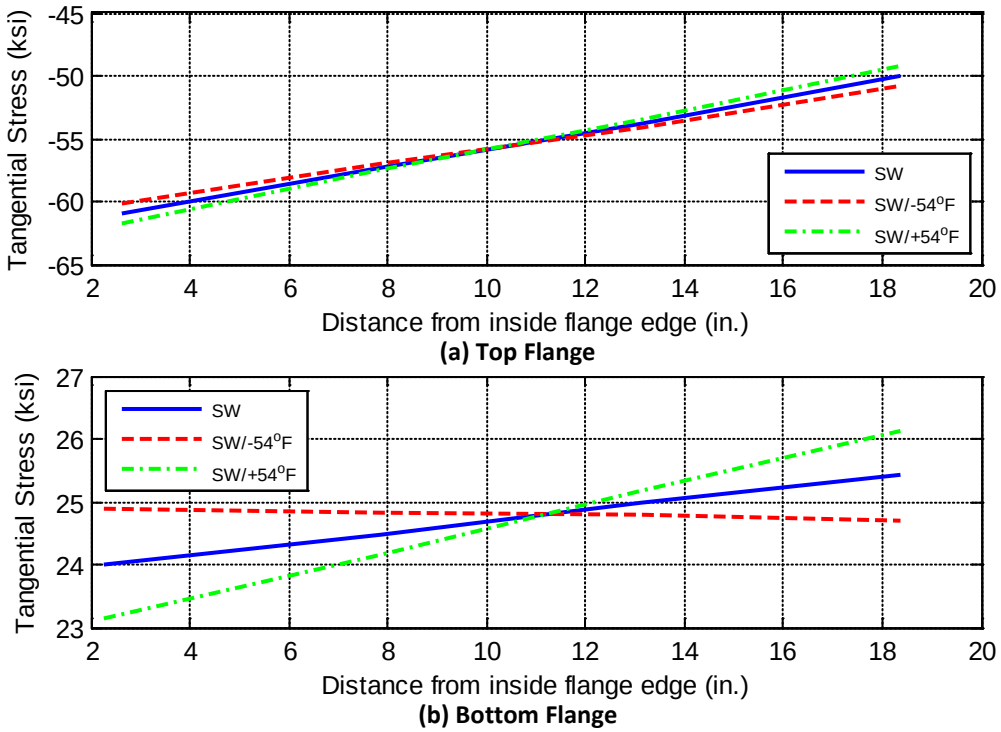


**Figure 3.34. Tangential Flange Stresses in Outside Girder (R = 200 ft.)**

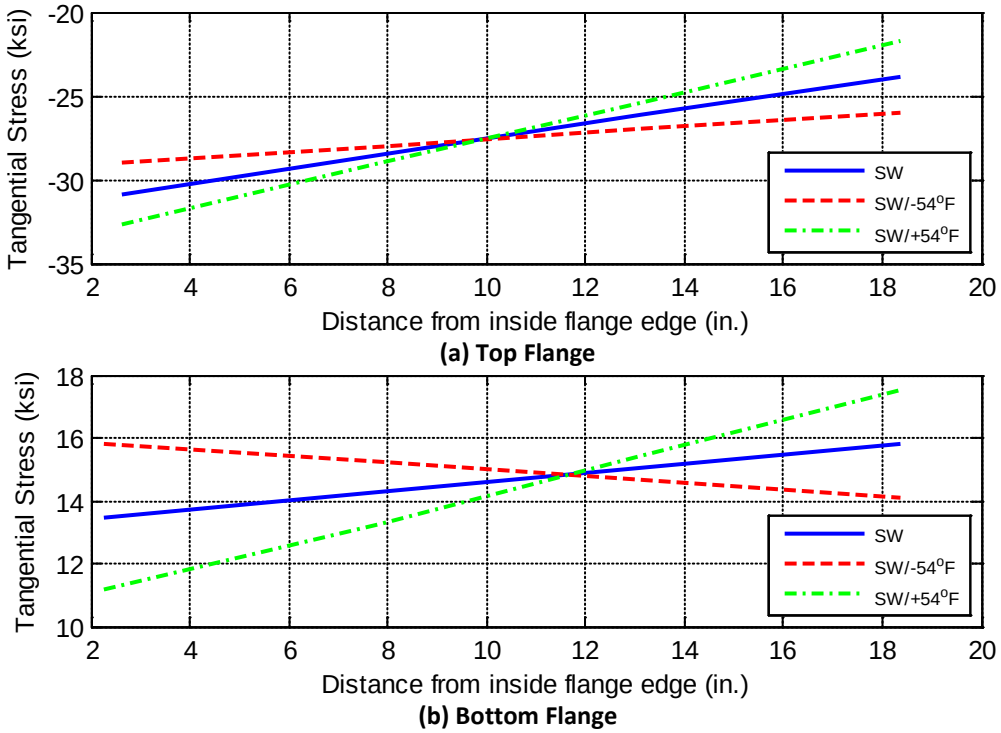


**Figure 3.35. Tangential Flange Stresses in Outside Girder (R = 500 ft.)**

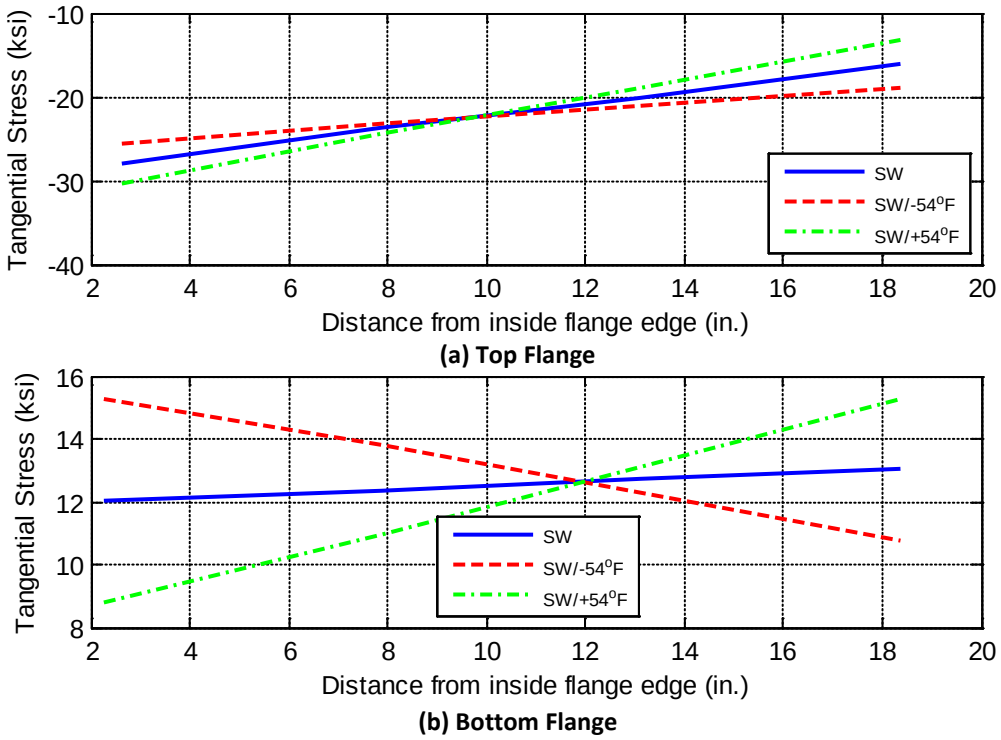


**Figure 3.36. Tangential Flange Stresses in Outside Girder (R = 700 ft.)**

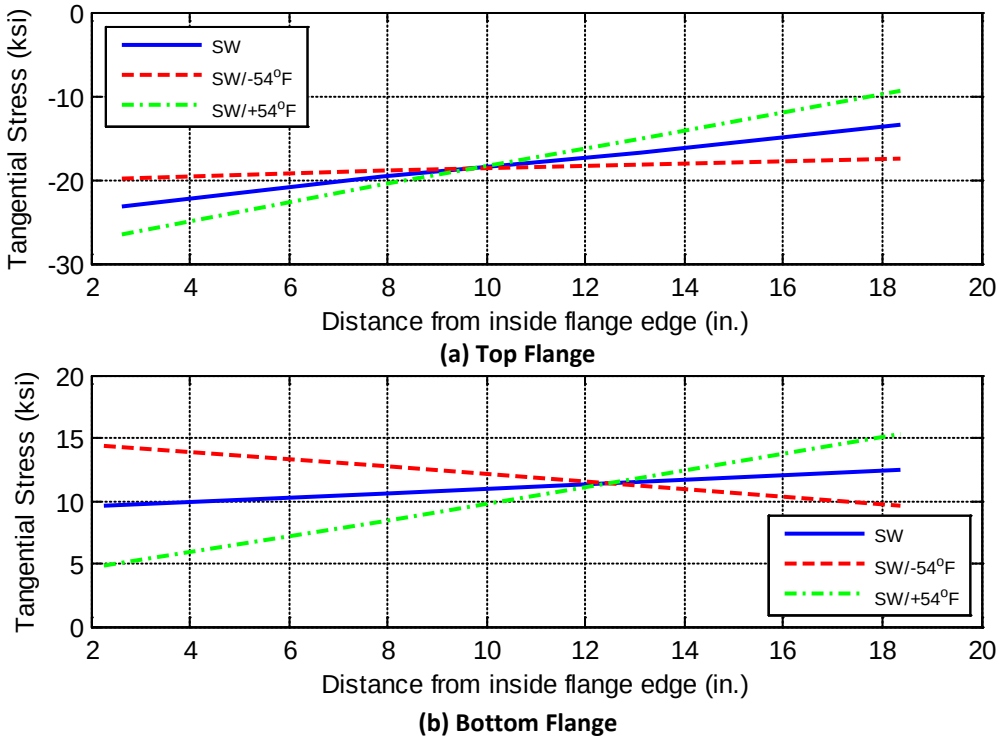


**Figure 3.37. Tangential Flange Stresses in Outside Girder (R = 1000 ft.)**

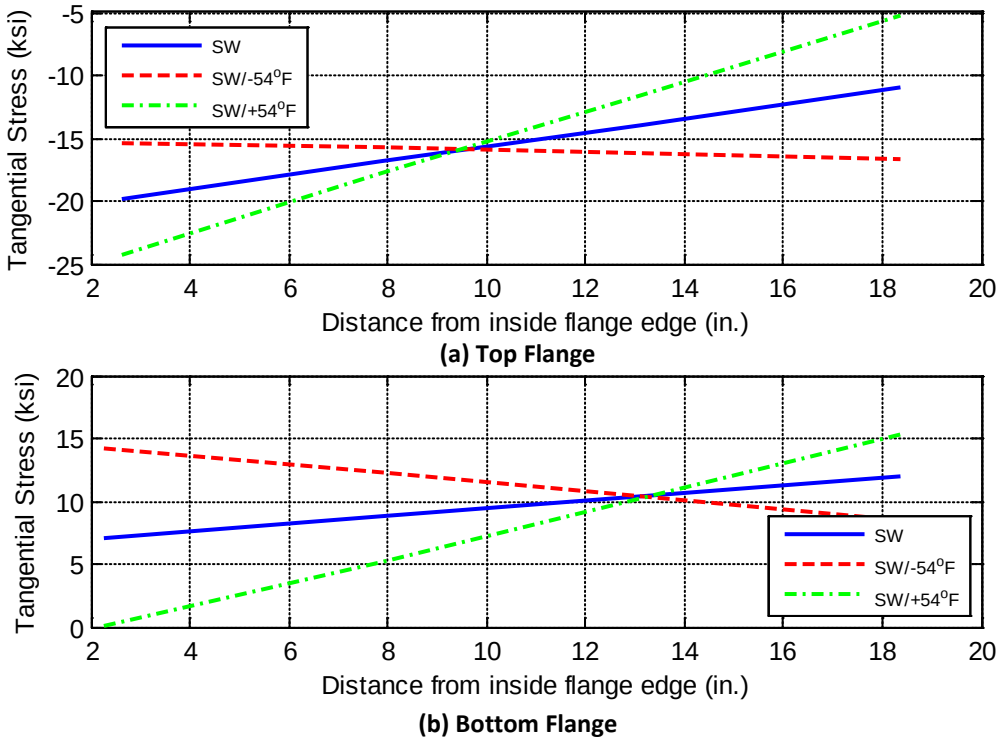


**Figure 3.38. Tangential Flange Stresses in Outside Girder (R = 1500 ft.)**

It is obvious from this elementary analysis that the addition of temperature loading to a two-girder curved section equipped with cross frames has an impact on the state of stress in the girder flanges. Of course, the level of this impact will be dependent on a number of factors that have not been investigated here, one being the boundary conditions of the section. Constraints, or lack thereof, provided by supports on the girders will have a significant effect on the thermal stresses that arise in the section. It appears that in this curved section, the majority of the axial load caused by thermal loading is carried by the girder flanges. Yet, as additional stresses are introduced into the girder flanges, the capacity of the flanges to carry other loads (deck weight, vehicle loads, etc.) would certainly be affected. Further studies must be performed to investigate how significantly the addition of thermal loading will impact the load carrying capacity of curved girders.

## 3.4 Conclusions

Results from the two brief FE studies presented in this section clearly indicate that thermal loading elicits a significant response in curved I-girder sections. The FE study on a simple, curved I-beam section revealed that:

- An increase in web panel slenderness of a curved I-beam section results in a decrease in the sections vertical moment carrying capacity.
- As the curvature of an I-beam section increases (radius of curvature decreases), maximum longitudinal stresses in the flanges increase, lateral bending moments in the flanges increase, and the moment carrying capacity of the section is decreased.
- Increase in temperature loading magnitude results in a decrease in vertical moment carrying capacity of the curved I-beam section.

Additionally, an analysis of the thermal loading effects on a curved I-girder section consisting of two transversely stiffened I-girders braced together with cross frames having fixed end boundary conditions lead to the conclusions:

- Thermal loading causes larger uniform lateral displacement at the girder mid-span for girders with smaller radii of curvature.
- A small amount of twist will occur in the girders under temperature loading with the magnitude being greater for sections with smaller degree of curvature.
- Sections with larger degrees of curvature experience greater torsional displacement under self-weight, stiffening the sections in the radial direction.
- Larger torsion from self-weight as degree of curvature increases highlights the need for intermediate supports during construction of curved steel I-girder bridges.

- For two girders connected with cross frames, thermal loading leads to different degrees of twist between the two girders at the support locations (ends of girder sections).
- Temperature loading has a larger impact on flange stresses as radius of curvature is increased, in particular, the magnitude of lateral flange bending moment induced in the top and bottom flanges by thermal loading is increasing as the curvature of the section is decreasing.
- Constraints on curved I-girders will affect how significant an impact thermal loading has on girder stresses; thus, further studies should be performed to investigate how boundary conditions impact the thermal stress state of the girder.
- Although temperature adds stress to curved I-girder flanges, further studies should be performed to understand the full magnitude of thermal loading effects on the moment carrying capacity of a curved I-girder bridge.

The information provided in this concise investigation is an adequate first step, but the effect of changing thermal conditions on curved I-girder bridges is a topic that must be investigated in much more detail. Additional thermal stresses and deformations could lead to a multitude of problems both during bridge construction as well as throughout the life cycle of the structure. A more broad study on a full-scale bridge should be performed to develop a better understanding of how changing temperature conditions might affect the I-girders when all components of a bridge are present.

# CHAPTER FOUR

# FINITE ELEMENT MODEL OF BUFFALO CREEK BRIDGE

## 4.1 Introduction

Finite element analysis in Chapter Three focused on smaller scale parametric studies of curved I-girder sections aimed at representing the behavior of the girders of curved I-girder bridges. Although results obtained in Chapter Three provide valuable information as to the response of curved I-sections to thermal loading, a better understanding of how changing temperature affects curved I-girder bridges could be better determined through a full scale case study of a bridge structure. The Buffalo Creek Bridge was chosen as the candidate for this case study. This section contains the detailed description of a three-dimensional finite element model created using the software package ADINA (2003) for use in investigating the behavior of the Buffalo Creek Bridge, which presents some modeling challenges due to its structural complexity. The main feature of this model is the detail with which all of the structural components were modeled in an effort to investigate the effects of thermal loading and how varying some bridge design parameters might decrease thermal stresses on the bridge. This section describes all of the procedures associated with creating the FE model.

## 4.2 Buffalo Creek Bridge

The Buffalo Creek Bridge in Logan County, West Virginia carries WV Route 10 over Buffalo Creek. The bridge is constructed of 8 curved I-girders, 1 stub girder, and is subdivided into 4 spans. Elevation changes exist on the structure in both the longitudinal and transverse directions as the bridge is designed with a 7.5% cross slope along with a north to south profile grade. Girders are continually braced with cross members along the length of each span with transverse web stiffeners at a few choice

locations in each span. The bridge deck was designed as an LRFD empirical concrete deck including a 6.5 in. thick reinforced concrete substrate divided into two distinct layers of reinforcement and a 2.0 in. thick micro-silica modified concrete overlay. The southern end of the bridge is supported by a semi-integral abutment (abutment 1) and the northern end is supported by a standard expansion joint abutment (abutment 2). Two column, reinforced concrete piers support the superstructure with piers 1 and 2 being oriented perpendicular to the curvature of the four center girders and pier 3 being skewed to line up parallel with abutment 2.

## 4.3 Bridge Superstructure Model

In many cases, the process of creating a finite element model that accurately represents the response of a large structure can be simplified by making some valid assumptions. For instance, a structure that is symmetrical about a certain point can be modeled by creating only one of the symmetrical sections and using symmetry boundary conditions to account for the additional symmetrical sections. However, this study requires that a full scale FE model of the structure be created mainly because the curvature and varying elevations of the bridge denies the structure from exhibiting any symmetry, thus, negating the possibility to make some assumptions that could save considerable modeling and computation time. Therefore, every effort has been made to reproduce the exact geometry of the Buffalo Creek Bridge when creating the FE model.

The initial challenge in creating the Buffalo Creek bridge model was reproducing the complicated girder geometry. As seen in Figure 4.1, the bridge consists of eight (8) full girders with one (1) stub girder and three (3) piers. Each of the eight (8) girders are steel, curved, I-beam girders with stiffeners along their length, with three girders (girders 3, 4, and 5) having a uniform radius of curvature and five girders (girders 1, 2, 6, 7, and 8) having varying radii of curvature. In addition to the bridge curvature, the structure has varying elevation changes (cross slopes) along both the longitudinal and

transverse directions. The point coordinates defining the girder shapes had to be extrapolated from the design drawings mathematically using the radii of curvature, girder spacing, and girder elevations.

This study consists of a number of FE models of differing configurations. The models can be separated into two major categories: those with fully rigid piers and those with pier flexibility modeled. Figure 4.1 shows a full model of the Buffalo Creek Bridge, complete with all three piers modeled. The piers were modeled using eight-node shell elements with the bearings represented using a series of spring elements. More discussion on the modeling of the bridge piers will be presented later in this chapter.

As a result of the large size of the model, every effort was made to minimize the computing cost associated with solving the model while maintaining the accuracy and usefulness of the results. Therefore, 8-node shell elements were used to model a majority of the bridge components including the girders, cross members at piers, abutment wall, deck, and piers. The majority of the area of the bridge girders is modeled using elements with lengths of approximately 3 ft. However, the element mesh is refined to a maximum length of 6 in. on the girders at the abutment, pier, and mid-span locations allowing a more thorough investigation of behavior in these areas. The sizes of the elements modeling the abutment wall vary and are chosen so that the ends of the girders and the abutment share nodal points, creating a rigid connection between the girders and the abutment. The main structure of the bridge piers are discretized as elements no larger than one foot on any edge. However, element subdivisions of the girder haunches are adjusted to allow a one-to-one node connection between the piers and the girders.

The modeling of the composite bridge deck is unique in that it is idealized as a multilayered shell element to accurately represent the separate layers of reinforcement. Use of the multilayered shell element allows the user to specify an arbitrary number of

individual layers to make up the thickness of the shell with each layer assigned different material properties. The multilayered shell element is a useful and efficient way to model a composite section without having to use a bulky 3D element. Being as the reinforced deck is a composite section, the properties of each layer of the deck are computed and used to form the multilayer shell. Shell elements making up the bridge deck are specified as having a maximum length of 3 ft. The process of computing these properties will be discussed later in this chapter.

The intermediate cross members consist of two horizontal members (top and bottom) and two diagonal members. For the intermediate cross members, the top horizontal and diagonal members are of type L4x3x3/8 and the bottom horizontal members are L4x3x1/2 L-beam sections. The top horizontal and diagonal members at each pier are L6x4x1/2 sections while the bottom horizontal member is an I-beam of type W24x192 with two stiffeners on each side of the web. The stresses within the cross members are not of paramount concern for this study so most of the cross member sections are discretized as Hermitian beam elements. All members except the bottom horizontal members at the pier are represented using beam elements by simply specifying the beam cross sectional properties and orientation. Bottom horizontal cross member sections at the piers cannot be represented in this way because of the presence of the bearing stiffeners. Consequently, the geometry of these cross members is replicated using 8-node shell elements.

Spring elements are utilized to represent the non-linear behavior of the soil behind semi-integral abutment 1. Along the abutment wall, grounded non-linear spring elements are created at each point of the abutment wall geometry. In ADINA (2003), a grounded spring element is a spring element that is connected to only one node. The force the spring exerts at this point is a function of the displacement of the node and the spring stiffness. Development of the nonlinear spring stiffness properties and their application to the model is discussed later in this chapter.

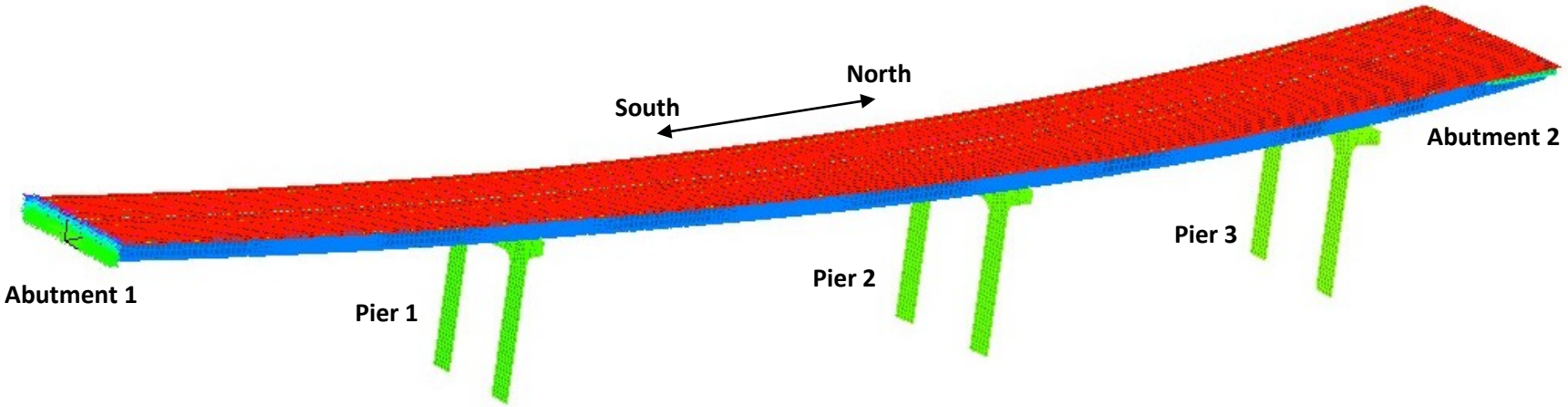


(a) Full FE model of Buffalo Creek Bridge

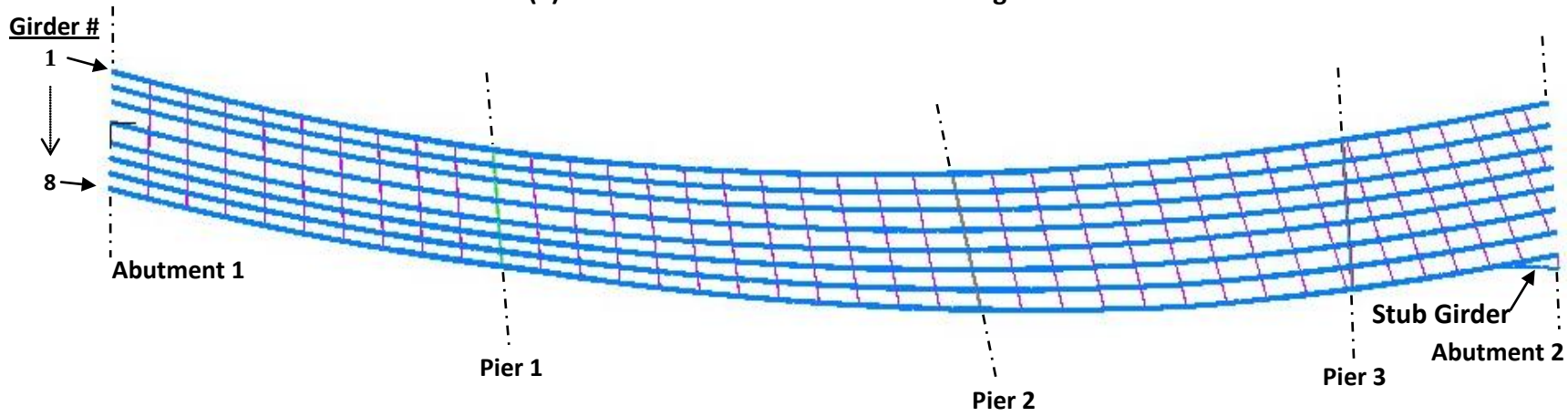


(b) Plan View of FE Model of Buffalo Creek Bridge Girders

Figure 4.1. FE Model of Buffalo Creek Bridge

## 4.4 Bridge Substructure Model

To further understand the behavior of the Buffalo Creek Bridge, it was deemed necessary to investigate how introducing pier flexibility will affect the behavior of the bridge superstructure. The concrete pier pillars were modeled using 8-node shell elements with every effort made to exactly replicate the pier geometry. Figure 4.2 shows a depiction of the model of Pier 1. The connection between the piers and girders is made via a set of linear springs that represent bridge bearings. For the rigid pier case, boundary conditions are placed on the top of pier haunches that prohibit any pier movement, simulating bridge bearings being completely stationary. For the case modeling pier flexibility, the bottom surfaces of the piers are fixed to simulate the pier being anchored to the bedrock.

Using the command 'spring-lines', ADINA allow springs acting in a specified degree of freedom to be defined between two nodes. The displacement of the nodes relative to each other in these specified degrees of freedom are tied together to the degree of the defined spring stiffness. ADINA also allows multiple springs to be defined between two nodes, allowing multiple degrees of freedom on the girders and piers to be linked together at one location. The top surface of the pier haunches and the bottom flange of the girders (at the locations of the piers) have their surfaces subdivided in such a way that there is one node on the top surface of the pier haunch exactly eight inches directly below each node on the girder bottom surface. This distance of eight inches is used because the thickness of the bearings on the bridge is eight inches. These corresponding girder and pier nodes are tied together with a series of springs intended to mimic the behavior of the bridge bearings.

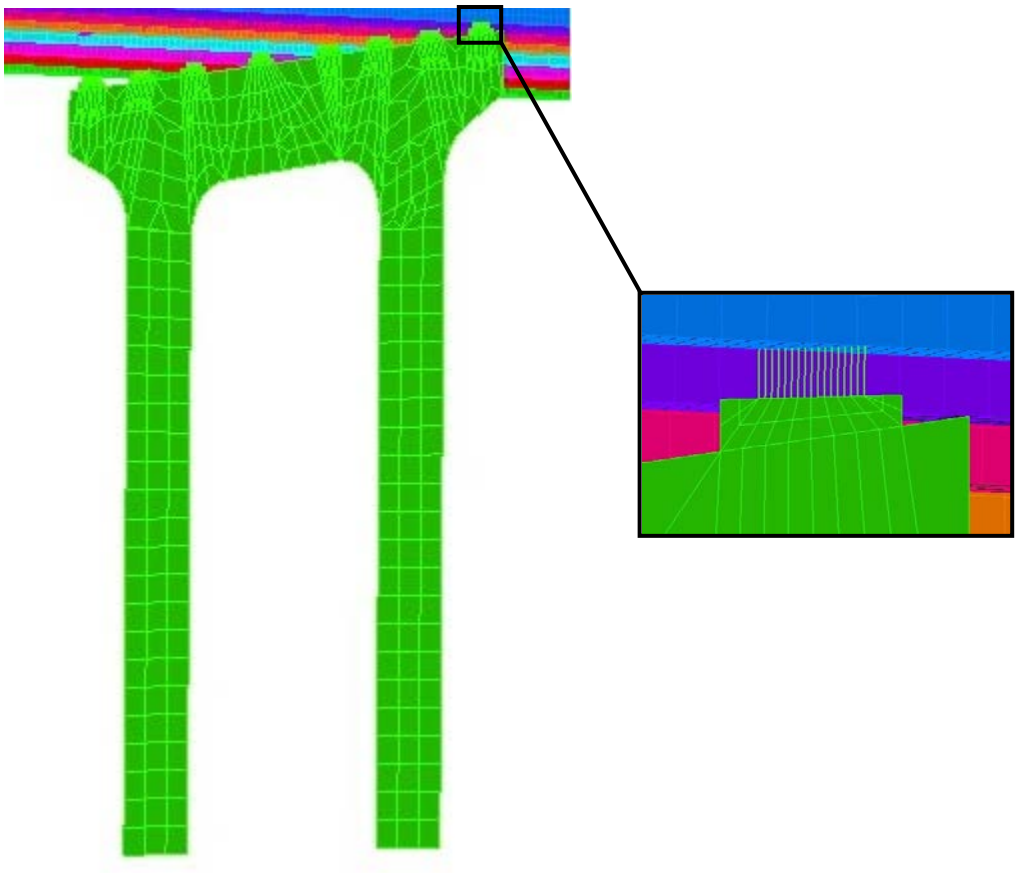

**Figure 4.2. FE Model of Buffalo Creek Bridge Pier 1**

For instance, to simulate fixed bearings (see Figure 4.4) six springs are modeled between each node, connecting the x-, y-, and z-translations and rotations. Since it is assumed for this study that the bridge bearings fully restrict movement in the directions they are intended to do so and allow full, free movement in all the other directions, the stiffness of the springs is set at an extremely high value ($k = 1x10^{21}$) which allows the spring to model a tied connection between the specified degrees of freedom. For the other types of bearings, springs are modeled between the pier haunch and girder nodes connecting the appropriate degrees of freedom to simulate each desired bearing type shown in Figure 4.4.

## 4.5 Material Model

The properties of the steel and concrete making up the Buffalo Creek Bridge are assumed to be general values as these will be sufficient under the encountered loading conditions. The steel and concrete material properties are given in Table 4.1. An elastic isotropic material model is used for the steel girders because the aim of this study is to investigate the pre-yield behavior of the Buffalo Creek Bridge.

**Table 4. 1. FE Model Material Properties**

| | Steel | Concrete |
|---|---|---|
| **Modulus of Elasticity (psi)** | $30\times10^6$ | $3\times10^6$ |
| **Poisson's Ratio** | 0.3 | 0.2 |
| **Density (slug/ft$^3$)** | 15.22 | 4.658 |
| **Coefficient of Thermal Expansion (/°F)** | $6.78 \times 10^{-6}$ | $6.2 \times 10^{-6}$ |

Throughout the bridge deck, the density of the steel reinforcement varies in the radial and transverse directions. As a result, the material properties of a section of the deck in the transverse direction will differ from those in the radial direction, making it necessary to model the deck using an orthotropic material. Additionally, since the reinforcement density changes from location to location within the deck, the deck is divided into sections with similar reinforcement densities and the orthotropic properties are calculated individually for each section. The deck is subdivided into three distinct layers: the 3.25 in. thick bottom layer, the 3.25 in. thick top layer, and the 2 in. thick overlay. Table 4.2 contains a summary of the layout of the concrete deck reinforcement.

**Table 4. 2. Deck Reinforcement Configuration**

| | | Transverse Reinforcement | Longitudinal Reinforcement |
|---|---|---|---|
| **Along Spans** | **Top Layer** | #4 rebar @ 1 ft. spacing | #5 rebar @ 0.30 m spacing |
| | **Bottom Layer** | #4 rebar @ 8 in. spacing | #5 rebar @ 0.30 m spacing |
| **Above Piers** | **Top Layer** | #4 rebar @ 1 ft. spacing | #5 rebar @ 0.20 m spacing<br>#6 rebar @ 0.20 m spacing |
| | **Bottom Layer** | #4 rebar @ 8 in. spacing | #5 rebar @ 0.30 m spacing<br>#4 rebar @ 0.30 m spacing |

For each section of like reinforcement density, an equivalent modulus of elasticity ($E_{eq}$), poisson's ratio ($\nu_{eq}$), density ($\rho_{eq}$), and coefficient of thermal expansion ($\alpha_{eq}$) are calculated using the following equations:

$$n = \frac{E_s}{E_c} \tag{4.1}$$

$$A_{eq} = A_c + (n-1)A_s \tag{4.2}$$

$$E_{eq} = \frac{(E_c A_c + E_s A_s)}{A_{eq}} \tag{4.3}$$

where $E_s$ and $E_c$ are the modulus of elasticity of steel and concrete respectively (from Table 4.1) and $A_s$ and $A_c$ are the cross sectional area in a particular cross section of the deck of steel and concrete respectively. The other equivalent properties (Poisson's ratio, density, and coefficient of thermal expansion) for the orthotropic sections were calculated using the same equations by substituting the appropriate property for $E$ into Equations 4.1 and 4.3. Applying each set of properties to the appropriate section and layer of the concrete deck is the final step in creating the material model for the reinforced concrete deck.

## 4.6 Boundary Conditions

Accurate modeling of the conditions at bridge supports is an integral part of FE analysis as slight changes in the boundary conditions can have a profound effect on the results. As previously mentioned, the models created for this case study can basically be divided into two categories: cases that model the piers as rigid members and cases that model the piers as flexible members. For the rigid pier case, the bridge piers will have no impact on structural response and the behavior of the bridge will be as if the bottom surface of the bridge bearing are fixed and cannot move. In the flexible pier case, bridge piers are free to deform as loading is placed on the structure and this deformation may impact the response of the superstructure. The boundary conditions applied to the Buffalo Creek models are chosen to reproduce the actual

support conditions as accurately as possible. Boundary condition locations which are referenced throughout this section are displayed in Figure 4.1.

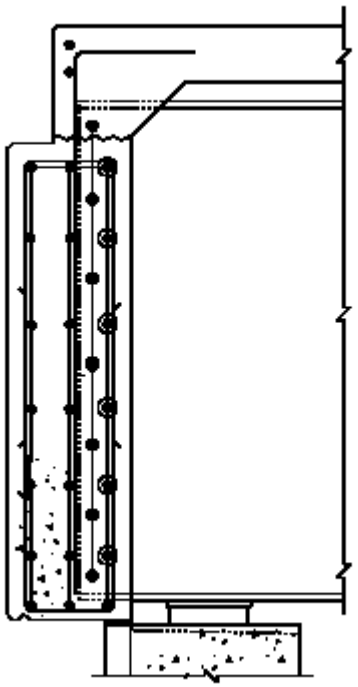

**Figure 4.3 Typical Semi-Integral Abutment Detail**

The abutment at the east end of the bridge, abutment 1, is constructed as a semi-integral abutment. Semi-integral abutments combine some of the characteristics of expansion joint abutments with integral abutments. As is the case with integral abutments, the abutment wall is cast around the girder ends creating a rigid connection between the girders and abutment wall. However, the abutment wall is not continuous from the bridge deck to the support piles as in integral abutment design. One section of the wall incases the girder ends while another section is just below the girder ends and provides vertical support to the girders as well as longitudinal and transverse support in the form of bearing joints. A schematic of a typical semi-integral abutment is shown in Figure 4.3. All of the supports on the Buffalo Creek Bridge come in the form of expansion joints with the exception of the soil behind the abutment wall. The

wall of abutment 1 is modeled as rigidly connected to the girder ends with the appropriate expansion joint modeled at each girder.

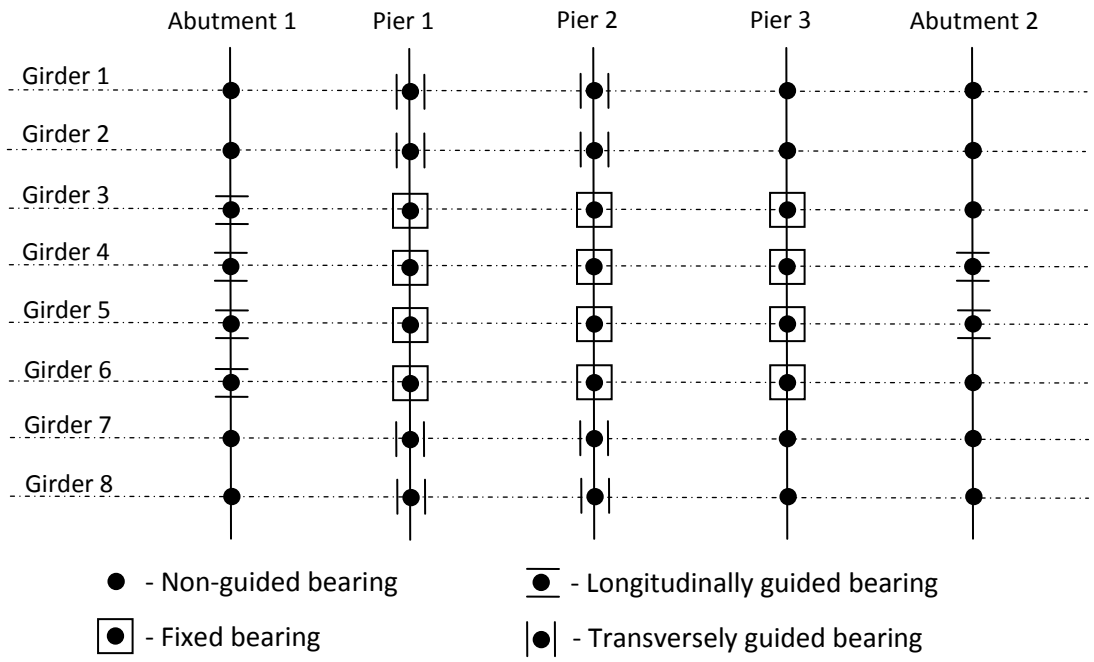


**Figure 4.4 Bearings at Supports**

The bearing supports consist of four types of connections between the girders and the piers: non-guided expansion bearings, fixed bearings, longitudinally guided expansion bearings, and transversely guided expansion bearings. Non-guided bearings provide only vertical support to the girders, fixed bearings create a fully fixed connection between the piers and the girders, longitudinally guided bearings provide vertical support as well as preventing transverse displacement and rotation about the longitudinal axis, and transversely guided bearings provide vertical support along with constraining longitudinal displacement and rotation about the transverse axis. Figure 4.4 indicates the type of bearings present along the length of the bridge at each support location for each girder.

Due to the curved shape of the Buffalo Creek Bridge, the constraints on the girder bottom flanges act in a different direction for each individual bearing at each individual location. To accurately represent the behavior of these bearings, individual skewed coordinate systems were created at each bearing location on each pier and at abutment 2 (thirty-two skewed coordinate systems in total) and applied to the appropriate nodes. As a result, once the boundary conditions (in the form of spring sets) are applied to these nodes, they will act so as the longitudinal direction is along the centerline of the bottom flange and the transverse direction is perpendicular to this centerline. This ensures that the boundary conditions are applied in the correct direction locally at the bearings and not just in the global coordinate systems.

In bridge design, it is assumed that the shear studs attached to the top flange of bridge girders will provide full composite action between the top flange of the bridge girders and the bottom surface of the concrete deck. Full composite action implies that under any given loading condition the displacement at locations where the deck and girder top flange come in contact are equal. For this study, full composite action is assumed between the girders and deck.

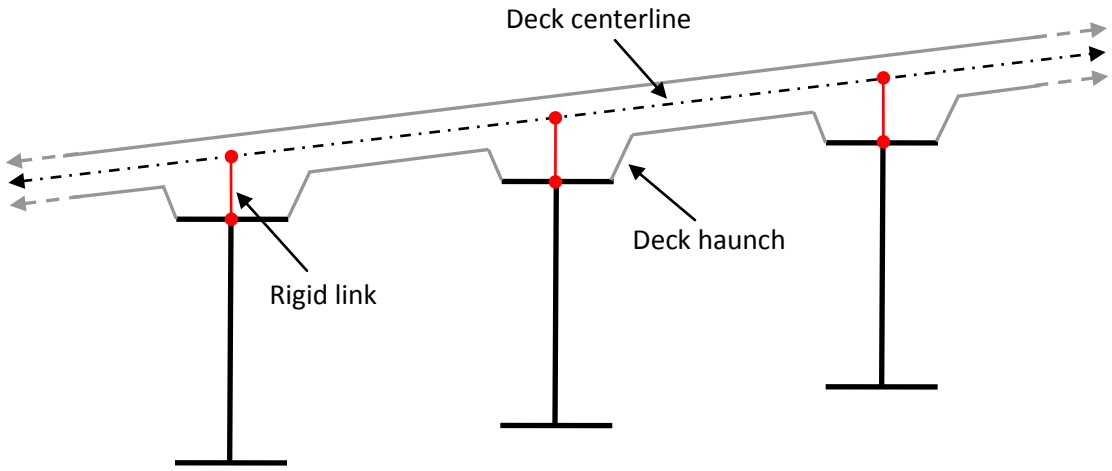


**Figure 4.5 Rigid Links Used for Deck-Girder Connection**

As stated previously, it is the desire of this study to model the composite deck as a 2D shell element. However, the varying elevation of the girders in the transverse direction makes it difficult to rigidly attach a smooth deck, modeled using shell elements, across the top flange

surfaces of the girders. A solution to this problem is obtained by idealizing the deck haunches as a set of rigid links as seen in Figure 4.5. Instead of modeling the 3D nature of the deck haunches and greatly adding to the solution time of the model, the deck haunches are replaced by rigid links which connect the top flange of the girders to 2D shell elements created to coincide with the deck centerline.

## 4.7 Soil-Abutment Interaction

Although expansion joints are present at abutment 1 allowing expansion and contraction of the structure, the soil behind the semi-integral abutment wall will produce a constant pressure on the abutment. This non-linear force on the abutment will resist the expansion and contribute to the contraction of the bridge and can be classified as states of active, passive, or at-rest pressure. An extensive literature review was conducted which revealed that the most accurate way to model the behavior of the soil backfill is by using a set of nonlinear springs known as a "Winkler" model. The literature review also concluded that the most widely used standards for computing the response curves of the soil backfill come from design manuals such as Clough and Duncan (1971), NCHRP report (Barker et al., 1991), and Husain and Bagnariol (1996) which are all based on the finite element analysis by Clough and Duncan (1971). For this study, the process outlined in Barker et al. (1991) was used in modeling the nonlinear response of the soil backfill.

The nonlinear behavior of the springs representing the soil is modeled by defining the spring stiffness with a nonlinear force versus deflection curve (f-d curve). The amount and direction of the abutment wall deflection will determine the amount of force exerted back on the wall by the backfill. When the abutment translation or rotation is in the direction of the backfill, the backfill will be in the passive pressure state. Conversely, when the abutment moves away from the soil, the backfill will be in the active pressure state. In the instance that the abutment is not moving, the pressure will be in the at-rest state. Naturally, the passive pressure applied by the

backfill will be significantly greater than the active pressure under equal deflection in the opposite direction.

According to Barker et al. (1991), the Rankine Theory can be used for calculating active and passive earth pressures on retaining walls when the wall friction angle is equal to the slope of the backfill surface, which is true in this case because the back of the abutment is vertical. First of all, when creating an f-d curve for soil force on a retaining wall, the type of soil behind the abutment wall must be known. In this study, the soil backfill is of type medium dense sand with an internal friction angle of $\phi_f = 39°$. Next, the approximate displacements required to reach minimum active and maximum passive earth pressure must be determined. For medium dense soil, the values are obtained from Clough and Duncan (1971) and listed in Table 4.3.

**Table 4. 3. Minimum Active and Maximum Passive Earth Pressure States**

| | Active | Passive |
|---|---|---|
| **Δ/H** | 0.002 | 0.02 |

where $\Delta$ is the movement of the top of the wall required to reach minimum or maximum pressure state and H is the height of the wall.

Now the coefficient of at-rest earth pressure, $K_o$, is calculated according to the equation

$$K_o = 1 - \sin\phi_f \qquad (4.4)$$

which is the value for the coefficient of lateral earth pressure when there is no wall deflection. The value for $K$ at the minimum active earth pressure, $K_a$, is calculated from the equation

$$K_a = \frac{1 - \sin\phi_f}{1 + \sin\phi_f} \qquad (4.5)$$

while the value for the maximum passive pressure, $K_p$, is determined using

$$K_p = \frac{1+\sin\phi_f}{1-\sin\phi_f} \qquad (4.6)$$

These three values are used in a MATLAB (2011) program to create a graph and a function value to calculate the coefficient of earth pressure at any state. The graph contains *Δ/H* values versus *K* values. It should be noted that for any values of *Δ/H* beyond the values required to reach minimum active and maximum passive pressure the value for *K* will not increase beyond $K_a$ and $K_p$ respectively. Figure 4.6 shows an example of the graph of the relationship between the wall movement and earth pressure coefficient used in this study.

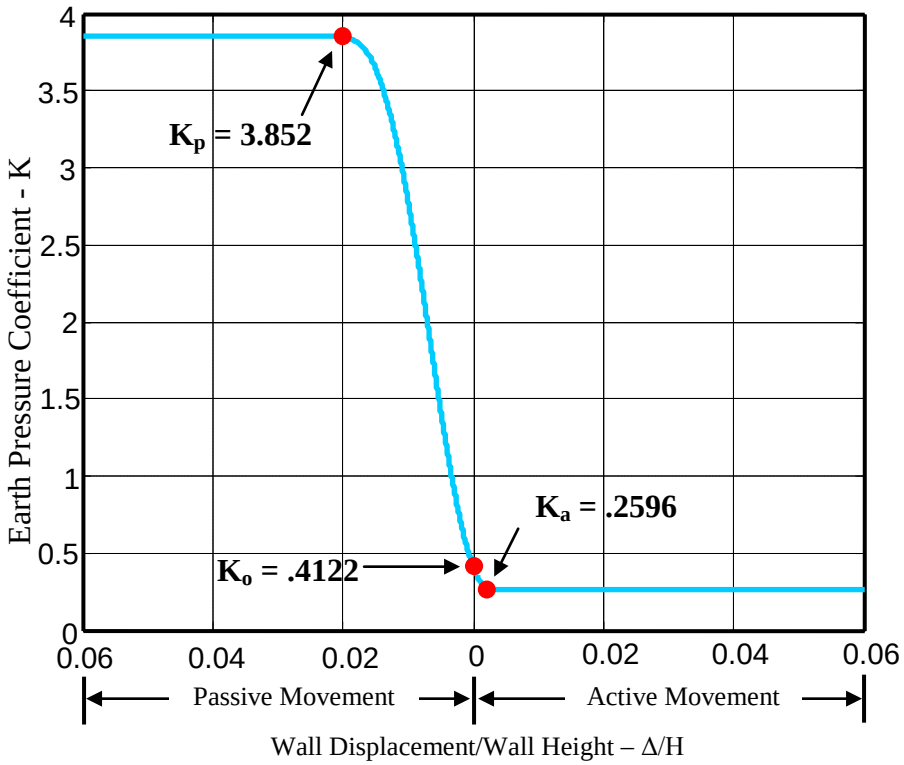


**Figure 4.6 Relationship Between Abutment Movement and Earth Pressure Coefficient**

The values for *K* interpolated using this process are used to determine the passive and active earth pressures exerted on the abutment walls using the equations:

$$p_a = K_a z \gamma \qquad (4.7)$$

$$p_p = K_p z \gamma \qquad (4.8)$$

where γ is the unit weight of the soil (force/length$^3$) and z is the depth below the soil (length). For medium dense sand, the value for γ is 130 lb/ft$^3$. However, since springs act upon a single point rather than an entire surface, the pressure over a prescribed area must be condensed into a concentrated force. For each surface, the concentrated force acting upon that element is calculated by multiplying Equations 4.7 and 4.8 by the area of the appropriate surface. This value is then divided by four to obtain the concentrated force acting upon each point making up the rectangular surface. The f-d curves created by this process are computed using Equations 4.9 and 4.10 and are then used as the non-linear stiffness properties of the appropriate spring elements on the wall of abutment 1. An example of a few f-d curves utilized by this model can be seen in Figure 4.7 and the abutment wall with attached springs is shown in Figure 4.8.

$$F_a = \frac{K_a \gamma A z}{4} \qquad (4.9)$$

$$F_p = \frac{K_p \gamma A z}{4} \qquad (4.10)$$

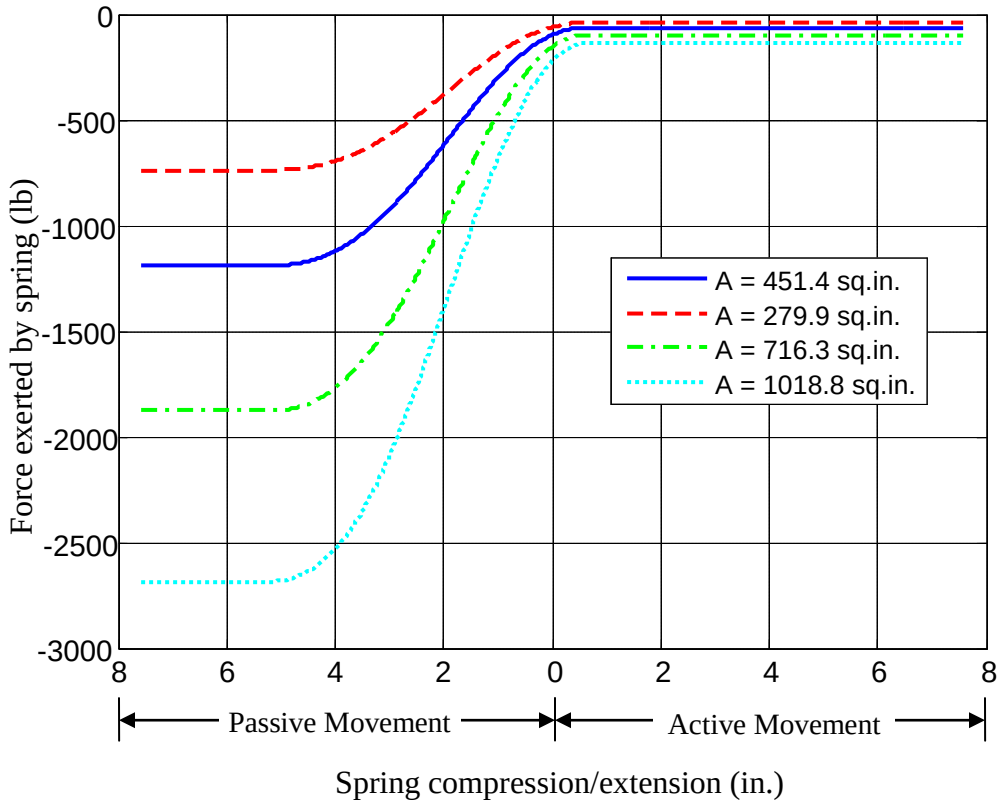


**Figure 4.7 F-d Curves at Depth of 31.8 in. Below Deck**

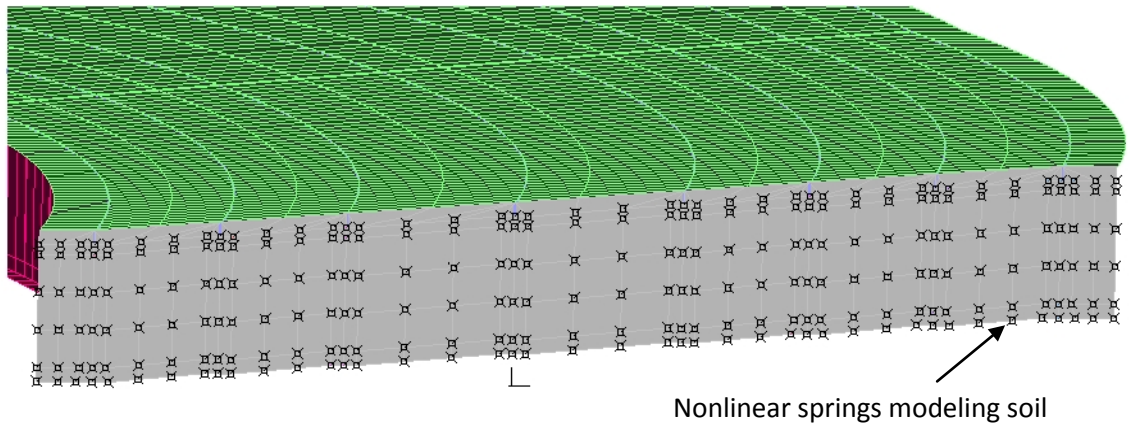


**Figure 4.8 Nonlinear Springs Used to Model Soil-Abutment Interaction**

# CHAPTER FIVE

# FINITE ELEMENT MODEL VALIDATION

## 5.1 Introduction

A critical step in performing a finite element structural analysis is validating the FE output by comparing outputs from the finite element model with experimentally measured responses. Ideally, the experimentally measured response comes from physically measuring a structures response under controlled or known conditions. Unfortunately, no such experimental values were available or were able to be measured for the Buffalo Creek Bridge.

An alternative to comparing FE results to experimental measurements is the comparison of FE calculated responses to theoretically determined responses. Theoretical measurements of varying types of responses can be calculated using a number of different methods. In this case, the Buffalo Creek Bridge girder camber tables in the bridge design sheets contain theoretically computed values for the vertical girder deflection under the weight of steel dead load along with the weight of steel dead load plus the concrete bridge deck weight.

For the purpose of model validation, the response of the FE model was investigated under steel superstructure gravity loading plus steel superstructure and reinforced concrete deck gravity loading. To mimic the construction sequence of the Buffalo Creek Bridge, gravity loading is applied in two steps: First, the model is solved with only the gravity load of the girders and cross members acting on the structure. Second, the weight of the concrete bridge deck is applied to the model that is already deformed under the weight of the steel superstructure. When computing the vertical camber values presented in the bridge design sheets, engineers do not account for how the deflections of the bridge piers will affect the girder displacement profile. Thus, the FE model with rigid bridge piers is used as the baseline model for the model verification study.

## 5.2 Steel Superstructure Gravity Load

The first step in model validation included subjecting the FE model of the steel superstructure (girders and cross members) of the Buffalo Creek Bridge to gravity loading and measuring the vertical girder deflections for comparison with the values in the bridge design sheets. Figures 5.1 to 5.8 include plots comparing FE computed deflected girder shapes with design calculated deflected girder shapes for individual bridge girders under self weight loading. For sake of comparison, a cubic spline interpolation of the FE measured deflected shape is performed at 1/10 points along each span corresponding to the locations at which deflection is given in the camber tables.

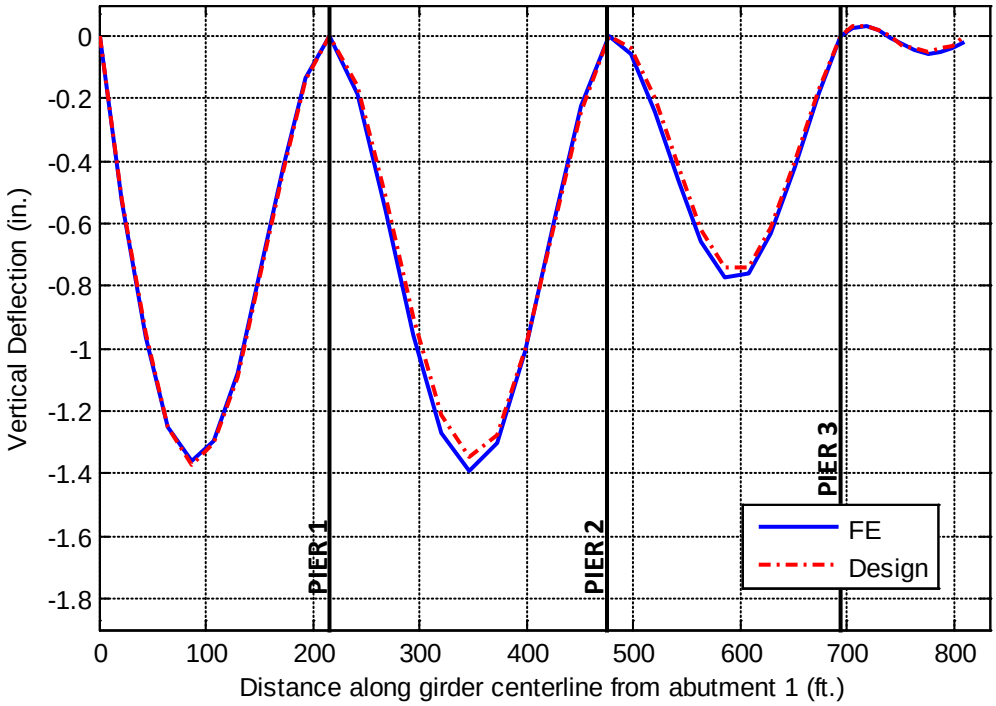


**Figure 5.1. FE and Design Calculated Self-Weight Deflections (Steel Superstructure Only) – Girder 1**

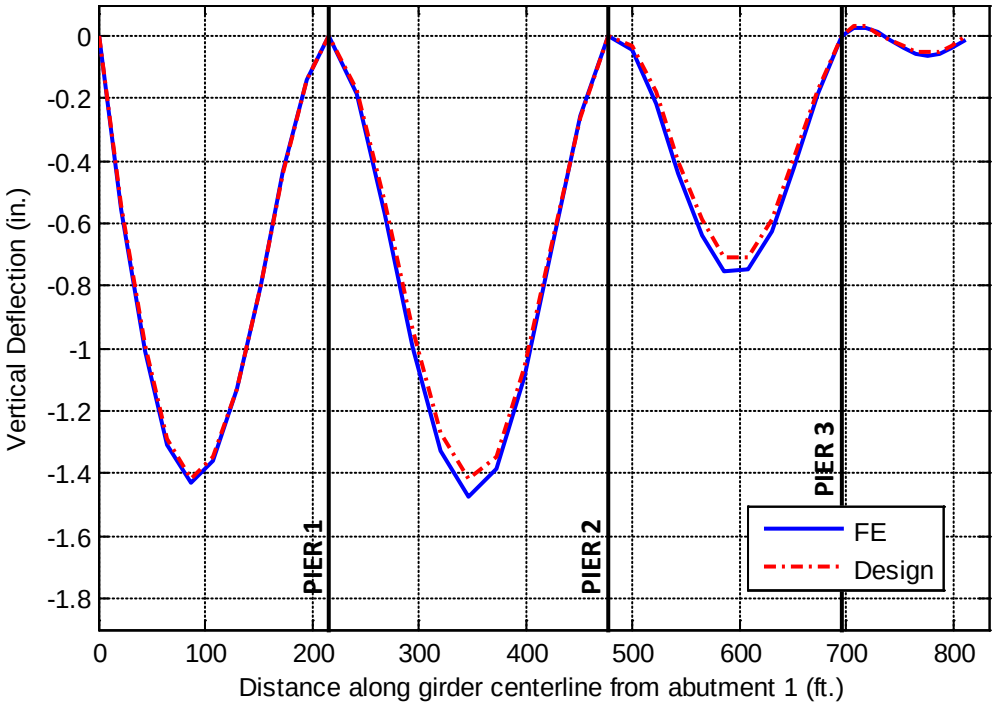


**Figure 5.2. FE and Design Calculated Self-Weight Deflections (Steel Superstructure Only) – Girder 2**

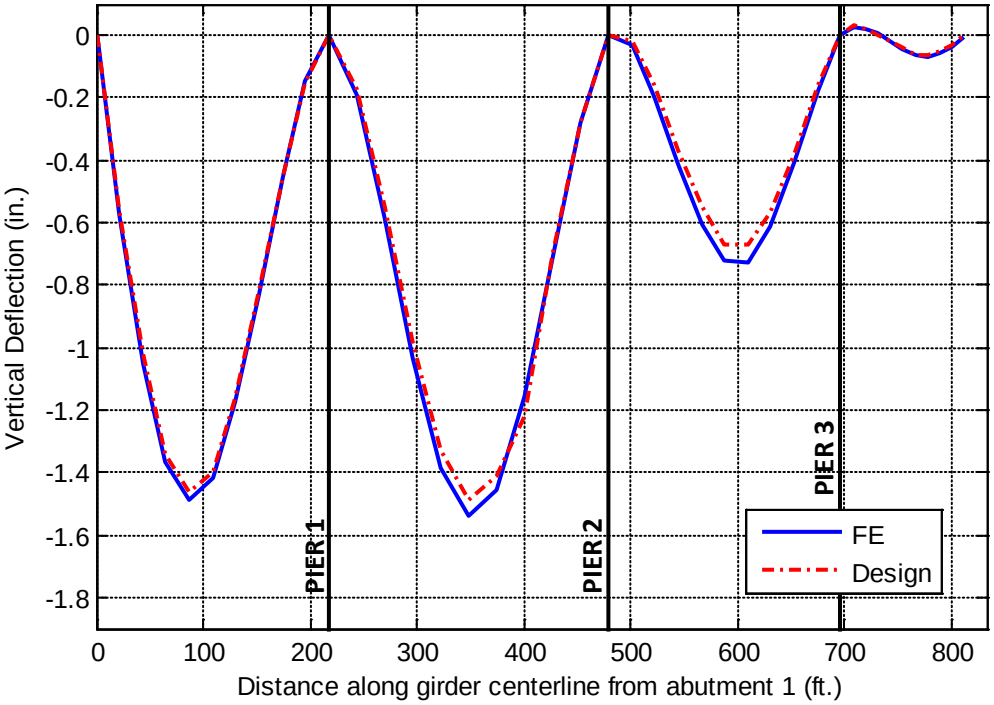


**Figure 5.3. FE and Design Calculated Self-Weight Deflections (Steel Superstructure Only) – Girder 3**

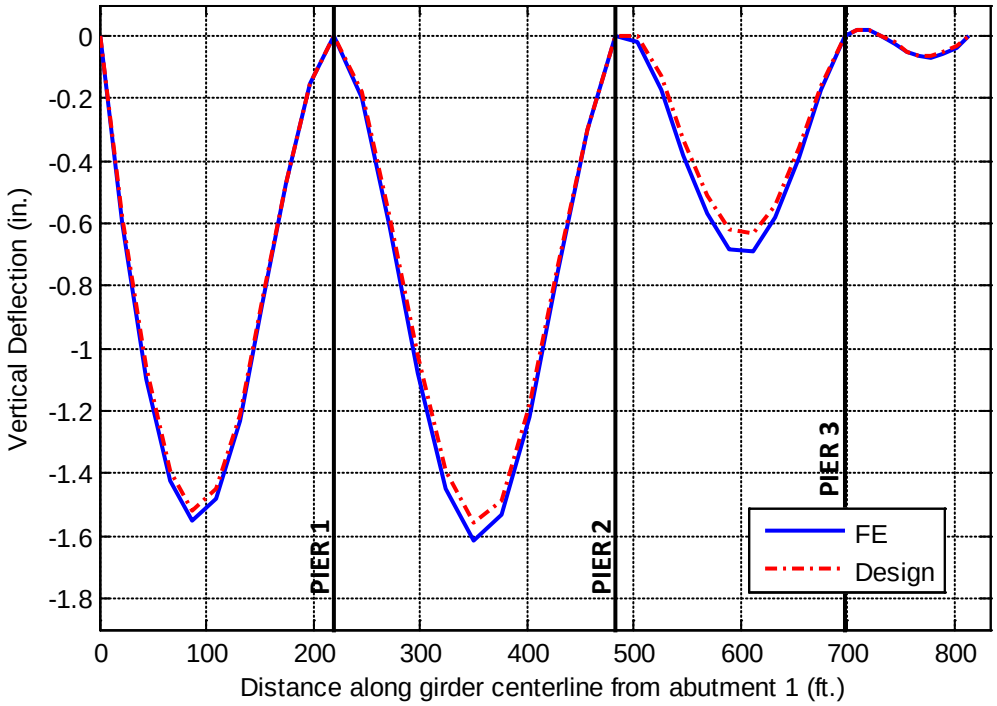


**Figure 5.4. FE and Design Calculated Self-Weight Deflections (Steel Superstructure Only) – Girder 4**

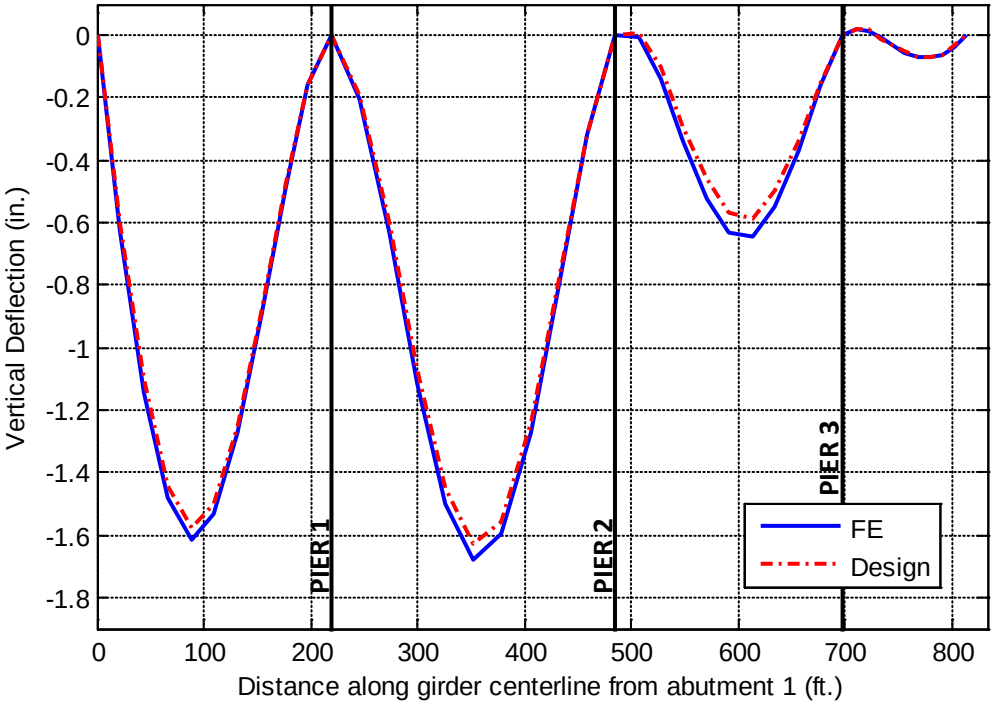


**Figure 5.5. FE and Design Calculated Self-Weight Deflections (Steel Superstructure Only) – Girder 5**

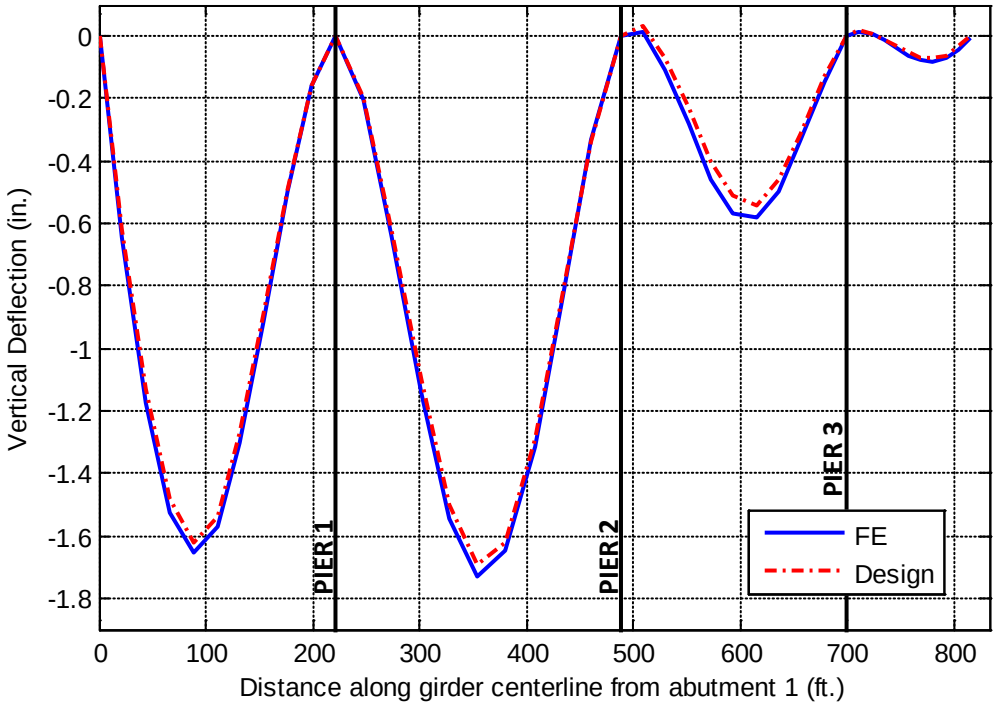


**Figure 5.6. FE and Design Calculated Self-Weight Deflections (Steel Superstructure Only) – Girder 6**

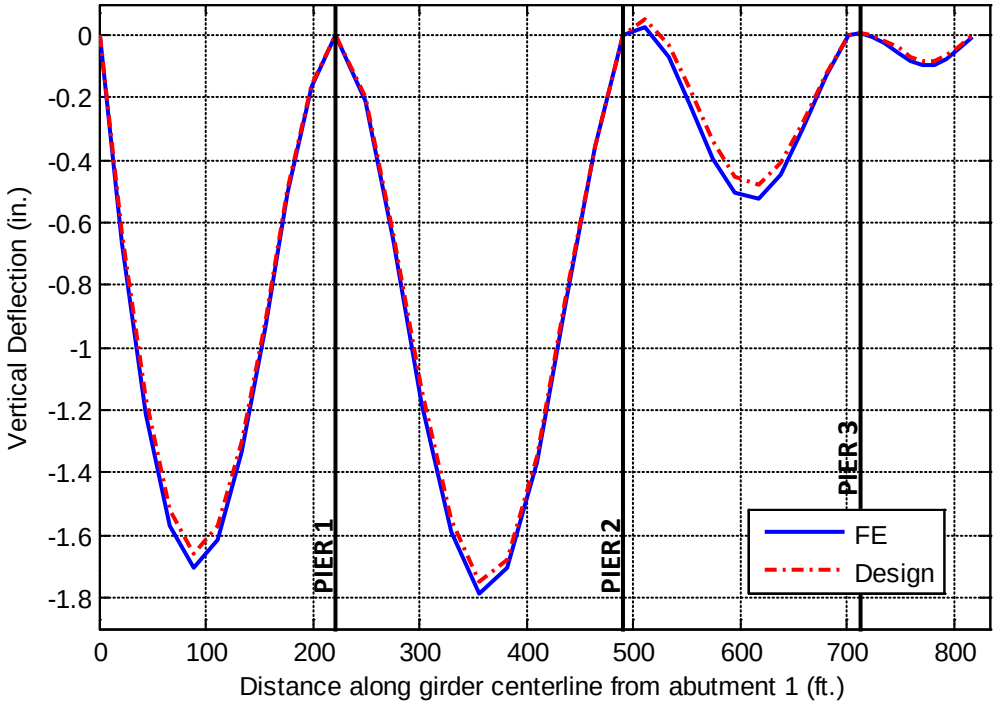


**Figure 5.7. FE and Design Self-Weight Deflections (Steel Superstructure Only) – Girder 7**

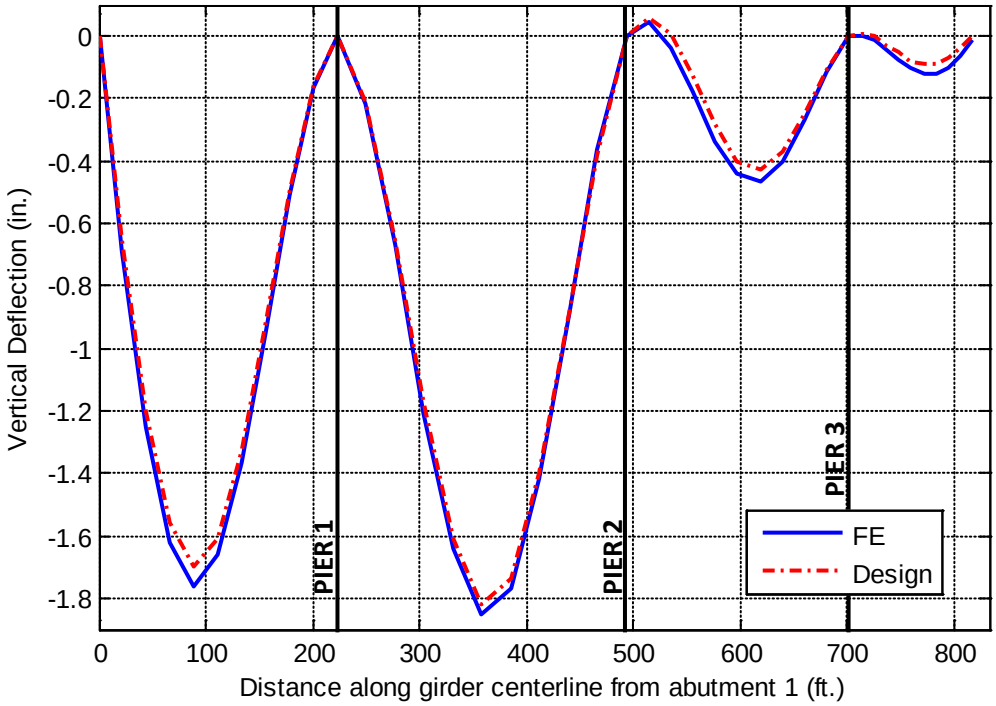


**Figure 5.8. FE and Design Calculated Self-Weight Deflections (Steel Superstructure Only) – Girder 8**

As Figures 5.1 to 5.8 show, the deflected shapes under steel superstructure gravity loading predicted by the FE analysis look to be a fairly good match to the deflection patterns given in the girder camber tables. However, the difference between these two sets of values must be quantified in order to verify the accuracy of the FE model. In this case, the greatest differences in the sets of values will occur roughly at the middle of each span where the vertical span deflections are the largest. Therefore, a comparison of these maximum vertical span deflection values is performed to investigate the degree of accuracy of this FE model. In Table 5.1, the column labels of 'MS1', 'MS2',' MS3', and 'MS4' correspond to values obtained and calculated at the middle of the first span, second span, third span, and fourth span, respectively. The rows labeled 'FE' contain vertical deflections calculated from the finite element analysis and the rows labeled 'DESIGN' contain design calculated vertical deflections given in the camber tables. The row labeled 'A. ERR' represents the values for the absolute error between the finite element deflection values and the camber deflection values, with the camber values serving as the exact

values and the finite element values serving as the approximate values. The percent error between the two sets of values, given in the row labeled '% ERR', is by definition the absolute error divided by the exact (camber) value multiplied by 100.

The percent error value is often used to determine how close an experimental value is to the exact value it is attempting to approximate. Examination of Table 5.1 indicates that all of the percent error values at the center of spans 1 and 2 are at or below 4.5% indicating an acceptable correlation between the two sets of values at these locations. On the other hand, the percent error values increase at the center of spans 3 and 4. Eleven of the 16 percent error values are below 10%. These slightly larger error values can be attributed to the fact that when dealing with small numbers and computing percent error, the error values can tend to get very large if the devisor, which in this case is the camber deflection value, is very small. As Table 5.1 shows, the camber deflection values in the center of spans 3 and 4 are all less than 1 inch and are much smaller compared to the camber deflection values at mid-spans 1 and 2. As a result, even a small difference in the FE and camber deflections will most likely result in a large percent error. However, even though the percent error between the FE and exact (camber) values is very high in some instances at mid-spans 3 and 4, the largest absolute error between the sets of values at these locations is only 0.06926 inches (approximately 1/15 of an inch), indicating a reasonable degree of accuracy for the FE calculated vertical defections in the center of spans 3 and 4.

**Table 5.1. Comparison of FE and Design Calculated Vertical Girder Deflections Due to Steel Superstructure and Gravity Loading**

| | | MS1 | MS2 | MS3 | MS4 |
|---|---|---|---|---|---|
| GIRDER 1 | DESIGN | -1.37 | -1.35 | -0.74 | -0.05 |
| | FE | -1.3704 | -1.3958 | -0.77962 | -0.055451 |
| | A. ERR | -0.0004 | -0.0458 | -0.03962 | -0.005451 |
| | % ERR | 0.03% | 3.39% | 5.35% | 10.90% |
| GIRDER 2 | DESIGN | -1.42 | -1.42 | -0.71 | -0.05 |
| | FE | -1.4386 | -1.4734 | -0.76282 | -0.061992 |
| | A. ERR | -0.0186 | -0.0534 | -0.05282 | -0.011992 |
| | % ERR | 1.31% | 3.76% | 7.44% | 23.98% |
| GIRDER 3 | DESIGN | -1.46 | -1.49 | -0.67 | -0.06 |
| | FE | -1.4982 | -1.5416 | -0.73694 | -0.066412 |
| | A. ERR | -0.0382 | -0.0516 | -0.06694 | -0.006412 |
| | % ERR | 2.62% | 3.46% | 9.99% | 10.69% |
| GIRDER 4 | DESIGN | -1.52 | -1.56 | -0.63 | -0.06 |
| | FE | -1.5668 | -1.6125 | -0.69899 | -0.068936 |
| | A. ERR | -0.0468 | -0.0525 | -0.06899 | -0.008936 |
| | % ERR | 3.08% | 3.37% | 10.95% | 14.89% |
| GIRDER 5 | DESIGN | -1.58 | -1.63 | -0.59 | -0.07 |
| | FE | -1.628 | -1.6748 | -0.65002 | -0.073047 |
| | A. ERR | -0.048 | -0.0448 | -0.06002 | -0.003047 |
| | % ERR | 3.04% | 2.75% | 10.17% | 4.35% |
| GIRDER 6 | DESIGN | -1.62 | -1.69 | -0.54 | -0.07 |
| | FE | -1.6734 | -1.7275 | -0.58721 | -0.079958 |
| | A. ERR | -0.0534 | -0.0375 | -0.04721 | -0.009958 |
| | % ERR | 3.30% | 2.22% | 8.74% | 14.23% |
| GIRDER 7 | DESIGN | -1.66 | -1.75 | -0.48 | -0.08 |
| | FE | -1.7235 | -1.7838 | -0.52409 | -0.095239 |
| | A. ERR | -0.0635 | -0.0338 | -0.04409 | -0.015239 |
| | % ERR | 3.83% | 1.93% | 9.19% | 19.05% |
| GIRDER 8 | DESIGN | -1.7 | -1.82 | -0.43 | -0.09 |
| | FE | -1.7799 | -1.846 | -0.46682 | -0.12545 |
| | A. ERR | -0.0799 | -0.026 | -0.03682 | -0.03545 |
| | % ERR | 4.70% | 1.43% | 8.56% | 39.39% |

## 5.3 Steel Superstructure and Reinforced Deck Gravity Load

The final step in FE model validation consists of adding the weight of the reinforced concrete bridge deck to the structure that is already deformed by the steel superstructure weight. Adding the weight of the reinforced concrete deck proved to be much more difficult than simply adding the deck to the model and using the mass proportional load feature in ADINA to simulate the deck weight due to gravity. Upon completion of the bridge construction, shear studs on the top flange of the girders are embedded within the reinforced concrete deck. Ideally, these embedded shear studs create full composite action between the top flange of the girders and the bottom surface of the deck, meaning two adjacent girder and deck locations will have identical deformations under all loading conditions (the strain profile of the deck and girders will be continuous through the thickness). Basically, the deck and girders will behave as if they are fully attached along the top flange surfaces of all the girders.

However, as the concrete deck is poured, the steel girders will incur deflections due to the weight of the concrete before the concrete cures and reaches full stiffness. As a result, the weight of the concrete deck will impose deflections upon the steel superstructure without providing any resistance to these deflections. Considering this, it was determined that the most accurate method to simulate the weight of the bridge deck on the girders was by representing the deck weight with a series of distributed loads on the top flanges of the girders.

To determine the magnitude of the distributed load placed on each girder, it is assumed that each girder will carry the weight of concrete obtained within a volumetric section spanning from the midway points between adjacent girders and the subject girder. Figure 5.9 shows a simplified example of how much area (multiply by the deck thickness to obtain volume) of concrete is carried by a uniformly curved girder. This volume of concrete represents a weight once the density is known. As Figure 5.9 demonstrates, Girder B carries half of the concrete volume between Girder B and Girder A along with half of the volume between Girder B and

Girder C. If the distance between the girders remains uniform along the length of the girders, the value of the distributed load on the top flange of Girder B has the value of:

$$\frac{(\rho_{conc})(t_{conc})(\frac{1}{2}d_1 + \frac{1}{2}d_2)}{w_{tf}} \qquad (5.1)$$

where $\rho_{conc}$ is reinforced concrete density, $t_{conc}$ is concrete thickness, and $w_{tf}$ is the width of the girder top flange. In this case shown in Figure 5.9, since the lateral distance between the girders is uniform, the amount of distributed load each girder carries corresponding to the weight of the deck carried by each girder is uniform along the entire length of the girder.

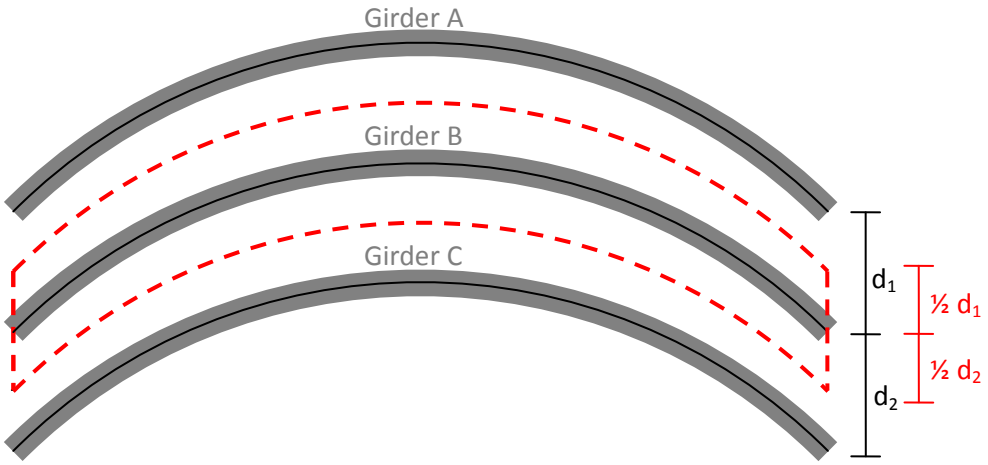


**Figure 5.9. Schematic of Area of Concrete Deck Carried by Specific Girder**

According to the design sheets, the thickness of the reinforced concrete deck is 8.5 inches. Yet, this thickness does not include the volume within the haunches of the stay-in-place (SIP) forms between the bridge girders. Figure 5.10 shows a typical cross section of the bridge deck SIP forms. SIP forms of this profile and length are placed in sequence along the length of the bridge. Because the haunches in the SIP forms increase the volume of concrete in the bridge

deck, an equivalent deck thickness is computed to account for this additional concrete. This is done by computing the combined area of the haunches (labeled #1 and #2 in Figure 5.10) which turns out to be 13.2 $in^2$. Over the 9 in. length, each SIP form adds an additional 13.2 $in^2$ of cross-sectional concrete area. Dividing the additional concrete cross sectional area by the length of the SIP forms results in an additional equivalent deck thickness of 1.08 in. Finally, a deck thickness of 9.58 in. is used in Equation 5.1 to calculate the distributed loads representing the weight of the bridge deck

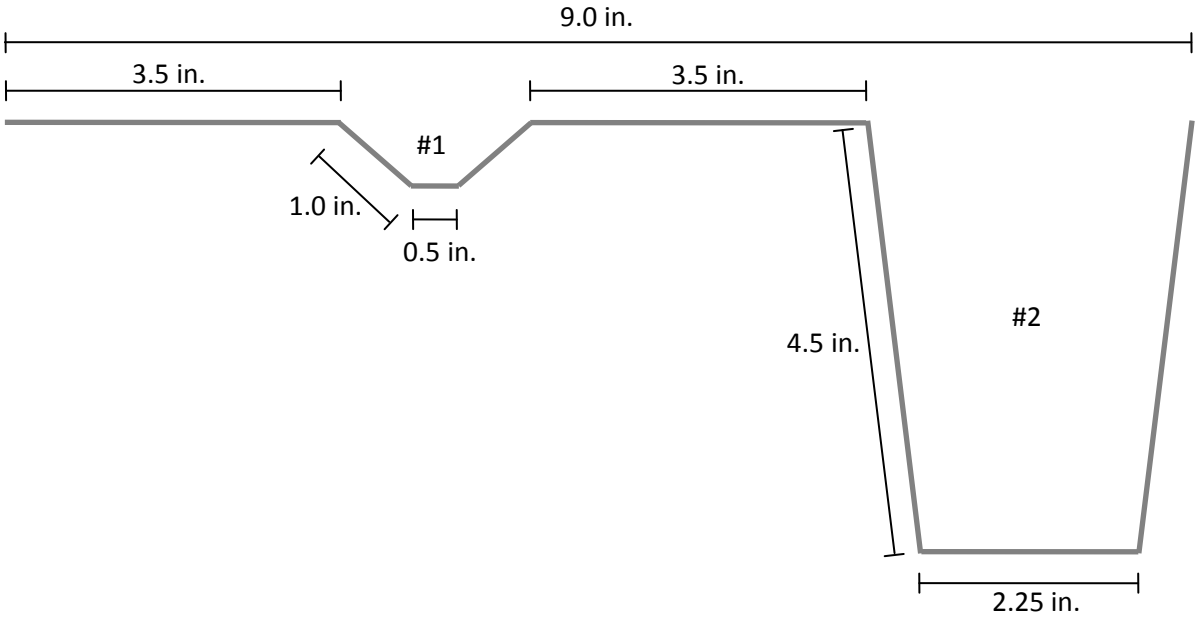


**Figure 5.10. Typical SIP Form Profile**

However, the distributed loads representing the bridge deck are not uniform because the girder spacing for the Buffalo Creek Bridge does not remain uniform along the length of the structure, which is shown in Figure 4.1. The same concept represented by Equation 5.1 applies when formulating the distributed loads representing the deck weight, except that for some sections the deck width carried by the girder becomes linearly variable along the girder length. In these cases, the distributed load will also vary linearly along the length of the girder as a function of the deck width carried by the girder. Deck widths at critical locations were determined by examining the design sheets and appropriate linearly varying distributed loads were formulated

based on girder spacing along the length of the bridge. An example of one linearly varying distributed load on the top flange of Girder 6 is shown in Figure 5.11.

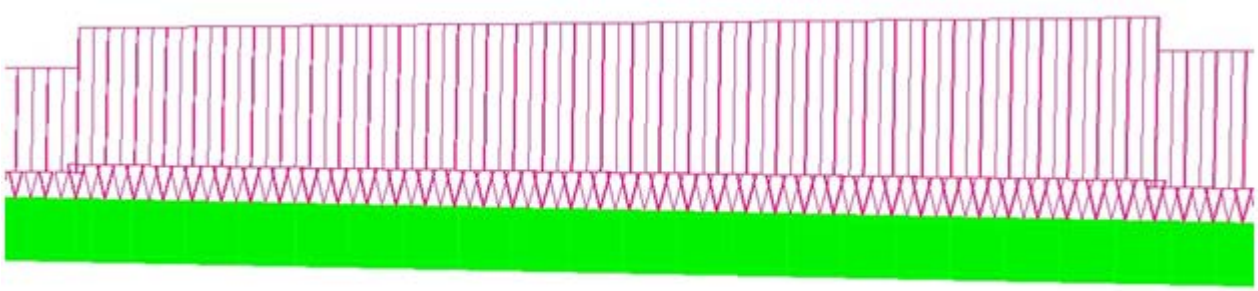

**Figure 5.11. Example of Linearly Varying Distributed Load Representing Deck Weight – Girder 6**

Deck weight loading is applied to the model subsequent to girder self-weight loading. The vertical girder deflections were measured and compared to the design calculated girder deflections given in the design sheets in the same manner as they were in Section 5.2. Comparisons of finite element and design calculated vertical girder deflections due to the gravity loading of the bridge deck and the steel superstructure are given in Figures 5.12 – 5.19. Visual inspection of these plots shows a good agreement between FE and theoretical values with Table 5.2 quantifying the displacements at the maximum displacement locations (mid-spans) and showing comparisons in the form of absolute and percent error.

Although the absolute errors between the FE and design measurements for deck and steel superstructure weight vertical deflections in Table 5.2 are higher than those in Table 5.1, the percent error values are within an acceptable range. Absolute error measurements are larger because the magnitude of the deflections under due to deck and steel weight are on the order of three times higher than those purely due to steel self-weight load. The FE predicted deflection values at mid-span 4 yield large percent error values when compared to camber values in the design sheets. This can mainly be attributed to the deflections at these locations being very small, but all of the absolute error values at mid-span 4 are less than 1/10 of an inch. As a result, even though the percent error values at mid-span 4 are large, the vertical girder deflection values due to deck and steel superstructure loading predicted by the FE analysis are considered to be acceptable.

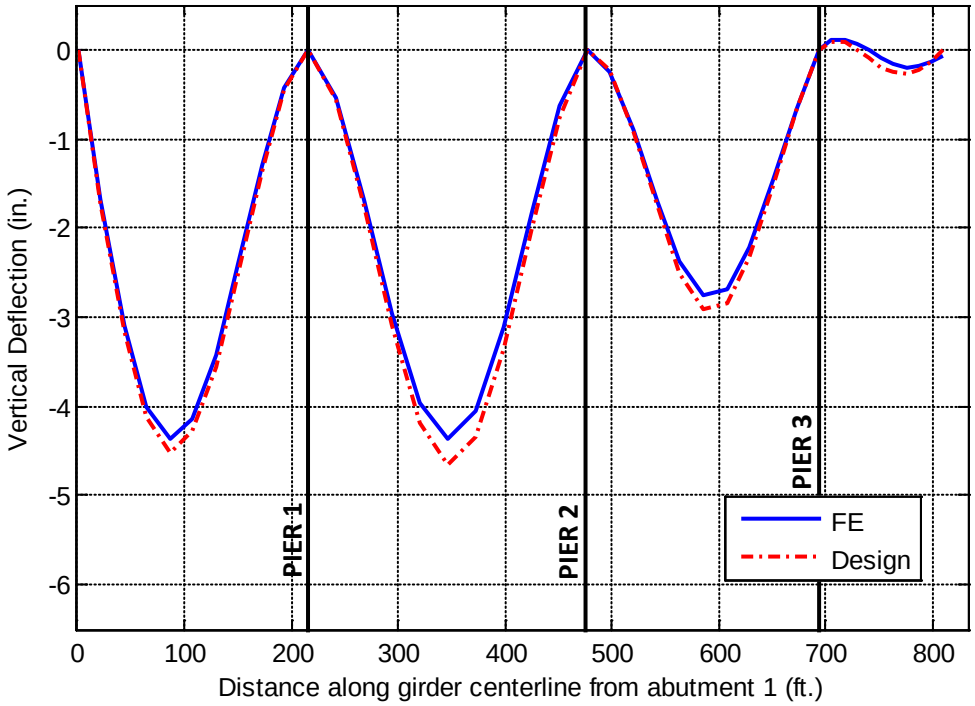


**Figure 5.12. FE and Design Calculated Self-Weight Deflections (Steel Superstructure and Deck) – Girder 1**

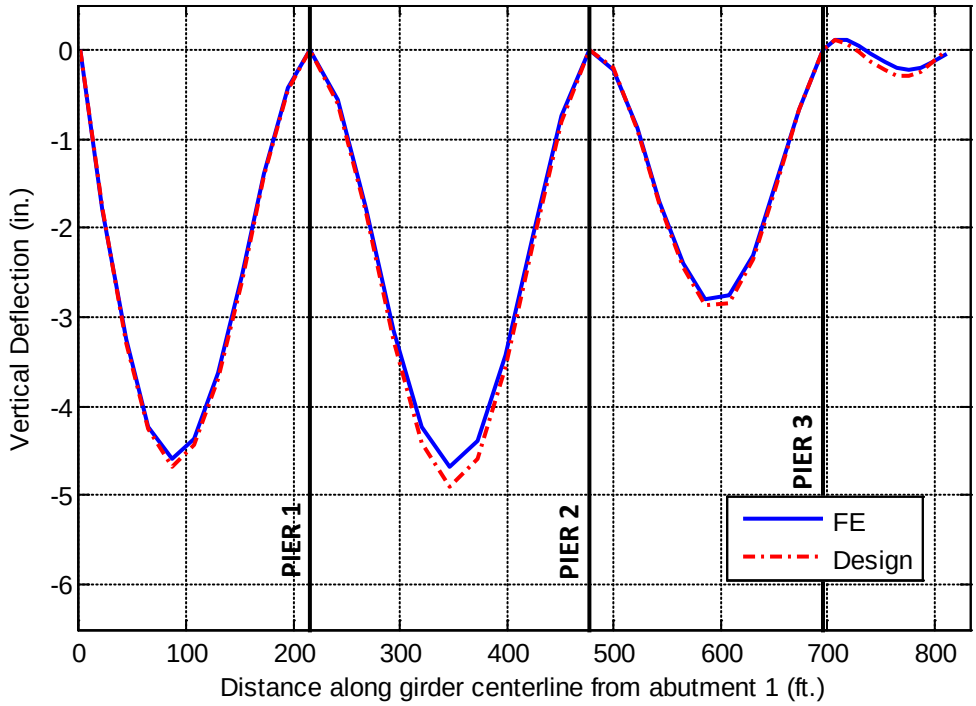


**Figure 5.13. FE and Design Calculated Self-Weight Deflections (Steel Superstructure and Deck) – Girder 2**

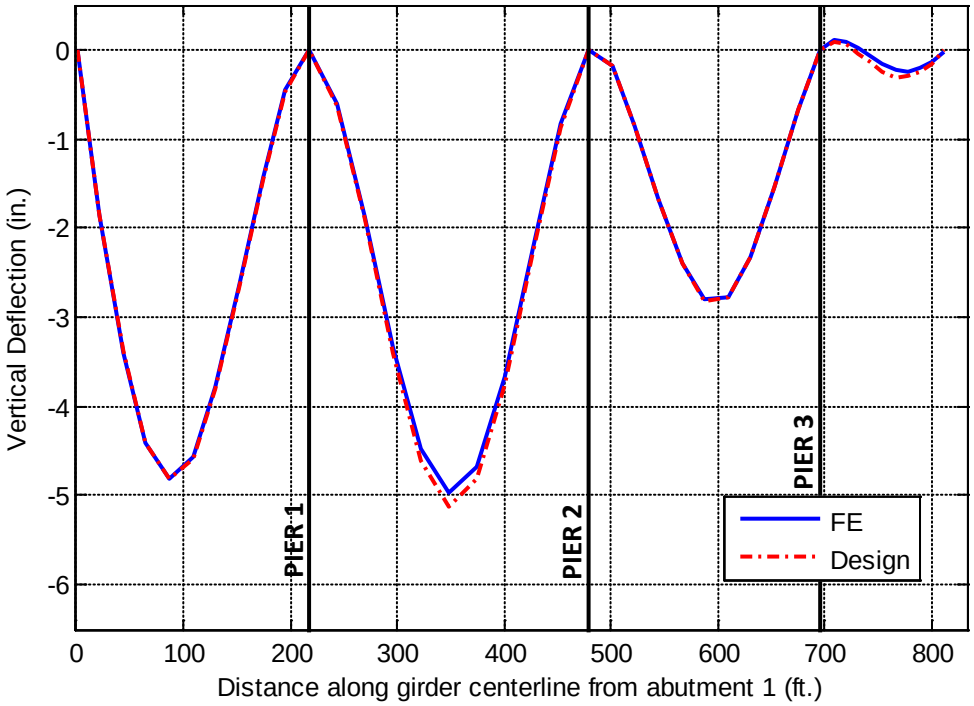


**Figure 5.14. FE and Design Calculated Self-Weight Deflections (Steel Superstructure and Deck) – Girder 3**

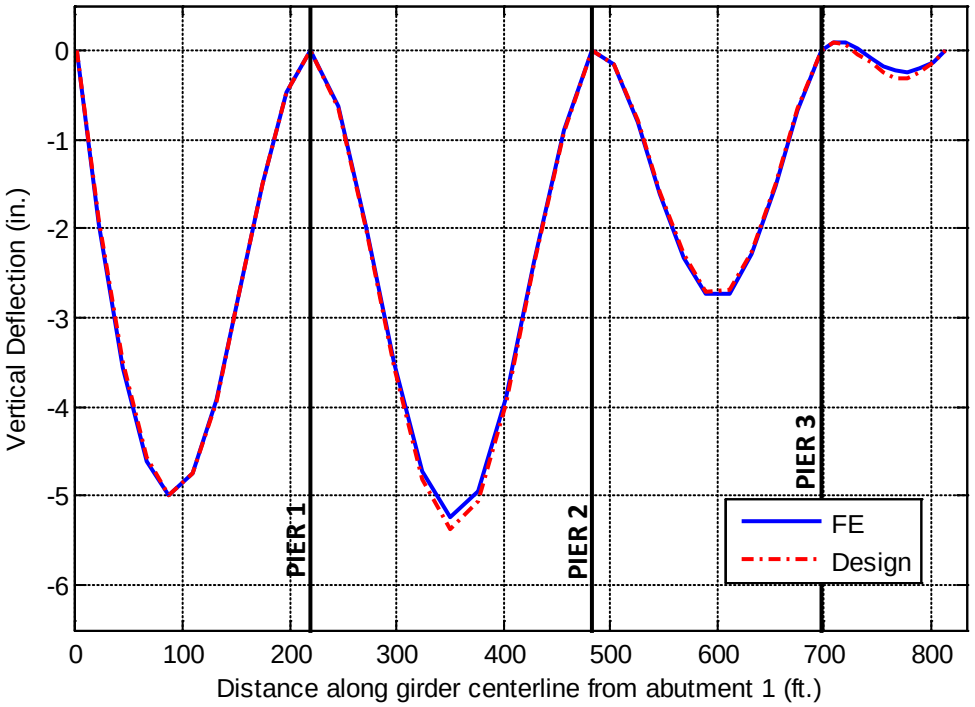


**Figure 5.15. FE and Design Calculated Self-Weight Deflections (Steel Superstructure and Deck) – Girder 4**

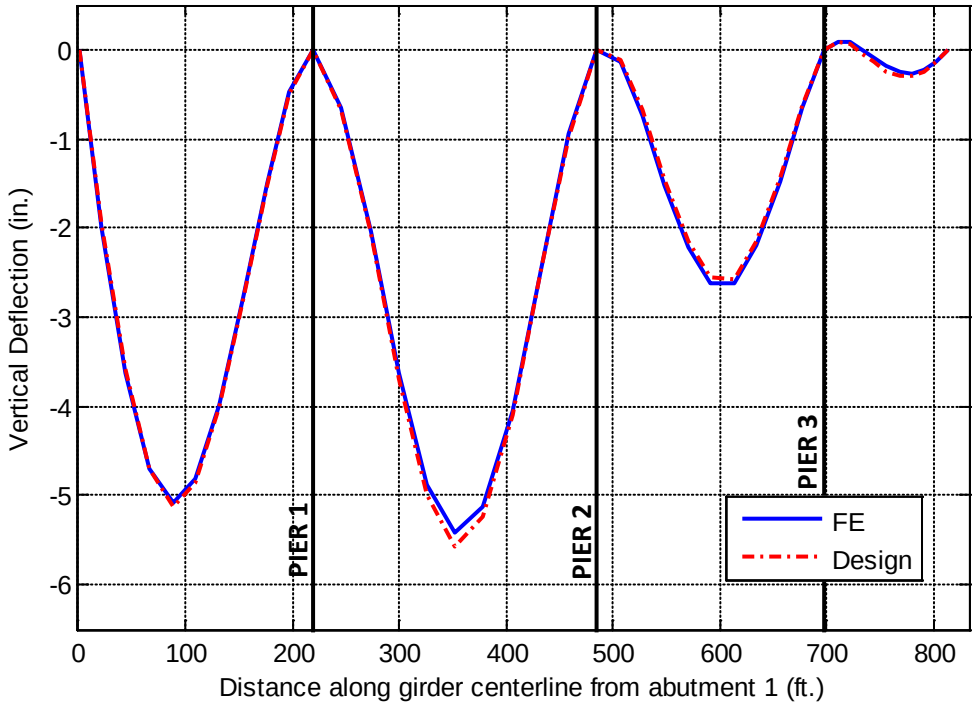


**Figure 5.16. FE and Design Calculated Self-Weight Deflections (Steel Superstructure and Deck) – Girder 5**

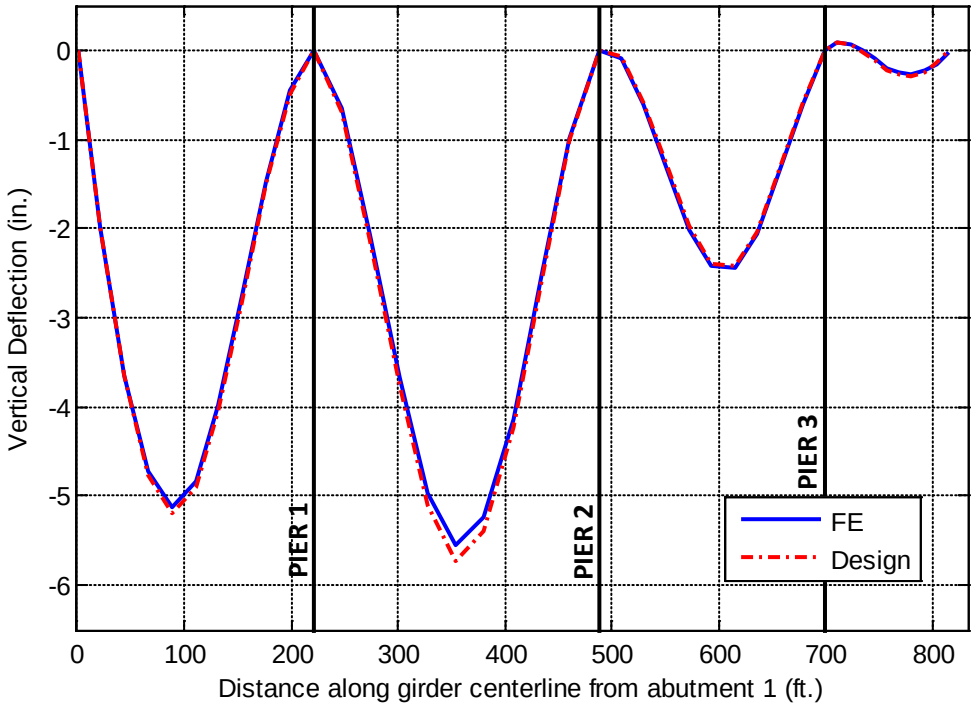


**Figure 5.17. FE and Design Calculated Self-Weight Deflections (Steel Superstructure and Deck) – Girder 6**

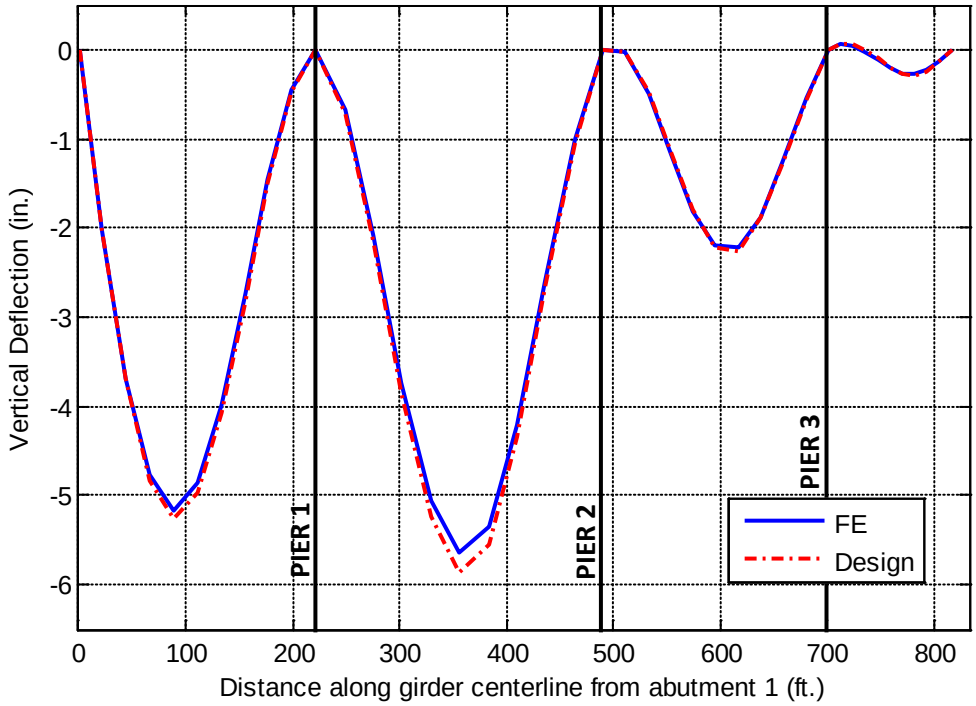


**Figure 5.18. FE and Design Calculated Self-Weight Deflections (Steel Superstructure and Deck) – Girder 7**

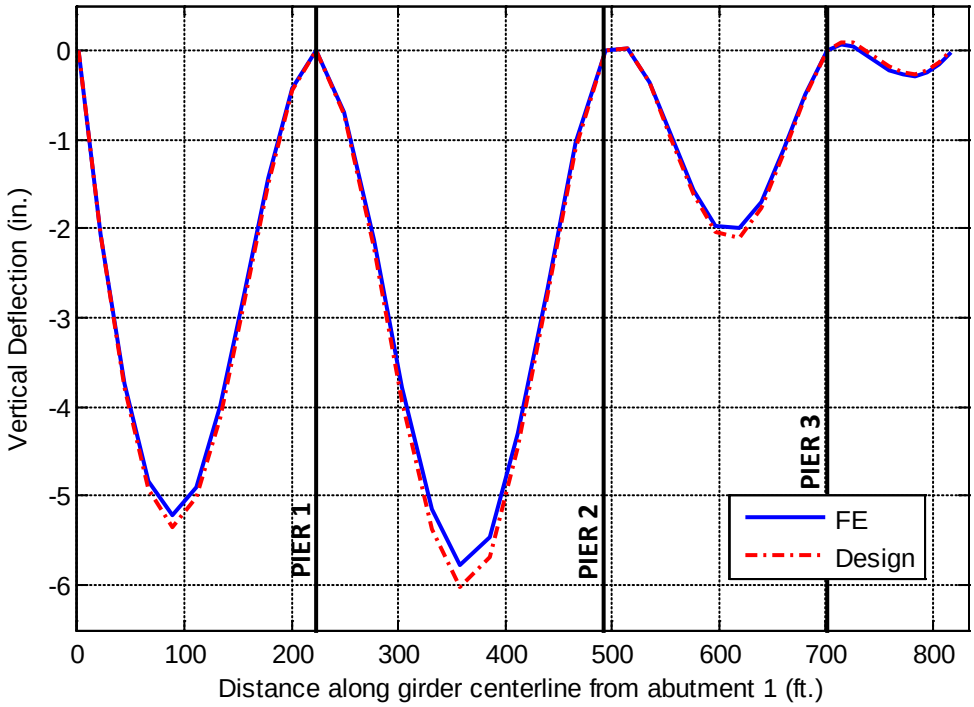


**Figure 5.19. FE and Design Calculated Self-Weight Deflections (Steel Superstructure and Deck) – Girder 8**

**Table 5.2. Comparison of FE and Design Calculated Vertical Girder Deflections Due to Steel Superstructure and Concrete Deck Gravity Loading**

| | | MS1 | MS2 | MS3 | MS4 |
|---|---|---|---|---|---|
| GIRDER 1 | DESIGN | -4.51 | -4.65 | -2.9 | -0.27 |
| | FE | -4.3759 | -4.3574 | -2.7805 | -0.19774 |
| | A. ERR | -0.1341 | -0.2926 | -0.1195 | -0.07226 |
| | % ERR | 2.97% | 6.29% | 4.12% | 26.76% |
| GIRDER 2 | DESIGN | -4.67 | -4.89 | -2.87 | -0.29 |
| | FE | -4.6126 | -4.684 | -2.8338 | -0.2322 |
| | A. ERR | -0.0574 | -0.206 | -0.0362 | -0.0578 |
| | % ERR | 1.23% | 4.21% | 1.26% | 19.93% |
| GIRDER 3 | DESIGN | -4.82 | -5.13 | -2.82 | -0.3 |
| | FE | -4.8191 | -4.9722 | -2.8399 | -0.24602 |
| | A. ERR | -0.0009 | -0.1578 | 0.0199 | -0.05398 |
| | % ERR | 0.02% | 3.08% | -0.71% | 17.99% |
| GIRDER 4 | DESIGN | -4.99 | -5.37 | -2.71 | -0.31 |
| | FE | -5.0144 | -5.2464 | -2.7843 | -0.24941 |
| | A. ERR | 0.0244 | -0.1236 | 0.0743 | -0.06059 |
| | % ERR | -0.49% | 2.30% | -2.74% | 19.55% |
| GIRDER 5 | DESIGN | -5.21 | -5.57 | -2.58 | -0.3 |
| | FE | -5.1069 | -5.4318 | -2.6672 | -0.26163 |
| | A. ERR | -0.1031 | -0.1382 | 0.0872 | -0.03837 |
| | % ERR | 1.98% | 2.48% | -3.38% | 12.79% |
| GIRDER 6 | DESIGN | -5.19 | -5.73 | -2.42 | -0.3 |
| | FE | -5.1379 | -5.5479 | -2.4747 | -0.27116 |
| | A. ERR | -0.0521 | -0.1821 | 0.0547 | -0.02884 |
| | % ERR | 1.00% | 3.18% | -2.26% | 9.61% |
| GIRDER 7 | DESIGN | -5.26 | -5.86 | -2.26 | -0.29 |
| | FE | -5.1777 | -5.6593 | -2.2497 | -0.28029 |
| | A. ERR | -0.0823 | -0.2007 | -0.0103 | -0.00971 |
| | % ERR | 1.56% | 3.42% | 0.46% | 3.35% |
| GIRDER 8 | DESIGN | -5.35 | -6.02 | -2.1 | -0.27 |
| | FE | -5.2383 | -5.7834 | -2.0234 | -0.29247 |
| | A. ERR | -0.1117 | -0.2366 | -0.0766 | 0.02247 |
| | % ERR | 2.09% | 3.93% | 3.65% | -8.32% |

## 5.4 Pier Bearing Performance Evaluation

As detailed in Chapter 4 each bearing providing a connection between the pier and the girder bottom flange is idealized using a set of linear springs. Unfortunately, there is no experimental or theoretical data available to validate quantitatively the accuracy of this method of bearing modeling. This section details and discusses two sample FE analysis of the Buffalo Creek Bridge performed in an effort to visually verify the use of spring sets to model the pier bearings.

The function of the pier bearings is to provide a connection between the piers and the bridge girders while allowing the girder flanges (at the bearings) to move only in a certain direction relative to the pier, based on the type of bearing (fixed, longitudinal, transverse, non-guided). It can be assumed that if, under loading, the springs sets idealizing the bearings allow girder displacement relative to pier displacement in the direction corresponding to the appropriate bearing at that pier-girder connection point, the use of the springs is accurately replicating the bearing behavior.

To perform this investigation, the bridge model with fixed piers described in Chapter Four is used. With the movement of the piers fixed on their top surfaces, it is relatively simple to investigate direction of the girder bottom flange displacement relative to the pier at the corresponding location. Because thermal loading will cause expansion and contraction of the bridge in both the radial and tangential directions, one model is solved with a uniform +45°F load applied to the entire model and a second model incorporates a -45°F uniform thermal load.

In order to investigate the use of springs to model the behavior of pier bearings, the displacements of the girder bottom flanges at the bearing locations are studied under the uniform thermal loads. Three points are chosen at each location, an extreme inside node, a center node, and an extreme outside node, as shown in Figure 5.20. Throughout the remainder of this section, these nodes collectively at each bearing location will be referred to as bottom flange nodes.

Figures 5.21-5.26 provide a comparison of the undisplaced (original) coordinates of the bottom flange nodes, in the z-x plane, with the coordinates of the bottom flange nodes displaced under uniform thermal loading. The black dashed line in Figures 5.21-5.26 represents the undisplaced pier centerline in the radial direction (relative to bridge curvature). The black dots represent the original, undisplaced z-x coordinated of the bottom flange nodes and the red and green dots show the displaced location of the bottom flange nodes under -45°F and +45°F uniform thermal load, respectively.

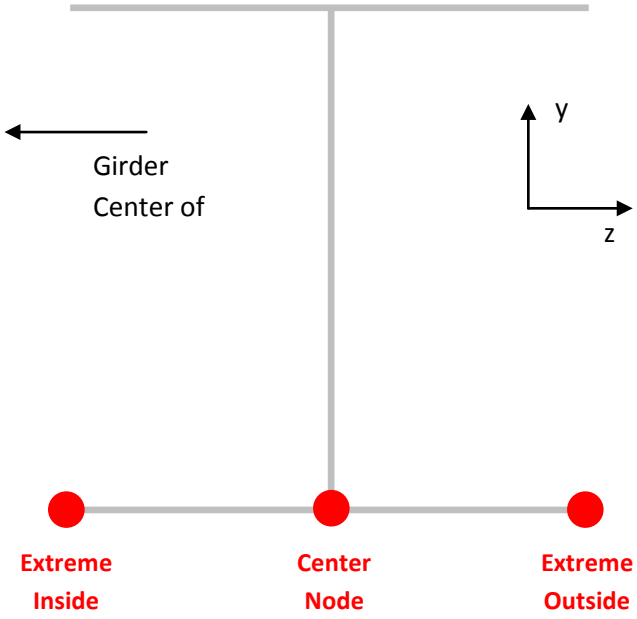


**Figure 5.20. Explanation of node locations used for bearing displacement analysis**

In Chapter 4, Figure 4.4 defines the types of bearings used at each location along each pier. The three types of bearings incorporated at the piers are fixed, transverse, and non-guided bearings. Fixed bearings tie the bottom surface of the girder with the top surface of the piers and do not allow the girders to have any movement relative to the top pier surface. At transverse bearing locations, the girder will be free to move in the transverse direction relative to the transverse pier centerline. Non-guided bearings do not restrict the movement of the girders in either the transverse or longitudinal directions and only provide support in the vertical direction, restricting vertical movement.

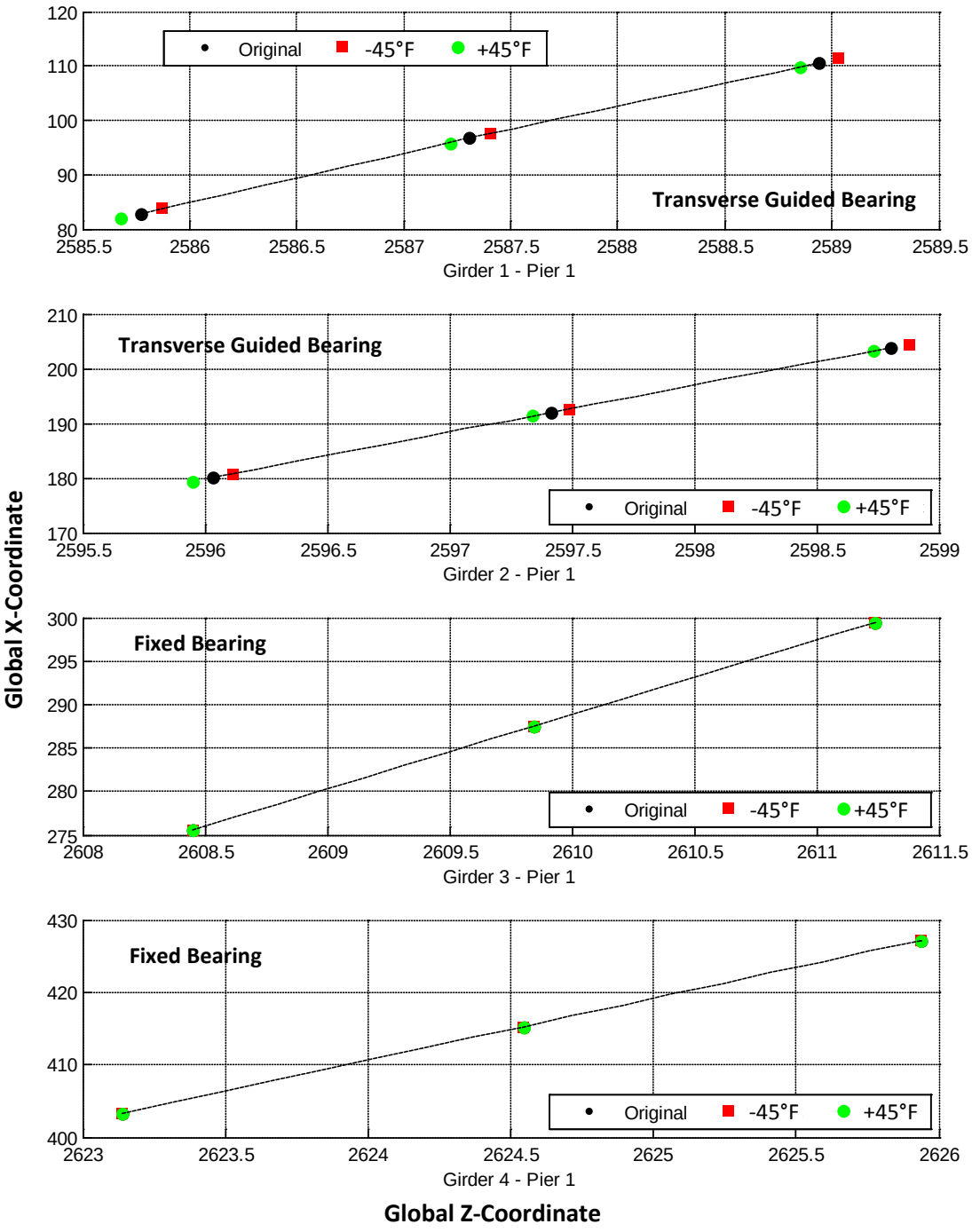


**Figure 5.21. Bottom Flange Displacements of Girders 1-4 at Pier 1 Under +/-45°F Thermal Loading with Pier Movement Fixed**

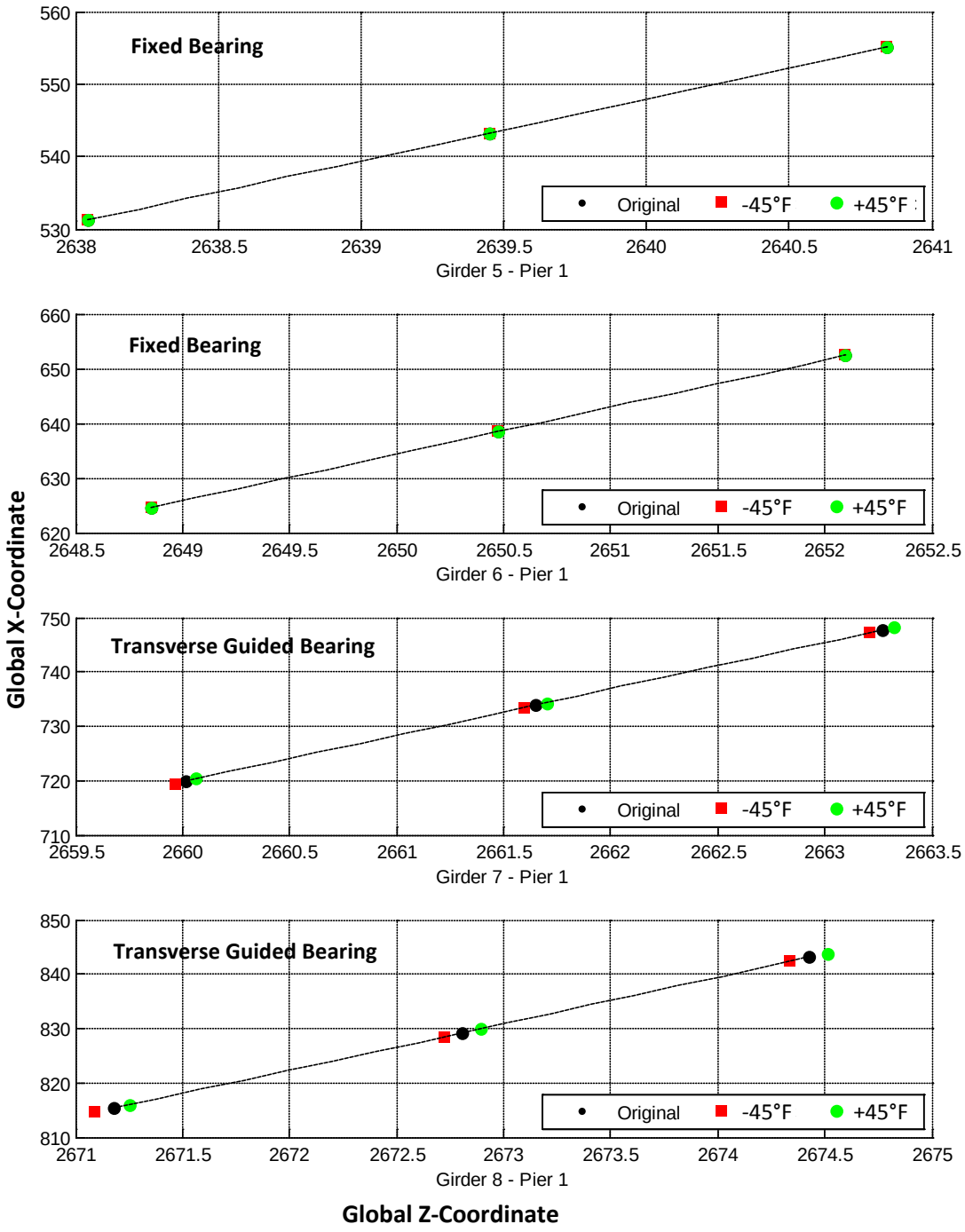


**Figure 5.22. Bottom Flange Displacements of Girders 5-8 at Pier 1 Under +/-45°F Thermal Loading With Pier Movement Fixed**

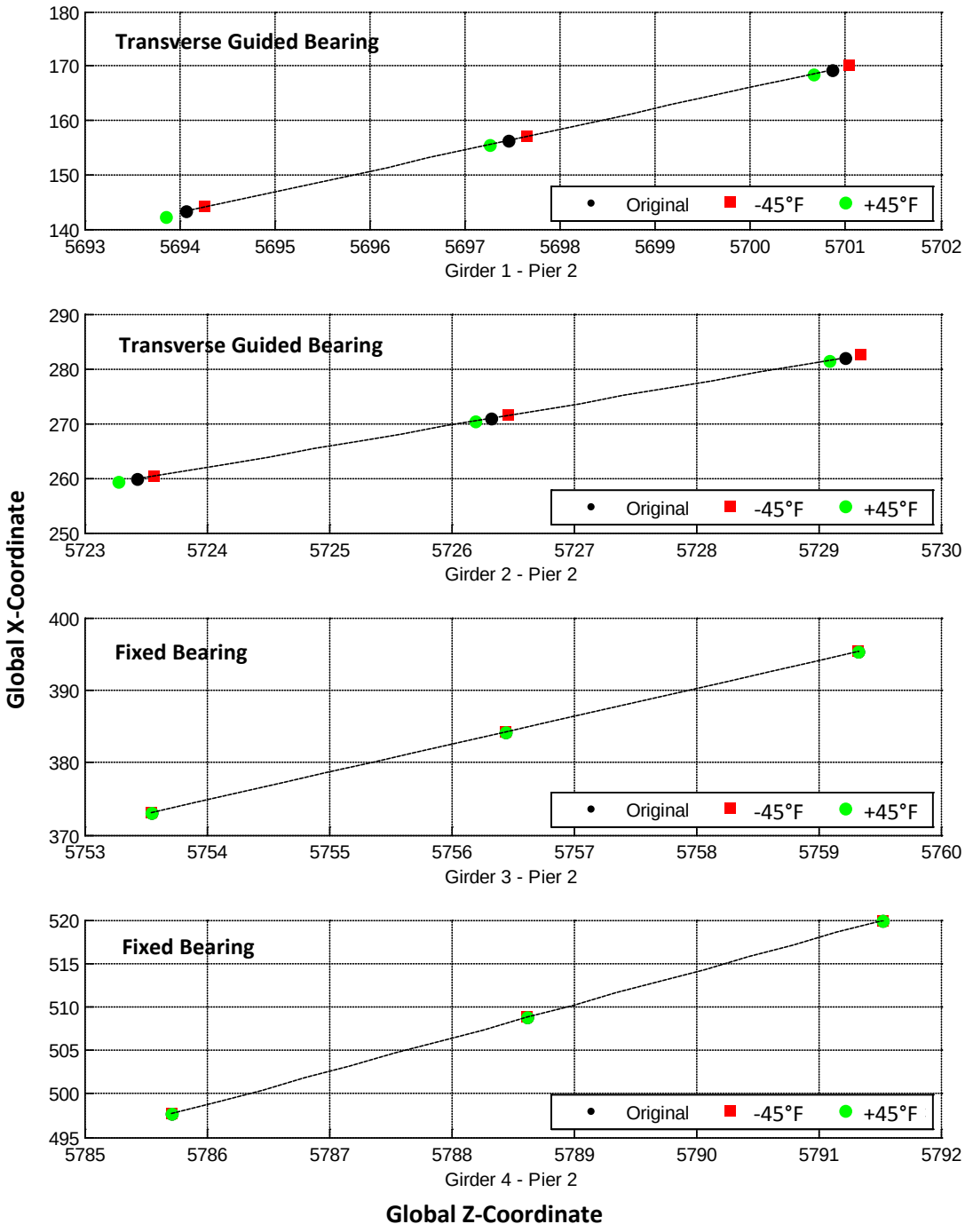


**Figure 5.23. Bottom Flange Displacements of Girders 1-4 at Pier 2 Under +/-45°F Thermal Loading With Pier Movement Fixed**

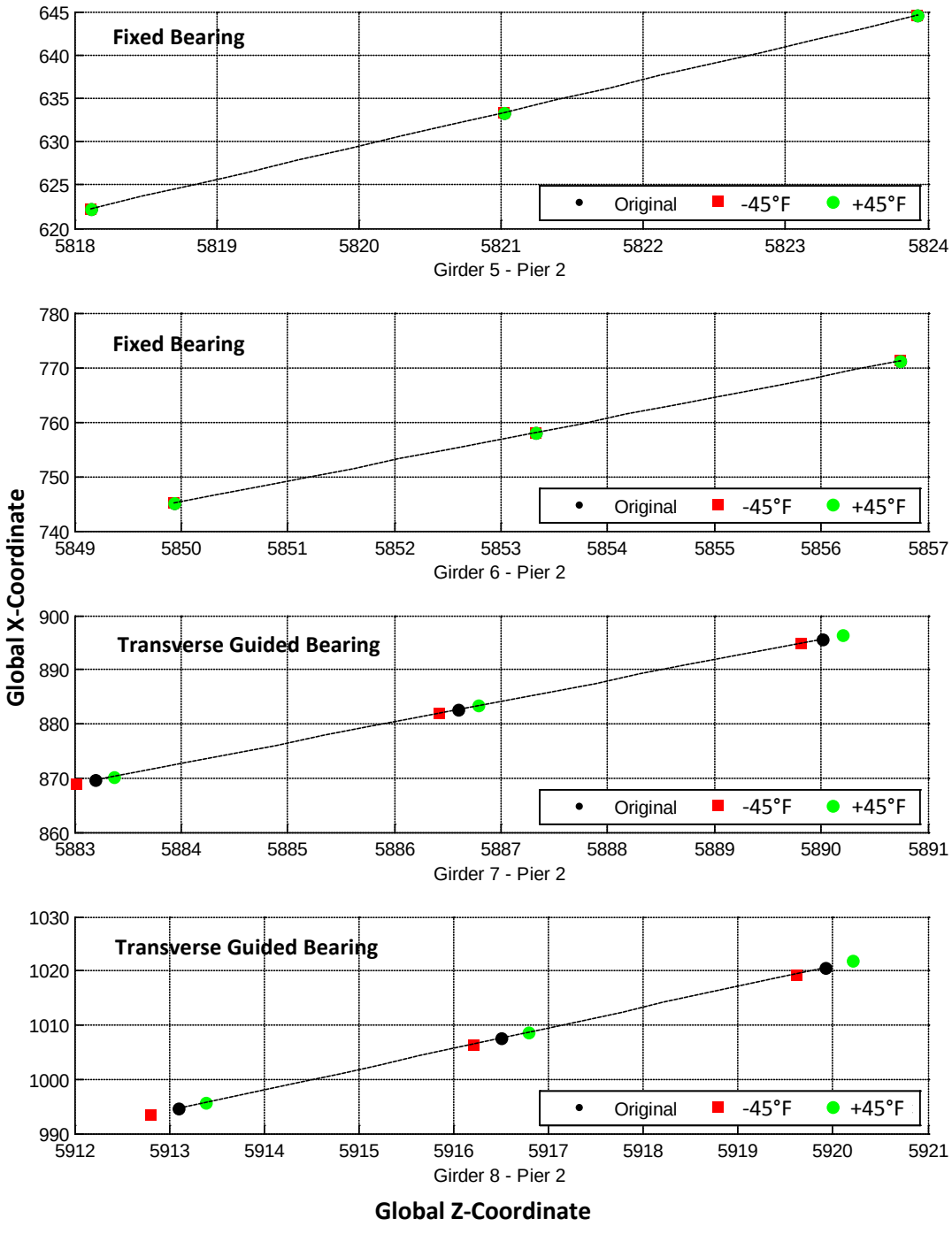


**Figure 5.24. Bottom Flange Displacements of Girders 5-8 at Pier 2 Under +/-45°F Thermal Loading With Pier Movement Fixed**

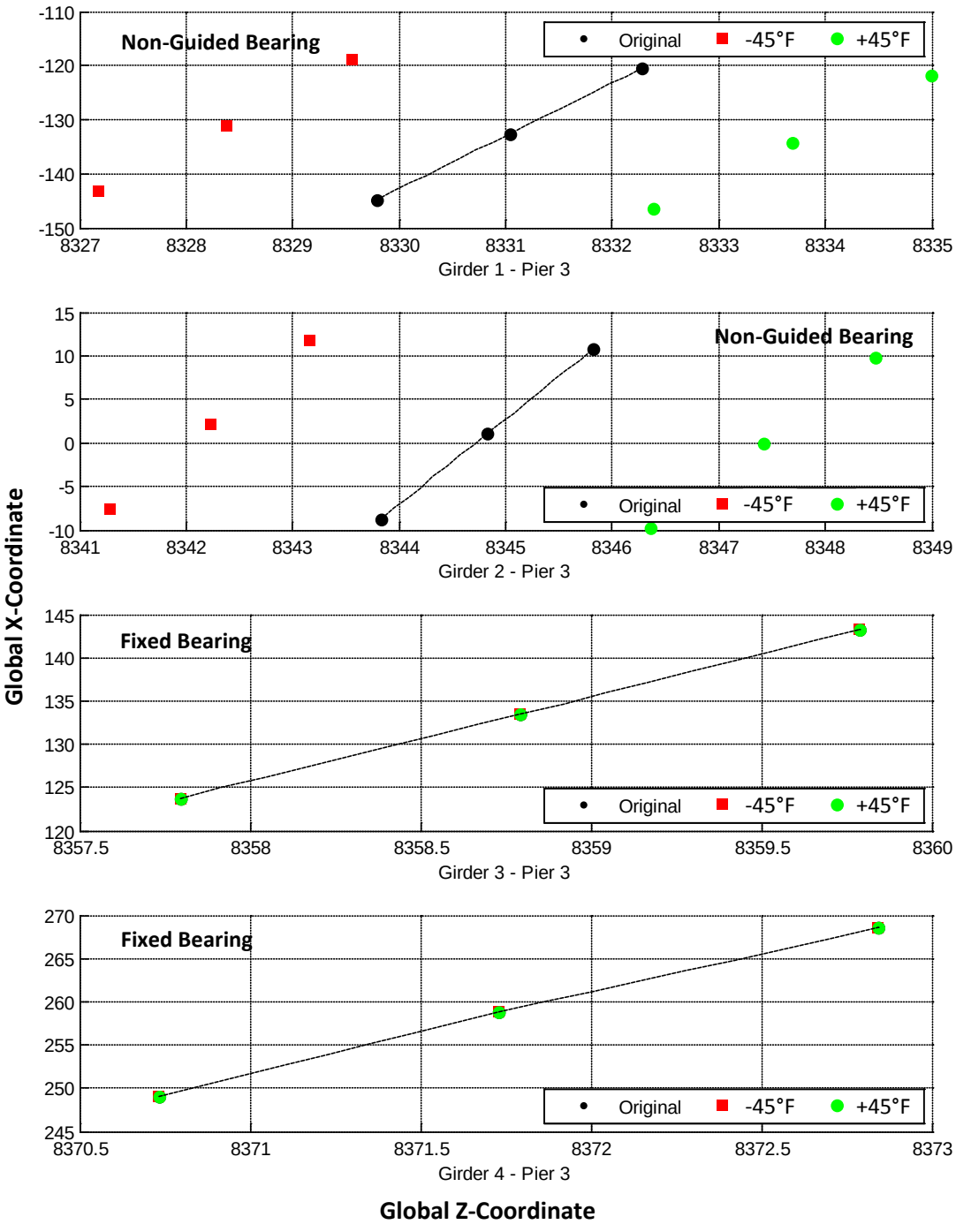


**Figure 5.25. Bottom Flange Displacements of Girders 1-4 at Pier 3 Under +/-45°F Thermal Loading With Pier Movement Fixed**

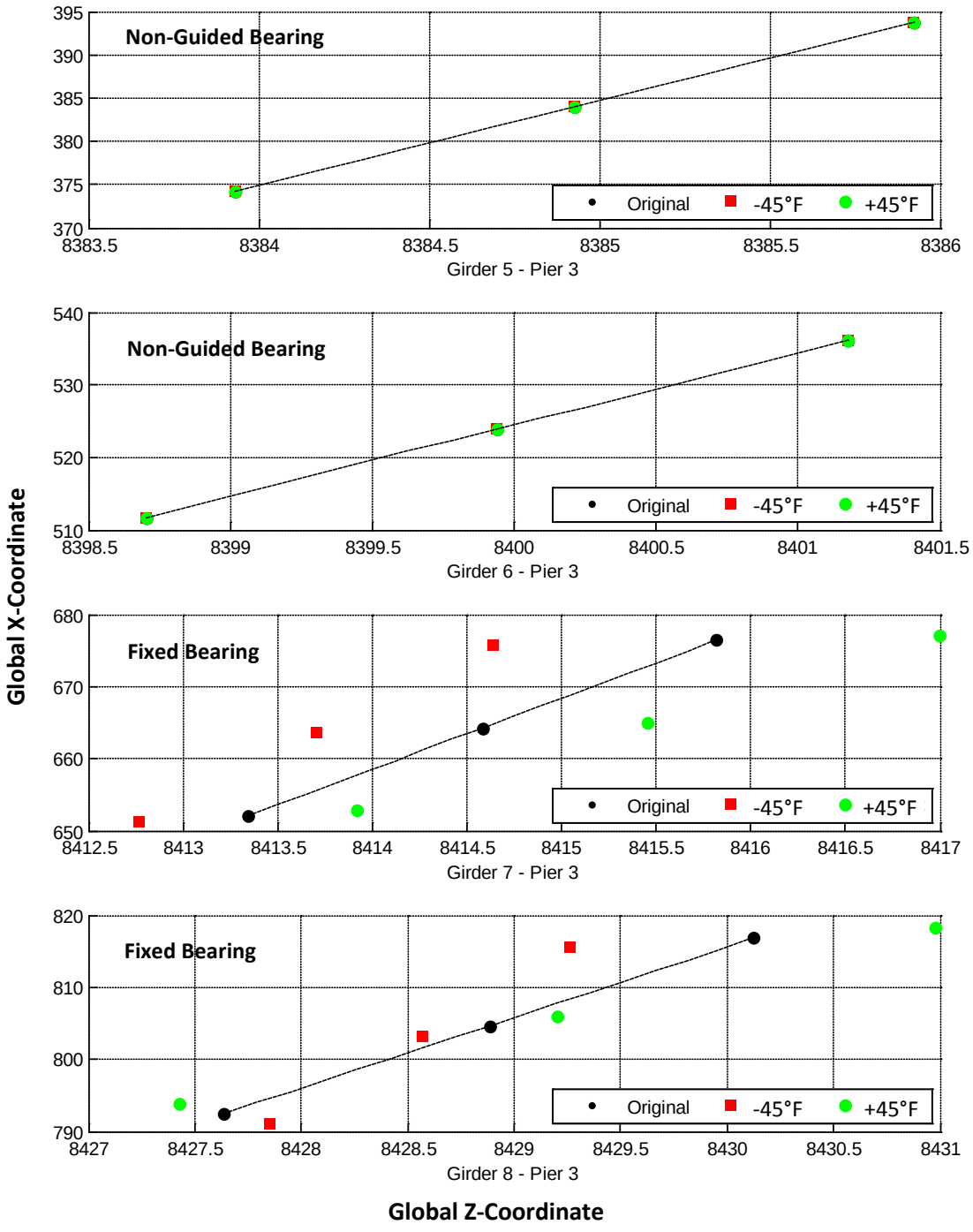


**Figure 5.26. Bottom Flange Displacements of Girders 5-8 at Pier 3 Under +/-45°F Thermal Loading With Pier Movement Fixed**

At the locations where transverse bearings are present (pier 1- girders 1, 2, 7, 8 and pier 2 – girders 1, 2, 7, 8) the girder nodes should only move in the transverse direction along the pier transverse centerline. There should be no displacement where fixed bearings are present (pier 1 – girders 3, 4, 5, 6, pier 2 – girders 3, 4, 5, 6, and pier 3 – girders 3, 4, 5, 6). Finally, displacement of the girders at non-guided bearings (pier 3 – girders 1, 2, 7, 8) should be in both the radial and transverse directions. Examination of the displacement of the bottom flange nodes under uniform thermal loading in Figures 5.21-5.26 provides evidence that the springs are only allowing girder movement in the appropriate direction for each particular bearing on the piers. Thus, it can be concluded that modeling the pier bearing using stiffened springs is an accurate method of replicating the ideal behavior of the pier bearings.

## 5.5 Conclusions

Although there are no experimental values available to compare with the analytical values obtained solving the FE models employed in this study, the results presented within the preceding chapter validate the accuracy of the FE model when compared with theoretical results. FE calculated girder gravity displacements match the camber gravity displacements given in the design sheets with enough precision to conclude that the FE model can accurately be used to model static loading of the Buffalo Creek Bridge. In addition, girder displacement values at bearing locations caused by uniform thermal loading show that springs modeling the bearings on the bridge piers apply boundary conditions on bridge girders acting in the appropriate directions.

# CHAPTER SIX

# BUFFALO CREEK BRIDGE OUT-OF-PLANE WEB DEFORMATIONS

## 6.1 Introduction

The webs of I-girder bridges are designed such that their main function is to maintain the relative distance between the top and bottom flanges under all anticipated loading conditions. Top and bottom flange sections of the I-girders are designed to carry the majority of the loading placed on the structure. Out-of-plane web deformations will have a negative effect on the load carrying capacity of bridges constructed using I-beams. According to White and Jung (2007) and Kala et al. (2005), while it is well known that steel I-girders maintain a certain level of post-buckling strength after initial buckling, large out-of-plane distortions will negatively influence the ultimate structural capacity of a steel I-girder.

I-girder out-of-plane distortions most often come in the form of lateral distortional buckling which is the combination of the local buckling and lateral buckling modes (See Figure 6.1). Local buckling is the instability mode resulting from changes in the geometry of the cross section while lateral buckling is defined as the lateral displacement and/or twist of the I-girder cross section. These two modes combined make up the distortional buckling mode.

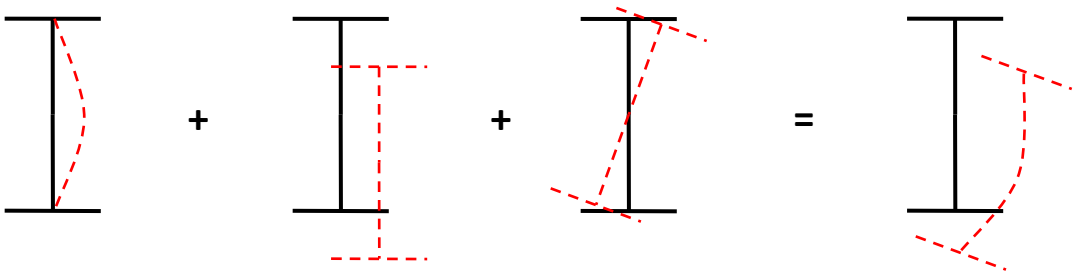


(a) Local Buckling (b) Lateral Buckling (c) Torsional Buckling (d) Distorsional Buckling

**Figure 6.1. Buckling Modes of I-Girders**

As stated previously, the design of a curved I-girder bridge differs greatly from the design of a comparable straight I-girder bridge because simply adding curvature to the structure adds complexities not present in straight I-girder bridges. The curved nature of the structure introduces a torsional component to the structural response, even under simple self-weight loads, that will not be present in straight girder bridges. The presence of buckling in the curved I-girder cross section prior to placing the bridge in-service is likely, and may lead to increased levels of girder buckling once in-service loads are introduced. The out-of-plane displacement will lead to subsequent in-service loading not being applied through the centroid of the I-girder cross section; thus, further increasing the out-of-plane distortion of the cross section. Although these initial out-of-plane distortions may not correspond to concerning high levels of stresses in the cross section and it is well known that steel girders maintain a certain level of post buckling strength after some initial buckling, the increase in out-of-plane distortion of the cross section will decrease the load carrying capacity of the I-girder.

This chapter focuses on investigating various displacements of the I-girders of the Buffalo Creek Bridge under self-weight, -45°F uniform thermal loading, and +45°F uniform thermal loading. Section 6.3 presents the lateral displacement profiles at the web centerline of each girder along the length of the girder under the forces of gravity. In Section 6.4, the out-of-plane web displacement profiles of each girder due to gravity loading are studied. Web cross-sectional displacements caused by gravity at various locations are investigated in Section 6.5. Sections 6.6, 6.7, and 6.8 present the same information as Sections 6.3, 6.4, and 6.5, respectively, only with the addition of -45°F and +45°F uniform thermal loading to gravity loading.

## 6.2 Lateral Displacement Calculation Algorithm

The complicated nature of the Buffalo Creek Bridge geometry requires that all of the bridge geometry be defined in the global Cartesian coordinate system when creating the geometry of the finite element model. Displacement values given in the Cartesian coordinate system will

not precisely represent lateral displacements perpendicular to the girder centerline because of the curved shape of the I-girders. As Figure 6.2 shows, simply studying displacement in the global z-direction will not yield an accurate representation of lateral displacement.

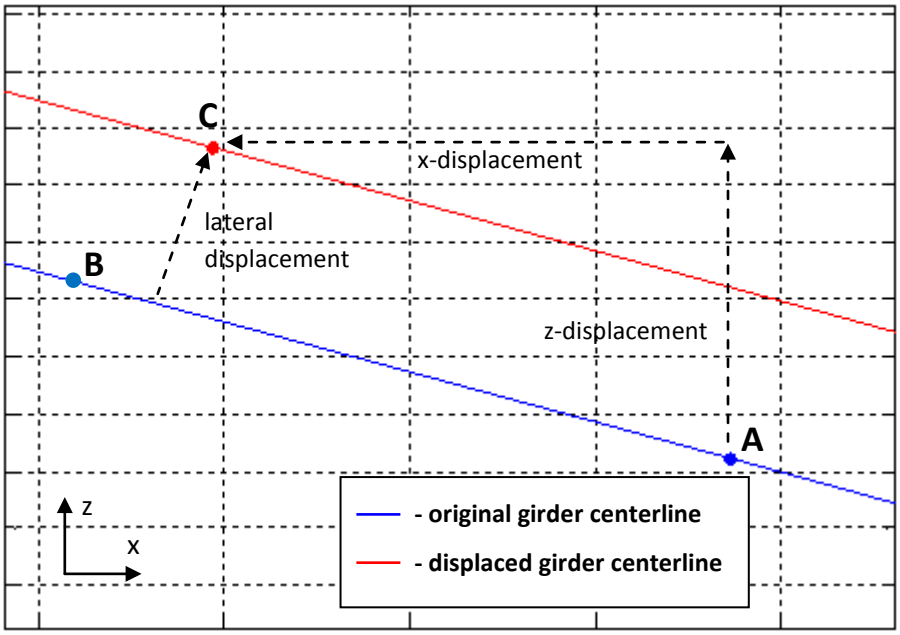


**Figure 6.2. Example of Web Centerline Nodal Displacement – Girder 4/Span 4**

To determine true lateral displacement at any node on the curved I-girders, an algorithm was developed in MATLAB (2011) that uses the original undisplaced nodal coordinates, displaced nodal coordinates, and the slope of the undisplaced girder centerline to determine the true lateral displacement of any node. The procedure followed by this algorithm is as follows (see examples of points A, B, and C in Figure 6.2):

1. Select nodes (coordinates in x-z plane)
    a. Original undisplaced node: *A*
    b. Original undisplaced subsequent node along girder centerline: *B*
    c. Displaced original node (displaced node A): *C*
2. Formulate vectors $\overline{BA}$ and $\overline{CA}$
    a. $\overline{BA} = B - A$
    b. $\overline{CA} = C - A$
3. Compute dot product of $\overline{BA}$ and $\overline{CA}$

a. $dot = \left(\overline{BA_x} * \overline{CA_x}\right) + \left(\overline{BA_z} * \overline{CA_z}\right)$

4. Compute pseudo-cross product of BA and CA
   a. $pX = \left(\overline{BA_x} * \overline{CA_z}\right) - \left(\overline{BA_z} * \overline{CA_x}\right)$
5. Compute the angle between AB and AC
   a. $\theta = a\tan 2\left(pX, dot\right)$
6. Use $\theta$ and length of $\overline{AB}$ to compute lateral displacement

This algorithm is used to determine the lateral displacement of all nodes, when necessary, throughout the remainder of this study.

## 6.3 I-Girder Lateral Displacement – Gravity Loading

This section investigates the lateral web displacement profiles, also referred to as global buckling, of all eight bridge girders under self-weight gravity loading. Boundary conditions are modeled as described in Figure 4.4 with both rigid pier and flexible pier results presented and compared. All web displacements are evaluated as close to the web centerline as the FE mesh will allow.

As Figure 6.1 shows, one component of distortional buckling is lateral bucking, which is the combination of lateral and vertical displacement of an I-girder section (see Figure 6.1 (b)). By design, I-girders are built to carry vertical loads with the force resultant of the loads applied through the cross-section, permitting the girder flanges to carry a majority of the load in the form of bending moments. The main function of the web is to maintain the relative distance between top and bottom flanges, and sustain the shear stresses in the cross-section. These vertical loads naturally result in vertical deflections of the I-girder cross section, especially at the center of each span. On the other hand, I-girders are not necessarily designed to carry loads in the lateral direction. These loads tend to cause buckling of the I-girder cross section, leading to a decrease in the load carrying capacity of the section. In the case of curved I-girder bridges, lateral deformation is practically unavoidable when uniform vertical loading is applied

across the top flange because the resultant force of this distributed load will not act through the plane of the I-girder web. Figures A.1 - A.8 in Appendix A present the lateral displacement at the web centerline of each span of each girder for models with rigid and flexible piers subjected to gravity loading.

Figures A.1 – A.8 show that, when subjected to dead weight loading only (steel girder and concrete deck self-weight), the Buffalo Creek Bridge I-girder webs experience global buckling. In Span 1 of Girder 8, the magnitude of this lateral displacement reaches 2.11 in. when the bridge piers are modeled as rigid, a magnitude representing more than three times the web thickness. Although these lateral deformations do not indicate that the I-girders are approaching the point of yielding at this level of loading, it should be noted that the I-girders are experiencing a certain level of buckling prior to any lateral, thermal, or live load forces being introduced on the structure.

The difference in magnitude of gravity induced global lateral web displacement between cases with rigid and flexible piers is evident in Figures A.1 to A.8. The largest disparity between displacements occurs in Spans 2 and 3, where one or both of ends of the span are supported by bearings designed to restrict longitudinal movement along the girder centerline. Although the bearing itself is designed to eliminate girder displacement at the pier, the flexibility of the piers will allow the girders to displace at these locations. This additional movement at the supports when modeling the piers as flexible members leads to an increase in the overall lateral deformation of the I-girders in these spans compared to when the piers are modeled as rigid members.

Results plotted in Figure 6.3 compare the maximum lateral web deformations in each span of the bridge for each girder when subjected to gravity loading. These results show that, for both rigid and flexible bridge piers, displacements in spans 1 and 2 increase slightly from girder 1 to 8 while displacements in span 3 and 4 decrease slightly from girder 1 to 8. This can be attributed to the fact that, in spans 1 and 2, the span length increases from girder 1 to 8 and in spans 3

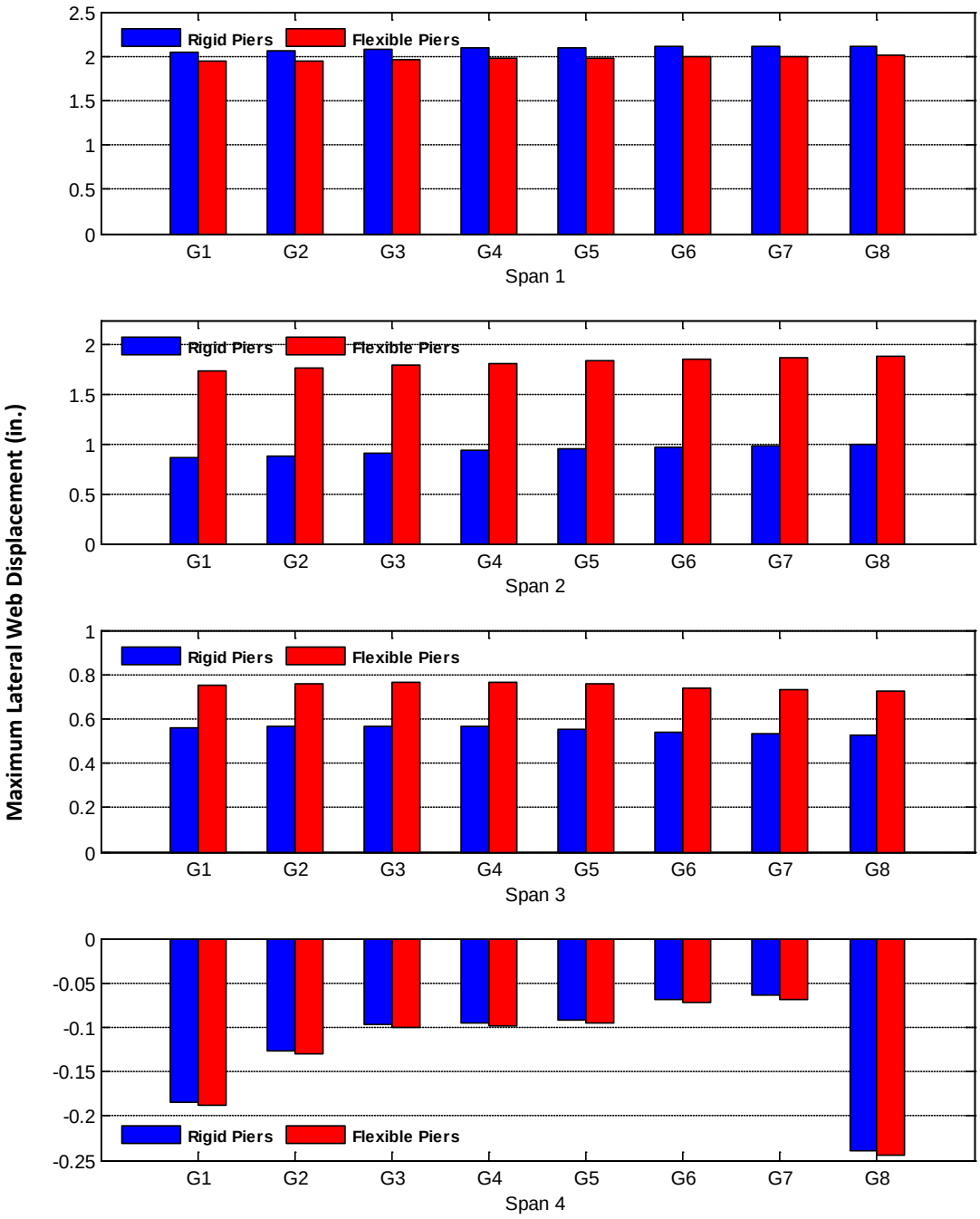


**Figure 6.3. Comparison of Maximum Lateral Web Deformations Due to Gravity Load**

and 4 the span length decreases from girder 1 to 8. For the curved girders, as the lengths of the spans between supports increases, the amount of global buckling caused by vertical gravity loading will also increase.

Figure 6.3 also shows that in span 1, rigid pier boundary conditions result in slightly larger lateral web displacements, in spans 2 and 3, flexible pier case results in significantly larger lateral web displacement than does the rigid pier case, and in span 4, flexible pier boundary conditions yield slightly larger lateral web displacements. The explanation for why flexible and rigid pier boundary conditions lead to the lateral web displacements behaving differently in each span can be found in the type of bearing supports at the end of each span and the span lengths. As vertical loading is applied (i.e. gravity loading), the curved shape of the I-girders causes forces in the longitudinal and transverse directions in the plane of the bridge to be transmitted to the bearings, with the majority of the force in the longitudinal direction. Consequently, where the bearings fix girder movement in the longitudinal direction (fixed and transversely guided bearings), these forces will be transmitted to the piers. When the piers are modeled as flexible members, the forces transmitted from the bearings lead to pier displacement. Because at these locations the girders are tied to the movement of the piers in the girder longitudinal and/or transverse direction, the ends of each span displace as the piers displace and as the ends of the spans displace, this will inherently cause the maximum lateral web displacement in the span to increase for a curved section. Figure 4.4 shows that the girder bottom flanges are tied to the piers in the longitudinal direction at all the bearings on piers 1 and 2 and at girders 3-6 on pier 3. Because both ends of span 2 are tied to the piers in the longitudinal direction, the largest increase in lateral web displacement occurs here when modeling the piers as flexible members rather than rigid members, with the largest difference of 50.6% occurring in girder 1. An increase in lateral web displacement between flexible and rigid pier models is also seen to a lesser degree in span 3, with the maximum difference of 27.4% occurring in girder 8. Spans 1 and 4 each have one end of the span free to move in the longitudinal direction, which significantly lessens the impact that modeling the piers as flexible members has on the lateral web displacement.

The design sheets for the Buffalo Creek Bridge present camber deviation values for each of the bridge girders representing the vertical deflection response of the girders to dead weight loading once the superstructure has been erected. These values were used in Chapter 5 to validate the finite element model. However, there are no provisions in the design sheets for the amount of sweep deviations occurring in the girders under the same loading conditions. According to the Bridge Welding Code (2007), sweep deviations are horizontal displacements from a perfectly straight (in this case curved) alignment. Section C-3.5.1.4 also states that most bridge members are flexible and allow some lateral adjustment during erection without damage. However, the finite element results plotted in Figure 6.3 show that gravity loading on the structure results in sweep deviations in the bridge girders of over 2 in. in span 1 of the Buffalo Creek Bridge.

Figure 6.4 contains bar graphs quantifying how the sweep deviation compares to the camber values in each span of each girder. The bars in Figure 6.4 represent, as a percentage, the magnitude of the measured sweep in relation to the magnitude of the measured camber. For instance, a location having a camber value of 1.0 in. and a sweep value of 1.0 in. will result in a 100% comparison. A location with a camber of 1.0 in. and a sweep of 0.75 in. will result in a 75% comparison. The closer the percentage values get to 100%, the closer the magnitude of sweep deviation is getting to matching the magnitude of camber deviation.

As Figure 6.4 shows, the magnitude of sweep deviation under dead weight loading is smaller than the camber deviation under the same loading conditions. The sweep deviation values should still be noted because they are representative of initial global buckling of the I-girders and in several locations the sweep magnitude is over 40% of the value of camber magnitude. Lateral deformations tend to be more detrimental to the structural integrity bridges and these lateral deformations under initial bridge construction were not accounted for in the design tables.

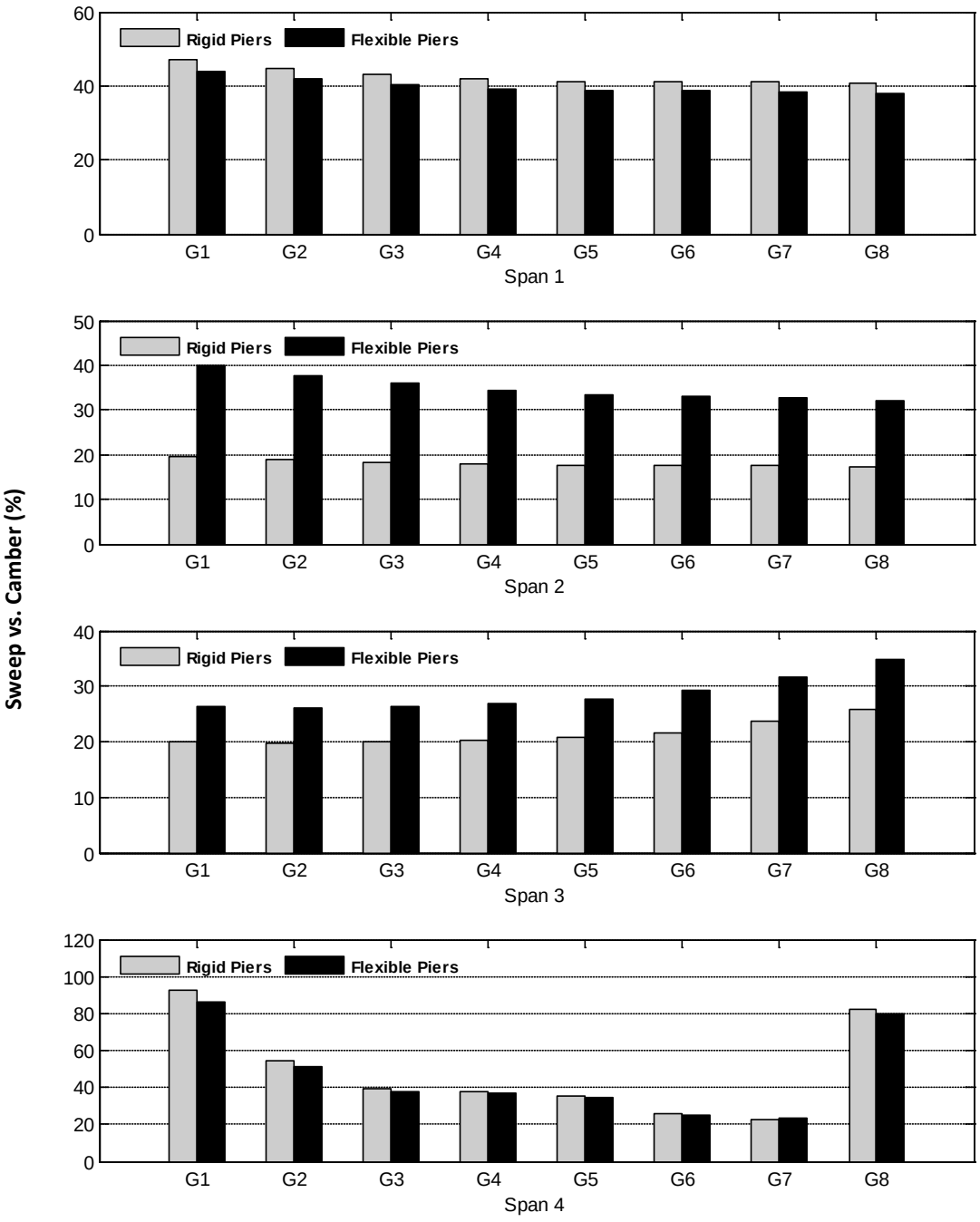


**Figure 6.4. Comparison of Camber and Sweep Deviations under Gravity Load**

## 6.4 Web Out-Of-Plane Displacement – Gravity Loading

The curved geometry of the Buffalo Creek Bridge leads to lateral girder displacements under even the smallest applications of vertical loads, such as gravity loading, and this is shown in Figures A.1 – A.8. Although bridge design does not account for lateral I-girder displacements, some lateral deformation of the I-girders should be expected because of girder curvature. However, I-girders are designed so that the flanges carry a majority of the loading and out-of-plane web deformation is minimized. Out-of-plane web deformation is defined as the I-girder web deforming laterally from the plane created between the top flange and bottom flange centerline and is a form of local buckling as shown in Figure 6.1. According to Helwig et al. (2007) in a study on the effects of initial imperfections on bridge girders, the effects of out-of-flatness (local buckling) reduce the initial stiffness of the (web) plate. Therefore, with larger initial imperfections there are larger displacements at low load levels. Additionally, imperfections result in larger deformations compared to relatively straight plates, and therefore often result in earlier yielding on the plate section. Although initial imperfections are often considered as imperfections from fabrication or erection, out-of-plane deformations caused by gravity loading are considered imperfections here because they are not accounted for during design procedures.

The first loading condition applied on the Buffalo Creek Bridge finite element model is the self-weight of the bridge superstructure. This loading condition represents the response of the bridge to the gravity load of the superstructure before the bridge deck cures and the concrete can contribute any stiffness to the system. Figures A.9 – A.16 show the out-of-plane web deformation along the web centerline for each of the four spans of each of the eight girders for models with both rigid and flexible piers subjected to only the self-weight of the bridge superstructure.

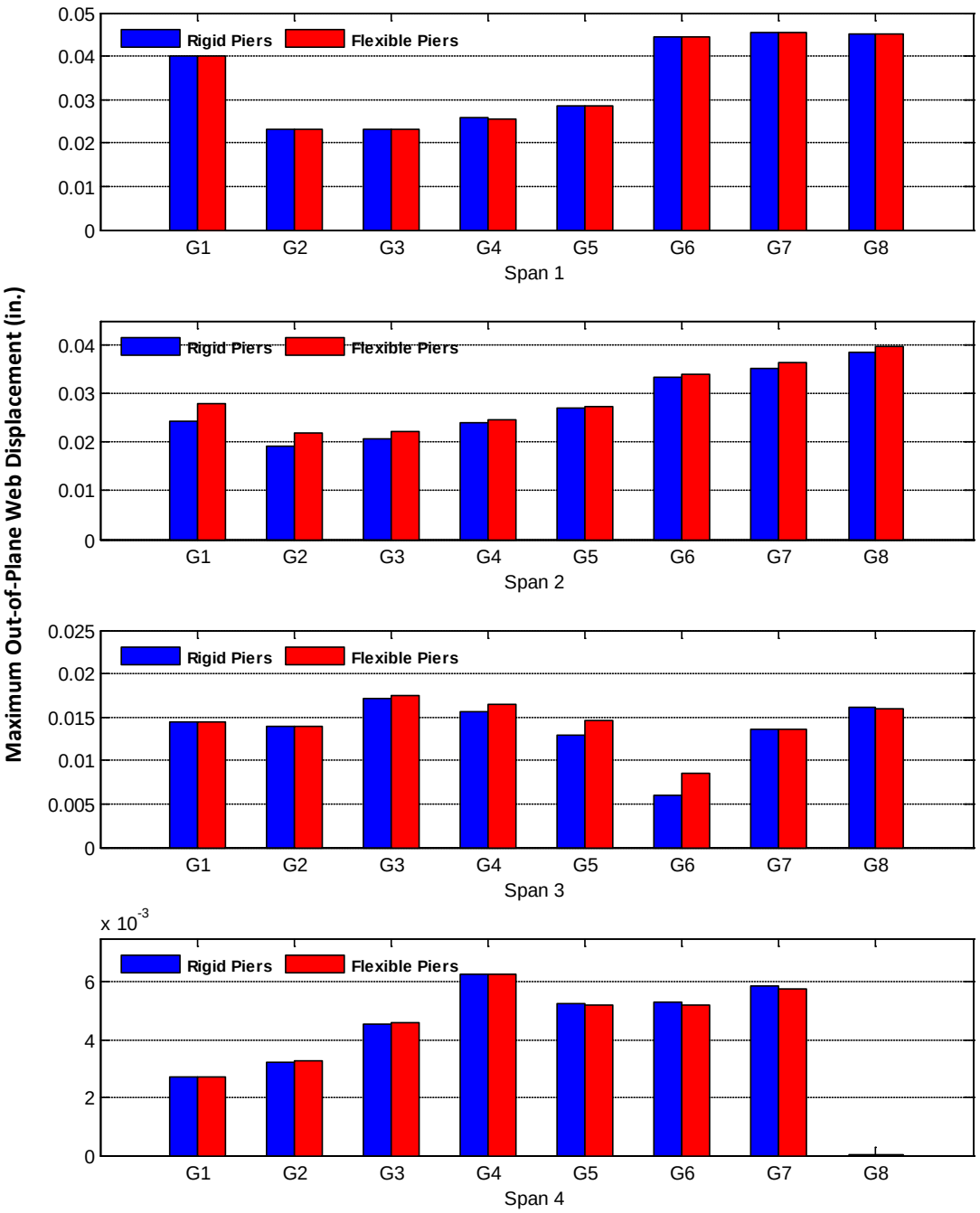


**Figure 6.5. Comparison of Maximum Out-of-Plane Web Deformations at Girder Mid-Spans Due to Gravity Load**

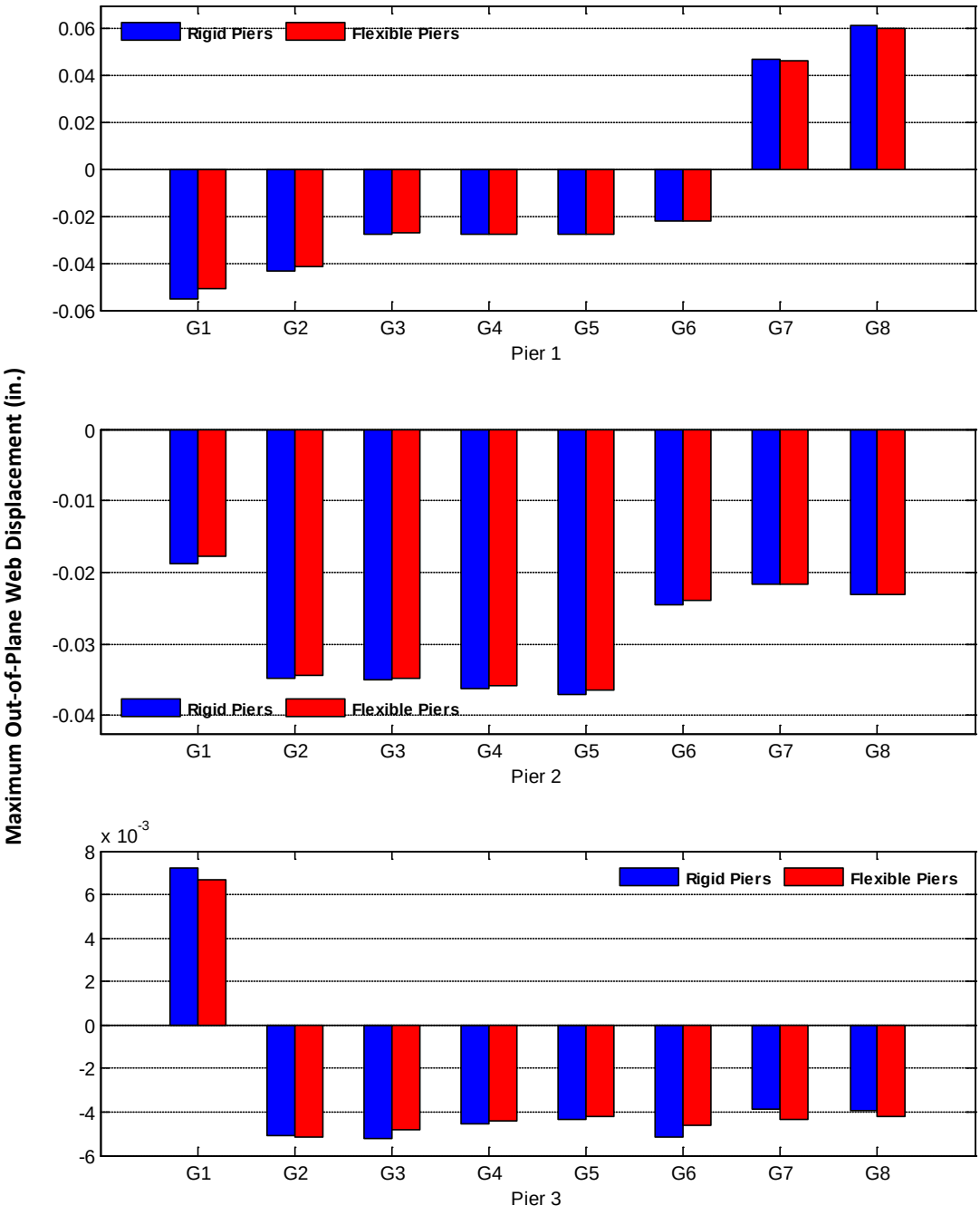


**Figure 6.6. Comparison of Maximum Out-of-Plane Web Deformations Near Piers Due to Gravity Load**

Figures A.9 – A.16 show that even during the early stages of construction, out-of-plane web deformation is occurring along the web centerline of the curved I-girders. Although there is out-of-plane deformation present, the magnitudes of these deformations are small, with the maximum value of 0.0616 in. in Span 2 of Girder 8, which is only 9% of the web thickness. Deflections of this magnitude likely will not have any effect on the capacity of the structure. However, it should be noted that the deflections shown in Figures A.9 – A.16 are occurring without consideration of any initial imperfections due to fabrication, lateral forces, or thermal forces. The consideration of any small initial imperfections that are sure to arise during fabrication would almost certainly increase the magnitude of the lateral web deflections. Although these displacement levels do not appear to be concerning, the presence of out-of-plane displacement and associated reduction in initial web stiffness under this initial loading could lead to reductions in I-girder load carrying capacity in later stages of the structures life.

Even though the out-of-plane displacement profiles plotted in Figures A.9 – A.16 show that modeling the bridge piers as rigid or flexible members doesn't have a significant impact on the out-of-plane web displacement when loaded with gravity, there are some observations that can be made from the plots. First, the profiles show areas along the length of each span, especially spans 1, 2, and 3, where the magnitude of the out-of-plane displacement is significantly less than the rest of the span. Cross referencing with the design sheets reveals that these areas of lesser out-of-plane displacement correspond to locations where intermediate stiffeners are present on the girder webs in between the cross members. Intermediate stiffeners on the girders obviously minimize the magnitude of out-of-plane displacement caused by gravity loading. Next, the plots show that the out-of-plane web displacement behavior of each span is different near the piers compared to in the center of the span. Under gravity loading, the girders will be subjected to a negative bending moment at the pier locations and a positive bending moment at the middle of each span. It appears from Figures A.9 – A.16 that I-girder sections under positive and negative bending moment experience out-of-plane web displacement in opposite directions. Finally, these out-of-plane web displacements in opposite

directions at the piers and mid-spans indicate that the girders are experiencing a degree of longitudinal buckling under self-weight loading.

Because the out-of-plane web displacement behavior in each span appears to differ between the area close to the piers and the middle of the span, the maximum out-of-plane web displacement will be investigated in these two areas separately. Figure 6.5 displays a series of bar graphs representing the maximum out-of-plane web displacement, for rigid and flexible pier models, at the middle of each span for each girder. Next, Figure 6.6 plots the same results taken at the locations near each pier on each girder.

Results given in Figures 6.5 and 6.6 confirm that modeling the bridge piers as rigid or flexible members does not have a significant impact on the out-of-plane web displacement caused by gravity loading. However, Figure 6.5 does clearly show that, for rigid and flexible pier models, the maximum out-of-plane web displacement at the mid-spans of spans 1 and 2 is less in girders 2-5 than in girder 1 and girder 6-8. In span 1 of girders 2-5, the bottom flange width in most of the span is 25 inches compared to a bottom flange width of 20 inches in girder 1 and girders 6-8. Span 2 of girders 2-5 has a bottom flange width of 24 inches in most of the span while span 2 of girder 1 and girders 6-8 has a bottom flange width of 20 inches. It is evident from the span 1 and span 2 results given in Figure 6.5 that as the girder bottom flange width increases, the magnitude of out-of-plane web displacement due to gravity loading decreases.

## 6.5 Web Cross-Section Displacement – Gravity Loading

To better understand the web buckling behavior of the Buffalo Creek Bridge girders, it is necessary to study the web displacement profiles at some critical locations. It is impractical to investigate the web lateral displacement profiles at every location on each girder; so, the results studied here focus on locations at the center of each span (mid-spans) and at each pier. These locations were chosen because this is where girders will experience the largest positive

and negative bending moments under normal loading conditions. Girder cross section displacement results at the mid-spans are investigated at locations as close as possible to the center of the span while still in the center of a web panel (See Figure 6.7). These locations were chosen because they are closest to the center of the span but the furthest away from the transverse stiffeners and will likely exhibit the most extreme lateral displacements in the respective panels. At the bridge piers, lateral web displacements are studied at the center of the panels on either side of the pier as well as directly over the piers.

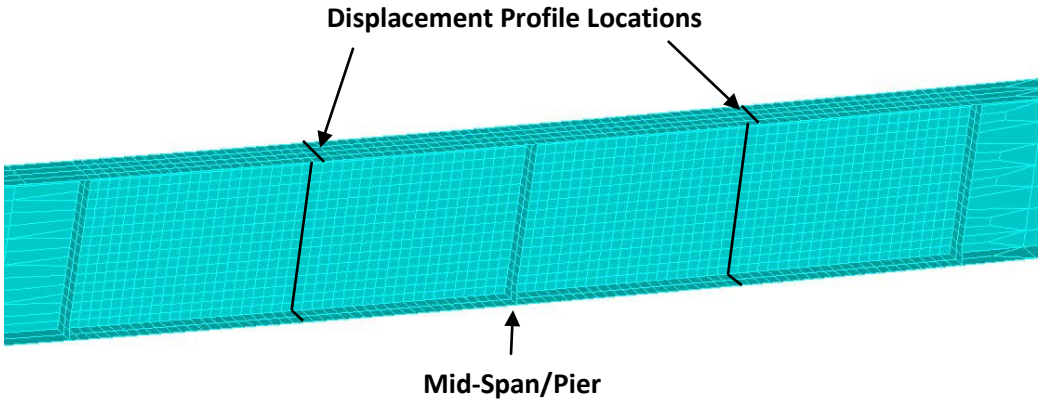


**Figure 6.7. Location of Cross Sectional I-Girder Displacement Profiles**

These profiles will provide greater insight into the overall buckling behavior present in the I-girder webs. Out-of-plane, or lateral, web displacements are computed at each location through the depth of the girder web using the algorithm discussed in Section 6.2. Plots A.17 – A.32 in Appendix A contain lateral, or radial in the case of curved I-girders, web displacement profiles at critical locations for each of the eight girders when the Buffalo Creek Bridge is loaded with self-weight. The plots compare profiles for models with the piers idealized as rigid and flexible members. A datum of 0.0 in Figures A.17 – A.32 represents the un-displaced I-girder web.

Figures A.17 – A.24 contain the web cross section displacement profiles at all four mid-spans of each girder. Because the displacement profiles in the panels on either side of the mid-span are

found to be very similar, only the profile for one panel at each mid-span is presented in the figures. Figures A.25 – A.32 contains the web displacement profiles at each of the three pier locations on each girder. At piers 1 and 2, displacement profiles are presented at the center of the web panel before the pier (Figure (a)/(b) – 1), at the web directly over the pier (Figure (a)/(b) – 2), and at the center of the web panel after the pier (Figure (a)/(b) – 3). At pier 3, displacement profiles are given at the center of the web panel before the pier (Figure (c) – 1) and at the web directly over the pier (Figure (c) – 2) because transverse stiffeners are present very close to pier 3 on the abutment 2 side (See Figure 4.1), minimizing the buckling behavior at this location.

Displacement profiles plotted in Figures A.17 – A.24 clearly show that superstructure self-weight loading is causing lateral-distortional buckling at the mid-spans of each girder. Modeling piers as rigid or flexible members will impact how much lateral displacement occurs, as was discussed previously in Section 6.3. It doesn't appear that pier flexibility has any effect on the local or torsional buckling of the web cross sections when loaded with gravity. Likewise, plots of web deformation at or near the bridge piers indicate that gravity loads are inducing lateral distortional buckling at these locations. At some locations, particularly directly over the piers, pier flexibility has a slight effect on the magnitude of local buckling and the degree of rotation of the cross section. Web sections directly over the piers experience a smaller amount of local buckling compared to web panels just before or just after the piers because there are vertical stiffeners on the web at these locations.

According to a study by White and Jung (2007), flexural resistance of steel I-girders is typically defined in steel design guidelines based on local and lateral-torsional buckling modes and lateral distortional buckling is not considered. This is due to a lack of a closed-form solution to accurately quantify lateral distortional buckling, which is also a problem in this study because it prohibits the numerical comparison of lateral-distortional buckling between different cross-sections of different models subjected to different loading conditions. However, results in Appendix A show that lateral-distortional I-girder buckling is occurring in several locations on

the Buffalo Creek Bridge under only gravity loading. This lines up with the conclusion made by Bradford (1992) that distortional buckling will occur at significantly lower load levels than lateral-torsional buckling. This lateral distortional buckling will negatively affect the load carrying capacity of the I-girders, and the study of I-girder stresses under the same loading conditions combined with thermal loading, detailed in subsequent chapters, will lead to more details as to how much girder capacity is affected by lateral torsional buckling.

## 6.6 I-Girder Lateral Displacement – Gravity and Thermal Loading

Results presented and discussed in Sections 6.3 – 6.5 show the behavior of the Buffalo Creek Bridge prior to the introduction of any thermal, lateral, or live loading. The following three sections will study the same behavior of the bridge once -45°F and +45°F uniform thermal loads are introduced. Thermal loading is added to the model after the structure has displaced under self-weight and the deck has fully cured, allowing it to contribute its full stiffness to the system. Just as in the previous section, two cases will be studied: modeling the piers as rigid members and modeling the piers as flexible members.

First, the lateral displacement profiles of girder web centerlines when subject to gravity loading followed by +/-45°F thermal loading are studied. Figures B.1 – B.8 contain lateral web displacement profiles for each span of each girder when loaded with self-weight followed by a uniform +45°F thermal load and Figures B.9 – B.16 contain plots of these profiles under self-weight and -45°F thermal loading. The impact of the addition of thermal loading to the bridge varies in each girder and also varies within each span based on pier flexibility. As such, this study will first detail the effects of thermal loading span-by-span before making conclusions about the effect temperature has on the lateral web displacement of the entire structure.

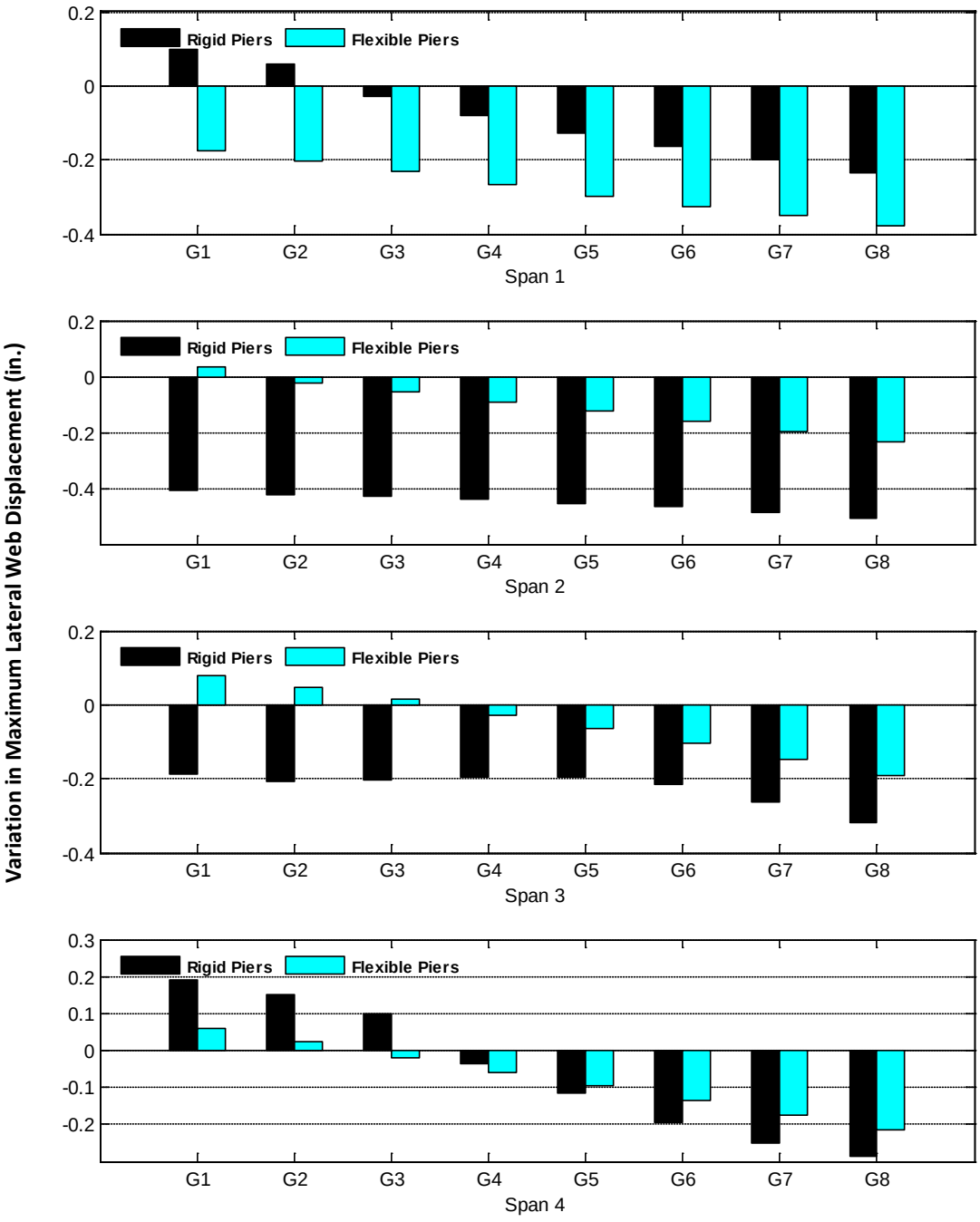


**Figure 6.8. Variation of Maximum Lateral Web Deformations with the Addition of -45°F Thermal Load**

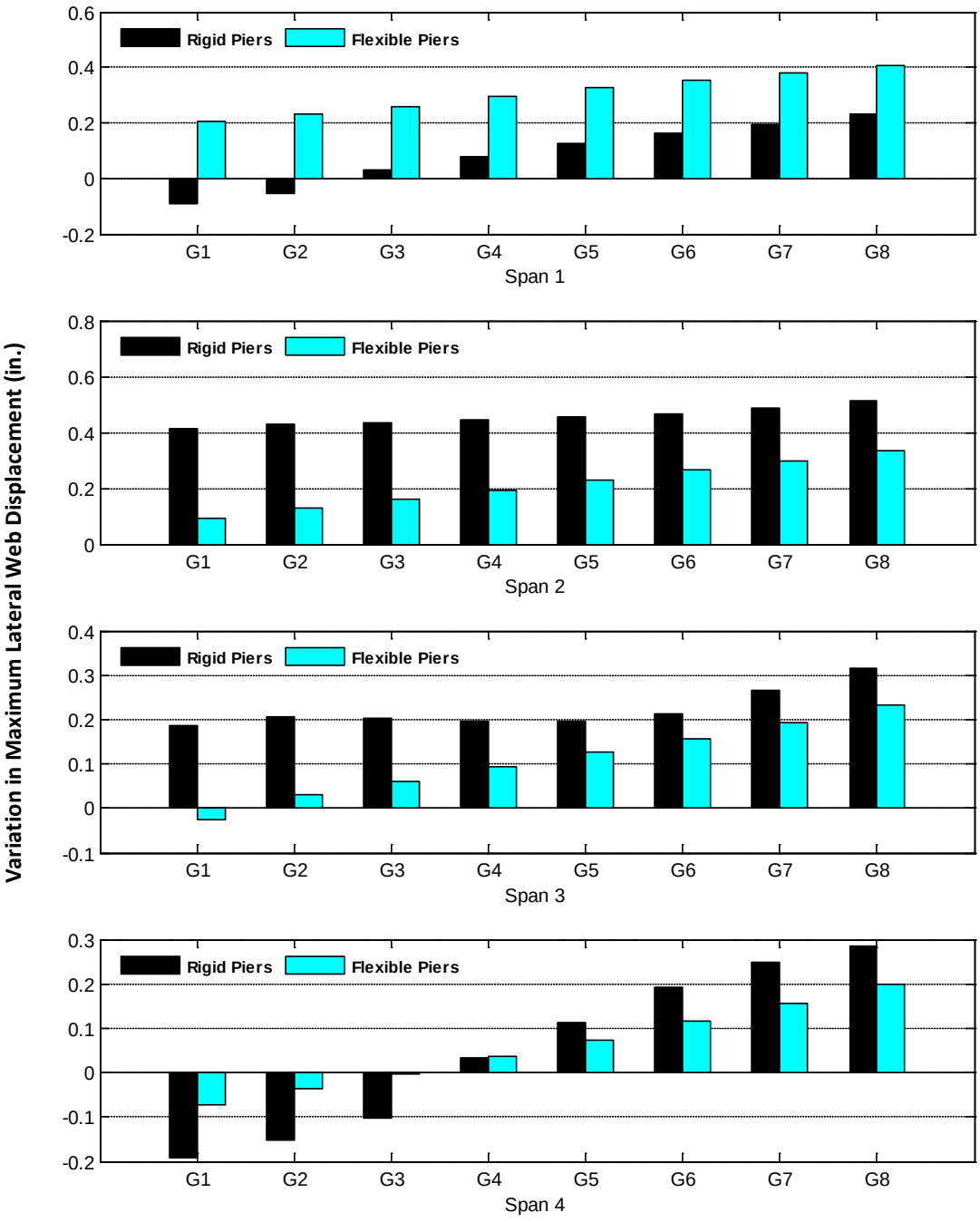


**Figure 6.9. Variation of Maximum Lateral Web Deformations with the Addition of +45°F Thermal Load**

**Table 6. 1. Percent Change in Lateral Web Centerline Displacement with Addition of -45°F Thermal Load**

| | | Span 1 | Span 2 | Span 3 | Span 4 |
|---|---|---|---|---|---|
| Girder 1 | Rigid | 5.3% | -50.2% | -33.9% | 828.3% |
| | Flexible | -9.4% | 1.9% | 10.8% | 437.9% |
| Girder 2 | Rigid | 3.3% | -50.8% | -37.4% | 477.2% |
| | Flexible | -10.7% | -1.5% | 6.7% | 143.4% |
| Girder 3 | Rigid | -1.5% | -49.9% | -36.3% | 406.5% |
| | Flexible | -12.0% | -3.3% | 2.0% | 201.6% |
| Girder 4 | Rigid | -3.9% | -47.1% | -35.5% | -92.9% |
| | Flexible | -13.7% | -5.3% | -3.9% | 457.6% |
| Girder 5 | Rigid | -6.2% | -47.6% | -35.5% | -288.8% |
| | Flexible | -15.4% | -7.2% | -8.8% | -2920.7% |
| Girder 6 | Rigid | -8.0% | -47.8% | -40.6% | -467.7% |
| | Flexible | -16.7% | -9.1% | -14.8% | -1289.4% |
| Girder 7 | Rigid | -9.7% | -49.1% | -60.6% | -666.2% |
| | Flexible | -17.8% | -11.1% | -21.0% | -522.9% |
| Girder 8 | Rigid | -11.4% | -50.9% | -75.1% | -661.7% |
| | Flexible | -19.3% | -13.1% | -27.1% | -704.0% |

**Table 6. 2. Percent Change in Lateral Web Centerline Displacement with Addition of +45°F Thermal Load**

| | | Span 1 | Span 2 | Span 3 | Span 4 |
|---|---|---|---|---|---|
| Girder 1 | Rigid | -5.1% | 50.6% | 33.9% | -828.5% |
| | Flexible | 10.6% | 5.6% | -4.0% | -809.4% |
| Girder 2 | Rigid | -3.1% | 51.1% | 37.4% | -477.4% |
| | Flexible | 11.9% | 7.6% | 4.5% | -227.7% |
| Girder 3 | Rigid | 1.4% | 50.2% | 36.3% | -406.7% |
| | Flexible | 13.2% | 9.3% | 9.2% | -9.9% |
| Girder 4 | Rigid | 3.8% | 47.4% | 35.5% | 92.8% |
| | Flexible | 14.8% | 11.2% | 14.1% | 240.9% |
| Girder 5 | Rigid | 6.1% | 47.9% | 35.6% | 288.7% |
| | Flexible | 16.5% | 13.1% | 19.5% | 2267.0% |
| Girder 6 | Rigid | 7.8% | 48.1% | 40.6% | 467.6% |
| | Flexible | 17.7% | 15.0% | 25.5% | 1091.2% |
| Girder 7 | Rigid | 9.5% | 49.4% | 60.6% | 666.1% |
| | Flexible | 19.0% | 16.8% | 32.0% | 307.7% |
| Girder 8 | Rigid | 11.2% | 51.1% | 75.2% | 661.7% |
| | Flexible | 20.3% | 18.7% | 32.9% | 424.2% |

Figures 6.8 and 6.9 are created to more clearly show how applying temperature to the Buffalo Creek Bridge immediately after completion of construction effects the overall lateral web displacement. The bar graphs in these figures represent the maximum magnitude of additional

lateral displacement in each girder span caused by thermal loading on the already gravity displaced profiles. The maximum lateral deformation was computed in a 100 foot section in the center of each span because this area is most often where maximum lateral displacement occurs and will provide the best location for consistent comparisons between adjacent spans. At these maximum displacement difference locations, the percentage of increase or decrease in the web lateral displacement caused by thermal loads is calculated and the results are given in Tables 6.1 and 6.2.

Displacement profiles of span 1 as well as Figures 6.8 and 6.9 show that thermal loading has a greater impact on span 1 lateral deformation when the piers are modeled as flexible members with thermal loading having an increasingly larger effect on the magnitude of lateral displacement going from girder 1 to girder 8. With a -45°F thermal load on the rigid pier model, lateral displacement increases in girders 1 and 2, but decreases at an increasing rate in girders 3-8. The opposite is true for the rigid pier case for +45°F thermal loading. Values in Table 6.1 show a decrease in lateral displacement up to 19.3% for flexible piers and 11.4% for rigid piers under uniform -45°F thermal loading and Table 6.2 reveals an increase of up to 20.5% for flexible piers and 11.2% for rigid piers under uniform +45°F thermal loading.

Although Figures A.1 – A.8 show that modeling the bridge piers as flexible members yields higher lateral web displacements in spans 2 and 3 under self-weight loading than modeling the piers as rigid members, results in Figures B.1 – B.16 show that rigid pier models experience significantly greater response to thermal loading. Results show that lateral web displacements in span 2 are more significantly impacted by thermal loading when the bridge piers are modeled as rigid. Just as in span 1, temperature loading has an increasingly larger effect on lateral web displacement in spans 2 from girder 1 to girder 8. Temperature increase leads to up to 18.7% greater lateral displacements in span 2 when the piers are modeled as flexible members and up to 51.1% greater lateral displacements when piers are modeled as rigid.

Conversely, temperature decrease causes up to a 13.1% decrease in lateral displacement in span 2 when the piers are flexible and up to a 50.9% decrease when the piers are rigid. Profile plots also show that when the girders in span 2 are supported by rigid piers and loaded with gravity and thermal loading, the I-girders begin to show signs of longitudinal buckling along the web centerline at the center of each span.

Plots of lateral web deformation profiles of span 3 shows that temperature loads have a larger effect on lateral web deformation when the piers are modeled as rigid as opposed to flexible. Loading the model with +45°F uniform temperature yields an increase in lateral web deformation for both rigid and flexible pier models (with the exception of a slight decrease in span 3 of girder 1), with the magnitude of increase growing larger from girder 1 to girder 8. The -45°F thermal load causes the lateral deformation of the rigid pier models to decrease for all girders. However, as temperature decreases on the bridge with flexible piers, the webs of the three inside girders (girders 1, 2, and 3) closest to the radius of curvature exhibit increased lateral displacement while the other girders show decreased lateral displacement. Uniform temperature loading of +45°F increases lateral web displacement by up to 75.2% for rigid pier models and by up to 39.2% for flexible pier models, while uniform temperature loading of -45°F decreases lateral web displacement by up to 75.1% for rigid pier models and by up to 27.1% for flexible pier models. Like span 2, the addition of thermal loading is causing longitudinal buckling to occur along the web centerline at the mid-span.

Results for span 4 indicate that the magnitude of the difference, be it increase or decrease, in lateral web deformation due to thermal loads is greater for models with rigid piers than those with flexible piers. Uniform temperature of +45°F decreases the lateral web displacement of girders 1-3 while increasing the lateral web displacement of girders 4-8. The converse of that is true for -45°F loading: increase in lateral web displacement in girders 1-3 and decrease in girders 4-8. Tables 6.1 and 6.2 show that temperature loading can significantly increase or decrease the lateral web deformation in span 4 for both rigid and flexible pier models. Lateral

displacement increases of up to 2267% and decreases as low as -2920.7% are calculated on girder 5 when the piers are flexible. When the piers are rigid, the web profile shows longitudinal buckling under temperature increase and decrease, but very little, if any, buckling is seen in girders 1-2 and 7-8.

Plots in Figures B.1 – B.16 and Figures 6.8 and 6.9 clearly show that the introduction of a uniform temperature load impacts the laterally displaced shape of the Buffalo Creek Bridge I-girders. Girder response to thermal loading varies from span to span based on how the piers are modeled. Previously discussed results indicate that changing the stiffness of the bridge piers changes how each span, and each girder, responds to a uniform thermal load. A study of Figure 4.4 reveals that the majority of the pier bearings restrict movement along the girder longitudinal direction (all except girders 1, 2, 7, and 8 on pier 3) and the sixteen centermost bearings fully restrict all girder movements. The types of bearings and flexibility of the piers becomes critical when studying thermal effects. As the temperature of the bridge changes, the superstructure will attempt to expand and contract accordingly. Just as curved girders exhibit a more complex response to vertical loading than do straight girders, the response of a curved I-girder to thermal loading will be different than the response of a comparable straight I-girder. Uniform thermal loading on straight I-girders leads to a majority of the thermal expansion and contraction occurring along the girder centerline, while the same loading on a curved I-girder will cause the I-girder to expand or contract in both the radial and tangential directions. Hence, bearing orientation and pier flexibility will play a vital role in how these thermal expansions and contractions are accommodated and how the overall structure responds to those expansions and contractions.

As bridge girders expand and contract under changing thermal conditions, this expansion and contraction will create forces on the bridge bearings according to the type of bearing at each location and the curvature of the superstructure. The fundamental difference between the two

models created in this study is how these forces affect structural response. When the piers are modeled with flexibility, the forces imposed on the bearings from girder expansion and contraction will lead to the piers displacing according to the magnitude of the forces and the orientation of the bearings. The displacement of the piers serves to dissipate some of the thermally induced forces in the I-girders. On the other hand, the only girder movement at the bridge supports when piers are modeled as rigid members is movement allowed by bearing design. Girder movement due to thermal expansion and contraction is not transferred to the bridge piers, thereby preventing the I-girders from transferring any thermal forces to the bridge piers.

Study of lateral web centerline displacement profiles in Figures B.1 – B.16 reveals the stark difference between how rigid and flexible pier models respond to uniform thermal loading. In the case where the piers are modeled as flexible members, the magnitude of additional lateral web displacement caused by uniform thermal loading appears to be consistent along the length of each span. This indicates that, while flexible piers will not allow full thermal expansion and contraction, they are allowing the superstructure to expand and contract as a continuous unit under thermal loads. In contrast, modeling the Buffalo Creek Bridge piers as rigid members causes each span to behave mostly independently because of the large number of fixed bearings on the piers. The fixed bearings combined with fixed piers will also restrict the thermal expansion and contraction of the associated girders.

In the case of span 1, bearings at abutment 1 are designed such that they should accommodate most thermal expansion and contraction. Slight resistance to longitudinal movement will be provided by the soil backfill and the longitudinally guided bearings on girders 2-6 will resist thermal expansion in the radial direction. Bearings on pier 1 restrict any girder movement in the longitudinal direction, but will accommodate transverse movement at girders 1, 2, 7, and 8. However, transverse movement at these locations will be minimal because the four innermost

girders are fixed at pier 1, and the outermost girders are tied to the four innermost girders by cross frames and the concrete bridge deck. For the rigid pier case, Figures 6.8 and 6.9 show that the magnitude of thermally induced lateral displacements in the girders of span 1 are the smallest when compared to spans 2-4.

Profiles of lateral web displacements of spans 2 and 3 clearly reveal that rigid pier model boundary conditions are restricting thermal expansion and contraction. All bearings on pier 1 and pier 2 restrict girder movement along the girder tangential direction which significantly restricts the thermal movements of the I-girders. As a result, temperature increase causes lateral web deformation to increase because expansion can only occur in the lateral direction. Furthermore, the resistance to thermal expansion leads to compressive stresses through the I-girder cross section which causes noticeable longitudinal buckling along the web centerline. As a uniform temperature drop is introduced, lateral web displacement in the span decreases as the span contracts. Just as boundary conditions resist thermal expansion of the girders in span 2, they will also resist girder contraction. This resistance to contraction creates tensile stress in the I-girders resulting in longitudinal buckling of the girder web. Although displacement magnitudes are smaller, the same behavior is observed in span 3. Boundary conditions on span 3 are very similar to those on span 2, except for free bearings on girders 1, 2, 7, and 8 on pier 3. However, the girders will not be fully free to move at these locations because they are tied to the four innermost girders by cross members and they are also tied together by the stiffness of the bridge deck. The lateral response of the girders in span 3 to thermal loading can be explained in the same manner as span 2.

Generally, thermal loading has a larger impact on the lateral web displacement in span 4 when the piers are modeled as rigid members. Figures B.1 – B.16 also show that introducing temperature to the rigid pier models leads to longitudinal buckling at the web centerline, with the largest magnitude of longitudinal buckling in girders 3-6 in the center of the bridge. Since

the end of span 4 supported by abutment 2 is made up of bearings that allow movement along the longitudinal centerline of the girders, it would expect that this would allow thermal expansion and contraction, minimizing any effects that would cause buckling. Figures B.1 – B.16 show that this is not the case, and one contributing factor to the buckling in span 4 is the length of span 4 compared to the length of the adjacent span. The unsupported length of the girders in span 4 is approximately 55% of the unsupported length of the girders in span 3. Although not a design criteria, a good rule of thumb for bridge design is for the length of the extreme spans (at the ends of the bridge) to be at least 80% of the adjacent span. Of course, this often times is not possible because the piers can only be placed in locations where the terrain will allow. Span 4 of the Buffalo Creek Bridge obviously does not meet these criteria. The larger unsupported length in span 3 naturally causes span 3 to experience greater vertical deflection than span 4 under self-weight loading. This leads to a negative bending moment in the girder at pier 3 that is not symmetrical about pier 3. Unlike at the other supports on the Buffalo Creek Bridge, the stress distribution through the web depth on the span 4 side of pier 3 is not mostly symmetrical about the web centerline as is the case on either side of piers 1 and 2, nor is the cross stress magnitude in the top and bottom flange at a cross section similar. When thermal loading is added, this unsymmetrical stress profile is exaggerated, leading to longitudinal web buckling. In span 4 of girders 3-6, the fixation of the girders at pier 3 further increases the degree of longitudinal buckling in span 4. A second contributing factor to the buckling of span 4 is the boundary conditions on the span. In theory when the piers are rigid, the bearings providing the boundary conditions to the girders in span 4 should allow for thermal expansion and contraction (see Figure 4.4). In reality, this will not be the case. Fixed bearings at girders 3-6 on Pier 3 combined with cross-members connecting the girders and the stiffened bridge deck will provide some degree of resistance to thermal movements. The combination of the length of span 4 compared to the adjacent span and the resistance to expansion and contraction provided by the boundary conditions and additional bridge superstructure components causes thermal stresses to arise in span 4 that, in theory, should be relieved by bridge movement at the bearings. These additional stresses cause lateral

deformation along with web bucking. Further evidence of these stress profiles is given in Chapter 7.

Results presented and discussed in this section along with plots in Appendix B reveal that the addition of thermal loading to the Buffalo Creek Bridge leads to additional lateral I-girder displacements. Overall, thermal loads increase or decrease global girder buckling to a lesser degree when the bridge piers are modeled as flexible members compared to when they are modeled as rigid members. Pier flexibility allows the entire superstructure to expand and contract as the temperature changes, but the rigid pier models isolate the thermal response to a mostly span-by-span case. As such, the most significant response to thermal loads is seen in spans 2 and 3 when the piers are modeled as rigid members. These spans experience the largest magnitude of thermally induced lateral displacement as well as a significant amount of longitudinal buckling from temperature loads.

## 6.7 Web Out-Of-Plane Displacement – Gravity and Thermal Loading

The previous section shows that the application of thermal loading, both +45°F and -45°F, has an effect on the overall lateral displacement of the Buffalo Creek Bridge I-girders. The next phase of this study looks to determine what impact, if any, temperature has on the out-of-plane displacement of the I-girder webs. Figures B.17 – B.36 in Appendix B contain plots of the out-of-plane web displacement at the web centerline of each span of each girder.

The same form of data analysis is used to create Figures 6.10 and 6.11 as was previously used to create Figures 6.8 and 6.9. These figures present a comparison of the maximum additional out-of-plane web displacement induced in each span of each girder when uniform thermal loading is added. Once again, at the locations of maximum displacement difference, the percentage of out-of-plane web displacement change as a result of thermal loads is calculated and the results are given in Tables 6.3 and 6.4.

As results in Section 6.4 indicate, modeling the bridge piers as either rigid or flexible members does not have a significant impact on out-of-plane web displacement under gravity loading only. However, the webs of the rigid and flexible pier models respond differently with the addition of thermal loads. In each of the web centerline out-of-plane displacement profiles plotted in Figures B.17 – B.32 there are areas where the out-of-plane web displacement is clearly higher than other locations. The areas of smaller out-of-plane displacement correspond to locations on the girders where transverse stiffeners are present. It is obvious from these plots that intermediate web stiffeners reduce the magnitude of out-of-plane web displacement caused by temperature loading.

Tables 6.3 and 6.4 show, in terms of percentage, positive and negative thermal loading has a larger impact on the out-of-plane web displacement when the bridge piers are modeled as rigid. However, at the center of span 1 and towards abutment 1, +45°F loads on rigid pier models decrease the amount of out-of-plane web displacement compared to gravity loading while +45°F loads on flexible pier models increase out-of-plane web displacement in the same regions. Closer to pier 1, rigid pier models out-of-plane web displacement increases in the negative direction while flexible pier models out-of-plane web displacement decreases compared to gravity loading results. For both cases of pier modeling, the opposite is true when -45°F loading is introduced.

At the locations where thermal loading has the most profound effect on the magnitude of out-of-plane web displacement, Table 6.4 shows that a +45°F thermal load applied on the bridge with rigid piers after gravity loading results in a 25% - 100% decrease in the displacement magnitude in span 1. Similar loading causes up to a 36% increase in out-of-plane web displacement when the piers have flexibility. Conversely, a temperature decrease leads to an increase in out-of-plane web displacement in models with rigid piers and a decrease in out-of-plane web displacement for models with flexible piers. Table 6.3 shows that a -45°F temperature drop can increase out-of-plane web displacement of rigid pier models by up to

117% over gravity loading. The same uniform temperature load decreases out-of-plane web displacement by up to 17% for flexible pier models.

In spans 2 and 3, thermal loading has a much larger effect on out-of-plane web displacements when the piers are modeled as rigid rather than flexible members, as is evidenced in Figures 6.10 and 6.11. Once again, areas on either side of the mid-span of the girders exhibit a much smaller magnitude of out-of-plane web displacement due to the presence of transverse stiffeners. For flexible pier models, out-of-plane web displacements in spans 2 and 3 of the girders increase by up to 69% when +45°F thermal loading is added to gravity loading, but decrease by up to 41% when -45°F thermal loading is added to gravity loading. The same is true for the case with rigid piers, but the magnitude of displacement increase and decrease is far greater. Results show an increase of up to 655% due to +45°F loading and a decrease of up to 653% due to -45°F thermal loading.

As is the case in spans 2 and 3, the addition of thermal loading has a larger impact on the out-of-plane web displacement of the girders of span 4 when the piers are modeled as rigid members rather than flexible members. This is shown in the profiles plotted in Figures B.17 – B.36 and in the results plotted in Figures 6.10 and 6.11. However, percentage change results in Tables 6.3 and 6.4 for span 4 can be somewhat misleading. The divisor in the equation determining percent change is the out-of-plane displacement under gravity loading. These values are very small, especially in comparison to temperature induced out-of-plane web displacements, leading to very high percent change values as a result of using very small numbers as divisors. In the case of rigid pier models loaded with +45°F uniform loading, out-of-plane web displacement increases away from the center of curvature in girder 1, increases toward the center of curvature (in negative direction) in girders 2-6, and seems to vary in girders 7 and 8. Results for -45°F uniform thermal loading appear to be fairly equal in magnitude but opposite in direction of the +45°F results.

The results explained in the preceding paragraphs of this section and the out-of-plane web displacement profiles in Figures B.17 – B.32 highlight how models with rigid and flexible piers behave differently when subjected to uniform thermal loading. Introducing pier flexibility causes temperature loading to have more of an overall structural effect on out-of-plane web displacement. On the other hand, when piers are assumed rigid, thermal loading seems to affect each span individually. All of the pier bearings supporting the four centermost girders are fixed bearings, serving to effectively tie the superstructure to the piers. Introduction of a uniform temperature increase or decrease onto the structure will cause the bridge to expand or contract, with the largest amount of expansion/contraction occurring along the bridge longitudinal direction because this is the longest bridge dimension.

As a result of this thermal expansion or contraction of the superstructure, forces will be transferred to the bridge piers according to the type of bearings present on the piers. Where the piers are modeled as flexible members, these forces transferred through the bearing cause the piers to displace. Results in Figures B.17 – B.32 show that the flexibility of the bridge piers greatly reduces the out-of-plane web deformation caused by thermal loading. Pier flexibility leads to thermal loading placing a level of global tensile (temperature decrease) or global compressive (temperature increase) forces along the length of each girder. Tensile forces placed on the I-girders by uniform -45°F thermal loading decrease the out-of-plane web displacement along the length of the girder. Conversely, compressive forces created by +45°F thermal loading increase the out-of-plane web deformation. When the bridge piers are modeled as flexible members, the effect that thermal loading has on the local web buckling is fairly consistent along the length of each girder.

On the other hand, modeling the bridge piers as rigid structures combined with the fixity of the pier bearings has the effect of causing each span to mostly behave individually when uniform temperature change is introduced. For span 1, the boundary conditions on the girders at abutment 1 provide only a slight resistance to movement in the longitudinal direction but the boundary conditions at pier 1 fully restrict girder movement in the longitudinal direction. As a

result, the span will expand under +45°F thermal loading, decreasing the out-of-plane web displacement at the mid-span and will contract under -45°F thermal loading, increasing mid-span out-of-plane web displacement. For the most part, the boundary conditions provided by the pier bearings fix the longitudinal movement of the girders in spans 2 and 3. Because the girders cannot to expand or contract when thermal conditions change, the thermal forces that are transferred to the piers in the flexible pier models instead remain in the girders. These additional thermal forces lead to the large amount of additional out-of-plane web displacements along the length of spans 2 and 3 seen in Figures B.17 – B.32.

Once again, as mentioned in Section 6.6, the boundary conditions on Span 4 would suggest that the girders in Span 4 are free to expand and contract under changing thermal conditions. Web out-of-plane displacement profiles in Appendix B indicate that this is not exactly true. Thermal loading leads to increased out-of-plane web displacement in either the positive or negative direction, depending on positive or negative temperature loading. With the addition of -45°F thermal loading, out-of-plane web displacement increases to the side of the web opposite the location of the transverse stiffeners (towards the center of curvature on girder 1, away from the center of curvature on girders 2-8). The opposite of this is true when a +45°F uniform thermal load is applied to the structure. Although, theoretically, the girders in Span 4 should be able to expand and contract to relieve thermally induced stresses, temperature loads are causing additional out-of-plane web displacements. Unsymmetrical bending moments about Pier 3 mentioned in Section 6.6 are partially responsible for these out-of-plane displacements along with thermal movement being restricted by a combination of the fixed bearings at Pier 3, rigid pier conditions, stiffened deck, and cross frames connecting the girders.

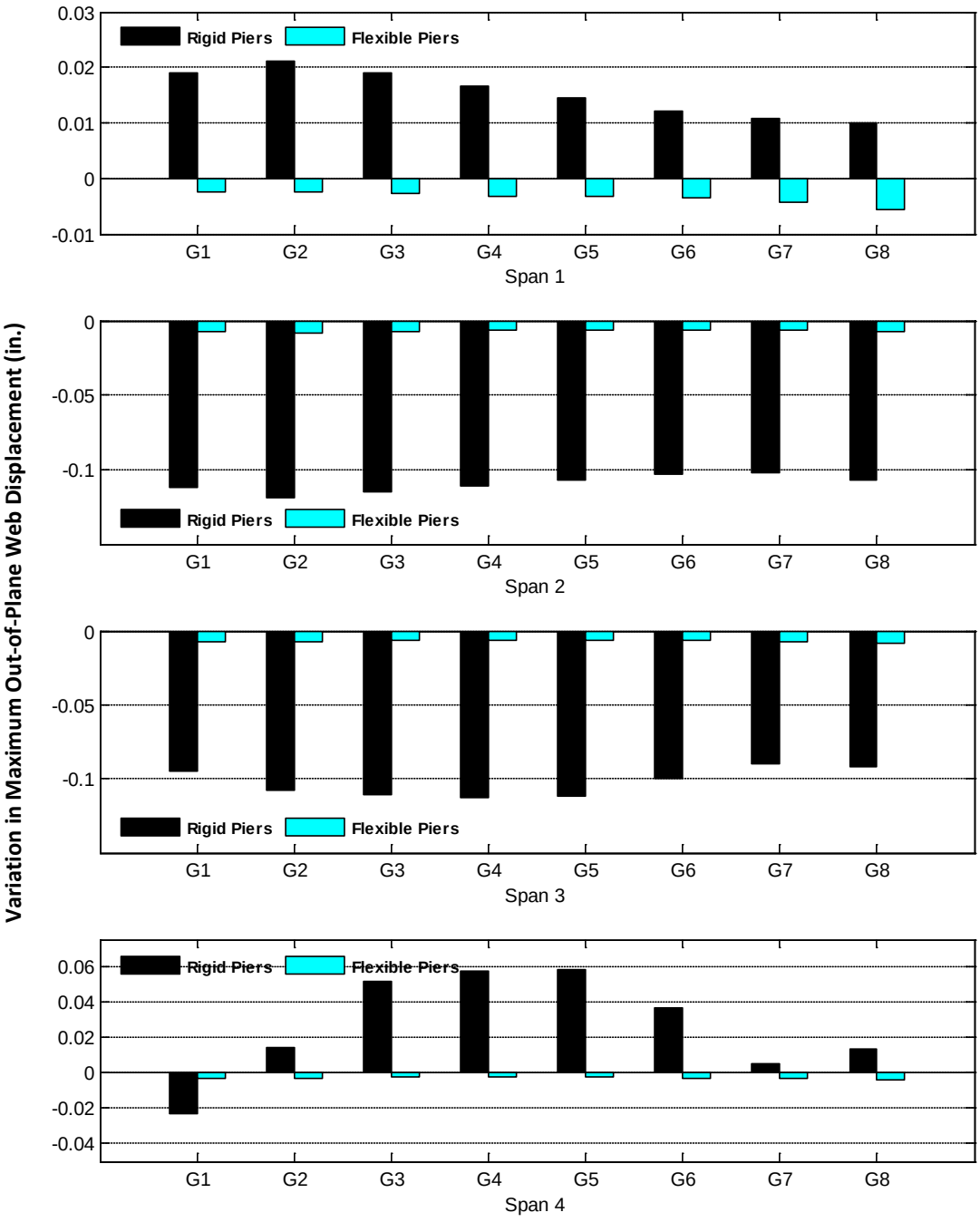


**Figure 6.10. Variation of Maximum Out-of-Plane Web Deformations with the Addition of -45°F Thermal Load**

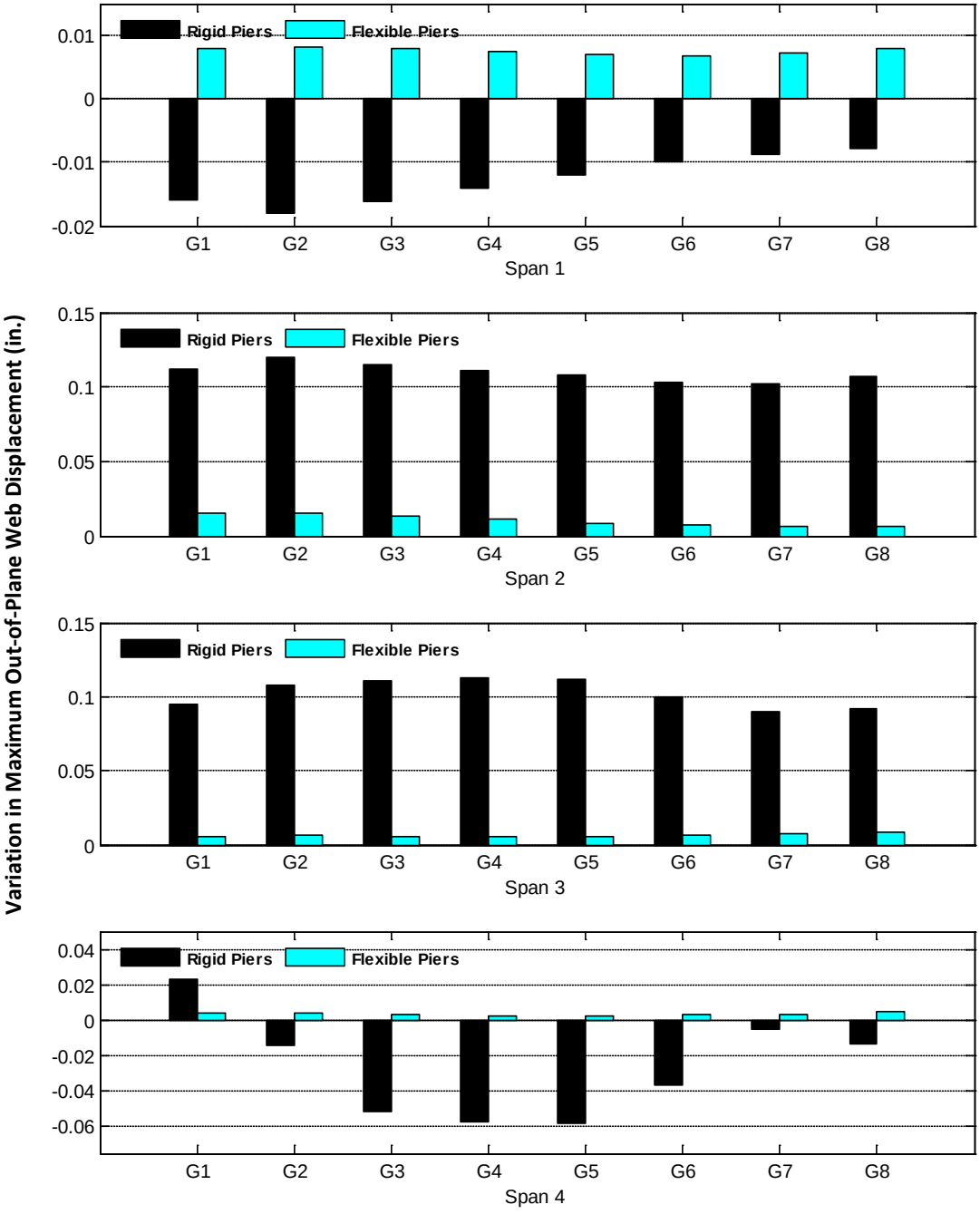


**Figure 6.11. Variation of Maximum Out-of-Plane Web Deformations with the Addition of +45°F Thermal Load**

**Table 6. 3. Percent Change in Out-of-Plane Web Centerline Displacement with Addition of -45°F Thermal Load**

| | | Span 1 | Span 2 | Span 3 | Span 4 |
|---|---|---|---|---|---|
| Girder 1 | Rigid | 62.03% | -490.08% | -756.54% | 22102.48% |
| | Flexible | -6.38% | -29.35% | -50.12% | 144146.58% |
| Girder 2 | Rigid | 117.21% | -653.82% | -776.67% | 446.10% |
| | Flexible | -11.55% | -41.71% | -57.32% | -597.60% |
| Girder 3 | Rigid | 107.98% | -572.96% | -645.33% | -2621.61% |
| | Flexible | -12.44% | -35.19% | -38.89% | 141.85% |
| Girder 4 | Rigid | 84.69% | -489.09% | -726.89% | -8743.08% |
| | Flexible | -15.62% | -29.29% | -41.33% | 1068.82% |
| Girder 5 | Rigid | 65.16% | -424.39% | -889.61% | -11249.91% |
| | Flexible | -11.84% | -24.35% | -45.06% | 326.17% |
| Girder 6 | Rigid | 36.95% | -322.85% | -1971.89% | 10080.48% |
| | Flexible | -11.08% | -18.77% | -86.17% | -62.95% |
| Girder 7 | Rigid | 33.41% | -304.24% | -694.23% | 169.64% |
| | Flexible | -13.59% | -18.46% | -55.79% | -117.03% |
| Girder 8 | Rigid | 32.03% | -293.46% | -1338.06% | -44.11% |
| | Flexible | -17.56% | -18.64% | -57.65% | 234.54% |

**Table 6. 4. Percent Change in Out-of-Plane Web Centerline Displacement with Addition of +45°F Thermal Load**

| | | Span 1 | Span 2 | Span 3 | Span 4 |
|---|---|---|---|---|---|
| Girder 1 | Rigid | -52.84% | 491.43% | 756.71% | -22102.85% |
| | Flexible | 20.76% | 53.14% | 38.99% | -164331.35% |
| Girder 2 | Rigid | -100.46% | 655.24% | 776.79% | -446.16% |
| | Flexible | 36.62% | 69.83% | 46.88% | 707.84% |
| Girder 3 | Rigid | -91.87% | 574.56% | 645.43% | 2621.83% |
| | Flexible | 34.61% | 60.30% | 32.03% | -174.74% |
| Girder 4 | Rigid | -71.40% | 490.53% | 727.02% | 8744.61% |
| | Flexible | 29.98% | 46.71% | 35.53% | -1088.46% |
| Girder 5 | Rigid | -54.79% | 425.67% | 889.81% | 11252.68% |
| | Flexible | 25.91% | 34.65% | 40.30% | 74.70% |
| Girder 6 | Rigid | -30.11% | 323.82% | 1972.35% | -10082.88% |
| | Flexible | 16.19% | 23.35% | 82.15% | 67.19% |
| Girder 7 | Rigid | -26.81% | 305.14% | 694.40% | -169.61% |
| | Flexible | 16.93% | 19.51% | 56.96% | 122.04% |
| Girder 8 | Rigid | -25.21% | 294.18% | 1338.26% | 44.13% |
| | Flexible | 25.07% | 17.56% | 60.86% | -257.15% |

Section 6.6 shows that I-girder local buckling is present on the Buffalo Creek Bridge after the introduction of gravity and thermal loading. The addition of thermal loads has a more significant impact on I-girder local buckling when the bridge piers are modeled as rigid members rather than flexible members. However, plots of the web out-of-plane displacement profiles for models with flexible piers show that pier movement does not relieve all thermal forces on the I-girders, which is assumed during design. Inevitably, the additional thermal displacements detailed in this section will lead to additional thermal stresses being placed on the girders, and this will be studied in Chapter 7. It is of note that local I-girder buckling is already present under these loading conditions, prior to any design loads being introduced on the structure.

## 6.8 Web Cross-Section Displacement – Gravity and Thermal Loading

In a similar manner as was done in Section 6.5 for the gravity loading case, it is necessary to study the web displacement profiles when the Buffalo Creek Bridge is loaded with thermal loading in addition to gravity loading. These web displacement profiles are investigated at the same locations on the girders (at mid-spans and piers) as were studied in Section 6.5. Figures B.33 – B.40 and Figures. B.41 – B.48 compare web displacement profiles at the center of each span for models with rigid and flexible piers when the bridge is loaded with +45°F and -45°F uniform thermal loading, respectively. Likewise, Figures B.49 - B.56 and Figures B.57 - B.64 offer the same web displacement profile comparisons at the bridge piers for +45°F and -45°F uniform thermal loading.

As was the case for gravity loading alone, Figures B.33 – B.48 give proof that the I-girders are experiencing lateral distortional buckling under only self-weight and thermal loading both when the piers are modeled as rigid and flexible members. Results show that the addition of thermal loading to the Buffalo Creek Bridge changes the web displacement profiles at all of the locations studied for both cases of modeling. Cross-section displacement profile plots in Appendix B

reveal that rigid pier models deflected web shapes are more significantly affected by thermal loading than is the flexible pier model deflected shape. Thermal loading has a noticeably more pronounced impact on local and torsional buckling of the I-girder cross section when the bridge piers are rigid. Although some cross section displacement profiles for the flexible pier models show changes in torsional and local buckling when thermal loading is added, the majority of the effect of thermal loading is seen in the lateral buckling of the cross section.

Plots in Appendix B give evidence that, with piers modeled as both rigid and flexible members, the I-girder web profiles are experiencing lateral distortional buckling under only self-weight and uniform thermal loading. Although there is no method in place to quantify this lateral distortional buckling, visual inspection of the web cross-section displacement plots leads to the conclusion that thermally induced lateral distortional buckling is more severe for bridge models with rigid piers. However, it is of concern that lateral distortional buckling is present for both loading cases because the loading conditions considered here are loads that will occur on the structure well before the bulk of the design loads are introduced. It is known that lateral distortional buckling of a web cross section will negatively affect the load carrying capacity of an I-girder section. So, if thermal loading is increasing the lateral distortional buckling in the I-girder cross section of the Buffalo Creek Bridge, it stands to reason that the addition of thermal loading is decreasing the load carrying capacity of the I-girders, before traffic is even introduced on the structure. However, the degree to which the buckling decreases the load carrying capacity cannot be determined from the displacement plots investigated in this study, but will be studied further in the following chapter when investigating the stresses in the Buffalo Creek Bridge.

## 6.9 Discussion and Conclusions

It is apparent from the results presented in the preceding sections that curved I-girder bridges are susceptible to experiencing lateral distortional buckling during bridge construction and at

the early stages of the life of the structure, prior to the introduction of any live loading. Both global and local buckling of the bridge I-girders is observed after the construction of the superstructure, but before any loading other than gravity loading is present on the bridge. At these initial stages, considering pier flexibility does not have a significant impact on local I-girder buckling but does lead to a larger magnitude of global buckling compared to considering the piers are rigid members. These are notable conclusions because previous studies attribute initial girder buckling and imperfections to fabrication errors/imperfections, transportation, erection, and a host of other factors. The study here shows that I-girder imperfections and initial buckling occurs in the curved I-girder bridge purely due to the weight of the superstructure, and is not a result of any imperfections or errors.

Adding a uniform thermal load to the gravity load displaced Buffalo Creek Bridge results in additional global and local buckling for both the rigid and flexible pier cases. When the piers are modeled as flexible members, thermal expansion and contraction cause movement in the piers. This movement allowed at the piers permits the entire superstructure to expand and contract more or less as one continuous unit as temperature changes, thereby reducing the impact that thermal loading has on the global and local I-girder buckling. However, combined with gravity loading effects, the case with flexible piers exhibits overall greater global girder buckling than the rigid pier case because of the movement allowed by the bridge piers. Conversely, thermal expansion and contraction are not accommodated by pier movement when the piers are rigid. The resistance to thermal movement by the fixed bearings leads to additional global and local bucking of the I-girders. Thermal loading causes a larger degree of lateral distortional buckling in the I-girder cross sections when the piers are modeled fully rigid. In addition, although the global buckling caused by gravity and thermal loading combined is greater for the flexible pier models, the impact thermal loading only has on I-girder global and local buckling is larger when the bridge piers are rigid.

Bridge design assumes that any thermal stresses placed on the bridge by changing temperature conditions will be relieved by allowing movement of the superstructure through the design of

the bridge bearings, pier movement, or some combination of the two. Results presented in this chapter show that even when these conditions are ideal, meaning the bearings are functioning exactly as they were designed and the piers are permitted to deform, thermal loading still causes lateral girder deformation and lateral distortional girder buckling. In reality, the Buffalo Creek Bridge's response to changing thermal conditions is likely somewhere between the fully rigid and fully flexible pier case presented here. Previous studies have assumed or concluded that initial buckling in I-girder bridges is caused by imperfections from fabrication, transportation, erection, or some other human factors. While this may still be the case, data and conclusions in this chapter clearly show that imperfections arise in curved I-girders before the introduction of design loads due simply to the self-weight of the structure and uniform thermal loading. When combined with the imperfections documented and studied by other researchers, the results given in this chapter will likely be more exaggerated.

# CHAPTER SEVEN

# BUFFALO CREEK BRIDGE I-GIRDER WEB STRESSES

## 7.1 Introduction

In theory, steel I-girder bridges are generally designed such that the bearing configuration allows the superstructure to expand and contract as a result of uniform thermal loading, minimizing or alleviating any thermal forces on the bridge. More specifically, the design sheets for the Buffalo Creek Bridge do not contain any calculations or values for thermal forces on the structure, the only thermal considerations are the amount of expansion and contraction of the bridge expansion joints. However, studies by McBride (2005) and Beckett (2011) show that bridge bearing design will not fully accommodate thermal movements and uniform thermal loading can induce significant levels of axial stress in the I-girders of both straight and curved steel I-girder bridges. As these stresses are not accounted for during design, their introduction combined with stresses considered during design may complicate the bridge behavior.

This chapter studies the effect that introducing uniform thermal loading to the Buffalo Creek Bridge will have on the state of stress in the steel I-girders. Section 7.2 presents results for how thermal loading effects the overall state of stress in the I-girder webs and what impact this has on girder stress capacity. Section 7.3 studies thermally induced longitudinal web stresses and how these stresses affect the web buckling behavior. Axial web stresses and I-girder capacity are investigated in Section 7.4 while Section 7.5 looks at how thermal loading effects bridge I-girder capacity in terms of bending and axial stresses.

## 7.2 Effective Web Stress

Results in Chapter 6 show that the bearings of the Buffalo Creek Bridge do not perform in a way that alleviates all thermal effects on the bridge girders, no matter if the piers are modeled as rigid or flexible members. Uniform thermal loads have been shown to increase both global and local bucking of the steel I-girders, and studies have previously shown that increase in the early age bucking of steel I-girders will be detrimental to their load carrying capacity. The degree to which these unanticipated thermal loads impact structural capacity can be investigated through the study of the effective stress in the I-girder sections. In ADINA (2009), the effective stress at a node is the measure of the overall state of stress at that node. ADINA (2009) computes effective stress by interpolating the stress components individually; then, after interpolation, ADINA (2009) computes effective stress using the formula:

$$\sigma_e = \sqrt{\frac{1}{2}\left(\left(\tau_{xx}-\tau_{yy}\right)^2+\left(\tau_{xx}-\tau_{zz}\right)^2+\left(\tau_{yy}-\tau_{zz}\right)^2+6\left(\tau_{xy}+\tau_{xz}+\tau_{yz}\right)\right)} \qquad (7.1)$$

where $\tau$ represents the individual stress components. At each location, the effective stress can be compared to the yield stress of the material to determine if the section has reached its material yield point.

The design of the Buffalo Creek Bridge accounts for the displacement, and associated stress, caused on the I-girders by the self-weight of the superstructure. However, design does not take into consideration any stresses induced on the I-girders via thermal loads. Any additional effective stress on the I-girders caused by thermal loading will decrease the capacity of the girders available to accommodate all subsequent loads. The first step in studying how thermal loading and thermal buckling impact the load carrying capacity of the Buffalo Creek Bridge I-girders is plotting the effective stress profile of the I-girder webs when subjected to gravity and both -45°F and +45°F thermal loading. Figures C.1 – C.8 contain effective web stress profiles at

the center of each girder span (same locations displacements were plotted in Chapter 6) in regions likely to experience the largest positive moment when the bridge is loaded with gravity and gravity followed by -45°F temperature loading. Figures C.9 – C.16 show similar plots but with +45°F temperature applied. Effective stress profiles in Figures C.17 – C.24 have been taken at the same pier locations, where the girders experience the largest negative moment, as the displacements in Chapter 6 and show results when the structure is loaded with gravity and gravity followed by -45°F temperature. Finally, Figures C.25 – C.32 plot pier effective stress profiles for gravity and gravity plus +45°F temperature.

Results in Figures C.1 – C.32 reveal that modeling the bridge piers as rigid or flexible members has little to no effect on the effective stress profiles at the girder mid-spans and piers under gravity loading. In fact, the difference in effective stress between the two types of modeling is such that no difference can be visually determined in the Figures in Appendix C. The effective stress profiles are also mostly symmetric about the web centerline for the gravity loading case, except directly over the bridge piers. Because effective stress is a measure of a sections overall state of stress, the symmetry of these effective stress profiles indicates the bending moment of the section being the dominant straining action on the cross section, which agrees with the design assumptions.. This is not exactly the case directly over the piers because of the influence of the bridge bearings and stiffeners. The addition of uniform thermal loading has minimal impact on the effective stress in the cross sections under investigation when the bridge piers have flexibility. However, web effective stress profiles are impacted by uniform temperature loading when the bridge piers are assumed rigid and profiles show that temperature loading, both -45°F and +45°F, cause the effective stress profiles to no longer exhibit symmetry about the web centerline, especially in the center of spans 2, 3, and 4. This is an indication that thermal loading may be introducing an axial stress component to the web stress profile.

As previously mentioned, effective stress at a location is useful in determining if the material has reached the point of yielding. The Buffalo Creek Bridge I-girder webs in the majority of

each span are constructed of AASHTO M270, Grade 50W structural steel with yield strength of 50 ksi. At each pier, I-girder webs are made with ASTM A709, Grade HPS70W structural steel with yield strength of 70 ksi. Investigation of the plots in Figures C.1 – C.32 reveals that the stress levels in the I-girder webs do not reach these critical yield stress levels at any locations under the effect of gravity and uniform thermal loading. Although the effective stress levels in the I-girder webs do not indicate yielding in the webs as a result of gravity and thermal loading, the additional magnitude of effective stress induced by thermal loads are stresses that are not accounted for during bridge design. This additional, unaccounted for level of stress prior to the introduction of design loads decreases the capacity of the I-girder webs available to handle design loading.

In order to determine the degree to which thermal loading affects the load carrying capacity of each I-girder section as it pertains to yielding of the web panel, the maximum effective stresses in I-girder web sections under each loading condition are calculated. Comparisons are made between the maximum effective web stress caused by gravity loading and maximum effective web stress caused by gravity and temperature loading and plotted in Figures 7.1 – 7.8. Bar graphs in Figures 7.1 – 7.8 overlay the maximum effective web stress at a specific cross section caused by self-weight with the maximum effective web stress at the same location due to gravity and temperature. Figures 7.1 and 7.2 plot effective stress comparisons at the girder mid-span cross sections, Figures. 7.3 and 7.4 plot comparisons at the pier 1 cross sections, Figures 7.5 and 7.6 plot comparisons at pier 2 cross sections, and Figures 7.7 and 7.8 plot comparison at pier 3 cross sections.

Figures 7.1 – 7.8 confirm that the maximum effective stresses in the I-girder cross sections of the Buffalo Creek Bridge studied here do not reach the level of the material yield stress under gravity and thermal loading and that thermal loading has a very small effect on the web maximum effective stress when the bridge piers have flexibility. However, when the bridge piers are modeled as rigid members, a uniform thermal load placed on the bridge model results

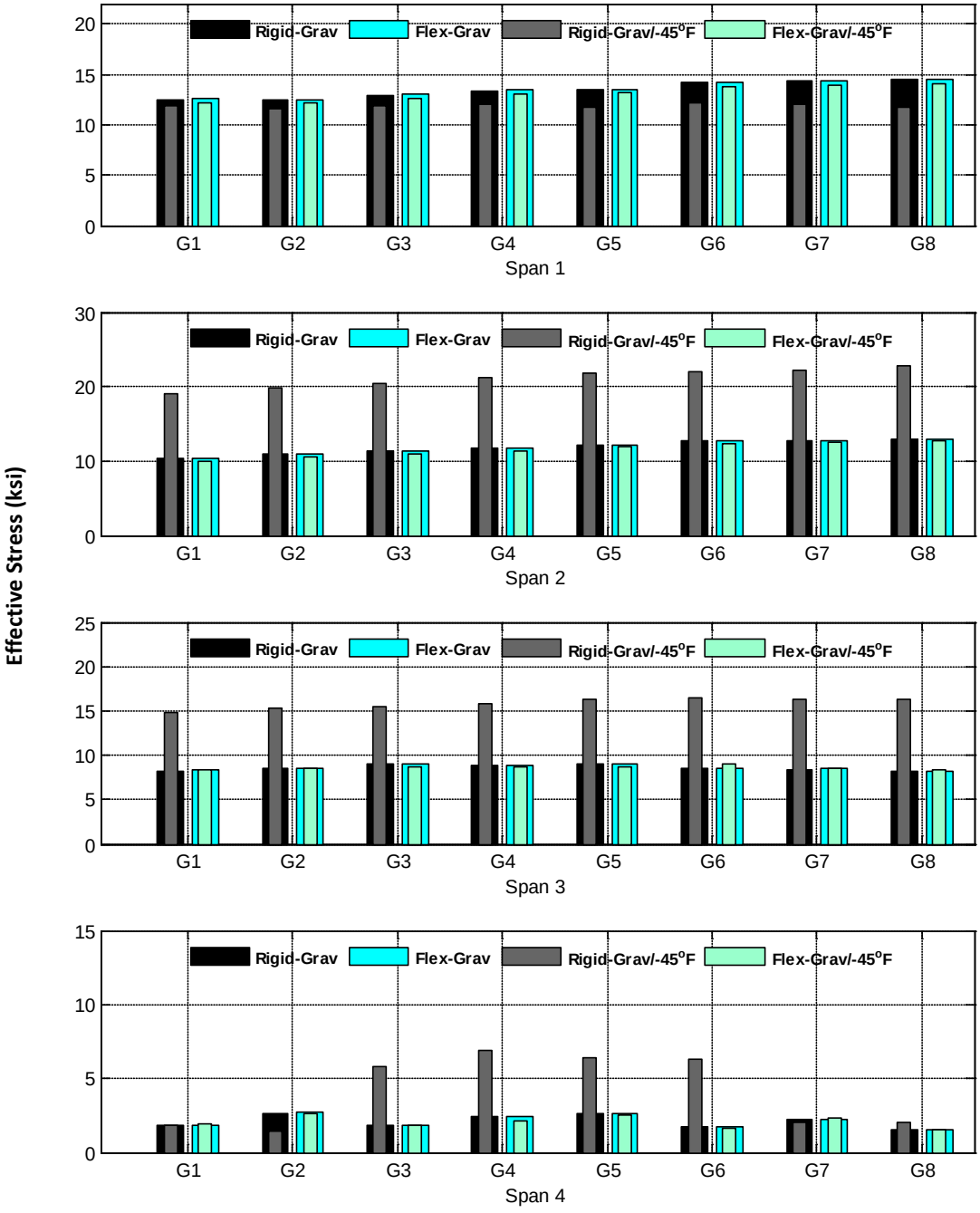


**Figure 7.1. Maximum Effective Web Stress Comparison – Mid-Spans – Gravity and -45°F Thermal Loading**

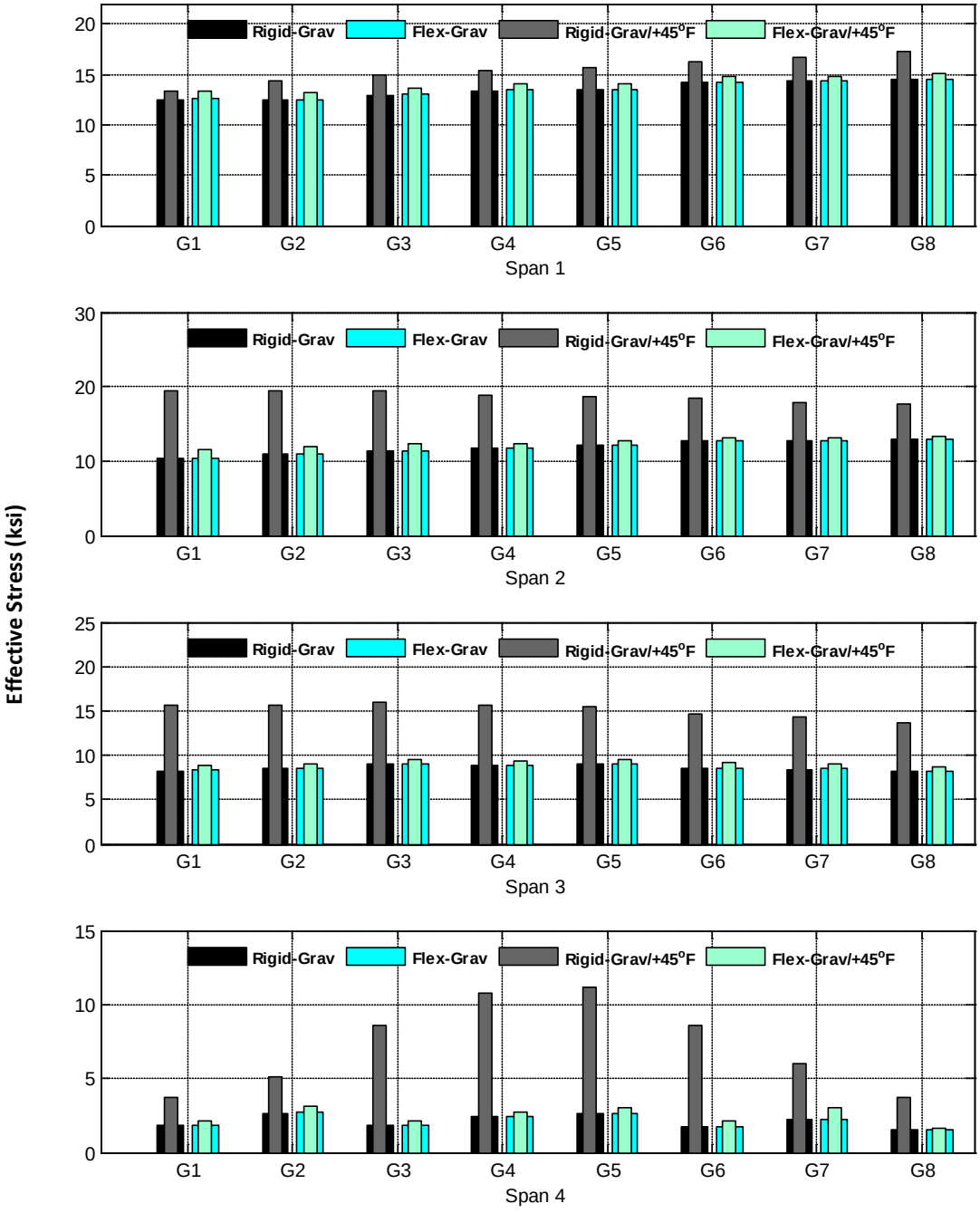


**Figure 7.2. Maximum Effective Web Stress Comparison – Mid-Spans – Gravity and +45°F Thermal Loading**

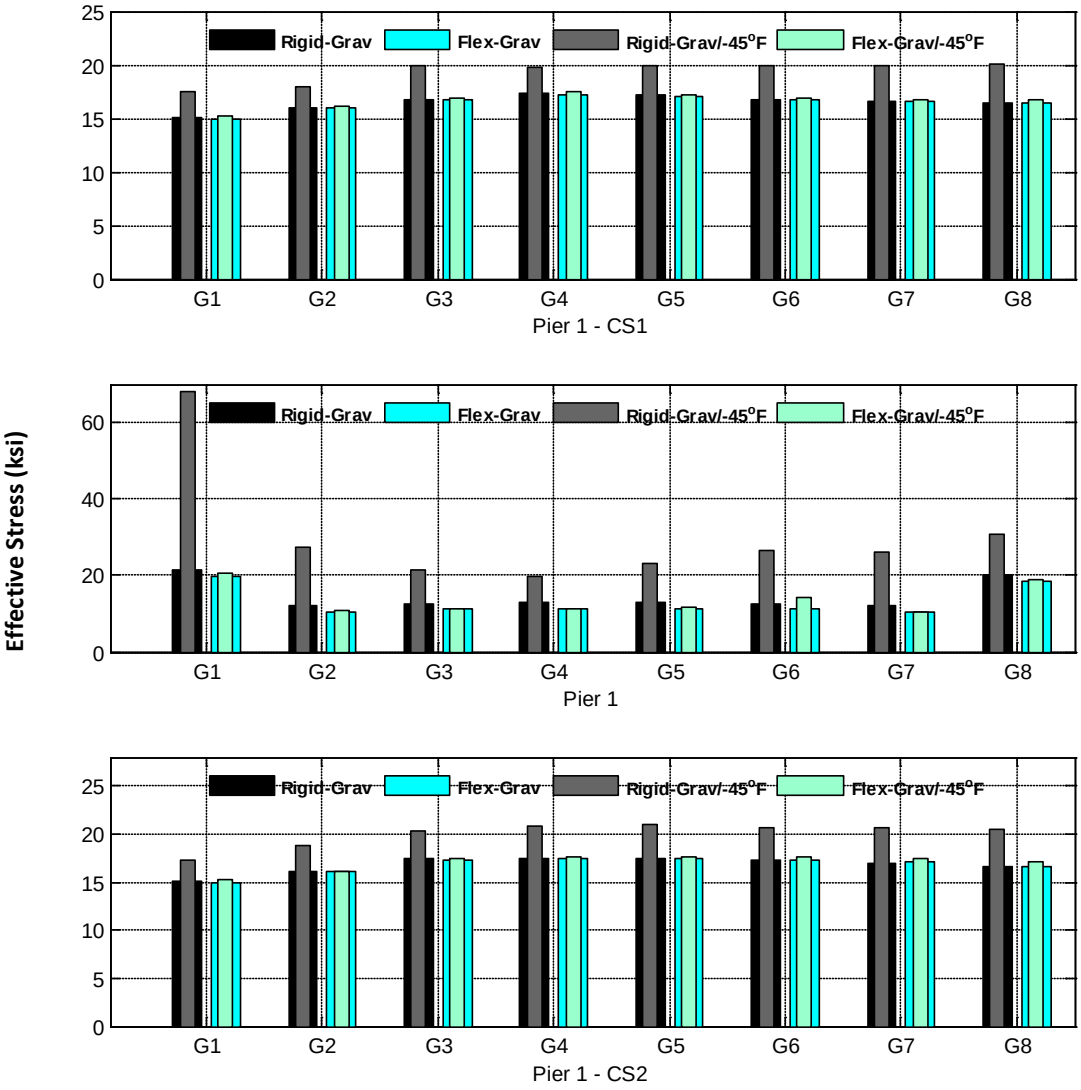


**Figure 7.3. Maximum Effective Web Stress Comparison – Pier 1 – Gravity and -45°F Thermal Loading**

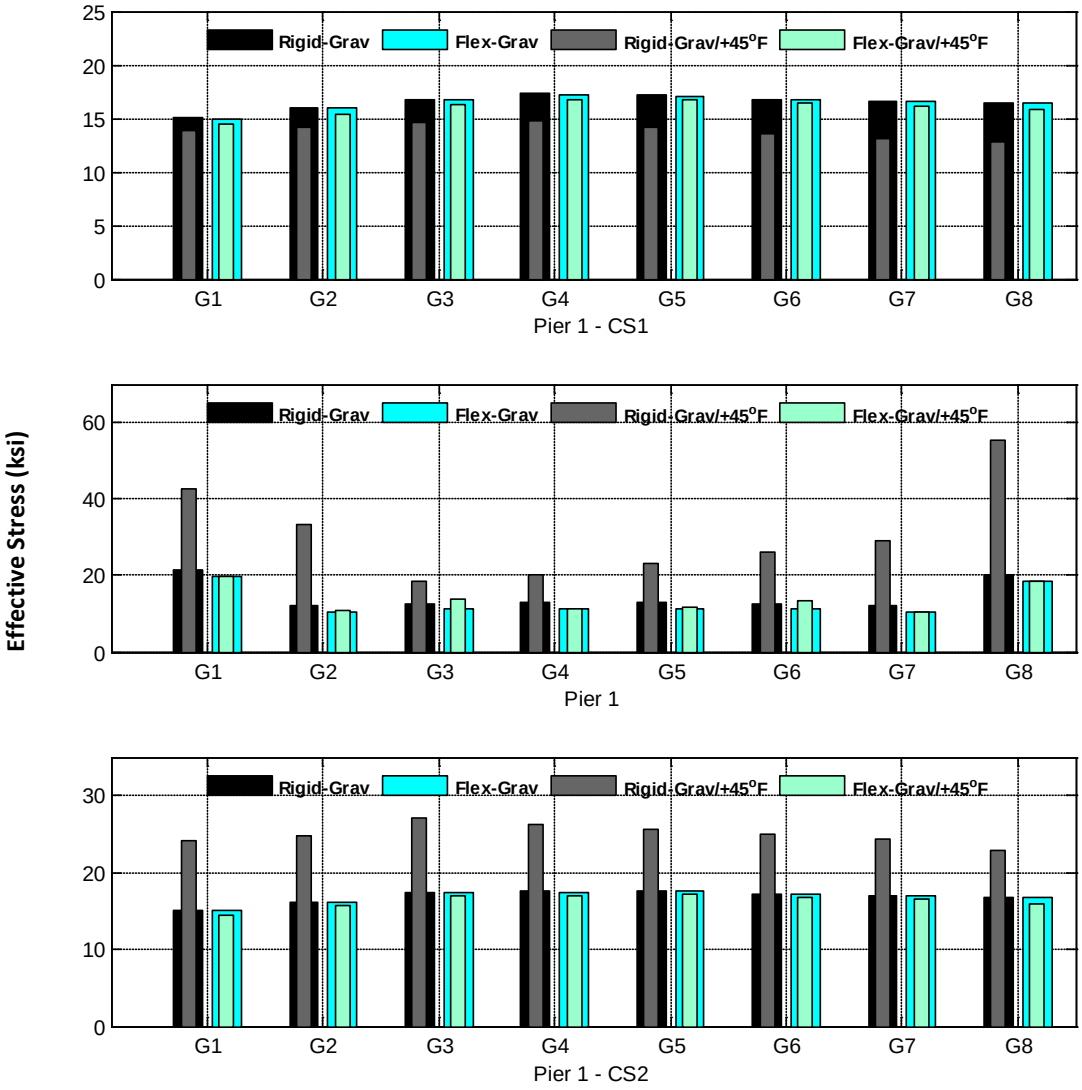


**Figure 7.4. Maximum Effective Web Stress Comparison – Pier 1 – Gravity and +45°F Thermal Loading**

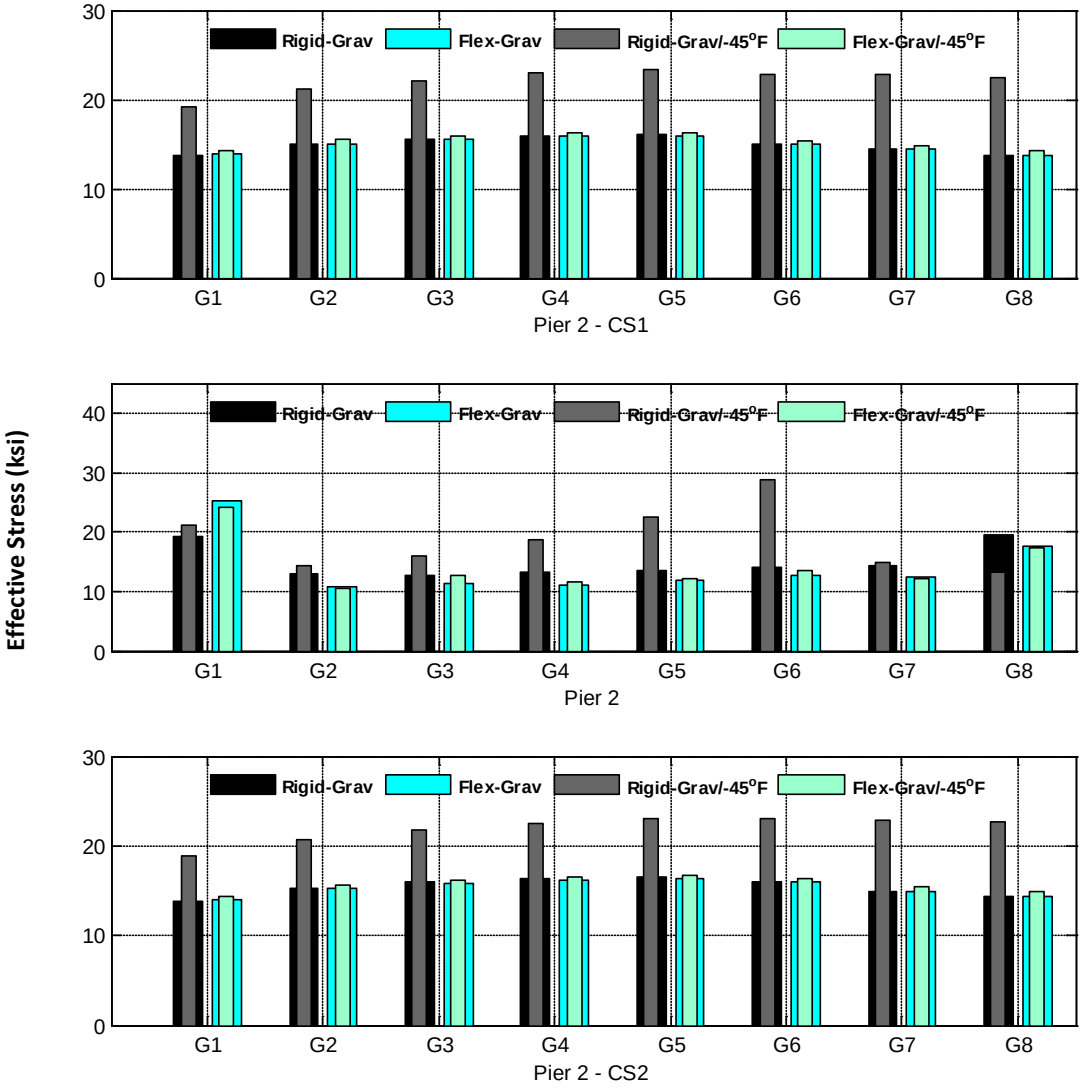


**Figure 7.5. Maximum Effective Web Stress Comparison – Pier 2 – Gravity and -45°F Thermal Loading**

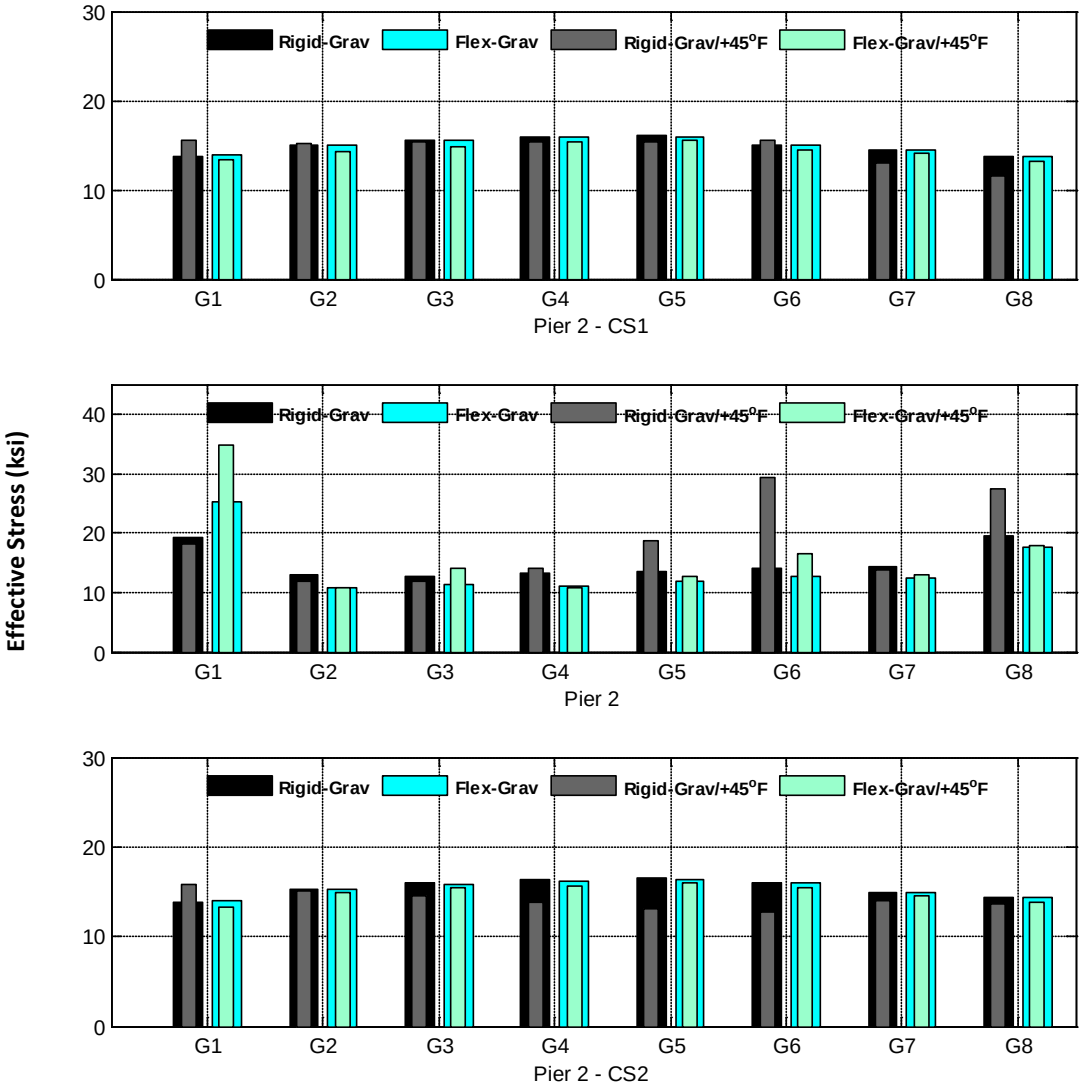


**Figure 7.6. Maximum Effective Web Stress Comparison – Pier 2 – Gravity and +45°F Thermal Loading**

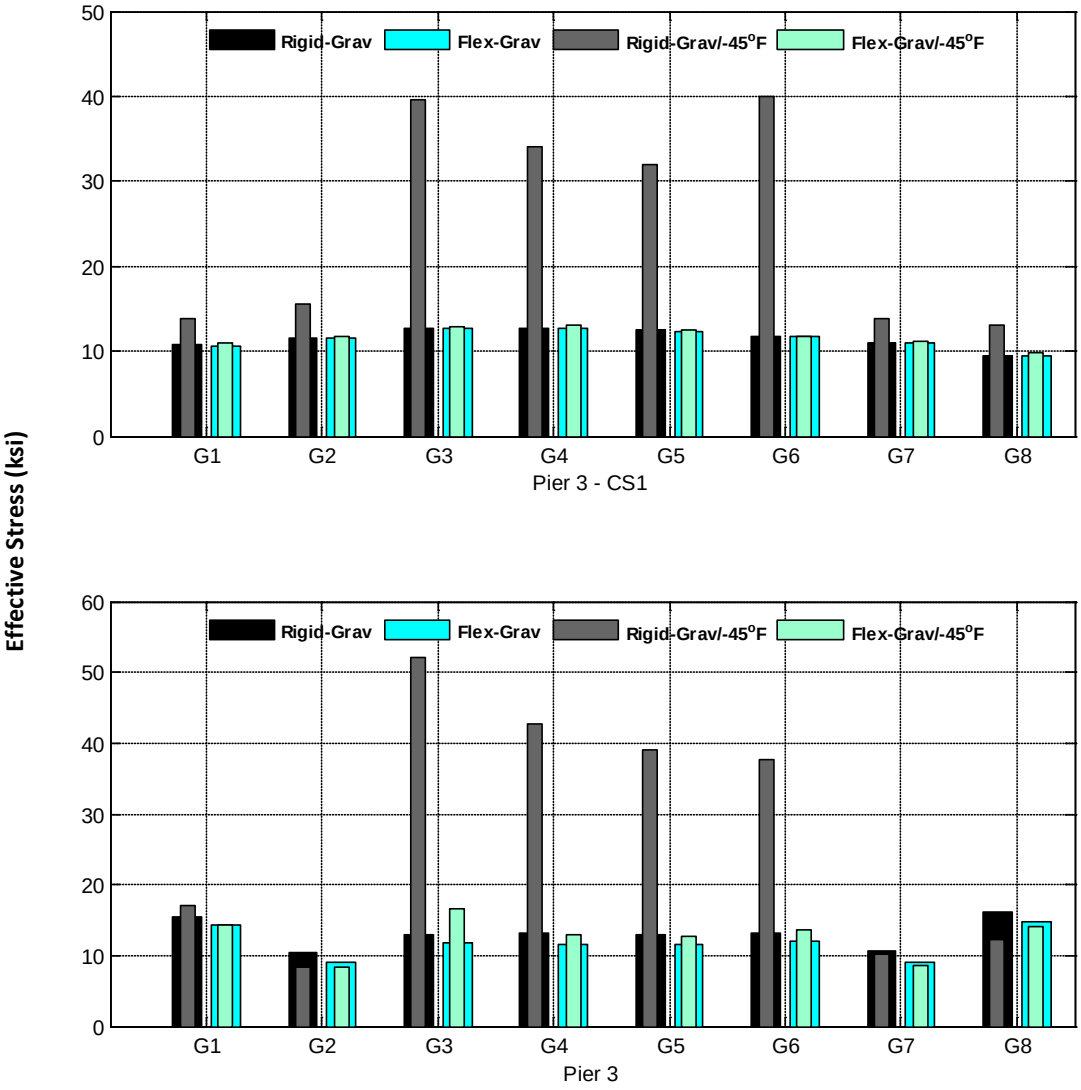


**Figure 7.7. Maximum Effective Web Stress Comparison – Pier 3 – Gravity and -45°F Thermal Loading**

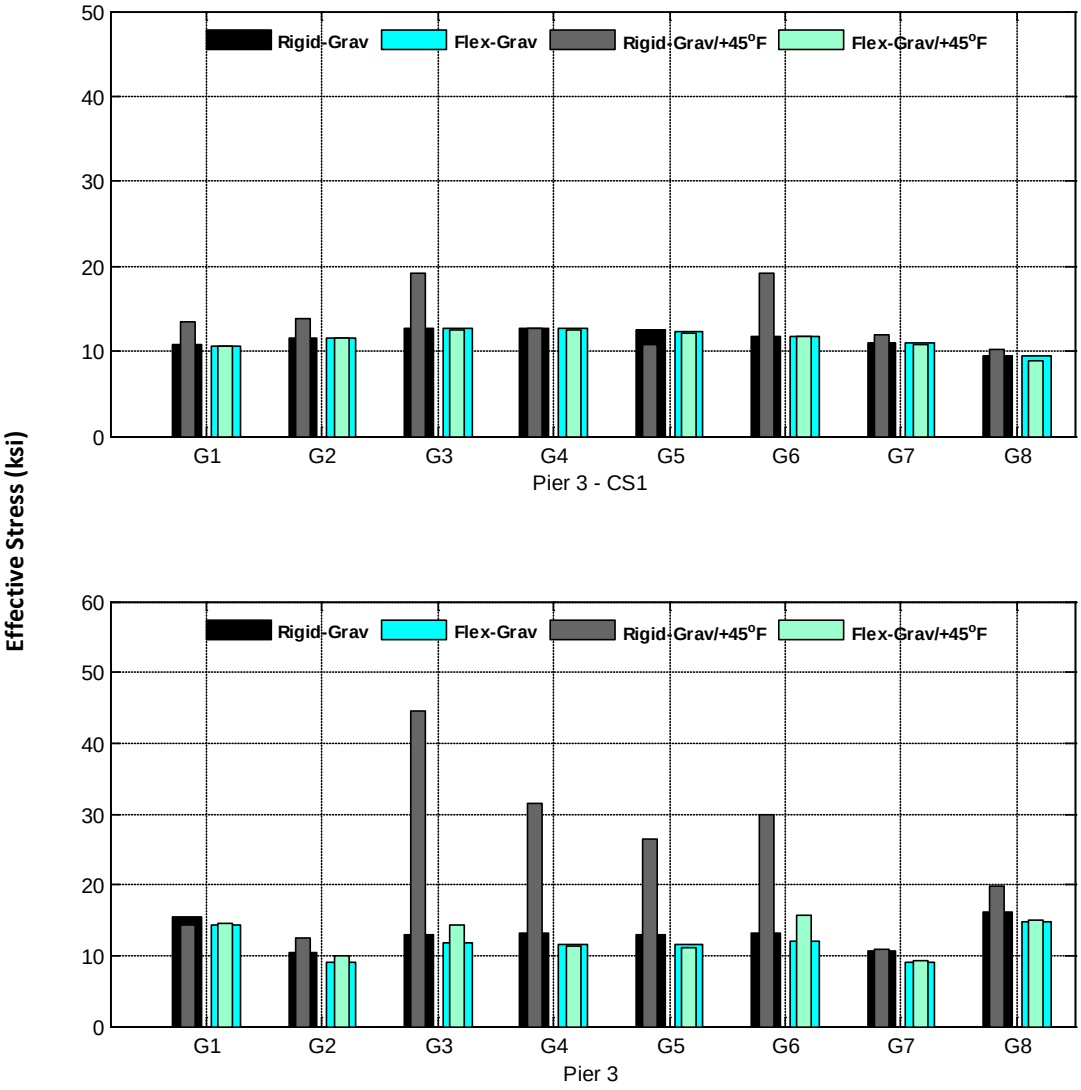


**Figure 7.8. Maximum Effective Web Stress Comparison – Pier 3 – Gravity and +45°F Thermal Loading**

in changes in the maximum effective web stress in each cross section. Once again, effective webs stresses caused by gravity and thermal loading do not lead to web stress levels exceeding the material yield stress. However, the loading cases studied are inducing effective web stresses approaching and even exceeding 50% of the material yield stresses (25 ksi at mid-spans and 35 ksi at and near the piers). Thermal stresses are typically assumed to be relieved through the design of the bearing orientation, so any thermally induced stresses are additional stresses that are not part of the overall stress state of the structure considered when the bridge was designed. Being that the material used, and thus the girders, can only experience a finite level of stress before reaching the yield point, the unaccounted for thermal stresses will lower the stress capacity available for the girders to handle design loads and other unexpected loads, and therefore, ultimately, lower the factor of safety that the bridge was designed with.

To what degree thermally induced web stresses reduce the load carrying capacity of the Buffalo Creek Bridge when the bridge piers are assumed rigid is determined by comparing the material yield stress to the gravity and thermal stress states. This comparison will be made by representing both the gravity and thermal stress magnitudes as percentages of allowable stress before material yielding. For instance, at the mid-span locations the web material yield stress is 50 ksi. If the gravity load causes a maximum effective stress in the web of 10 ksi, this represents 20% of the allowable material yield stress. At that same location, if the addition of thermal loading raises the maximum effective stress to 15 ksi, then the web stress level is at 30% of the allowable material yield stress, with thermal stress consuming 10% of the capacity. The additional capacity consumed by thermal loading is investigated in this study because, as mentioned earlier, web stress levels due to the weight of the superstructure are already accounted for during bridge design and stress levels due to temperature loading are not.

Results in Tables 7.1 and 7.2 represent the percentage of maximum yield strength of each cross section that is consumed by stresses resulting from uniform thermal loading on the Buffalo Creek Bridge with piers modeled as rigid members. The flexible pier loading case is not studied here because the impact of thermal loading on the effective web stress for this case was found

to be very small. For the cases studied, at some locations the impact of temperature is very small or may even reduce the overall maximum effective stress in the web compared to gravity loading effective stress levels. On the other hand, there are many locations where the magnitude of increase in maximum effective stress with the addition of temperature is significant.

First, stresses at the middle of each span that are plotted in Figures C.1 – C.16, 7.1, and 7.2 will be investigated followed by the stresses at the piers plotted in Figures C.17 – C.32 and 7.3 – 7.6. Results for mid-span maximum effective web stresses plotted in Figures 7.1 and 7.2 show that uniform thermal loading has a less significant impact on the maximum effective web stress in span 1 than in any of the other three spans. For both rigid and flexible pier models, temperature decrease slightly decreases web effective stress and temperature increase slightly increases effective web stress. The largest stress levels are seen when the rigid pier models are loaded with +45°F loading and the stresses range from 13.3 ksi (26.6% of yield strength) in girder 1 to 17.2 ksi (34.4% of yield strength) in girder 8. Uniform positive thermal loading increases maximum effective web stress between 6.4% and 18.6% over gravity load while uniform negative thermal loading decreases maximum effective web stress from -4.8% to -18.7% compared to gravity loads. As shown in Table 7.1, when bridge piers are rigid and the bridge is loaded with +45°F thermal loading, the stresses in span 1 caused by temperature will consume between 1.67% and 5.48% of the available web stress capacity.

Girders in span 2 show a larger response to thermal loading than those in spans 1, in terms of maximum effective web stress, when the bridge piers are rigid. With flexible piers, temperature decrease slightly decreases the web stress level and temperature increase slightly increases web stresses, although the magnitude is very small and not investigated any further in this section. On the other hand, both positive and negative temperature loading increase the maximum effective web stress when piers are rigid. When loaded with gravity loading followed by -45°F thermal loading, the maximum effective web stresses in span 2 range from 19.0 ksi (38% of yield strength) in girder 1 to 22.8 ksi (45.6% of yield strength) in girder 8. Gravity

**Table 7. 1. Percent of Maximum Yield Strength in Mid-Span I-Girder Webs Consumed by Thermal Loading**

| | | Span 1 | Span 2 | Span 3 | Span 4 |
|---|---|---|---|---|---|
| -45°F | Girder 1 | -1.25% | 17.41% | 13.33% | 0.15% |
| | Girder 2 | -1.68% | 18.04% | 13.71% | -2.50% |
| | Girder 3 | -2.13% | 18.29% | 12.78% | 7.90% |
| | Girder 4 | -2.77% | 18.90% | 13.82% | 8.98% |
| | Girder 5 | -3.46% | 19.10% | 14.61% | 7.61% |
| | Girder 6 | -4.00% | 18.53% | 15.93% | 9.32% |
| | Girder 7 | -4.64% | 19.10% | 15.81% | -0.44% |
| | Girder 8 | -5.36% | 19.66% | 16.16% | 1.12% |
| +45°F | Girder 1 | 1.67% | 18.40% | 14.92% | 3.85% |
| | Girder 2 | 3.88% | 17.10% | 14.43% | 4.96% |
| | Girder 3 | 3.88% | 16.08% | 13.99% | 13.47% |
| | Girder 4 | 3.96% | 14.20% | 13.42% | 16.60% |
| | Girder 5 | 4.31% | 12.77% | 13.07% | 17.06% |
| | Girder 6 | 4.19% | 11.39% | 12.13% | 13.86% |
| | Girder 7 | 4.79% | 10.38% | 11.90% | 7.46% |
| | Girder 8 | 5.48% | 9.58% | 11.09% | 4.45% |

**Table 7. 2. Percent of Maximum Yield Strength in Pier I-Girder Web Consumed by Thermal Loading**

| | | Pier 1/CS1 | Pier 1 | Pier 1/CS2 | Pier 2/CS1 | Pier 2 | Pier 2/CS2 | Pier 3/CS1 | Pier 3 |
|---|---|---|---|---|---|---|---|---|---|
| -45°F | Girder 1 | 3.46% | 66.57% | 3.16% | 7.78% | 2.79% | 7.12% | 4.48% | 2.39% |
| | Girder 2 | 2.78% | 21.81% | 3.84% | 8.74% | 1.87% | 7.72% | 5.83% | -2.93% |
| | Girder 3 | 4.61% | 12.72% | 4.13% | 9.35% | 4.70% | 8.44% | 38.55% | 55.94% |
| | Girder 4 | 3.44% | 9.85% | 4.76% | 9.93% | 7.74% | 8.88% | 30.35% | 42.39% |
| | Girder 5 | 4.03% | 14.85% | 4.96% | 10.58% | 13.15% | 9.39% | 27.87% | 37.14% |
| | Girder 6 | 4.46% | 20.13% | 5.03% | 11.18% | 21.27% | 10.19% | 40.23% | 34.94% |
| | Girder 7 | 4.83% | 19.94% | 5.16% | 12.02% | 0.75% | 11.25% | 4.16% | -0.38% |
| | Girder 8 | 5.21% | 15.07% | 5.42% | 12.56% | -8.90% | 11.79% | 5.21% | -5.39% |
| +45°F | Girder 1 | -1.87% | 30.29% | 12.91% | 2.43% | -1.49% | 2.76% | 3.91% | -1.43% |
| | Girder 2 | -2.56% | 30.36% | 12.31% | 0.20% | -1.47% | -0.48% | 3.32% | 2.94% |
| | Girder 3 | -3.01% | 8.54% | 13.98% | -0.37% | -1.43% | -1.96% | 9.18% | 45.21% |
| | Girder 4 | -3.59% | 10.14% | 12.55% | -0.77% | 1.24% | -3.68% | -0.15% | 26.43% |
| | Girder 5 | -4.17% | 14.75% | 11.68% | -0.88% | 7.56% | -4.81% | -2.38% | 19.15% |
| | Girder 6 | -4.57% | 19.35% | 11.15% | 0.67% | 22.04% | -4.61% | 10.63% | 23.91% |
| | Girder 7 | -4.93% | 24.36% | 10.40% | -1.97% | -0.71% | -1.18% | 1.51% | 0.59% |
| | Girder 8 | -5.28% | 50.37% | 8.98% | -2.98% | 11.27% | -1.05% | 0.96% | 5.45% |

loading followed by +45°F thermal loading results in maximum effective web stresses in span 2 from 19.5 ksi (39% of yield strength) in girder 1 to 17.7 ksi (34.4% of yield strength) in girder 8.

A uniform temperature drop of -45°F increases maximum effective web stress in span 2 by between 76.7% (girder 8) and 84.5% (girder 1) and a uniform temperature increase of +45°F also increases maximum effective web stress in span 2 by between 37.2% (girder 8) and 89.3% (girder 1) compared to gravity loading stress levels. Table 7.1 results show that effective web stresses as a result of -45°F loading account for up to 19.6% of allowable stresses in the I-girder webs while effective web stresses from +45°F loading accounts for up to 18.4% of allowable stresses in the I-girder webs.

The effect that thermal loading has on the maximum effective web stress in the girders of span 3 is similar to the effect it has on span 2, with only the magnitude of the stresses being different. In span 3, gravity followed by -45°F loading results in maximum effective web stresses ranging from 14.9 ksi (29.8% of yield stress) in girder 1 to 16.2 ksi (32.4% of yield stress) in girder 8. Adding a +45°F load to gravity yields maximum effective web stresses from 15.7 ksi (31.4% of yield) in girder 1 to 13.7 ksi (27.4% of yield stress) in girder 8. Introducing -45°F to the model increases stress levels by between 81.7% (girder 1) and 100% (girder 8) and adding +45°F loading increases stress levels by between 69.1% (girder 8) and 91.5% (girder 1). Stress levels induced in the girders of span 3 from uniform -45°F temperature alone consume up to 16.16% of the web stress capacity and stress levels in the girders of span 3 via +45°F temperature alone consume up to 14.92% of the web capacity.

Girder web effective stresses in span 4 are affected differently by thermal loading than the girders in spans 1-3. One similarity is that when the bridge piers are flexible, temperature change has a minimal effect on web effective stresses with temperature decrease causing a slight stress decrease and temperature increase causing a slight stress increase. As Figures 7.1 and 7.2 show, +45°F loading has a greater impact on the maximum effective web stress than -45°F loading. The effective web stresses of the four innermost girders are impacted the most

significantly by thermal loads. Uniform -45°F thermal loading combined with gravity loading creates maximum effective web stresses in span 4 reaching up to 6.9 ksi (13.8% of yield stress) which occurs in girder 4 while gravity loading combined with +45°F thermal loading leads to maximum effective web stresses up to 11.1 ksi (22.2% of yield stress) in girder 5. In the center of span 4 at girder 4, the maximum effective web stress increases by 184% when -45°F thermal load is applied to the structure. Furthermore, a +45°F load on the structure causes the maximum effective web stress in girder 4 to increase by 340%. The degree to which thermal loading increases effective stress over the stress levels from gravity loading in span 4 is larger than the percentage of increase in previous spans, but the overall magnitude of gravity and thermally induced stresses is smaller. Table 7.1 shows, in bridge span 4, that effective web stress from -45°F thermal loading alone consumes up to 9.32% of the web stress capacity in girder 6 and effective web stress from +45°F thermal loading alone accounts for 17.06% of the web stress capacity in girder 5.

Results discussed in the preceding paragraphs and plotted in Figures C.1 – C.16, 7.1, and 7.2 reveal that thermal loading affects the overall state of stress of the I-girder webs at the center of bridge spans to varying degrees based on the boundary conditions on the girders. When the boundary conditions are such that pier flexibility allows movement of the girders at the piers, thermal loading has a very small effect on the overall stress state of the webs at girder mid-spans. Overall, with flexible piers, positive uniform thermal loading slightly increases and negative uniform thermal loading slightly decreases the effective web stresses at the girder mid-spans. Thermal loading, both positive and negative, has a measureable effect on both the effective web stress profiles and the maximum effective web stress at girder mid-spans when the bridge piers are rigid. The impact on effective stress is the most significant in spans 2 and 3 because bridge bearings on piers 1 and 2 restrict the majority of thermal expansion and contraction, leading to increased compressive and tensile stress levels, respectively. Boundary conditions on girders at abutments 1 and 2 allow girder movement such that thermal stresses in the span can be relieved. Thermal loading has very little effect on the effective stresses in the mid-spans of span 1 girders. However, some stress increases and changes in stress profiles

are shown in span 4, especially in girders 3-6. The same things that caused buckling in span 4 under thermal loading (length of span 4 compared to span 3 combined with bearing fixity at pier 3 and cross member and deck fixity) prevent span 4 from fully expanding and contracting as the temperature on the structure changes, causing thermal stresses to arise in span 4.

Plots in Figures C.17 – C.32 show that effective stress magnitudes at and near the bridge piers are slightly higher than those in the adjacent spans. The difference between self-weight induced effective web stress profiles for rigid and flexible pier models is shown to be very small in Figures C.17 – C.32. Figures 7.3 – 7.8 do, however, show that at the bridge piers the rigid pier case experiences a slightly larger maximum effective web stress than the flexible pier case when loaded with gravity. Just as was the case in the bridge spans, temperature loads have a very small impact on the maximum effective stress in the web cross sections when bridge piers are flexible. Some web effective stress profiles from the flexible pier models are slightly altered by the addition of temperature.

As previously mentioned, placing thermal loading on the Buffalo Creek Bridge models with rigid piers leads to changes in the web effective stress profiles and maximum effective web stresses near and at bridge piers. Directly over the bridge piers, plots show spikes in the effective web stress profiles, especially at the bottom of the webs. These spikes correspond to stress concentrations arising in the girders as a result of bearing constraints on the girders at the piers. The magnitude of these stress concentrations is largest at locations with fixed bridge bearings (Figure 4.4). Effective stress fringe plots in Figures 7.9 and 7.10 show examples of effective stress concentrations at two locations. Most of these stress concentrations represent maximum effective stress values in the web cross section at the piers and are reflected in the plots in Figures 7.3 – 7.8 and the values in Table 7.2. These are the reason that maximum effective stresses vary from girder to girder directly over each pier.

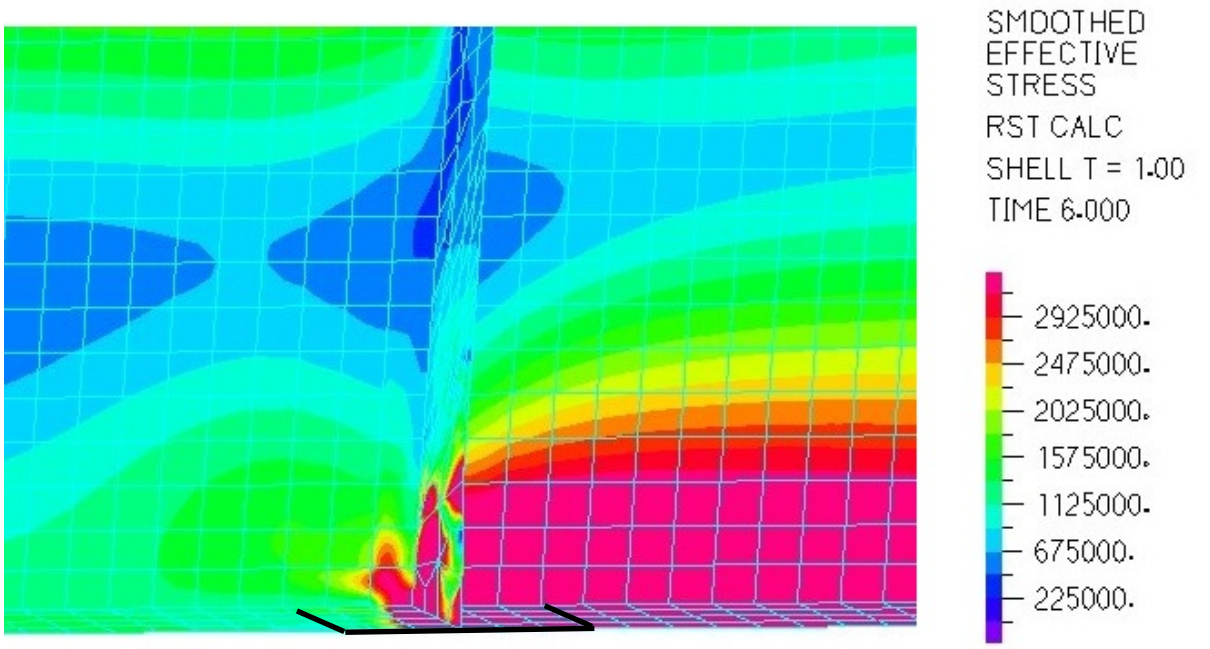


**Figure 7.9. Web Effective Stress Concentration – Girder 3 – Pier 1 – Rigid Piers - +45°F Loading**

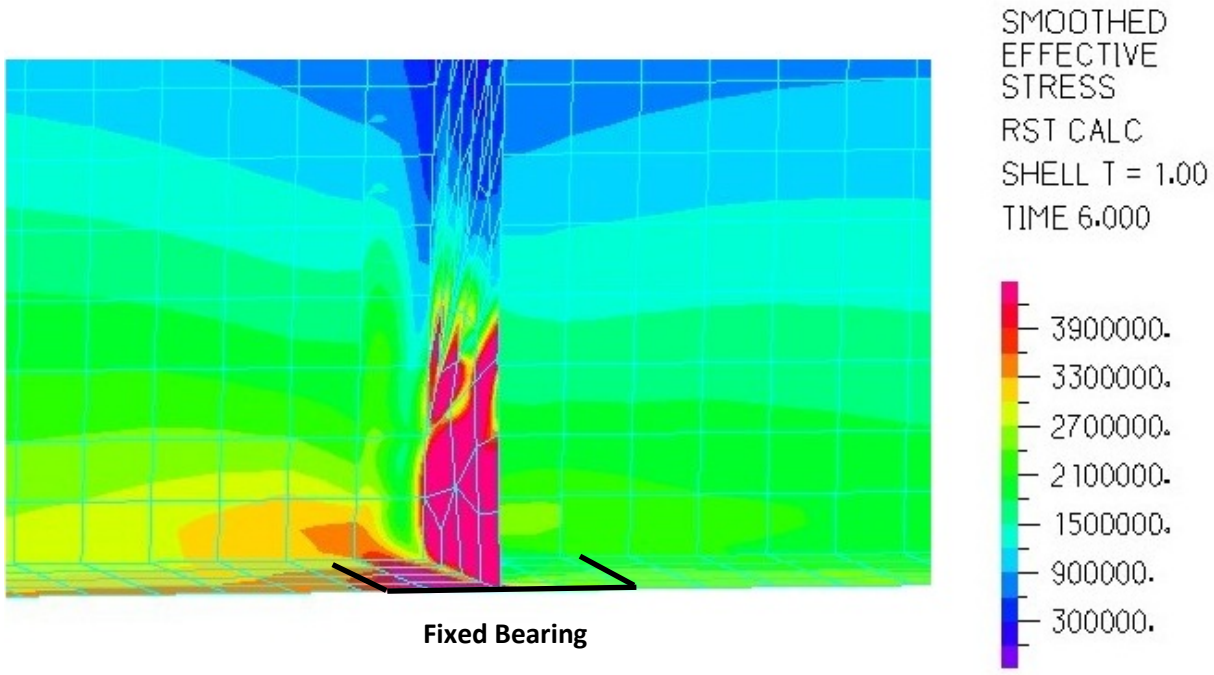


**Figure 7.10. Web Effective Stress Concentration – Girder 6 – Pier 2 – Rigid Piers - +45°F Loading**

When the piers are rigid, a temperature decrease of -45°F almost uniformly increases the maximum effective web stresses at and adjacent to the piers. However, most of the stress values are well below the material yield strength of the web at the piers (70 ksi). On girder 1 at pier 1, -45°F causes a stress concentration of 67.93 ksi (97% of yielding) and on girder 3 at pier 3 the -45°F load leads to a stress concentration of 52.0 ksi (74.3% of yielding). In cross sections adjacent to pier 1, the temperature drop leads to effective stresses that consume between 3.16% and 5.42% of material maximum yield strength. The effects of -45°F loading in cross sections adjacent to pier 2 are somewhat larger with thermal loading stresses accounting for between 7.12% and 12.56% of the total material yield strength. At and near pier 3, -45°F loading increases the maximum effective stresses such that temperature stresses account for up to 55.95% of the total allowable material yield stress.

Effective stress at and near the piers when the piers are rigid and the bridge is subjected to +45°F loading do not display the symmetry of the -45°F results. On the span 1 side of pier 1, the effective stress decreases with thermal loading increase while on the span 2 side of pier 1, the thermal contribution to effective stress leads to maximum values accounting for between 8.98% and 13.98% of material strength. Stress concentrations directly over pier 1 cause the magnitude of maximum effective stress to vary, with the magnitude reaching 55.56 ksi at girder 8, which corresponds to thermal stresses consuming 50.37% of the total material yield stress. At and near pier 2, +45°F thermal loading has a small impact on the maximum effective stresses. On either side of the pier, most girders exhibit a decrease in maximum effective stress, with the few increases being very small. Directly over pier 2, once again +45°F loads do not have a large effect on the stress, but at girder 6 cause a stress concentration of 29.34 ksi. Maximum effective stress values from +45°F loading also vary at and near pier 3, with the most significant impact of temperature seen in girders 3-6 directly over the piers, where the stress reaches a maximum of 44.48 ksi in girder 3. Thermal effective stresses consume between 19.15% and 45.21% of the total material yield stress at girders 3-6 at pier 3.

Results in the preceding paragraphs of this section show that, although not considered during the bridge design, thermal loading on the Buffalo Creek Bridge has an effect on the overall state of stress in the I-girders. The impact of thermal loading, in terms of effective stress magnitude, is less when the bridge piers are modeled as flexible as opposed to rigid members. Pier flexibility permits more global thermal expansion and contraction of the entire structure, relieving stresses that arise as a result of constraining thermal movement. On the other hand, modeling the bridge piers as rigid members leads to evident increases in web effective stresses at both the center of girder spans and at the piers. At the center of the bridge spans, the largest thermal loading impact to effective stresses is seen in the center two spans (spans 2 and 3) because the boundary conditions on the girders in these spans will restrict most thermal expansion and contraction. At the mid-spans, thermal loading alone has been shown to induce web stresses that account for up to 19.6% of the material yield strength. In the area of the bridge piers, thermal loads produce the largest increase in effective stress at the locations of fixed bearings. These fixed bearings combined with the rigid piers lead to stress concentrations in the webs. Thermally induced effective stresses alone at the bridge piers are shown to consume up to 66.57% of the material yield strength.

Although the loading conditions studied here are not shown to induce stress levels in the girders that exceed the material yield strength, the effective stress levels calculated here are worth noting. In reality, the thermally induced effective stress levels are likely somewhere between the flexible and rigid pier results because the bridge bearings will likely not function as ideally designed, providing restraint to girder movement in some locations that were meant to move freely. Likewise, results will most likely not be as severe as the rigid pier results presented here. However, the rigid pier results are considered the worst case scenario and this is the case used by bridge designers when performing loading calculations. Results in this section clearly show that thermal loading, both positive and negative, leads to an increase in the effective stresses in I-girder webs. These are stresses that, although they do not put the girders in a state of yielding, will decrease the capacity of the I-girders and possibly reduce their ability to handle other types of loading which the bridge was designed for.

## 7.3 I-Girder Longitudinal Web Stresses

Longitudinal stresses in I-girder sections are a combination of bending and axial stress components. Design of steel I-girder bridges considers bending stresses as they are a result of flexural forces, such as self-weight dead loading and design live loading, on the structure. On the other hand, axial forces on the I-girder are mostly neglected because they are mainly a result of constrained thermal expansion and contraction, and bridge design assumes that boundary conditions on the bridge superstructure function in a way that relieves all thermal stresses. However, previous studies by McBride (2005), Shoukry *et al*. (2005), and Beckett (2011) found that significant levels of axial stresses can be induced on steel I-girders as a result of constrained thermal expansion and contraction.

Although design assumes I-girder axial stresses, especially during construction, to be at or very near zero, out-of-plane deformations observed in Chapter Six indicate that this may not be the case for the Buffalo Creek Bridge. Results show that thermal loading leads to additional out-of-plane I-girder web deformations, indicating that thermal expansion and contractions are not being fully relieved, which will lead to axial stresses in the superstructure. These unforeseen axial stresses may jeopardize the structural integrity of the bridge by decreasing the girder capacity to handle design flexural loads and as well as any other unforeseen loads that may arise.

Figures C.33 – C.64 display longitudinal web stress profiles as computed by the FE analysis at the same locations where effective stresses were studied in Section 7.2 and out-of-plane displacements were studied in Chapter Six. Results in these plots compare longitudinal web stress profiles for rigid and flexible pier models loaded with gravity loading and gravity loading followed by either +45°F or -45°F uniform thermal loading. As expected, longitudinal web stress results show that flexural girder stresses develop in the cross-section as a result of the gravity loading of the structure. The evidence of this is the symmetry of the longitudinal web

stress profiles about the web centerline when the only loading is the self-weight of the superstructure. However, the addition of thermal loading can lead to the stress profiles no longer being symmetric about the web centerline. This indicates that thermal loading, or more specific, the structural resistance to thermal movements, is creating axial stresses in the cross section. The magnitude of additional axial and bending stresses in the girder cross sections caused by thermal loading will be investigated in a later section.

Profiles indicate that thermal loading on FE models with rigid piers results in more significant changes in longitudinal stress than thermal loading on models with flexible piers. It easy to see from Figures C.33 – C.64 that temperature loading increases the axial stress component in the web cross sections, especially in the center two spans. However, it appears that thermal loading may also have an effect on the bending component of the longitudinal web stress profiles in some locations, especially in spans 1 and 4.

Bridge design guidelines do not require designers to thoroughly investigate I-girder webs for flexural loading because the webs of I-girders are mainly designed to carry shear forces. AASHTO (2003) and AASHTO (2010) require that steel I-girder webs under flexure must be analyzed for bend-buckling. Bend-buckling may occur in I-girder web sections when bending forces placed on the I-girders lead to longitudinally compressive web stresses that may lead to web plate buckling. Web bend-buckling analysis in AASHTO (2003) and AASHTO (2010) define the web bend-buckling resistance ($F_{cr}$) as:

$$F_{cr} = \frac{0.9Ek}{\left(\frac{D}{t_w}\right)^2} \leq F_y \qquad (7.2)$$

where $E$ = Modulus of Elasticity (ksi)

$k$ = Bend-buckling coefficient = $\frac{9}{(D_c/D)^2}$

$D$ = Web depth (in.)

$D_c$ = Depth of web in compression (in.)

$t_w$ = Web thickness (in.)

$F_y$ = Material yield strength (ksi)

The bend-bucking resistance factor limits the magnitude of longitudinal stress in the web in order to avoid web buckling. For composite sections subjected to positive flexure (mid-span locations), AASHTO (2010) does not require bend-buckling resistances to be checked after the web is in its final composite condition if the webs do not require longitudinal stiffeners. Furthermore, according to AASHTO (2010), for loads applied at the fatigue and service limit states after the deck has hardened or is made composite, the increased compressive stresses in the web tend to be compensated for by the increase in $F_{cr}$ resulting from the corresponding decrease in $D_c$. $F_{cr}$ for these sections is generally close to, or larger than, $F_{yc}$ (web compressive yield strength) at the strength limit state. Therefore, AASHTO (2010) does not require web bend-buckling to be checked after the structure is in the composite state. In this case, this would be after the bridge deck is poured and has fully cured. It should be noted that the thickness of the deck haunches is not accounted for in Equation 7.2. In negative bending areas, this additional depth will increase the value for $D_c$ and $D$, decreasing $F_{cr}$. In positive bending regions, the haunch depth will increase $D$ while not effecting $D_c$, thus increasing $F_{cr}$. As it will be shown that negative moment regions are the most sensitive to web bend buckling, neglecting haunch depth will yield a conservative analysis.

Although design criteria states that it is not necessary, nor required, this study proceeds with performing the bend-buckling analysis on the Buffalo Creek Bridge I-girders after the structure is deformed under self-weight loading, the bridge deck has cured, and both a -45°F and +45°F thermal load is placed on the structure. AASHTO (2010) does not consider web bend-buckling in this case, nor does AASHTO (2010) consider thermal loading. Previous results in this chapter, along with results in Chapter Six, show good evidence that thermal loads induce additional stresses in the web cross sections. More particularly, positive thermal loading increases the

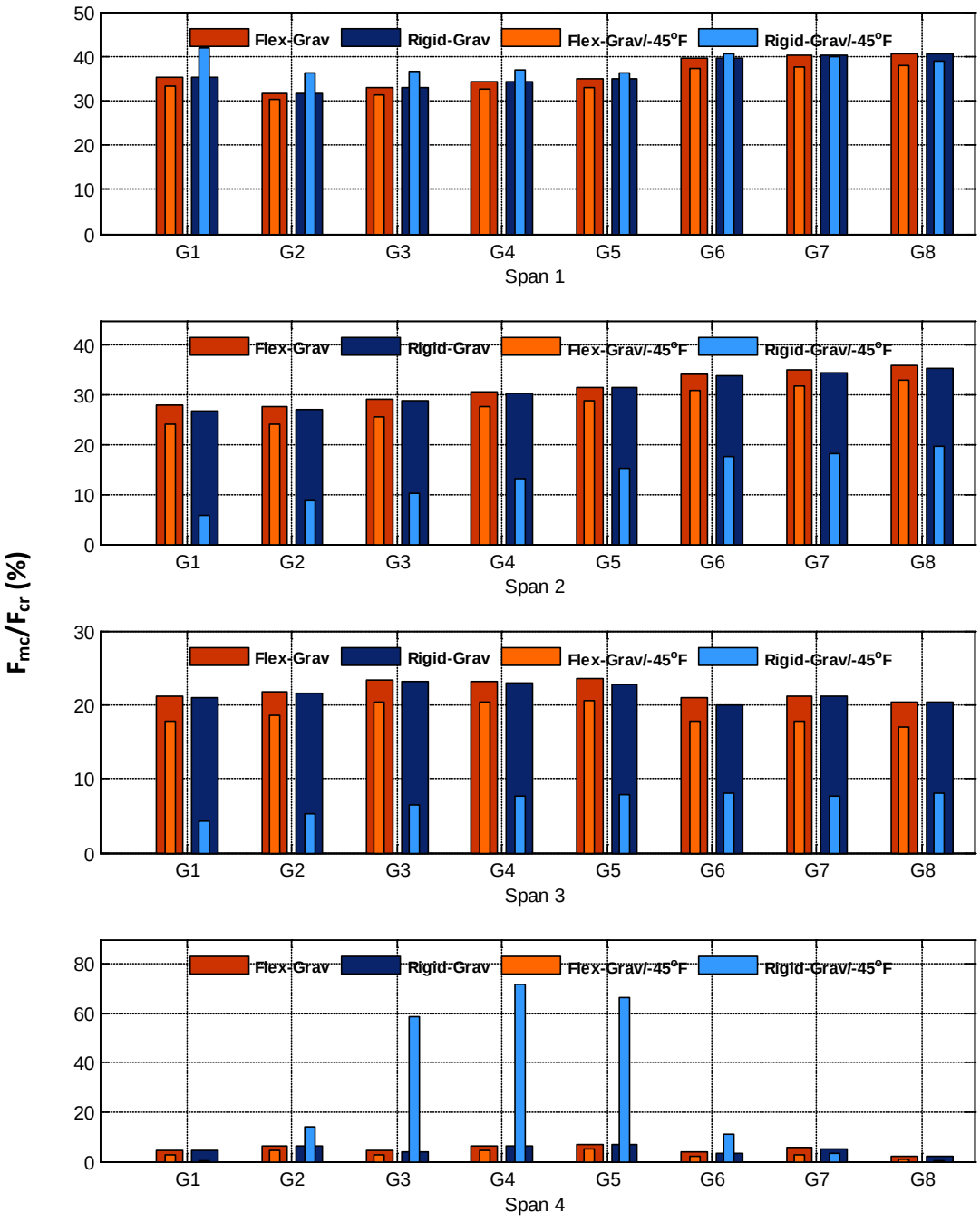


**Figure 7.11. Maximum Longitudinal Compressive Stress Versus Web Bend-Buckling Resistance Factor at Mid-Spans – Gravity and -45°F Loading**

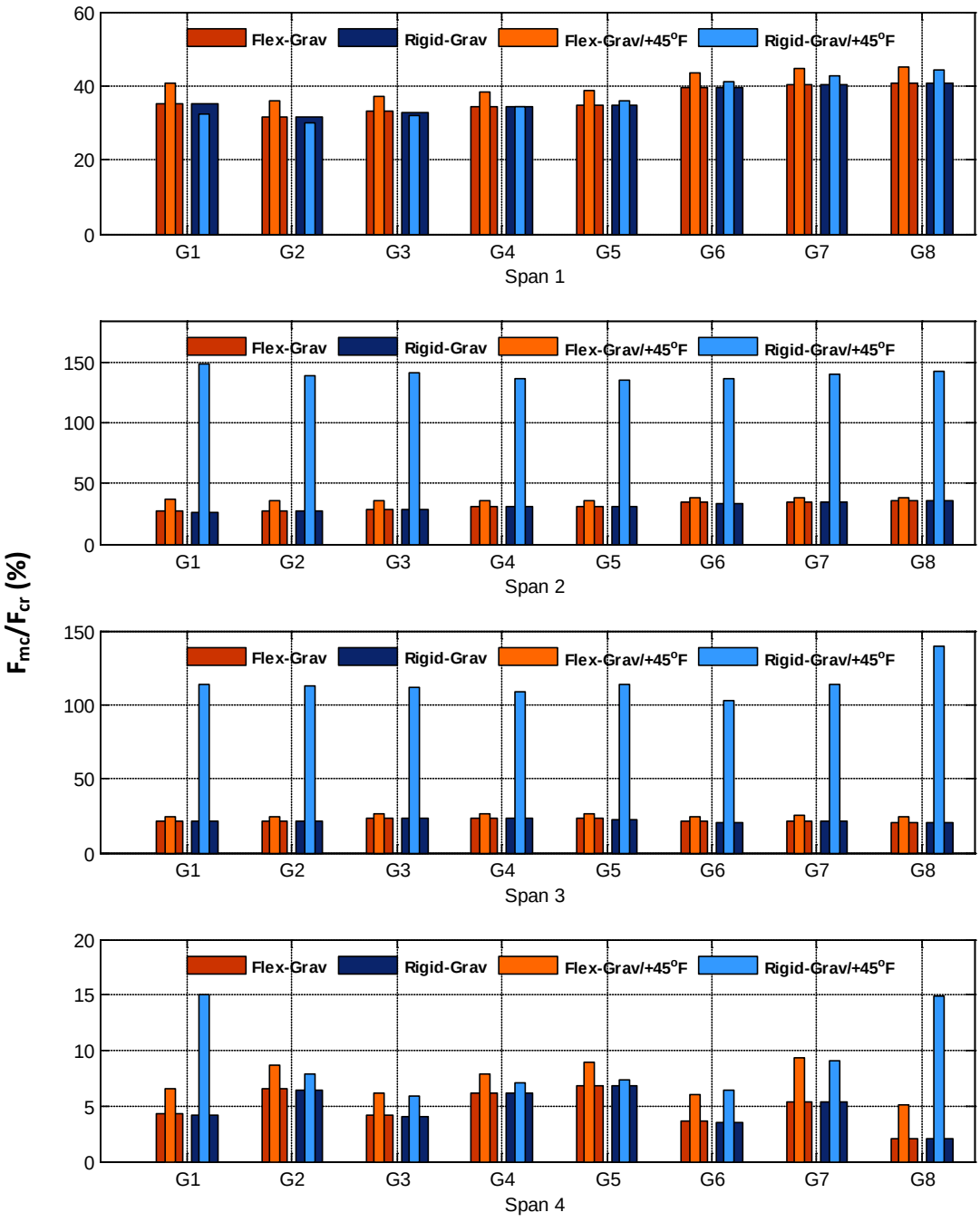


**Figure 7.12. Maximum Longitudinal Compressive Stress Versus Web Bend-Buckling Resistance Factor at Mid-Spans – Gravity and +45°F Loading**

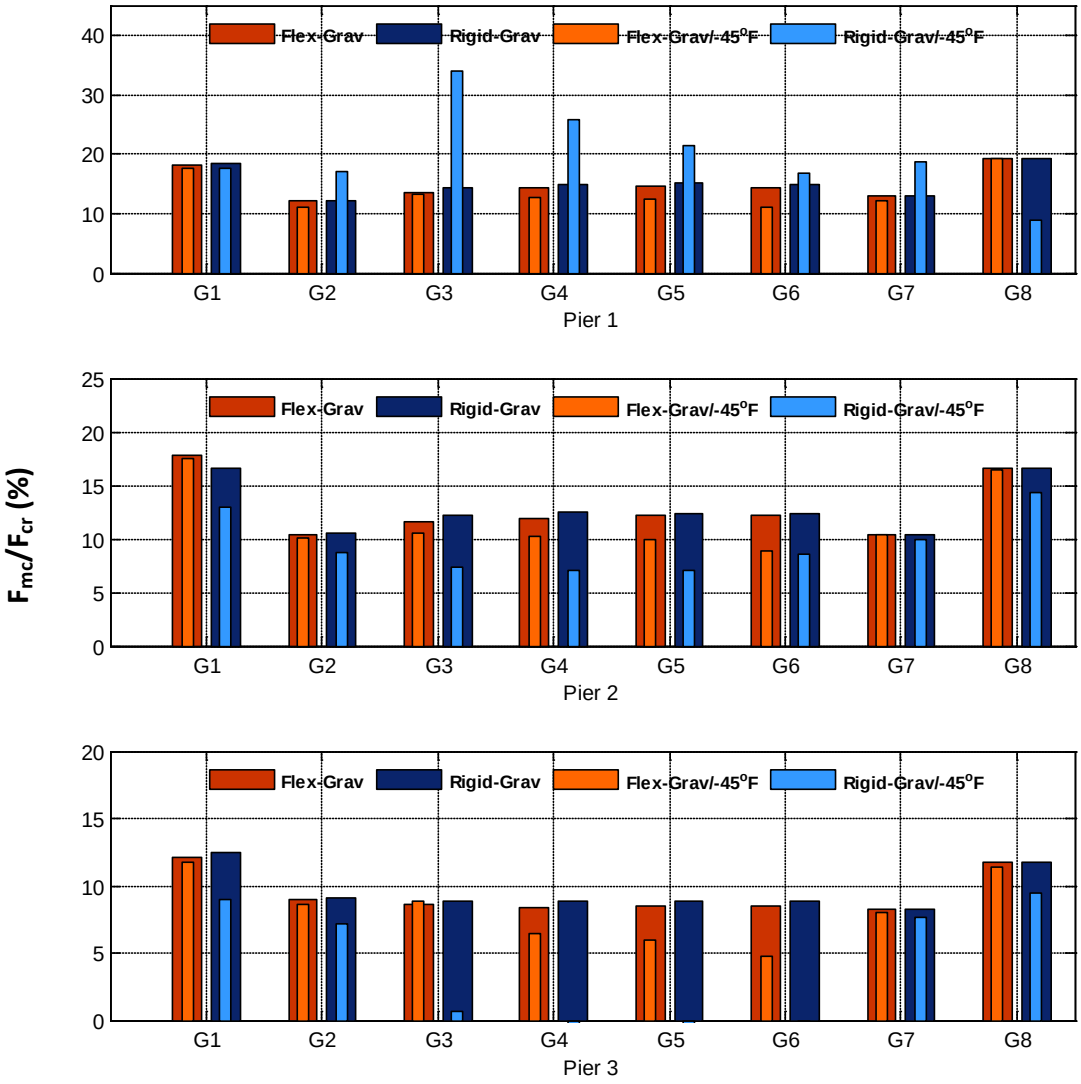


**Figure 7.13. Maximum Longitudinal Compressive Stress Versus Web Bend-Buckling Resistance Factor at Piers – Gravity and -45°F Loading**

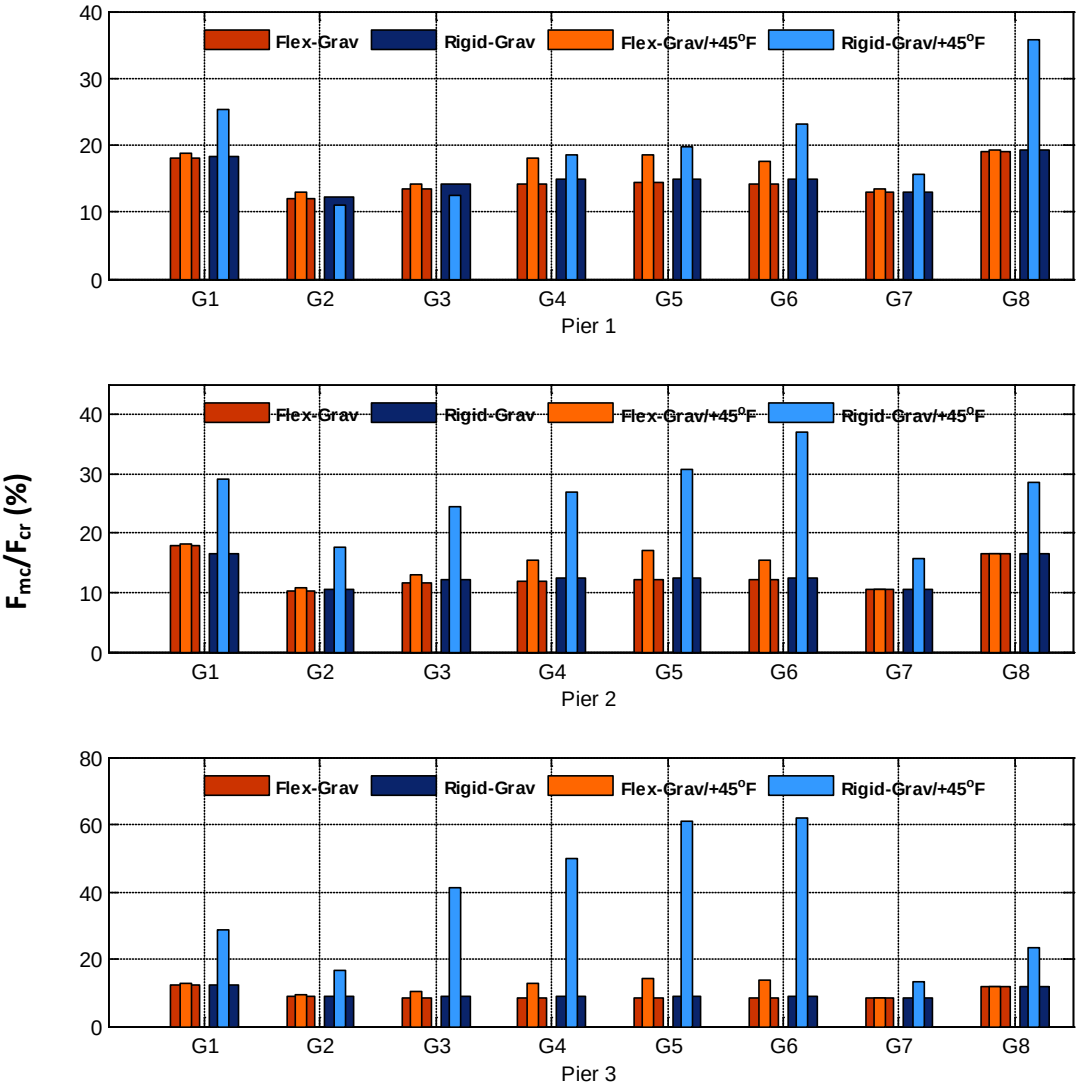


**Figure 7.14. Maximum Longitudinal Compressive Stress Versus Web Bend-Buckling Resistance Factor at Piers – Gravity and +45°F Loading**

level of compressive stress in the I-girder webs in spans 2-4 and negative thermal loading increases compressive stresses in span 1, which could both have an effect on the web bend-buckling behavior.

At all mid-span and pier locations discussed in previous analyses, the web bend-buckling resistance factor ($F_{cr}$) was computed for each load case based upon the FE computed longitudinal web stress profiles in Figures C.33 – C.64. The web bend-buckling resistance factor is a function of the depth of the web in compression at any given state of loading. As the depth of the web in compression decreases, the web bending buckling resistance factor increases, and vice versa. For each case of loading, web bend-buckling resistance values are compared to the maximum compressive stresses ($F_{mc}$) to determine if the section meets web bend-buckling criteria. Results are presented at mid-spans (Figures 7.11 and 7.12) and directly over the piers (Figures 7.13 and 7.14) as a ratio between $F_{mc}$ and $F_{cr}$ in terms of a percentage.

The impact of thermal loading on maximum compressive stress to web bend-buckling factor ratio is mostly a function of the axial stresses induced in the I-girder webs by changing thermal conditions. If temperature adds compressive stress in a cross section, the ratio of maximum compressive stress to web bend-buckling factor increases because the magnitude of maximum compressive stress increases while the depth of the web in compression increases, resulting in a decrease in $F_{cr}$. Increases in this ratio indicate that the section is moving closer to being in a state that does not satisfy the web bend-buckling resistance criteria. The opposite is true when thermal loading creates additional tensile stresses in the cross section, the ratio in Figures 7.11 – 7.14 decreases.

Results show that thermal loading has a greater effect on ratios in Figures 7.11 – 7.14 when the piers are modeled as rigid members, which should be expected, because thermal loading has a larger effect on longitudinal stresses when the piers are modeled as rigid rather than flexible. Although temperature has an effect on web bend-buckling in each cross section for each type of boundary condition, the most significant impact is found when a +45°F temperature load is

placed upon the Buffalo Creek Bridge model with rigid piers. As Figure 7.12 shows, positive thermal loading leads to compressive stress profiles in the girders of spans 2 and 3 that fail the AASHTO (2010) guidelines for web bend buckling. These two spans are supported by boundary conditions that restrict a large degree of the girder movement, leading to increased compressive stresses as thermal expansion of the girders is resisted.

These results contradict the statement made in AASHTO (2010) that the designer need not study web-bend buckling for cross sections in positive flexure once the deck has cured and acts compositely with the bridge girders because the increase in compressive stresses in the web are compensated for by the increase in the web bend-buckling resistance factor (Equation 7.3) resulting from the decrease in depth of the web in compression. This statement does not hold true when considering axial stresses caused by thermal loading. For instance, when constrained thermal expansion causes increased uniform compressive axial stresses in the cross section, both the level of compressive stress in the section and the depth of the web in compression will increase (i.e. at mid-span 2 in Figure C.41). Increasing the depth of the web in compression lowers the $F_{cr}$ value. Therefore, in the case of increased compressive thermal stresses on a composite section, an increase in compressive stress can be accompanied by a decrease in the web bend-bucking resistance factor, making it more likely the section will not meet web bend-buckling criteria.

Clearly, results show that when the bridge supports are rigid, the structure has deformed under self-weight, and the bridge deck has cured, a uniform temperature increase on the bridge leads to compressive stress levels in the center two spans that cause the section to fail AASHTO (2010) design criteria. On the other hand, web bend-buckling results at these same locations for the case of flexible piers do not show as significant an increase in the $F_{mc}/F_{cr}$ ratio. Although assumptions are made during design that thermal effects on the structure will be relieved through the bridge boundary conditions and movement of the bridge piers, results in the study by Beckett (2010) reveal that bearings on curved I-girder bridges may “lock-up” and boundary conditions on curved I-girder bridges will likely not function as they were ideally designed.

Furthermore, designers do not take into account the flexibility of the piers when performing bridge design calculations, in particular, web bend-buckling calculations. Although the behavior of the bridge in response to thermal loading will likely fall somewhere between the rigid and flexible pier case, the rigid pier case studied here will be the worst case scenario and would be the case used in design.

Analysis in this section reveals that thermal loading placed on the Buffalo Creek Bridge after the construction of the superstructure may have an impact on the web bend-buckling resistance analysis of the I-girders. Guidelines set forth in AASHTO (2003) and AASHTO (2010) allowing designers to neglect web bend-buckling behavior in certain bridge sections once the bridge deck is composite with the girders were found to be erroneous. Because the guidelines do not consider axial stresses from thermal loads, uniform compressive web stress increases resulting from constrained thermal expansion are also not considered. These axial compressive stresses will have a significant impact on the web bend-buckling behavior of an I-girder section because they will both decrease the web bend-buckling resistance factor governing the amount of compressive stress allowed in the cross section before the section will buckle and increase the magnitude of compressive stress in the same cross section. Any additional compression induced on the I-girders as a result of thermal loading is of concern because this will decrease the maximum compressive stress to web bend-buckling resistance factor ratio. Subsequent design loading cases increasing compressive stress levels in the cross section will only further reduce this ratio, endangering the structural integrity of the bridge.

## 7.4 I-Girder Axial Stresses

Longitudinal stress profiles in Figures C.33 – C.64 are a combination of the bending and axial stresses in each web cross section. Bending stresses are mainly a result of flexural loading and can be either linear or nonlinear through the cross section depending on several factors that can affect the bending behavior of a member. On the other hand, axial stresses are uniform

through the cross section and are likely a result of constraints placed on the expansion and/or contraction of the member. In this study, self-weight loading will be the major cause of bending stresses in the web cross sections and thermal loading will be the major contributor to axial stresses in the cross section.

Prior girder displacement and stress results have clearly shown that the bearing arrangement of the Buffalo Creek Bridge does not allow free thermal movements as was assumed in design. This section of the study will break down the longitudinal stress profiles into their axial and bending components to better identify how significant the impact of thermal loading is on structural capacity. Thermally induced axial stresses on the bridge girders represent stresses that were not accounted for by bridge designers, which may compromise the structures ability to handle design flexural loads or any other unforeseen loading conditions that may arise.

Axial stress in any web cross section can be determined using Equation 7.3 which integrates the longitudinal stresses through the cross section and averages this axial force by dividing by the cross sectional area of the section.

$$\sigma_{axial} = \frac{\int \sigma dA}{A} \qquad (7.3)$$

*A* is the cross sectional area I-girder section and $\sigma$ is the longitudinal stress measured at a specific location in the cross section.

Axial stresses are calculated in the positive moment regions (center of each span) and the negative moment regions (at each pier) for all three stages of loading and presented and compared in Figures 7.15 – 7.18. Although flexural loading does primarily induce bending stresses in I-girder, results show that axial stresses appear in the cross sections when the bridge is loaded with gravity. Under the self-weight of the superstructure, both the positive and negative moment regions develop axial tensile stresses in the cross section.

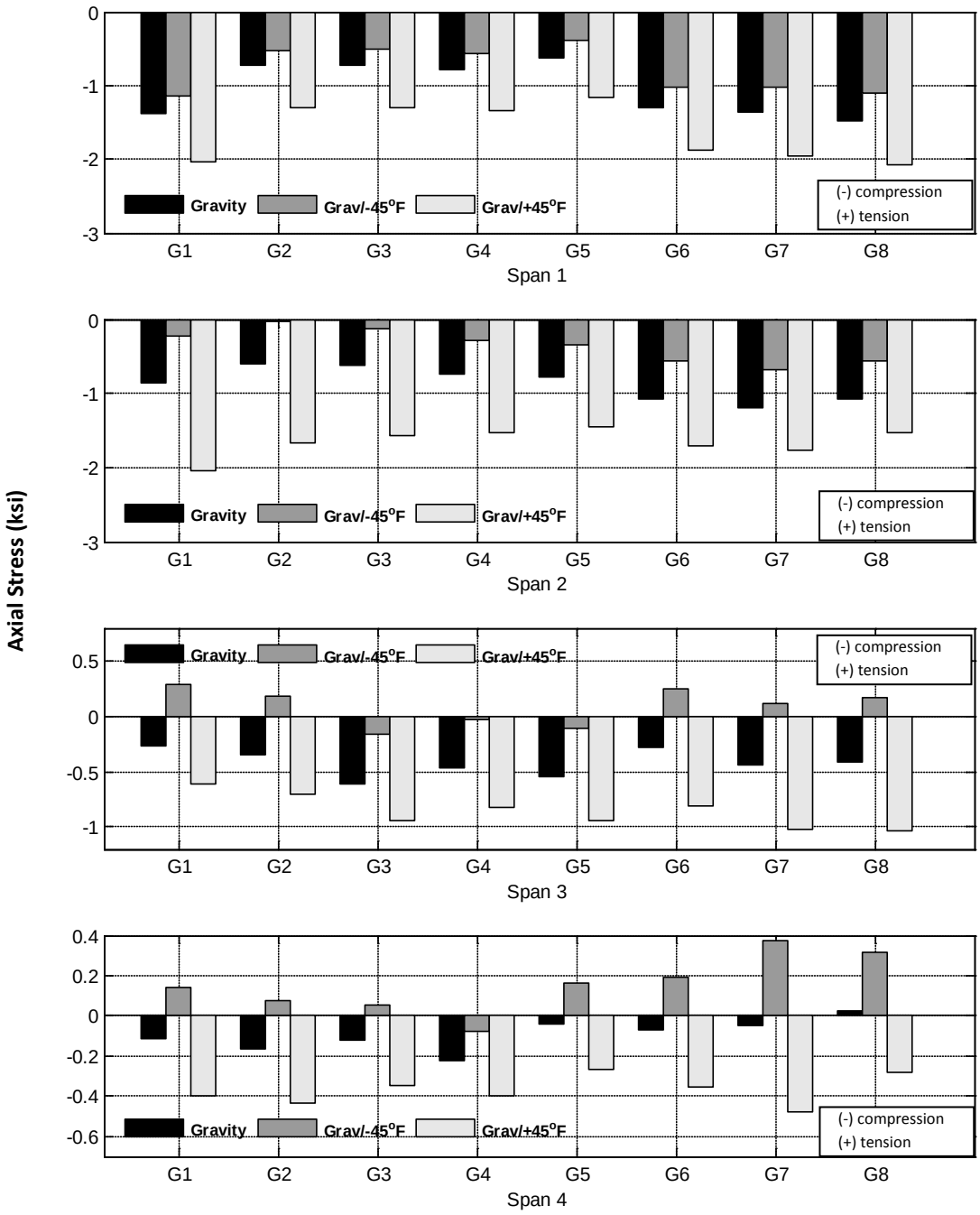


**Figure 7.15. Axial Web Stress Comparison – Mid-Spans – Flexible Piers**

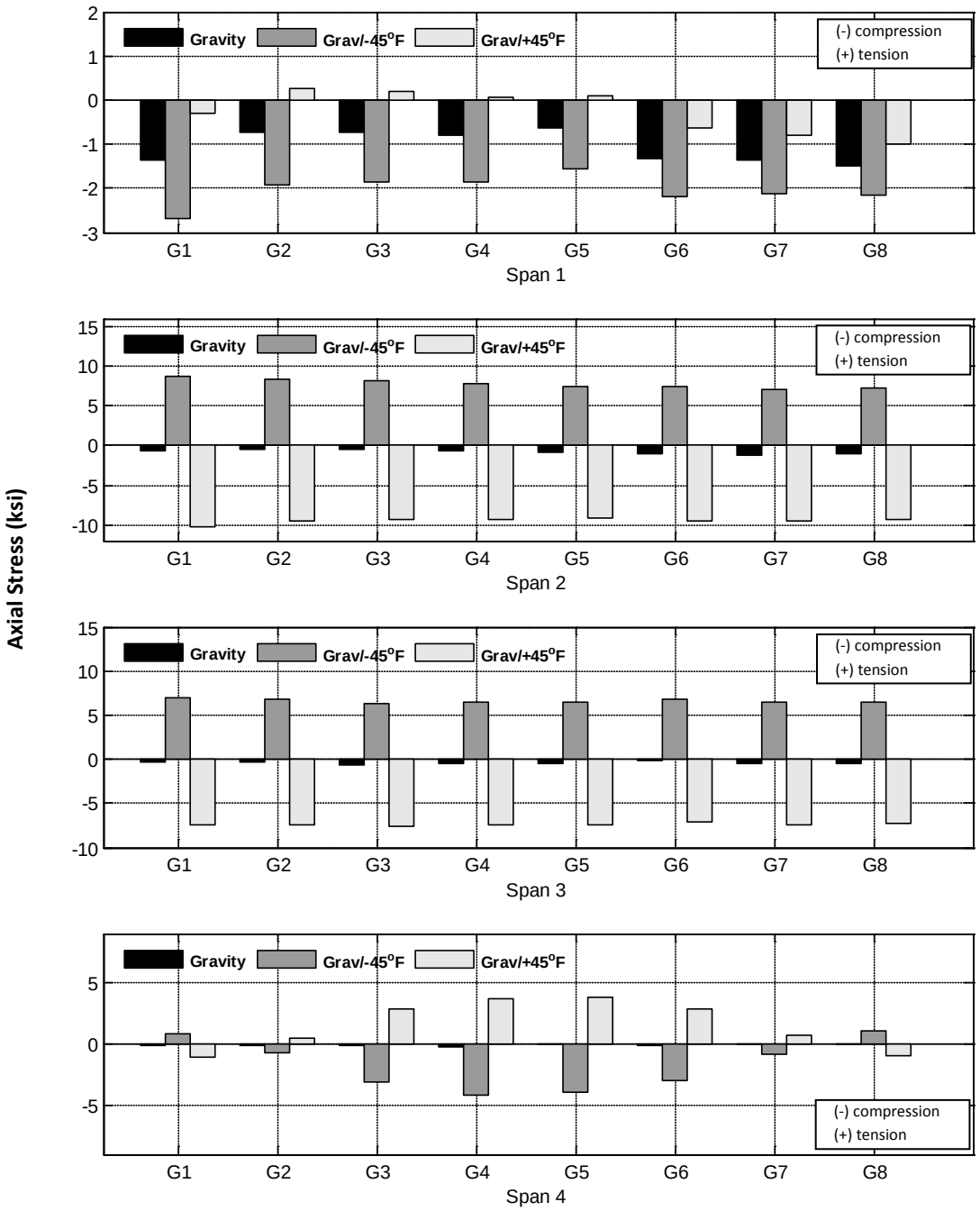


**Figure 7.16. Axial Web Stress Comparison – Mid-Spans – Rigid Piers**

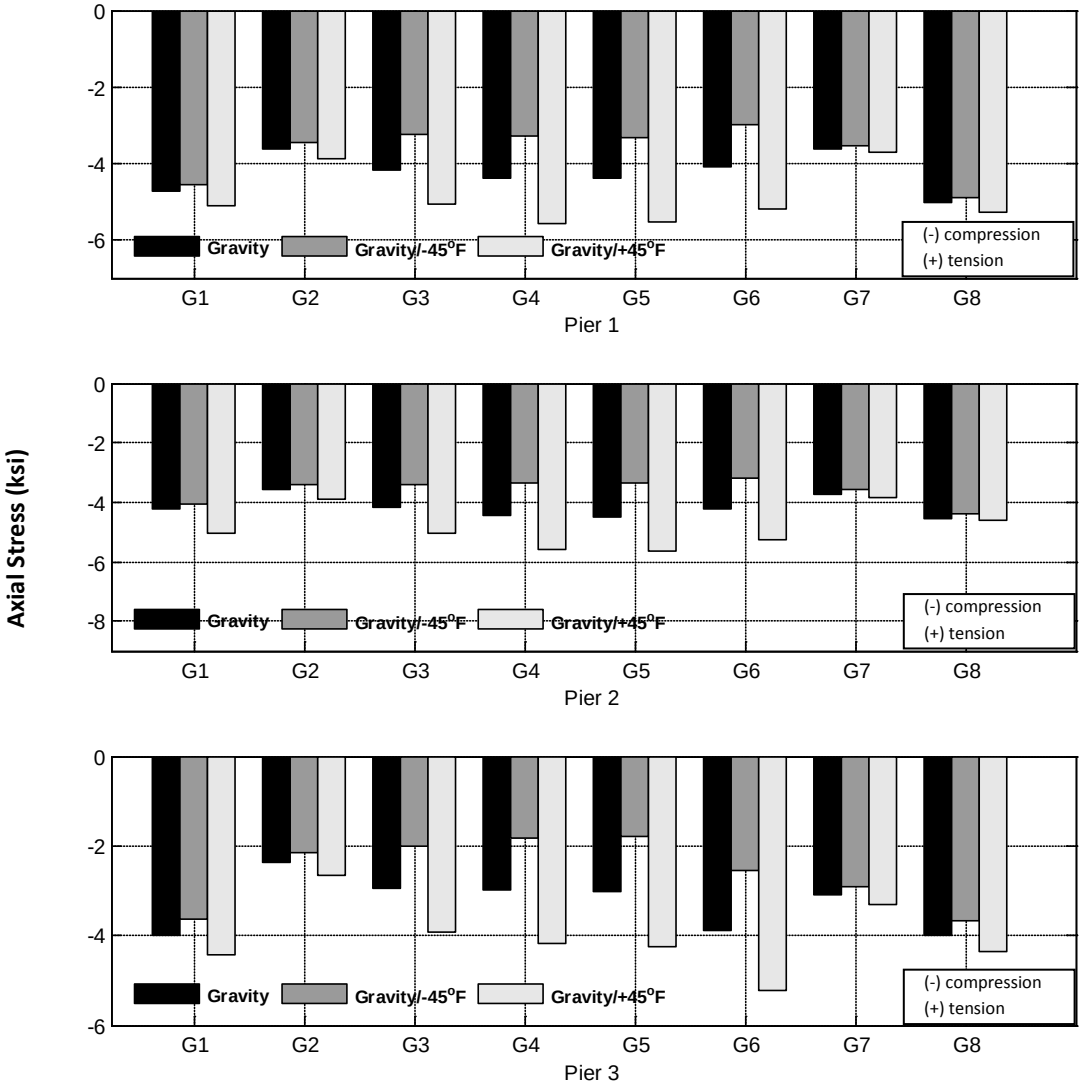


**Figure 7.17. Axial Web Stress Comparison – Piers – Flexible Piers**

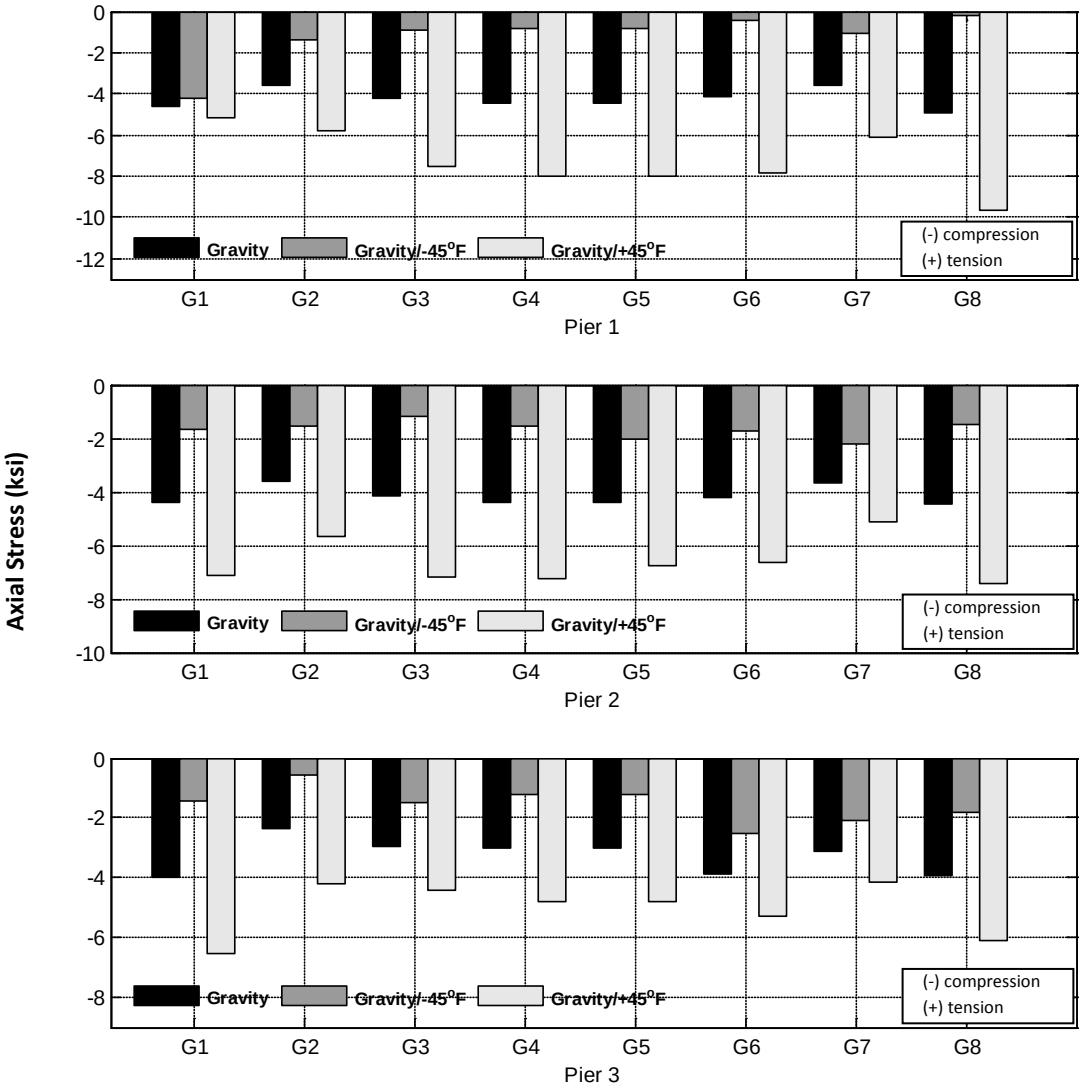


**Figure 7.18. Axial Web Stress Comparison – Piers – Rigid Piers**

The primary concern in this investigation is the magnitude of thermally induced axial stresses that arise in the bridge girders. As Figures 7.15 and 7.16 show, pier flexibility greatly reduces the effect that thermal loading has on the axial stress magnitude at the midspans. Just as was previously observed when studying thermally induced web displacements, results for flexible pier models axial stresses indicate that the flexibility of the piers allows the structure to expand and contract as one continuous body as thermal conditions change. Decreasing temperature (-

45°F) contracts the entire superstructure, adding tensile axial stress to the cross section and increasing temperature (+45°F) expands the structure and adds compressive axial stress to the mid-span cross sections.

Introducing thermal loading to the model with rigid piers causes a significant amount of axial stress to arise in the positive moment regions. Study of the results in Figures 7.15 and 7.16 reveals that axial stress magnitudes caused by gravity loading are fairly similar between flexible and rigid pier models. The same results also show that thermal loading on the bridge with rigid piers has a much more significant effect on the state of axial stress than when the bridge piers are flexible. Once again, the rigidity of the piers causes each span to respond for the most part individually to thermal loading, based on the boundary conditions on that particular span. Because spans 1 and 4 have one end mostly free to expand and contract along the bridge centerline, the temperature decrease of -45°F adds compressive axial stresses to the span as it contracts and the temperature increase of +45°F adds tensile axial stresses to the span as it expands. In span 1, -45°F loading increases the compressive axial stress by 168% while +45°F loading decreases the level of compressive axial stress in the girders by up to 136%, even putting four of the girders into a state of axial tension. For the girders of span 4, the most significant impact of thermal loading on the axial state of stress is seen in girders 3-6 because the bearings on pier 3 fix the movement of these girders. Negative temperature conditions of -45°F cause axial compressive stresses in span 4 to reach as much as -4.16 ksi, and yield an increase of up to 8,639% from the levels of gravity loading. Introducing a +45°F temperature load leads to levels of tensile stress up to 3.81 ksi, and up to a 8,461% change in the magnitude of axial stress compared to gravity values. Because boundary conditions on spans 2 and 3 are such that most girder movement along the bridge centerline at the piers is constrained, changing thermal conditions induce a large level of axial stress in the girders in these spans. As temperature increases on the bridge, compressive stresses arise in spans 2 and 3 as the boundary conditions resist thermal expansion. Conversely, tensile stresses arise in spans 2 and 3 as temperature drops and the boundary conditions resist girder contraction. In span 2, -45°F loading leads to axial tensile stress levels up to 8.79 ksi, a 1,807% change from the gravity

compressive stress state. Temperature increase of +45°F increases compressive stress levels to up to 10.17 ksi, a 1.813% increase in compressive web stress. Span 3 shows tensile stress up to 6.9 ksi from -45°F loading, a 2,191% change in axial stress compared to the gravity state, and experiences compressive stresses of up to 7.52 ksi, a 4,709% increase in compressive stress from the gravity state of axial stress.

At web locations directly over the piers, the initial gravity loading creates a state of axial compression in the girder webs in both the rigid and flexible pier cases. Axial stress magnitude is very similar between the rigid and flexible pier cases when considering only self-weight loading. At the piers, the same axial stress behavior as is seen at the mid-spans is observed when adding thermal loading to the model with flexible piers: temperature decrease decreases compressive axial stresses and temperature increase the magnitude of compressive axial stresses at the piers. For the flexible pier case, the impact of thermal loading at the piers is smaller compared to the rigid pier case, with -45°F decreasing axial compression stress by up to 26.6% at pier 1, up to 29.8% at pier 2, and up to 40.2% at pier 3, and +45°F loading increasing axial compressive stress by up to 27.5% at pier 1, up to 26.1% at pier 2, and up to 40.9% at pier 3.

Thermal loading has a similar effect on axial stresses at the piers for the case when piers are rigid as it does when the piers are flexible, only the magnitude of the thermal effects is larger. At all of the piers, -45°F loading adds tensile axial stress to the gravity axial stress state of the cross section and +45°F thermal loading adds compressive axial stress to the gravity stress state. A temperature decrease of -45°F decreases the compressive axial stress levels at the piers by up to 96.3% at pier 1, 71.6% at pier 2, and 76.5% at pier 3. Conversely, a temperature increase of +45°F increases the compressive axial I-girder stresses by up to 96.5% at pier 1, 72.2% at pier 2, and 76.5% at pier 3. Temperature decrease and increase on the bridge impacts the amount of axial stress in the I-girders at the piers at a similar magnitude, but with temperature decrease adding tension and temperature increase adding compression.

Results in Figures 7.15 – 7.18 reveal that placing a thermal load on the Buffalo Creek Bridge will result in additional axial stress in the I-girder cross sections at both the mid-spans and piers, axial stresses that are not accounted for during bridge design. At both locations, the effect of thermal loading on axial stress is larger when the bridge piers are modeled as rigid members. Spans with boundary conditions that restrict girder movement along the bridge centerline experience the largest variation in axial web stress with the introduction of temperature. At the piers, the girders experience axial compressive stress under gravity and both cases of thermal loads, with -45°F reducing the magnitude of compressive axial stress and +45°F increasing the magnitude of axial compressive stress.

Being as thermally induced axial stresses are not accounted for during bridge design, their presence on the Buffalo Creek Bridge may impact the structural capacity of the bridge in terms of being able to handle subsequent design loads and any other unforeseen loading conditions that may arise. AASHTO (2010) specifies the compressive resistance factor of steel I-beams via Equations 7.4 – 7.6 as the threshold of compressive stress a member can withstand. To perform this analysis, the I-girders are treated as pure compression members, the unbraced length (*l*) is the length between cross-members, and the boundary condition as a pinned-pinned connection.

$$P_n = 0.66^{\lambda} F_y A_s \qquad (7.4)$$

$$\lambda = \left( \frac{Kl}{r_s \pi} \right)^2 \frac{F_y}{E} \qquad (7.5)$$

$$P_r = \phi_c P_n \qquad (7.6)$$

where $F_y$ = Material yield stress (ksi)

$A_s$ = Gross cross sectional area (in.$^2$)

$K$ = Effective length factor

$r_s$ = Radius of gyration of the member (in.)

$E$ = Modulus of elasticity (ksi)

$\varphi_c$ = Resistance factor for compression (0.90)

Axial girder stresses presented in Figures 7.15 – 7.18 indicate that compressive axial stresses are present at the piers and mid-spans in the Buffalo Creek Bridge I-girders due to gravity and gravity followed by thermal loading. Furthermore, loading the bridge with self-weight followed by +45°F thermal loading leads to the highest level of compressive axial stresses. Measured axial compressive stresses are combined with the computed compressive resistance factor from Equation 7.6 of each section to determine the compressive resistance ratio of each section. This ratio is representative of how much of the I-girder sections compressive resistance is consumed under the specified state of loading, with a value of 100% indicating that the state of loading under consideration has caused the compressive stress in the section to reach its compressive stress capacity. Figures 7.19 – 7.22 contain the compressive resistance ratios at the center of each span and directly over the piers corresponding to the axial mid-span stress values in Figures 7.15 – 7.18.

Naturally, because the thermally induced compressive axial stresses are larger when the bridge piers are modeled as rigid members as opposed to flexible members, the compressive resistance ratio will also be larger for the case with rigid members. Figure 7.15 and 7.16 show that gravity plus +45°F thermal loading uniformly results in the highest level of compressive stresses at the bridge mid-spans. As such, when the flexible pier model is loaded with self-weight loading and +45°F thermal loading, up to 5.94% of the compressive capacity of the I-girders is consumed at mid-span 1, up to 5.90% at mid-span 2, up to 3.29% at mid-span 3, and up to 1.34% at mid-span 4. On the other hand, in the case of rigid bridge piers, the maximum compressive stresses occur in mid-spans 1 and 4 when the bridge is loaded with -45°F loading and in mid-spans 2 and 3 when the bridge is loaded with +45°F loading. These loading conditions result in compressive resistance ratios of up to 7.69% at mid-span 1, up to 29.8% at mid-span 2, up to 23.9% at mid-span 3, and up to 11.7% at mid-span 4, as shown in Figure 7.20.

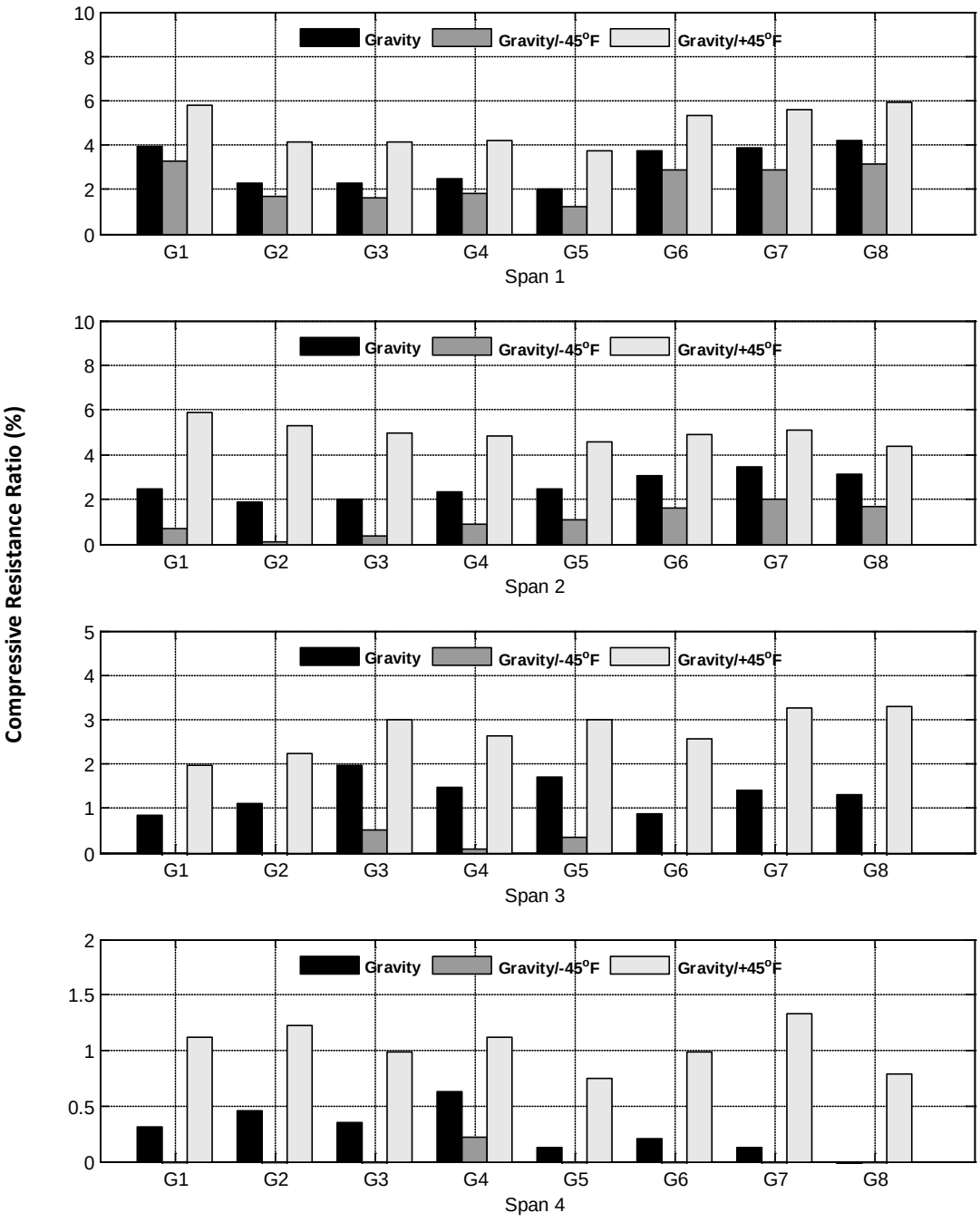


**Figure 7.19. Compressive Resistance Ratios – Mid-Spans – Flexible Piers**

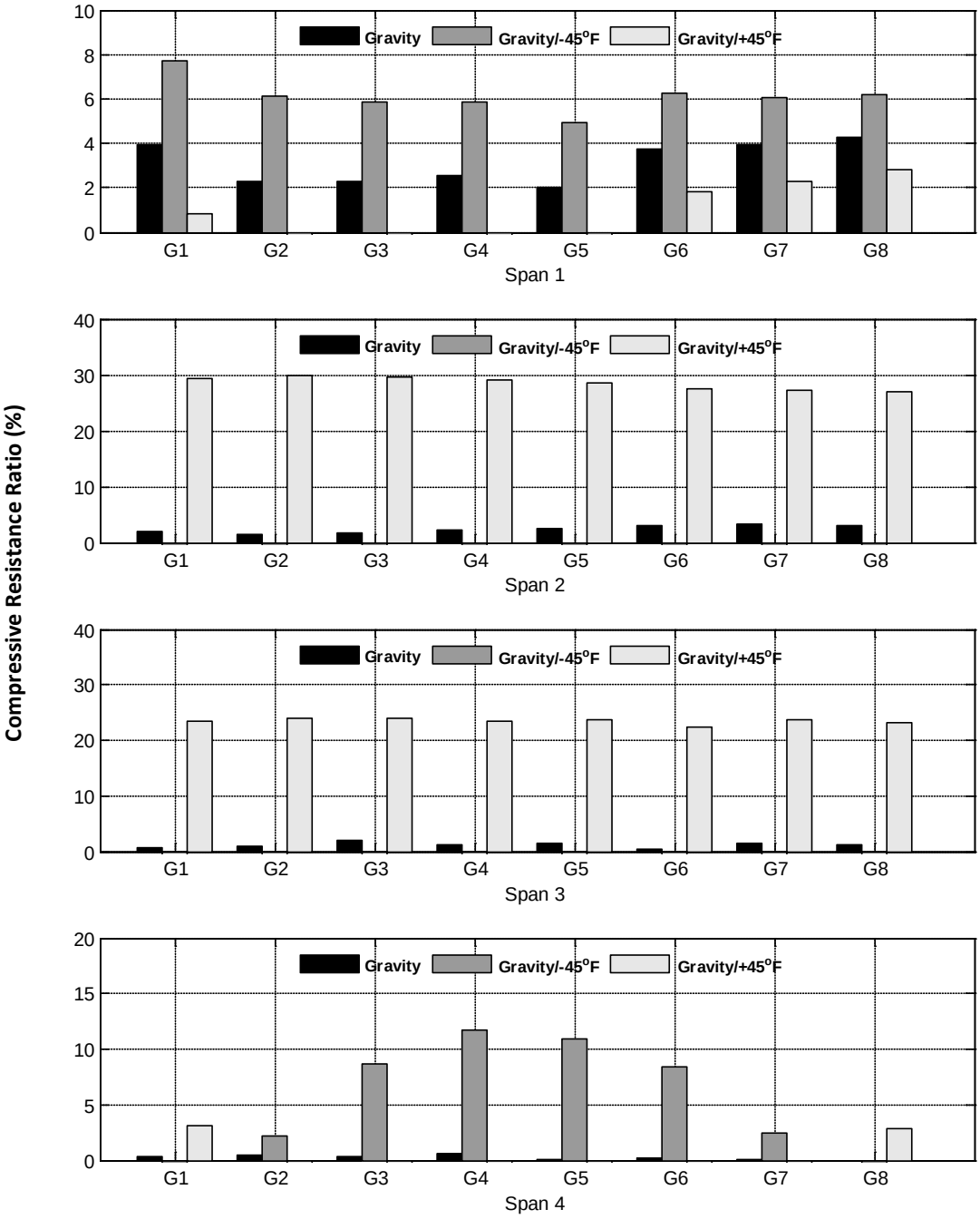


**Figure 7.20. Compressive Resistance Ratios – Mid-Spans – Rigid Piers**

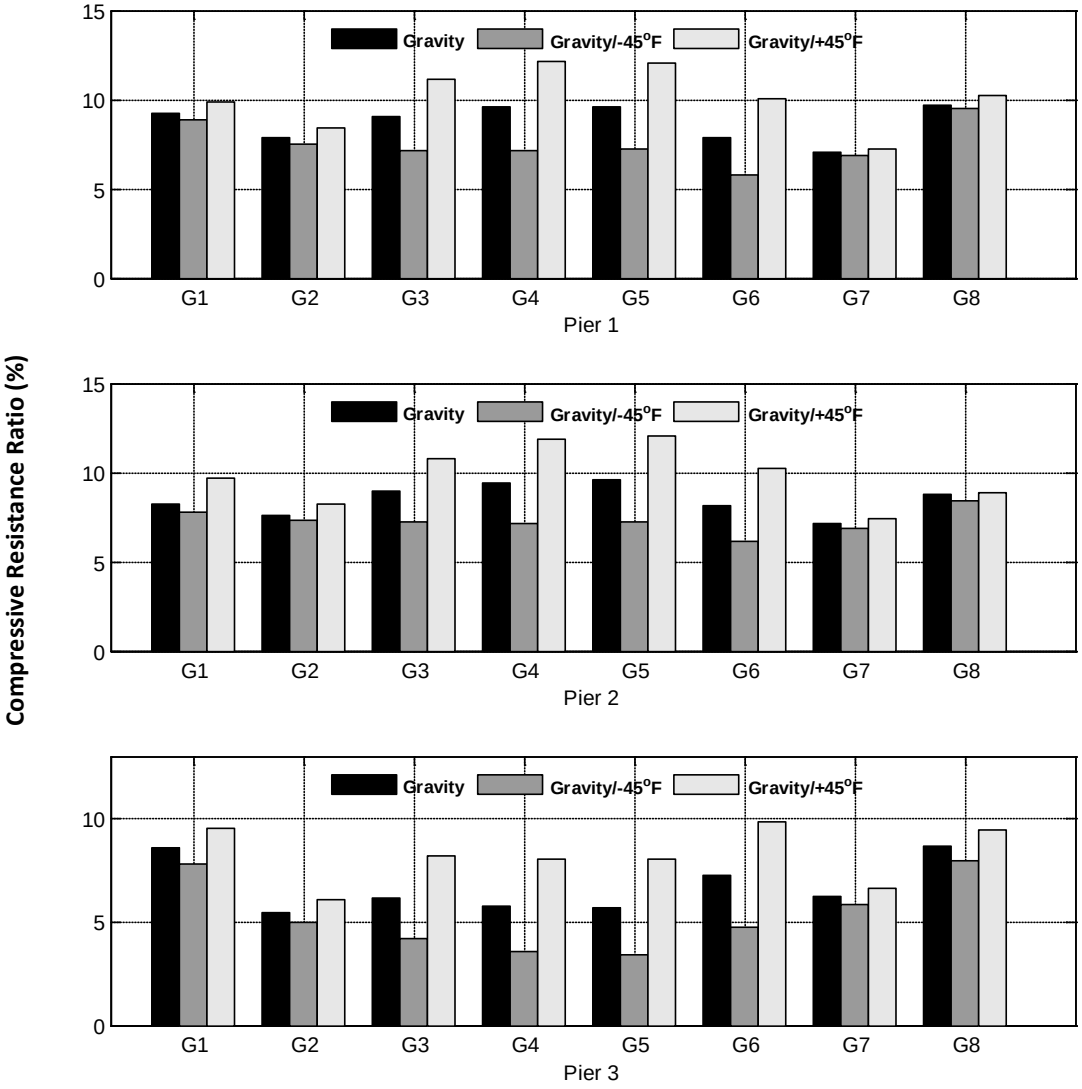


**Figure 7.21. Compressive Resistance Ratios – Piers – Flexible Piers**

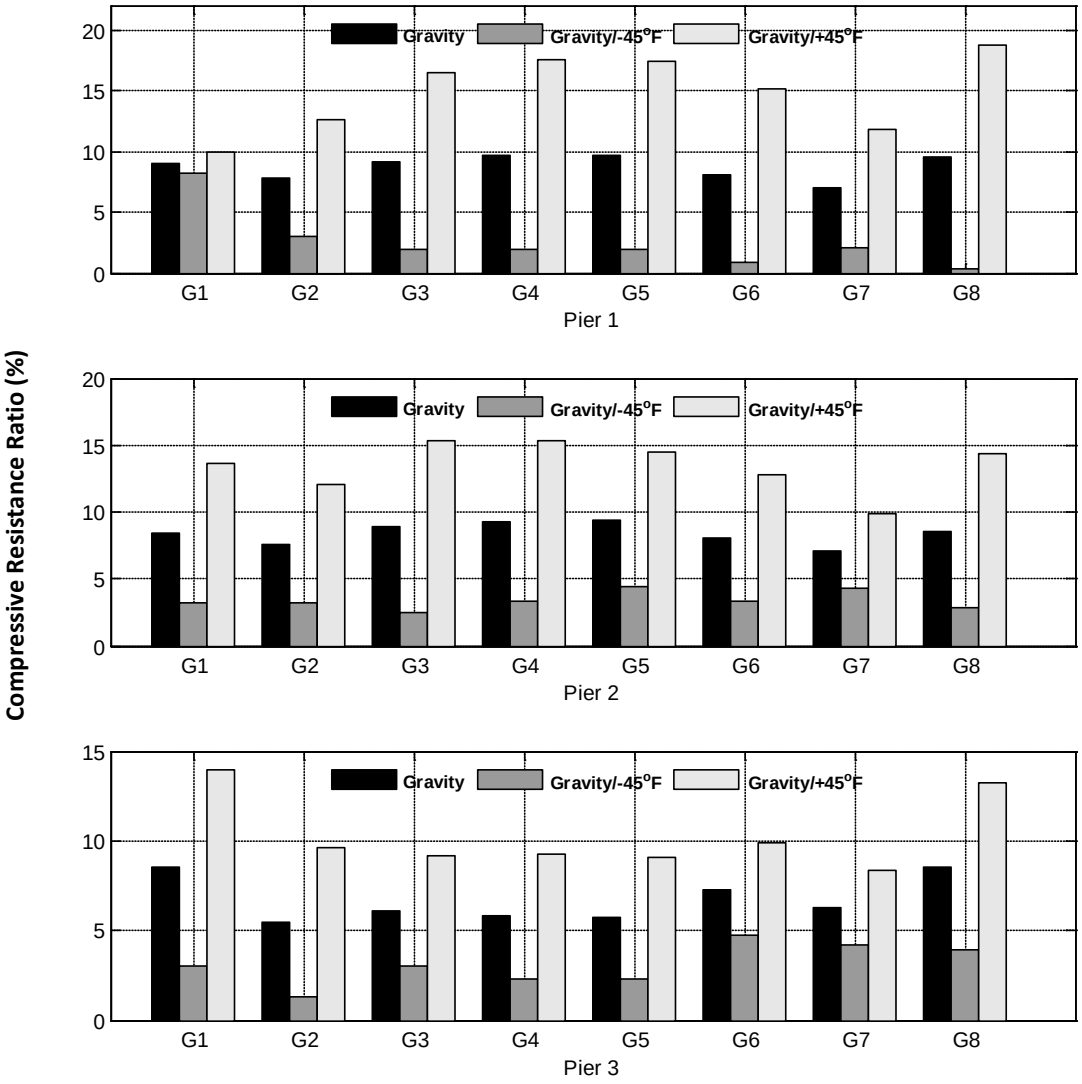


**Figure 7.22. Compressive Resistance Ratios – Piers – Rigid Piers**

Although the largest magnitude of compressive axial stresses due to thermal loading occurs in spans 2 and 3 when +45°F loading is employed, the I-girders are in a more constant, uniform state of axial compression at the piers. For both rigid and flexible pier cases, temperature decrease or increase only decreases or increases, respectively, the magnitude of axial I-girder compression at the bridge piers. Just as was the case at the mid-spans, the largest compressive axial stresses at the piers occur when the rigid pier model is subjected to gravity followed by

+45°F thermal loading. However, even though pier flexibility relieves some axial compressive stresses at the piers, gravity and +45°F thermal loading leads to compressive resistance ratios up to 12.1% at pier 1, 12.6% at pier 2, and 9.83% at pier 3 when the bridge piers are flexible. When bridge piers are rigid members, compressive resistance ratios reach 18.7% at pier 1, 15.4% at pier 2, and 14.0% at pier 3.

It is evident from the results in Figures 7.19 – 7.22 that stresses caused by restrained thermal loading are consuming some of the compressive capacity of the I-girders. Previous results have shown that girder axial stresses are larger when bridge piers are modeled rigidly, which obviously leads to larger compressive stress ratios for the rigid pier case compared to the flexible pier case. In reality, the level of thermal compressive I-girder stresses is mostly likely somewhere between the level for the rigid and flexible pier cases. Clearly, thermal loads on the Buffalo Creek Bridge, especially +45°F loading, will lead to axial girder stresses that consume some of the compressive capacity of the I-girders. This could become problematic as additional unforeseen axial stresses arise on the structure or additional flexural loads are incurred on the structure, because the presence of these axial compressive stresses will lower the load carrying capacity of the bridge. In addition, any increase in compressive stress levels makes the webs more susceptible to buckling. These results indicate that bridge designers should not neglect the effect that thermal loading has on the state of axial stress on the bridge.

## 7.5 Impact of Thermal Loading on I-Girder Capacity

To expand upon the axial stress results presented in the previous section, this section investigates how thermal loading affects the overall bridge capacity. The capacity of an I-girder web plate can be quantified using the relationship presented in Equation 7.7.

$$\frac{\sigma_a}{P_r} + \frac{\sigma_b}{F_{cr}} \leq 1.0 \qquad (7.7)$$

In Equation 7.7, $\sigma_a$ is the maximum axial compressive stress measured in the cross section, $P_r$ is the maximum allowable axial stress derived from Equations 7.4 – 7.6, $\sigma_b$ is the maximum bending stress measured in the cross section, and $F_{cr}$ is the maximum allowable bending stress of a web plate without longitudinal stiffeners as defined in Article 6.2.1 of AASHTO (2003) and calculated in Equation 7.2. This value is taken to be the lesser of the web bend-buckling resistance factor and the material yield strength. Equation 7.7 represents a structural capacity ratio for the I-girders, whereby if the ratio exceeds 1.0, the girders allowable capacity has been exceeded and the girder may be considered to be unstable. Web cross section longitudinal stress profiles in Figures C.49 – C.64 will be analyzed using Equation 7.7 to determine how thermal loading might be affecting girder stability.

To determine the level of bending stress in a particular cross section, the magnitude of axial stress in the cross section calculated using Equation 7.3 must first be removed from the longitudinal stress profile. However, even after the removal of the axial stress component from the overall stress profile, web bending stress profiles directly over the piers show varying degrees of nonlinear behavior at the top and bottom flange of the web panels. These stress nonlinearities are not directly related to bending stresses, rather they represent stress concentrations in the webs caused by the bridge bearings. Examples of these web concentrations can be seen in Figures 7.23 and 7.24. The largest magnitude of stress concentrations occur in the webs of girders 3-6 at the piers because the bearings on the piers supporting girders 3-6 are fixed bearings, as is shown in Figure 4.4.

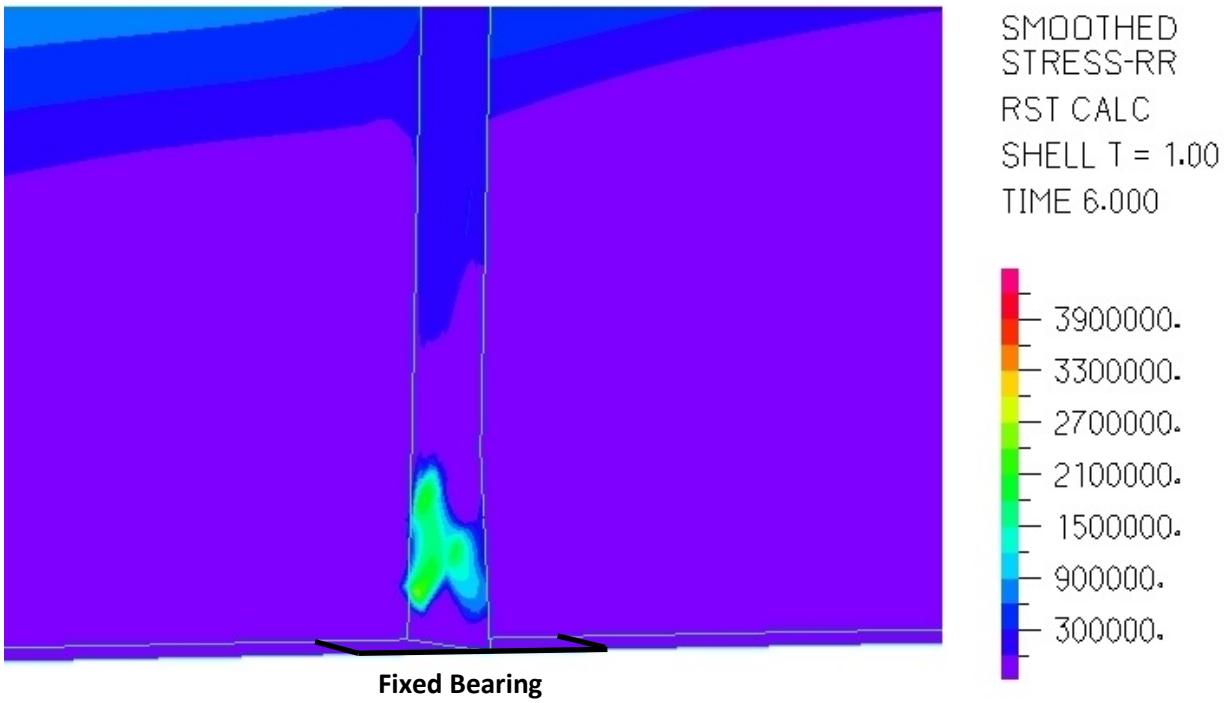


**Figure 7.23. Web Stress Concentration – Girder 3 – Pier 1 – Rigid Piers - +45°F Loading**

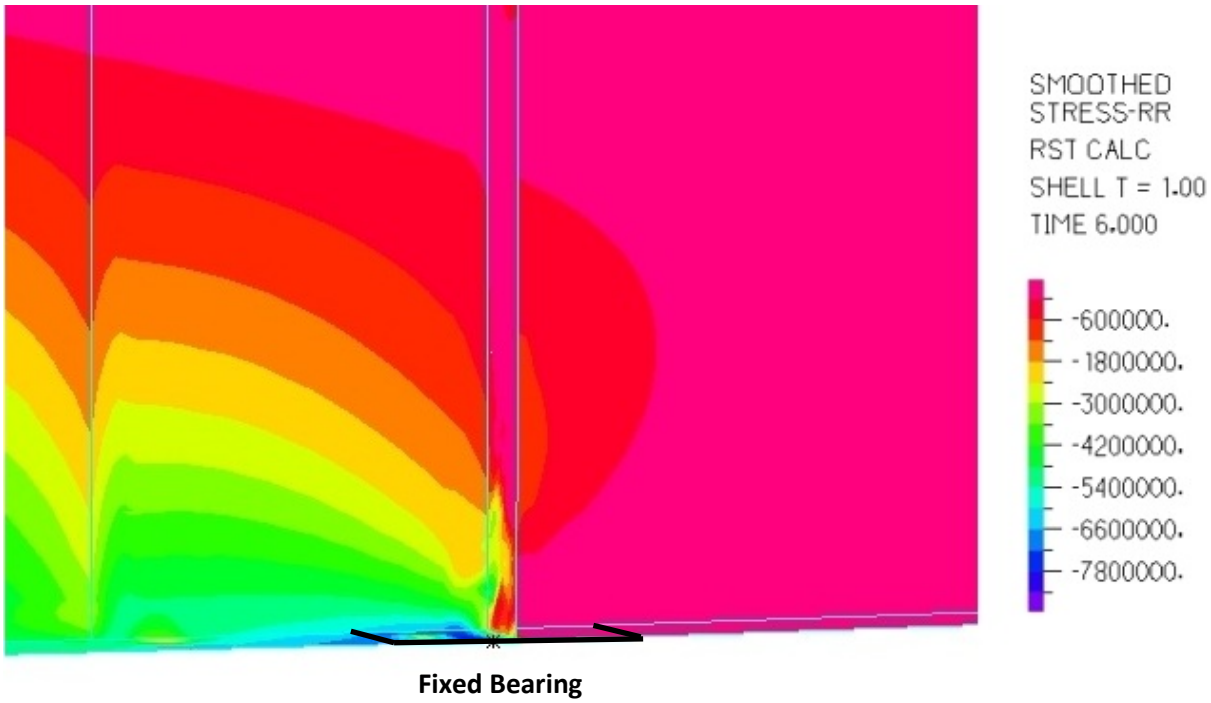


**Figure 7.24. Web Stress Concentration – Girder 6 – Pier 3 – Rigid Piers - +45°F Loading**

**Table 7. 3. Girder Capacity Ratios at Mid-Spans**

| | | -45°F | | | | | | +45°F | | | | | |
|---|---|---|---|---|---|---|---|---|---|---|---|---|---|
| | | Flexible | | | Rigid | | | Flexible | | | Rigid | | |
| | | $\sigma_a/\sigma_{ac}$ | $\sigma_b/\sigma_{ba}$ | Total Ratio | $\sigma_a/\sigma_{ac}$ | $\sigma_b/\sigma_{ba}$ | Total Ratio | $\sigma_a/\sigma_{ac}$ | $\sigma_b/\sigma_{ba}$ | Total Ratio | $\sigma_a/\sigma_{ac}$ | $\sigma_b/\sigma_{ba}$ | Total Ratio |
| Girder 1 | MS1 | 0.032 | 0.318 | 0.350 | 0.077 | 0.352 | 0.429 | 0.058 | 0.368 | 0.426 | 0.009 | 0.329 | 0.338 |
| | MS2 | 0.007 | 0.245 | 0.252 | - | 0.215 | 0.215 | 0.059 | 0.320 | 0.379 | 0.294 | 0.799 | **1.093** |
| | MS3 | - | 0.192 | 0.192 | - | 0.173 | 0.173 | 0.020 | 0.235 | 0.254 | 0.236 | 0.648 | **0.884** |
| | MS4 | - | 0.034 | 0.034 | - | 0.018 | 0.018 | 0.011 | 0.062 | 0.074 | 0.031 | 0.122 | 0.153 |
| Girder 2 | MS1 | 0.017 | 0.301 | 0.317 | 0.061 | 0.320 | 0.381 | 0.041 | 0.343 | 0.384 | - | 0.318 | 0.318 |
| | MS2 | 0.001 | 0.253 | 0.254 | - | 0.241 | 0.241 | 0.053 | 0.324 | 0.377 | 0.298 | 0.786 | **1.084** |
| | MS3 | - | 0.200 | 0.200 | - | 0.183 | 0.183 | 0.022 | 0.241 | 0.263 | 0.239 | 0.652 | **0.891** |
| | MS4 | - | 0.052 | 0.052 | 0.022 | 0.070 | 0.092 | 0.012 | 0.086 | 0.098 | - | 0.096 | 0.096 |
| Girder 3 | MS1 | 0.016 | 0.312 | 0.328 | 0.059 | 0.324 | 0.383 | 0.041 | 0.353 | 0.394 | - | 0.336 | 0.336 |
| | MS2 | 0.004 | 0.266 | 0.270 | - | 0.259 | 0.259 | 0.050 | 0.328 | 0.377 | 0.295 | 0.775 | **1.071** |
| | MS3 | 0.005 | 0.210 | 0.216 | - | 0.188 | 0.188 | 0.030 | 0.250 | 0.280 | 0.240 | 0.634 | **0.874** |
| | MS4 | - | 0.032 | 0.032 | 0.087 | 0.297 | 0.384 | 0.010 | 0.061 | 0.071 | - | 0.122 | 0.122 |
| Girder 4 | MS1 | 0.018 | 0.324 | 0.342 | 0.058 | 0.327 | 0.385 | 0.042 | 0.363 | 0.405 | - | 0.357 | 0.357 |
| | MS2 | 0.009 | 0.277 | 0.286 | - | 0.276 | 0.276 | 0.048 | 0.330 | 0.379 | 0.291 | 0.753 | **1.044** |
| | MS3 | 0.001 | 0.215 | 0.216 | - | 0.198 | 0.198 | 0.026 | 0.253 | 0.279 | 0.235 | 0.639 | **0.874** |
| | MS4 | 0.002 | 0.050 | 0.052 | 0.117 | 0.319 | 0.435 | 0.011 | 0.077 | 0.088 | - | 0.149 | 0.149 |
| Girder 5 | MS1 | 0.012 | 0.332 | 0.345 | 0.050 | 0.325 | 0.374 | 0.037 | 0.374 | 0.411 | - | 0.379 | 0.379 |
| | MS2 | 0.011 | 0.291 | 0.302 | - | 0.295 | 0.295 | 0.046 | 0.338 | 0.383 | 0.287 | 0.749 | **1.035** |
| | MS3 | 0.003 | 0.210 | 0.213 | - | 0.204 | 0.204 | 0.030 | 0.250 | 0.280 | 0.238 | 0.622 | **0.860** |
| | MS4 | - | 0.058 | 0.058 | 0.109 | 0.242 | 0.352 | 0.007 | 0.091 | 0.099 | - | 0.159 | 0.159 |
| Girder 6 | MS1 | 0.029 | 0.361 | 0.390 | 0.062 | 0.348 | 0.411 | 0.054 | 0.404 | 0.457 | 0.018 | 0.415 | 0.433 |
| | MS2 | 0.016 | 0.307 | 0.323 | - | 0.307 | 0.307 | 0.049 | 0.353 | 0.402 | 0.275 | 0.752 | **1.027** |
| | MS3 | - | 0.189 | 0.189 | - | 0.202 | 0.202 | 0.026 | 0.234 | 0.260 | 0.225 | 0.580 | **0.804** |
| | MS4 | - | 0.024 | 0.024 | 0.084 | 0.057 | 0.141 | 0.010 | 0.058 | 0.068 | - | 0.117 | 0.117 |
| Girder 7 | MS1 | 0.029 | 0.363 | 0.393 | 0.061 | 0.343 | 0.404 | 0.056 | 0.409 | 0.465 | 0.023 | 0.428 | 0.451 |
| | MS2 | 0.020 | 0.310 | 0.330 | - | 0.313 | 0.313 | 0.051 | 0.353 | 0.404 | 0.274 | 0.741 | **1.015** |
| | MS3 | - | 0.191 | 0.191 | - | 0.201 | 0.201 | 0.033 | 0.239 | 0.272 | 0.237 | 0.603 | **0.840** |
| | MS4 | - | 0.034 | 0.034 | 0.024 | 0.019 | 0.043 | 0.013 | 0.084 | 0.098 | - | 0.107 | 0.107 |
| Girder 8 | MS1 | 0.031 | 0.360 | 0.391 | 0.062 | 0.331 | 0.393 | 0.059 | 0.406 | 0.466 | 0.028 | 0.434 | 0.462 |
| | MS2 | 0.016 | 0.325 | 0.341 | - | 0.330 | 0.330 | 0.044 | 0.358 | 0.402 | 0.269 | 0.743 | **1.013** |
| | MS3 | - | 0.181 | 0.181 | - | 0.203 | 0.203 | 0.033 | 0.228 | 0.261 | 0.231 | 0.695 | **0.926** |
| | MS4 | - | 0.016 | 0.016 | - | 0.096 | 0.096 | 0.008 | 0.042 | 0.050 | 0.028 | 0.116 | 0.144 |

**Table 7. 4. Girder Capacity Ratios at Piers (G1-G4)**

| | | -45°F | | | | | | +45°F | | | | | |
|---|---|---|---|---|---|---|---|---|---|---|---|---|---|
| | | Flexible | | | Rigid | | | Flexible | | | Rigid | | |
| | | $\sigma_a/\sigma_{ac}$ | $\sigma_b/\sigma_{ba}$ | Total Ratio | $\sigma_a/\sigma_{ac}$ | $\sigma_b/\sigma_{ba}$ | Total Ratio | $\sigma_a/\sigma_{ac}$ | $\sigma_b/\sigma_{ba}$ | Total Ratio | $\sigma_a/\sigma_{ac}$ | $\sigma_b/\sigma_{ba}$ | Total Ratio |
| Girder 1 | P1/CS1 | - | 0.199 | 0.199 | 0.037 | 0.277 | 0.314 | 0.012 | 0.198 | 0.209 | - | 0.157 | 0.157 |
| | P1 | 0.088 | 0.316 | 0.404 | 0.081 | 0.432 | 0.513 | 0.099 | 0.320 | 0.418 | 0.100 | 0.277 | 0.377 |
| | P1/CS2 | - | 0.314 | 0.314 | - | 0.124 | 0.124 | 0.011 | 0.201 | 0.212 | 0.138 | 0.485 | 0.622 |
| | P2/CS1 | - | 0.181 | 0.181 | - | 0.184 | 0.184 | 0.024 | 0.206 | 0.231 | 0.086 | 0.311 | 0.397 |
| | P2 | 0.078 | 0.343 | 0.421 | 0.033 | 0.331 | 0.363 | 0.097 | 0.387 | 0.484 | 0.137 | 0.403 | 0.540 |
| | P2/CS2 | - | 0.183 | 0.183 | - | 0.185 | 0.185 | - | 0.170 | 0.170 | 0.087 | 0.319 | 0.406 |
| | P3/CS1 | 0.011 | 0.148 | 0.159 | - | 0.145 | 0.145 | 0.026 | 0.175 | 0.200 | 0.089 | 0.282 | 0.370 |
| | P3 | 0.078 | 0.215 | 0.293 | 0.030 | 0.229 | 0.259 | 0.095 | 0.223 | 0.318 | 0.140 | 0.417 | 0.557 |
| Girder 2 | P1/CS1 | - | 0.207 | 0.207 | 0.041 | 0.278 | 0.319 | 0.015 | 0.210 | 0.225 | - | 0.162 | 0.162 |
| | P1 | 0.075 | 0.248 | 0.323 | 0.030 | 0.226 | 0.256 | 0.084 | 0.248 | 0.332 | 0.126 | 0.317 | 0.443 |
| | P1/CS2 | - | 0.261 | 0.261 | - | 0.142 | 0.142 | 0.013 | 0.212 | 0.225 | 0.163 | 0.500 | 0.663 |
| | P2/CS1 | - | 0.195 | 0.195 | - | 0.209 | 0.209 | 0.019 | 0.198 | 0.217 | 0.094 | 0.296 | 0.391 |
| | P2 | 0.073 | 0.240 | 0.313 | 0.032 | 0.273 | 0.306 | 0.082 | 0.241 | 0.324 | 0.121 | 0.338 | 0.459 |
| | P2/CS2 | - | 0.196 | 0.196 | - | 0.211 | 0.211 | 0.004 | 0.190 | 0.195 | 0.088 | 0.286 | 0.373 |
| | P3/CS1 | 0.062 | 0.159 | 0.221 | - | 0.154 | 0.154 | 0.079 | 0.179 | 0.258 | 0.154 | 0.289 | 0.443 |
| | P3 | 0.050 | 0.179 | 0.229 | 0.013 | 0.178 | 0.191 | 0.061 | 0.196 | 0.256 | 0.096 | 0.321 | 0.417 |
| Girder 3 | P1/CS1 | 0.006 | 0.223 | 0.228 | 0.056 | 0.315 | 0.371 | 0.008 | 0.217 | 0.224 | - | 0.162 | 0.162 |
| | P1 | 0.071 | 0.257 | 0.328 | 0.019 | 0.197 | 0.216 | 0.111 | 0.276 | 0.387 | 0.164 | 0.355 | 0.520 |
| | P1/CS2 | - | 0.204 | 0.204 | - | 0.151 | 0.151 | 0.023 | 0.239 | 0.262 | 0.183 | 0.557 | 0.740 |
| | P2/CS1 | - | 0.203 | 0.203 | - | 0.222 | 0.222 | 0.011 | 0.200 | 0.211 | 0.095 | 0.297 | 0.392 |
| | P2 | 0.073 | 0.254 | 0.326 | 0.025 | 0.297 | 0.322 | 0.108 | 0.263 | 0.371 | 0.153 | 0.351 | 0.504 |
| | P2/CS2 | - | 0.201 | 0.201 | - | 0.230 | 0.230 | 0.014 | 0.203 | 0.217 | 0.081 | 0.271 | 0.352 |
| | P3/CS1 | - | 0.174 | 0.174 | 0.168 | 0.447 | 0.615 | 0.011 | 0.198 | 0.208 | - | 0.200 | 0.200 |
| | P3 | 0.042 | 0.199 | 0.241 | 0.031 | 0.254 | 0.284 | 0.082 | 0.236 | 0.318 | 0.092 | 0.235 | 0.327 |
| Girder 4 | P1/CS1 | 0.001 | 0.227 | 0.228 | 0.043 | 0.304 | 0.347 | 0.012 | 0.226 | 0.238 | - | 0.172 | 0.172 |
| | P1 | 0.071 | 0.273 | 0.344 | 0.019 | 0.242 | 0.260 | 0.121 | 0.310 | 0.431 | 0.175 | 0.438 | 0.613 |
| | P1/CS2 | - | 0.131 | 0.131 | - | 0.162 | 0.162 | 0.020 | 0.232 | 0.251 | 0.175 | 0.532 | 0.707 |
| | P2/CS1 | - | 0.205 | 0.205 | - | 0.233 | 0.233 | 0.012 | 0.206 | 0.218 | 0.097 | 0.303 | 0.400 |
| | P2 | 0.071 | 0.263 | 0.334 | 0.033 | 0.313 | 0.345 | 0.119 | 0.294 | 0.412 | 0.154 | 0.365 | 0.519 |
| | P2/CS2 | - | 0.206 | 0.206 | - | 0.246 | 0.246 | 0.013 | 0.207 | 0.220 | 0.071 | 0.251 | 0.322 |
| | P3/CS1 | - | 0.169 | 0.169 | 0.119 | 0.380 | 0.499 | 0.006 | 0.186 | 0.192 | - | 0.068 | 0.068 |
| | P3 | 0.035 | 0.208 | 0.243 | 0.023 | 0.277 | 0.300 | 0.080 | 0.259 | 0.339 | 0.093 | 0.231 | 0.324 |

**Table 7. 5. Girder Capacity Ratios at Piers (G5-G8)**

| | | -45°F | | | | | | +45°F | | | | | |
|---|---|---|---|---|---|---|---|---|---|---|---|---|---|
| | | Flexible | | | Rigid | | | Flexible | | | Rigid | | |
| | | $\sigma_a/\sigma_{ac}$ | $\sigma_b/\sigma_{ba}$ | Total Ratio | $\sigma_a/\sigma_{ac}$ | $\sigma_b/\sigma_{ba}$ | Total Ratio | $\sigma_a/\sigma_{ac}$ | $\sigma_b/\sigma_{ba}$ | Total Ratio | $\sigma_a/\sigma_{ac}$ | $\sigma_b/\sigma_{ba}$ | Total Ratio |
| Girder 5 | P1/CS1 | - | 0.224 | 0.224 | 0.034 | 0.290 | 0.324 | 0.012 | 0.225 | 0.237 | - | 0.169 | 0.169 |
| | P1 | 0.072 | 0.274 | 0.346 | 0.019 | 0.249 | 0.268 | 0.120 | 0.303 | 0.424 | 0.174 | 0.439 | 0.613 |
| | P1/CS2 | - | 0.072 | 0.072 | - | 0.171 | 0.171 | 0.020 | 0.233 | 0.252 | 0.169 | 0.518 | 0.688 |
| | P2/CS1 | 0.000 | 0.207 | 0.207 | - | 0.239 | 0.239 | 0.014 | 0.207 | 0.221 | 0.100 | 0.306 | 0.406 |
| | P2 | 0.072 | 0.267 | 0.338 | 0.044 | 0.332 | 0.376 | 0.120 | 0.300 | 0.421 | 0.144 | 0.337 | 0.481 |
| | P2/CS2 | - | 0.208 | 0.208 | - | 0.254 | 0.254 | 0.011 | 0.207 | 0.218 | 0.066 | 0.236 | 0.303 |
| | P3/CS1 | - | 0.175 | 0.175 | 0.129 | 0.465 | 0.594 | 0.005 | 0.187 | 0.193 | - | 0.008 | 0.008 |
| | P3 | 0.034 | 0.213 | 0.247 | 0.023 | 0.300 | 0.324 | 0.080 | 0.253 | 0.333 | 0.091 | 0.197 | 0.288 |
| Girder 6 | P1/CS1 | - | 0.221 | 0.221 | 0.023 | 0.285 | 0.308 | 0.011 | 0.221 | 0.232 | - | 0.164 | 0.164 |
| | P1 | 0.058 | 0.266 | 0.324 | 0.009 | 0.239 | 0.248 | 0.101 | 0.269 | 0.370 | 0.152 | 0.437 | 0.588 |
| | P1/CS2 | - | 0.038 | 0.038 | - | 0.171 | 0.171 | 0.012 | 0.225 | 0.237 | 0.140 | 0.506 | 0.646 |
| | P2/CS1 | - | 0.200 | 0.200 | - | 0.233 | 0.233 | 0.011 | 0.201 | 0.212 | 0.095 | 0.337 | 0.432 |
| | P2 | 0.062 | 0.265 | 0.327 | 0.033 | 0.330 | 0.363 | 0.102 | 0.252 | 0.354 | 0.128 | 0.277 | 0.405 |
| | P2/CS2 | - | 0.197 | 0.197 | - | 0.245 | 0.245 | - | 0.191 | 0.191 | 0.052 | 0.226 | 0.277 |
| | P3/CS1 | 0.011 | 0.163 | 0.174 | 0.192 | 0.448 | 0.640 | 0.017 | 0.170 | 0.187 | - | 0.197 | 0.197 |
| | P3 | 0.048 | 0.203 | 0.250 | 0.047 | 0.293 | 0.340 | 0.098 | 0.204 | 0.302 | 0.099 | 0.144 | 0.242 |
| Girder 7 | P1/CS1 | - | 0.219 | 0.219 | 0.020 | 0.280 | 0.300 | 0.011 | 0.220 | 0.231 | - | 0.161 | 0.161 |
| | P1 | 0.069 | 0.250 | 0.319 | 0.021 | 0.229 | 0.250 | 0.072 | 0.257 | 0.330 | 0.118 | 0.416 | 0.534 |
| | P1/CS2 | - | 0.015 | 0.015 | - | 0.175 | 0.175 | 0.010 | 0.218 | 0.228 | 0.137 | 0.490 | 0.627 |
| | P2/CS1 | - | 0.192 | 0.192 | - | 0.239 | 0.239 | 0.007 | 0.188 | 0.195 | 0.081 | 0.280 | 0.361 |
| | P2 | 0.069 | 0.243 | 0.312 | 0.043 | 0.278 | 0.321 | 0.074 | 0.245 | 0.319 | 0.099 | 0.336 | 0.436 |
| | P2/CS2 | - | 0.195 | 0.195 | - | 0.237 | 0.237 | 0.008 | 0.192 | 0.199 | 0.084 | 0.292 | 0.376 |
| | P3/CS1 | 0.008 | 0.142 | 0.150 | - | 0.151 | 0.151 | 0.020 | 0.169 | 0.189 | 0.056 | 0.222 | 0.278 |
| | P3 | 0.059 | 0.167 | 0.226 | 0.042 | 0.177 | 0.219 | 0.066 | 0.174 | 0.241 | 0.083 | 0.271 | 0.354 |
| Girder 8 | P1/CS1 | - | 0.218 | 0.218 | 0.015 | 0.279 | 0.293 | 0.010 | 0.217 | 0.228 | - | 0.159 | 0.159 |
| | P1 | 0.095 | 0.321 | 0.416 | 0.004 | 0.241 | 0.245 | 0.102 | 0.321 | 0.423 | 0.187 | 0.533 | 0.720 |
| | P1/CS2 | - | 0.003 | 0.003 | - | 0.180 | 0.180 | 0.010 | 0.209 | 0.219 | 0.129 | 0.461 | 0.590 |
| | P2/CS1 | - | 0.188 | 0.188 | - | 0.241 | 0.241 | 0.007 | 0.177 | 0.184 | 0.076 | 0.260 | 0.336 |
| | P2 | 0.084 | 0.286 | 0.371 | 0.029 | 0.279 | 0.308 | 0.089 | 0.285 | 0.374 | 0.143 | 0.491 | 0.635 |
| | P2/CS2 | - | 0.190 | 0.190 | - | 0.232 | 0.232 | 0.006 | 0.180 | 0.185 | 0.087 | 0.292 | 0.380 |
| | P3/CS1 | 0.072 | 0.126 | 0.199 | 0.035 | 0.139 | 0.174 | 0.088 | 0.147 | 0.236 | 0.126 | 0.211 | 0.337 |
| | P3 | 0.080 | 0.200 | 0.279 | 0.039 | 0.200 | 0.240 | 0.094 | 0.207 | 0.301 | 0.132 | 0.390 | 0.522 |

For the purposes of this study, calculating the bending stress in a cross section assumes that the bending stress components of the longitudinal stress profile is mostly linear. Therefore, any stress concentrations are removed from the bending stress profiles prior to calculating the bending stress magnitude in the cross section. As for axial stresses, these values have already been computed and discussed in Section 7.4. The axial component of Equation 7.7 is only concerned with compressive axial stresses. In Tables 7.3 – 7.5, cells containing a dash mark represent cross sections that are axially in tension under the specified load state.

It was previously mentioned that, under the loading conditions put forth in this study, it would be expected that axial stresses in the I-girder webs would be a result of temperature loads and bending stresses a result of flexural loading. However, just as results in Section 7.4 show that gravity loads on the structure do create a small degree of axial stress in the I-girder webs, thermal loads placed on the Buffalo Creek Bridge will cause increases or decreases in bending stress magnitude, depending on the thermal load. As Table 7.3 shows, results for the axial capacity ratio ($\sigma_a/P_r$) at the mid-span locations follow closely the axial stress results previously presented in this chapter. The larger the axial compressive stress at a particular location in Figures 7.15 and 7.16, the larger the percentage of axial capacity that is consumed under the specified loading state, leading to a larger axial capacity ratio at that location for that state of loading. Whereas the axial capacity ratios are primarily a function of the axial compressive stress magnitude at a location, the bending stress capacity ratio ($\sigma_b/F_{cr}$) is a function of the bending stress magnitude and the longitudinal stress profile. Not only does the bending stress capacity ratio change as the bending stress in the section changes, the web bend-buckling resistance ($F_{cr}$) changes as the stress profile changes. As the depth of the web in compression increases, the value for $F_{cr}$ decreases (see Equation 7.2). Interestingly, at the center of spans 2 and 3, a +45°F thermal load slightly decreases the bending stress magnitude in the web cross section. However, as Figures C.41 – C.48 show, the depth of the web in compression increases, decreasing the bend-buckling resistance for the particular cross section. As a result, even though the bending stress magnitude decreases, the bending capacity ratio increases.

Therefore, not only are thermally induced axial stresses impacting the structural capacity of the bridge by introducing axial forces on the I-girders not accounted for during design, but they are also decreasing the I-girder capacity to handle flexural loads by introducing uniform compressive stresses that decrease the flexural capacity of the I-girder. Ratios in Table 7.3 show that, in the majority of cases, gravity and thermal loads consume more of the girders available capacity when the bridge piers are modeled as rigid members. The most significant results in Table 6.3 occur at the center of spans 2 and 3 when the bridge piers are rigid and the bridge is loaded with gravity followed by +45°F thermal loading. The high level of compressive axial stress from constrained thermal expansion in these spans combined with the decrease in $F_{cr}$ caused by these axial stresses leads to total capacity ratios exceeding 0.8 in span 3 of all girders and 1.0 in span 2 of all girders.

To be thorough, I-girder capacity ratios were computed at all the locations at and near the piers where longitudinal stress profiles are presented in Figures C.49 – C.64. For the most part, thermal loading has the largest impact on I-girder web capacity directly over the piers as these locations incur larger thermally induced axial stress. As was the case at the mid-spans, the most significant effect on girder capacity at the piers is found when the bridge piers are rigid and +45°F loading is applied. However, even when flexible piers are used, gravity and thermal loading are shown to consume greater than 10% of the I-girders axial capacity in several locations directly over the piers. Once again, increasing compressive axial stress levels decrease available girder capacity through increasing levels of axial stress and decreasing available bending capacity. Although stress levels at bridge piers do not lead to cross sections exceeding combined axial and bending capacity, results show web capacities exceeding 50% in several cross sections, meaning that stresses on the section have already exceeded half of the structural capacity under only gravity and thermal loading.

The effect thermal loading has on the capacity of the Buffalo Creek Bridge I-girders is directly correlated to how much axial compressive stress the temperature load creates in the girders. Not only does an increase in axial compressive stress lead to an increase in the axial capacity

ratio component of the girder capacity equation, but it also increases the bending capacity ratio component through a decrease in the web bend-buckling value ($F_{cr}$). Since previous results have shown that thermal increases induce compressive axial stresses in I-girders boundary conditions do not allow thermal expansion and contraction, these cases will likely have the girder capacity most negatively impacted by thermal loads. In fact, results in Table 6.3 show that a temperature increase causes the girder capacity ratios to exceed 1.0 in all cases in mid-spans 2 and 0.80 in all cases in mid-span 3 when the bridge piers are rigid and the bridge is loaded with self-weight and a +45°F uniform thermal load. This is certainly of concern because these results show that the stresses on the Buffalo Creek Bridge I-girders could exceed the allowed capacity prior to any design or live loading being introduced on the structure. On the other hand, as expected, it appears that modeling the piers with full flexibility decreases the girder capacity ratios. This would be expected because previous results have also shown that pier flexibility decreases thermal axial stresses in the bridge I-girders. However, results are likely somewhere between the rigid pier and flexible pier results and designers would consider the piers as rigid members.

## 7.6 Discussion and Conclusions

The case study on the state of stress of the Buffalo Creek Bridge when subjected to self-weight and thermal loading reveals that changing thermal conditions on the structure will result in an increase in the magnitude of stress on the bridge. Design assumes that stresses caused by changing thermal conditions are relieved through the expansion and contraction of the bridge superstructure allowed by the design of the boundary conditions. While these results show that the magnitude of thermal stresses induced on the Buffalo Creek Bridge is reduced when the bridge piers are modeled as flexible members, this movement still does not fully relieve thermal stresses in the I-girder webs. In reality, actual bridge thermal stress states will likely be somewhere between the rigid and flexible pier state presented here because the bridge piers will exhibit some degree of flexibility, but the bridge bearings are not likely to function ideally

as designed and will not allow full, free thermal expansion and contraction at bearings designed to do so. In fact, the study by Beckett (2010) found that bearings on curved I-girder bridges can "lock-up" when subjected to unexpected thermal expansion and contraction.

Although results presented in this chapter reveal that thermal loading will lead to stresses in the I-girder webs of the Buffalo Creek Bridge, in most cases the level of stress is not such that failure or yielding is of concern. However, in the rigid pier case, results show that thermal loading leads to overall stress levels in several locations that exceed 50% of the material yield strength. Positive thermal loading leads to compressive longitudinal stresses in the center two spans, spans 2 and 3, causing mid-span webs to fail the AASHTO (2010) web bend-buckling guidelines. This indicates that I-girder webs could be experiencing buckling during construction and prior to any live loading on the bridge. Furthermore, results show that the stipulation in AASHTO (2010) that the bridge designer need not study web bend-buckling for cross sections in positive flexure once the deck has cured and acts compositely with the bridge deck was proven to be erroneous. This does not hold true when considering rigid piers and forces from thermal loading because axial compressive stresses lead to an increase in the stress magnitude in the cross-section while decreasing the web bend-buckling resistance as the depth of the web in compression increases. These axial forces from thermal loading are, in-fact, reducing the magnitude of flexural capacity of the cross section. Study of the overall I-girder capacity, in terms of axial and bending stresses, discloses the results that gravity loading followed by a +45°F thermal load leads to the total I-girder web capacity ratio exceeding the allowable capacity at eight mid-span locations while exceeding 80% of capacity at all locations in the center two spans. The capacity consumed is a direct correlation to the degree of axial stress thermal loading induces in the section. Increase in the axial stress magnitude increases the axial stress ratio as the axial stress magnitude increases while increasing the bending stress ratio by decreasing the allowing bending stress in the web as the depth of the web in compression increases.

As stated, in the majority of cases studied here, the introduction of thermal loading will not cause I-girder sections to yield. However, results have shown unequivocally that thermal loading leads to an increase in overall, longitudinal, axial, and bending stresses in the web cross sections of the Buffalo Creek Bridge. These magnitudes could likely be higher for in-service applications as relatively mild temperature increases and decreases of 45°F were chosen for this study. Stresses presented here that are caused by thermal loads are additional stresses not considered by designers, and therefore consume I-girder capacity that was designed to accommodate the design loads. As I-girders only have a finite capacity available to handle all load combinations that can arise, results here show that thermal loading on the Buffalo Creek Bridge in the early stages of construction before the introduction of any traffic or live loading will decrease the bridge capacity, and in some cases, may lead to premature buckling of the I-girder webs. The analysis in this chapter clearly shows that changing thermal conditions should be considered by bridge designers in the design of bridge I-girders and bridge boundary conditions. Design should consider the impact that constrained thermal expansion and contraction will have on I-girder stresses and either accommodate for these stresses levels through girder design or the redesign of boundary conditions to better accommodate changing thermal conditions.

# CHAPTER EIGHT

# CONCLUSIONS AND FUTURE RESEARCH

## 8.1 Conclusions

The main focal point of this research study has been to investigate the impact changing thermal conditions will have on the I-girders of curved steel I-girder bridges. The initial phase of the research focused on a couple of smaller scale parametric studies aimed at determining how thermal loading effects the web deformations and web and flange stresses a of a single curved I-section and of a two curved I-girder section representative of a small bridge section. This was followed by a full scale case study utilizing detailed finite element modeling techniques to study the effects that thermal loading has on the Buffalo Creek Bridge I-girders after completion of construction but prior to any traffic loading. Two models were created, one idealizing the bridge piers as rigid members and the other idealizing the bridge piers as flexible members, to study how changing thermal conditions will impact these two cases differently. The Buffalo Creek Bridge case study looks at how thermal loads affect local and global out-of-plane web deformations, both along the length of the girders and through the depth of the web, as well as the state of stress in the I-girder webs in terms of overall effective stresses, longitudinal stresses, and pure axial and bending stresses.

The first small scale parametric study reported on in Chapter Three on single curved I-sections with varying web slenderness and radii of curvature yielded the following initial conclusions:

1. As the web panel slenderness of a curved I-girder section increases, the vertical moment carrying capacity of the section decreases.
2. Increasing the degree of curvature in an I-girder (decreasing radius of curvature), results in increasing longitudinal stresses and lateral bending moments in the flanges when

subjected to a uniform vertical bending moment, decreasing the moment carrying capacity of the section.

3. When boundary conditions on the I-girder section are such that one end is free to move along the longitudinal centerline, thermal effects on the section are greatly reduced.
4. Increasing the magnitude of thermal loading on the I-girder section already loaded with self-weight leads to an increase in out-of-plane web deformation, an increase in the nonlinearity of the web longitudinal stress profile, an increase in the tensile or compressive stress (depending on thermal increase or decrease) in the flanges, and an increase in the lateral flange bending moment. Temperature loads lead to an enlarged level of stresses in the webs and flanges, thereby reducing the load carrying capacity of the I-section by reducing the amount of further loading the I-girder flanges can accommodate.

A second parametric study is modeled after The Horizontally Curved Steel I-Girder Design Example in the *AASHTO Guide Specifications* (2003) and consists of two curved I-girders braced together using cross frames. Cases with varying radii of curvature are subjected to uniform thermal loading to determine how sections with varying degrees of curvature respond to changing temperature conditions. The following conclusions are derived from this section of the study:

1. The larger the degree of curvature of the curved section, the greater the initial torsional buckling caused by self weight. This initial torsional deformation stiffens the I-girder sections in the lateral direction, causing the magnitude of lateral web displacement caused by thermal loading to decrease as the degree of curvature of the section increases. Overall, the smaller the radius of curvature, the larger the torsional buckling at the I-girder mid-spans caused by gravity and temperature loads.
2. For a two girder section, which is a common configuration for construction of curved I-girder bridges, changing temperature conditions leads to the girders experiencing different degrees of torsional bucking at their ends. This could be problematic in that as

temperature conditions change during the construction of a curved I-girder bridge, non-uniform girder deformation at the end of these sections could lead to problems fitting up and connecting these sections, possibly leading to locked in stresses as a result of having to force these sections into place.

3. Thermal loading has a larger impact on flange longitudinal stresses as the degree of curvature decreases (radius of curvature increases). As the degree of curvature of the section decreases, temperature loads have an increasing effect on the lateral flange bending moment magnitude in both the top and bottom flanges of the I-girders. Positive thermal loading creates additional lateral bending moments such that the maximum longitudinal stresses are the greatest at the flange tips. These additional longitudinal stresses will inevitably decrease the load carrying capabilities of the I-girders and could even lead to warping of the girder flanges.

The main focus of this research study is a case study on what effects thermal loading has on the Buffalo Creek Bridge, a curved I-girder bridge in Logan County, West Virginia. More specifically, the investigation focused on how the I-girder webs respond to thermal loading in terms of deformations and stresses and how this may impact the integrity. Conclusions drawn from the finite element modeling results are as follows:

1. Results show a level of global buckling, in the form of lateral web displacement, in the I-girders after only self-weight loading on the superstructure. Overall, pier flexibility yields greater global I-girder lateral bucking under self-weight loading, but lateral web deformation is present for both the flexible and rigid pier cases. In fact, the magnitude of these displacements in span 1 is at least 2.0 in. in most cases, a value approximately three times the web thickness.
2. Design sheets consider the camber deviation of the I-girders due to self-weight loading, but no calculations are made for the lateral deformation from gravity. Results found that lateral deformations reach up to 40% of the magnitude of camber values. For curved steel I-girder bridges, lateral camber values should be considered as the

curvature of the structure will typically always lead to lateral deformations being present and lateral deformations, although small at this stage, are typically more detrimental to I-girder capacity.

3. At the stage of gravity loading, web out-of-plane displacement, or local buckling, is observed in the I-girder webs. These deformations can be thought of as initial imperfections comparable to imperfections from fabrication because they are not considered during design. This initial local buckling of the webs reduces the initial web stiffness, will lead to larger displacements at lower load levels, and reduces the load carrying capacity of the I-girder. In reality, the initial imperfections in the web will likely be larger than shown in this study as the fabrication and erection imperfections that are sure to arise would be exaggerated with the onset of gravity loading.
4. Girder web cross-section displacement profiles reveal that lateral-distortional buckling is present in the I-girder webs after the Buffalo Creek Bridge displaces under self-weight loading. At mid-span cross sections, pier flexibility has a greater impact on lateral buckling when compared to the rigid pier case, but does not impact the local or torsional buckling. At and near piers, pier flexibility has a slight effect on all three buckling modes, but smaller local buckling occurs at the piers because of the transverse stiffeners. This early stage web buckling is of concern because it will certainly be exaggerated as additional loading is added to the structure; thus, reducing the load carrying capacity of the I-girders.
5. Analysis of web displacements shows that idealizing the bridge piers as rigid or flexible members causes the structure to respond in two distinctly different ways to temperature loading. Pier flexibility allows the superstructure to expand and contract as one uniform structure. When the piers are rigid, the fixity of the pier bearings leads to each span responding, for the most part, individually to thermal loading.
6. The introduction of uniform thermal loading to the Buffalo Creek Bridge has a quantifiable impact on the lateral web displacement magnitude. Uniform -45°F loading, in most cases, decreases the magnitude of global web buckling as the superstructure contracts. On the other hand, as the superstructure attempts to expand under +45°F

uniform loading, global web buckling increases. Due to the contribution of pier movements, lateral web deformations exhibit a larger response to changing temperature in span 1 when the piers are flexible. In spans 2-4, rigid pier model lateral displacements exceed those of the flexible model as the resistance at the supports to expansion and contraction causes the I-girders to displace laterally.

7. Positive uniform thermal loading (+45°F) increases lateral web displacements by up to 75.2% over gravity displacements in spans 1-3 when piers are rigid and by up to 32.9% over gravity displacements in spans 1-3 when piers are flexible. In span 4, +45°F loads increase global buckling by up to 661.7% for the rigid pier case and up to 2,267% for the flexible pier case. These results are of concern because the additional thermally induced lateral web displacements are unaccounted for during bridge design. The study here shows they will occur prior to any live, in-service loads on the structure. This could lead to the bridge exhibiting problems when subjected to in-service loading as these premature deformations prevent the I-girders from carrying these live loads in the manner they were intended, leading to further exaggerated, damaging lateral displacements.
8. Thermal loads, both positive and negative, have a much greater impact on web out-of-plane deformations when bridge piers are rigid rather than flexible. When piers are modeled as flexible, temperature increase slightly increases the magnitude of web out-of-plane deformation and temperature decrease slightly decreases the magnitude of web out-of-plane deformation. Conversely, with rigid piers, temperature increase and decrease both increase the magnitude of web out-of-plane deformation, just in opposite directions. Pier flexibility allows some of the forces of thermal expansion and contraction to be transferred to the piers, lessening their impact on the girders. In the case of rigid piers, these forces remain in the girders, and lead to additional local web buckling.
9. Thermal loading increases web out-of-plane displacement magnitude by up to 1,972% in spans 1-3 when piers are rigid and by up to 86% in spans 1-3 when piers are flexible. Just as was the case for gravity loading, initial out-of-plane web deformations reduce

the initial web stiffness and lower the load carrying capacity of the I-girders. Additionally, these results show that pier flexibility combined with bearing design will not fully accommodate thermal movements, as is often assumed in design.

10. For both rigid and flexible pier cases, thermal loading has an effect on the displaced web cross section profiles. Rigid pier model web cross section profiles are more significantly impacted by thermal loads, especially in terms of the local and torsional buckling modes. Flexible models do not show significant changes in the web local and torsional buckling modes due to temperature, but thermal loading does induce additional lateral web buckling. Once again, displacement results show that pier flexibility allows larger lateral girder displacements, which will transfer thermal forces from the girders to the bridge piers, causing pier movement. These forces remain in the girders in the rigid pier case, increasing local and torsional web buckling. The increase in lateral distortional buckling in the I-girders again shows that thermal loading will reduce the load carrying capacity of the I-girders prior to any in-service loading on the bridge.
11. Girder displacement results reveal that curved I-girder bridges are susceptible to global, local, and lateral distortional buckling during construction and shortly after completion. Previous studies have attributed initial girder buckling to fabrication errors/imperfections, transportation, erection, and/or a host of other factors. Results show that those imperfections and initial buckling occur purely due to superstructure weight. The addition of thermal loading after construction is complete will increase the degree of imperfections and buckling in the I-girders, depending on the magnitude of thermal loading and the boundary conditions on the superstructure.
12. Compared to the rigid pier case, pier flexibility greatly reduces the magnitude of thermally induced effective stresses in the I-girder webs as a result of the piers allowing expansion and contraction of the superstructure. On the other hand, assuming the piers as rigid members leads to measureable increases in the overall state of stress in the webs. The larger the number of degrees of freedom constrained by the bearings on a span, the larger the magnitude of stress thermal loading induces in the web.

13. Thermal effective stresses alone at girder mid-spans account for up to 19.6% of the material yield strength and stress concentrations at piers from thermal loading were shown to consume up to 66.57% of the material yield strength. These stresses are of concern because the additional thermal effective stresses on the Buffalo Creek Bridge revealed in this study are not considered by designers and could lead to problems later in the life of the structure.
14. Most bridge designs assume that bearing design relieves any axial stresses that may arise from changing thermal conditions, but this study shows that uniform temperature loads will lead to axial stress in the I-girder cross sections. The more restraint placed on the I-girder movement at the supports via the bearings and the degree of pier flexibility, the larger the magnitude of axial stress in I-girder webs as a result of thermal loading.
15. AASHTO (2007) requires that I-girder webs be checked for web bend-buckling, but does not require web bend-buckling be checked after girders are in a composite state with the deck. The statement is made in AASHTO (2007) that once the deck has cured and acts compositely with the bridge girders, the compressive stress increase in the web is compensated for by the increase in web bend-buckling resistance factor. Results in this study found this statement to be false when considering uniform axial compressive stresses induced by thermal loading. These axial compressive web stresses not only increase the maximum compressive web stress magnitude, they also increase the depth of the web in compression, decreasing the web bend-buckling resistance factor Therefore, when subjected to thermally induced axial compressive stresses, a section is more likely to not meet web bend-buckling criteria; hence, more likely to experience premature buckling. In fact, a +45°F load on the rigid pier model leads to stress profiles at the center of spans 2 and 3 that do not satisfy bend-buckling guidelines in Section 6.10.1.9 of AASHTO (2007) even after the girders are composite with the deck.
16. Gravity and thermal loading induced axial compressive stresses account for up to 5.99% of the I-girder compressive capacity when the piers are flexible and up to 29.53% when the piers are rigid. Once again, this is consumed capacity that is unaccounted for in design and stresses that will decrease the safety factor of the bridge and could

negatively impact the structural integrity of the bridge. In addition, increasing compressive stresses in the webs only makes the web panels more susceptible to buckling under subsequent loads.

17. The effect thermal loading has on the overall capacity of the Buffalo Creek Bridge I-girders in terms of web stresses is directly proportional to the amount of axial compressive stress the thermal load induces in the web. Not only does this increase the axial capacity ratio by increasing axial stress magnitude, but it also increases the bending capacity ratio by decreasing the web bending capacity value.
18. For the rigid pier case, gravity followed by +45°F thermal loading yields capacity ratios in spans 2 and 3 that exceed 0.75, with girders 1-4 having capacity ratios exceeding 1.0, indicating the girders stresses are greater than girder capacity. Even when the piers have flexibility, gravity and +45°F temperature loading yield capacity ratios in span 2 exceeding 0.70 and in span 3 exceeding 0.50.
19. Thermal I-girder stress and deformation results presented in this study reveal I-girder responses that are typically assumed to be relieved through bridge design. Detail of typical design procedures and design software is not adequate to reveal the structural behavior documented in this study. This research produces a methodology, in terms of a detailed finite element analysis, that should be used by bridge designers and owners alike to validate bridge design, especially in cases with complicated or unorthodox designs or geometries. Because of the complexities that arise in curved bridges, all curved bridge designs should be validated using a detailed, full-scale, 3D finite element analysis.

## 8.2 Future Research Suggestions

1. The case study presented here should be further expanded to investigate what effect changing thermal conditions will have on the I-girder flanges during and at the completion of construction. Although results here show that temperature at this early

stage can impact I-girder capacity in terms of the web, a large portion of the loading carried by the I-girders is carried by the flanges. How thermal loading and the associated web deformations and stresses effect the state of stress in the flanges should be studied.

2. Typically, if temperature is considered in the design of a bridge, it is assumed to be a uniform temperature load, although AASHTO (2007) acknowledges that temperature changes likely do not occur uniformly. AAASHTO (2007) also states that temperature gradient need not be investigated for all types of structures. The same case study performed here should be performed with a temperature gradient applied through the depth of the concrete deck and I-girders and the thermal I-girder web deformations and web and flange stresses studied.
3. The analysis of the Buffalo Creek Bridge performed in this study should be continued by introducing live loading to the finite element models and studying the same web displacement and stress results presented here. Live-loading could come in the form of AASHTO truck loading or uniformly distributed load, or some combination of the two. Furthermore, the state of stress in the girder flanges after gravity, thermal, and truck loading is applied on the bridge could be studied.
4. As was stated in this dissertation, configuration of the bridge bearings is a critical factor in how much thermal stress will arise in the bridge superstructure. The finite element models produced for this study could be modified to examine how different bearing configurations, for both the flexible and rigid pier cases, might lessen the impact of thermal loading while still maintaining the overall integrity of the bridge structure.
5. A more detailed investigation, possibly another case study, could be executed to study how thermal loading at the early stages of construction of curved I-girder bridges might impact the fit-up of curved girders or curved sections making up a full curved I-girder bridge. Explore whether fit-up problems will lead to locked-in stresses that will persist throughout the life of the structure and how these stresses might affect structural integrity.

6. The finite element models developed here could easily be used to look into what impact thermal loading has on the state of stress in the bridge deck. Especially for curved structures, changing thermal conditions that lead to transverse girder displacements may lead to longitudinal deck cracking at the early age of the structure. The impact that thermal loads have on deck stresses just after construction and after the introduction of live loading should be studied.
7. As stated, the boundary conditions in terms of the bearings and piers in this study represent two ideal conditions where the bearings are functioning perfectly as designed. In reality, this will not happen as there will be some degree of frictional resistance at the bridge bearings attributed to the geometry and material in the bearings along with the curvature of the superstructure. With some experimental of field measured results, an effort could be made to create a model that more accurately represents the function of the bridge bearings and piers.
8. Results clearly show that the presence of transverse stiffeners on web panels significantly decreases the web out-of-plane deformations caused by thermal loads. Action could be taken to determine if more transverse stiffeners on the webs of curved I-girders would reduce the thermal deformations and stresses in the I-girders and if this is a cost effective way to minimize thermal effects on curved I-girder bridges.
9. Further studies could be performed to determine if it is necessary to include lateral camber values for I-girders in the design sheets for curved I-girder bridges. The curvature of the I-girders will naturally lead to lateral deformations under all types of loading, and if these deformations were accounted for during design, that may minimize any fit-up problems that would arise during construction which could decrease additional stresses caused in the I-girders by forcing the girders together when there is not a proper fit.
10. A large scale study on curved I-girder bridges should be performed in an effort to produce a more complete design standard for curved bridges. This study should include all plausible loading conditions and combinations and study how changing bridge characteristics such as radius of curvature, cross frame spacing, transverse stiffener

spacing, web thickness, bearing arrangement, etc. effect structural response to these loading conditions. Although this would be a vast and time consuming study, a better understanding of the design of curved bridges is critical.

# REFERENCES


1. ABAQUS Manual (1988). Version 4-7, Hibbitt, Karlsson, and Sorensen, Inc., Pawtucket, RI.

2. Abdel-Sayed, M. (1973). Curved Webs Under Combined Shear and Normal Stresses, *Journal of the Structural Division*, ASCE, vol. 99, no. ST3, March, pp. 511-525.

3. ADINA Research and Development, Inc. (2003). "Theory and Modeling Guide, Volume 1: ADINA." *Rep. No. ARD 03-07*, Watertown, Mass.

4. ADINA Research and Development, Inc. (2009). "Theory and Modeling Guide, Volume 1: ADINA." *Rep. No. ARD 09-07*, Watertown, Mass.

5. American Association of State Highway and Transportation Officials (1977). *Standard Specifications for Highway Bridges*, 12th ed., Washington , D. C.

6. American Association of State Highway and Transportation Officials (1980). *Guide Specifications for Horizontally Curved Highway Bridges*, 1ST ed., Washington, D. C.

7. American Association of State Highway and Transportation Officials (1983). *Standard Specifications for Highway Bridges*, Washington , D. C.

8. American Association of State Highway and Transportation Officials (1987). *Guide Specifications for Horizontally Curved Highway Bridges*, Washington, D.C.

9. American Association of State Highway and Transportation Officials (1992). *Standard Specifications for Highway Bridges*, 15th ed., Washington , D. C.

10. American Association of State Highway and Transportation Officials (1993). *Guide Specifications for Horizontally Curved Highway Bridges*, 2nd ed., Washington, D. C.

11. American Association of State Highway and Transportation Officials (2003). *Guide Specifications for Horizontally Curved Highway Bridges*, 3rd ed., Washington, D. C.

12. American Association of State Highway and Transportation Officials (1998). *LRFD Bridge Design Specifications*, Washington, D. C.

13. American Association of State Highway and Transportation Officials (2002). *Standard Specifications for Highway Bridges*, 17th ed., Washington, D. C.

14. American Association of State Highway and Transportation Officials (2004). *AASHTO LRFD Bridge Design Specifications,* 2nd Ed., Washington, D. C.

15. American Association of State Highway and Transportation Officials (2006). *AASHTO LRFD Bridge Design Specifications*, 3rd Ed., Washington, D. C.

16. American Association of State Highway and Transportation Officials (2007). *AASHTO LRFD Bridge Design Specifications*, 4th Ed., Washington, D. C.

17. American Association of State Highway and Transportation Officials (2010). *AASHTO LRFD Bridge Design Specifications*, 5th Ed., Washington, D. C.

18. American Association of State Highway and Transportation Officials (2006). *AASHTO LRFD Design Examples – Horizontally Curved Steel Bridges*, Washington, D. C.

19. American Association of State Highway and Transportation Officials/AWS D.1M/D1.5:2008 (2007). *Bridge Welding Code*, American Welding Society (AWS) D1 Committee on Structural Welding, 5th Edition, Washington, D.C.

20. Armstrong, W. L. (1972). Dynamic Testing of Curved Bridge – Huyck Stream, *Journal of the Structural Division*, ASCE, vol. 98, no. 9, pp. 2015-2030.

21. ASCE-AASHTO Task Committee on Curved Girders. (1977). Curved I-Girder Bridge Design Recommendations, *American Society of Civil Engineers*, vol. 103, no. ST5, 1137-1167.

22. Barr, B. J., N. Yanadori, M. W. Halling and K. C. Womack (2007). Live-Load Analysis of a Curved I-Girder Bridge, *Journal of Bridge Engineering*, vol. 12, no. 4, July, pp. 477-484.

23. Beckett, C. L. (2011). Effect of Temperature Variation on the Structural Capacity of a Multi-Span Horizontally Curved Steel I-Girder Bridge, Masters Thesis, West Virginia University, Morgantown, WV.

24. Bell, B. J. and D. G. Linzell (2007). Erection Procedure Effects on Deformation and Stresses in Large-Radius, Horizontally Curved, I-Girder Bridge, *Journal of Bridge Engineering*, vol. 12, no. 4, July, pp. 467-476.

25. Bridge Software Development International, Ltd. (BSDI), (2000). *Bridge Software Development International Product Scope*, BSDI, Coopersburg, Pa.

26. Brockenbrough, R. L. (1986). Distribution Factors for Curved I-Girder Bridges, *Journal of Structural Engineering*, vol. 112, no. 10, Oct., pp. 2200-2215.

27. Chang, C. J., D. W. White, F. Beshah and W. Wright (2005). Design Analysis of Curved I-Girder Bridge Systems – An Assessment of Modeling Strategies, *Proceedings – 2005 Annual Stability Conference*, Structural Stability Research Council, March, 2005, Montreal, Quebec, Canada, pp. 349-369.

28. Chavel, B. W. and C. J. Earls (2002a). Stability of Curved Steel I-Girder Bridge Components During Erection, *2002 Annual Stability Conference*, Structural Stability Research Council, April 24-27, Seattle, Washington, pp. 75-93.

29. Chavel, B. W. and C. J. Earls (2002b). Evaluation of Erection Procedures of the Horizontally Curved Steel I-Girder Ford City Veterans Bridge, *Report No. FHWA-PA-2002-003-97-04 (74)*, The Pennsylvania Department of Transportation, Harrisburg, Pennsylvania.

30. Chavel, B. W. and C. J. Earls (2003). Investigation of Construction Issues and Inconsistent Detailing in Horizontally Curved I-Girder Bridges, *TRB Annual Meeting*, Washington, D. C.

31. Chavel, B. W. and C. J. Earls (2006a). Construction of a Horizontally Curved Steel I-Girder Bridge. Part I: Erection Sequence, *Journal of Bridge Engineering*, vol. 11, no. 1, pp. 81-90.

32. Chavel, B. W. and C. J. Earls (2006b). Construction of a Horizontally Curved Steel I-Girder Bridge. Part II: Inconsistent Detailing, *Journal of Bridge Engineering*, vol. 11, no. 1, pp. 91-98.

33. Cullen, L. E. (2007). An Evaluation of the Strength Characteristics of Horizontally Curved Steel I-Girder Bridges, Masters Thesis, West Virginia University, Morgantown, WV.

34. Culver, C. G. and R. E. Frampton (1970). Local Instability of Horizontally Curved Members, *Journal of the Structural Division*, ASCE, vol. 96, no. ST2, Feb, pp. 245-265.

35. Culver, C. G. and G. Nasir (1971). Inelastic Flange Buckling of Curved Plate Girders, *Journal of the Structural Division*, ASCE, vol. 97, no. ST4, April, pp. 1239-1256.

36. Culver, C. G. (1972). Design Recommendations for Curved Highway Bridges, *Project 68-32*, Commonwealth of Pennsylvania Department of Transportation, Harrisburg, PA..

37. Culver, C. G., C. L. Dym and D. K. Brogan (1972). Bending Behavior of Cylindrical Web Panels, *Journal of the Structural Division*, ASCE, vol. 98, no 10, pp. 2291-2308.

38. Culver, C. G., C. L. Dym and T. Uddin (1973). Web Slenderness Requirements for Curved Girders, *Journal of the Structural Division*, ASCE, vol. 99, no. 3, pp. 417-430.

39. Daniels, J. H., J. W. Fisher and B. T. Yen (1980). Fatigue of Curved Steel Bridge Elements, Design Recommendations for Fatigue of Curved Plate Girder and Box Girder Bridges, *Rep. No. FHWA-RD-79-138*, Offices of Research and

Development Structural and Applied Mechanics Division, Federal Highways Administration, Washington, D. C.

40. Davidson, J. S. (1996). "Nominal Bending and Shear Strength of Horizontally Curved Steel I-Girder Bridges", Ph.D. Dissertation, Auburn University, Auburn, Alabama.

41. Davidson, J. S., M. A. Keller and C. H. Yoo (1996). Cross-Frame Spacing and Parametric Effects in Horizontally Curved I-Girder Bridges, *Journal of Structural Engineering*, vol. 122, no. 9, Sept., pp. 1089-1096.

42. Davidson, J. S. and C. H. Yoo (1996). Local Buckling of Curved I-Girder Flanges, *Journal of Structural Engineering*, vol. 122, no. 8, Aug., pp. 936-947.

43. Davidson, J. S., S. R. Ballance and C. H. Yoo (1999a). Analytical Model of Curved I-Girder Web Panels Subjected to Bending, *Journal of Bridge Engineering*, vol. 4, no. 3, Aug., pp. 204-212.

44. Davidson, J. S., S. R. Ballance and C. H. Yoo (1999b). Finite Displacement Behavior of Curved I-Girder Webs Subjected to Bending, *Journal of Bridge Engineering*, vol. 4, no. 3, Aug, pp. 213-220.

45. Davidson, J. S., S. R. Ballance and C. H. Yoo (2000a). Behavior of Curved I-Girder Webs Subjected to Combined Bending and Shear, *Journal of Bridge Engineering*, vol. 5, no. 2, May, pp. 165-170.

46. Davidson, J. S., S. R. Ballance and C. H. Yoo (2000b). Effects of Longitudinal Stiffeners on Curved I-Girder Webs, *Journal of Bridge Engineering*, vol. 5, no. 2, May, pp. 171-178.

47. Davidson, J. S. and C. H. Yoo (2000). Evaluation of Strength Formulations for Horizontally Curved Flexural Members, *Journal of Bridge Engineering*, vol. 5, no. 3, Aug., pp. 200-207.

48. Davidson, J. S. and C. H. Yoo (2002). Stability of Horizontally Curved I-Girder Web Panels, *2002 Annual Stability Conference*, Structural Stability Research Council, April 24-27, Seattle, Washington, pp. 95-118.

49. Davidson, J. S. and C. H. Yoo (2003). Effects of Distortion on Strength of Curved I-Shaped Bridge Girders, *Transportation Research Record*, no. 1845, pp. 48-56.

50. Davidson, J. S., R. S. Abdalla, and M. Madhavan (2004). Stability of Curved Bridges During Construction, *UTCA Report 03228*, University Transport Center for Alabama, University of Alabama, Tuscaloosa, Alabama.

51. Davidson, J. S. and M. Madhaven (2005). Flange Compactness Definition for Horizontally Curved Bridge Girders, *Proceedings: 2005 Annual Stability Conference*, Structural Stability Research Council, March 6-9, 2005, Montreal, Quebec, Canada, pp. 185-203.

52. DePolo, D. S. and D. G. Linzell (2005). Evaluation of Live Load Lateral Flange Bending Distribution for a Horizontally Curved I-Girder Bridge, *2005 Annual Meeting – Transportation Research Board*, Washington, D. C.

53. DeSantiago, E, J. Mohammadi, H. M. O. Albaijat (2005). Analysis of Horizontally Curved Bridges Using Simple Finite-Element Models, *Practice Periodical on Structural Design and Construction*, vol. 10, no. 1, Feb., pp. 18-21.

54. Domalik, D. E., J. F. Shura and D. G. Linzell (2005). The Design and Field Monitoring of a Horizontally Curved Steel Plate Girder Bridge, *2005 Annual Meeting – Transportation Research Board*, Washington, D. C.

55. Galambos, T. V., J. F. Hajjar, W. H. Huang, B. E. Pulver, R. T. Leon and B. J. Rudie (2000). Comparison of Measured and Computed Stresses in a Steel Curved Girder Bridge, *Journal of Bridge Engineering*, vol. 5, no. 3, August, pp. 191-199.

56. Grubb, M. A., J. M. Yadlosky and S. R. Duwadi (1996). Construction Issues in Steel Curved-Girder Bridges, *Transportation Research Record*, no. 1544, pp. 64-70.

57. Hanshin Expressway Public Corp. (1988). *Guidelines for the Design of Horizontally Curved Bridges (Draft)*.

58. Hajjar, J. P., T. V. Galambos, W. H. Huang, B. E. Pulver, R. T. Leon and B. J. Rudie (1999). Measured Versus Computed Stresses in a Curved Steel Bridge, *Structural Engineering in the 21$^{st}$ Century: Proceedings of the 1999 Structures Congress*, April 18-21, New Orleanes, LA, pp. 231-234.

59. Heins, C. P. and K. R. Spates (1970). Behavior of Single Horizontally Curved Girder, *Journal of the Structural Division*, ASCE, vol. 96, no. ST7, pp. 1511-1524.

60. Heins, C. P. and J. O. Jin (1982). Load Distribution of Braced Curved I Girder Bridges, AISI Project 308, Effects of Bracing on I Girder Bridges, Institute for

Physical Science and Technology, University of Maryland, College Park, MD, June, 1982.

61. Heins, C. P. and J. O. Jin (1984). Live Load Distribution of Braced Curved I-Girders, *Journal of Structural Engineering*, vol. 110, no. 3, March, pp. 523-530.

62. Helwig, T., Herman, R., Zhang, Y, Espinoza, O., and B. Mercan (2007). Fabricated Plate Tolerances for Steel Bridges, *2007 World Steel Bridges Symposium*, New Orleans, LA, Dec. 5-7, 2007. CD Distribution.

63. Hibbett, Karlsson and Sorensen, Inc. ABAQUS/Standard User's Manual, Version 6.3, 2002.

64. Hilton, M. H. (1984). Deflection and Camber Loss in Heat-Curved Girders, *Transportation Research Record*, No. 950, Vol. 2, Transportation Research Board, National Research Council, Washington, D. C., pp. 51-59.

65. Howell, T. D. and C. J. Earls (2007). Curved Steel I-Girder Bridge Response During Construction Loading: Effects of Web Plumbness, *Journal of Bridge Engineering*, vol. 12, no. 4, July, pp. 485-493.

66. Kang, Y. J. and C. H. Yoo (1990). Flexural Stress of Curved Bridge Girders, *Proceedings – 1990 Annual Technical Session, Structural Stability Research Council*, St. Louis, MO, pp. 55-61.

67. Keller, M. A. (1994). Parametric Study of Horizontally Curved I-Girder Systems Including Lateral Bracing Effects, Masters Thesis, Auburn University, Auburn, Alabama.

68. Kim, W. S., J. A. Laman and D. G. Linzell (2007a). Live Load Radial Moment Distribution for Horizontally Curved Bridges, *Journal of Bridge Engineering*, vol. 12, no. 6, Nov., pp. 727-736.

69. Kim, Y. D., S. K. Jung and D. W. White (2007b). Transverse Stiffener Requirements in Straight and Horizontally Curved Steel I-Girders, *Journal of Bridge Engineering*, vol. 12, no. 2, March, pp. 174-183.

70. Krzmarzick, D. P. and J. F. Hajjar (2006). Load Rating of Composite Steel Curved I-Girder Bridges through Load Testing with Heavy Trucks, *Report No. MN/RC-2006-40*, Minnesota Department of Transportation, St. Paul, Minnesota.

71. Lay, M. G. (1965). Flange Local Buckling in Wide Flange Shapes, *Journal of the Structural Division*, ASCE, pp. 95-116.

72. Linzell, D. G. (1999). Studies of Full-Scale Horizontally Curved Steel I-Girder Bridge Systems Under Self Weight, Ph. D. Dissertation, School of Civil and Environmental Engineering, Georgia Institute of Technology, Atlanta, GA, 1999.

73. Linzell, D. G., Laman, J. A. and D. L. Nevling (2002). Evaluation of Level of Analysis Methodologies for Horizontally Curved I-Girder Bridges through Comparison with Measured Response of an In-Service Structure – Instrumentation and Field Test Plan. PTI Report No. 2002-32, Prepared for Professional Service Industries, Inc. for the Federal Highways Administration, April 2002.

74. Linzell, D. G., A. Zurieck and R. T. Leon (2003). Comparison of Measured and Predicted Response of Manufactured Circular Steel Tubular Members Under

Concentric and Eccentric Compressive and Tensile Loads, *Engineering Structures*, vol. 25, no. 8, pp. 1019-1031.

75. Linzell, D., D. Hall and D. White (2004a). Historical Perspective on Horizontally Curved I Girder Bridge Design in the United States, *Journal of Bridge Engineering*, vol. 9, no. 3, pp. 218-229.

76. Linzell, D. G., R. T. Leon and A. H. Zurieck (2004b). Experimental and Analytical Studies of Horizontally Curved Steel I-Girder Bridge During Erection, *Journal of Bridge Engineering*, vol. 9, no. 6, pp. 521-530.

77. Madhavan, M. and J. S. Davidson (2003). Elastic Local Buckling of Curved I-Girder Flanges, *Proceedings: Structural Stability Research Council*, Baltimore, MD, pp. 599-617.

78. Madhavan, M. and J. S. Davidson (2005). Elastic Buckling of Centerline-Stiffened Plates Subjected to a Linearly Varying Stress Distribution, *Proceedings – 2005 Annual Stability Conference*, North American Steel Construction/Structural Stability Research Council, Montreal, Quebec.

79. Madhavan, M. and J. S. Davidson (2007). Elastic Bucking of I-Beam Flanges Subjected to a Linearly Varying Stress Distribution, *Journal of Constructional Steel Research*, vol. 63, no. 10, pp. 1373-1383.

80. Maneetes, H. and D. G. Linzell (2006). Cross Frame and Lateral Bracing Influence on Curved Steel Bridge Free Vibration Response, *Journal of Constructional Steel Research*, vol. 59, no. 9, pp. 1101-1117.

81. MATLAB Student Version (2011). MATLAB User's Manual, *The Mathworks, Inc.*, Version 7.12.0.635, March 18, 2011.

82. Mariani, N., J. D. Mozer, C. L. Dym and C. G. Culver (1983). Transverse Stiffener Requirements for Curved Webs, *Journal of the Structural Division*, ASCE, vol. 99, no. ST4, April, pp. 757-771.

83. McBride, K. C. (2005). Thermal Stresses in the Superstructure of Integral Abutment Bridges, Masters Thesis, West Virginia University, Morgantown, WV.

84. McElwain, B. A. and J. A. Laman (2000). Experimental Verification of Horizontally Curved I-Girder Bridge Behavior, *Journal of Bridge Engineering*, vol. 5, no. 4, Nov, pp. 284-292.

85. MDX (2004). MDX Version 6 User Manual: Curved and Straight Bridge Design and Rating. September 27 Edition. www.mdxsoftware.com.

86. Mertlich, T. B., M. W. Halling and P. J. Barr (2007). Dynamic and Static Behavior of a Curved-Girder Bridge with Varying Boundary Conditions, *Journal of Performance of Constructed Facilities*, vol. 21, no. 3, June, pp. 185-192.

87. Moorty, S. and C. W. Roeder (1992). Temperature-Dependent Bridge Movements, *Journal of Structural Engineering*, vol. 118, no. 4, April, pp. 1090-1105.

88. MSC/NASTRAN (1994). *Reference Manual*, Version 68, vol. I, II, III, The MacNeal-Schwindler Corp., Los Angeles, CA.

89. Mikami, I and K. Furunishi (1984). Nonlinear Behavior of Cylindrical Web Panels, *Journal of Engineering Mechanics*, vol. 110, no. 2, Feb., pp. 239-251.

90. Nakai, H., T. Kitada, R. Ohminami and T. Kawai (1986). A Study on Analysis and Design of Web Plates in Curved Bridges Subjected to Bending, *Proc. JSCE*, Tokyo, vol. 368, no. 1-5, pp. 235-244. (In Japanese).

91. National Steel Bridge Alliance (NSBA), (1996). "Chapter 12: V-load Analysis – An Approximate Procedure, Simplified and Extended, for Determining Moments and Shear in Designing Horizontally Curved Open-Frame Highway Bridges." *Highway Structures Design Handbook*, vol. 1, Ch. 12, NSBA, Chicago.

92. Nevling, D., D. Linzell and J. Laman (2006). Examination of Level of Analysis Accuracy for Curved I-Girder Bridges Through Comparisons for Field Data, *Journal of Bridge Engineering*, vol. 11, no. 2, March, pp. 160-168.

93. Roeder, C. W. and S. Moorty (1990). Thermal Movements in Bridges, *Transportation Research Record*, no. 1290, pp. 135-143.

94. SAP Users Group (1977). SAPV2 – A Structural Analysis Program for Static and Dynamic Response of Linear Systems – Users Manual, University of Southern California, Oct.

95. Schelling, D., A. H. Namini and C. C. Fu (1986). Construction Effects on Bracing on Curved I-Girders, *Journal of Structural Engineering*, vol. 115, no. 9, Sept., pp. 2145-2165.

96. Schilling, C. G. (1996). Yield Interaction Relationships for Curved I-Girders, *Journal of Bridge Engineering*, vol. 1, no. 1, Feb, pp. 26-33.

97. Shanmugam, N. E., V. Thevendran, J. Y. Richard Liew and L. O. Tan (1995). Experimental Study on Steel Beams Curved in Plan, *Journal of Structural Engineering*, vol. 121, no. 2, pp. 249-259.

98. Shoukry, S. N., G. W. William, and M. Y. Riad, (2005). Early Age Cracking in Concrete Bridge Decks, Final Report No. T646-76-4.56, West Virginia Division of Highways, Charleston, WV, USA.

99. Shura, J. F. and D. G. Linzell (2006). Behavior of Horizontally Curved Steel Plate Girder Bridge During Steel Erection and Deck Placement, *2006 Annual Meeting – Transportation Research Board*, Washington, D. C.

100. Stegmann, T. H. and T. V. Galambos (1976). Load Factor Design Criteria for Curved Steel Girders of Open Cross Section, *Washington University Research Report No. 43*, Washington University, St. Louis, MO.

101. Tan, C. P. and S. Shore (1968). Dynamic Response of a Horizontally Curved Bridge, *Journal of the Structural Division*, ASCE, vol. 94, no. 3, pp. 761-781.

102. Thanasattayawibul, N. (2006). Curved Integral Abutment Bridges, Ph.D. Dissertation, Department of Civil and Environmental Engineering, University of Maryland, College Park, MD.

103. Tilley, M. R., F. W. Barton and J. P. Gomez (2006). Dynamic Analysis and Testing of a Curved Girder Bridge, *Rep. No. FHWA/VTRC 06-R32*, Virginia Department of Transportation, Richmond, VA and Federal Highway Administration, Washington, D. C.

104. *V-Load Analysis, An Approximate Procedure, Simplified and Extended for Determining Moments and Shears in Designing Horizontally-Curved Open-*

*Framed Highway Bridges*. (1984). USS Highway Structures Design Handbook, Volume 1, Chapter 12, United States Steel Corporation, Pittsburgh, Pennsylvania.

105. Washizu, K. (1975). *Variational Methods in Elasticity and Plasticity*, 2nd ed., Pergamon Press.

106. Womack, K., M. Halling and S. Bott (2001). Static and Dynamic Testing of a Curved, Steel Girder Bridge in Salt Lake City, Utah. *Report No. UT-00.13*, Utah Department of Transportation, Salt Lake City, Utah.

107. Womack, K. and B. Crookston (2003). Method of Analysis Comparison Study for a Curved, Steel Girder Bridge, *Report No. UT-03.02*, Utah Department of Transportation, Salt Lake City, Utah.

108. Yoo, C. H. and C. P. Heins (1973). Users Manual for the Static Analysis of Curved Bridge Girders, *Civil Engineering Report, No. 55*, University of Maryland, College Park, MD.

109. Yoo, C. H. and J. S. Davidson (1997). Yield Interaction Equations for Nominal Bending Strength of Curved I-Girders, *Journal of Bridge Engineering*, vol. 2, no. 2, May, pp. 37-44.

110. Yoo, C. H., Y. J. Kang and J. S. Davidson (1996). Buckling Analysis of Curved Beams by Finite Element Discretization, *Journal of Engineering Mechanics*, vol. 112, no. 8, Aug., pp. 762-770.

111. Yoo, C. H. and P. C. Littrell (1986). Cross-Bracing Effects in Curved Stringer Bridges, *Journal of Structural Engineering*, vol. 112, no. 9, Sept., pp. 2127-2140.

112. Yoo, C. H. and P. A. Pfeiffer (1983). Elastic Stability of Curved Members, *Journal of Structural Engineering*, vol. 109, no. 12, Dec, pp. 2922-2940.

113. Zhang, H., D. Huang and T. L. Wang (2005). Lateral Load Distribution in Curved Steel I-Girder Bridges, *Journal of Bridge Engineering*, vol. 10, no. 3, pp. 281-290.

114. Zureick, A. (1994). Curved Steel Bridge Research Project. Interim Report I: Synthesis. *Rep. No. FHWA-RD-93-129*, HDR Engineering, FHWA, 109 p.

115. Zureick, A. and R. Naqib (1999). Horizontally Curved Steel I-Girders State-of-the-Art Analysis Methods, *Journal of Bridge Engineering*, vol. 4, no. 1, pp. 38-47.

116. Zureick, A., D. Linzell, R. T. Leon and J. Burrell (2000). Curved Steel I-Girder Bridges: Experimental and Analytical Studies, *Engineering Structures*, vol. 22, no. 2, pp. 180-190.

# Appendix A

## GIRDER DEFORMATIONS UNDER GRAVITY LOADING

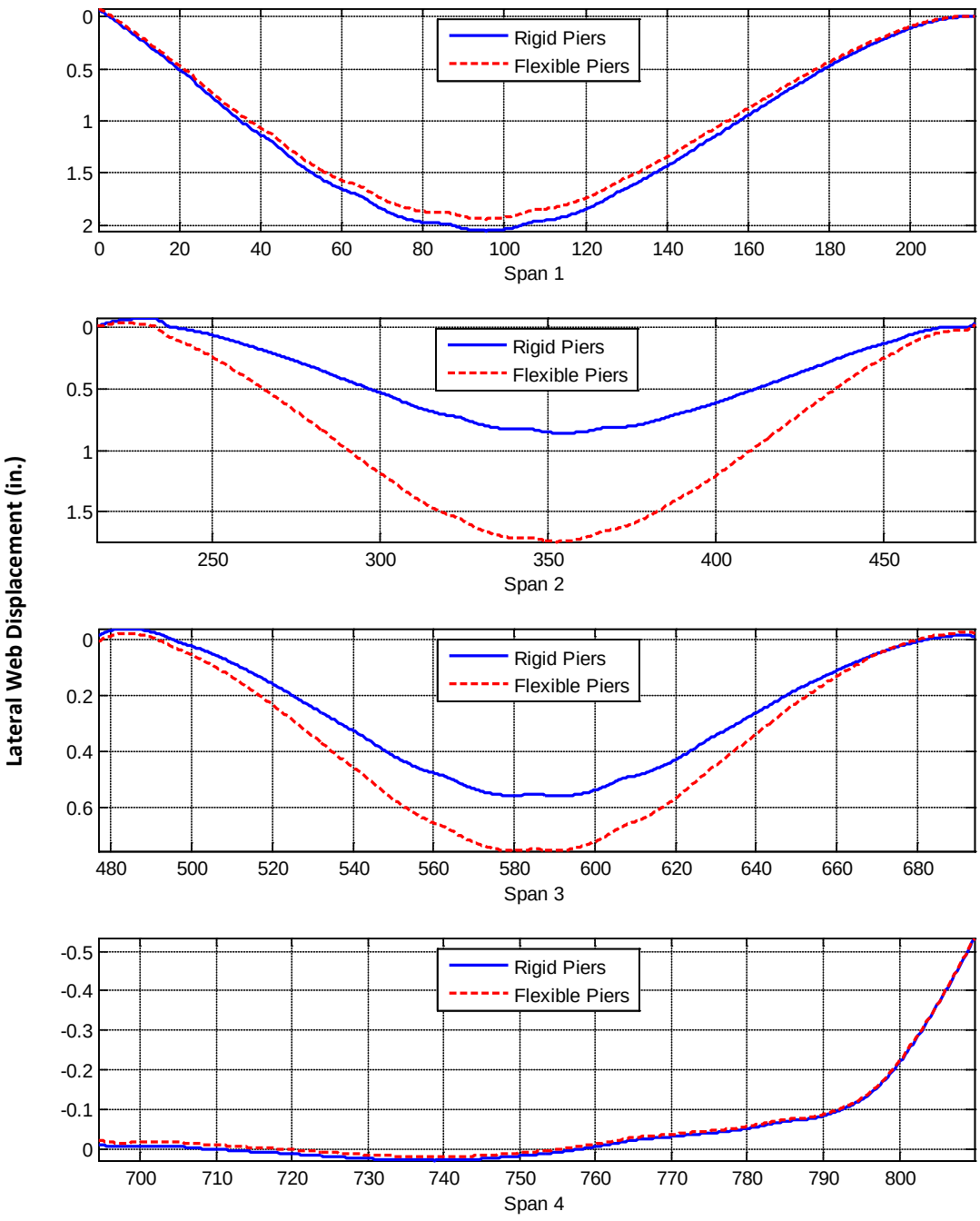


**Figure A.1. Girder 1 Lateral Web Centerline Displacement Due to Gravity Load**

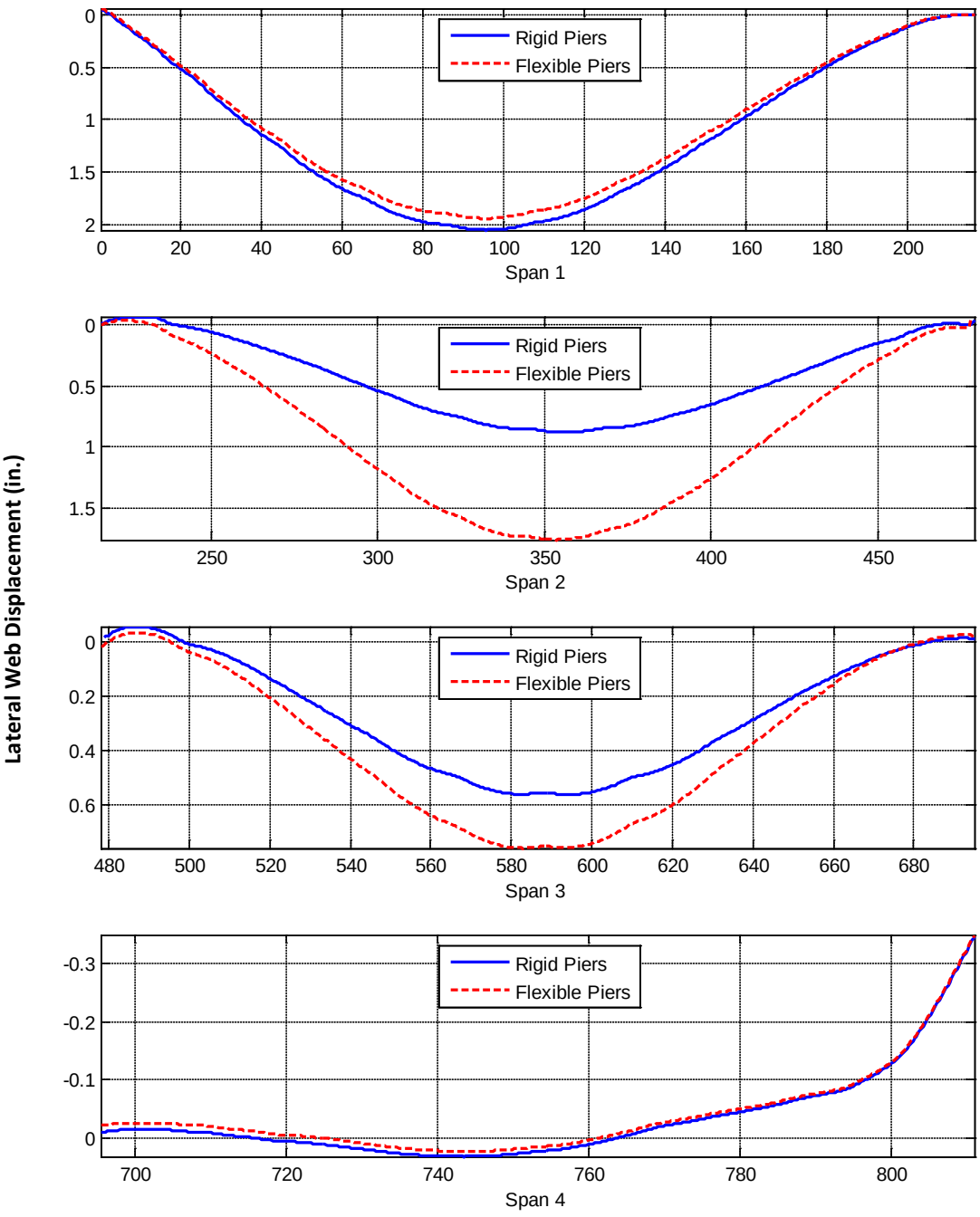


**Figure A.2. Girder 2 Lateral Web Centerline Displacement Due to Gravity Load**

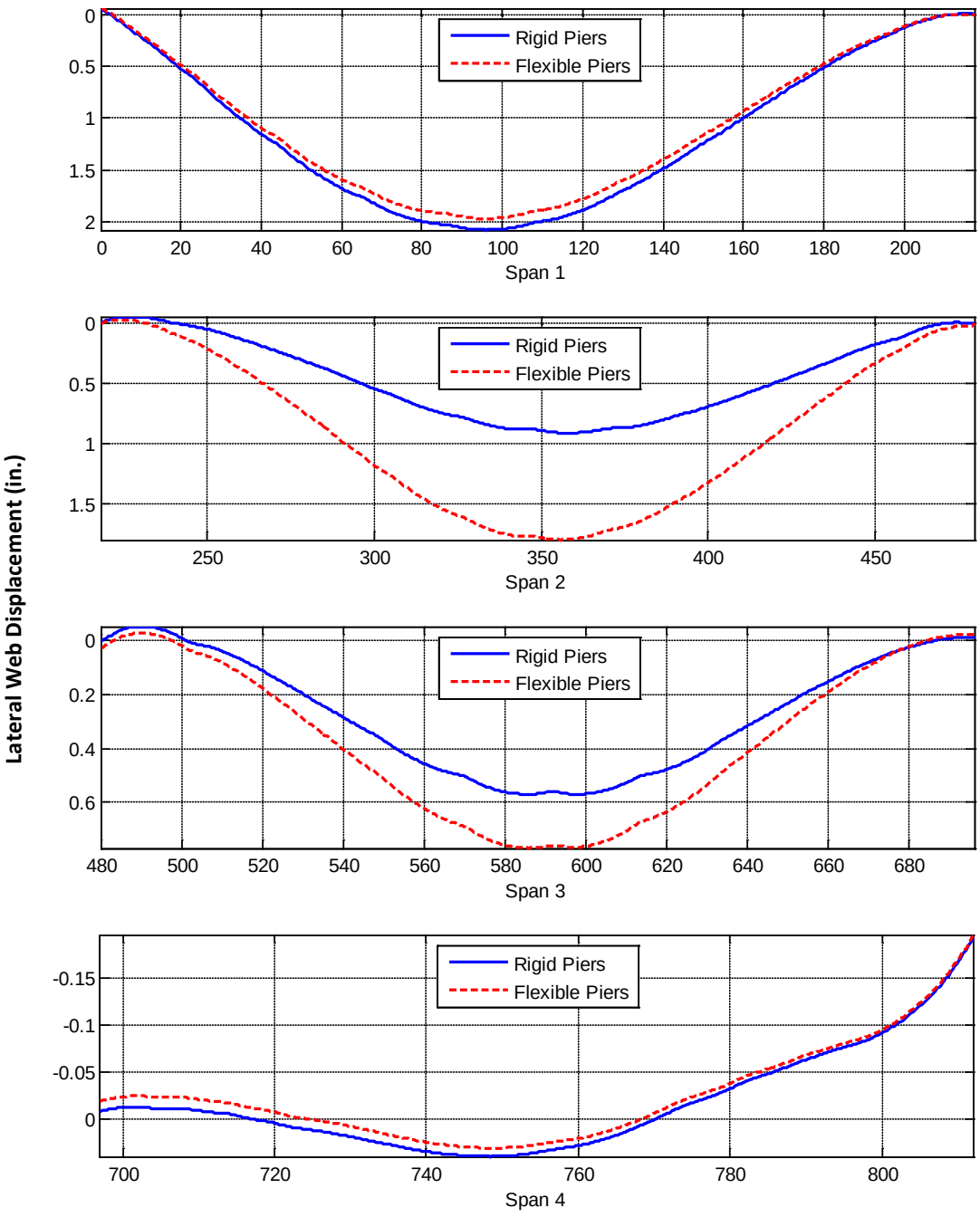


**Figure A.3. Girder 3 Lateral Web Centerline Displacement Due to Gravity Load**

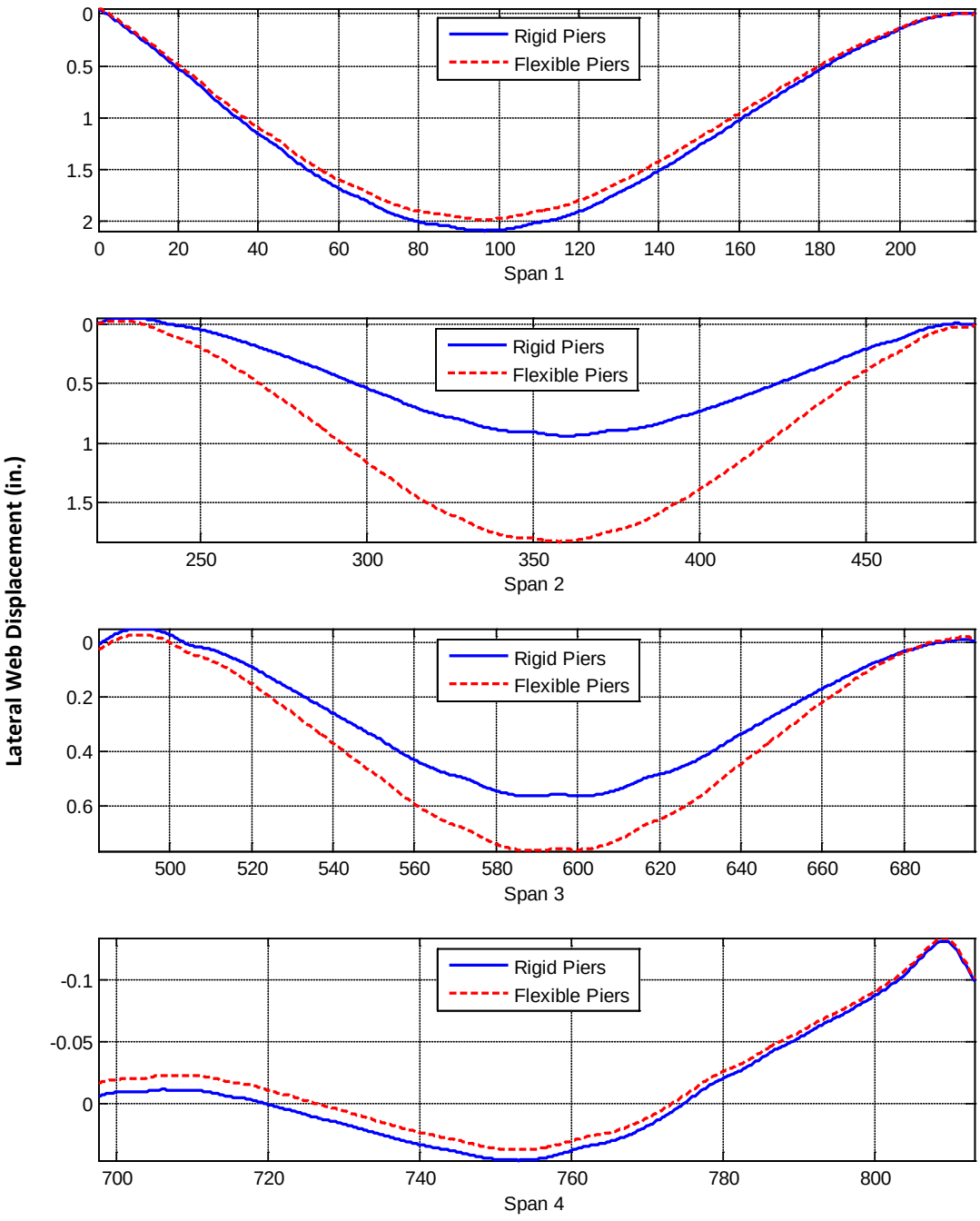


**Figure A.4. Girder 4 Lateral Web Centerline Displacement Due to Gravity Load**

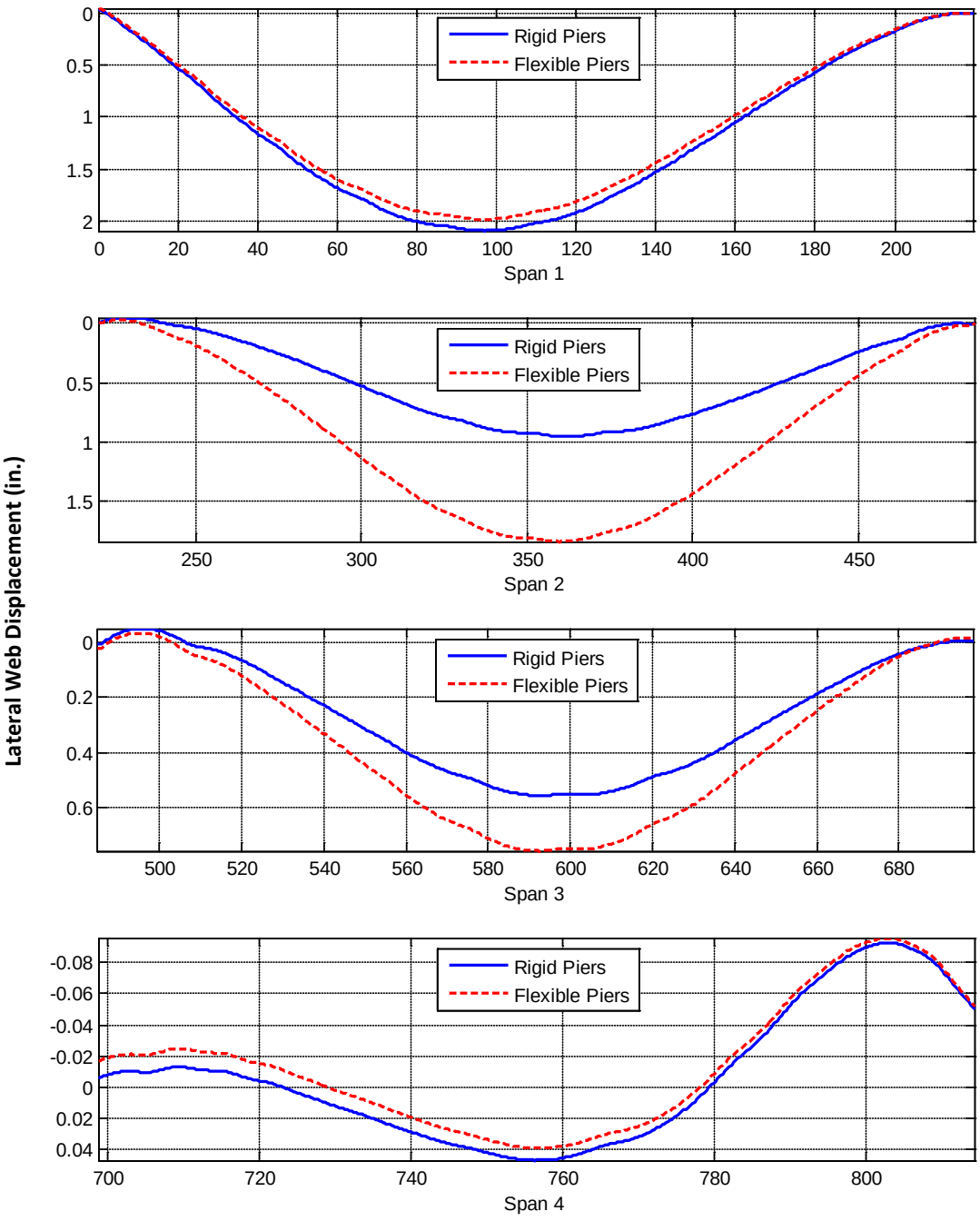


**Figure A.5. Girder 5 Lateral Web Centerline Displacement Due to Gravity Load**

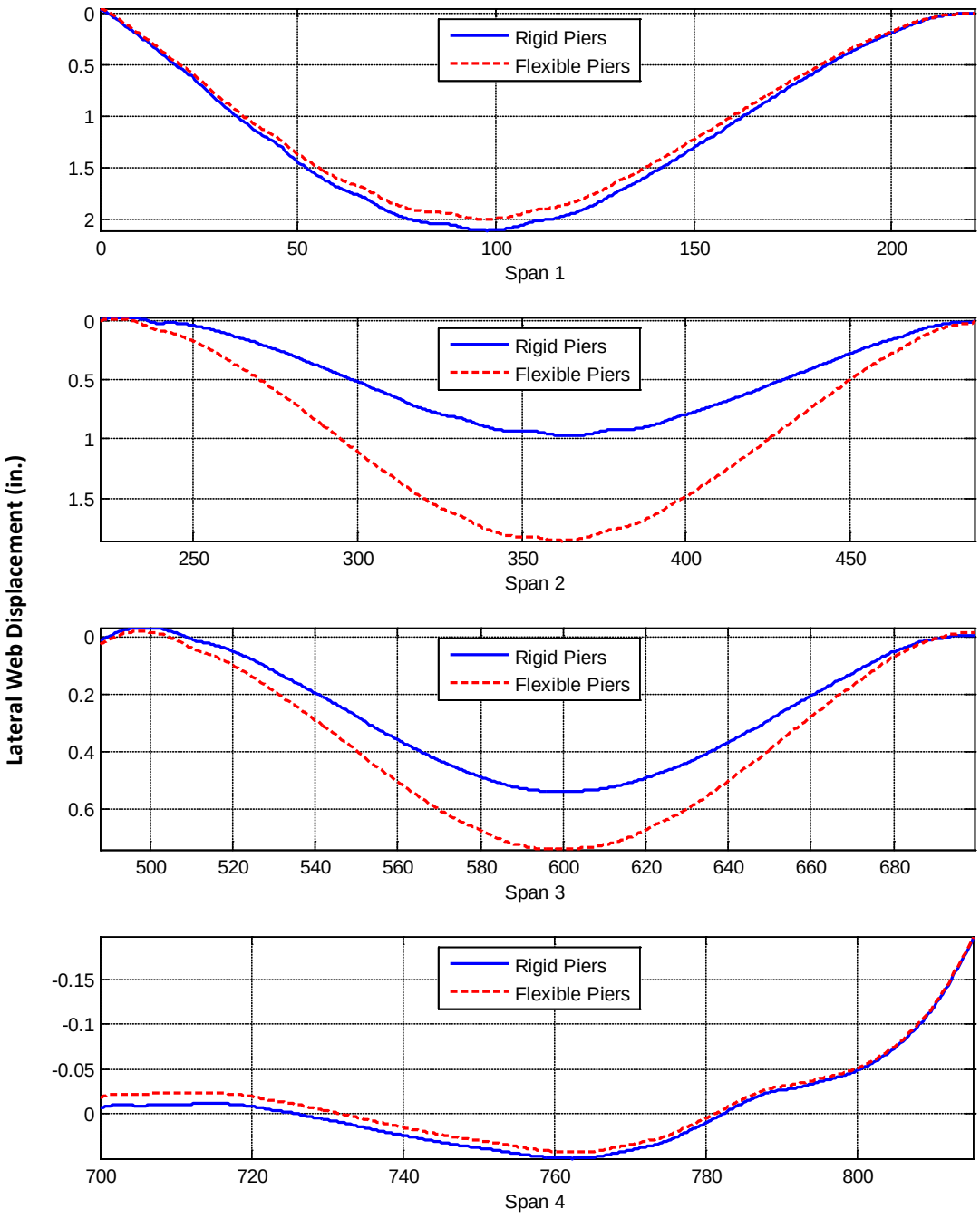


**Figure A.6. Girder 6 Lateral Web Centerline Displacement Due to Gravity Load**

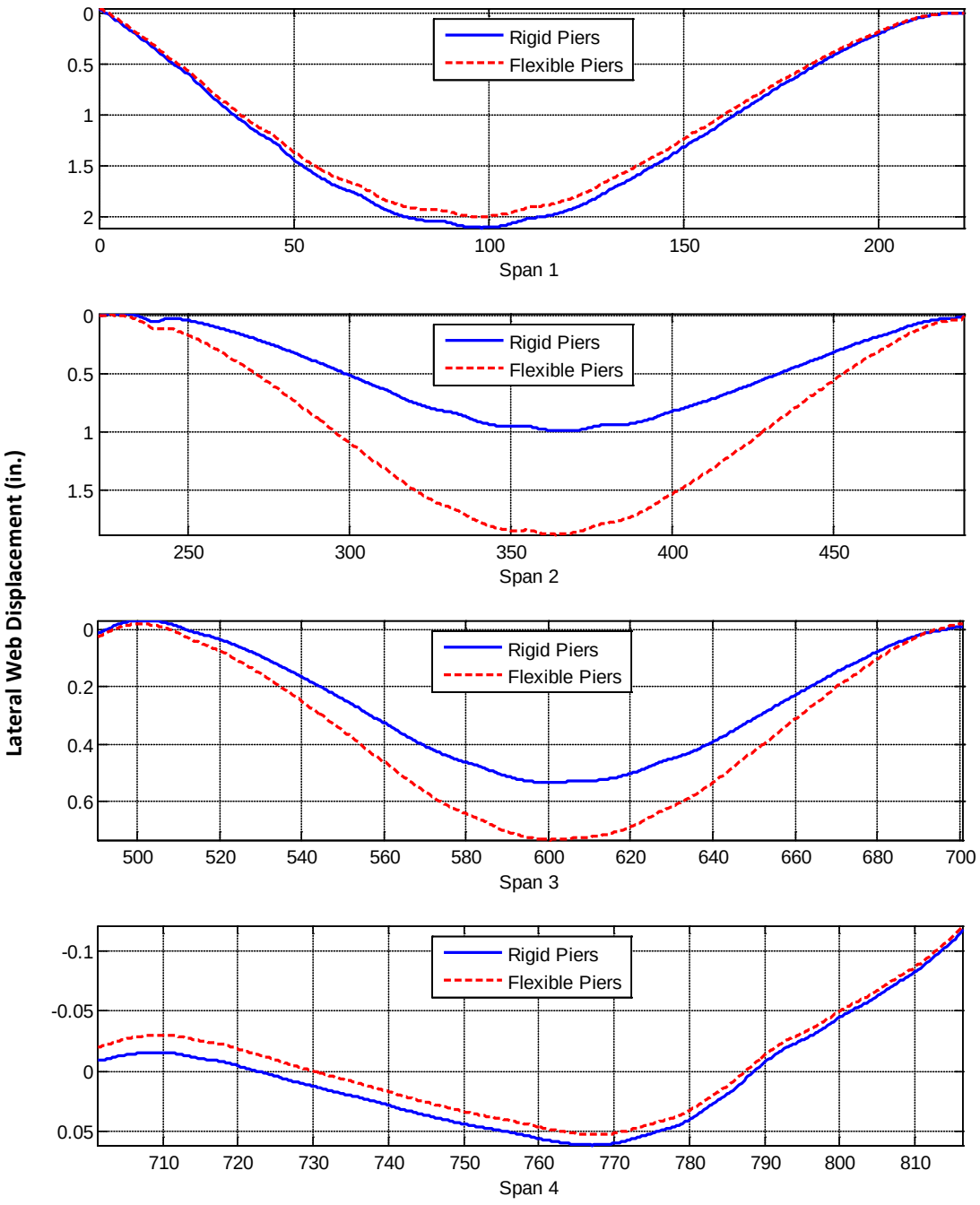


**Figure A.7. Girder 7 Lateral Web Centerline Displacement Due to Gravity Load**

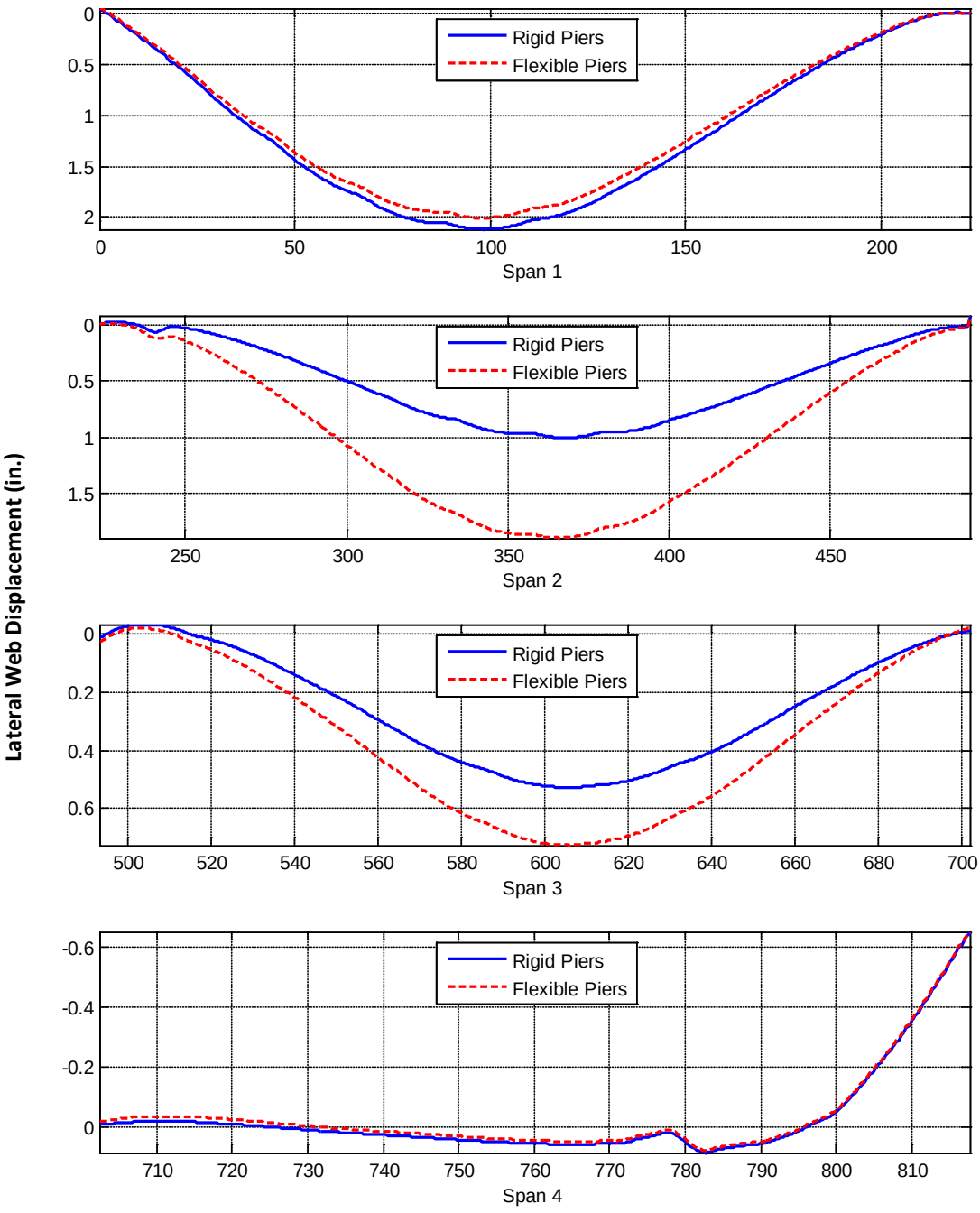


**Figure A.8. Girder 8 Lateral Web Centerline Displacement Due to Gravity Load**

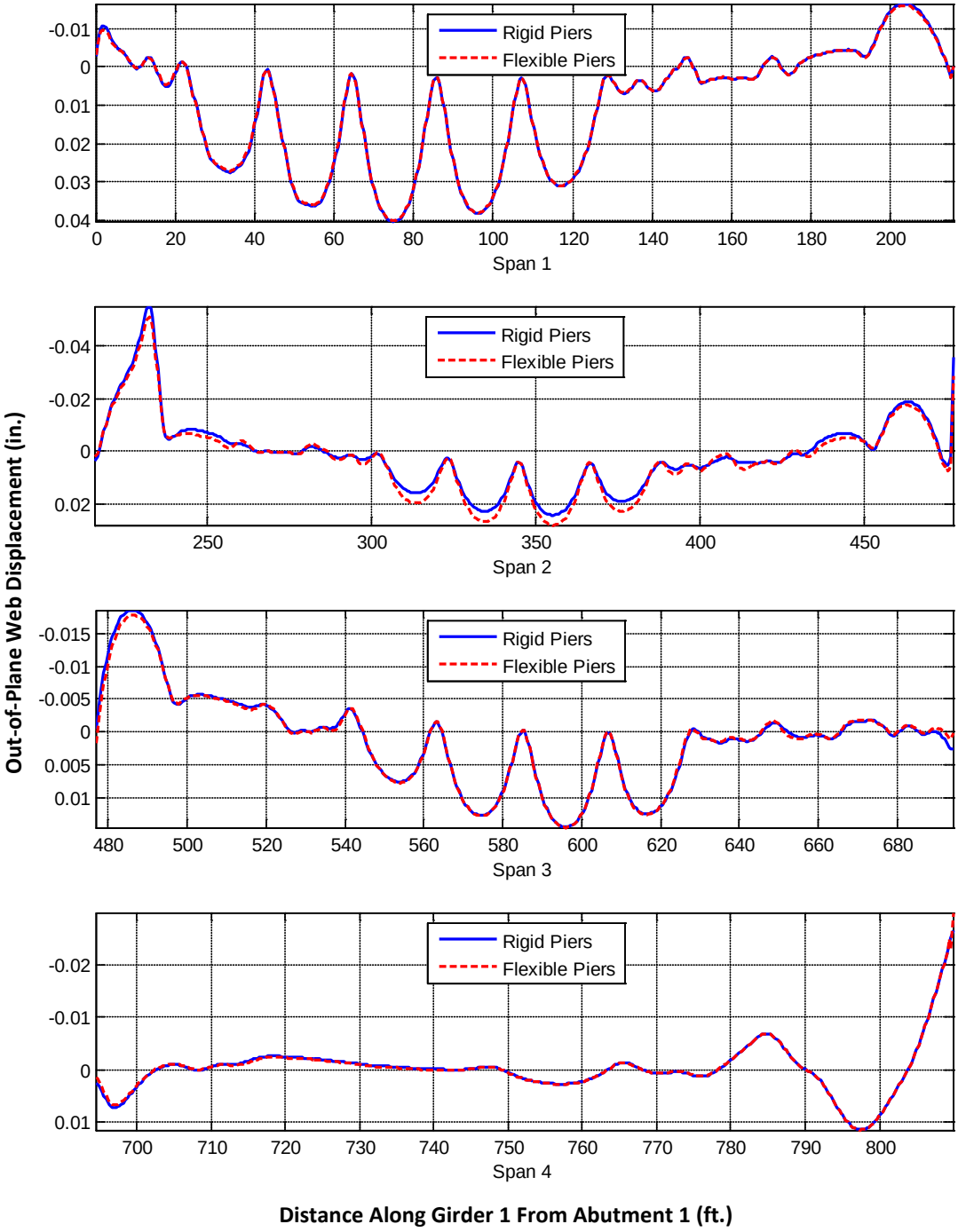


**Figure A.9. Girder 1 Out-of-Plane Web Centerline Displacement Due to Gravity Load**

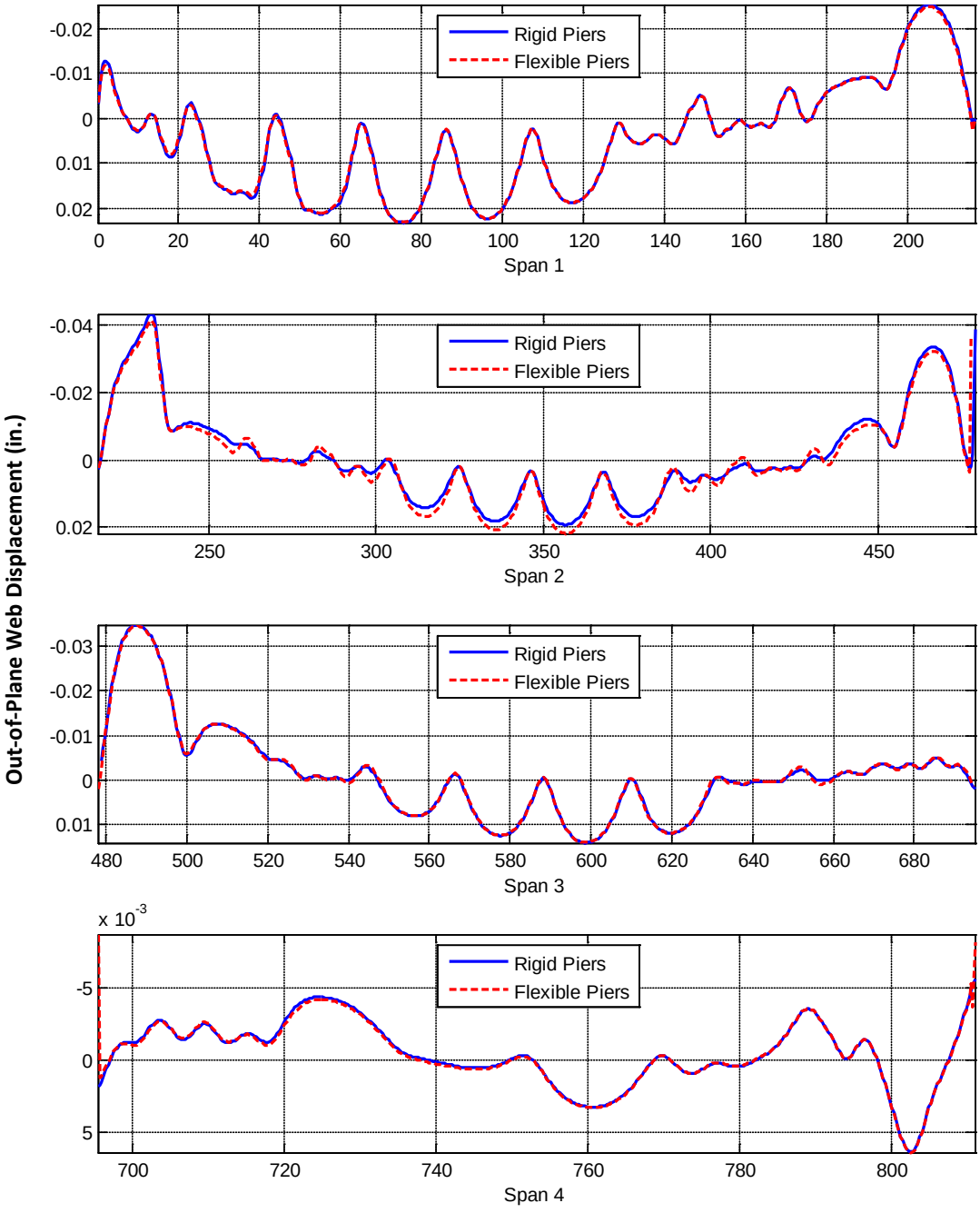


**Figure A.10. Girder 2 Out-of-Plane Web Centerline Displacement Due to Gravity Load**

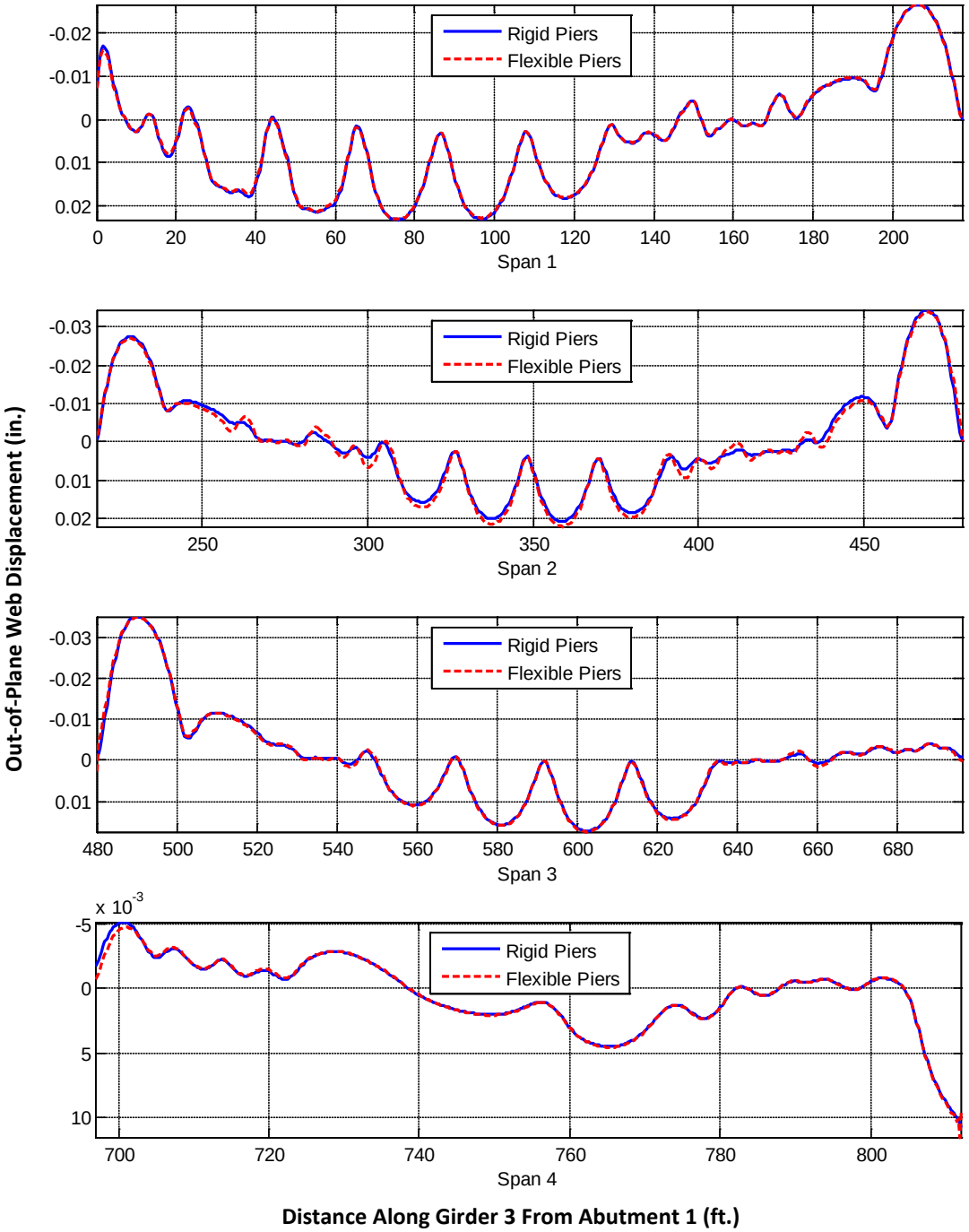


**Figure A.11. Girder 3 Out-of-Plane Web Centerline Displacement Due to Gravity Load**

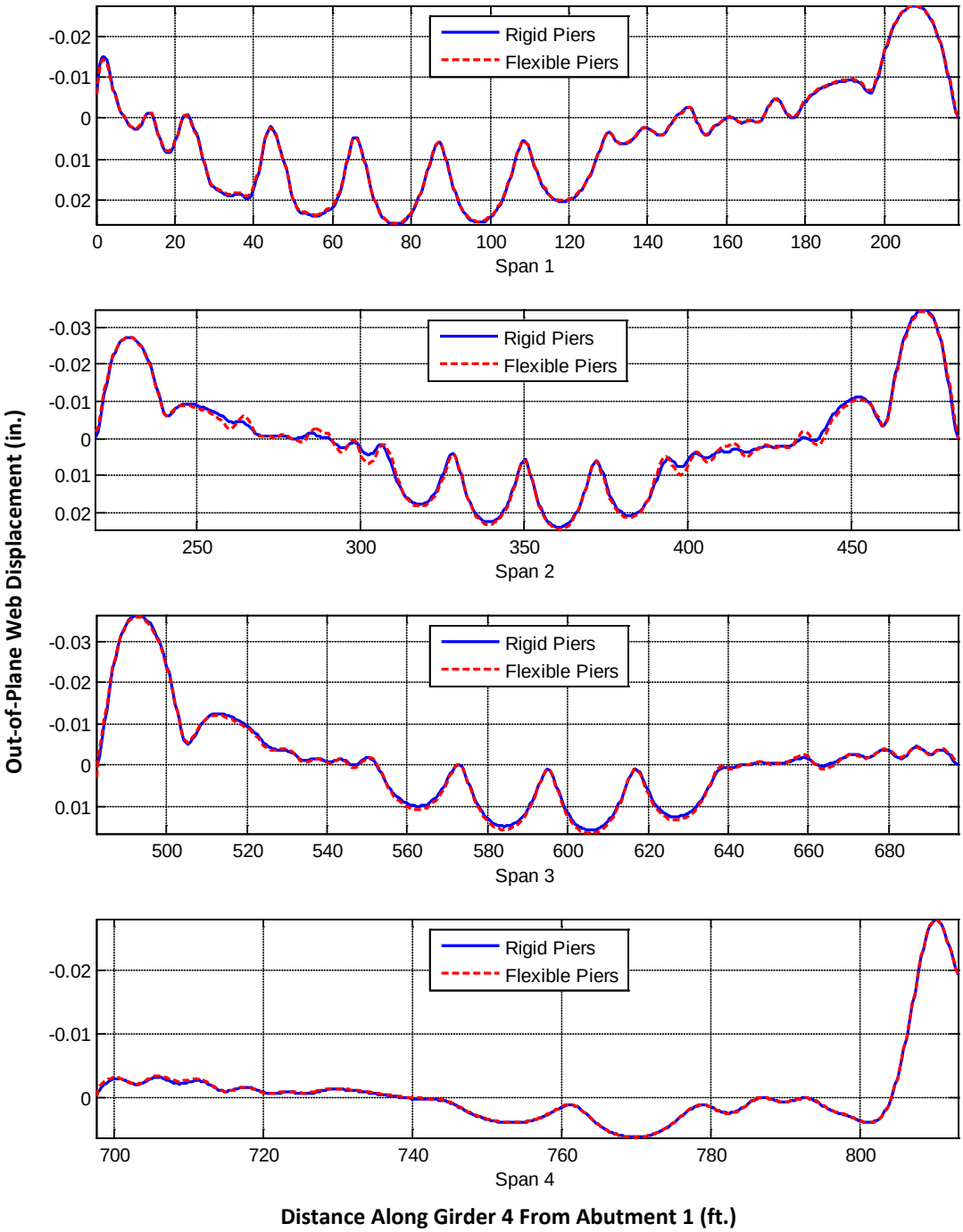


**Figure A.12. Girder 4 Out-of-Plane Web Centerline Displacement Due to Gravity Load**

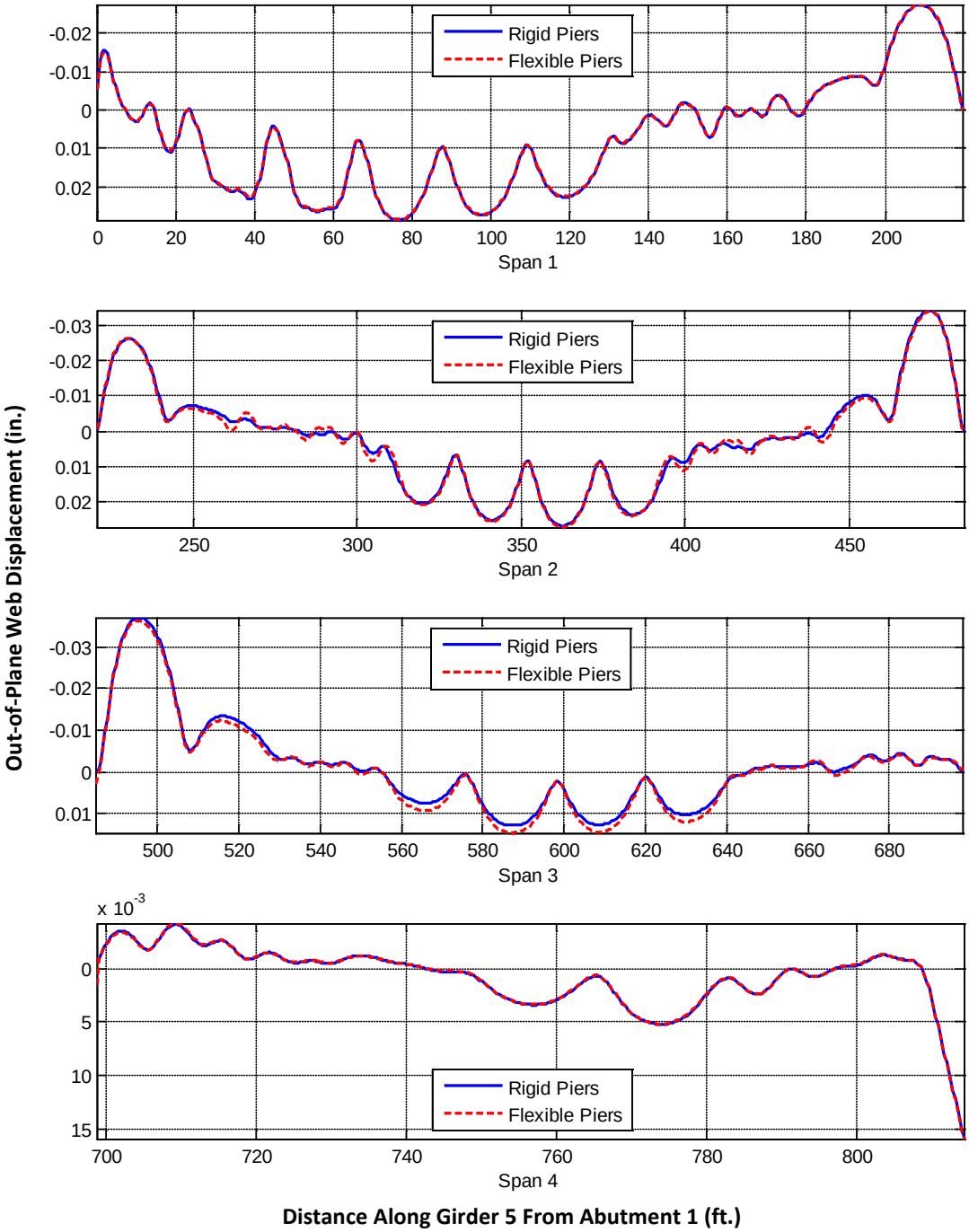


**Figure A.13. Girder 5 Out-of-Plane Web Centerline Displacement Due to Gravity Load**

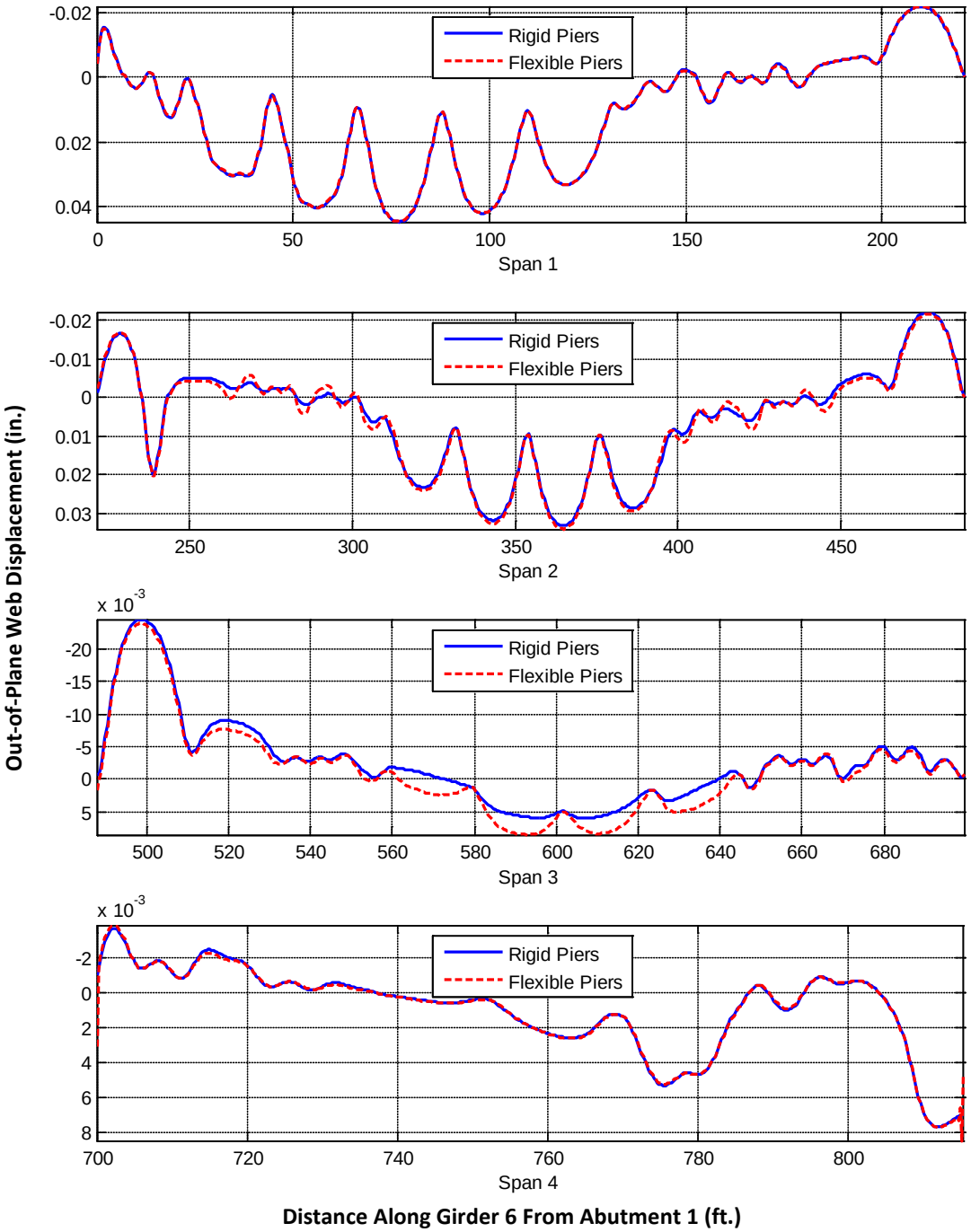


**Figure A.14. Girder 6 Out-of-Plane Web Centerline Displacement Due to Gravity Load**

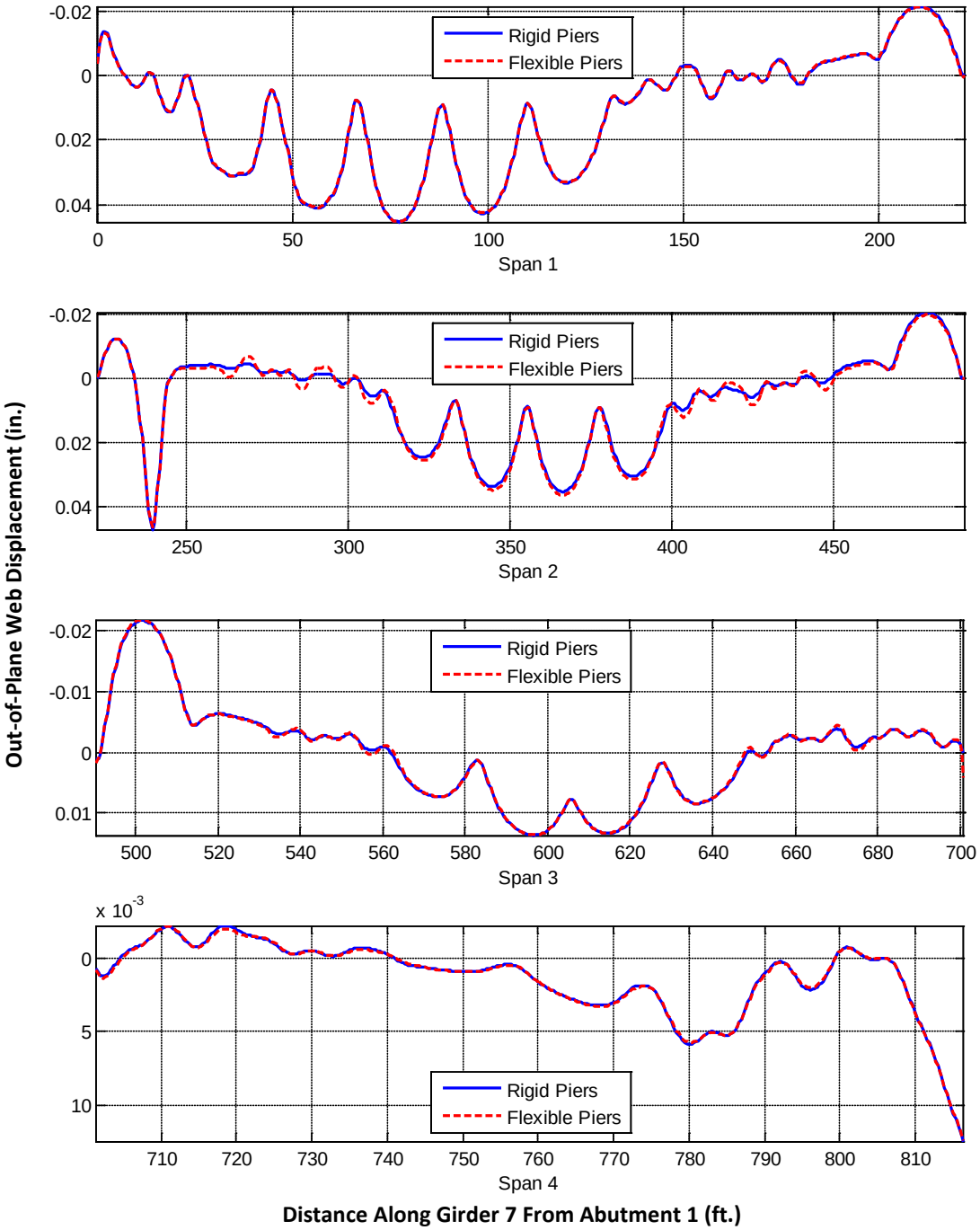


**Figure A.15. Girder 7 Out-of-Plane Web Centerline Displacement Due to Gravity Load**

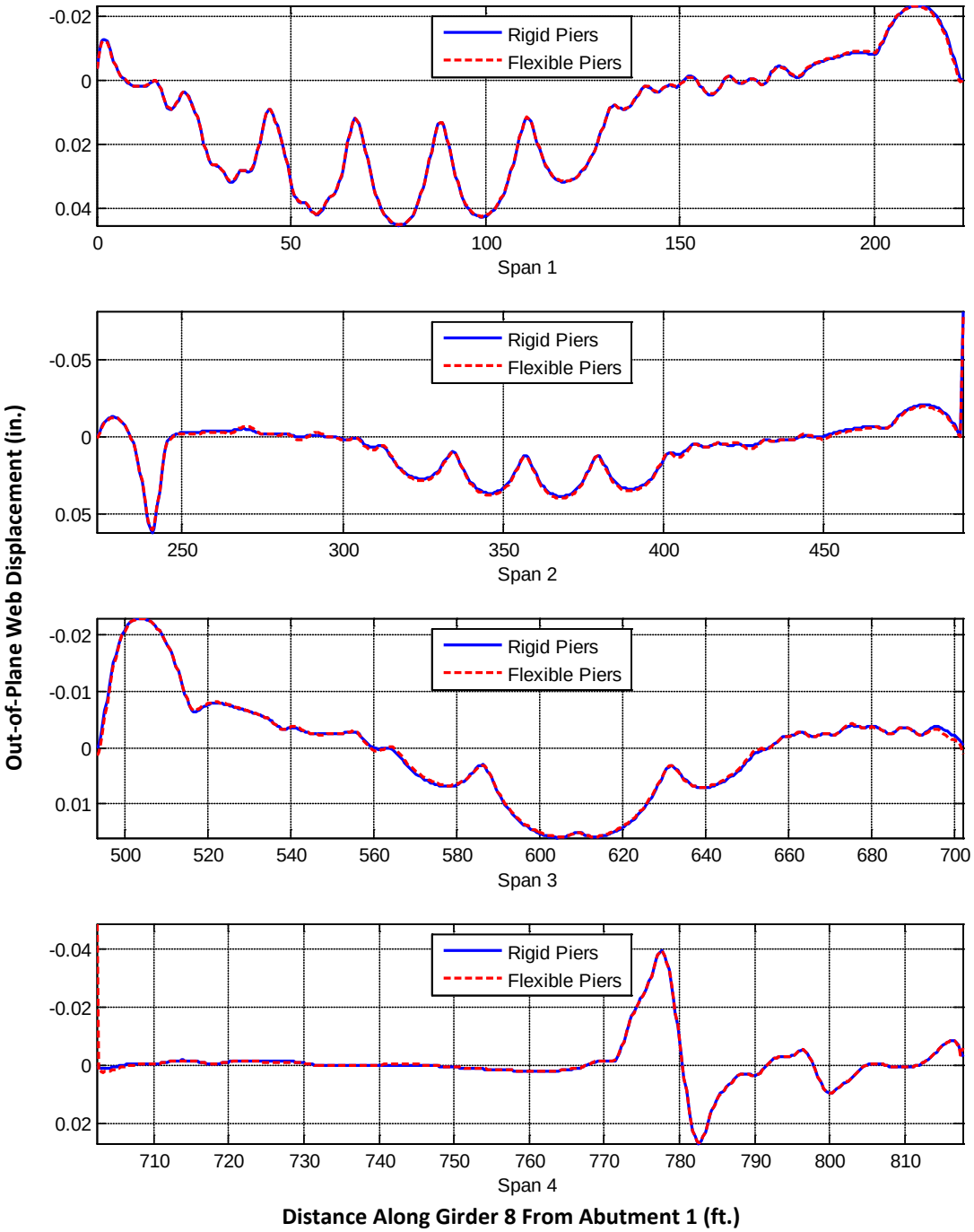


**Figure A.16. Girder 8 Out-of-Plane Web Centerline Displacement Due to Gravity Load**

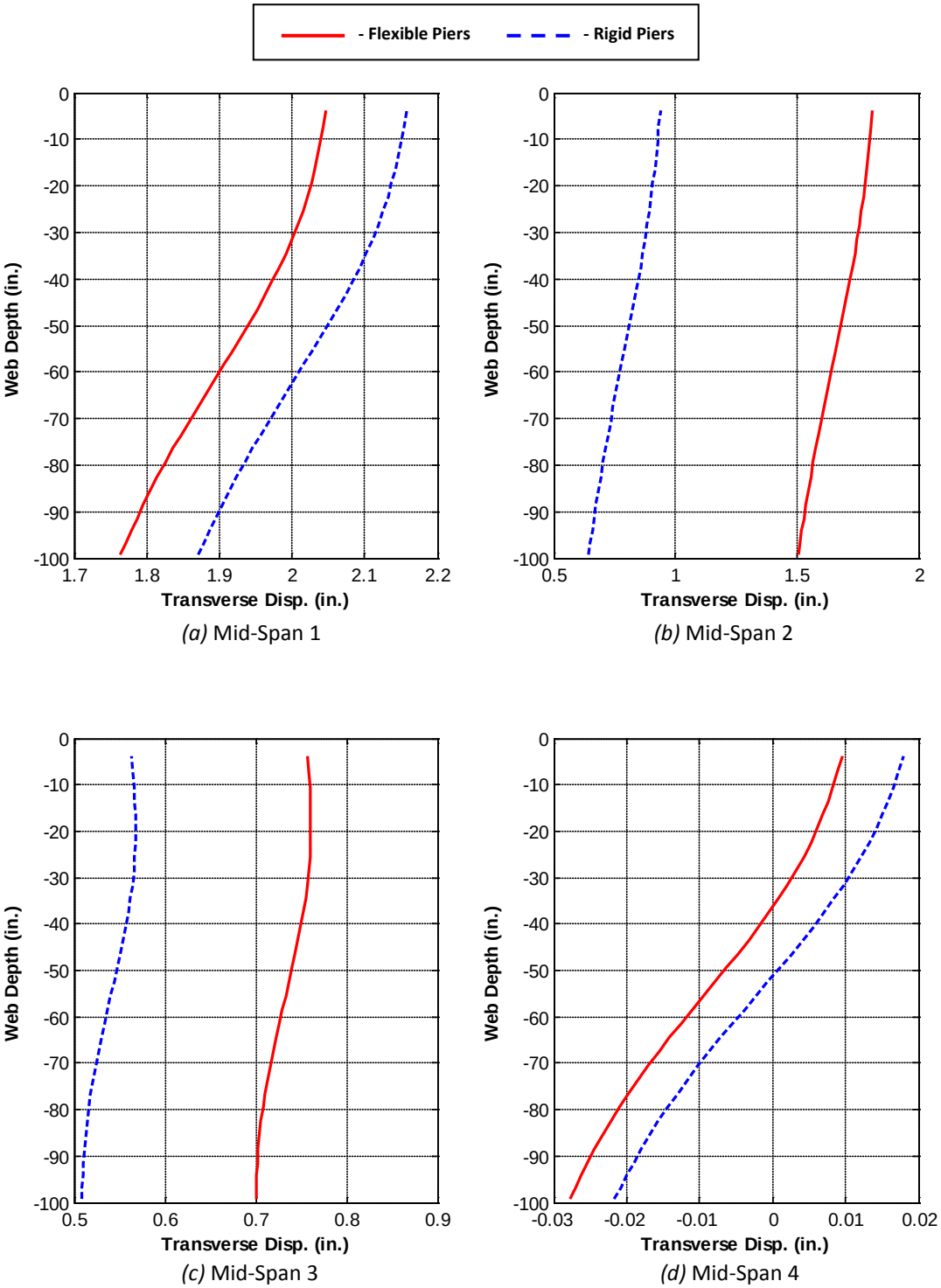


*(a)* Mid-Span 1

*(b)* Mid-Span 2

*(c)* Mid-Span 3

*(d)* Mid-Span 4

**Figure A.17. Web Displacement Profiles at Mid-Spans of Girder 1**

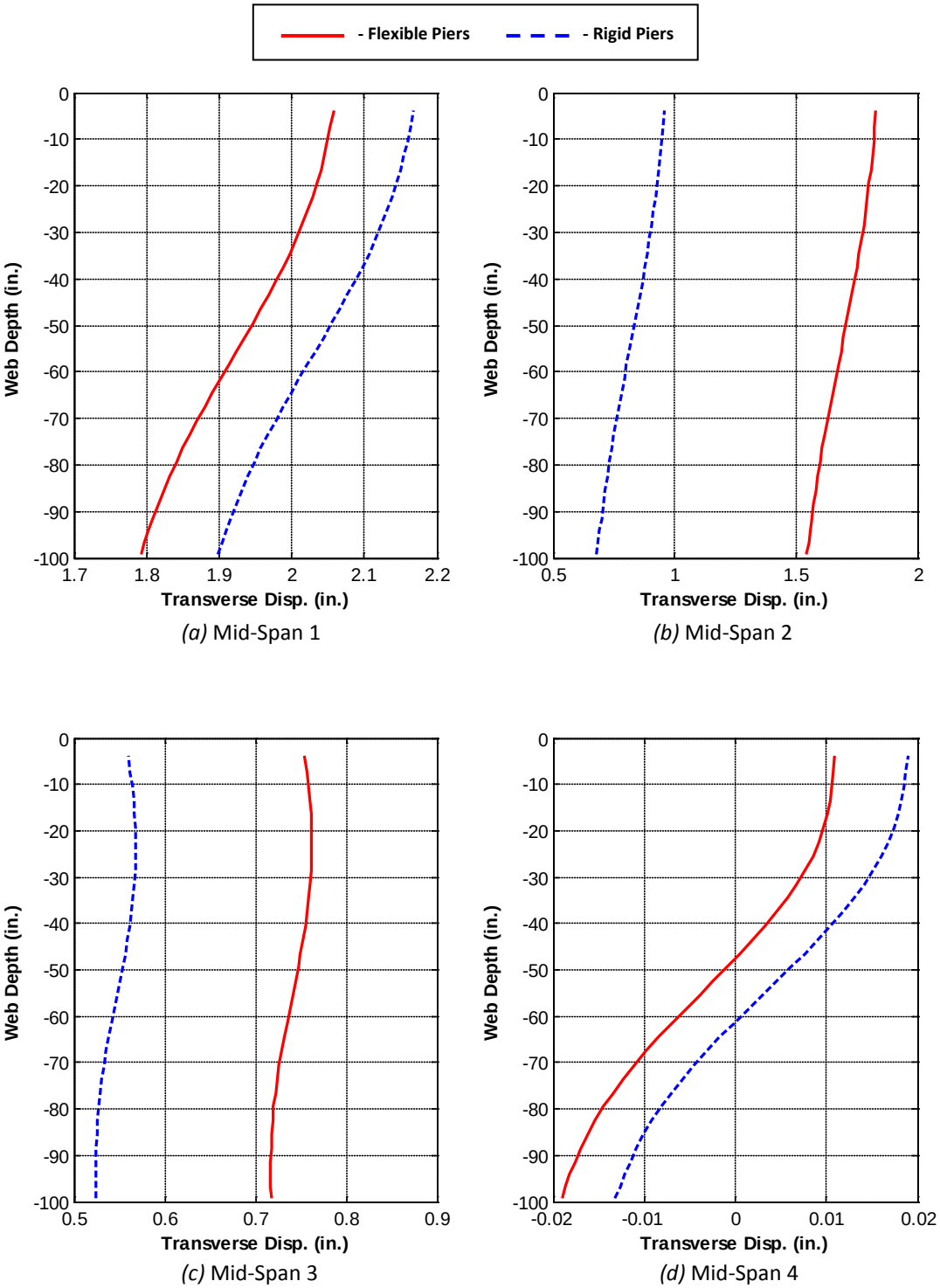


*(a)* Mid-Span 1

*(b)* Mid-Span 2

*(c)* Mid-Span 3

*(d)* Mid-Span 4

**Figure A.18. Web Displacement Profiles at Mid-Spans of Girder 2**

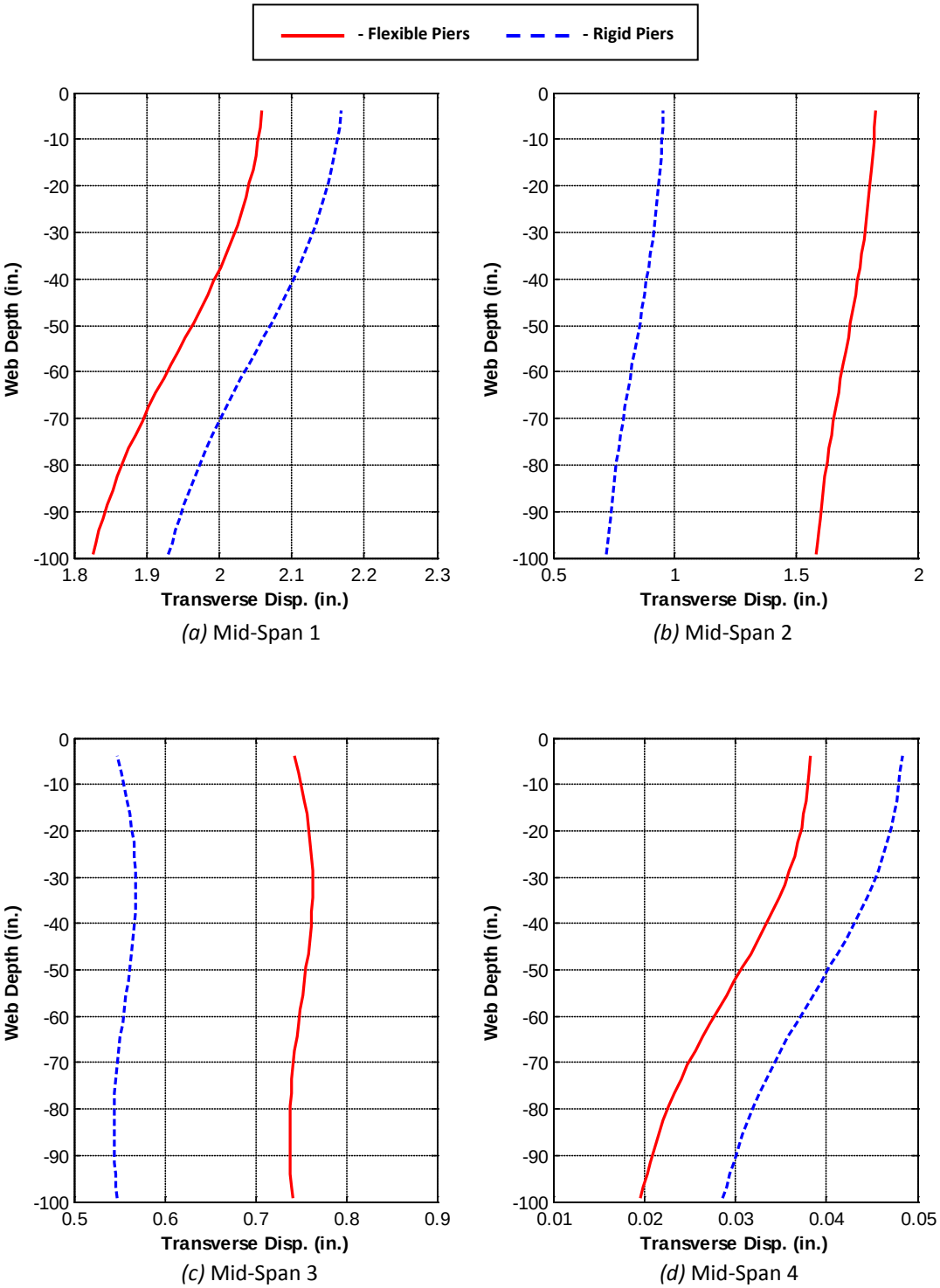


*(a)* Mid-Span 1

*(b)* Mid-Span 2

*(c)* Mid-Span 3

*(d)* Mid-Span 4

**Figure A.19. Web Displacement Profiles at Mid-Spans of Girder 3**

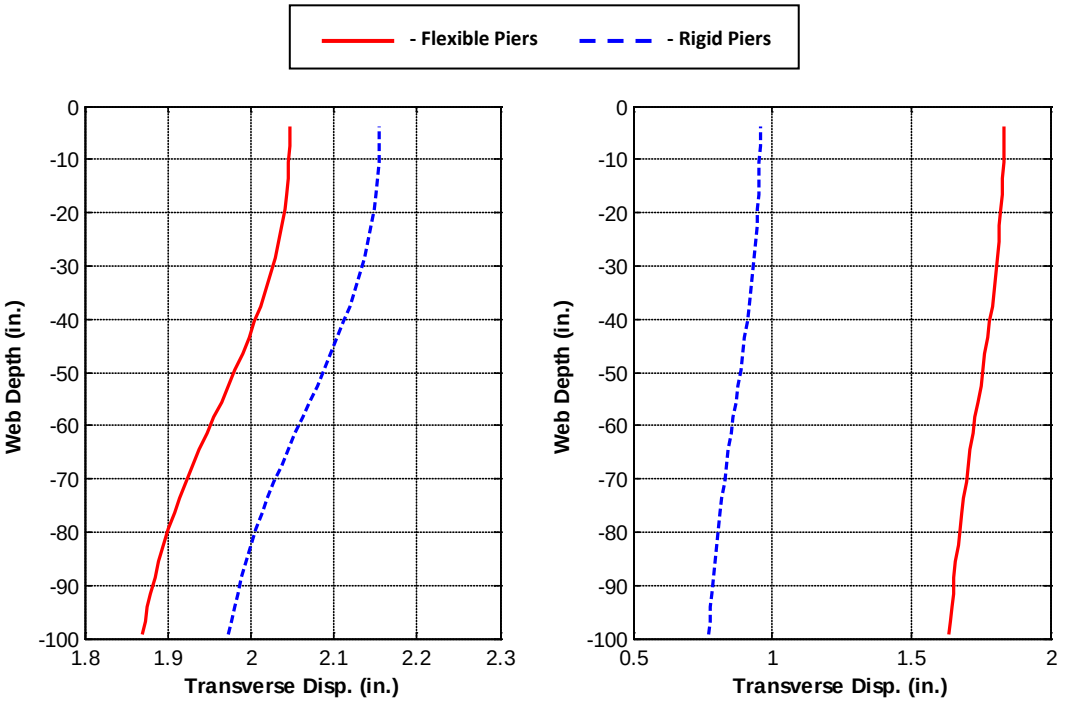


*(a)* Mid-Span 1

*(b)* Mid-Span 2

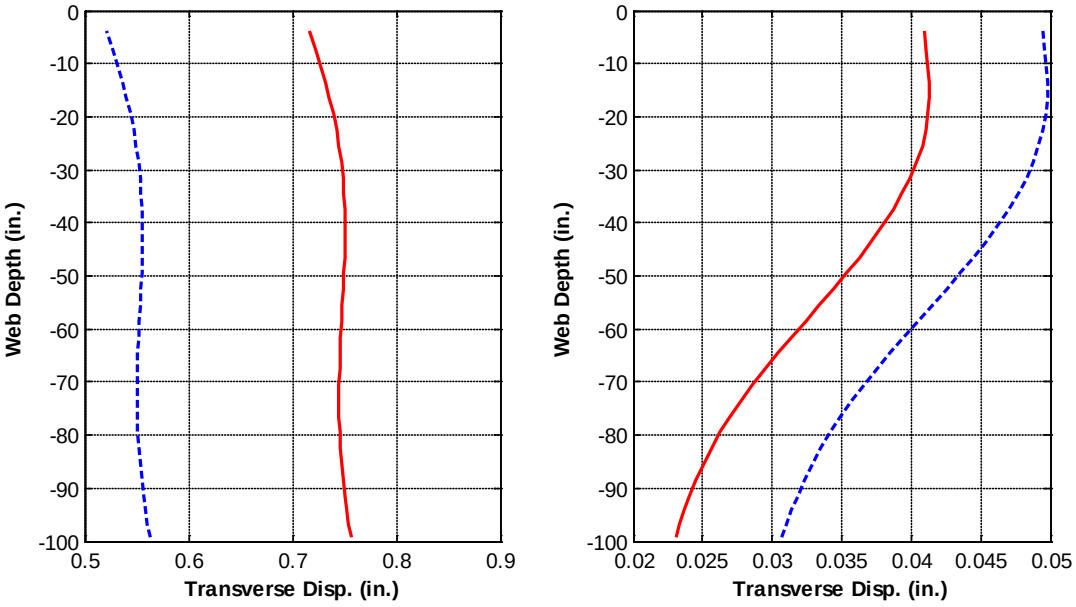


*(c)* Mid-Span 3

*(d)* Mid-Span 4

**Figure A.20. Web Displacement Profiles at Mid-Spans of Girder 4**

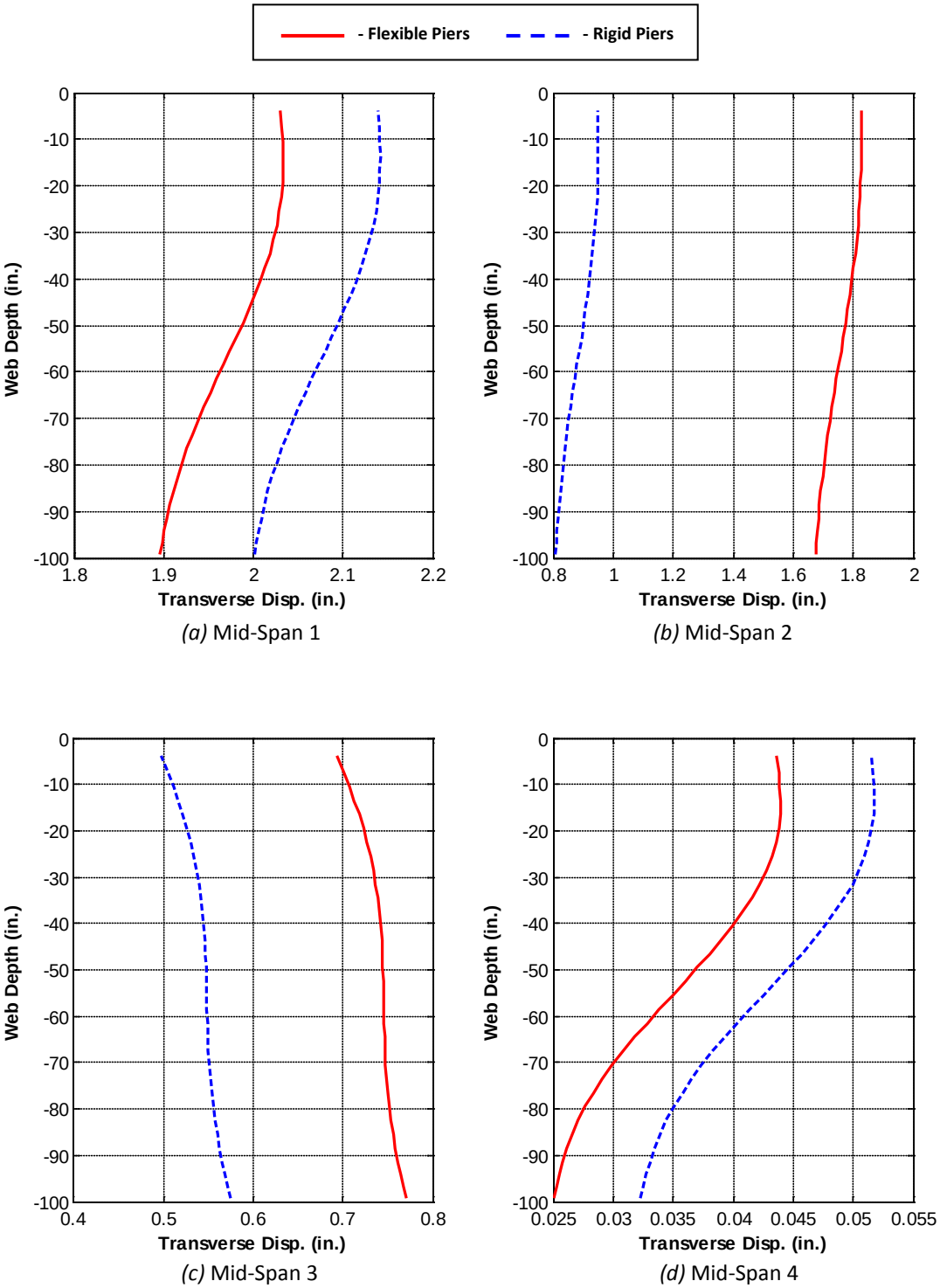


*(a)* Mid-Span 1

*(b)* Mid-Span 2

*(c)* Mid-Span 3

*(d)* Mid-Span 4

**Figure A.21. Web Displacement Profiles at Mid-Spans of Girder 5**

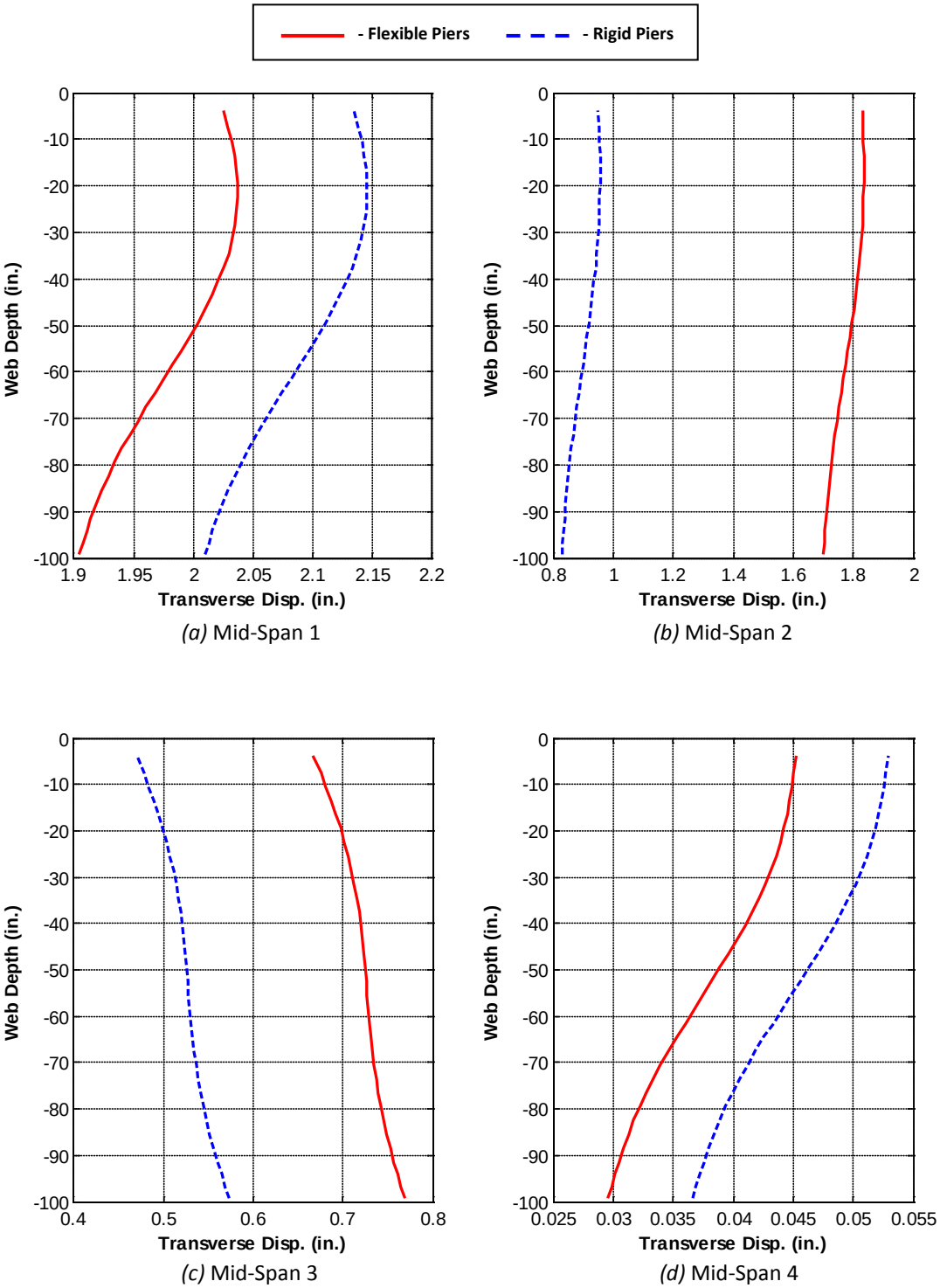


*(a)* Mid-Span 1

*(b)* Mid-Span 2

*(c)* Mid-Span 3

*(d)* Mid-Span 4

**Figure A.22. Web Displacement Profiles at Mid-Spans of Girder 6**

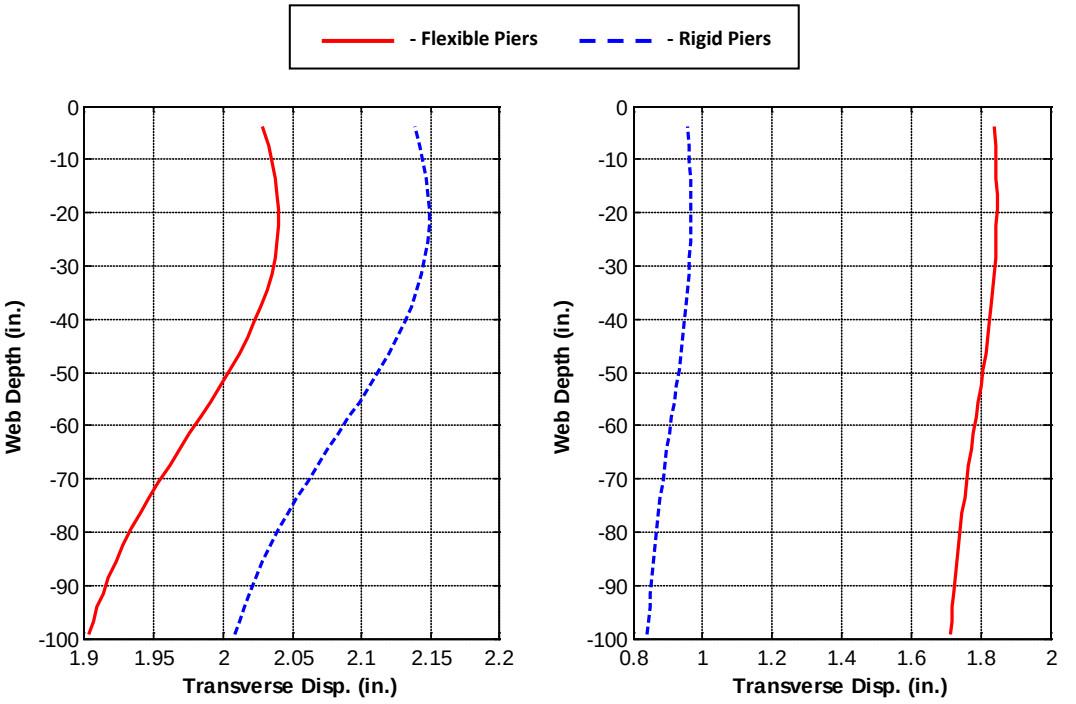


*(a)* Mid-Span 1

*(b)* Mid-Span 2

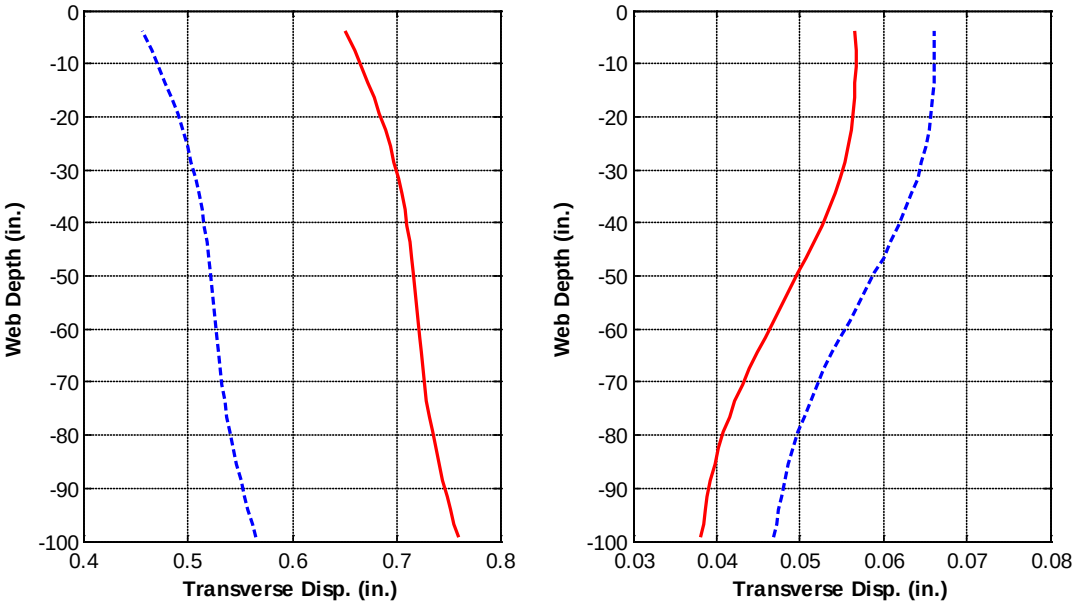


*(c)* Mid-Span 3

*(d)* Mid-Span 4

**Figure A.23. Web Displacement Profiles at Mid-Spans of Girder 7**

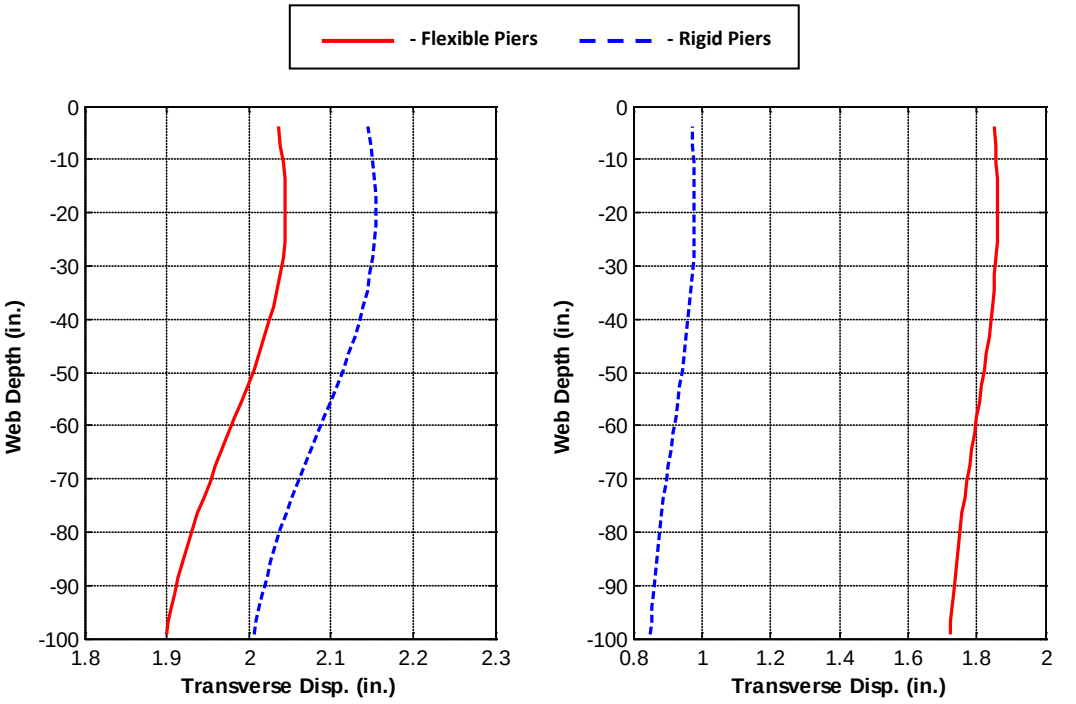


*(a)* Mid-Span 1

*(b)* Mid-Span 2

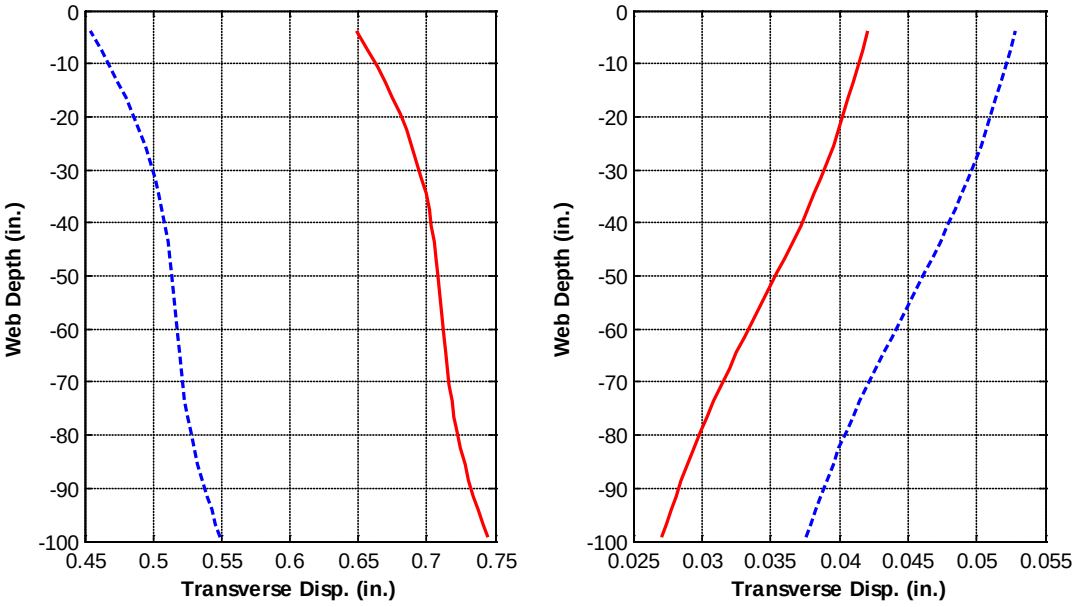


*(c)* Mid-Span 3

*(d)* Mid-Span 4

**Figure A.24. Web Displacement Profiles at Mid-Spans of Girder 8**

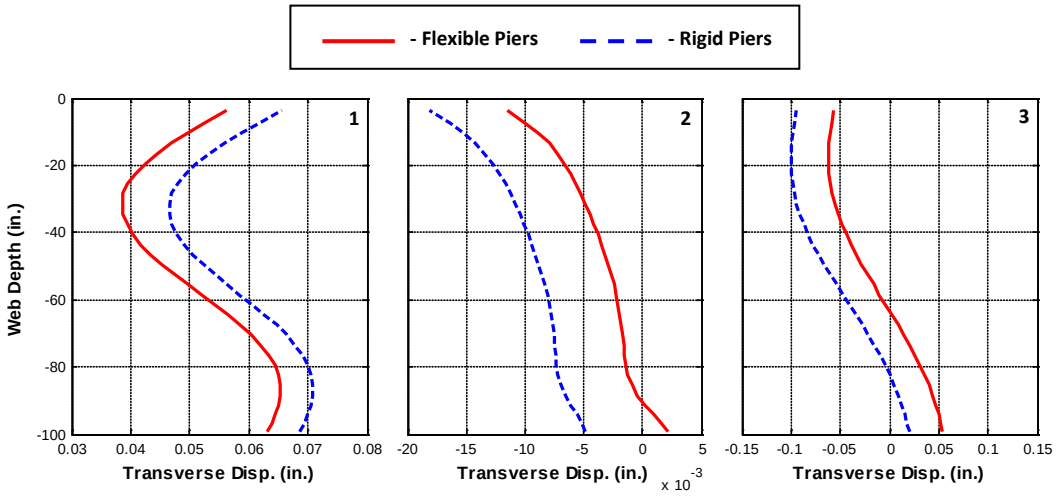


*(a)* Pier 1

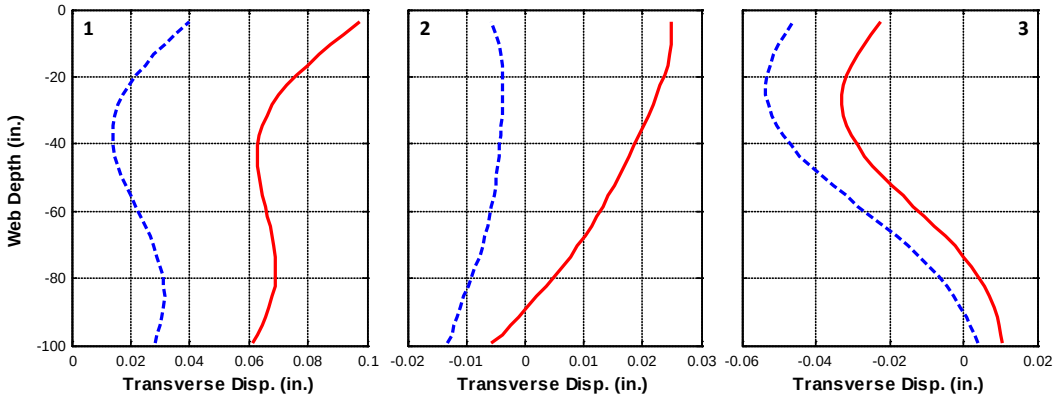


*(b)* Pier 2

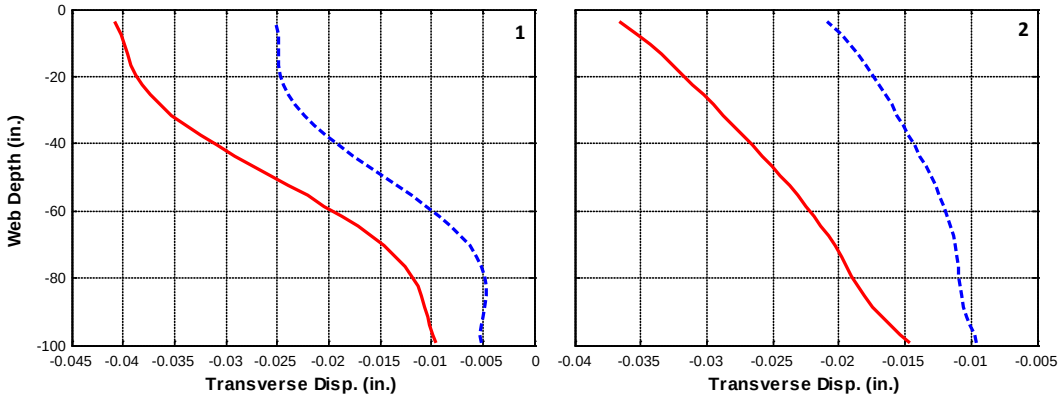


*(c)* Pier 3

**Figure A.25. Web Displacement Profiles at Piers of Girder 1**

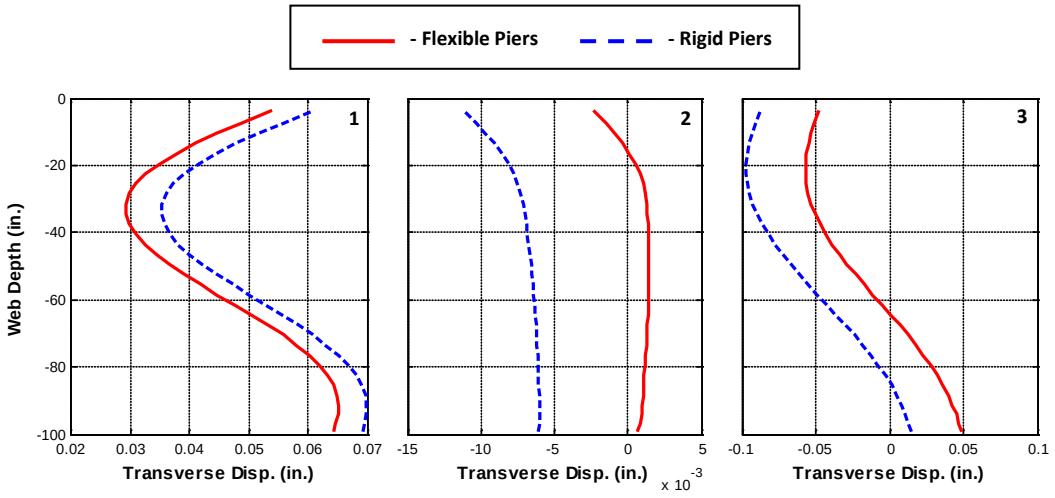


*(a)* Pier 1

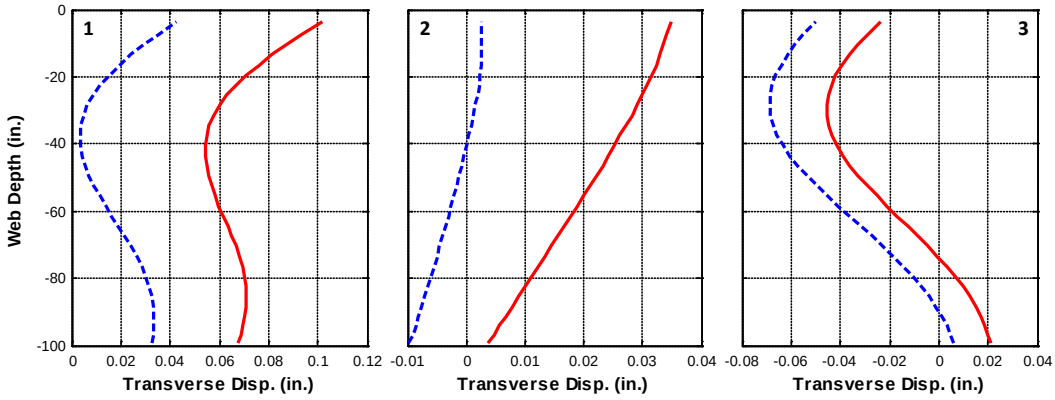


*(b)* Pier 2

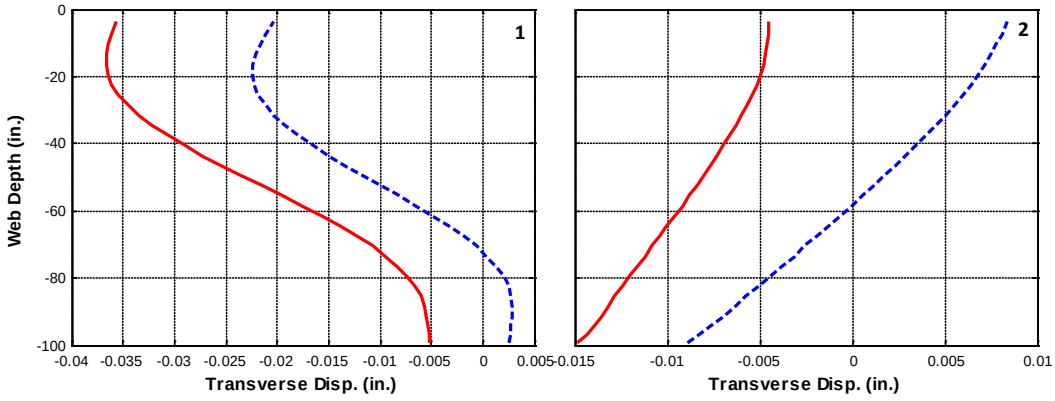


*(c)* Pier 3

**Figure A.26. Web Displacement Profiles at Piers of Girder 2**

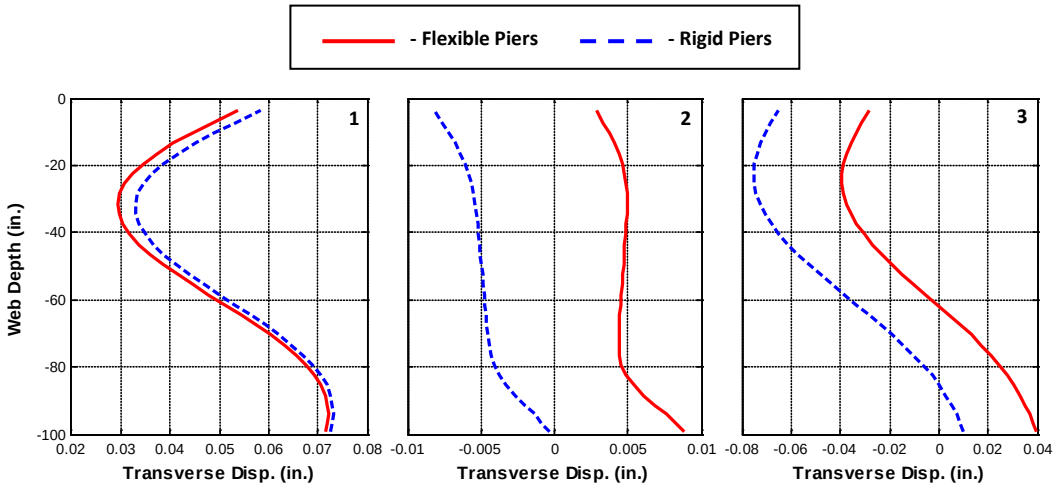


*(a)* Pier 1

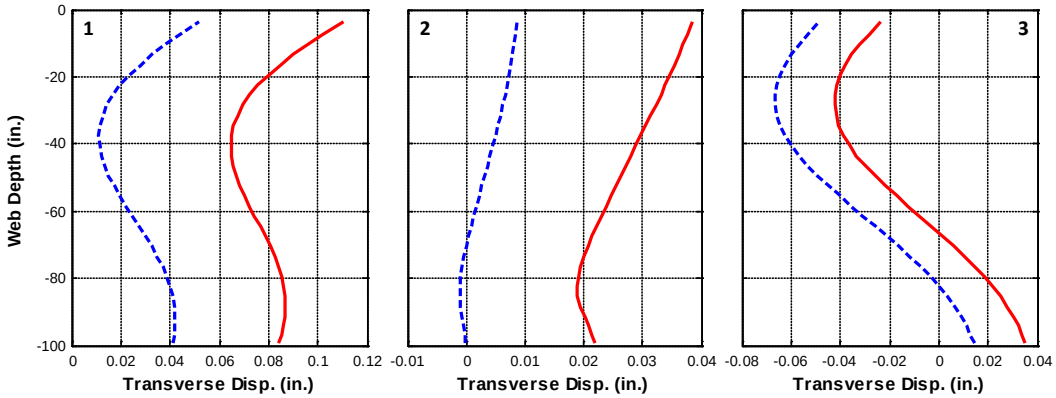


*(b)* Pier 2

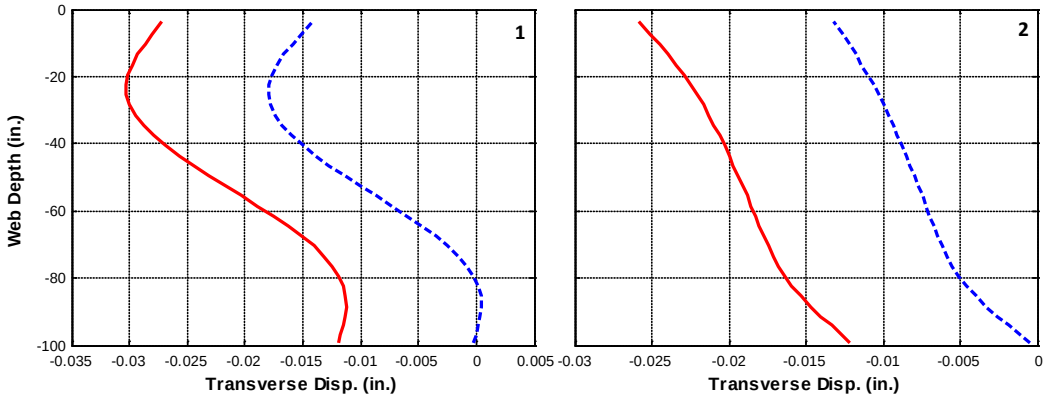


*(c)* Pier 3

**Figure A.27. Web Displacement Profiles at Piers of Girder 3**

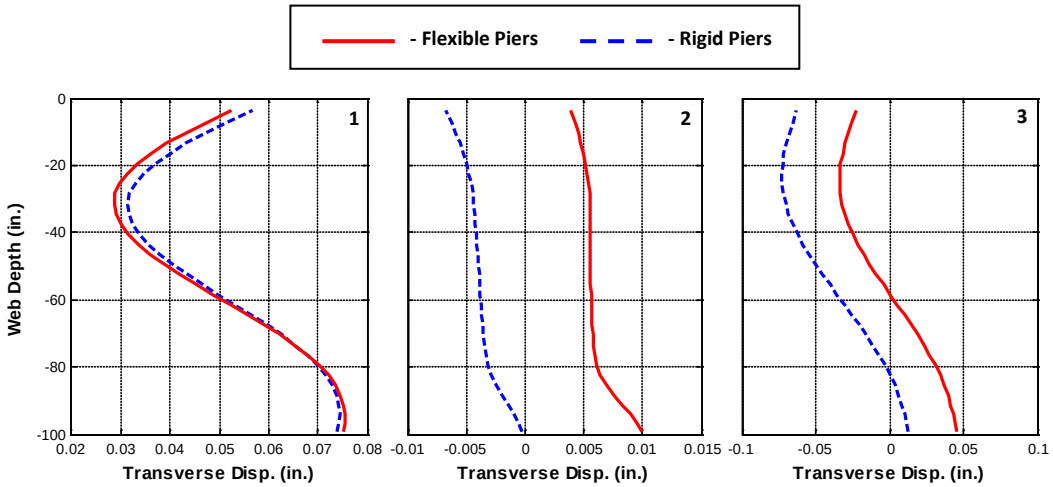


*(a)* Pier 1

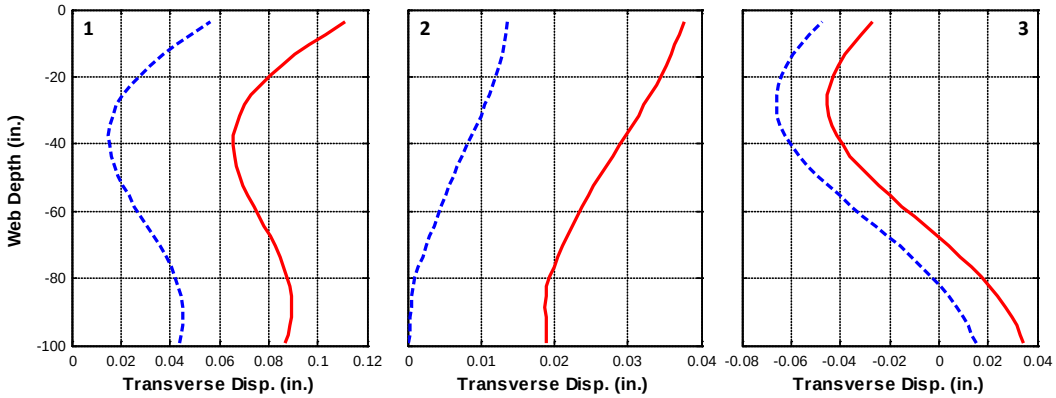


*(b)* Pier 2

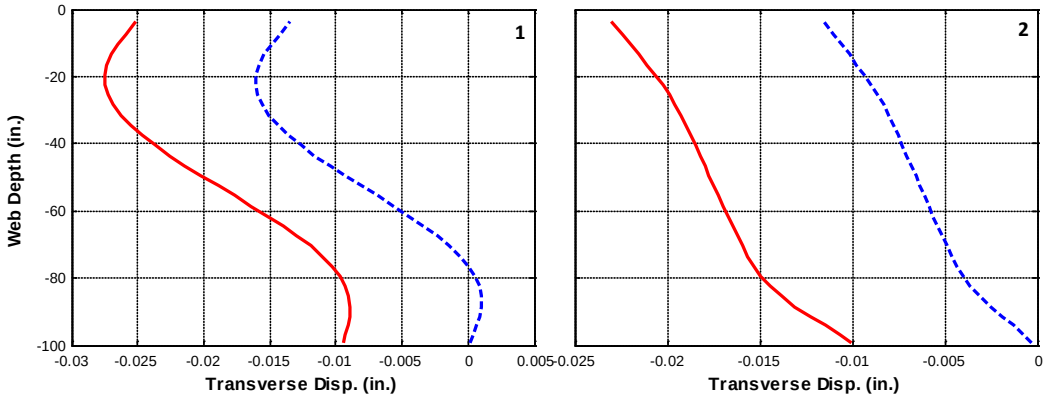


*(c)* Pier 3

**Figure A.28. Web Displacement Profiles at Piers of Girder 4**

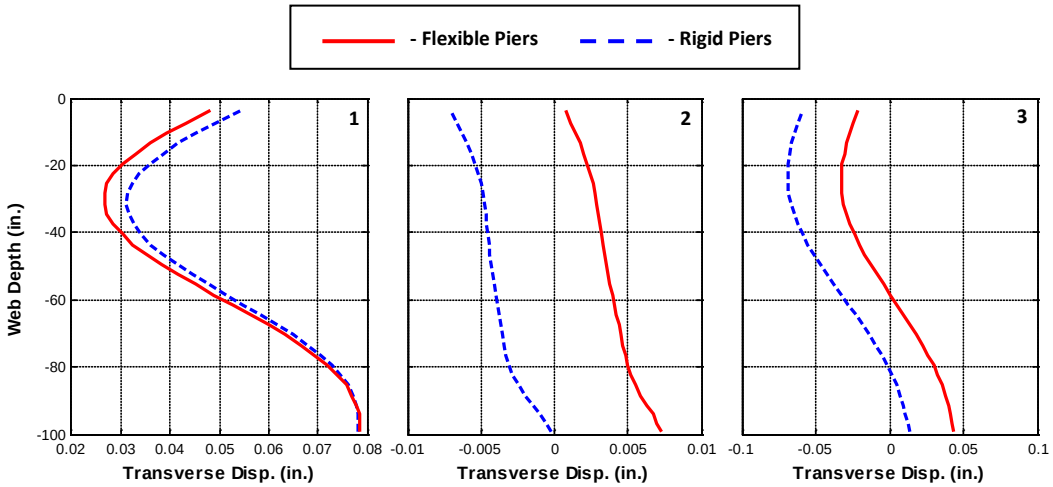


*(a)* Pier 1

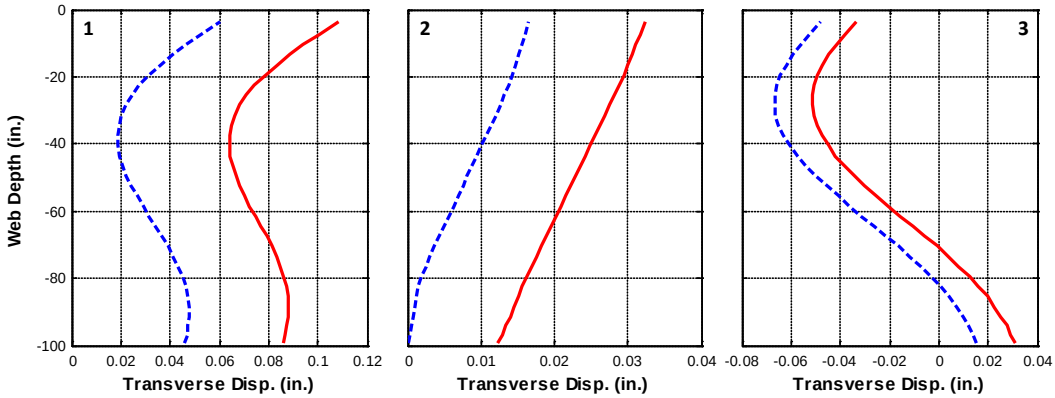


*(b)* Pier 2

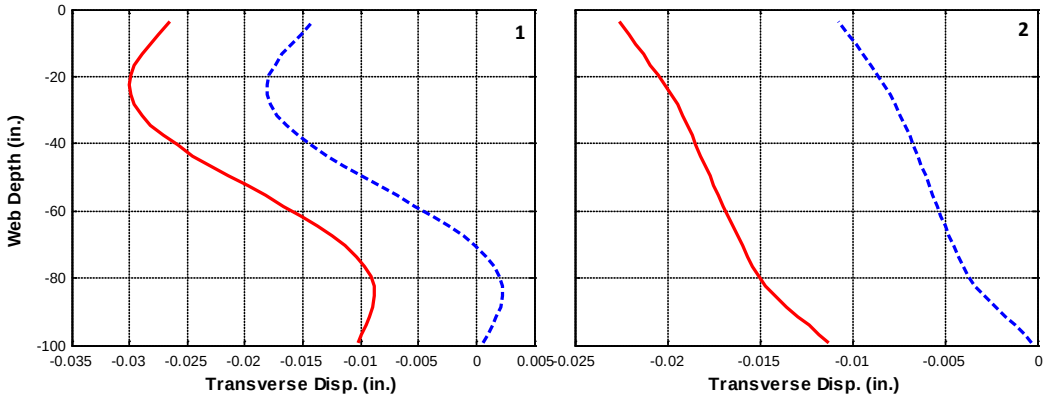


*(c)* Pier 3

**Figure A.29. Web Displacement Profiles at Piers of Girder 5**

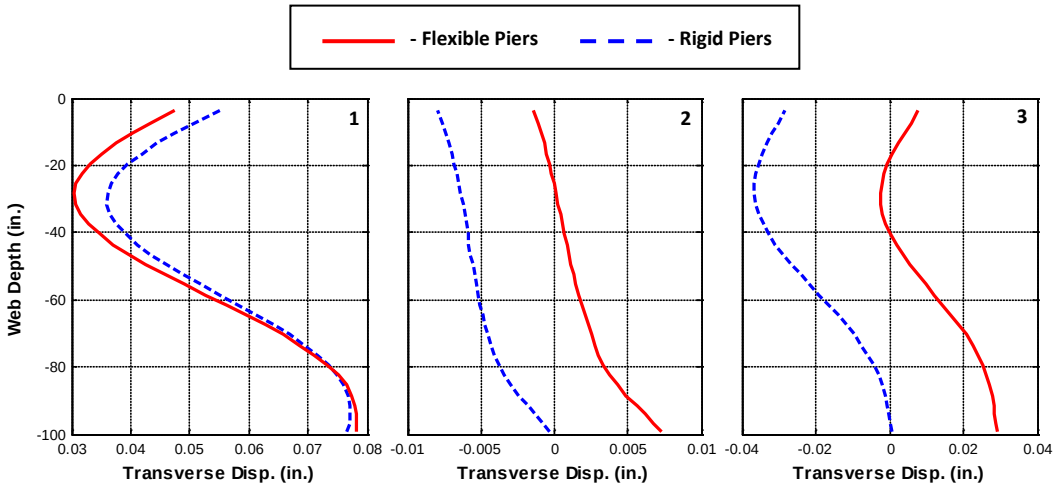


*(a)* Pier 1

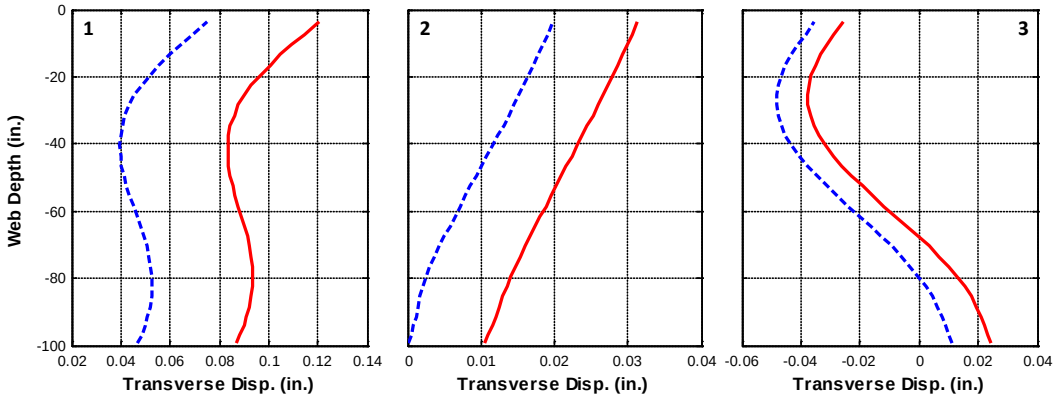


*(b)* Pier 2

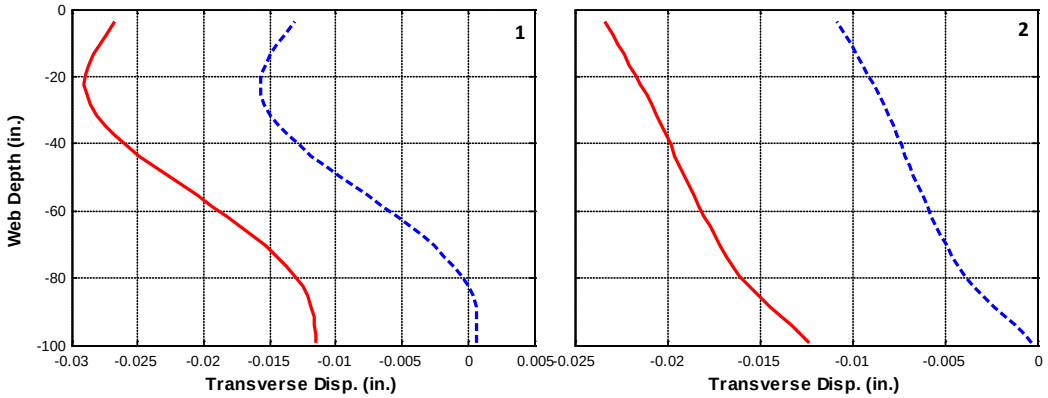


*(c)* Pier 3

**Figure A.30. Web Displacement Profiles at Piers of Girder 6**

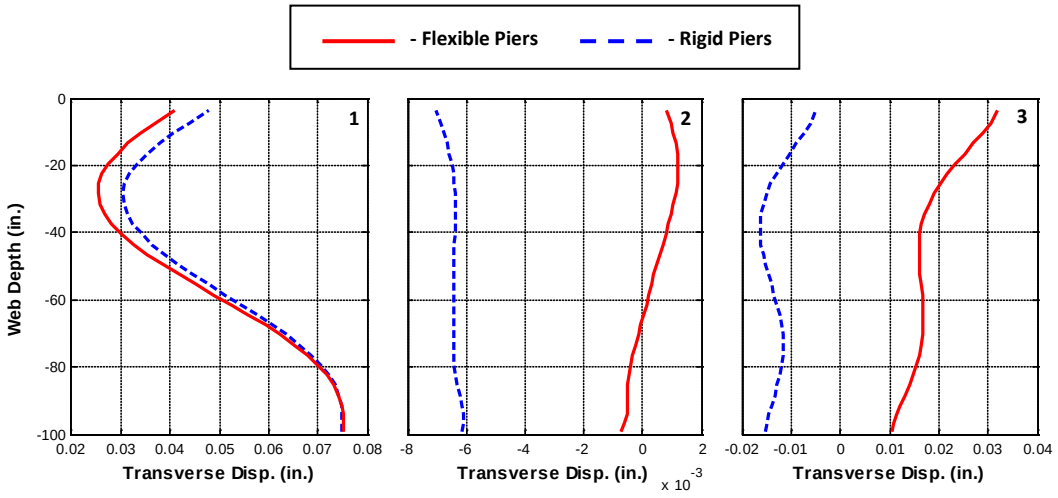


*(a)* Pier 1

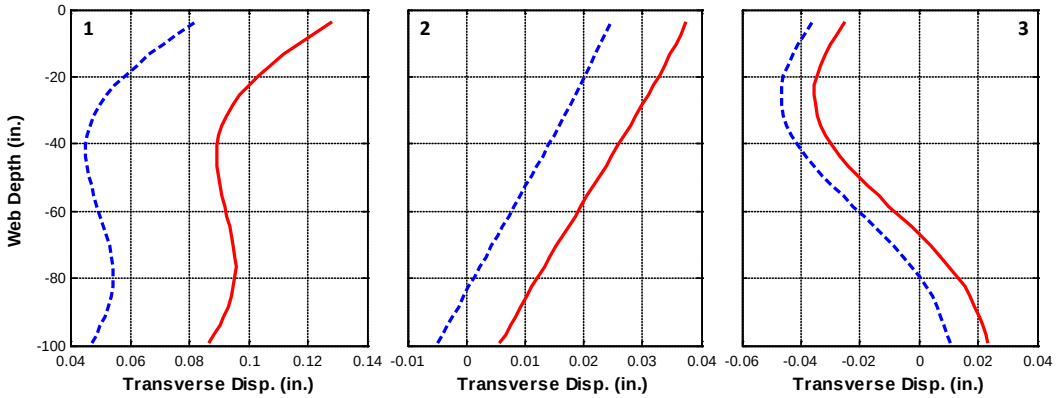


*(b)* Pier 2

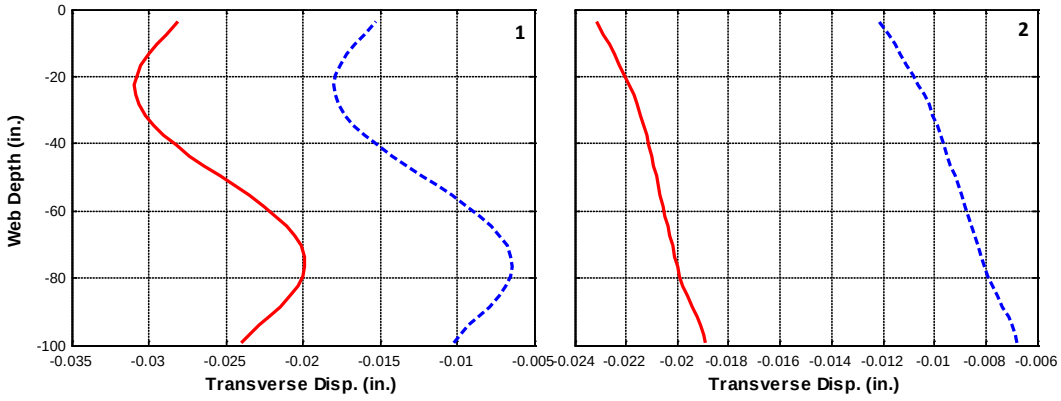


*(c)* Pier 3

**Figure A.31. Web Displacement Profiles at Piers of Girder 7**

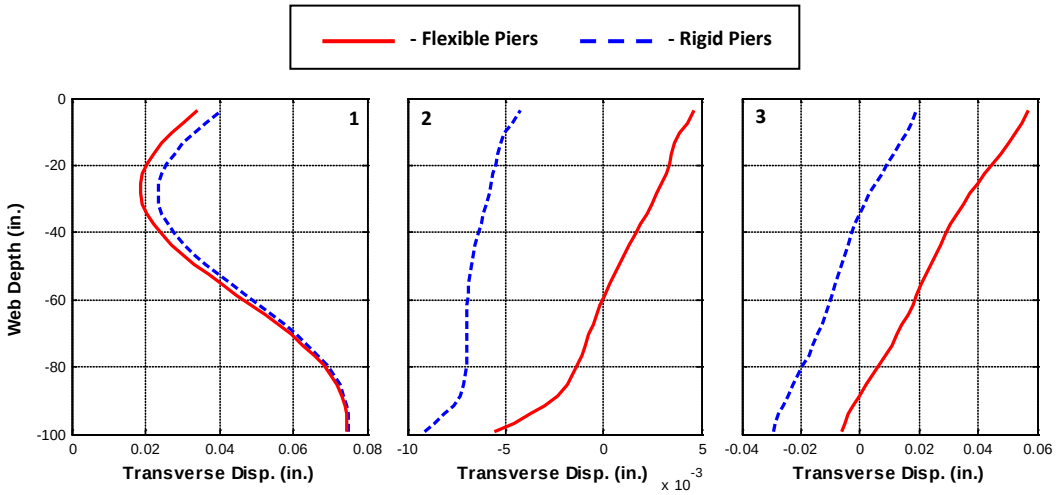


*(a)* Pier 1

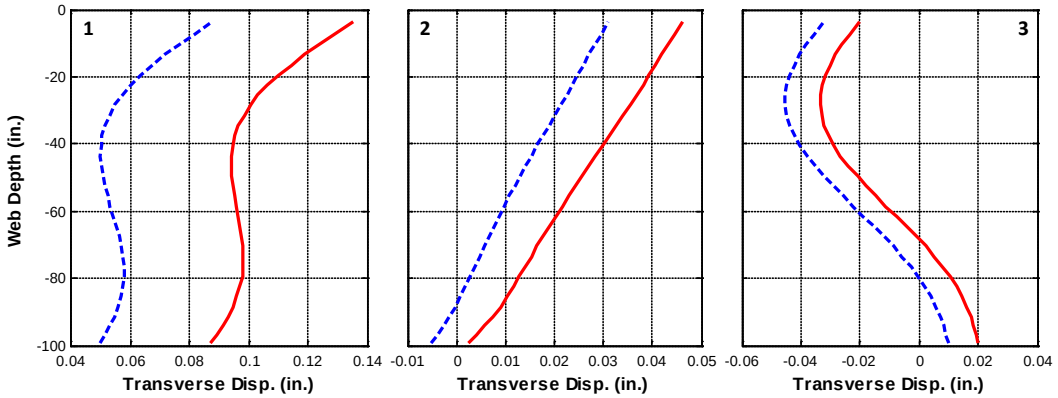


*(b)* Pier 2

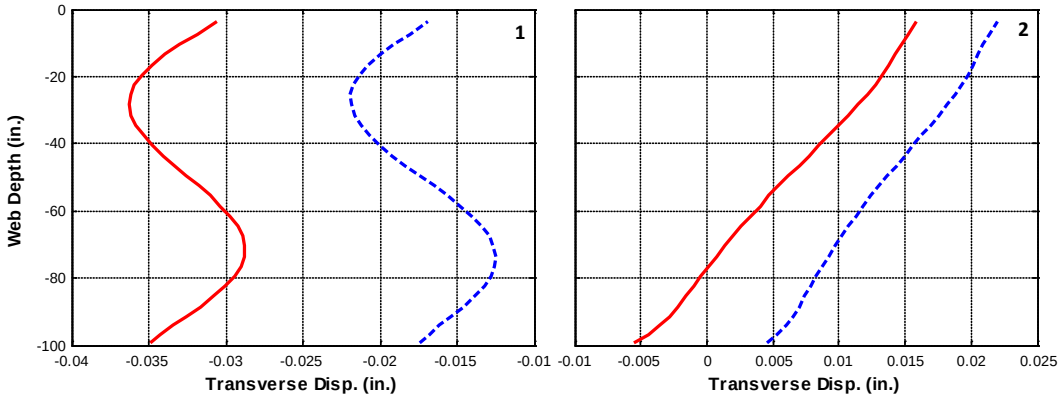


*(c)* Pier 3

**Figure A.32. Web Displacement Profiles at Piers of Girder 8**

# APPENDIX B

## GIRDER DEFORMATIONS UNDER GRAVITY AND THERMAL LOADING

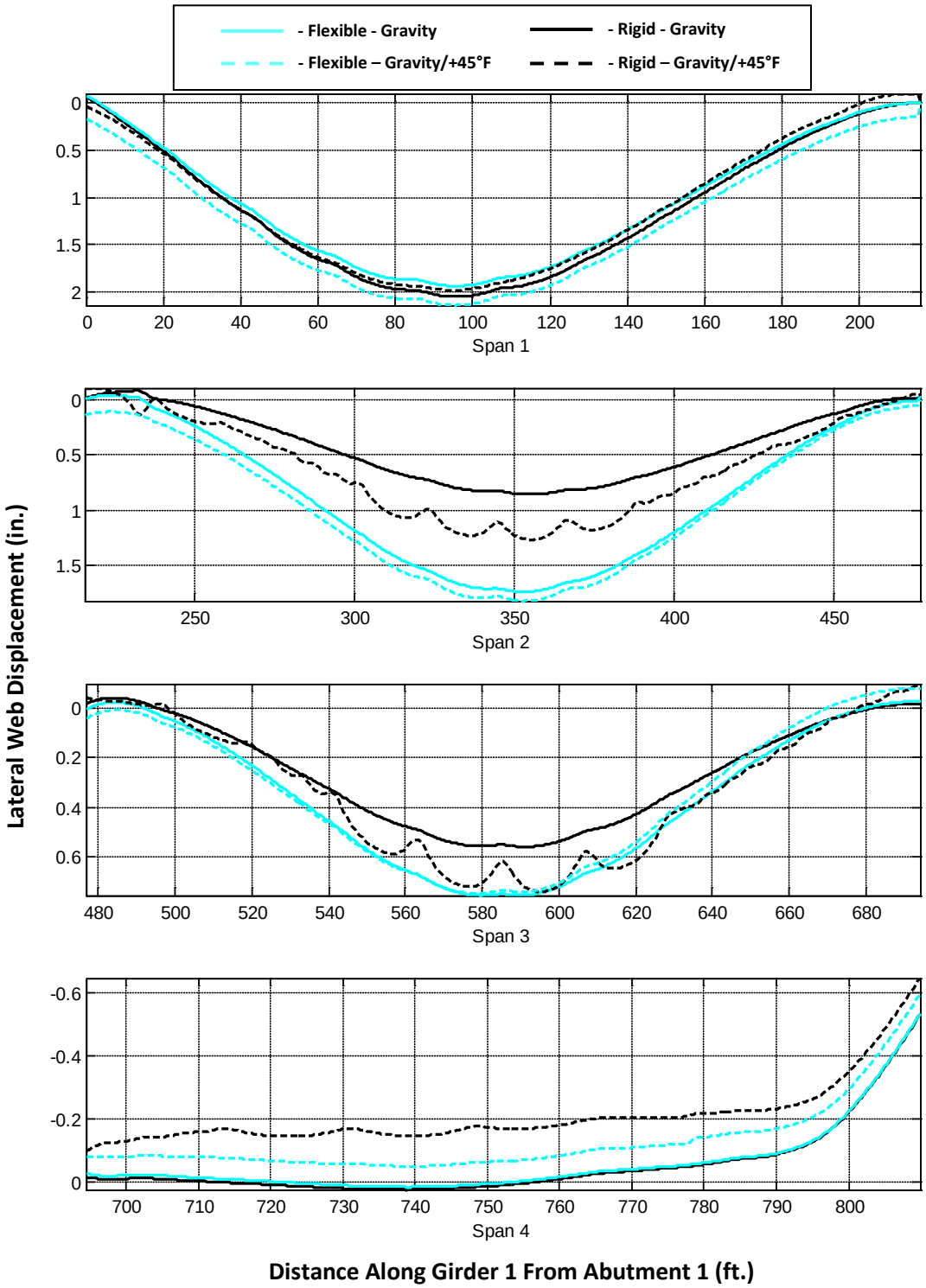


**Figure B.1. Girder 1 Lateral Web Centerline Displacement Due to Gravity and +45°F Thermal Load**

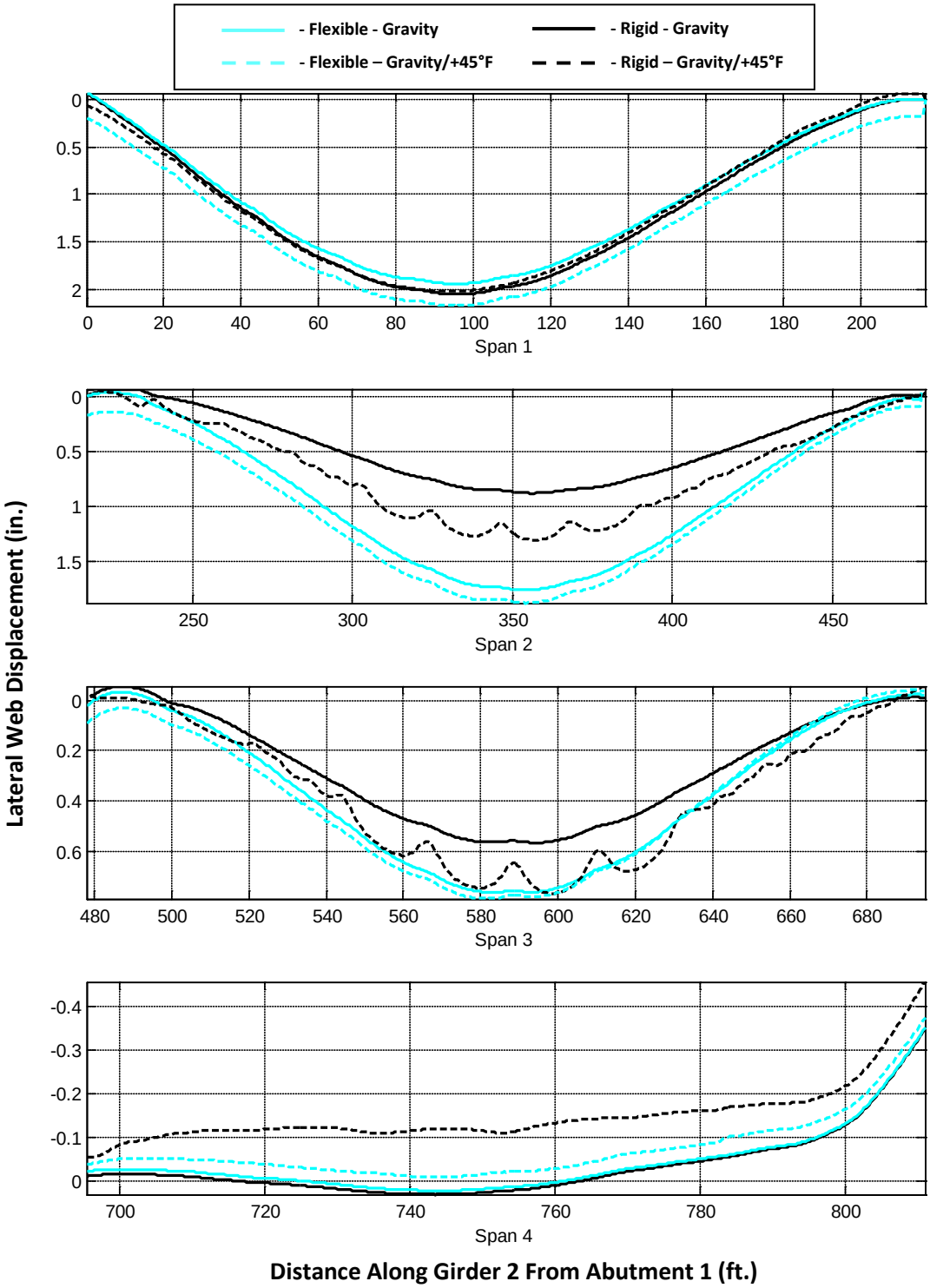


**Figure B.2. Girder 2 Lateral Web Centerline Displacement Due to Gravity and +45°F Thermal Load**

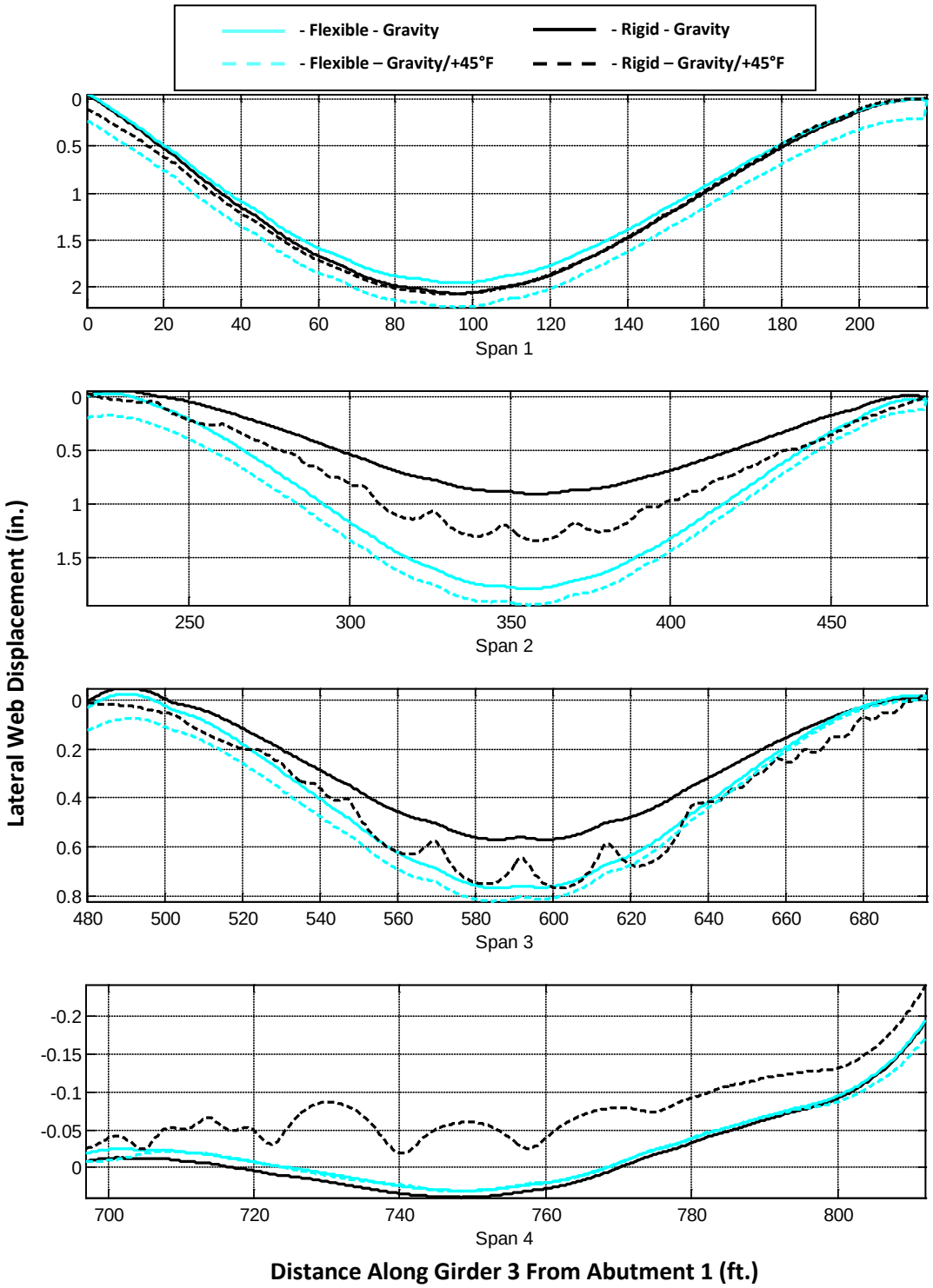


**Figure B.3. Girder 3 Lateral Web Centerline Displacement Due to Gravity and +45°F Thermal Load**

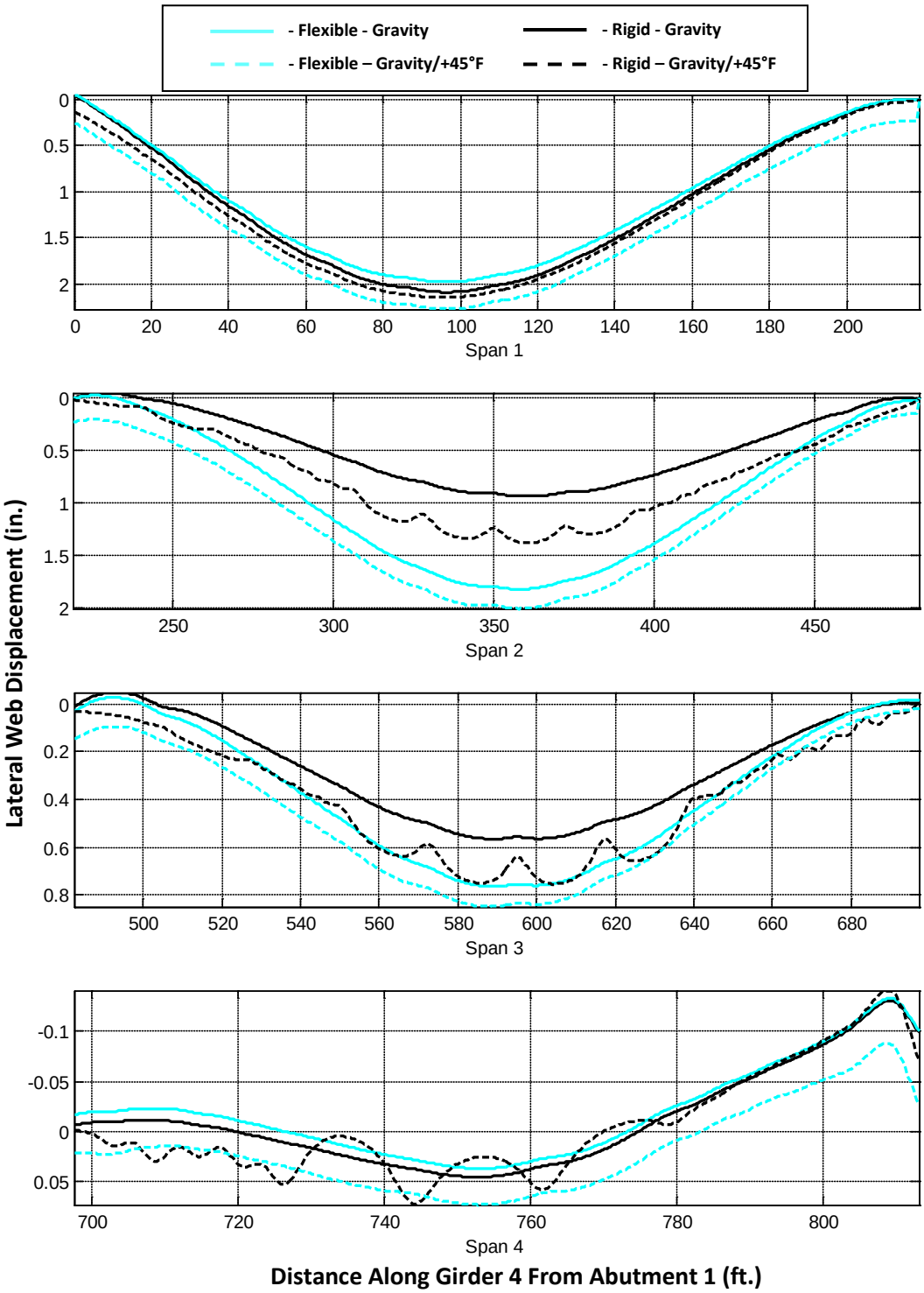


**Figure B.4. Girder 4 Lateral Web Centerline Displacement Due to Gravity and +45°F Thermal Load**

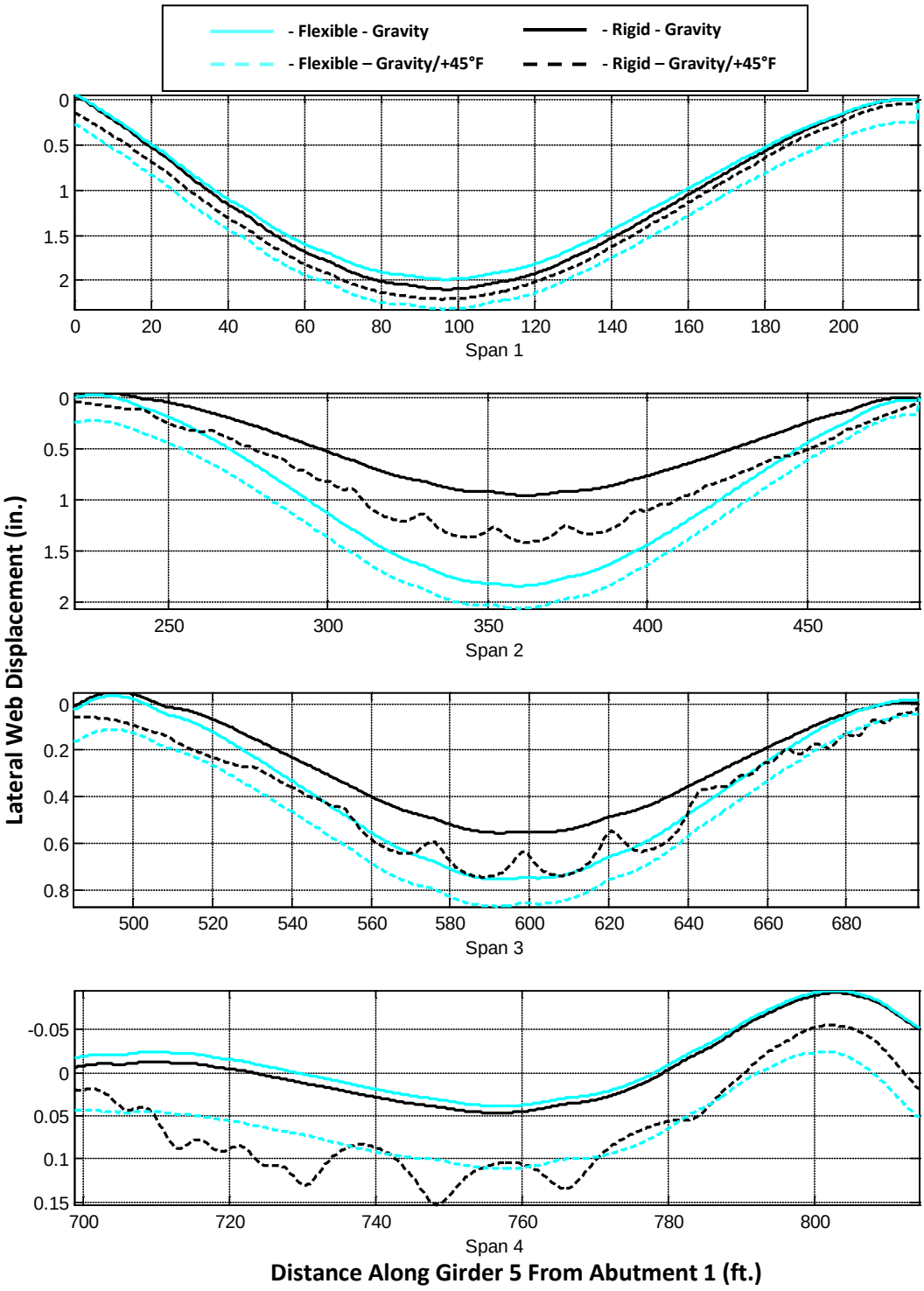


**Figure B.5. Girder 5 Lateral Web Centerline Displacement Due to Gravity and +45°F Thermal Load**

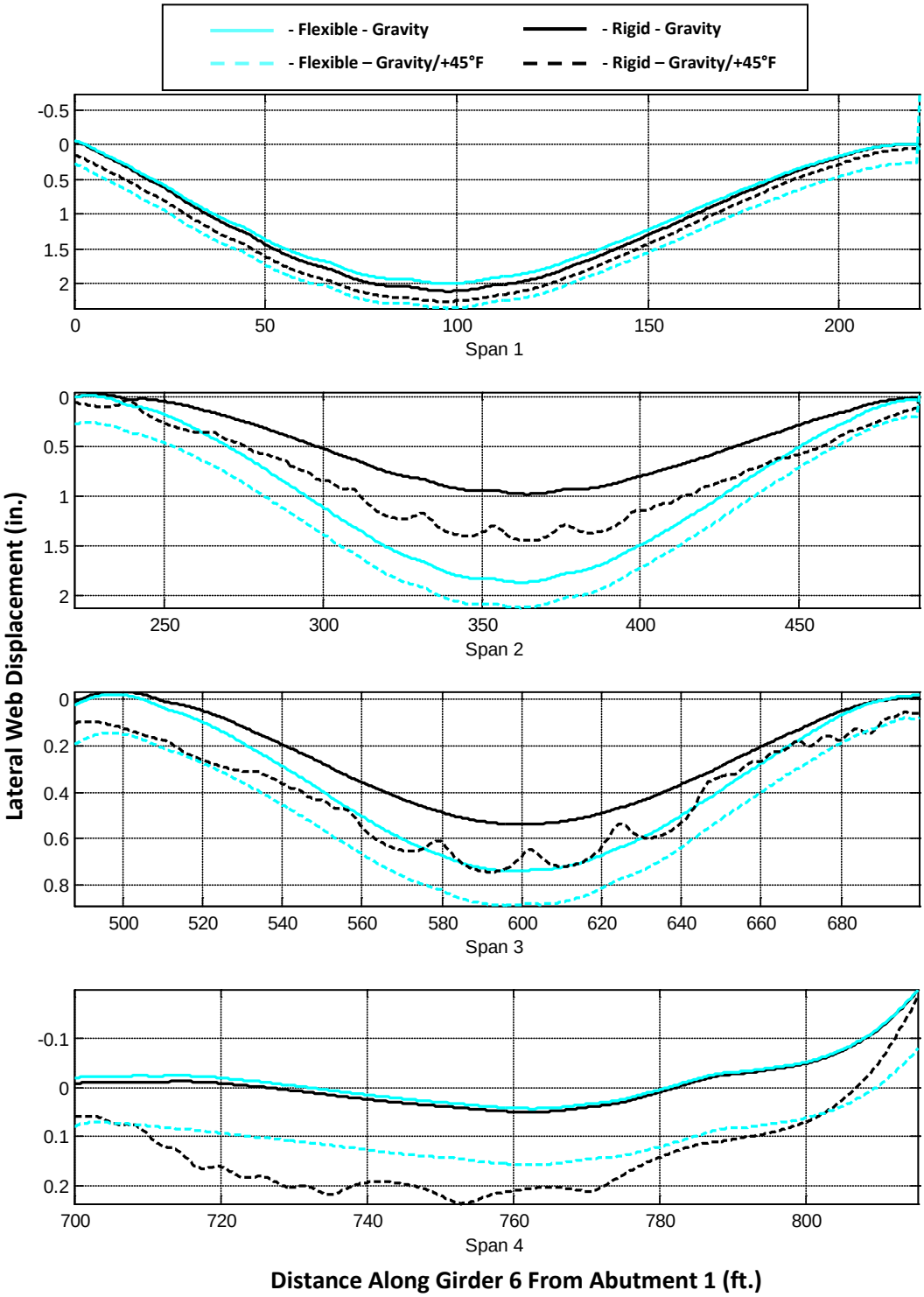


**Figure B.6. Girder 6 Lateral Web Centerline Displacement Due to Gravity and +45°F Thermal Load**

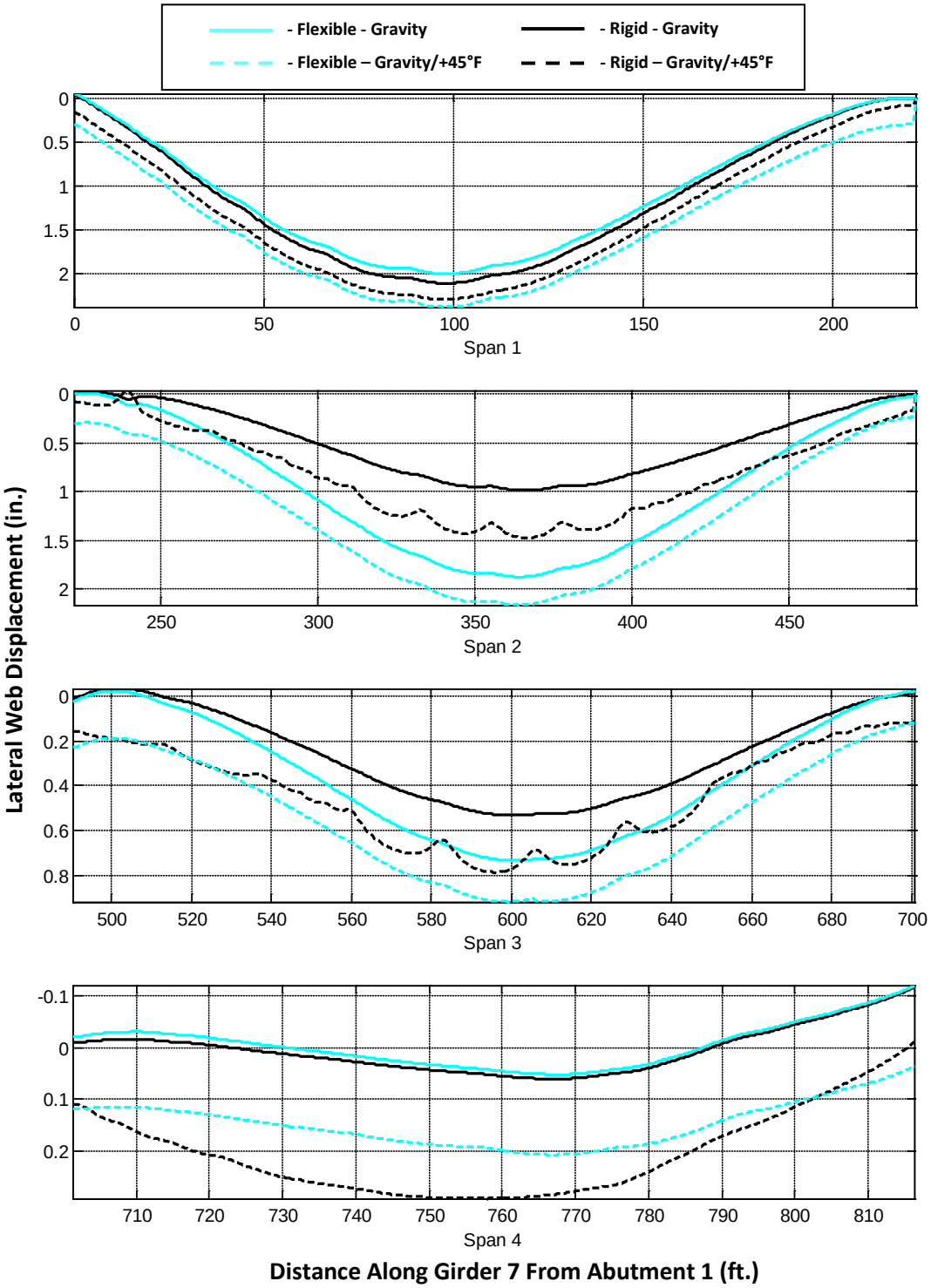


**Figure B.7. Girder 7 Lateral Web Centerline Displacement Due to Gravity and +45°F Thermal Load**

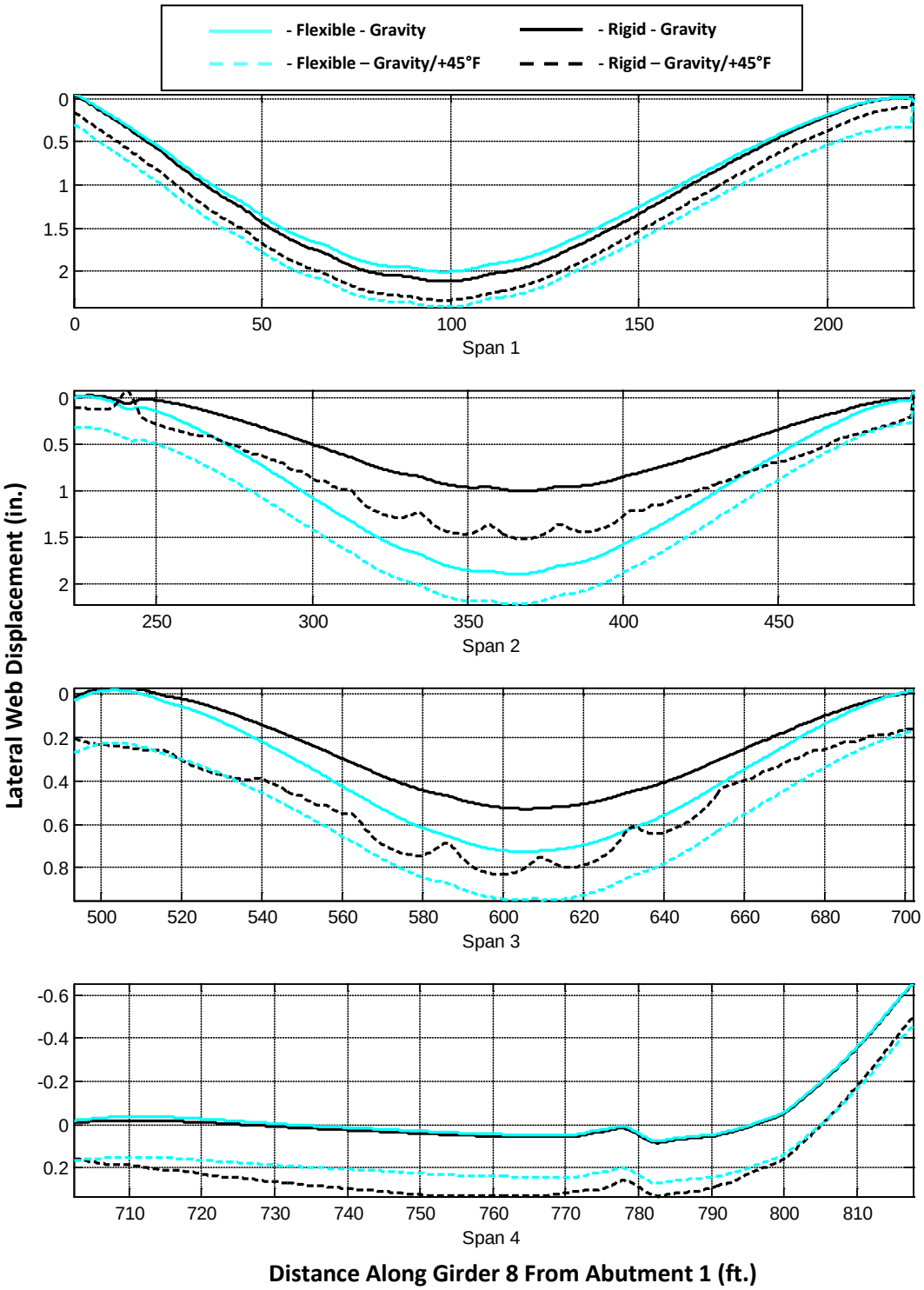


**Figure B.8. Girder 8 Lateral Web Centerline Displacement Due to Gravity and +45°F Thermal Load**

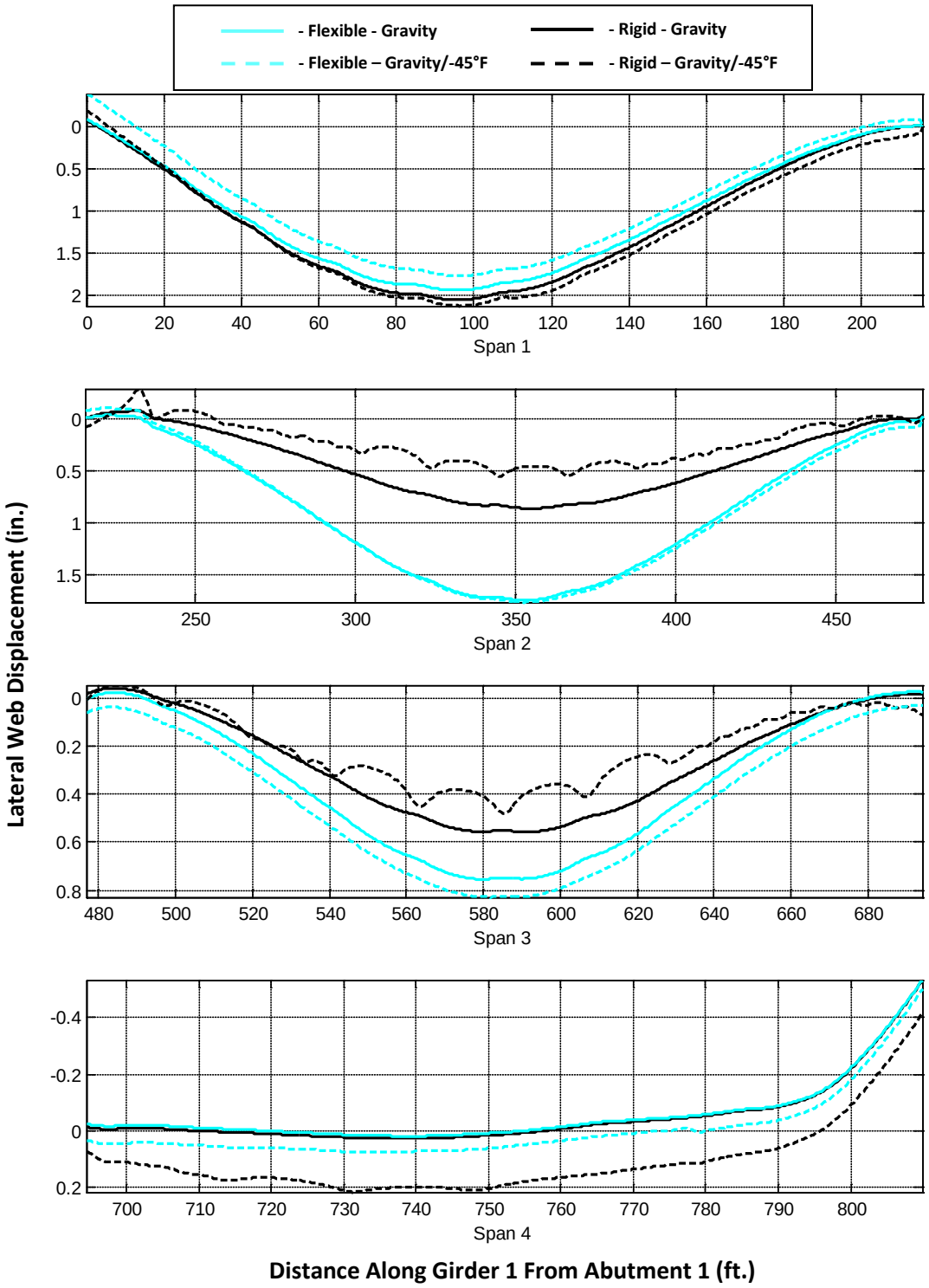


**Figure B.9. Girder 1 Lateral Web Centerline Displacement Due to Gravity and -45°F Thermal Load**

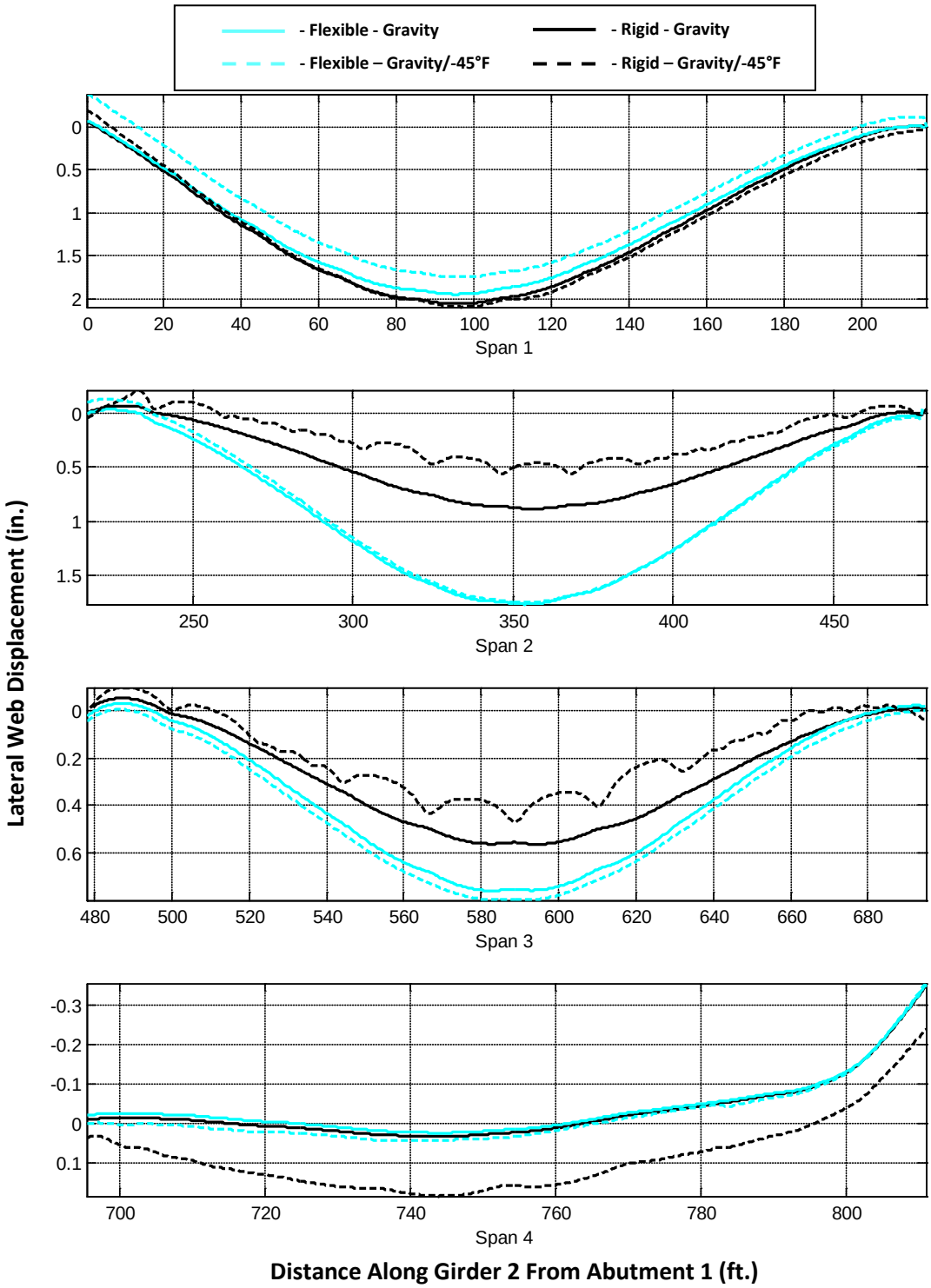


**Figure B.10. Girder 2 Lateral Web Centerline Displacement Due to Gravity and -45°F Thermal Load**

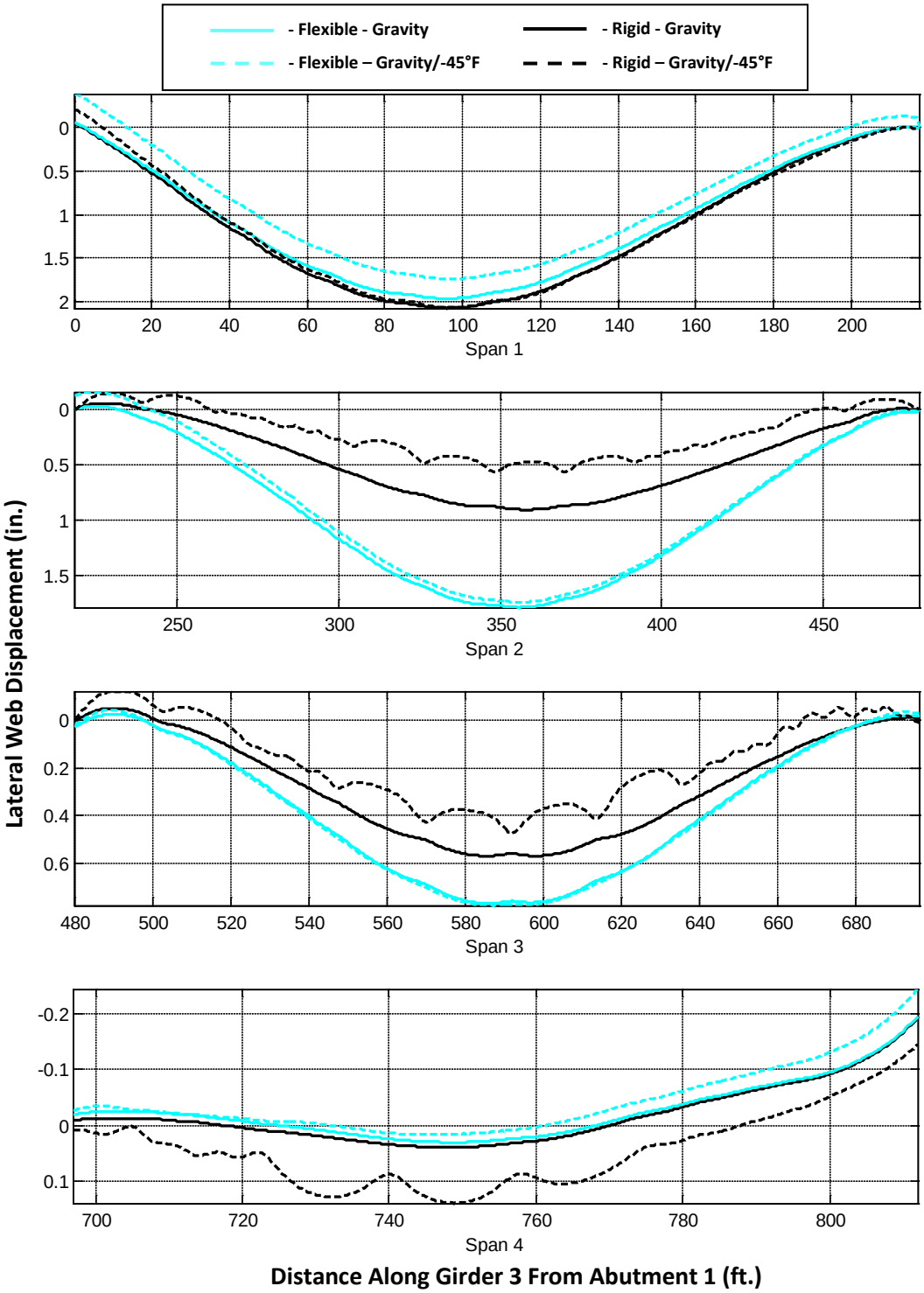


**Figure B.11. Girder 3 Lateral Web Centerline Displacement Due to Gravity and -45°F Thermal Load**

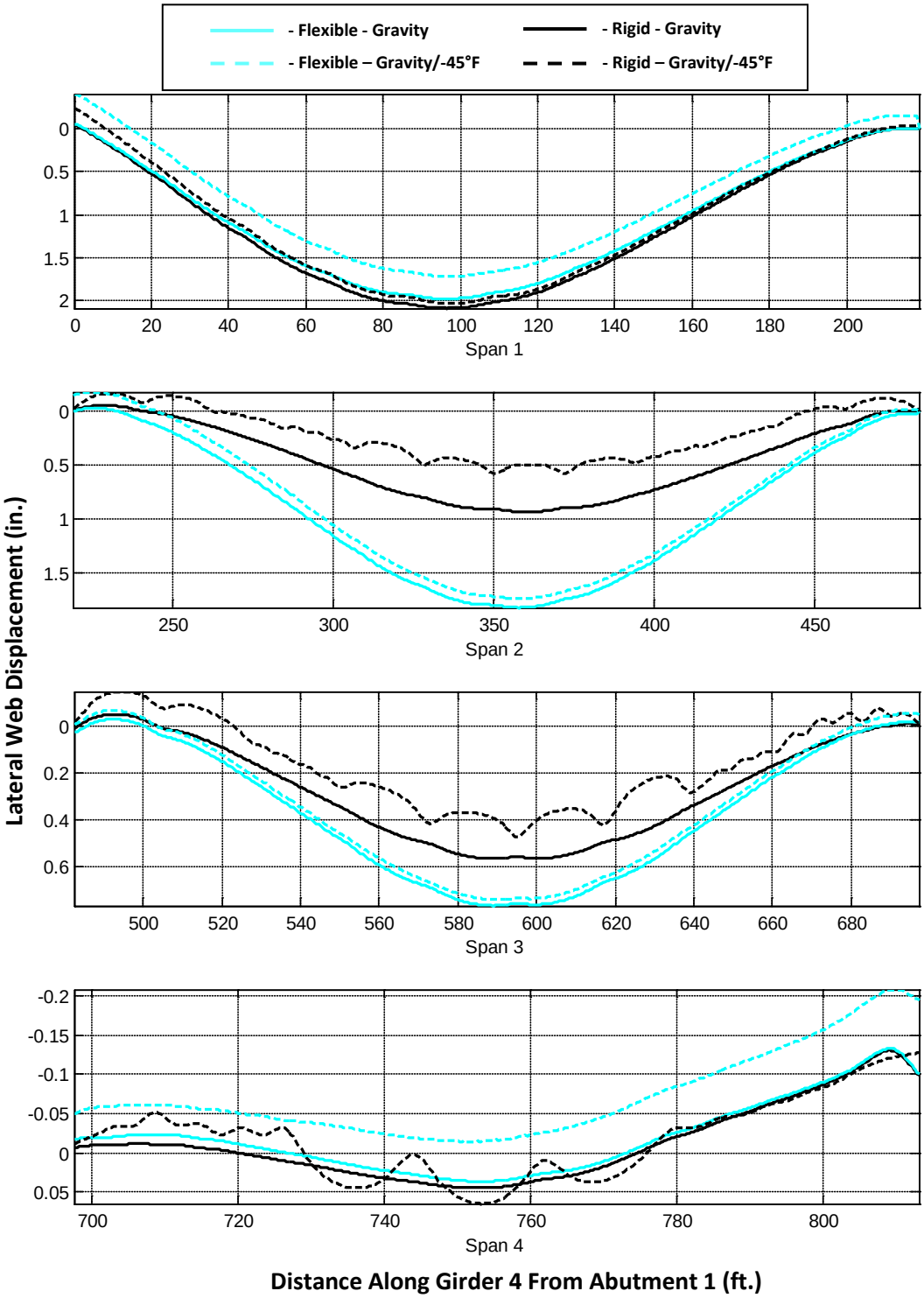


**Figure B.12. Girder 4 Lateral Web Centerline Displacement Due to Gravity and -45°F Thermal Load**

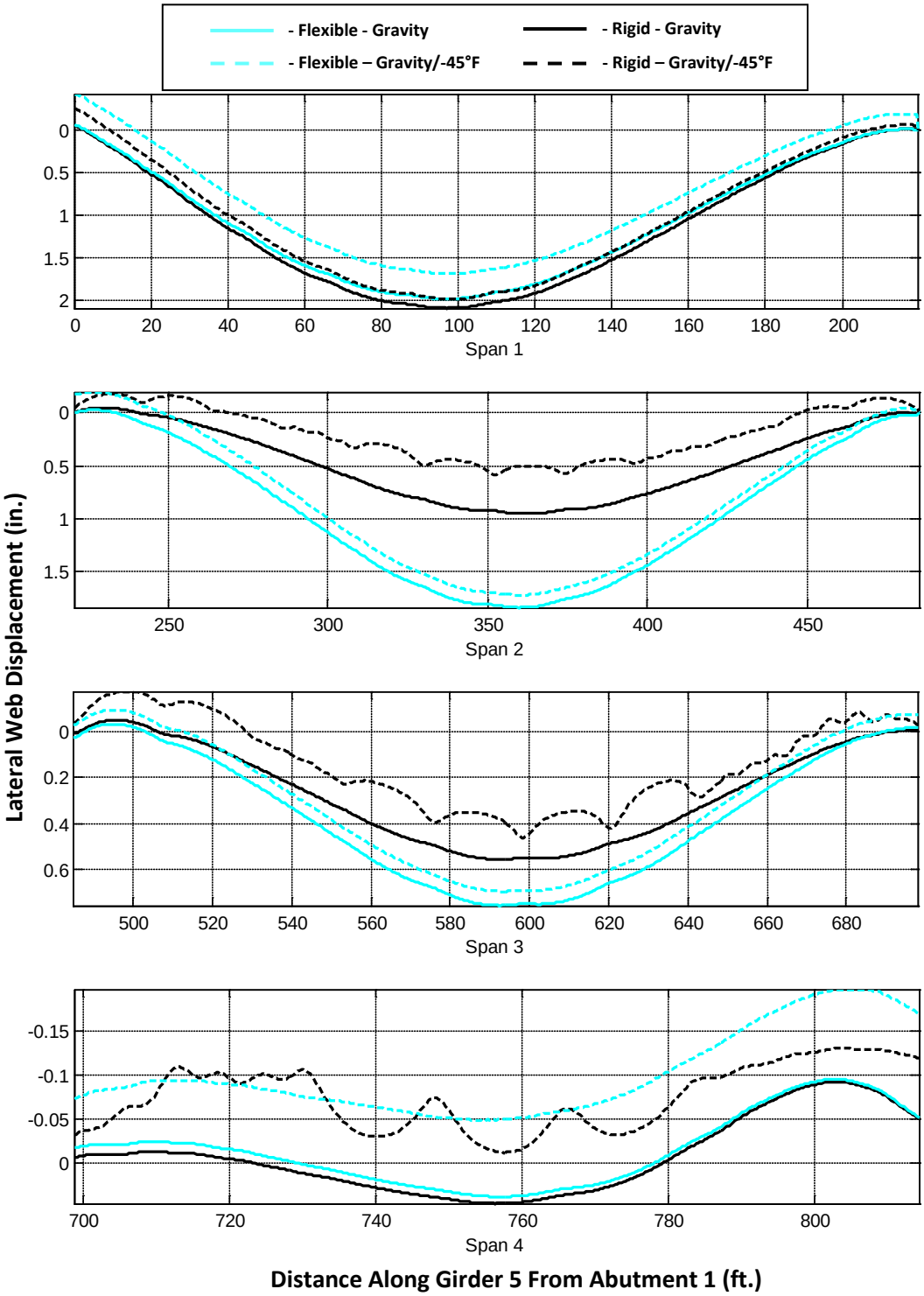


**Figure B.13. Girder 5 Lateral Web Centerline Displacement Due to Gravity and -45°F Thermal Load**

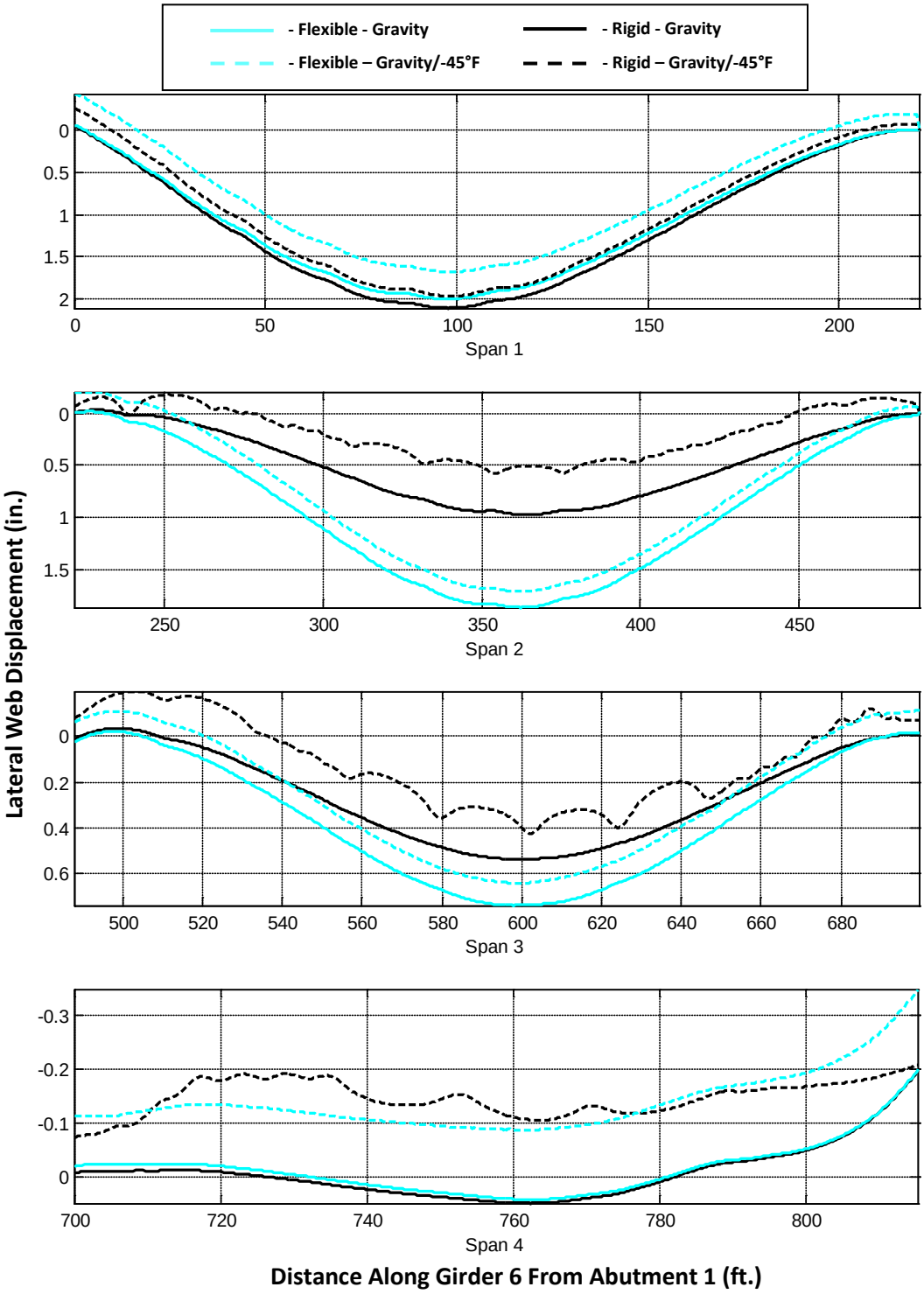


**Figure B.14. Girder 6 Lateral Web Centerline Displacement Due to Gravity and -45°F Thermal Load**

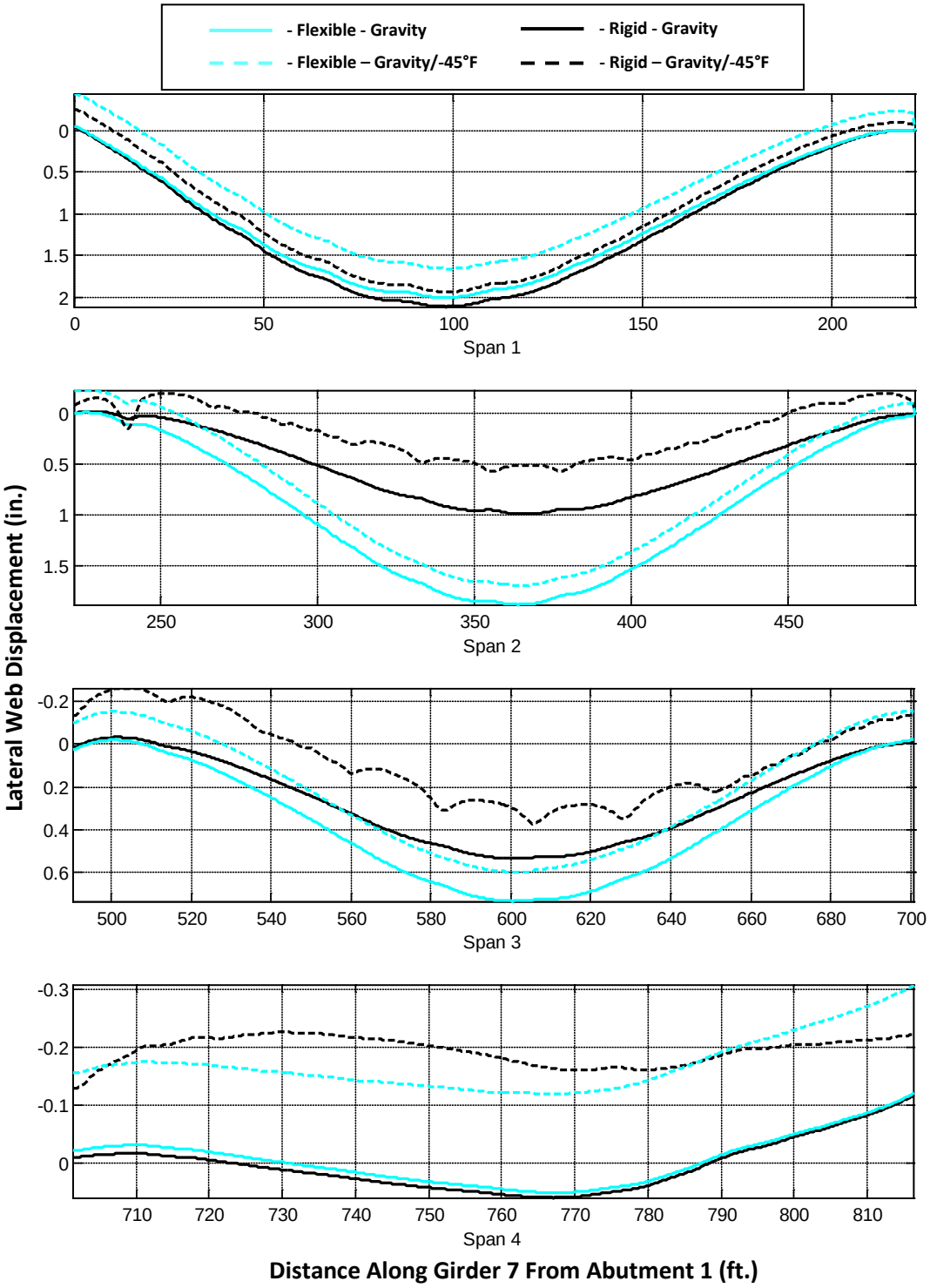


**Figure B.15. Girder 7 Lateral Web Centerline Displacement Due to Gravity and -45°F Thermal Load**

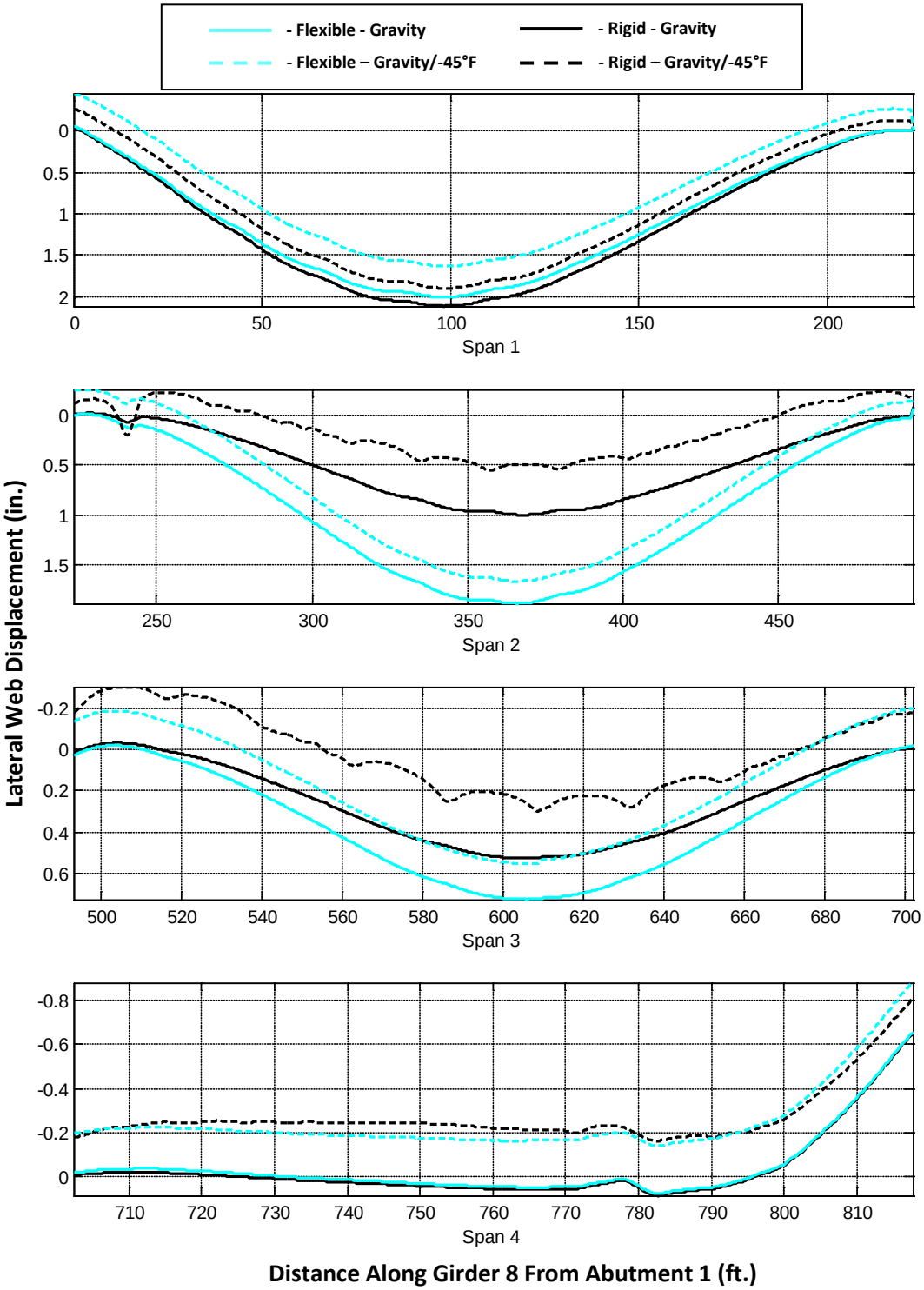


**Figure B.16. Girder 8 Lateral Web Centerline Displacement Due to Gravity and -45°F Thermal Load**

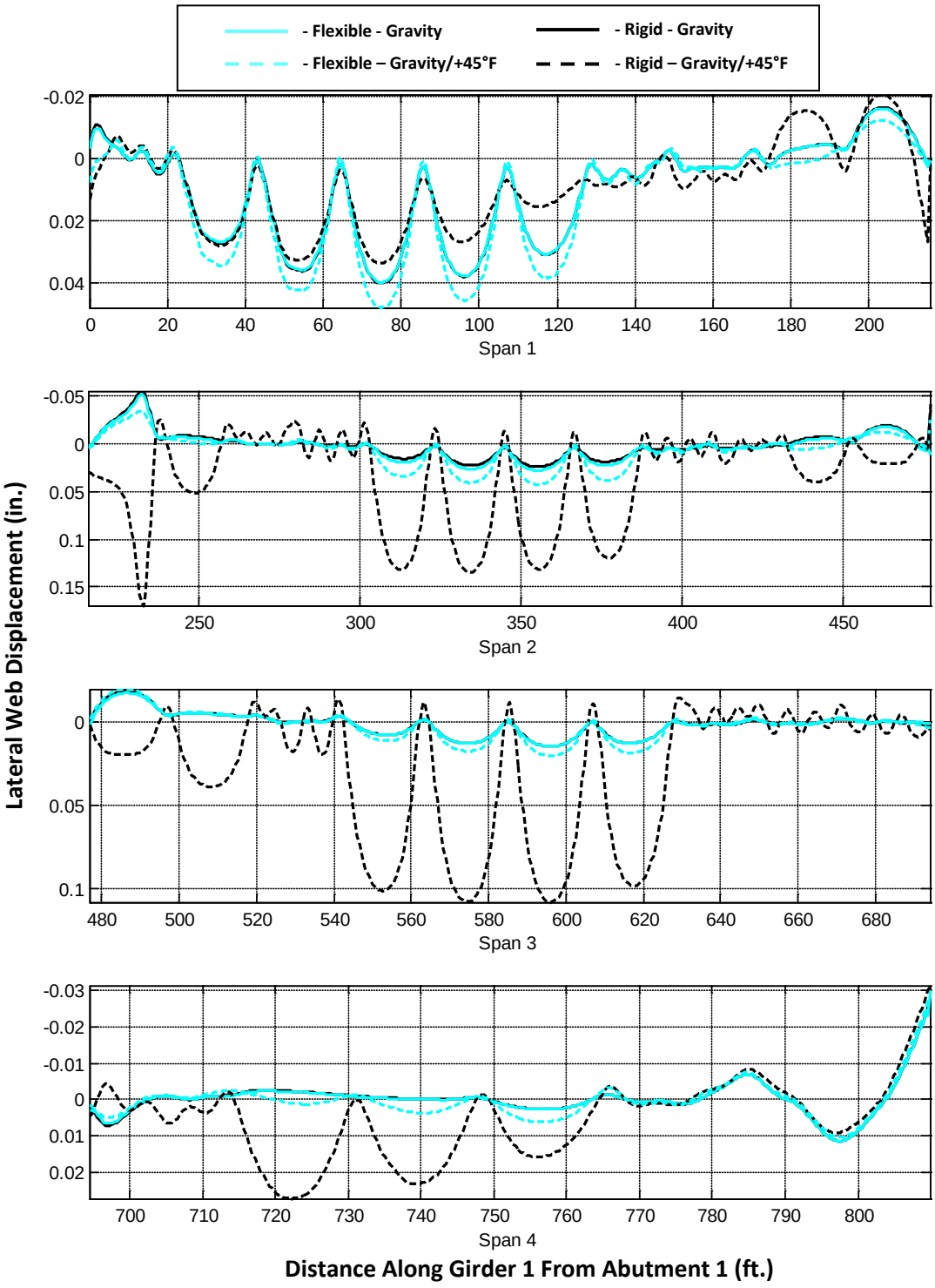


**Figure B.17. Girder 1 Out-of-Plane Web Centerline Displacement Due to Gravity and +45°F Thermal Load**

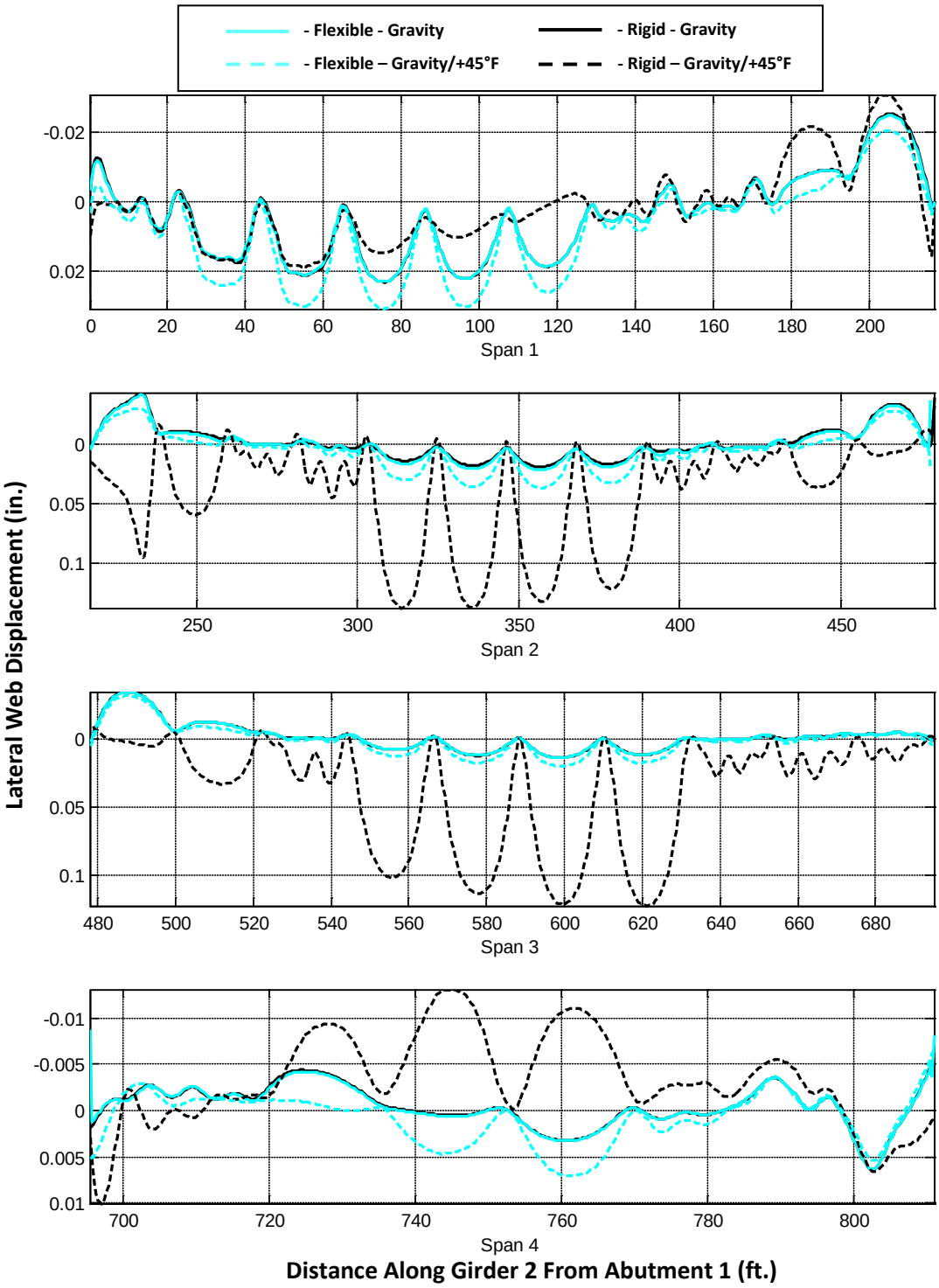


**Figure B.18. Girder 2 Out-of-Plane Web Centerline Displacement Due to Gravity and +45°F Thermal Load**

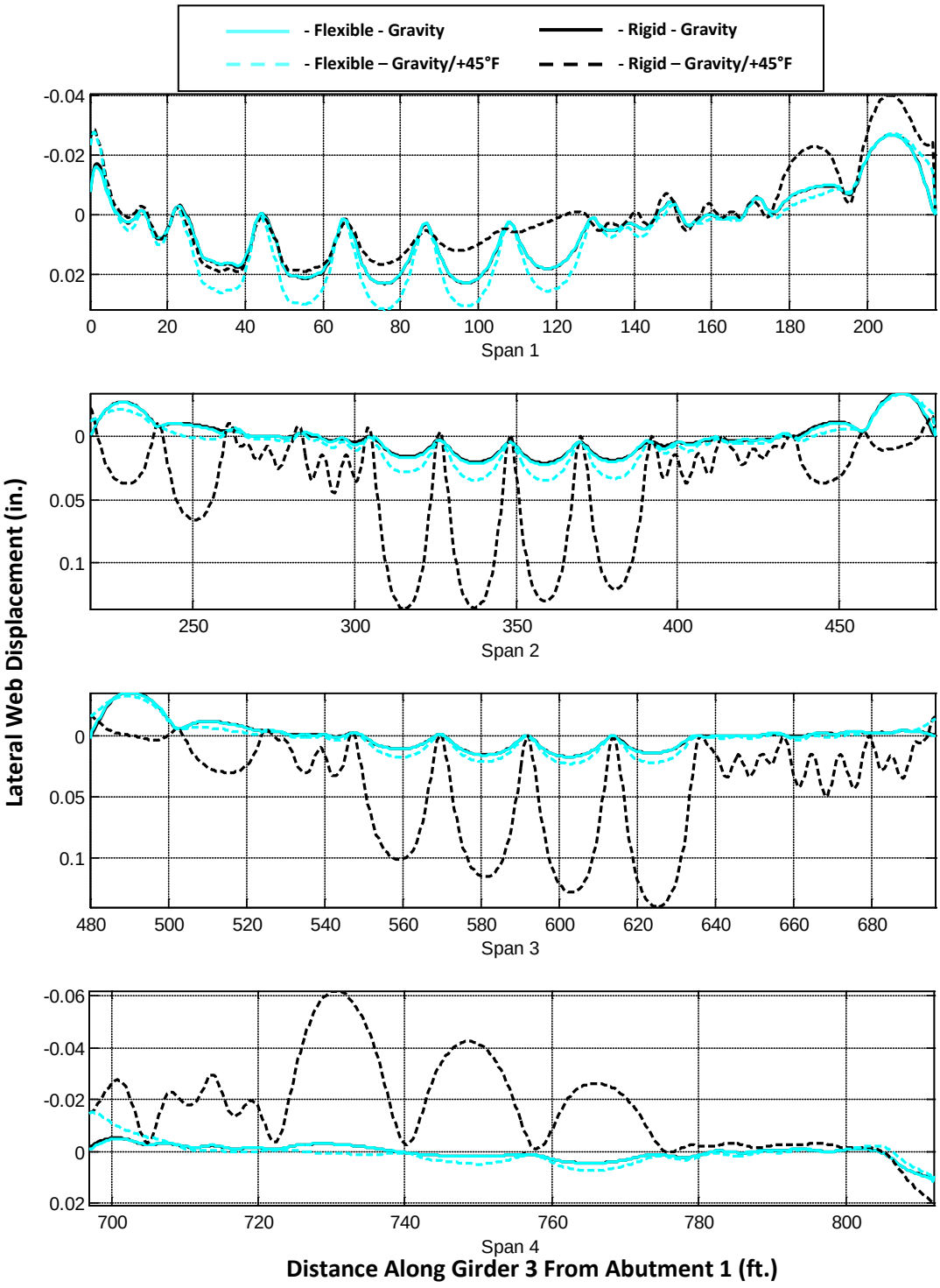


**Figure B.19. Girder 3 Out-of-Plane Web Centerline Displacement Due to Gravity and +45°F Thermal Load**

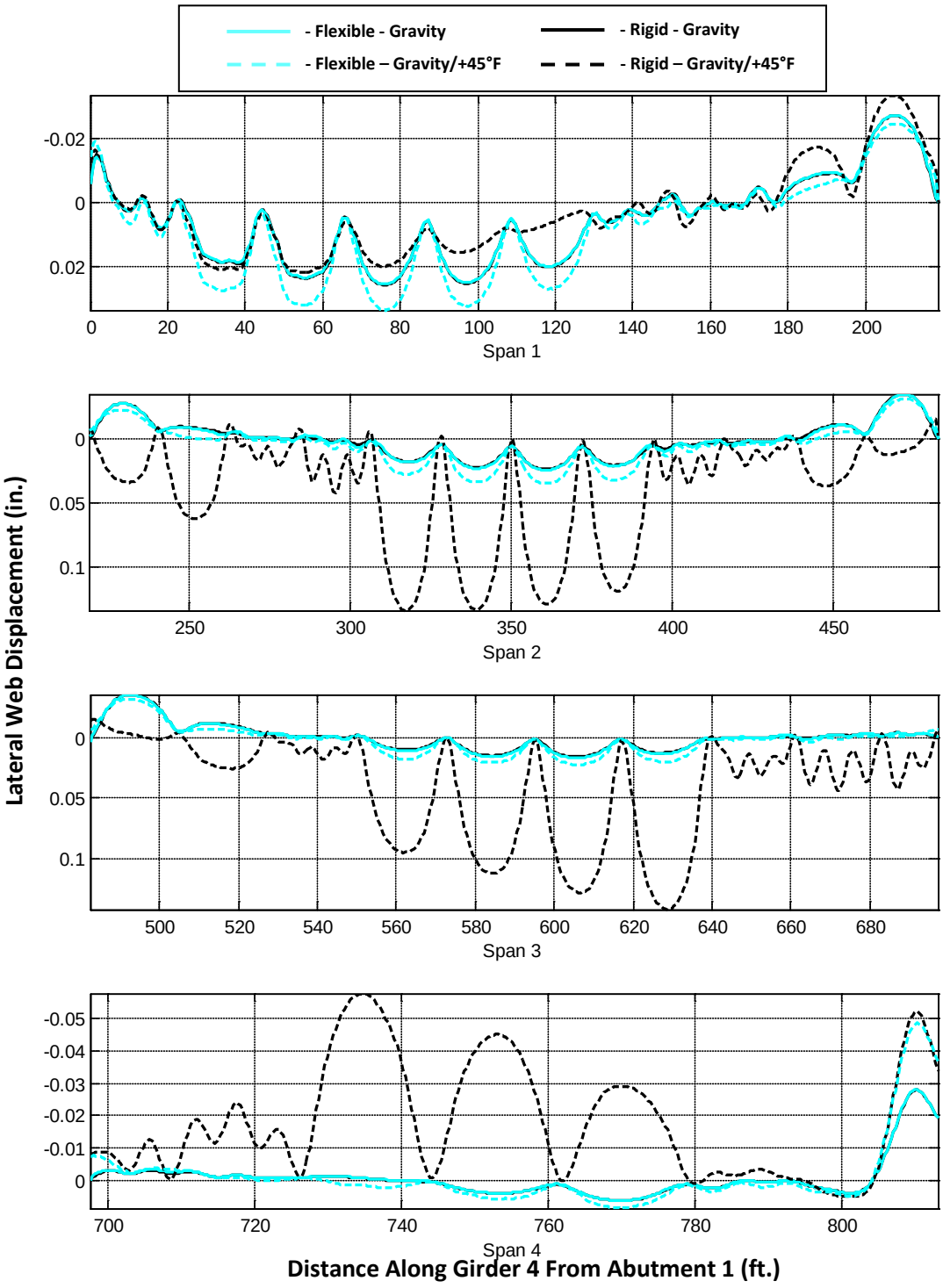


**Figure B.20. Girder 4 Out-of-Plane Web Centerline Displacement Due to Gravity and +45°F Thermal Load**

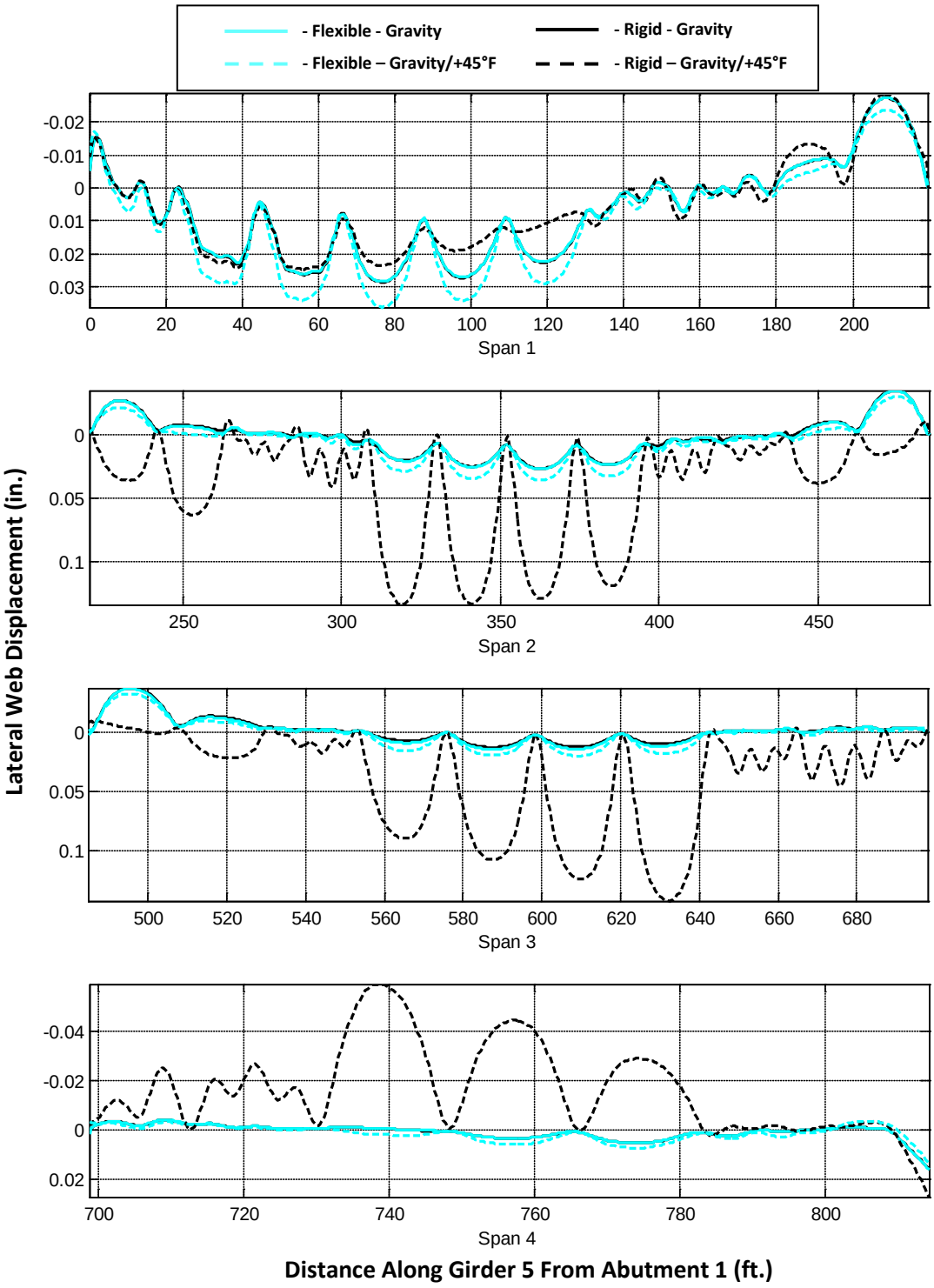


**Figure B.21. Girder 5 Out-of-Plane Web Centerline Displacement Due to Gravity and +45°F Thermal Load**

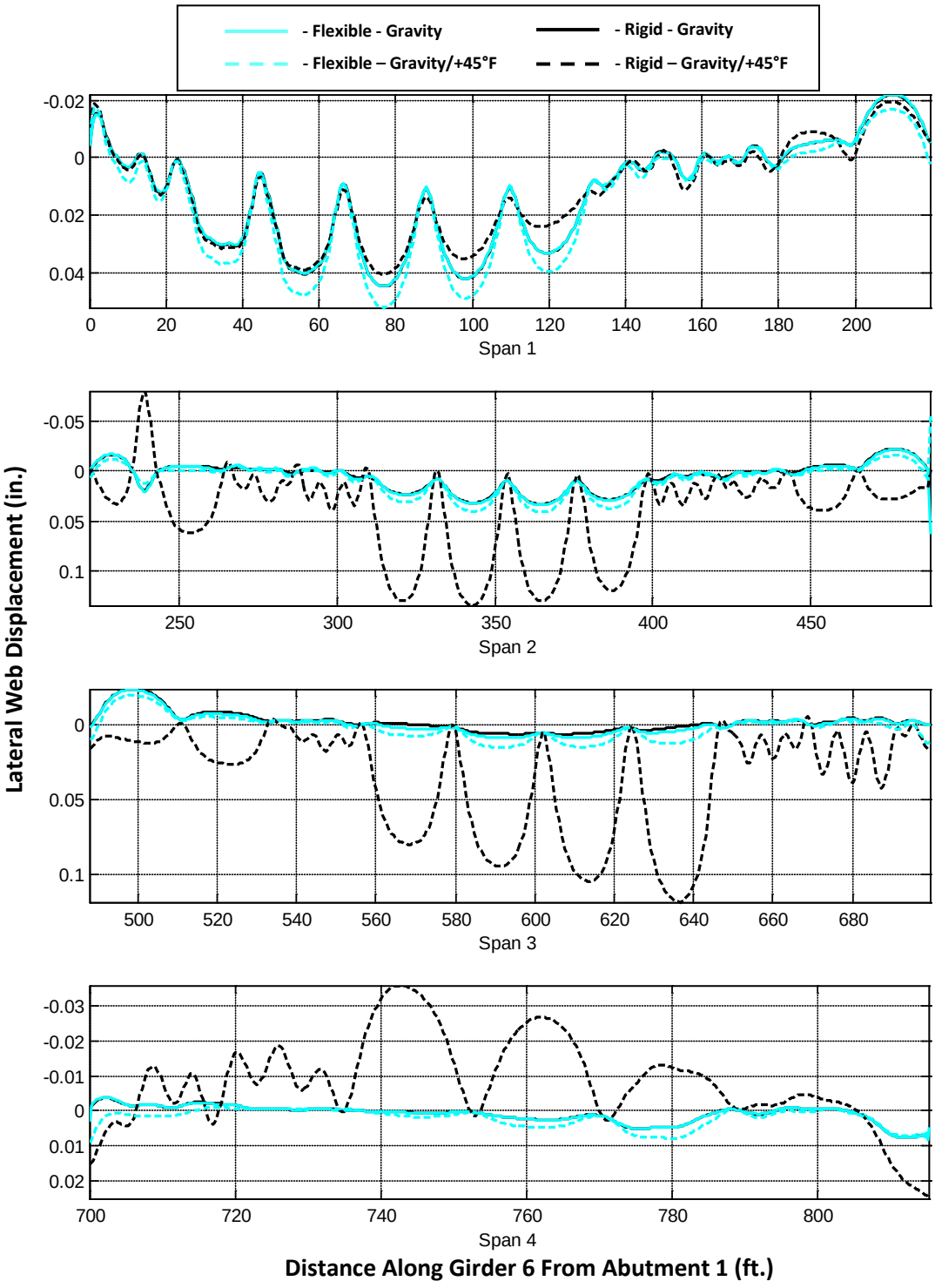


**Figure B.22. Girder 6 Out-of-Plane Web Centerline Displacement Due to Gravity and +45°F Thermal Load**

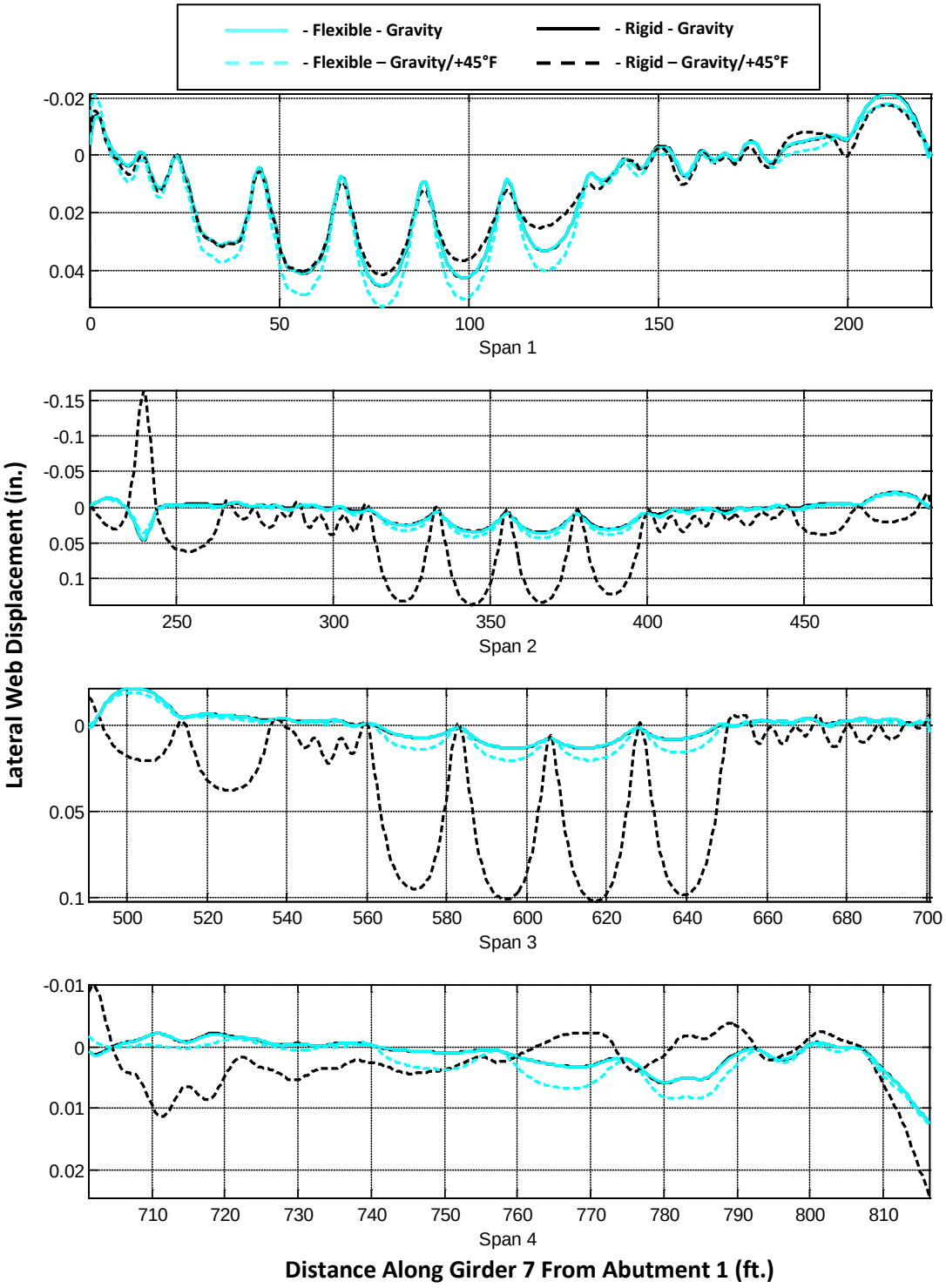


**Figure B.23. Girder 7 Out-of-Plane Web Centerline Displacement Due to Gravity and +45°F Thermal Load**

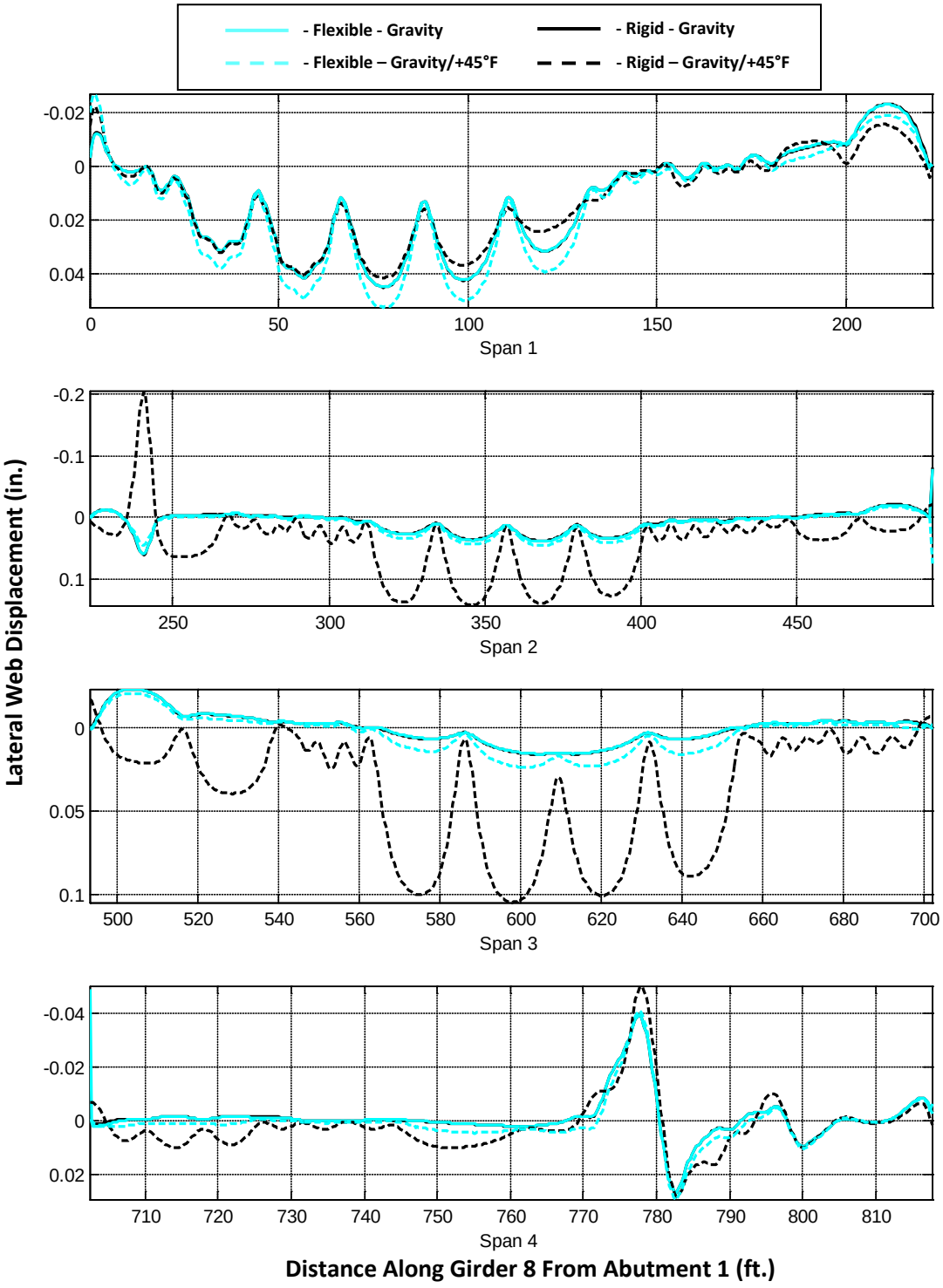


**Figure B.24. Girder 8 Out-of-Plane Web Centerline Displacement Due to Gravity and +45°F Thermal Load**

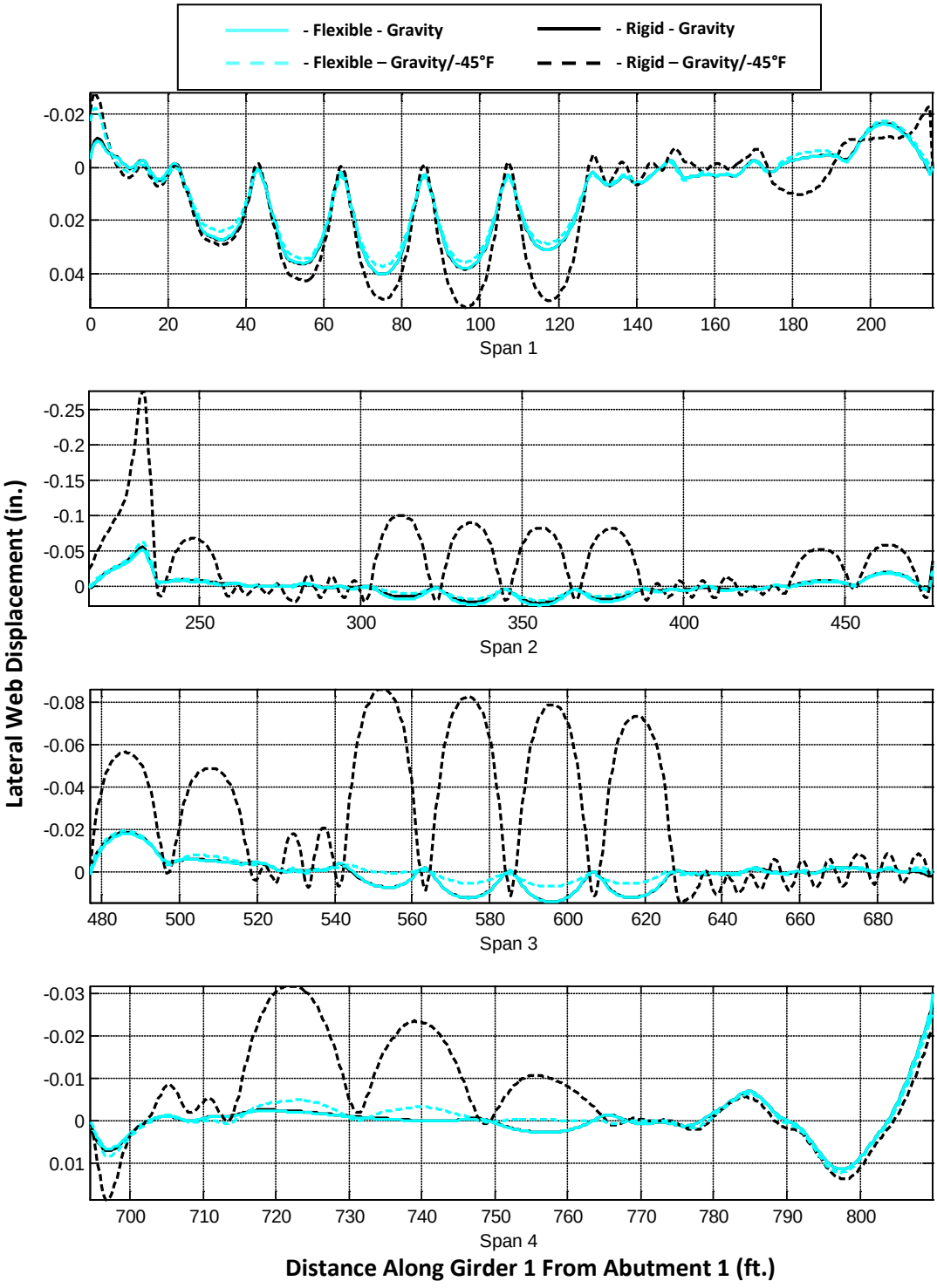


**Figure B.25. Girder 1 Out-of-Plane Web Centerline Displacement Due to Gravity and -45°F Thermal Load**

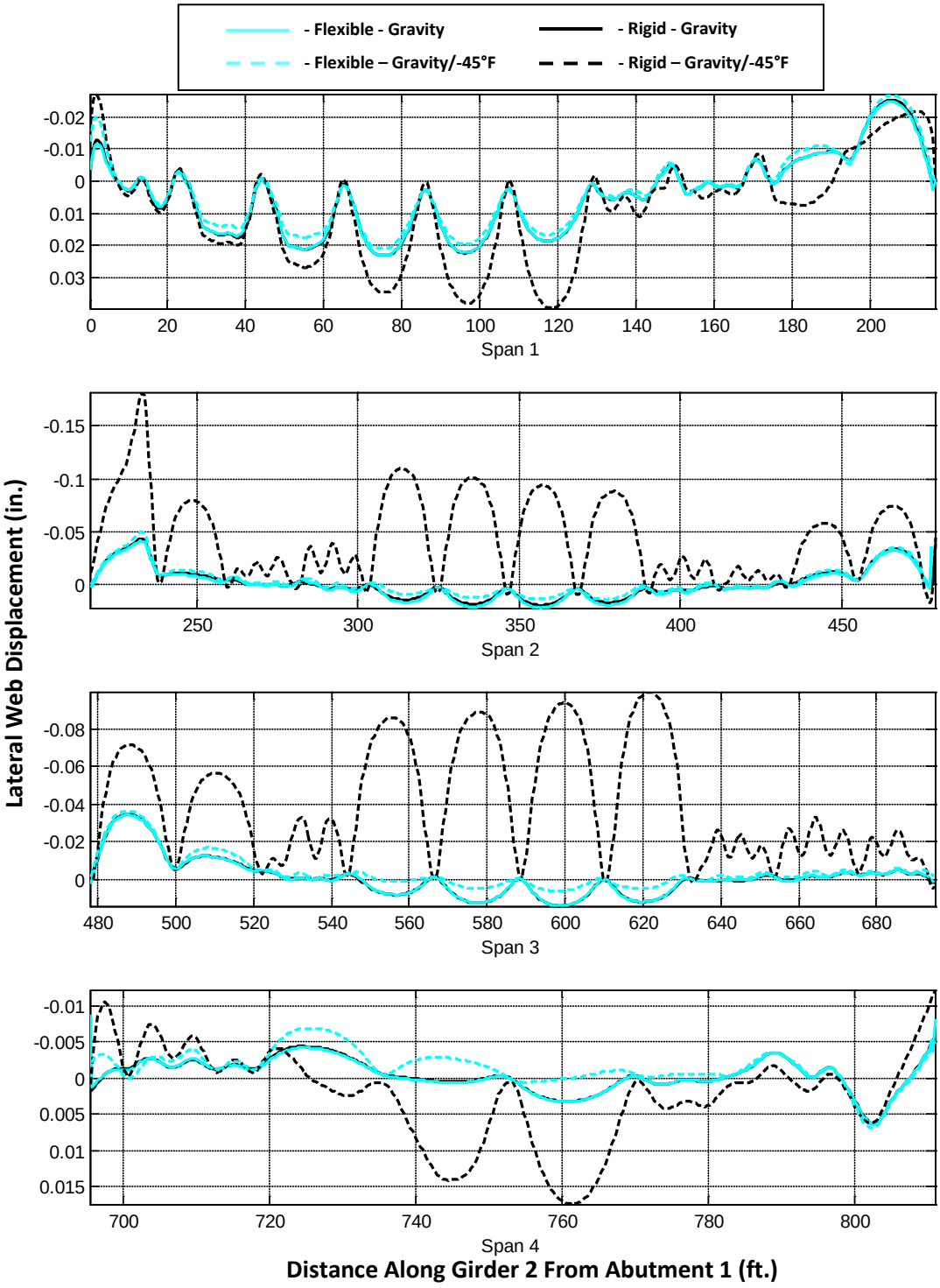


**Figure B.26. Girder 2 Out-of-Plane Web Centerline Displacement Due to Gravity and -45°F Thermal Load**

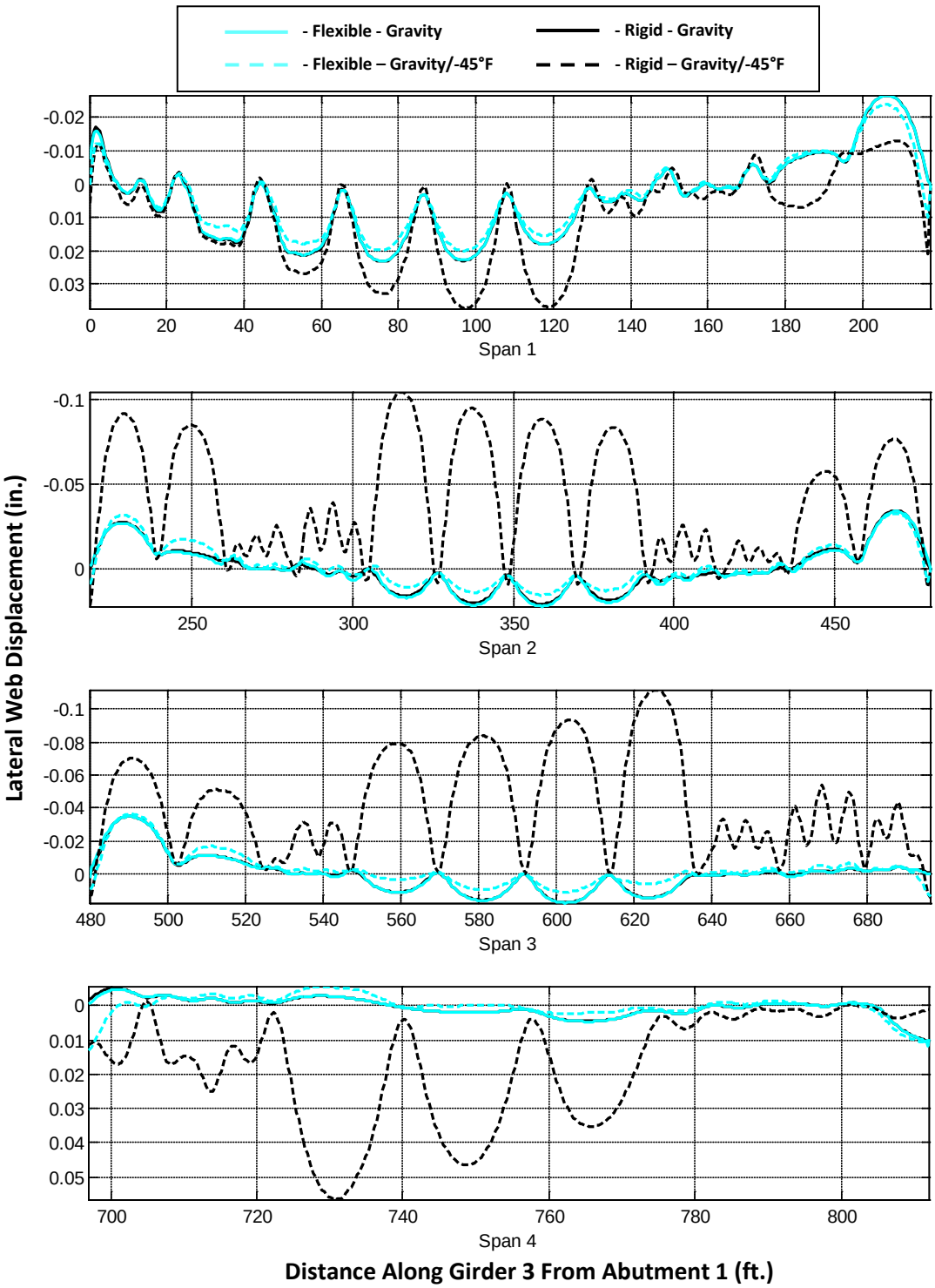


**Figure B.27. Girder 3 Out-of-Plane Web Centerline Displacement Due to Gravity and -45°F Thermal Load**

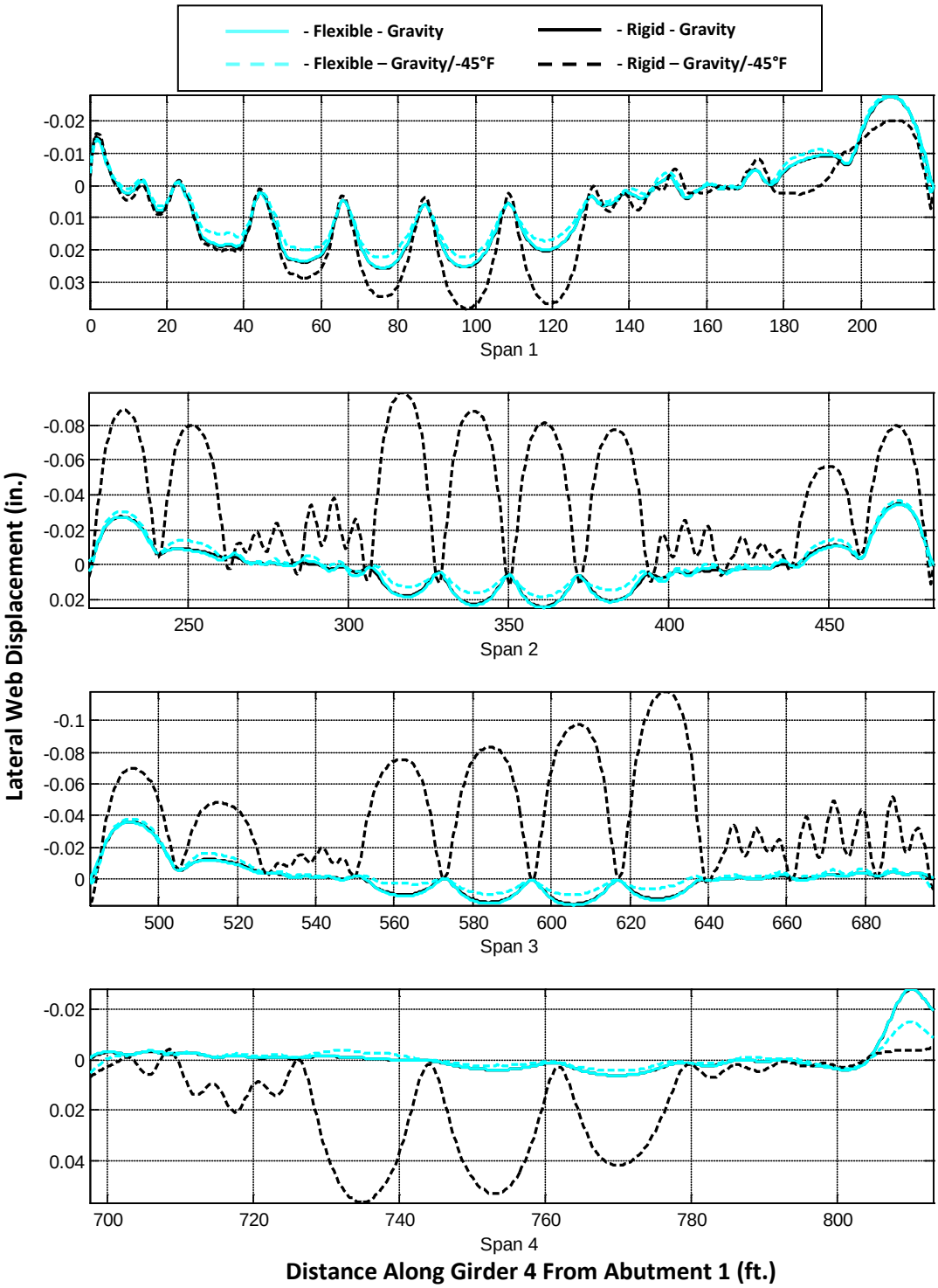


**Figure B.28. Girder 4 Out-of-Plane Web Centerline Displacement Due to Gravity and -45°F Thermal Load**

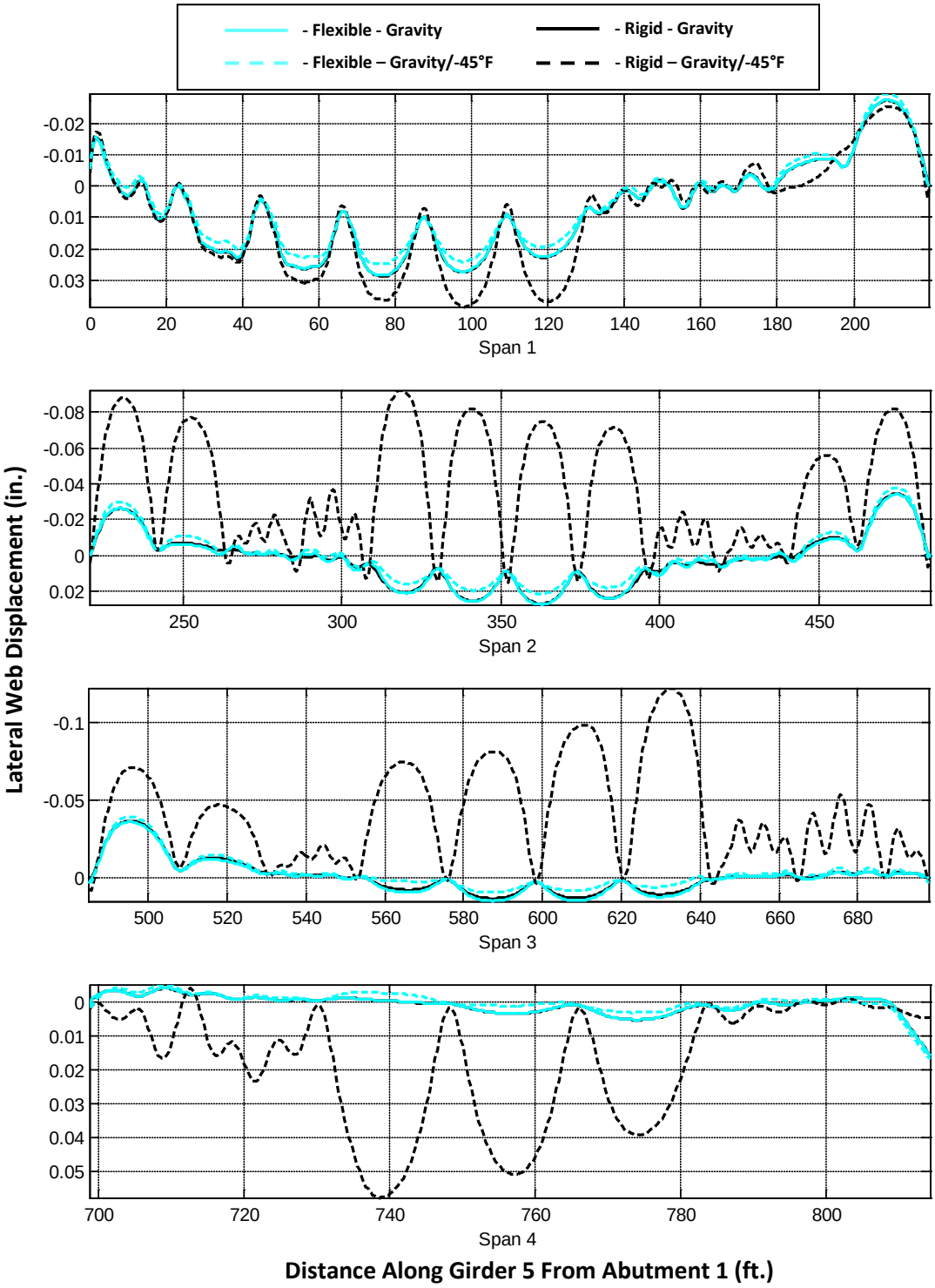


**Figure B.29. Girder 5 Out-of-Plane Web Centerline Displacement Due to Gravity and -45°F Thermal Load**

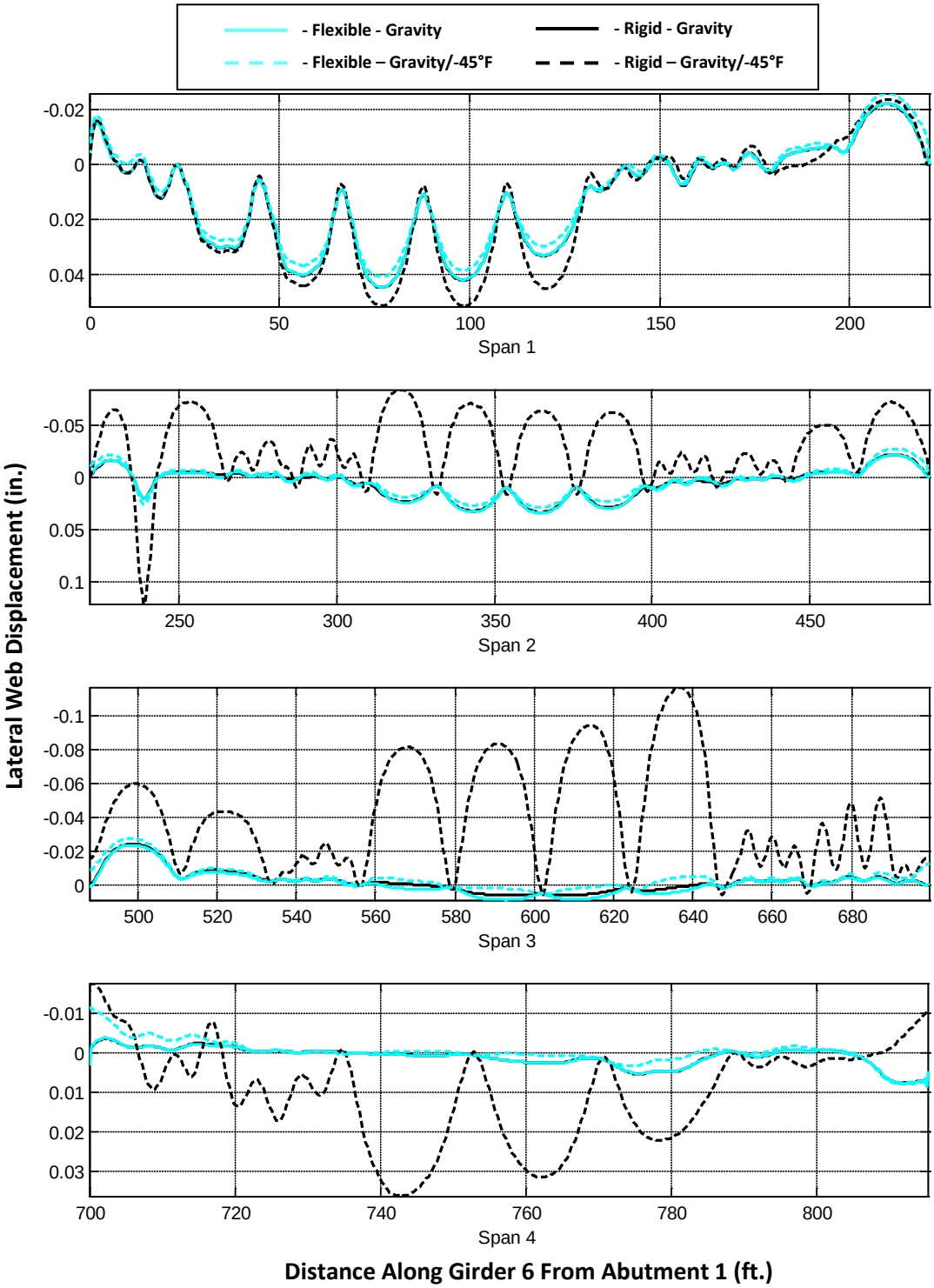


**Figure B.30. Girder 6 Out-of-Plane Web Centerline Displacement Due to Gravity and -45°F Thermal Load**

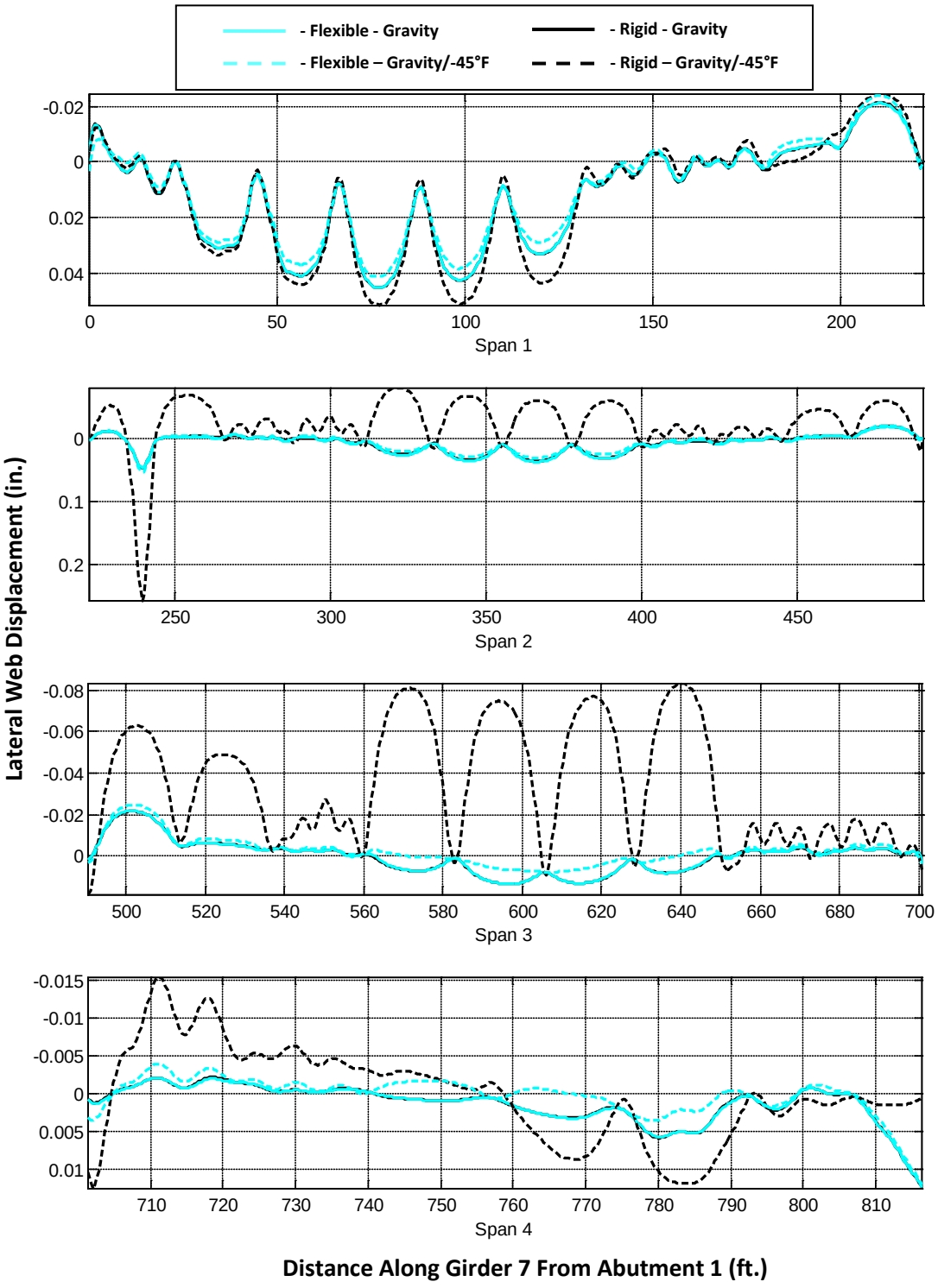


**Figure B.31. Girder 7 Out-of-Plane Web Centerline Displacement Due to Gravity and -45°F Thermal Load**

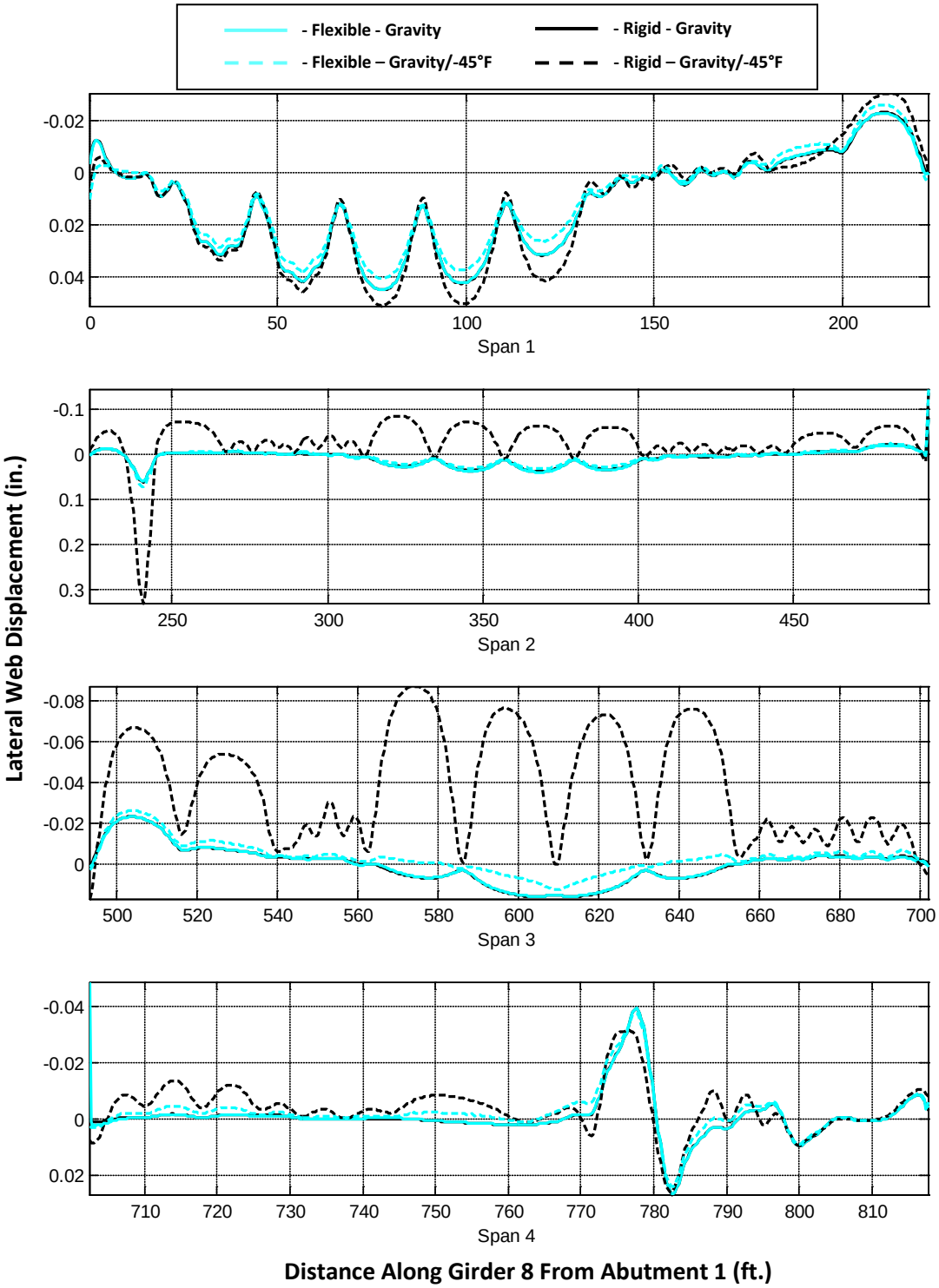


**Figure B.32. Girder 8 Out-of-Plane Web Centerline Displacement Due to Gravity and -45°F Thermal Load**

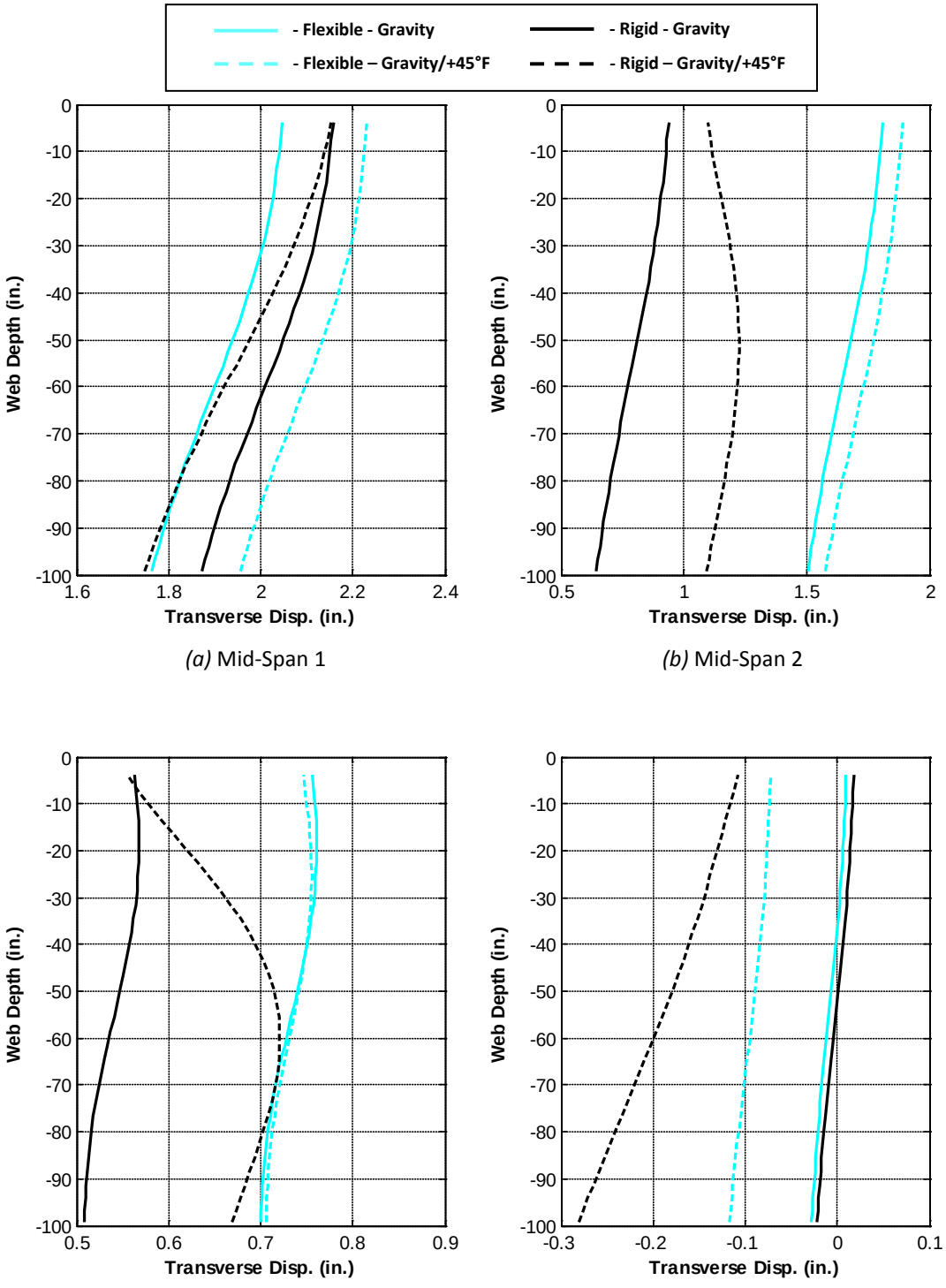


*(a)* Mid-Span 1

*(b)* Mid-Span 2

*(c)* Mid-Span 3

*(d)* Mid-Span 4

**Figure B.33. Web Displacement Profiles at Mid-Spans of Girder 1 – Gravity and +45°F Loading**

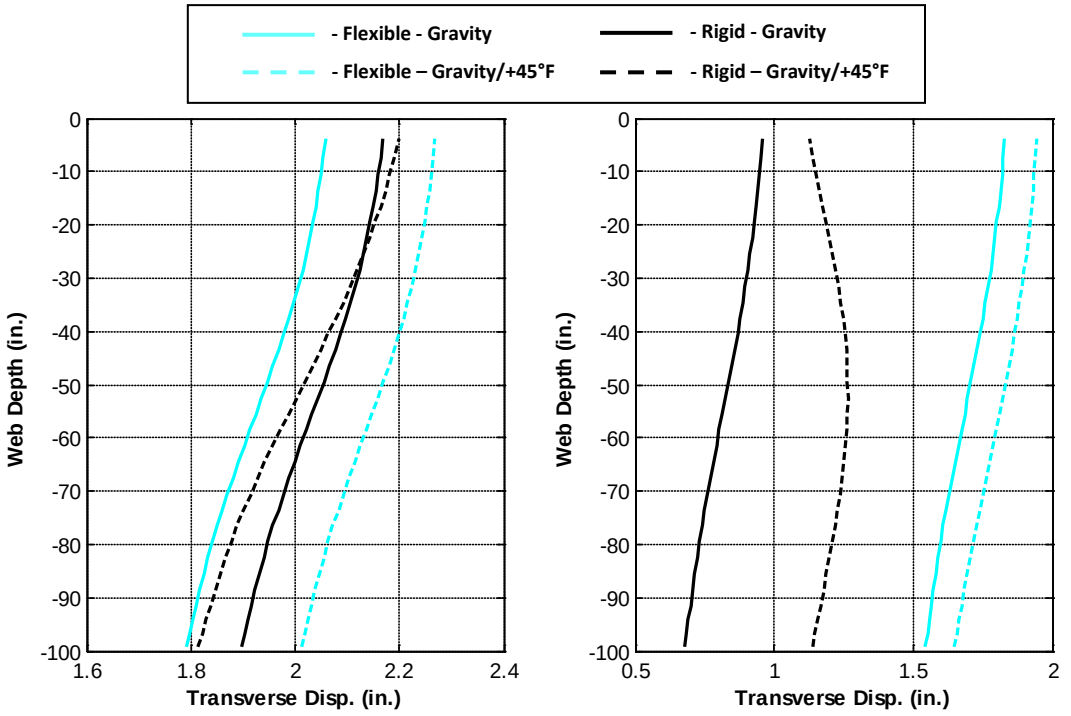


*(a)* Mid-Span 1

*(b)* Mid-Span 2

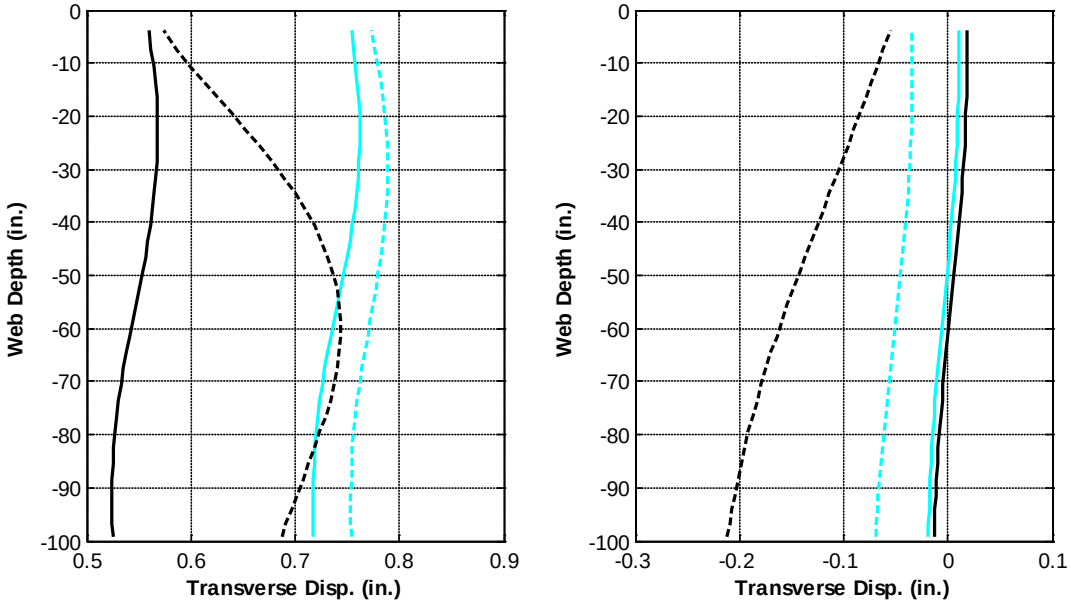


*(c)* Mid-Span 3

*(d)* Mid-Span 4

**Figure B.34. Web Displacement Profiles at Mid-Spans of Girder 2 – Gravity and +45°F Loading**

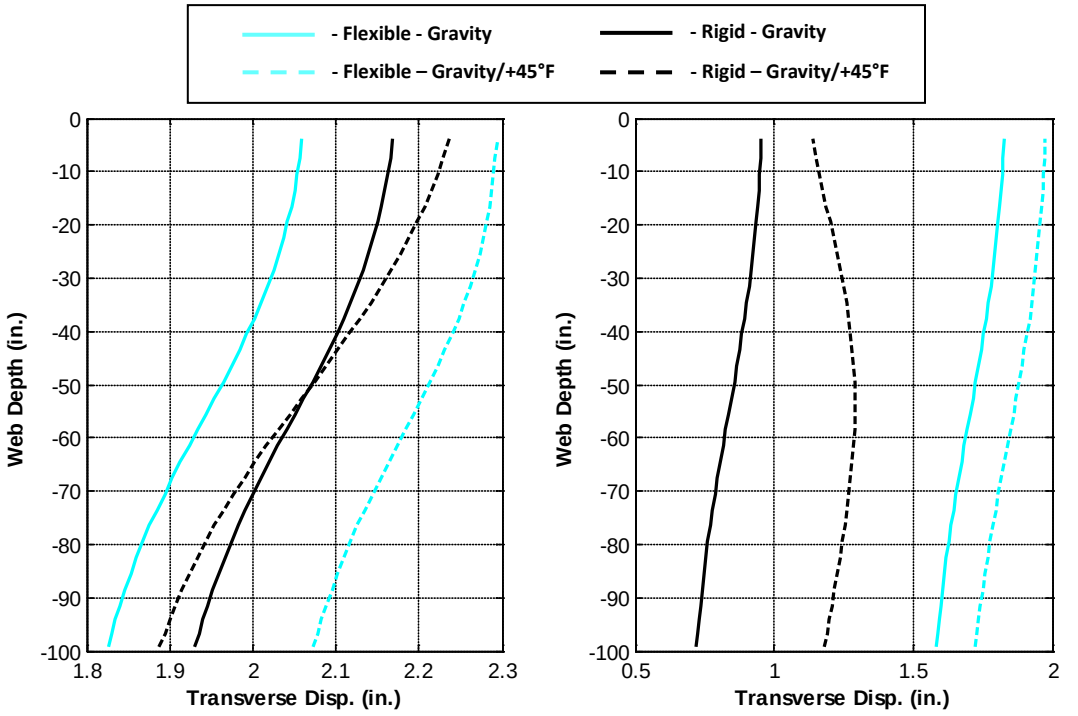


*(a)* Mid-Span 1

*(b)* Mid-Span 2

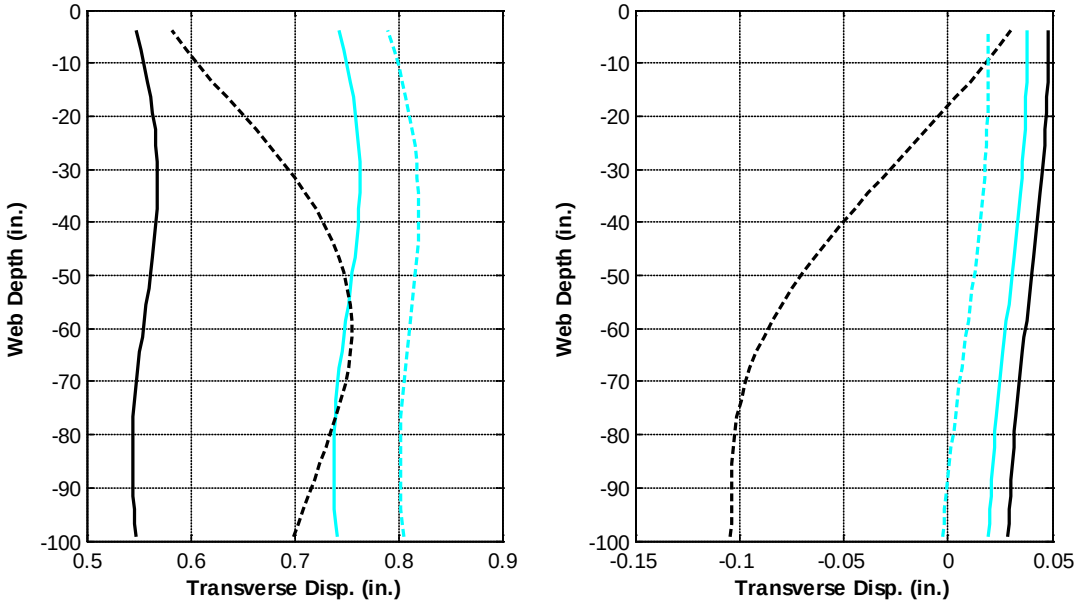


*(c)* Mid-Span 3

*(d)* Mid-Span 4

**Figure B.35. Web Displacement Profiles at Mid-Spans of Girder 3 – Gravity and +45°F Loading**

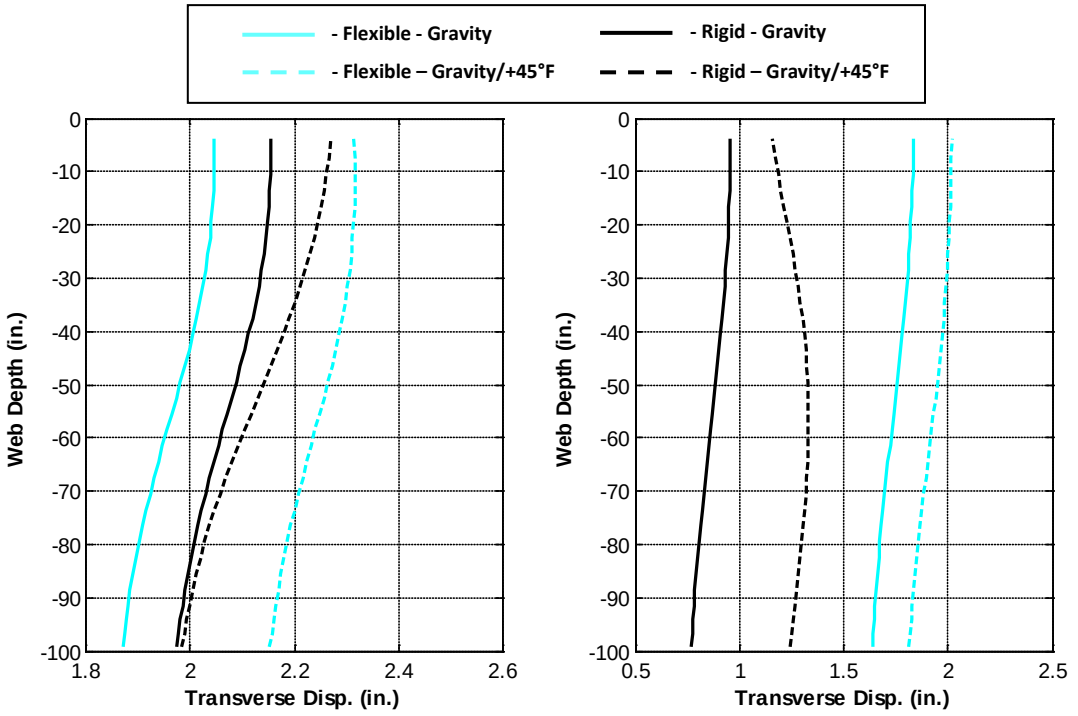


*(a)* Mid-Span 1

*(b)* Mid-Span 2

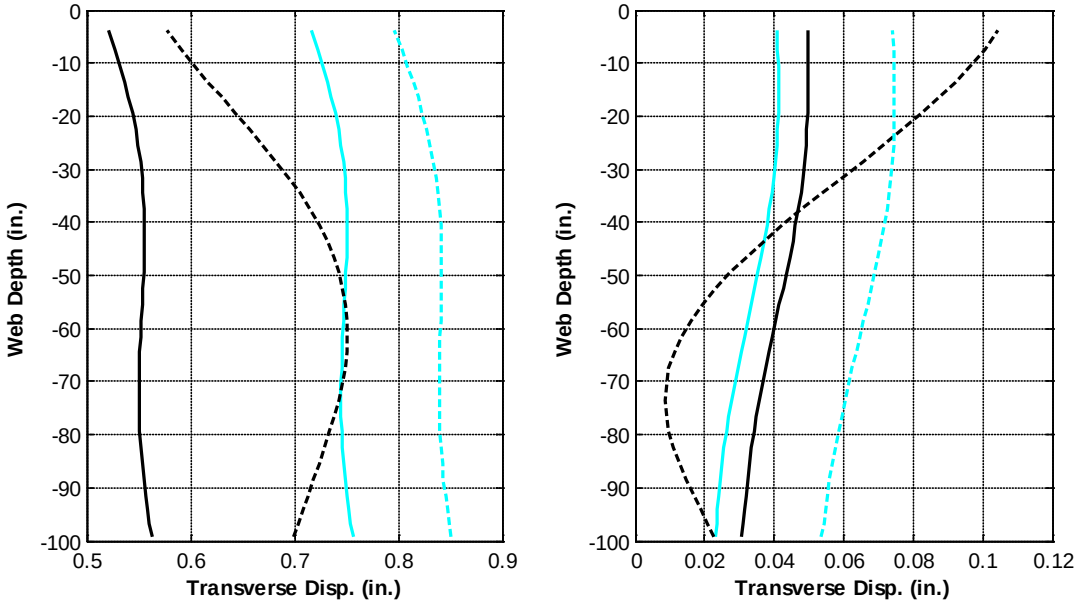


*(c)* Mid-Span 3

*(d)* Mid-Span 4

**Figure B.36. Web Displacement Profiles at Mid-Spans of Girder 4 – Gravity and +45°F Loading**

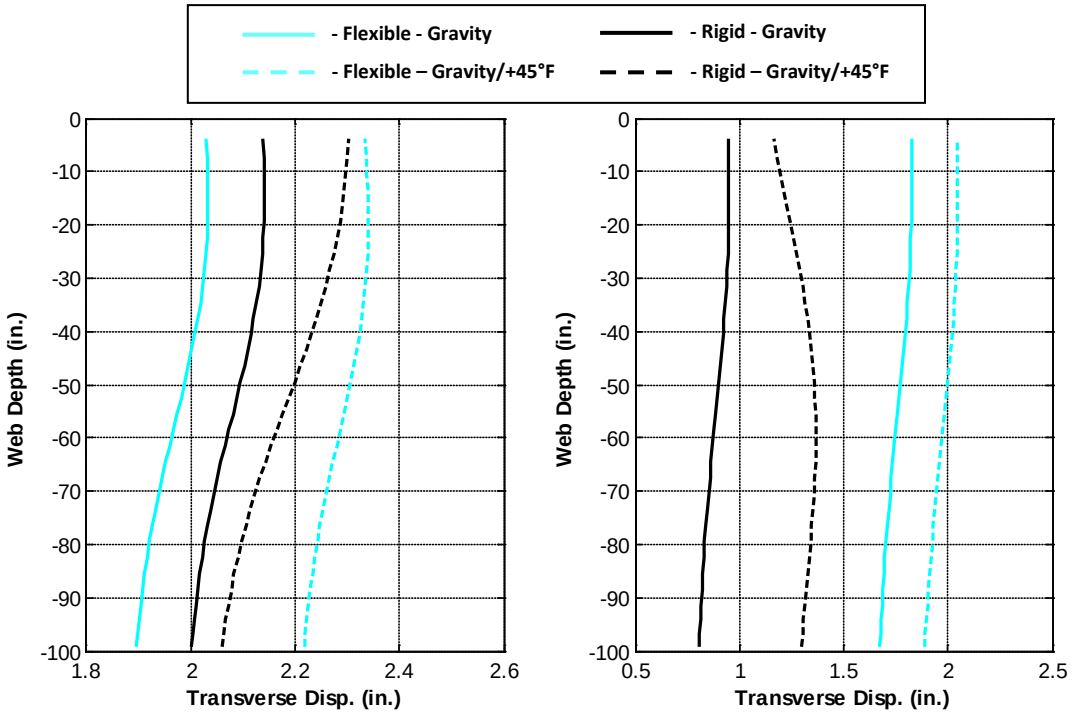


*(a)* Mid-Span 1

*(b)* Mid-Span 2

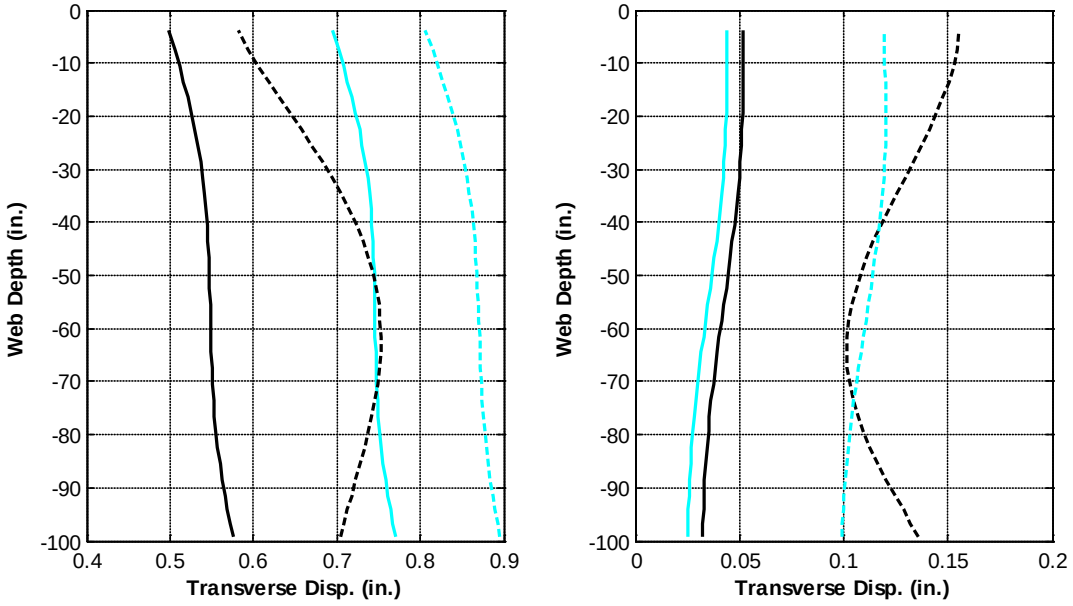


*(c)* Mid-Span 3

*(d)* Mid-Span 4

**Figure B.37. Web Displacement Profiles at Mid-Spans of Girder 5 – Gravity and +45°F Loading**

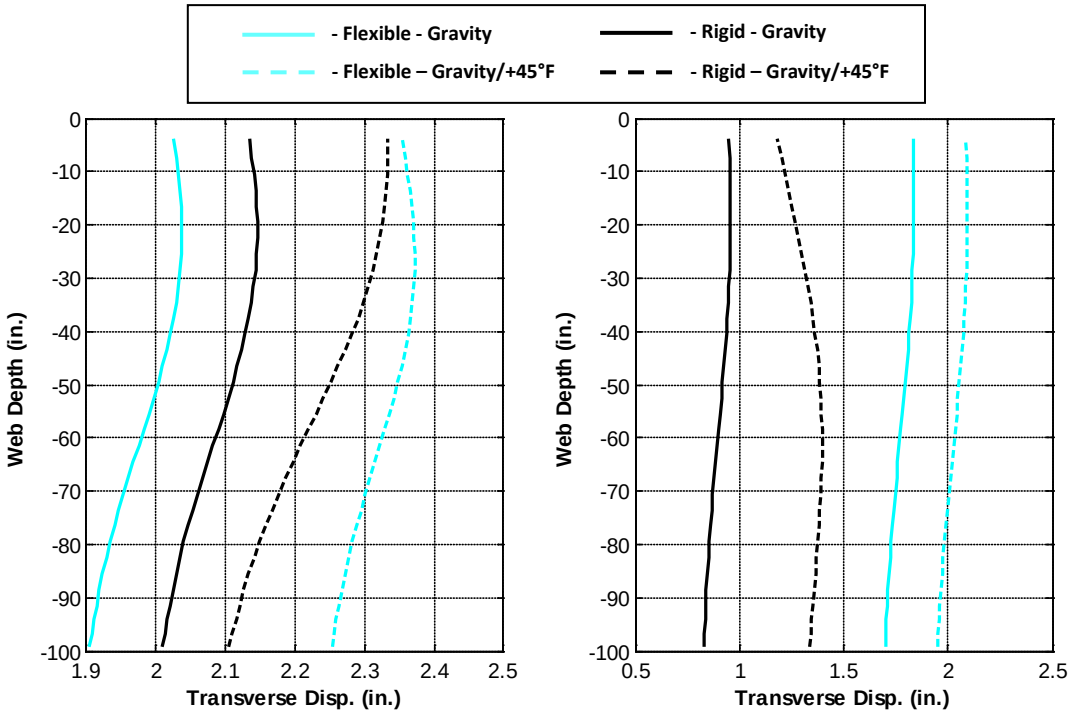


*(a)* Mid-Span 1

*(b)* Mid-Span 2

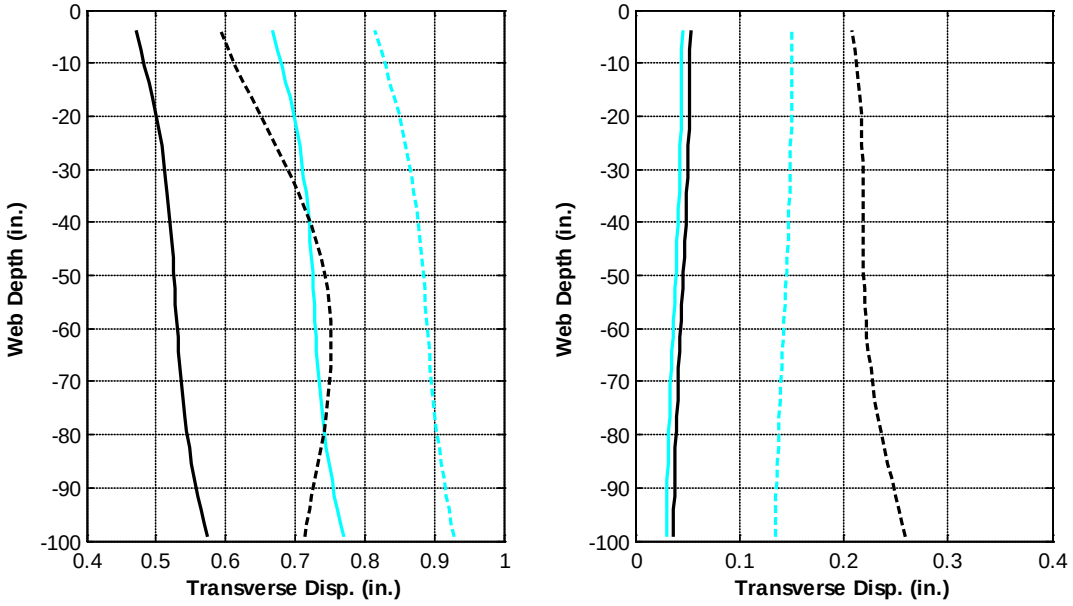


*(c)* Mid-Span 3

*(d)* Mid-Span 4

**Figure B.38. Web Displacement Profiles at Mid-Spans of Girder 6 – Gravity and +45°F Loading**

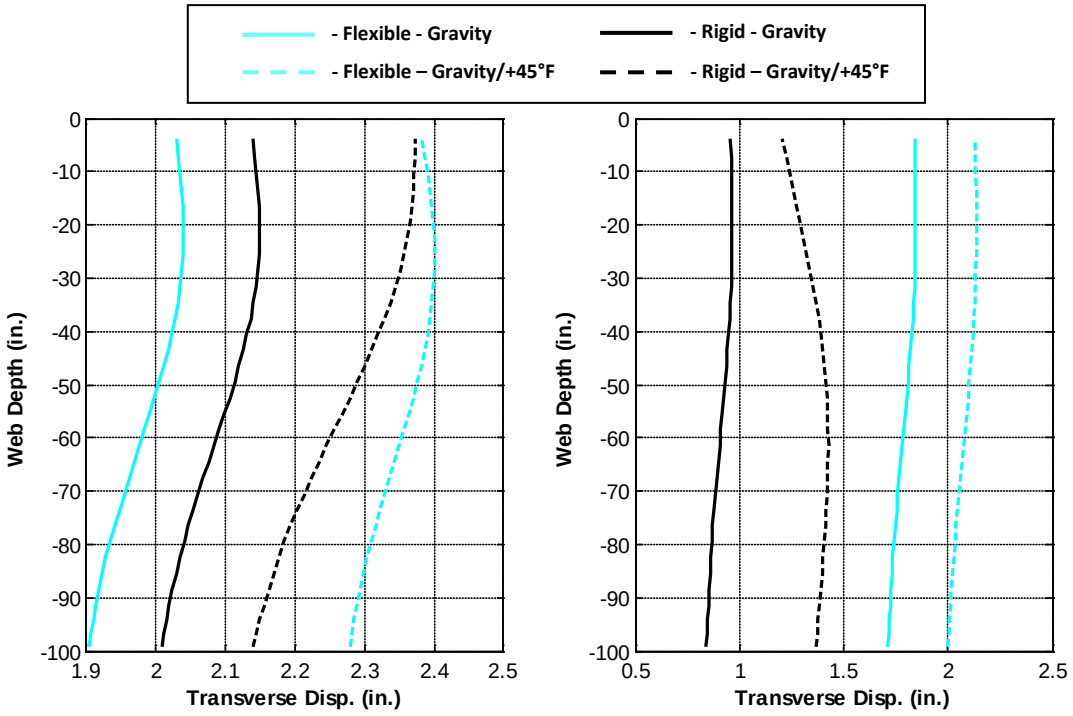


*(a)* Mid-Span 1

*(b)* Mid-Span 2

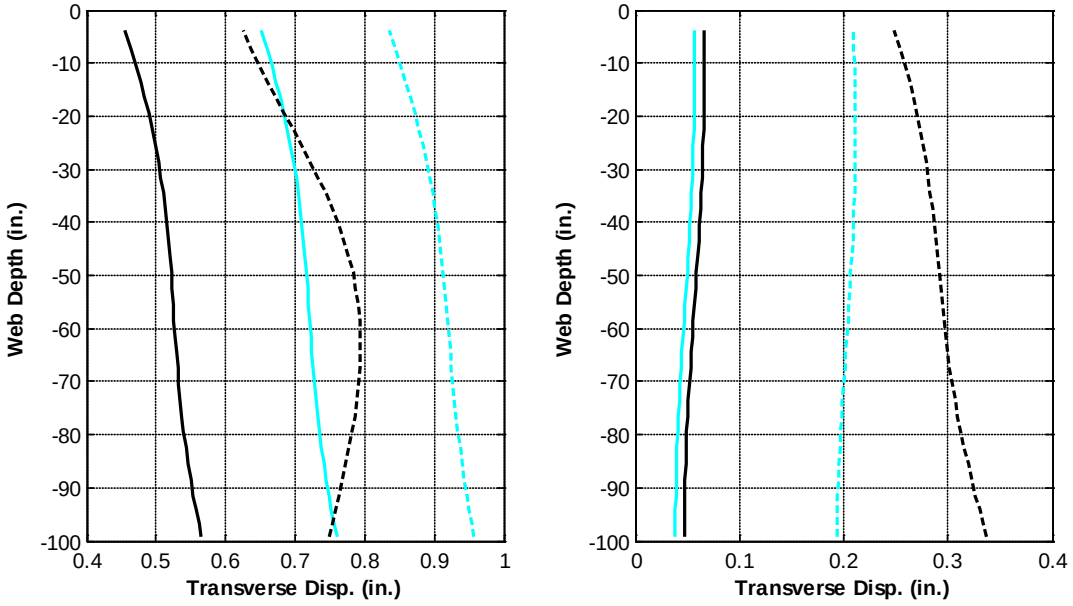


*(c)* Mid-Span 3

*(d)* Mid-Span 4

**Figure B.39. Web Displacement Profiles at Mid-Spans of Girder 7 – Gravity and +45°F Loading**

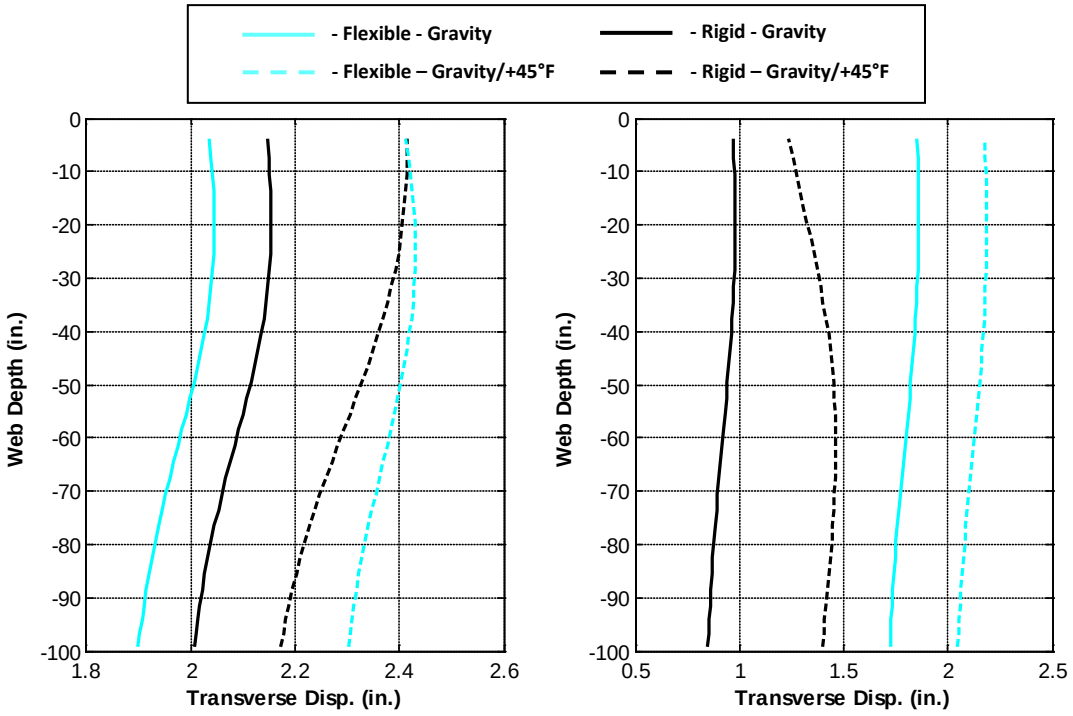


*(a)* Mid-Span 1

*(b)* Mid-Span 2

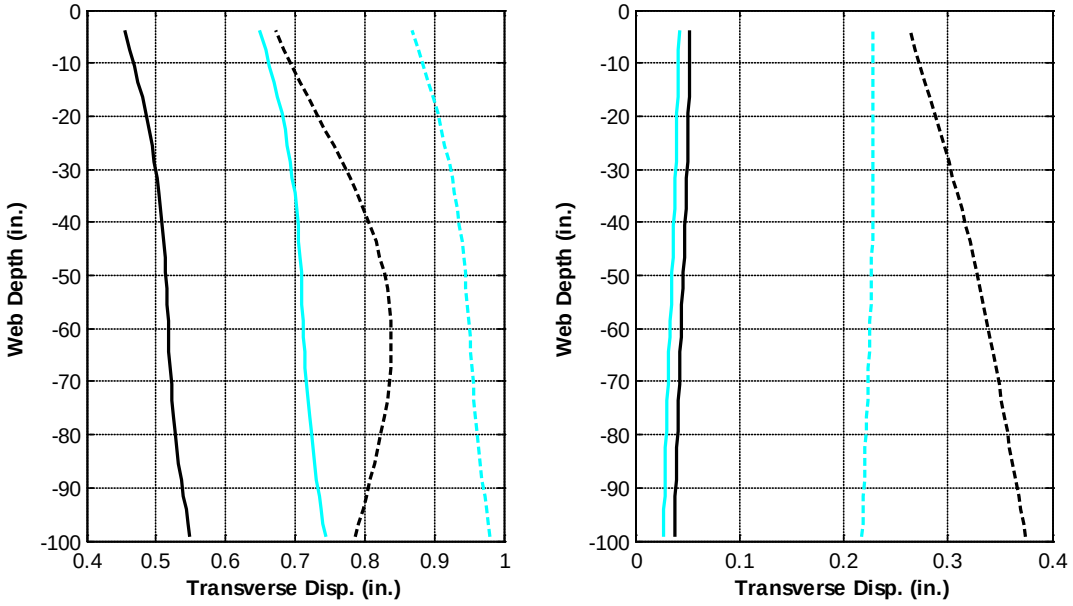


*(c)* Mid-Span 3

*(d)* Mid-Span 4

**Figure B.40. Web Displacement Profiles at Mid-Spans of Girder 8 – Gravity and +45°F Loading**

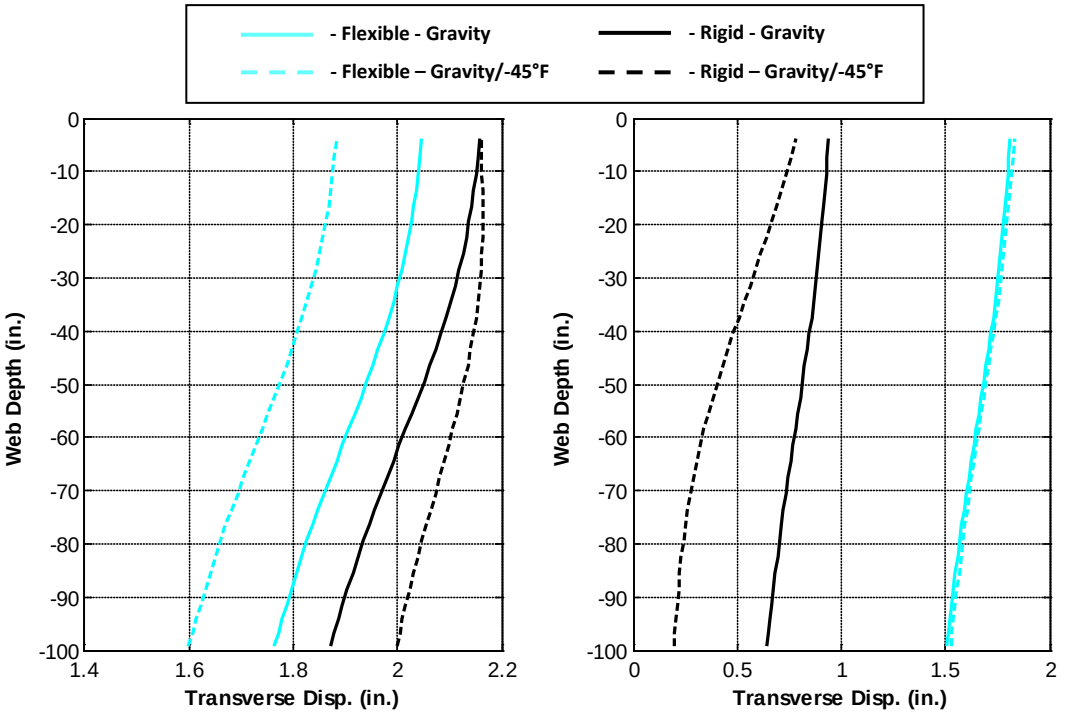


*(a)* Mid-Span 1 *(b)* Mid-Span 2

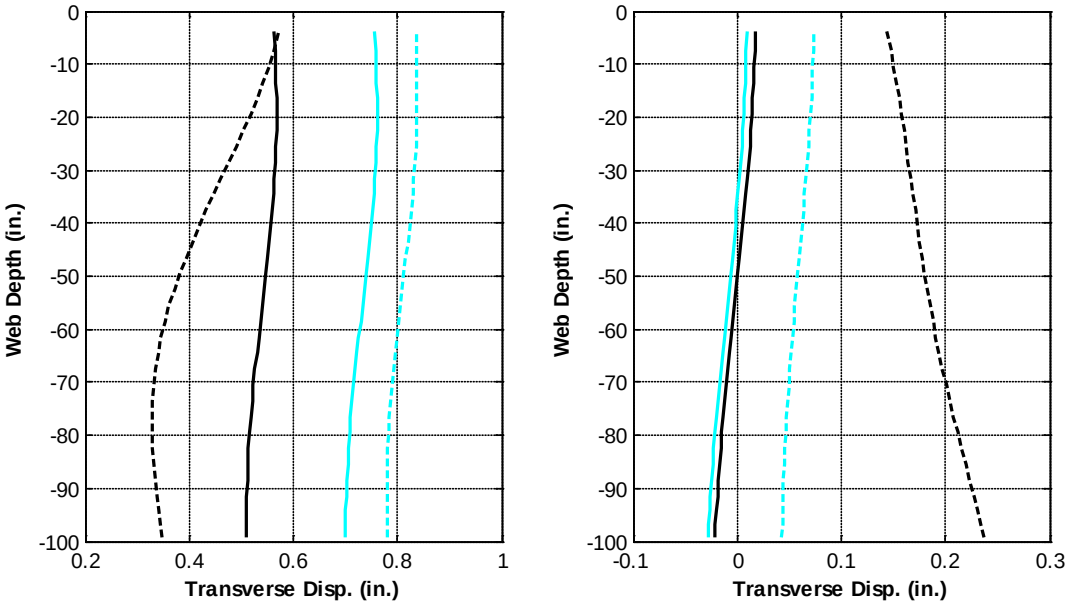


*(c)* Mid-Span 3 *(d)* Mid-Span 4

**Figure B.41. Web Displacement Profiles at Mid-Spans of Girder 1 – Gravity and -45°F Loading**

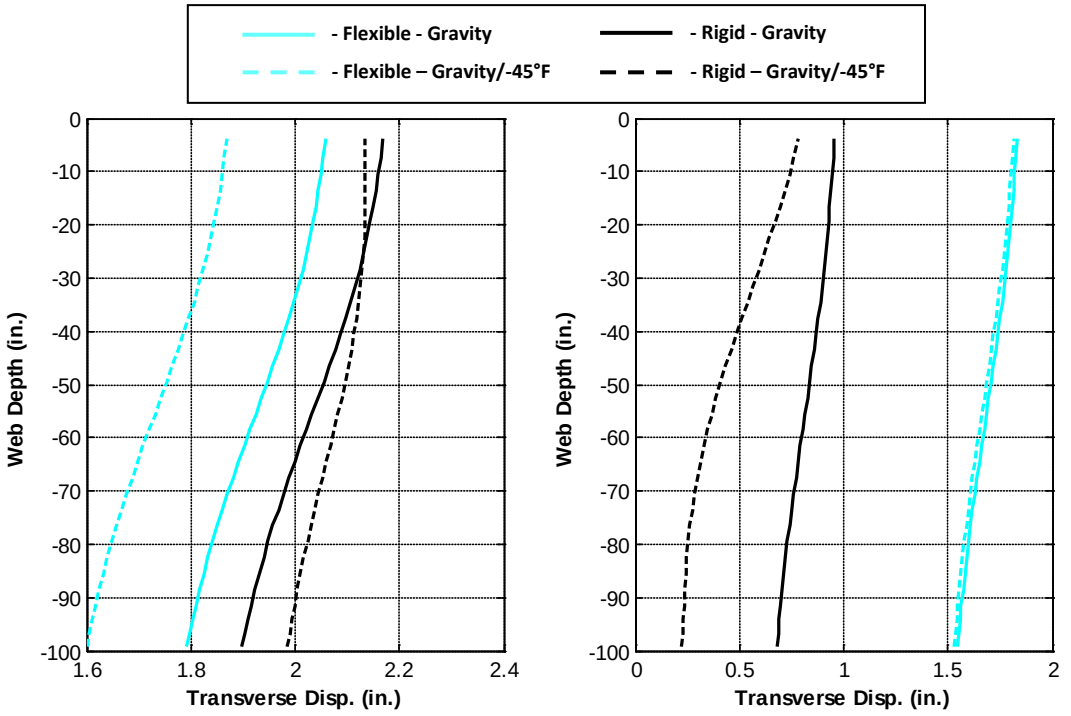


*(a)* Mid-Span 1

*(b)* Mid-Span 2

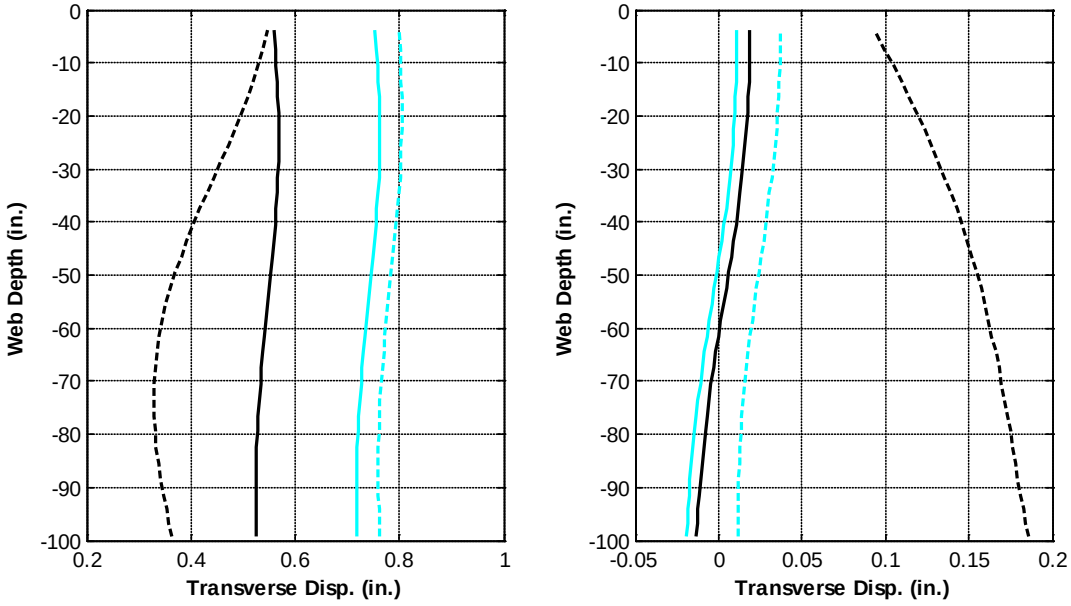


*(c)* Mid-Span 3

*(d)* Mid-Span 4

**Figure B.42. Web Displacement Profiles at Mid-Spans of Girder 2 – Gravity and -45°F Loading**

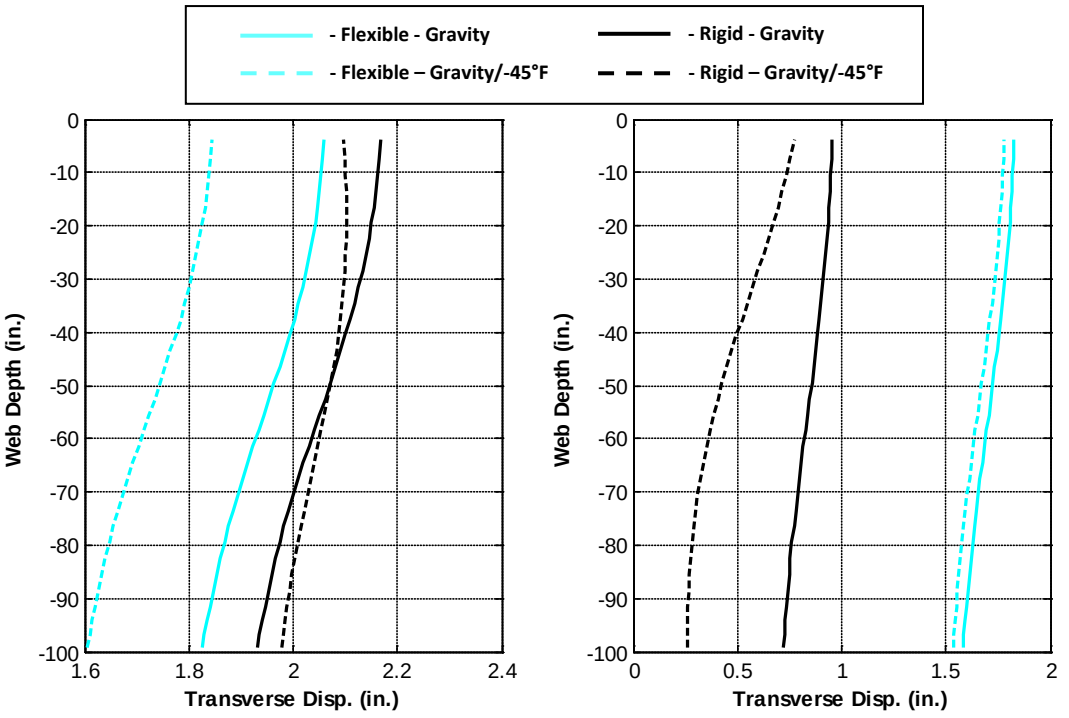


*(a)* Mid-Span 1

*(b)* Mid-Span 2

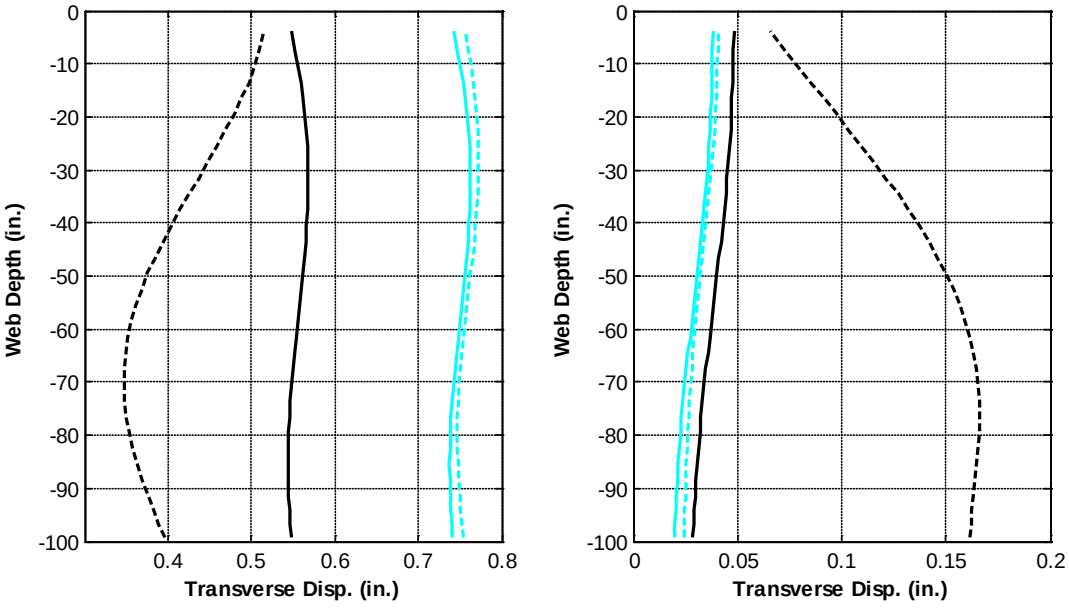


*(c)* Mid-Span 3

*(d)* Mid-Span 4

**Figure B.43. Web Displacement Profiles at Mid-Spans of Girder 3 – Gravity and -45°F Loading**

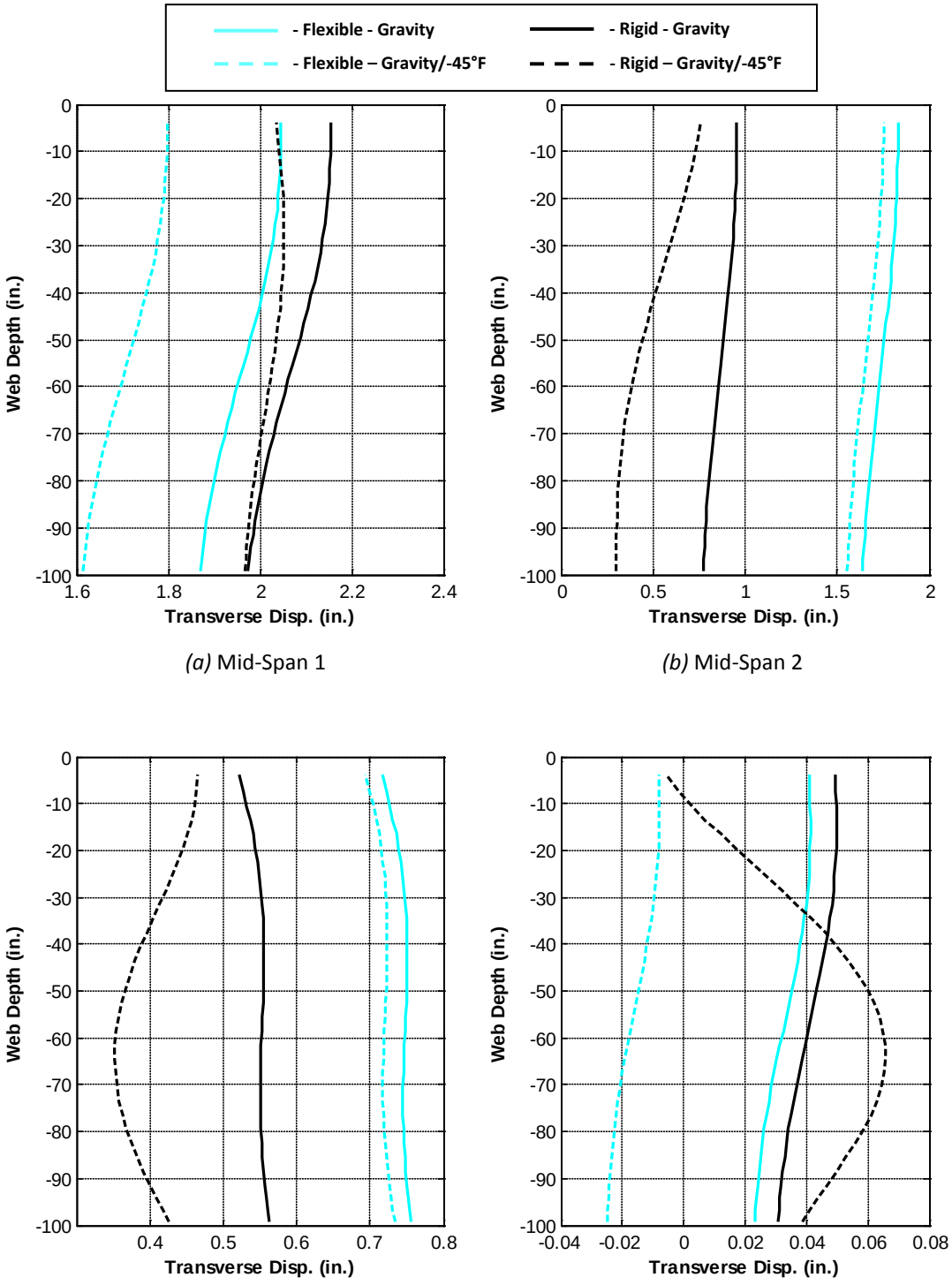


*(a)* Mid-Span 1

*(b)* Mid-Span 2

*(c)* Mid-Span 3

*(d)* Mid-Span 4

**Figure B.44. Web Displacement Profiles at Mid-Spans of Girder 4 – Gravity and -45°F Loading**

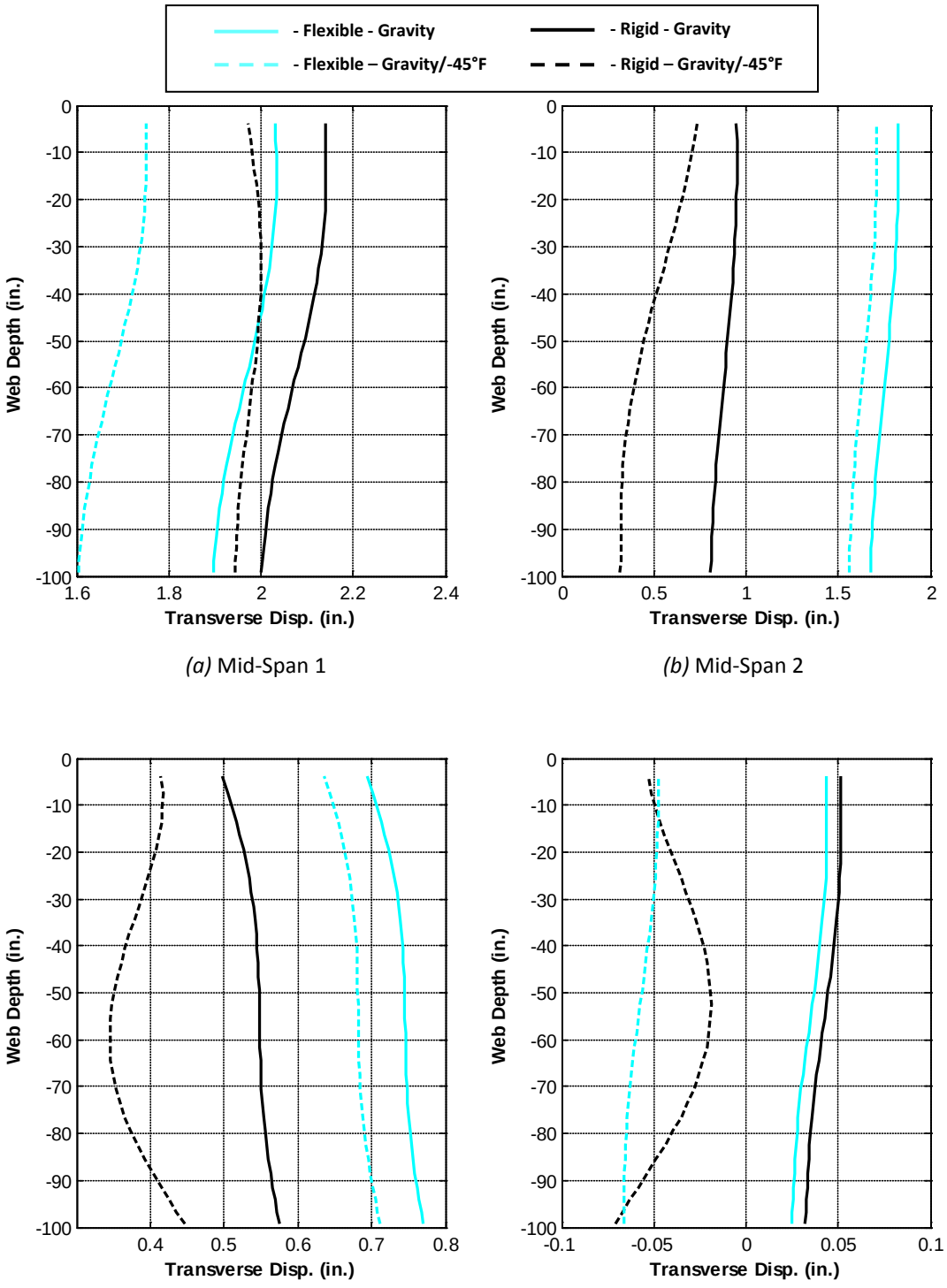


*(a)* Mid-Span 1

*(b)* Mid-Span 2

*(c)* Mid-Span 3

*(d)* Mid-Span 4

**Figure B.45. Web Displacement Profiles at Mid-Spans of Girder 5 – Gravity and -45°F Loading**

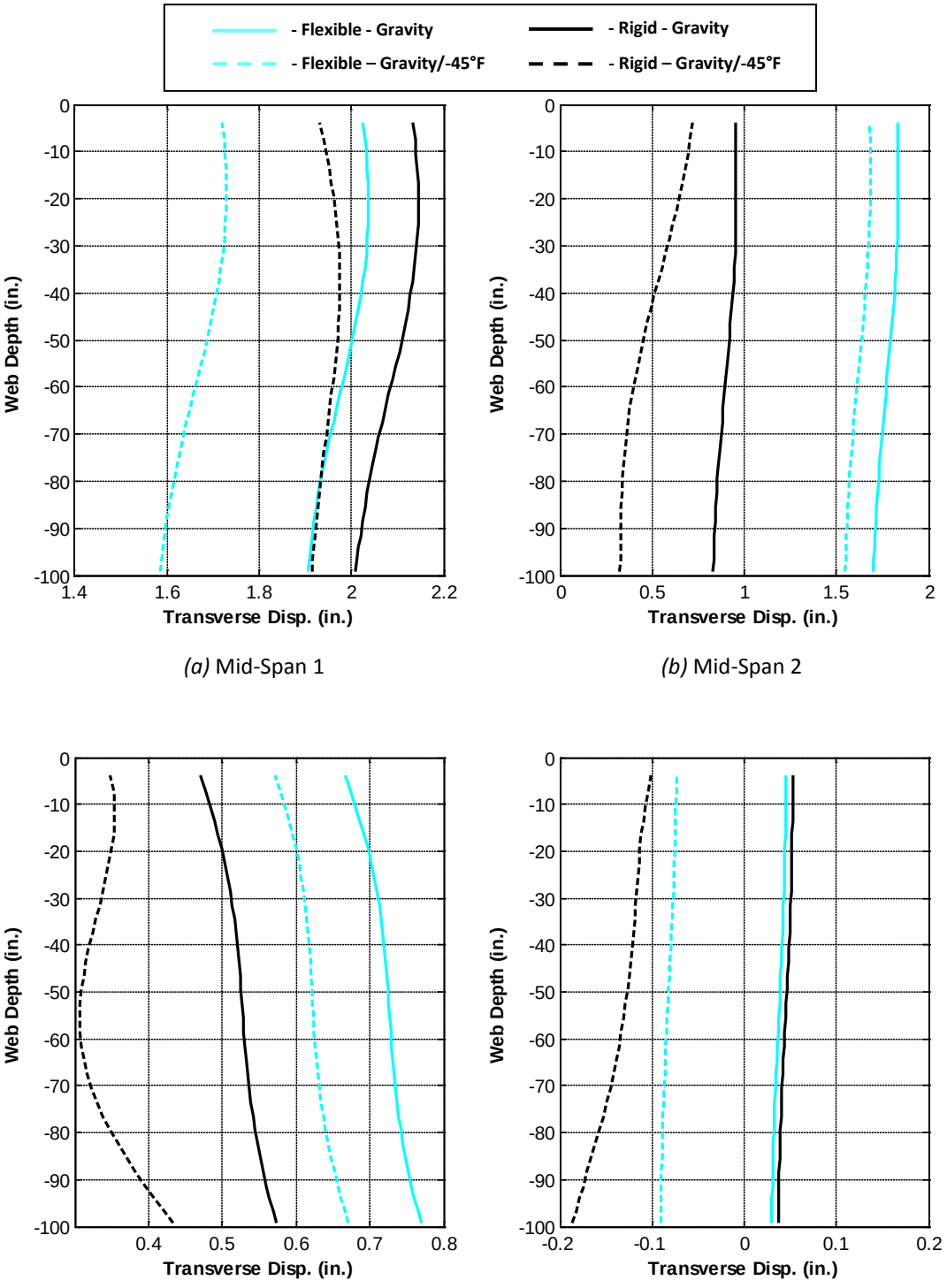


*(a)* Mid-Span 1

*(b)* Mid-Span 2

*(c)* Mid-Span 3

*(d)* Mid-Span 4

**Figure B.46. Web Displacement Profiles at Mid-Spans of Girder 6 – Gravity and -45°F Loading**

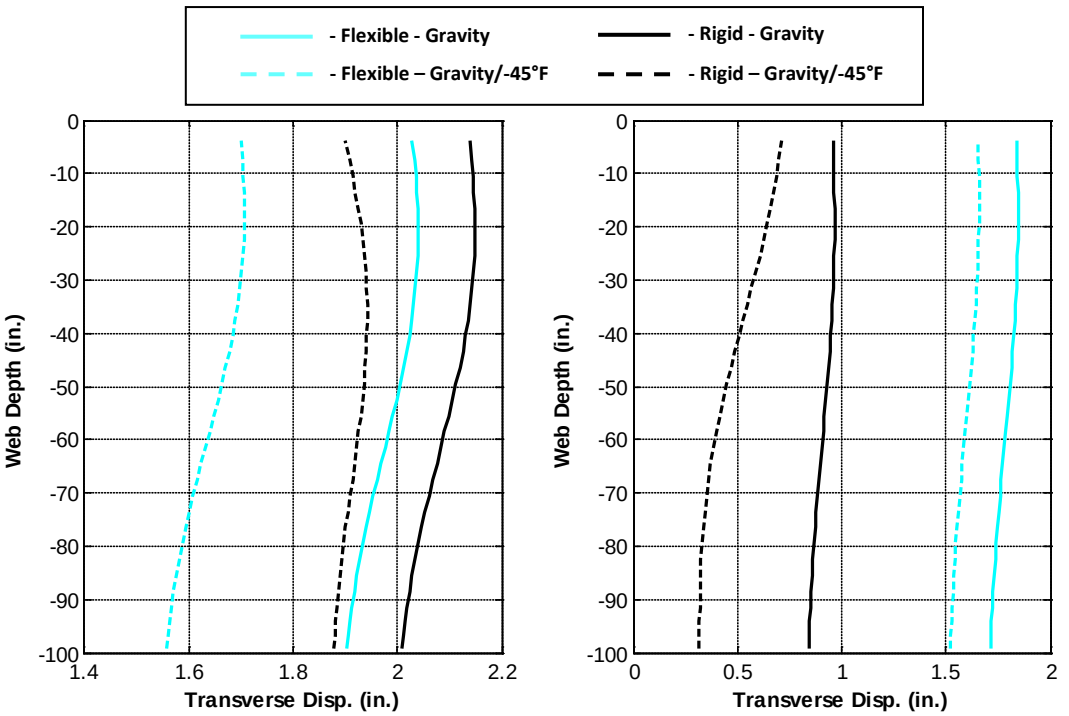


*(a)* Mid-Span 1

*(b)* Mid-Span 2

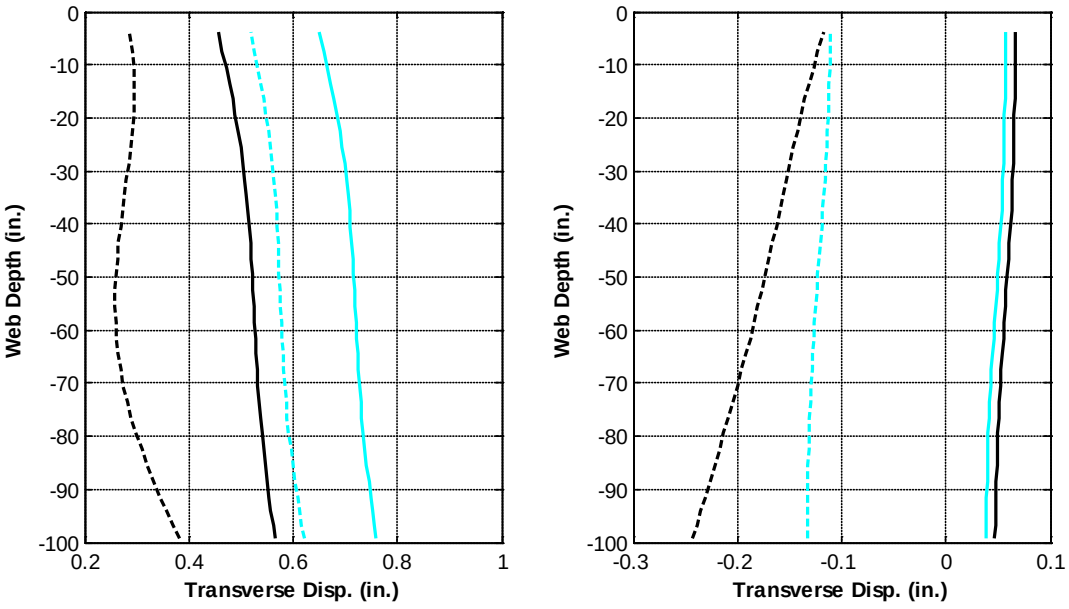


*(c)* Mid-Span 3

*(d)* Mid-Span 4

**Figure B.47. Web Displacement Profiles at Mid-Spans of Girder 7 – Gravity and -45°F Loading**

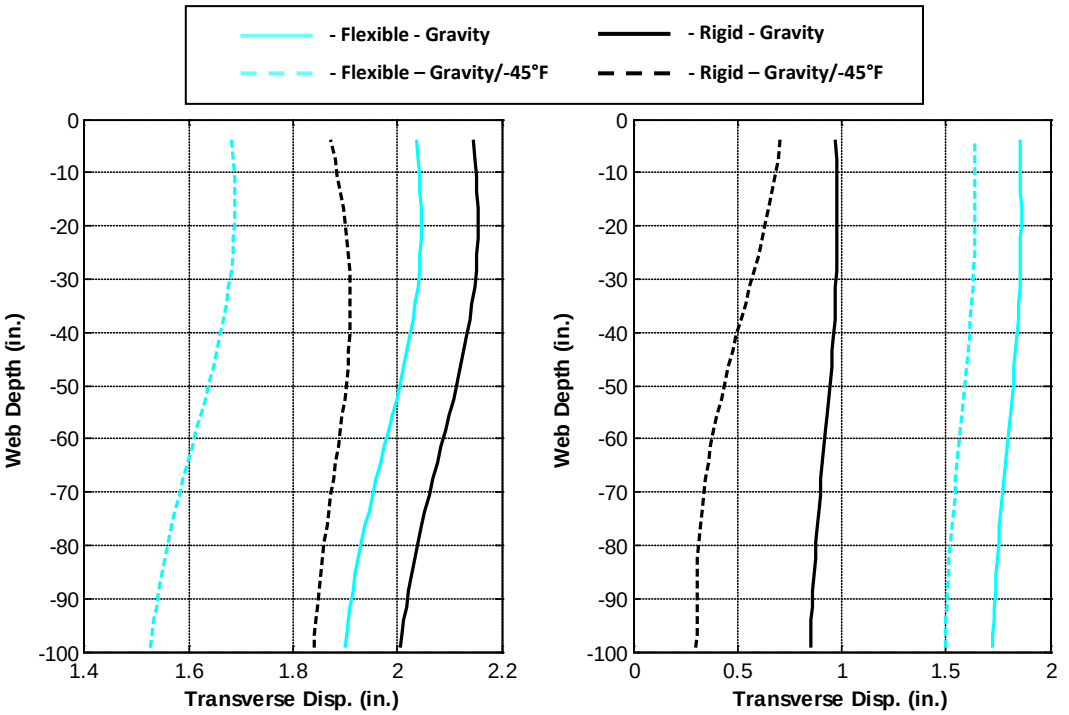


*(a)* Mid-Span 1

*(b)* Mid-Span 2

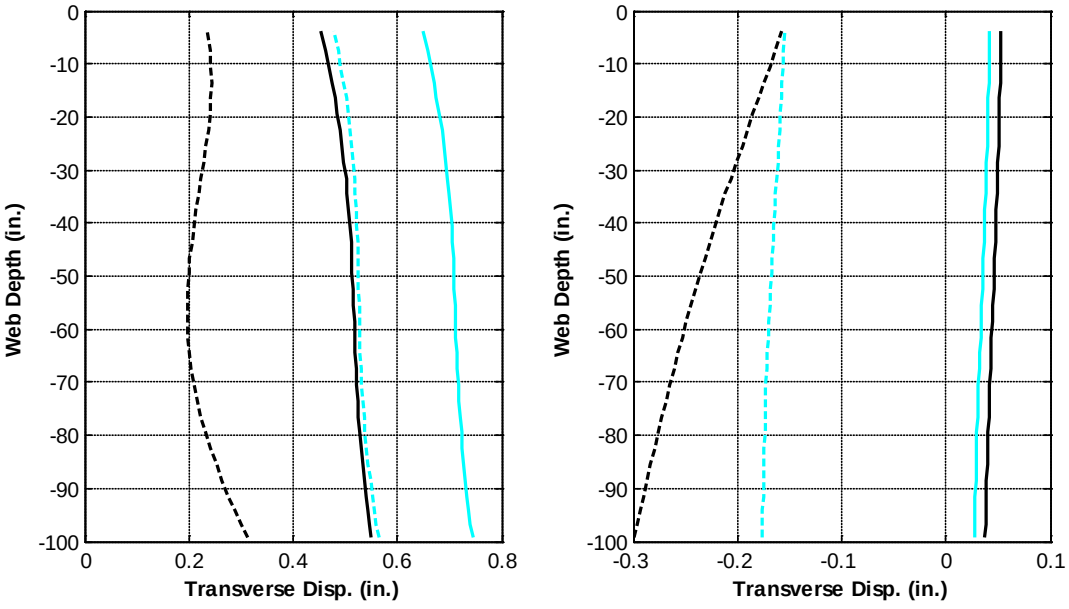


*(c)* Mid-Span 3

*(d)* Mid-Span 4

**Figure B.48. Web Displacement Profiles at Mid-Spans of Girder 8 – Gravity and -45°F Loading**

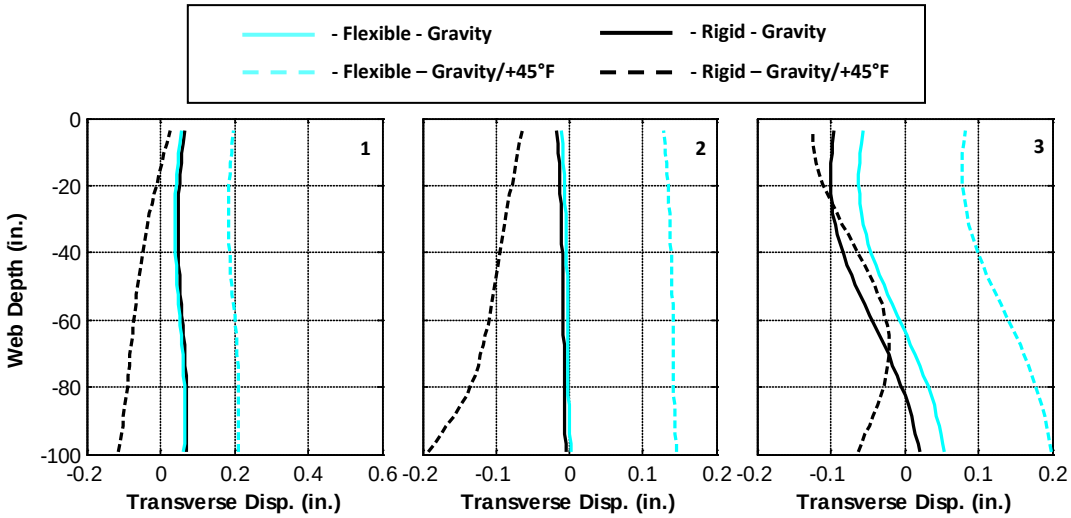


*(a)* Pier 1

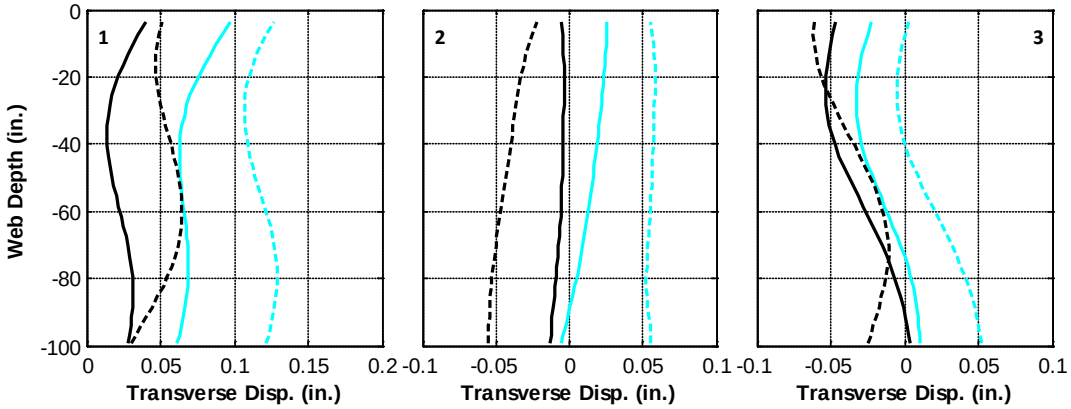


*(b)* Pier 2

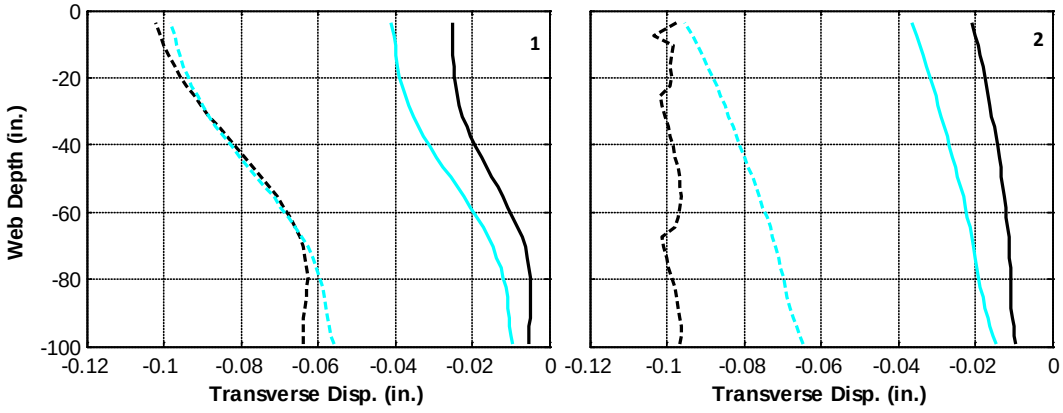


*(c)* Pier 3

**Figure B.49. Web Displacement Profiles at Piers of Girder 1 – Gravity and +45°F Loading**

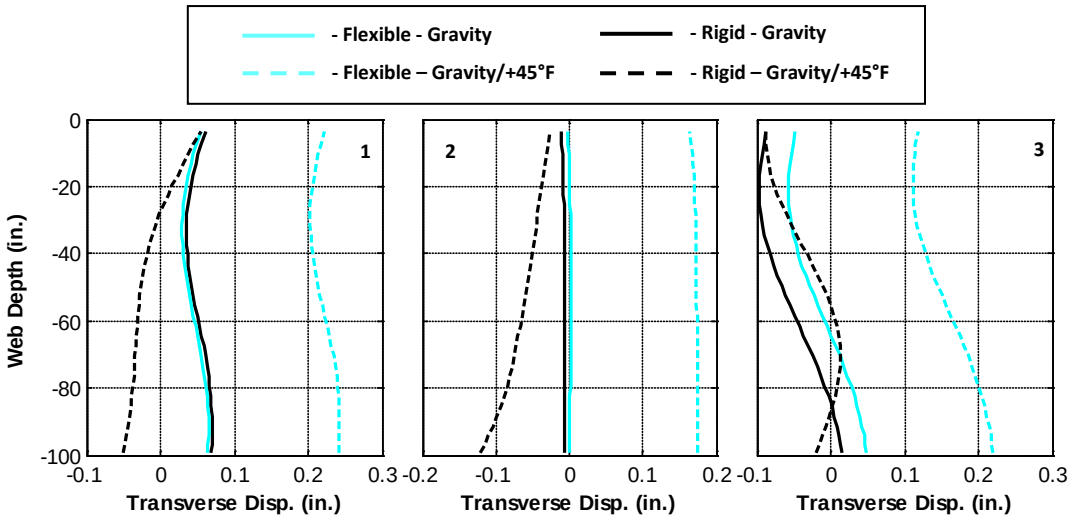


*(a)* Pier 1

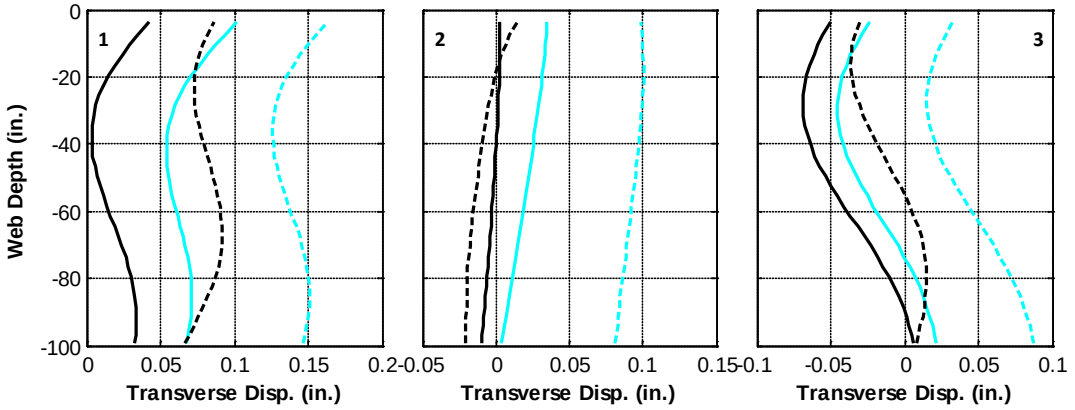


*(b)* Pier 2

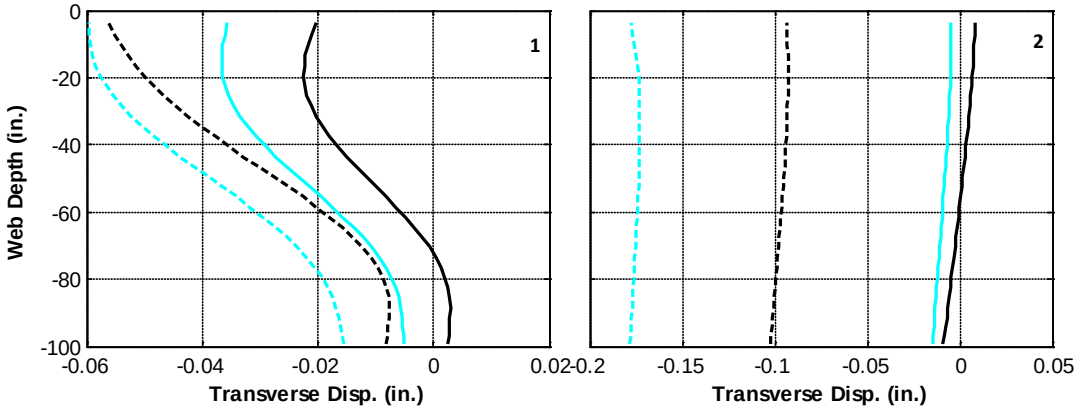


*(c)* Pier 3

**Figure B.50. Web Displacement Profiles at Piers of Girder 2 – Gravity and +45°F Loading**

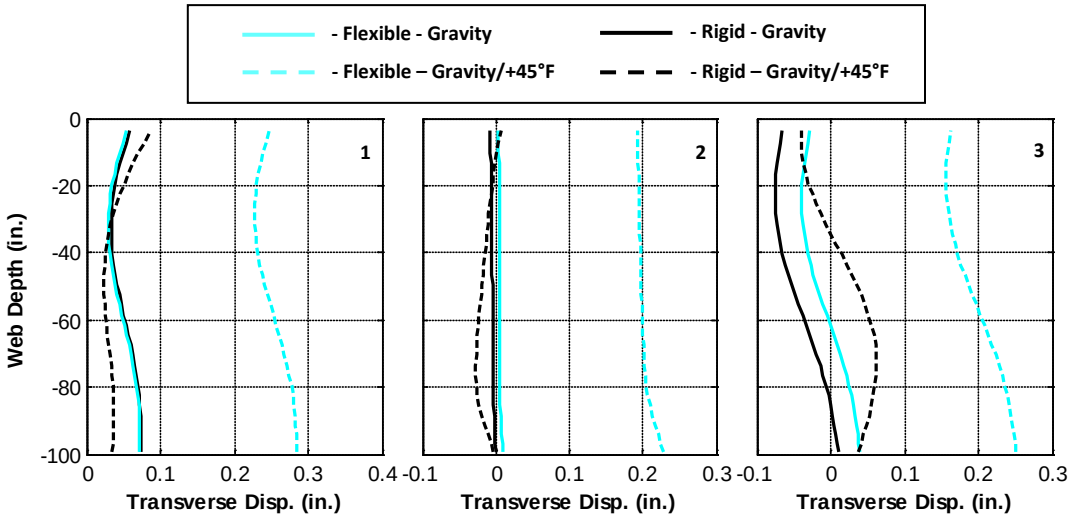


*(a)* Pier 1

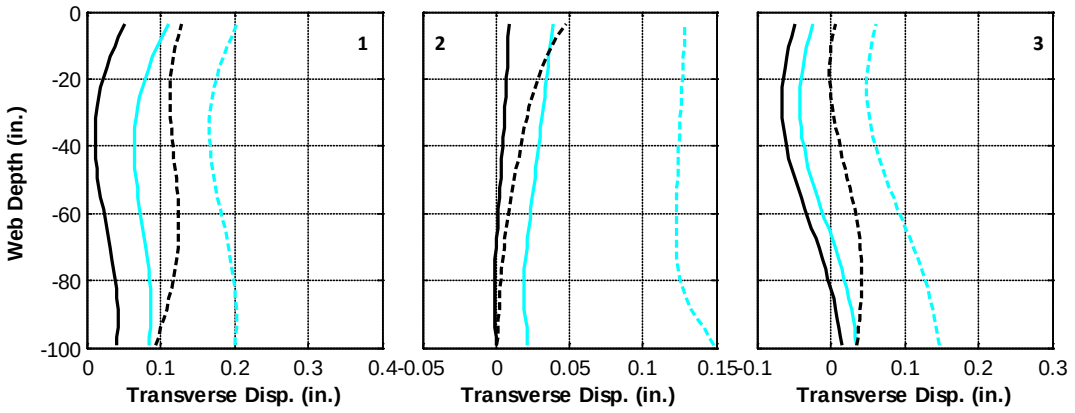


*(b)* Pier 2

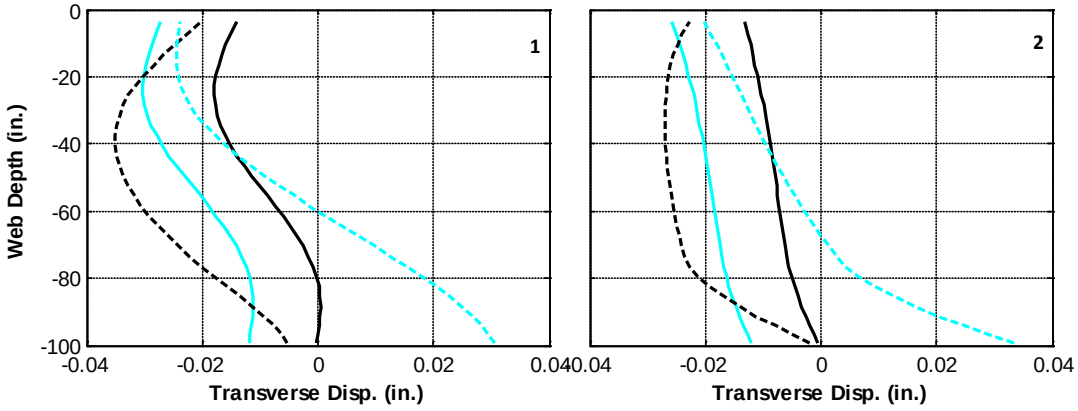


*(c)* Pier 3

**Figure B.51. Web Displacement Profiles at Piers of Girder 3 – Gravity and +45°F Loading**

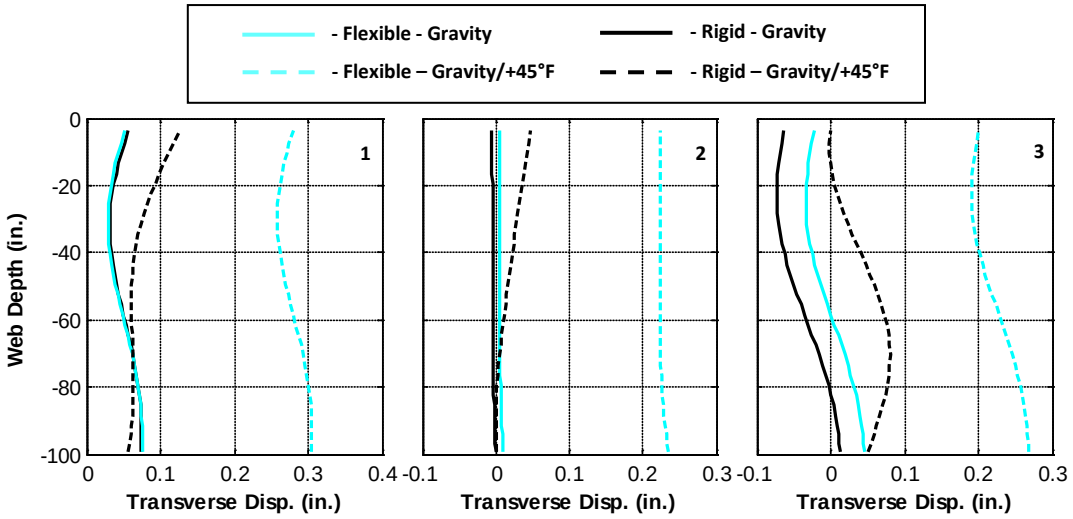


*(a)* Pier 1

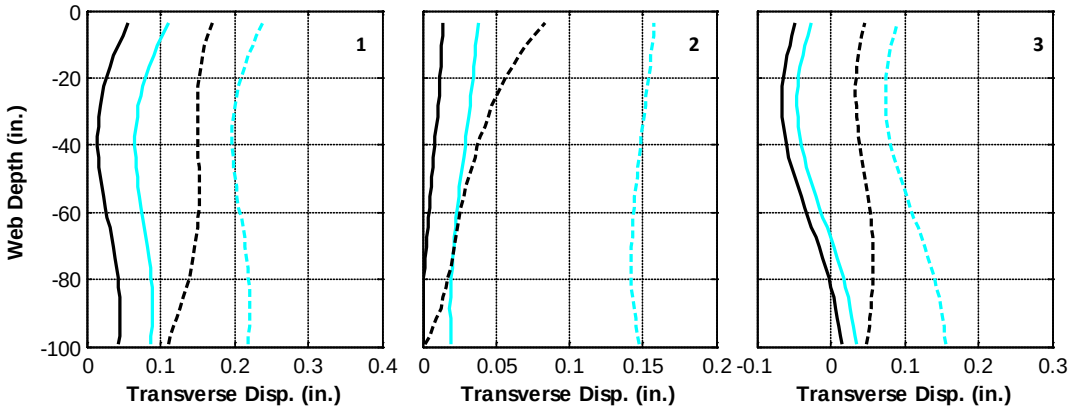


*(b)* Pier 2

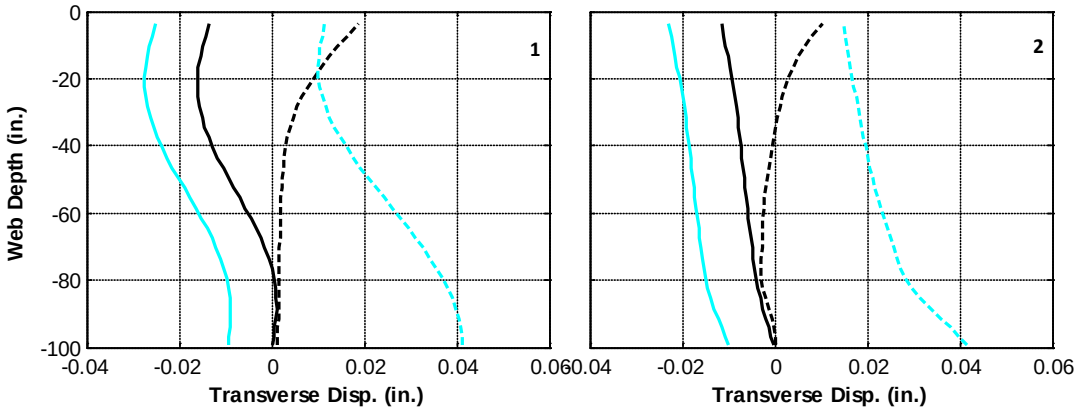


*(c)* Pier 3

**Figure B.52. Web Displacement Profiles at Piers of Girder 4 – Gravity and +45°F Loading**

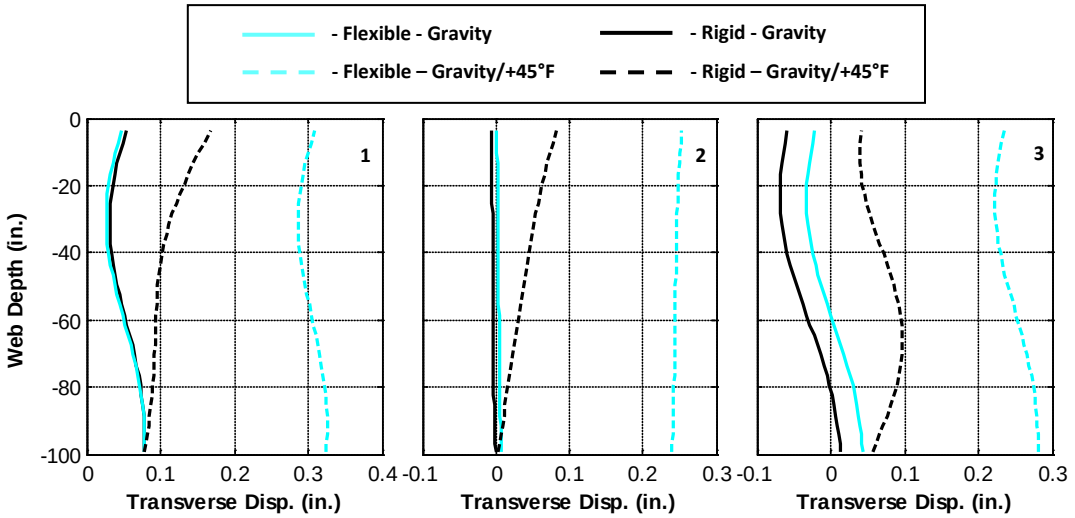


*(a)* Pier 1

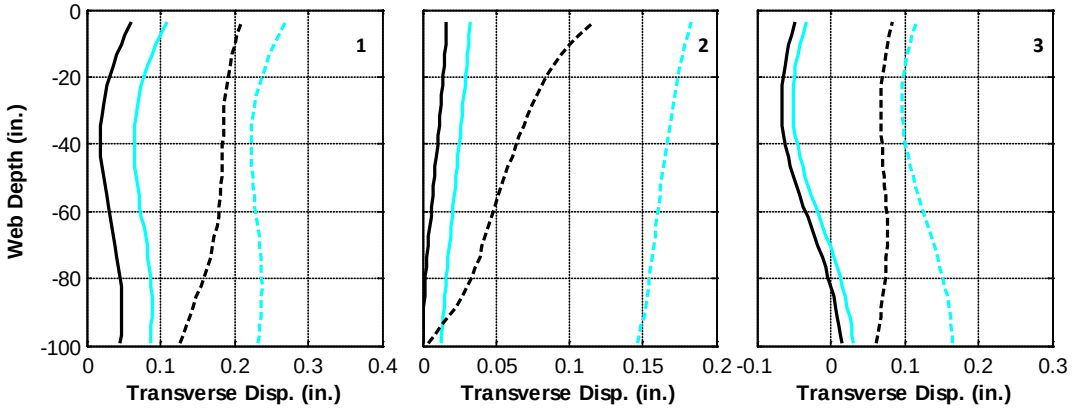


*(b)* Pier 2

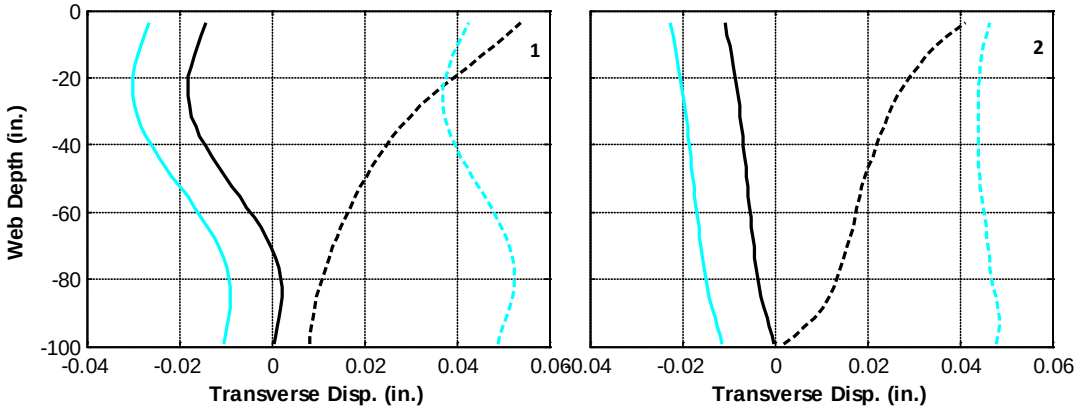


*(c)* Pier 3

**Figure B.53. Web Displacement Profiles at Piers of Girder 5 – Gravity and +45°F Loading**

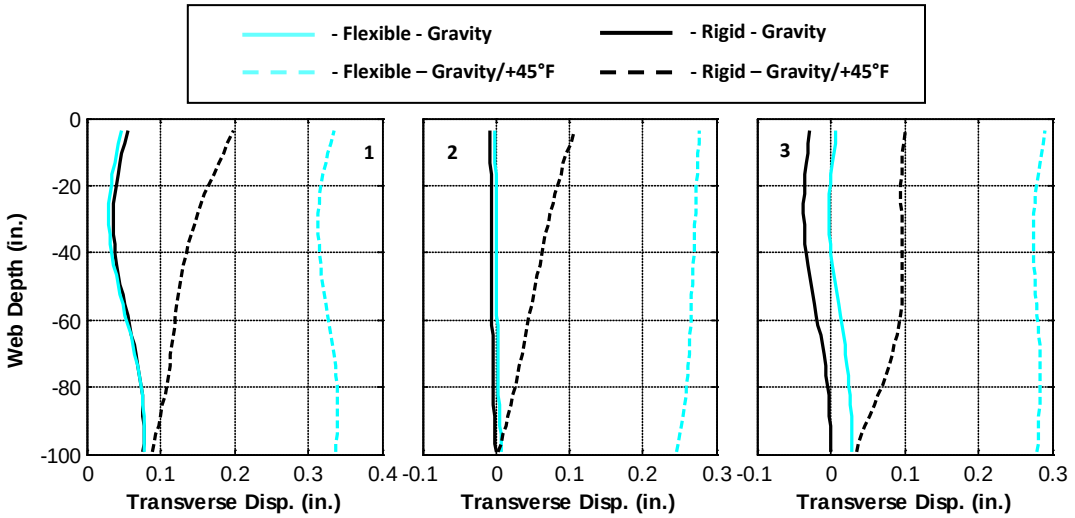


*(a)* Pier 1

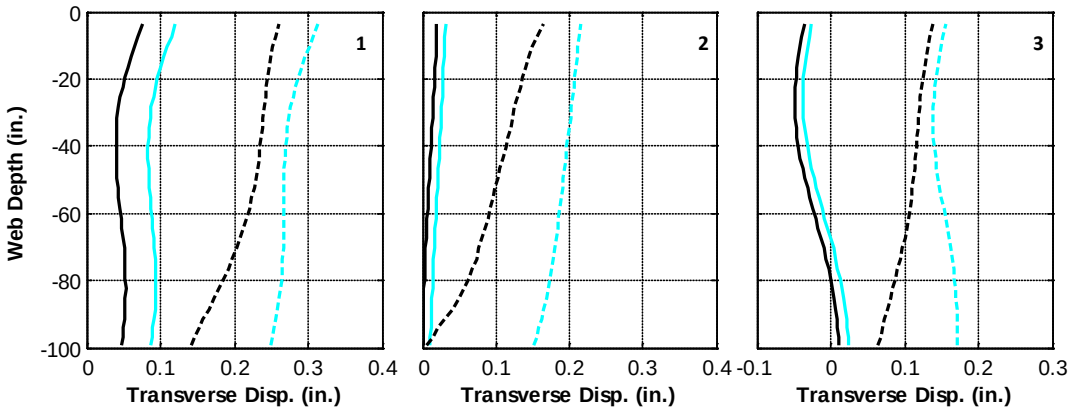


*(b)* Pier 2

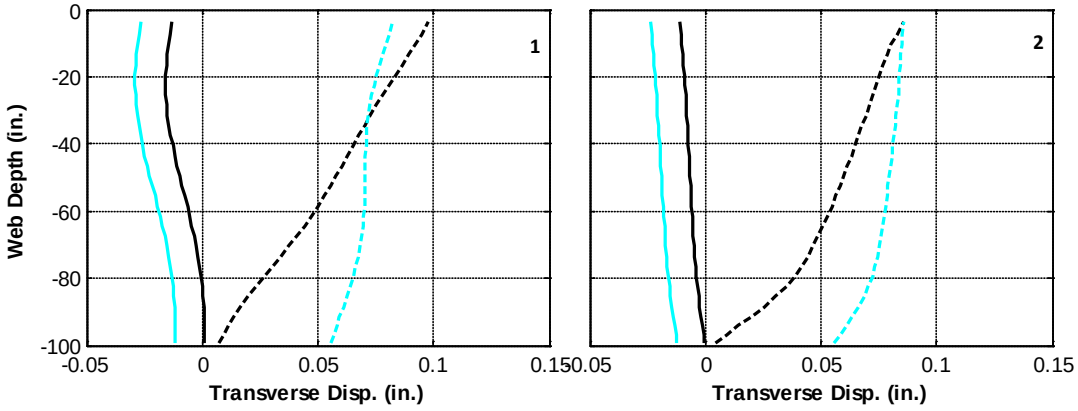


*(c)* Pier 3

**Figure B.54. Web Displacement Profiles at Piers of Girder 6 – Gravity and +45°F Loading**

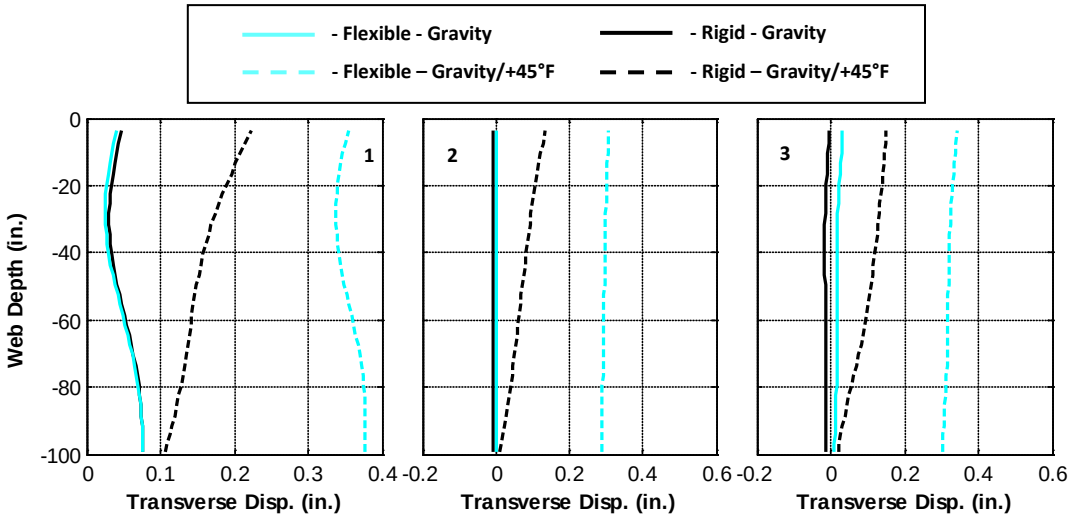


*(a)* Pier 1

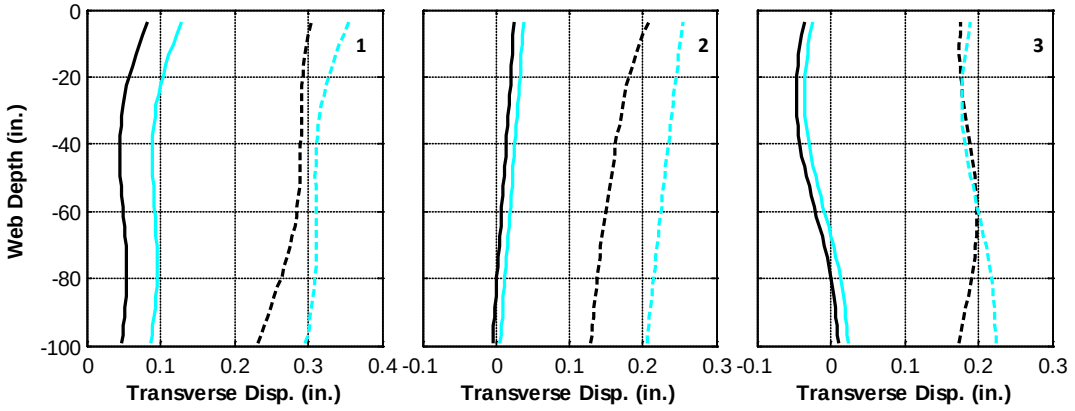


*(b)* Pier 2

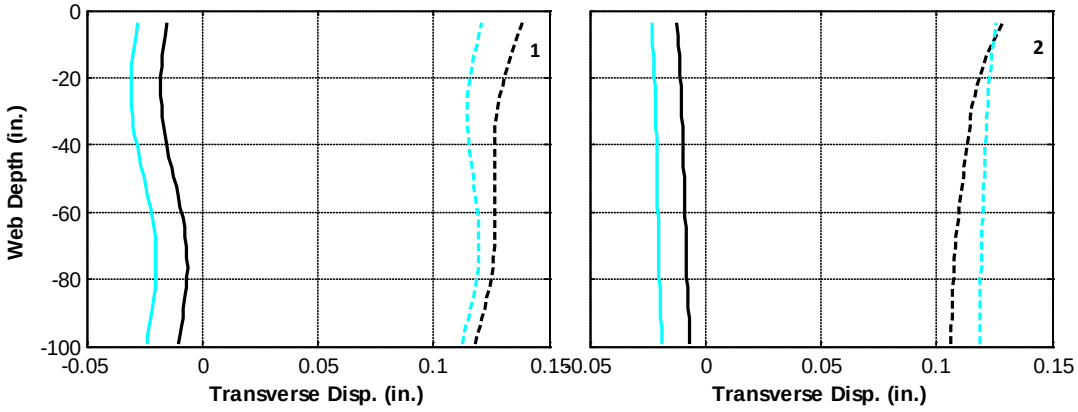


*(c)* Pier 3

**Figure B.55. Web Displacement Profiles at Piers of Girder 7 – Gravity and +45°F Loading**

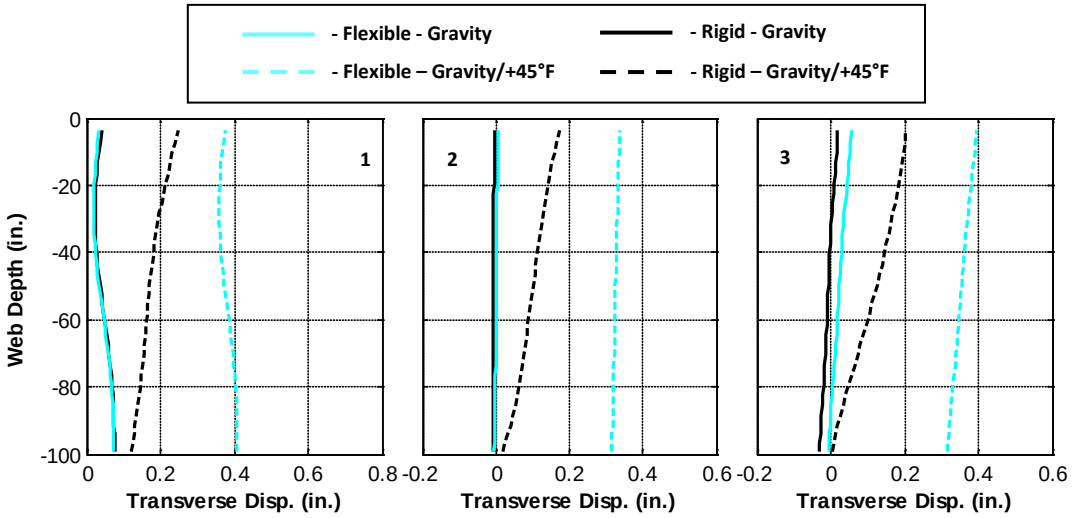


*(a)* Pier 1

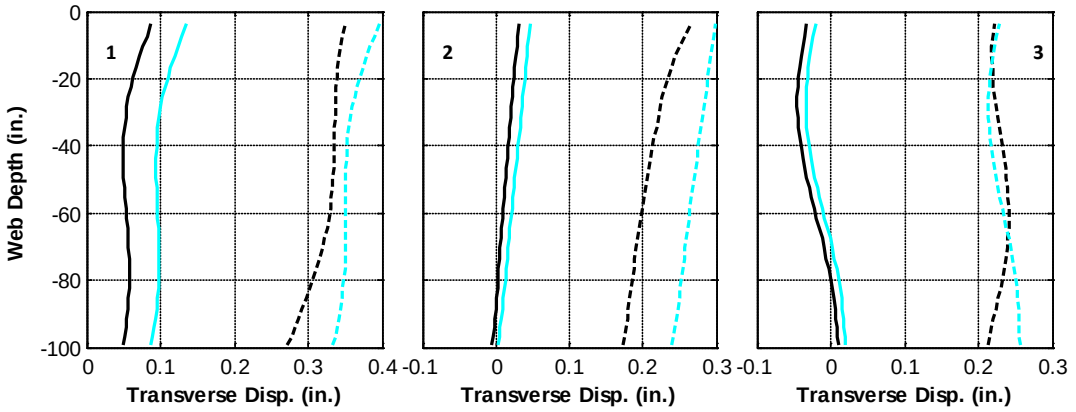


*(b)* Pier 2

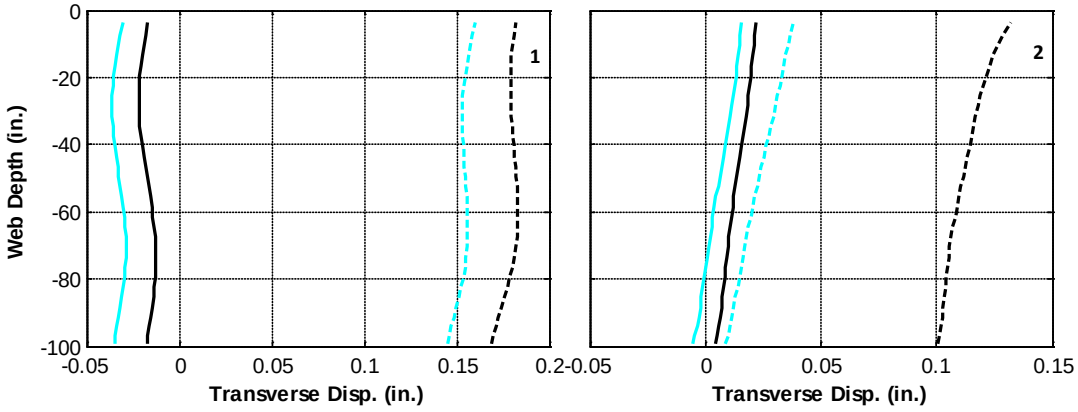


*(c)* Pier 3

**Figure B.56. Web Displacement Profiles at Piers of Girder 8 – Gravity and +45°F Loading**

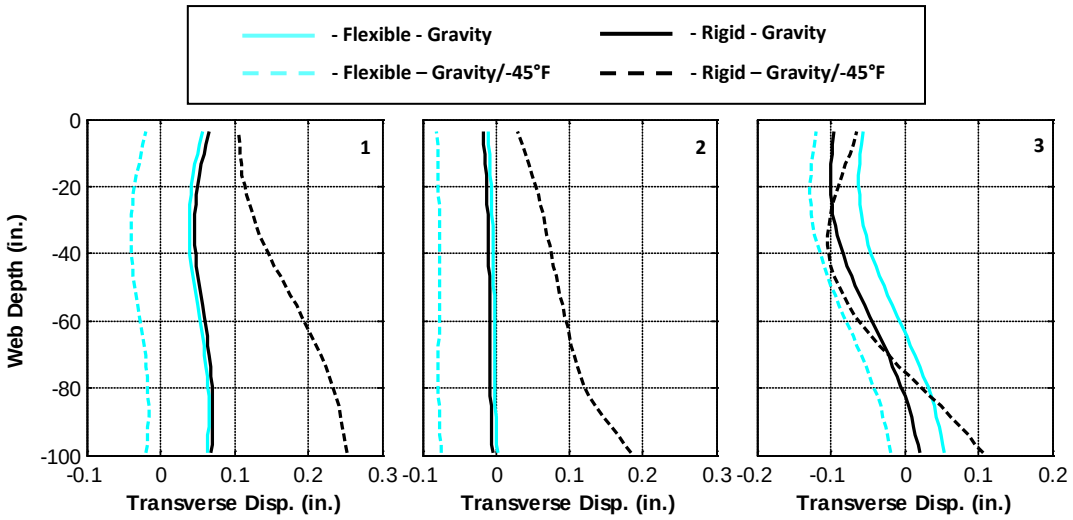


*(a)* Pier 1

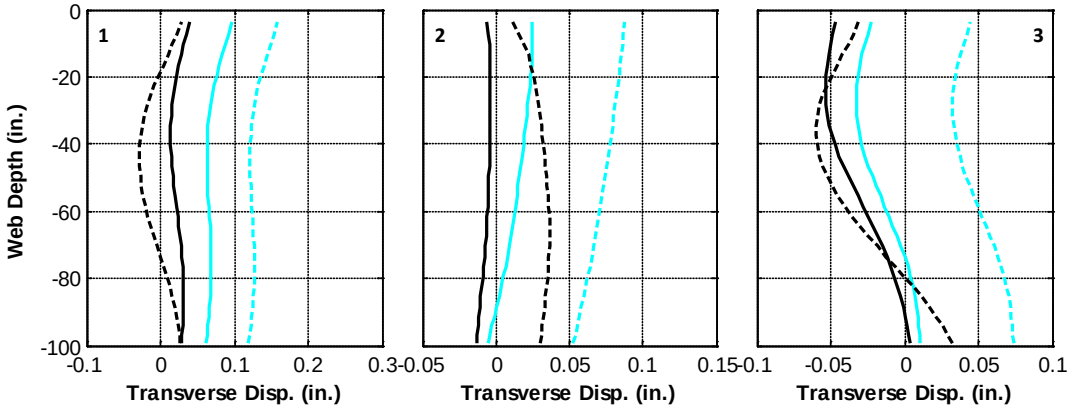


*(b)* Pier 2

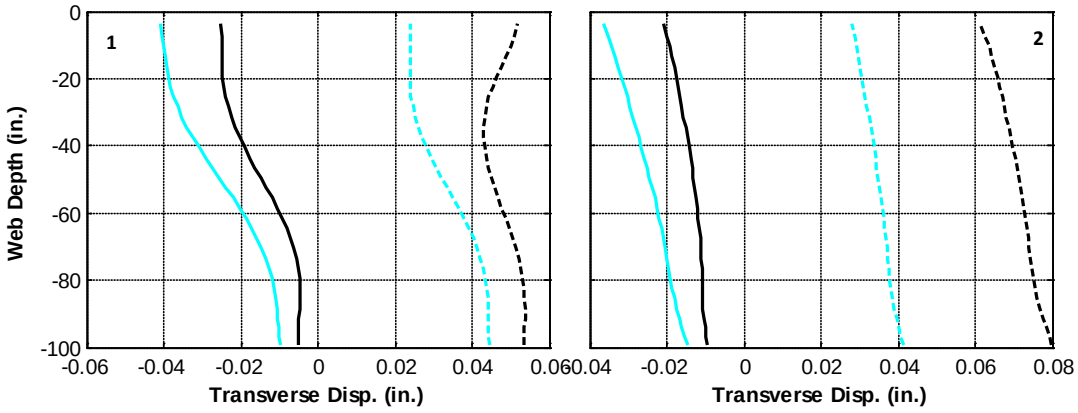


*(c)* Pier 3

**Figure B.57. Web Displacement Profiles at Piers of Girder 1 – Gravity and -45°F Loading**

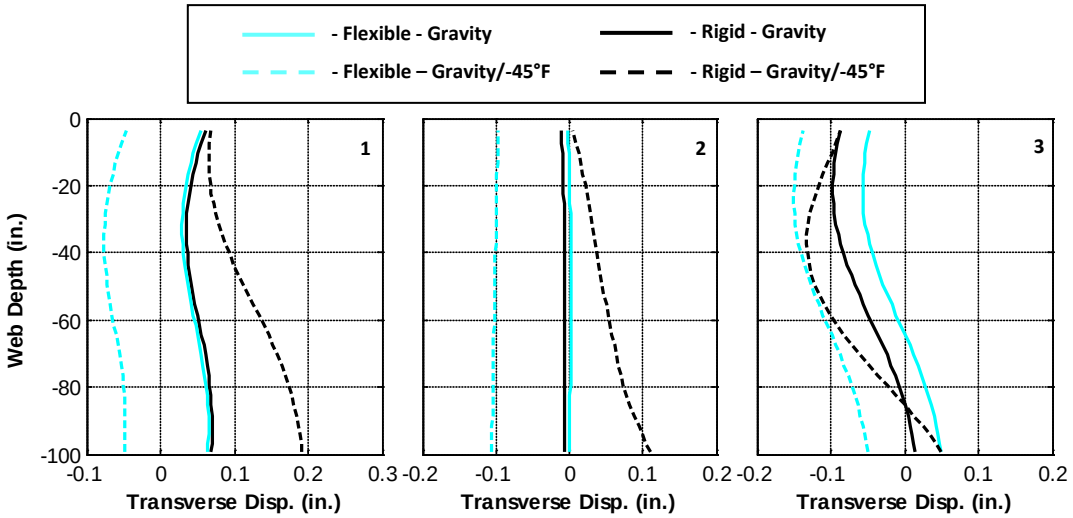


*(a)* Pier 1

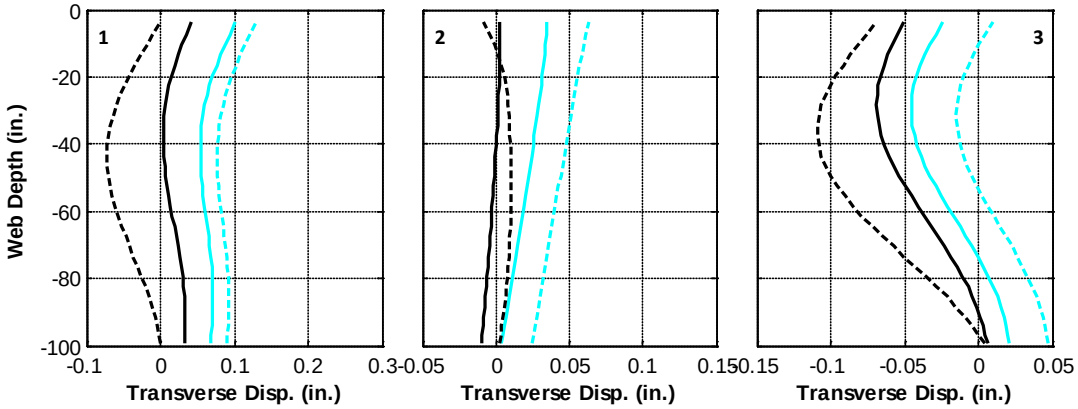


*(b)* Pier 2

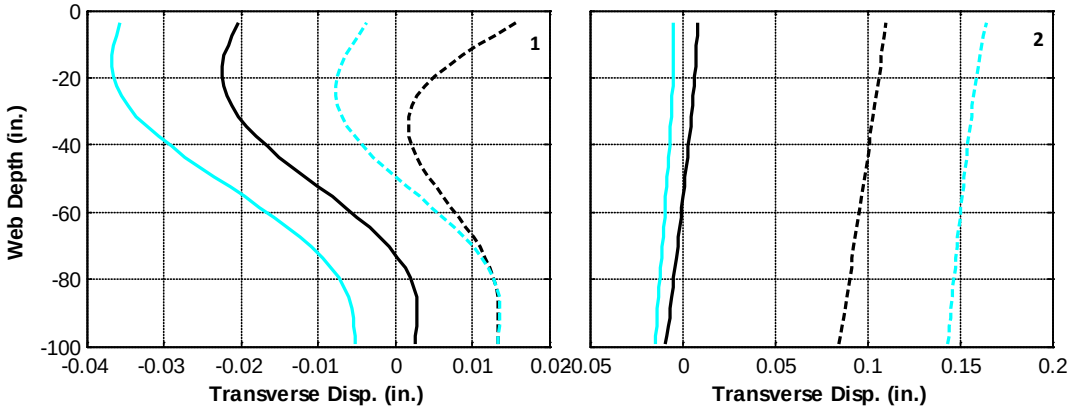


*(c)* Pier 3

**Figure B.58. Web Displacement Profiles at Piers of Girder 2 – Gravity and -45°F Loading**

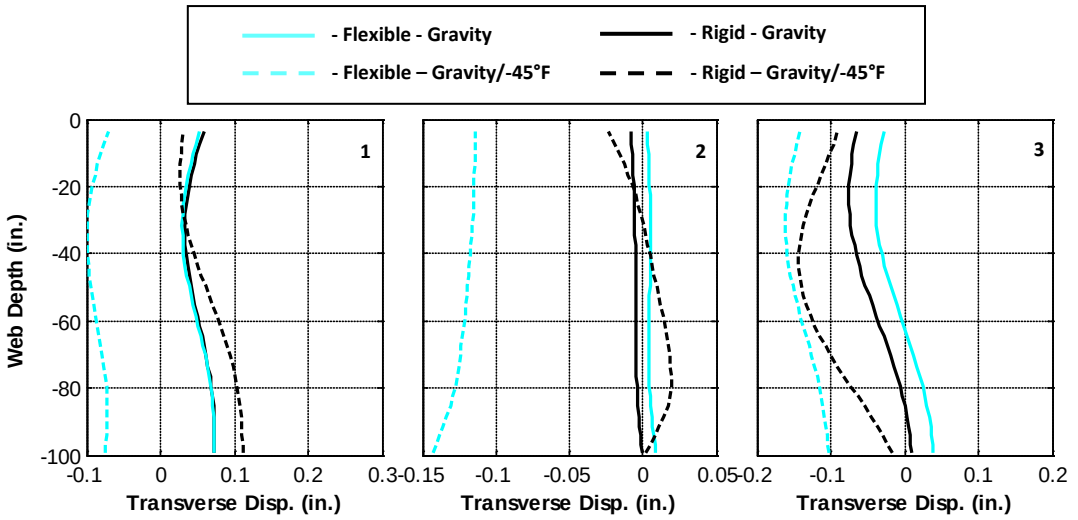


*(a)* Pier 1

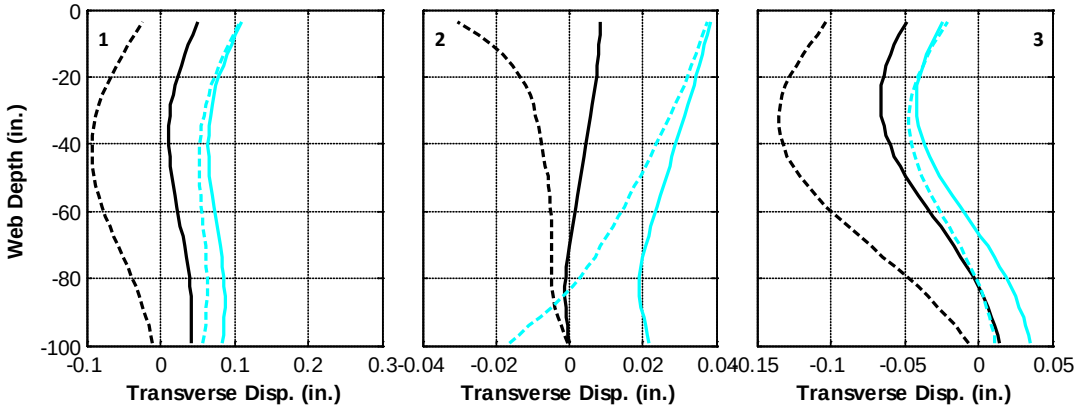


*(b)* Pier 2

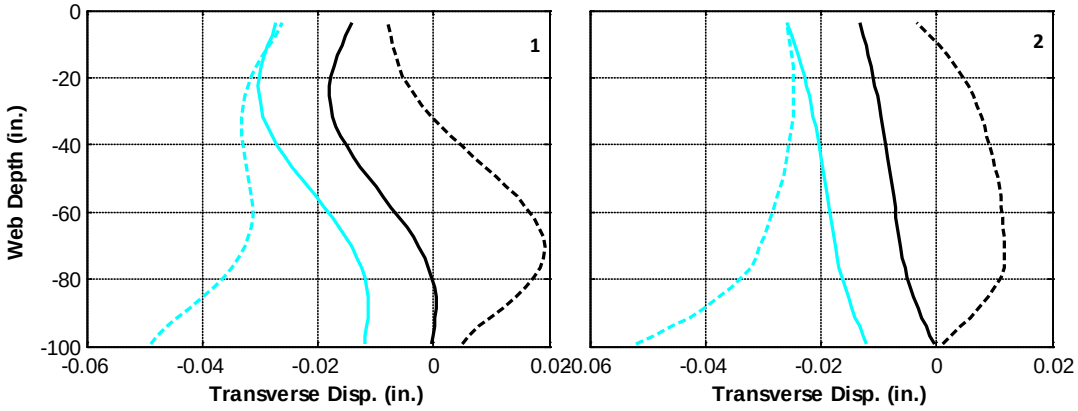


*(c)* Pier 3

**Figure B.59. Web Displacement Profiles at Piers of Girder 3 – Gravity and -45°F Loading**

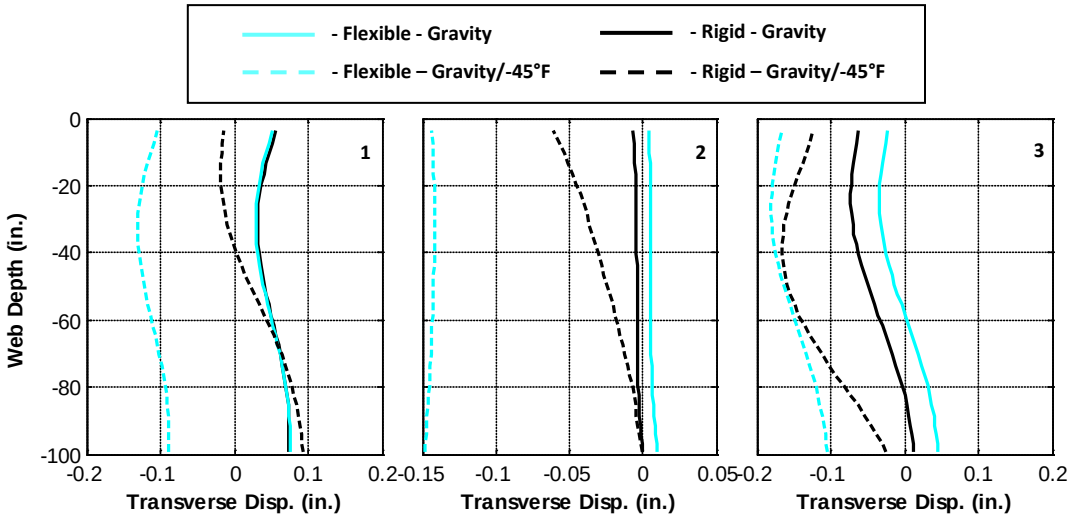


*(a)* Pier 1

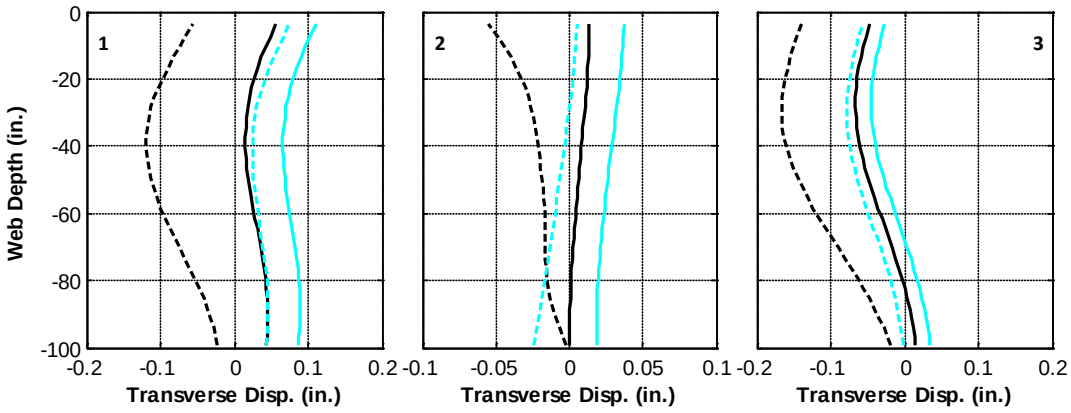


*(b)* Pier 2

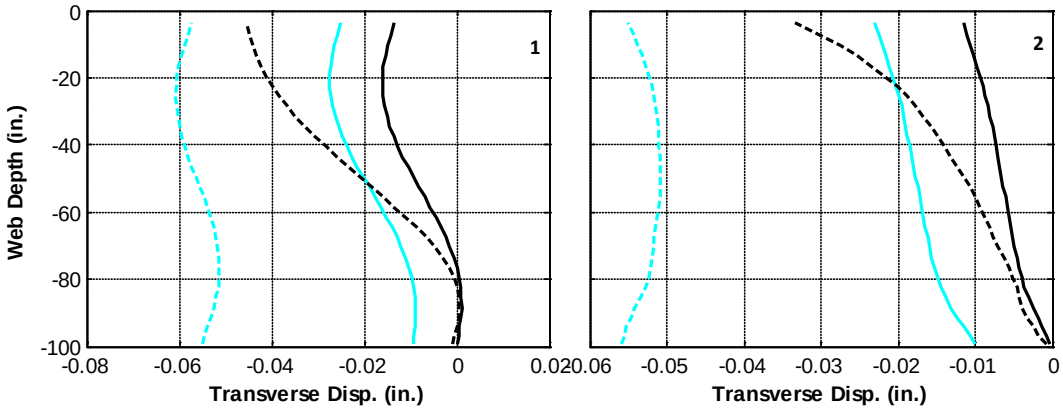


*(c)* Pier 3

**Figure B.60. Web Displacement Profiles at Piers of Girder 4 – Gravity and -45°F Loading**

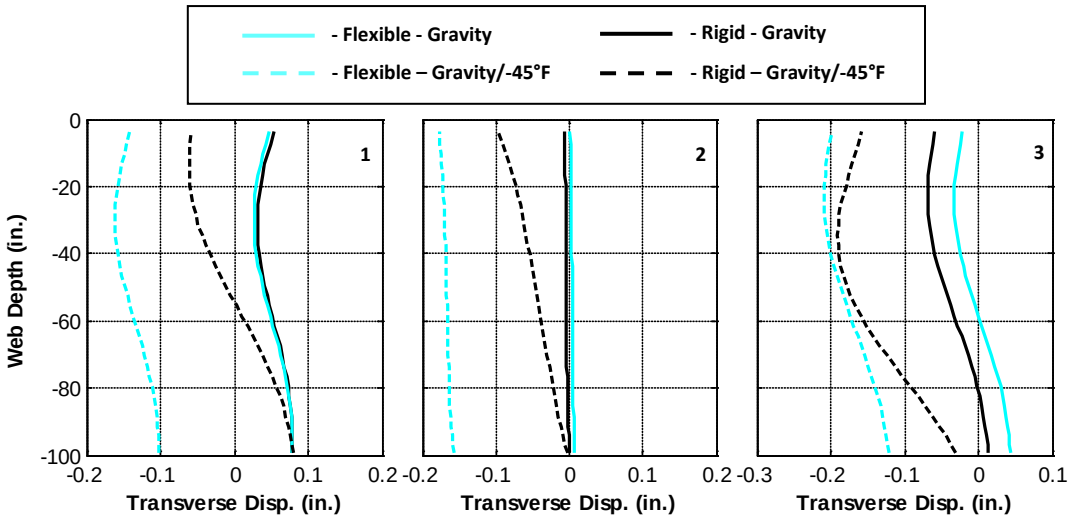


*(a)* Pier 1

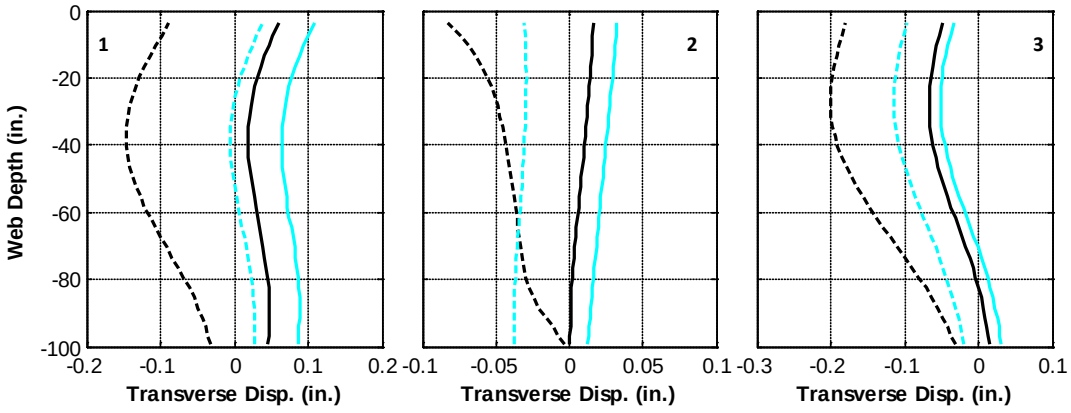


*(b)* Pier 2

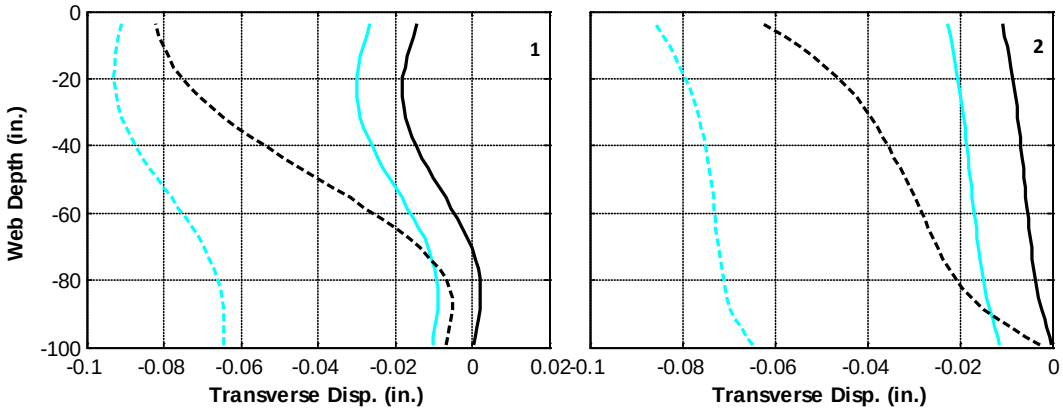


*(c)* Pier 3

**Figure B.61. Web Displacement Profiles at Piers of Girder 5 – Gravity and -45°F Loading**

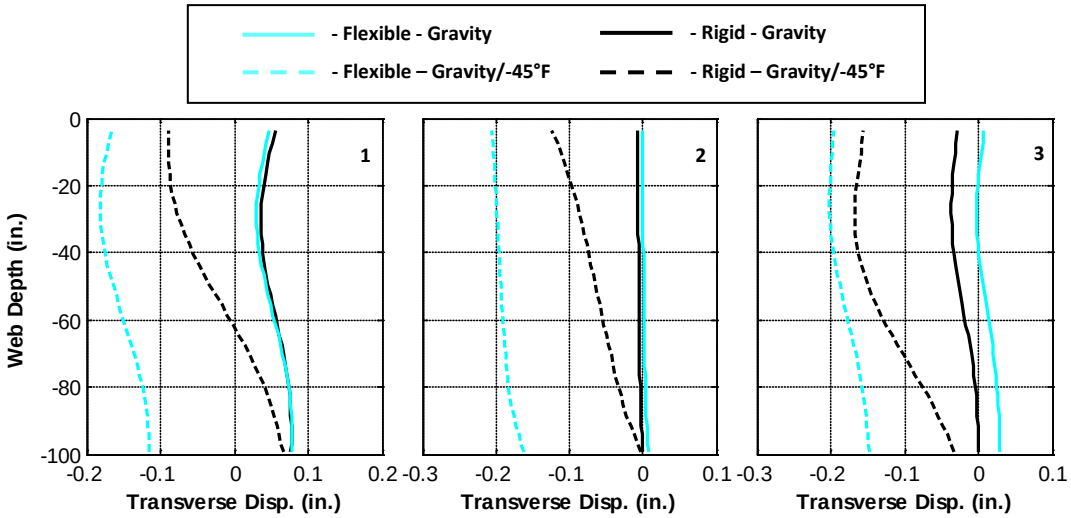


*(a)* Pier 1

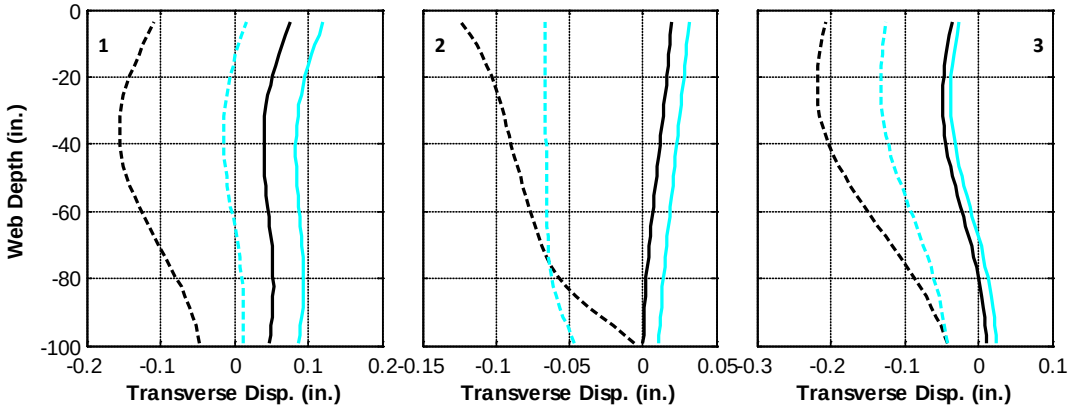


*(b)* Pier 2

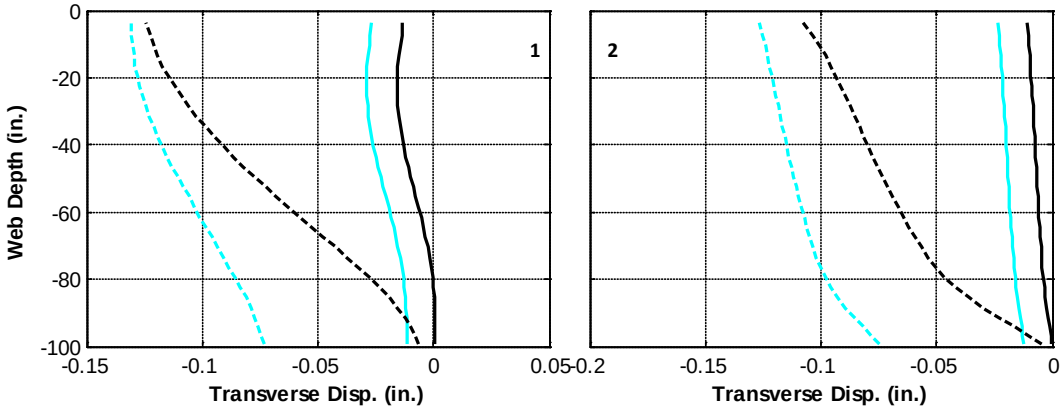


*(c)* Pier 3

**Figure B.62. Web Displacement Profiles at Piers of Girder 6 – Gravity and -45°F Loading**

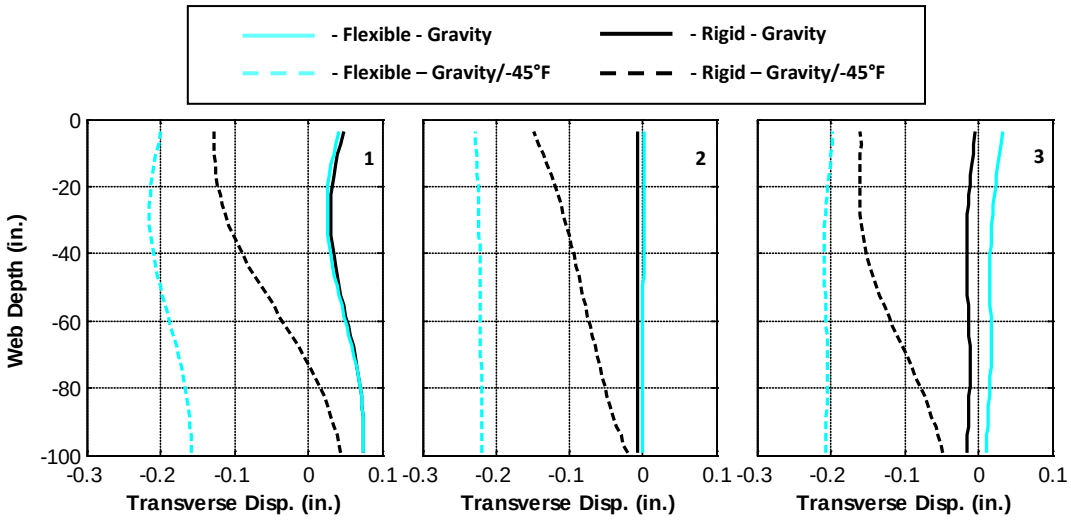


*(a)* Pier 1

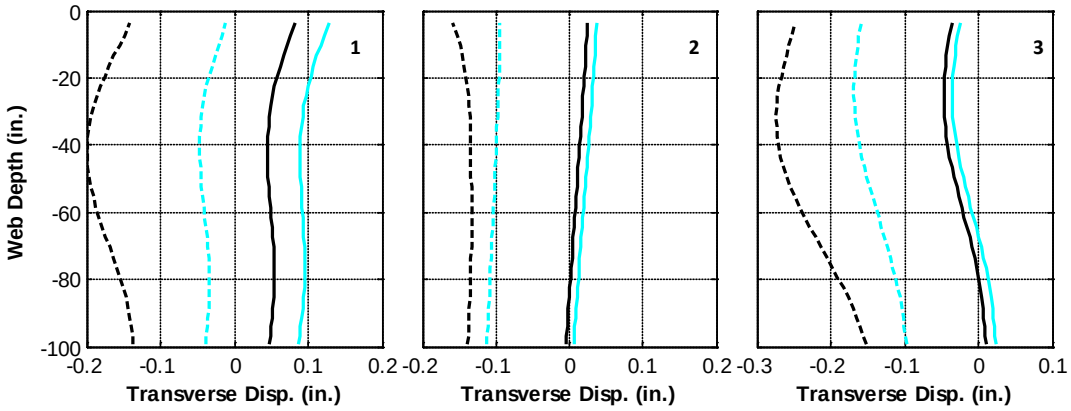


*(b)* Pier 2

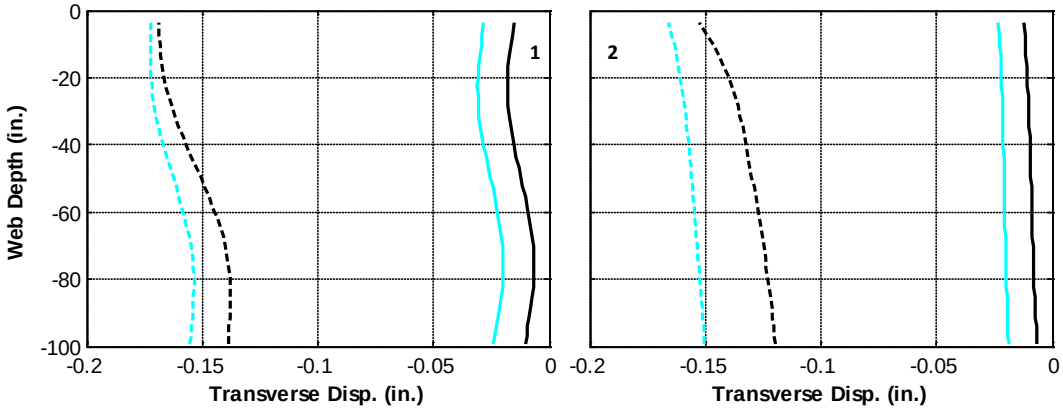


*(c)* Pier 3

**Figure B.63. Web Displacement Profiles at Piers of Girder 7 – Gravity and -45°F Loading**

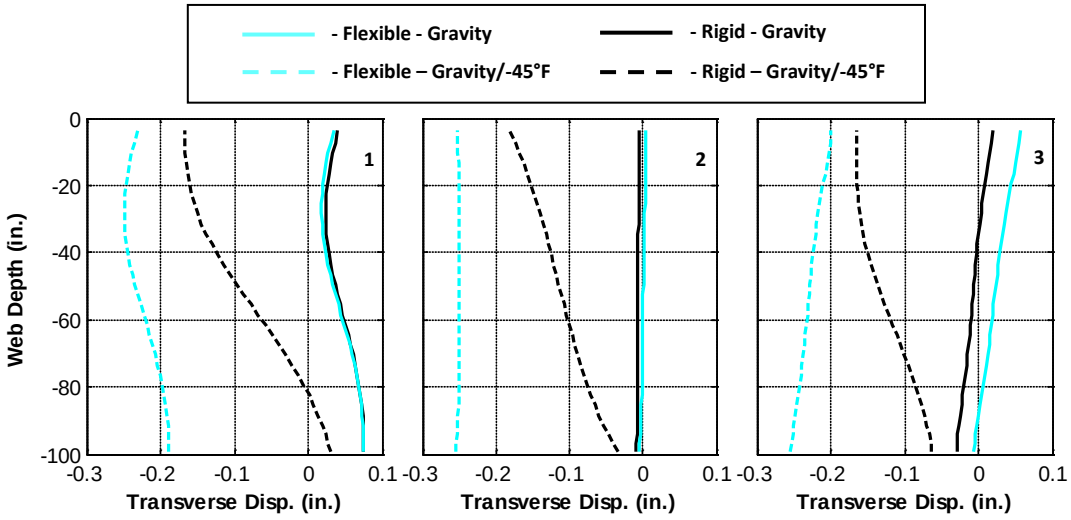


*(a)* Pier 1

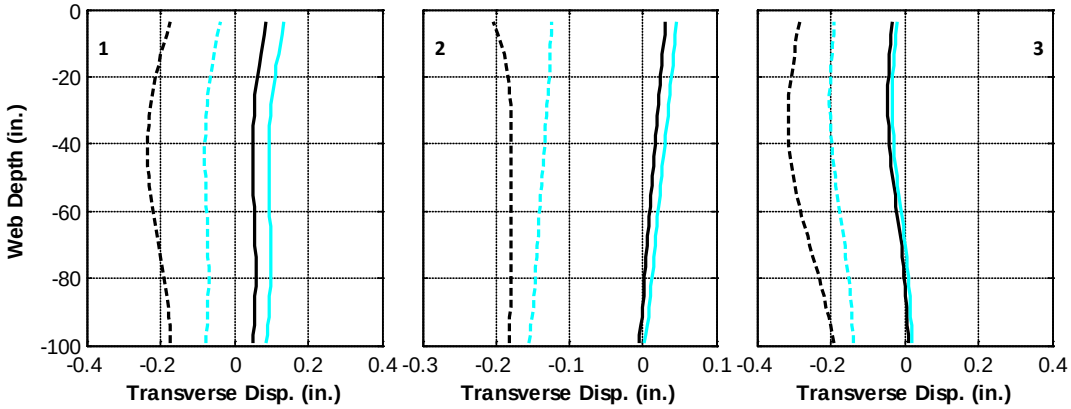


*(b)* Pier 2

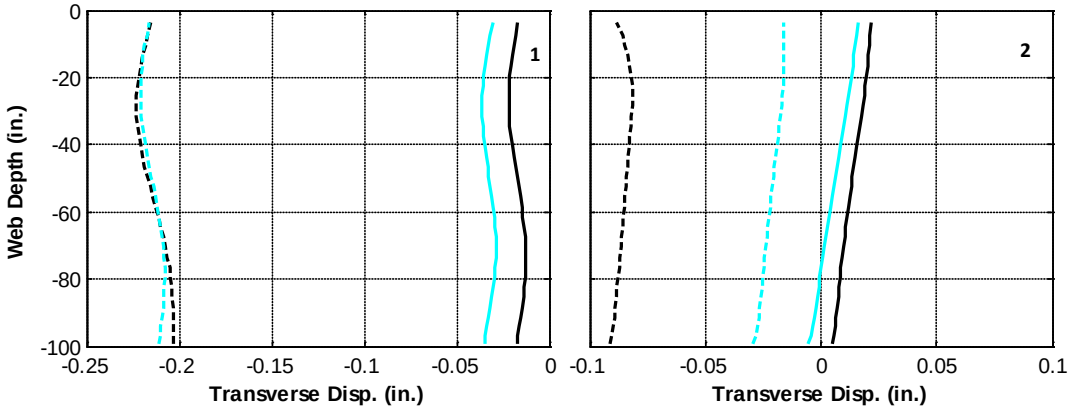


*(c)* Pier 3

**Figure B.64. Web Displacement Profiles at Piers of Girder 8 – Gravity and -45°F Loading**

# Appendix C

## GIRDER STRESS PROFILES UNDER GRAVITY AND THERMAL LOADING

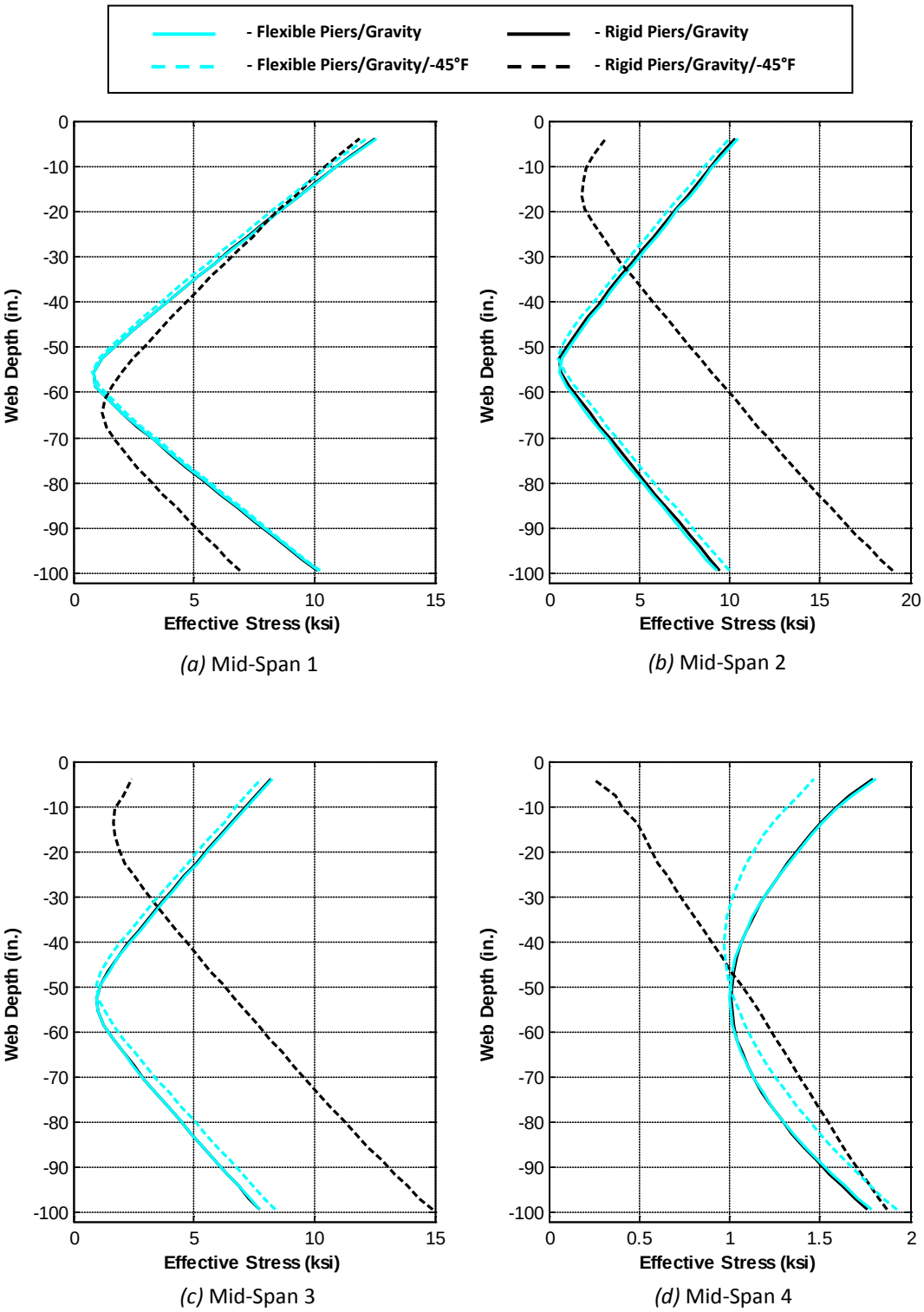


*(a)* Mid-Span 1

*(b)* Mid-Span 2

*(c)* Mid-Span 3

*(d)* Mid-Span 4

**Figure C.1. Girder 1 Mid-Span Web Effective Stress Profiles – Gravity and -45°F Loading**

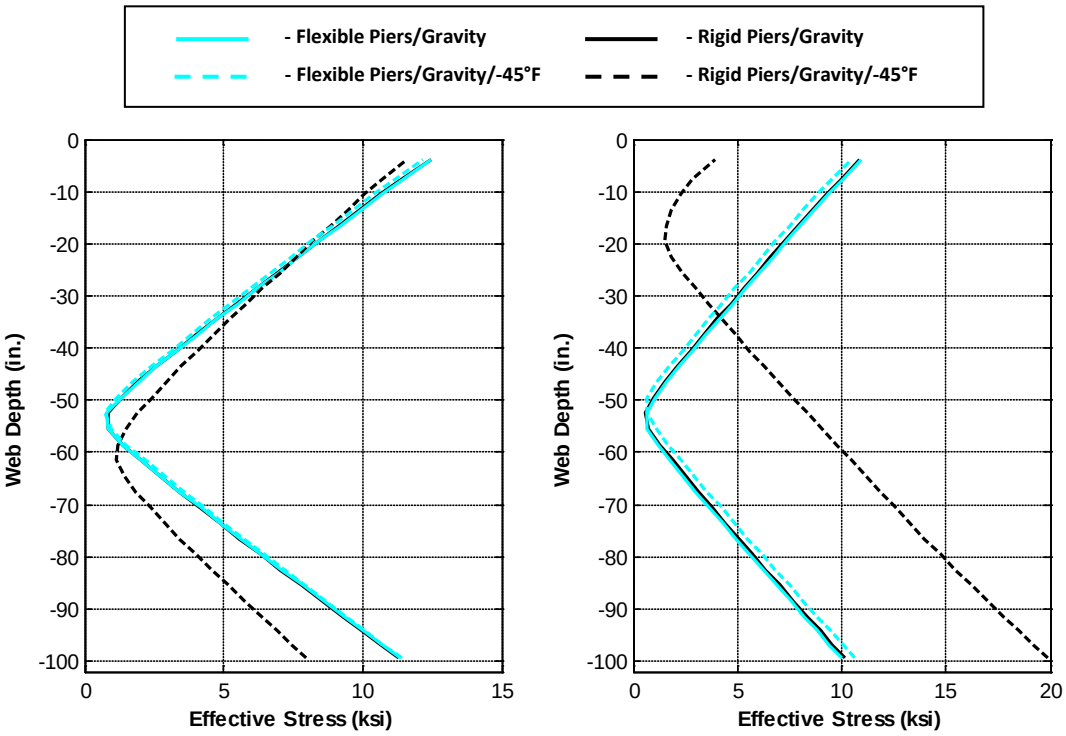


*(a)* Mid-Span 1

*(b)* Mid-Span 2

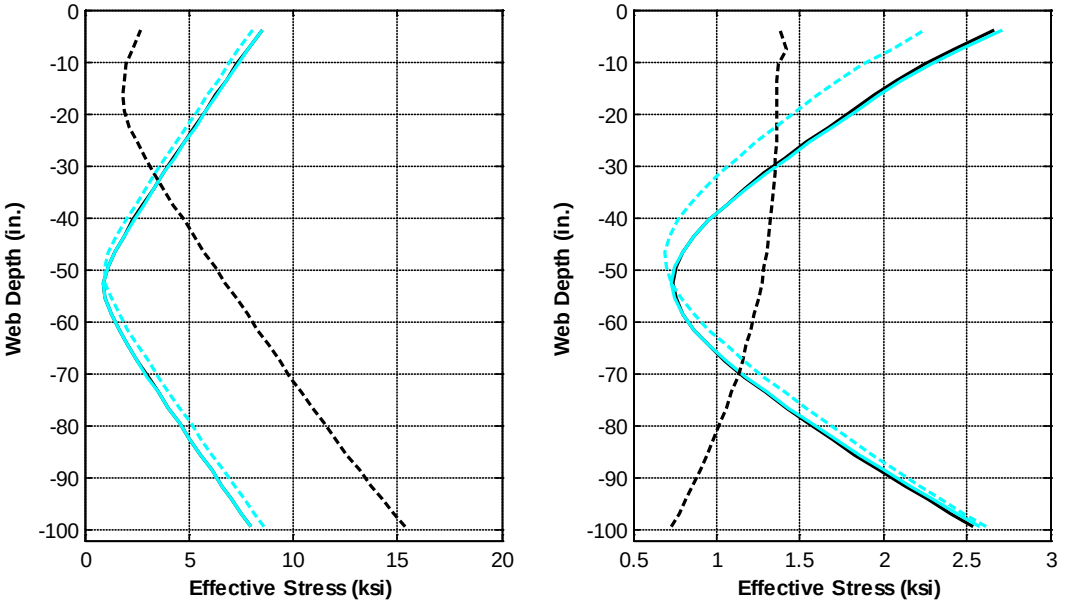


*(c)* Mid-Span 3

*(d)* Mid-Span 4

**Figure C.2. Girder 2 Mid-Span Web Effective Stress Profiles – Gravity and -45°F Loading**

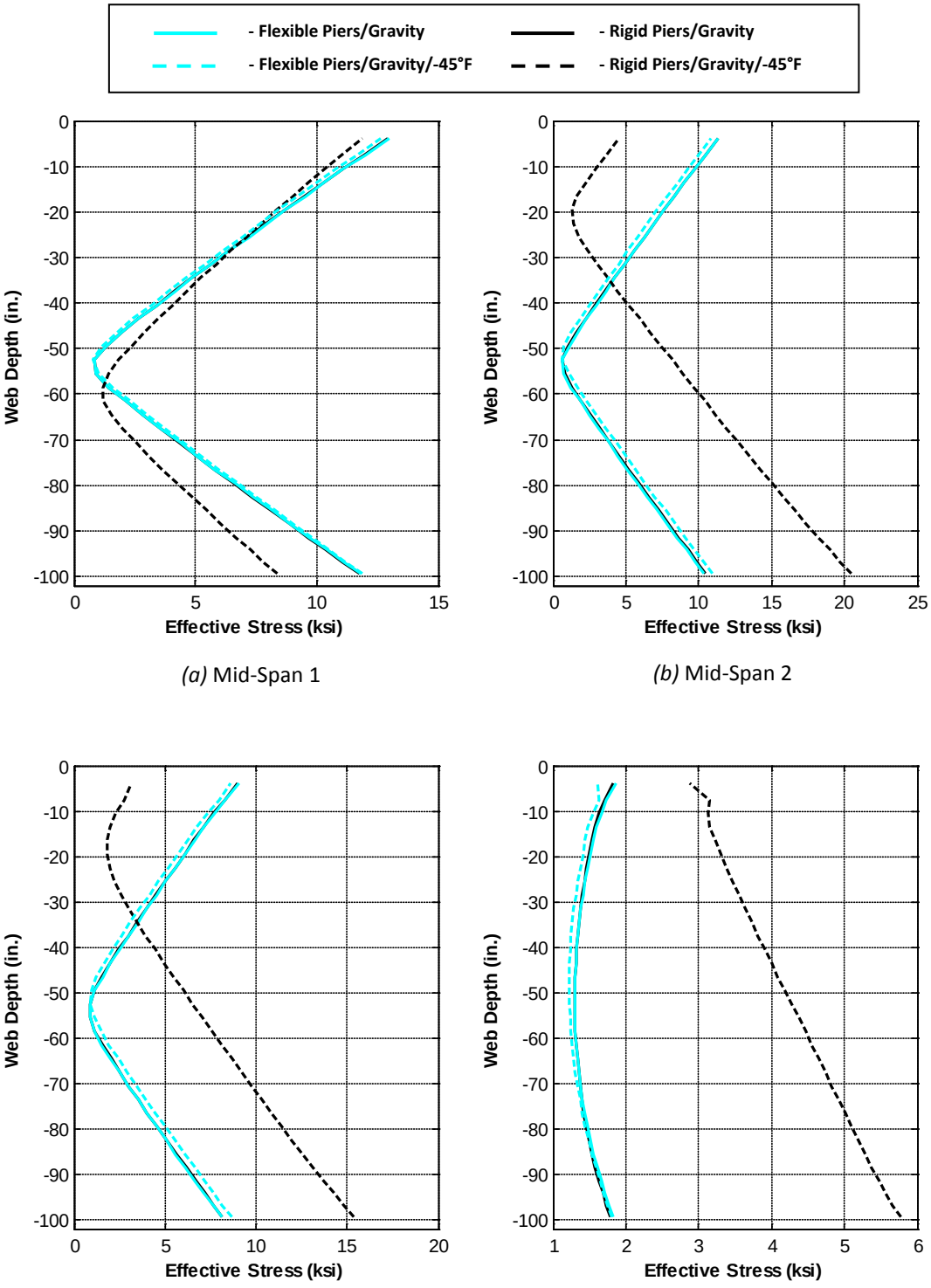


*(a)* Mid-Span 1

*(b)* Mid-Span 2

*(c)* Mid-Span 3

*(d)* Mid-Span 4

**Figure C.3. Girder 3 Mid-Span Web Effective Stress Profiles – Gravity and -45°F Loading**

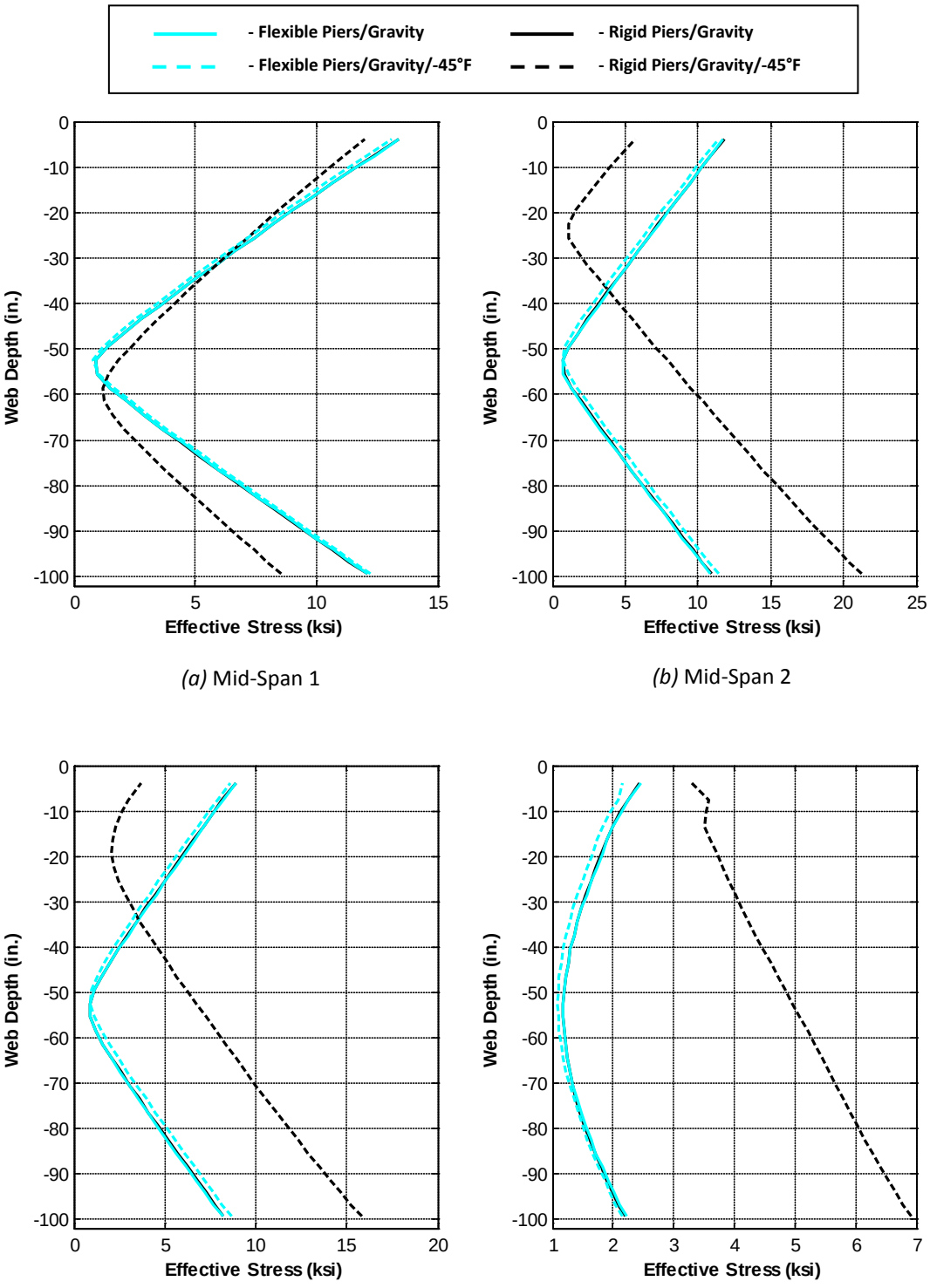


*(a)* Mid-Span 1

*(b)* Mid-Span 2

*(c)* Mid-Span 3

*(d)* Mid-Span 4

**Figure C.4. Girder 4 Mid-Span Web Effective Stress Profiles – Gravity and -45°F Loading**

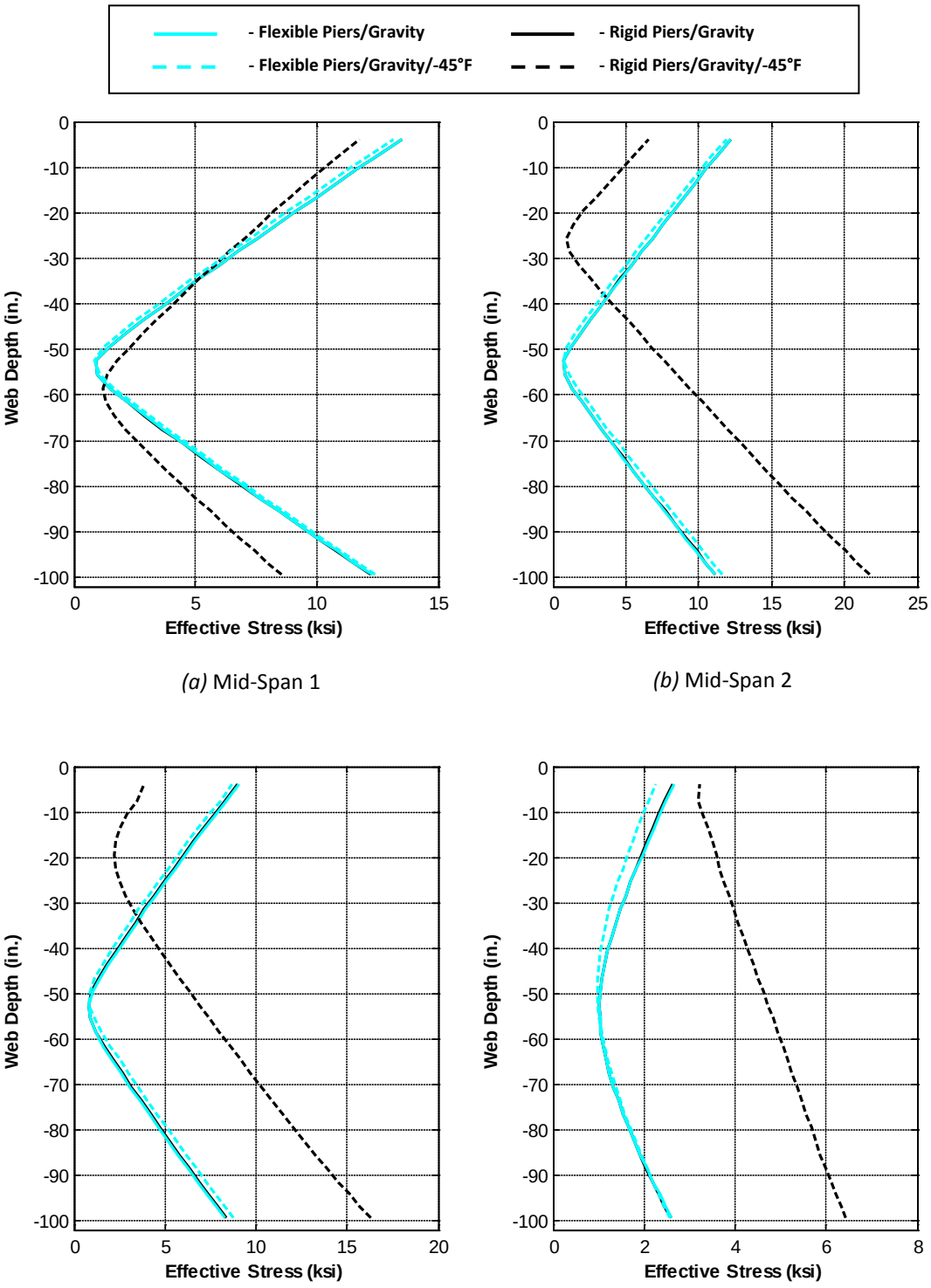


*(a)* Mid-Span 1

*(b)* Mid-Span 2

*(c)* Mid-Span 3

*(d)* Mid-Span 4

**Figure C.5. Girder 5 Mid-Span Web Effective Stress Profiles – Gravity and -45°F Loading**

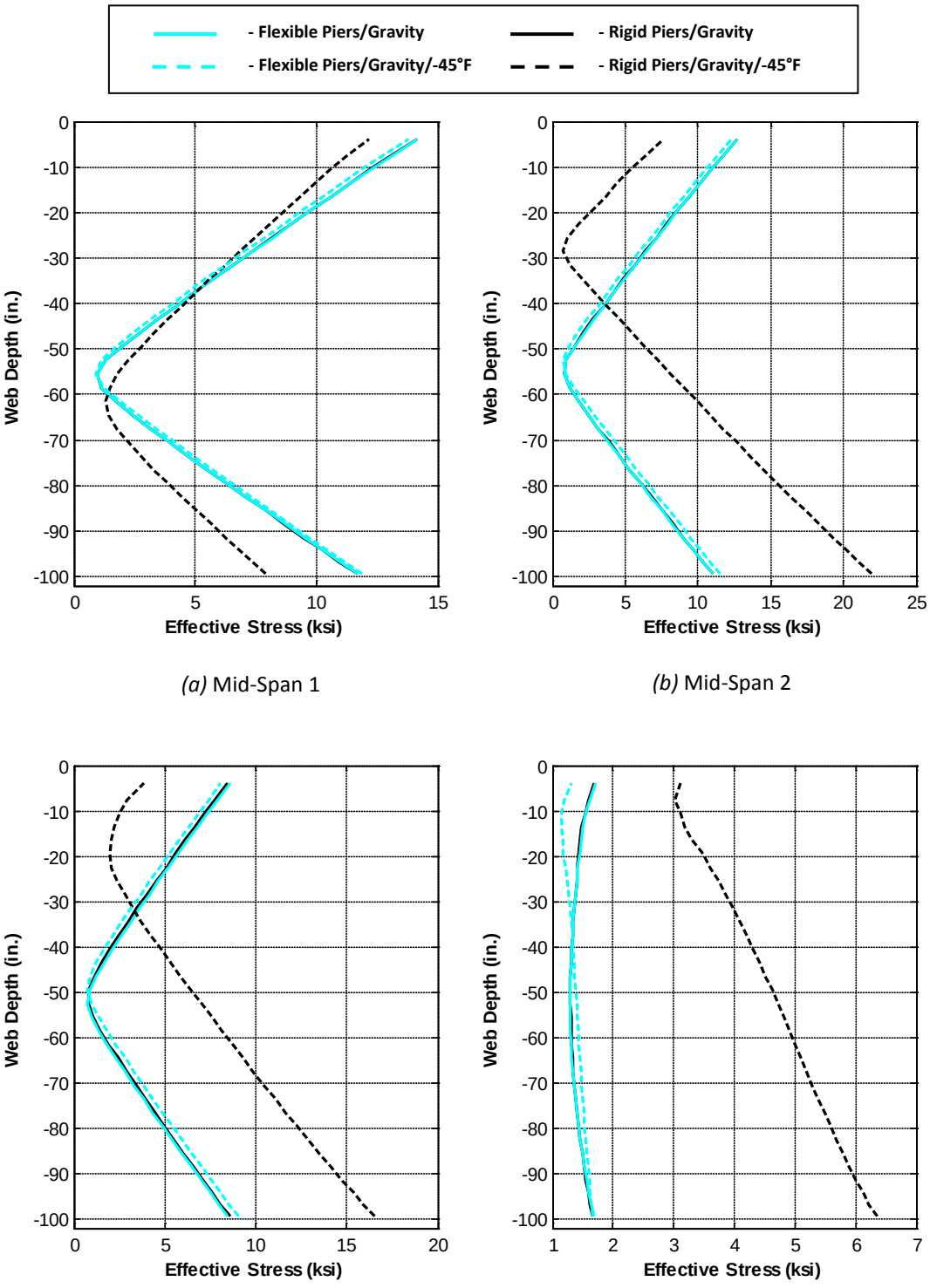


*(a)* Mid-Span 1

*(b)* Mid-Span 2

*(c)* Mid-Span 3

*(d)* Mid-Span 4

**Figure C.6. Girder 6 Mid-Span Web Effective Stress Profiles – Gravity and -45°F Loading**

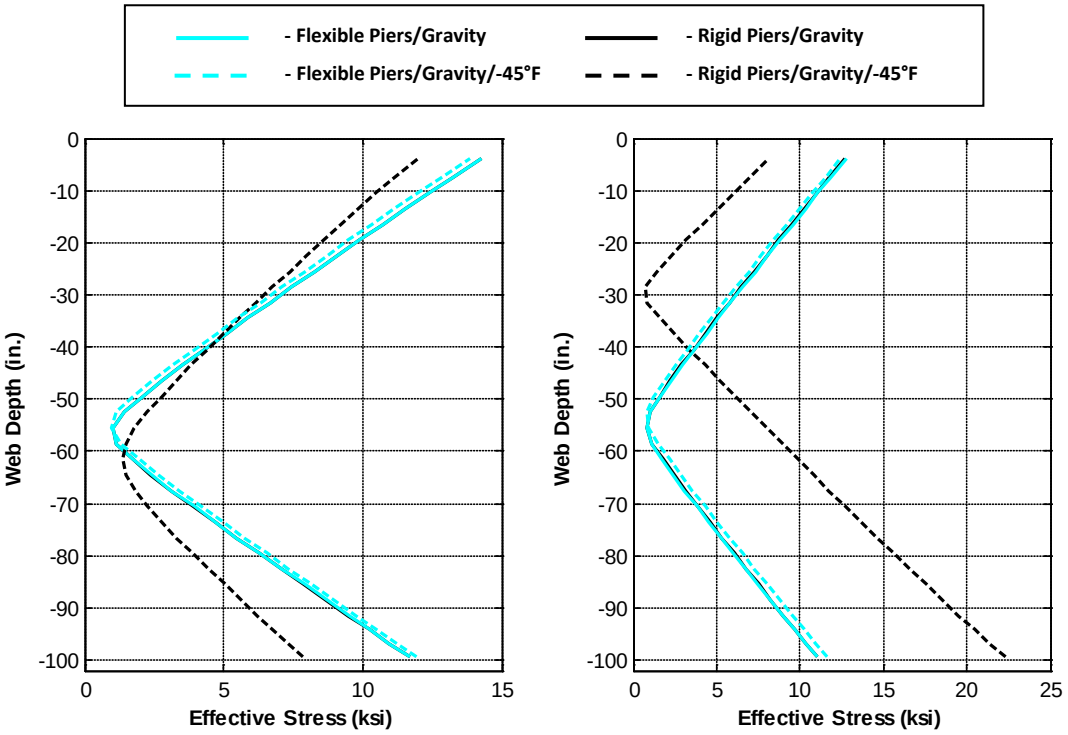


*(a)* Mid-Span 1

*(b)* Mid-Span 2

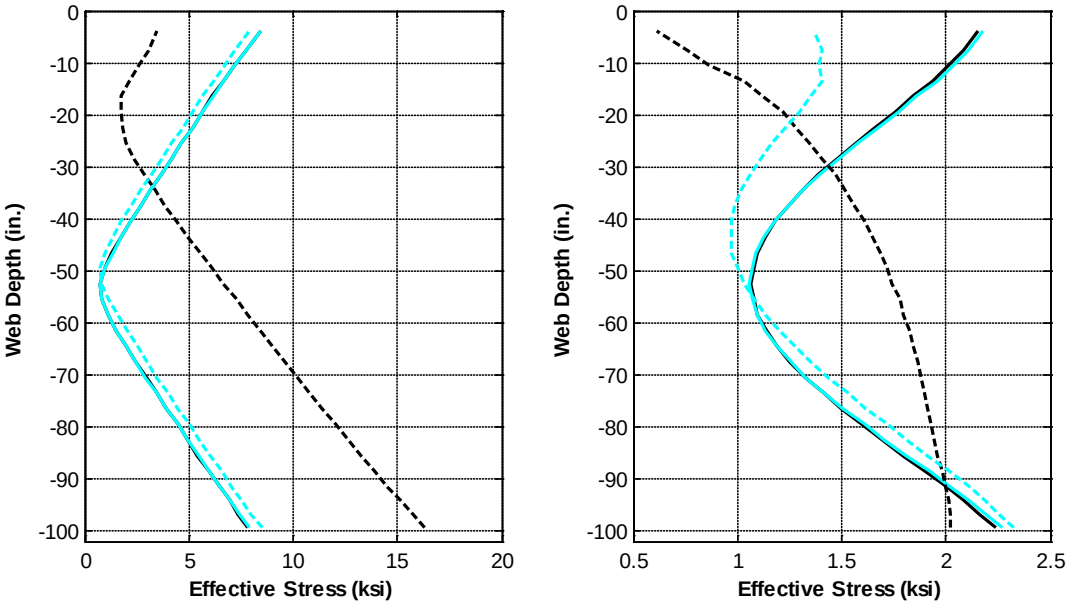


*(c)* Mid-Span 3

*(d)* Mid-Span 4

**Figure C.7. Girder 7 Mid-Span Web Effective Stress Profiles – Gravity and -45°F Loading**

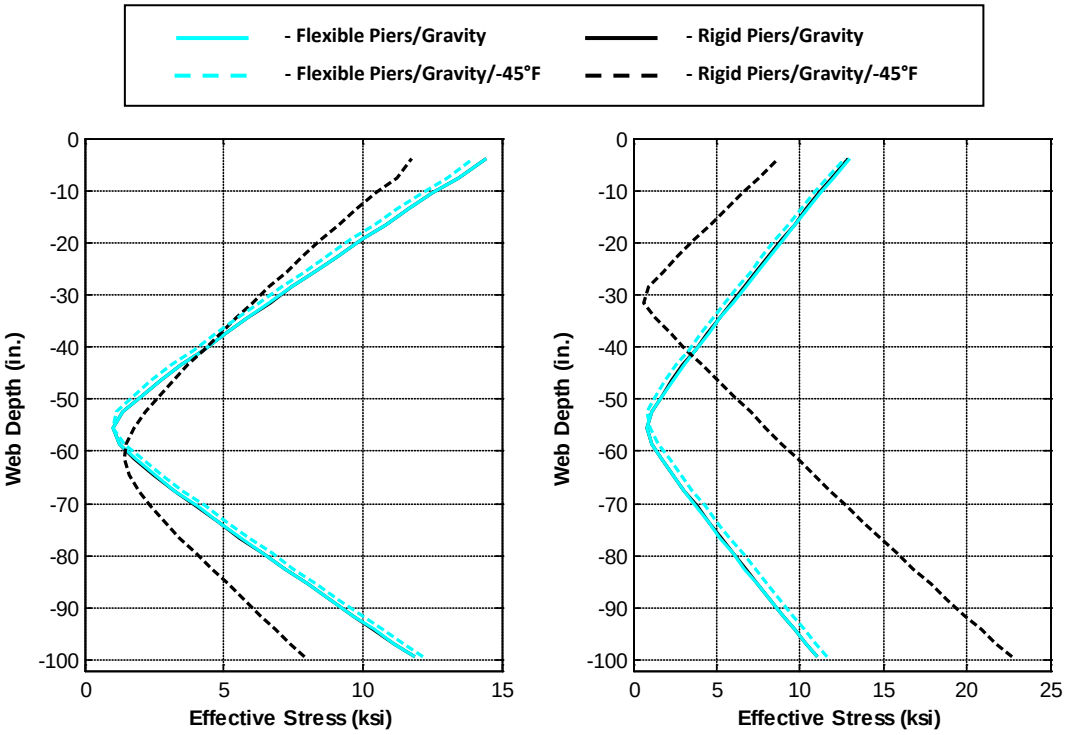


*(a)* Mid-Span 1

*(b)* Mid-Span 2

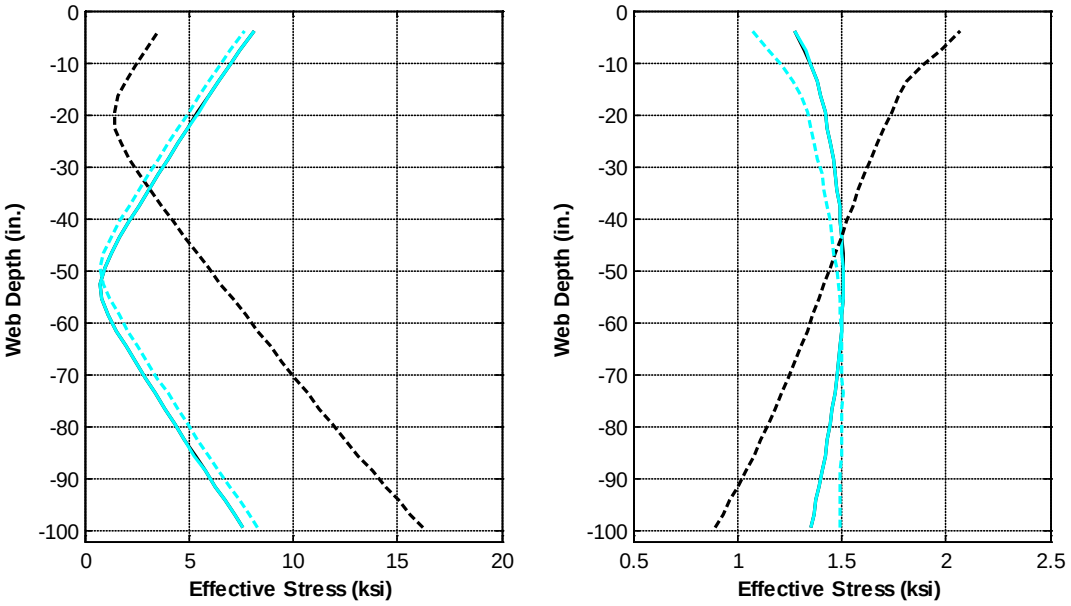


*(c)* Mid-Span 3

*(d)* Mid-Span 4

**Figure C.8. Girder 8 Mid-Span Web Effective Stress Profiles – Gravity and -45°F Loading**

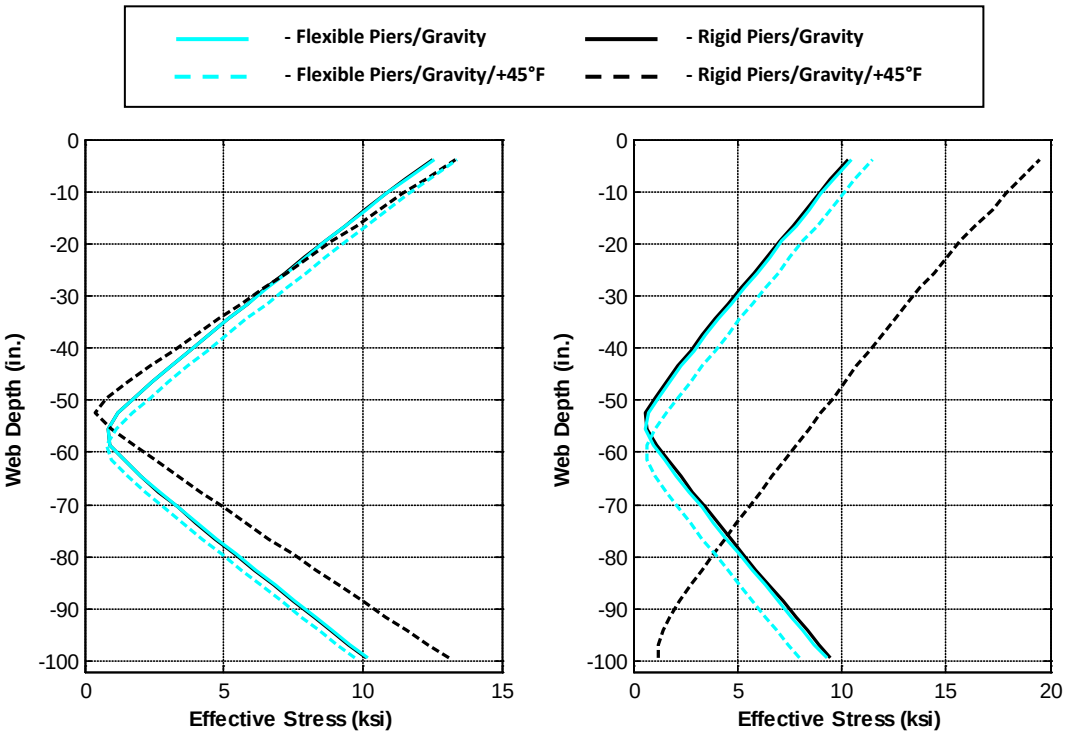


*(a)* Mid-Span 1

*(b)* Mid-Span 2

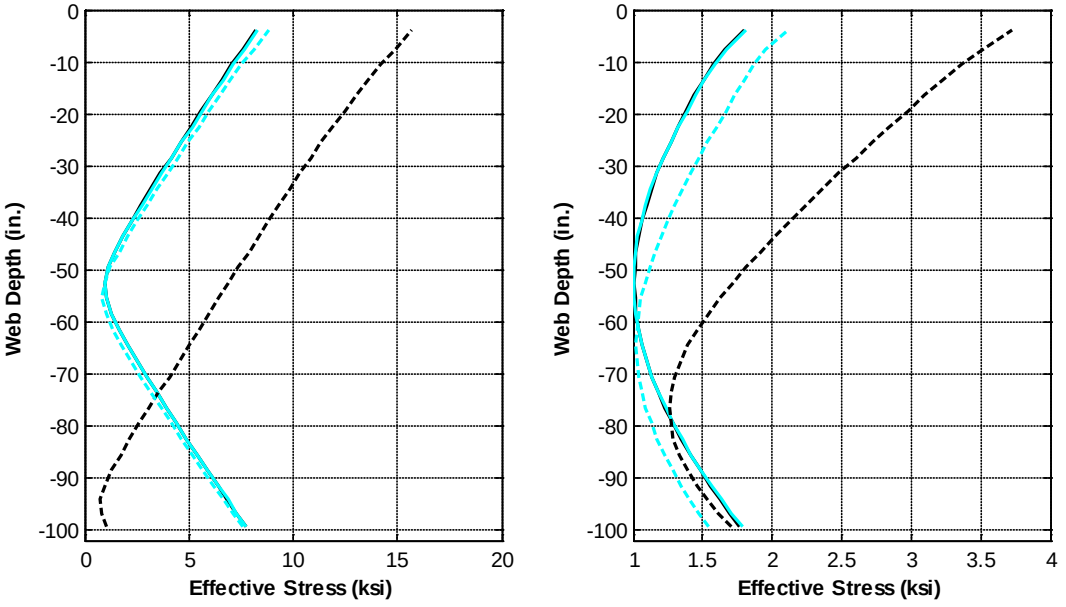


*(c)* Mid-Span 3

*(d)* Mid-Span 4

**Figure C.9. Girder 1 Mid-Span Web Effective Stress Profiles – Gravity and +45°F Loading**

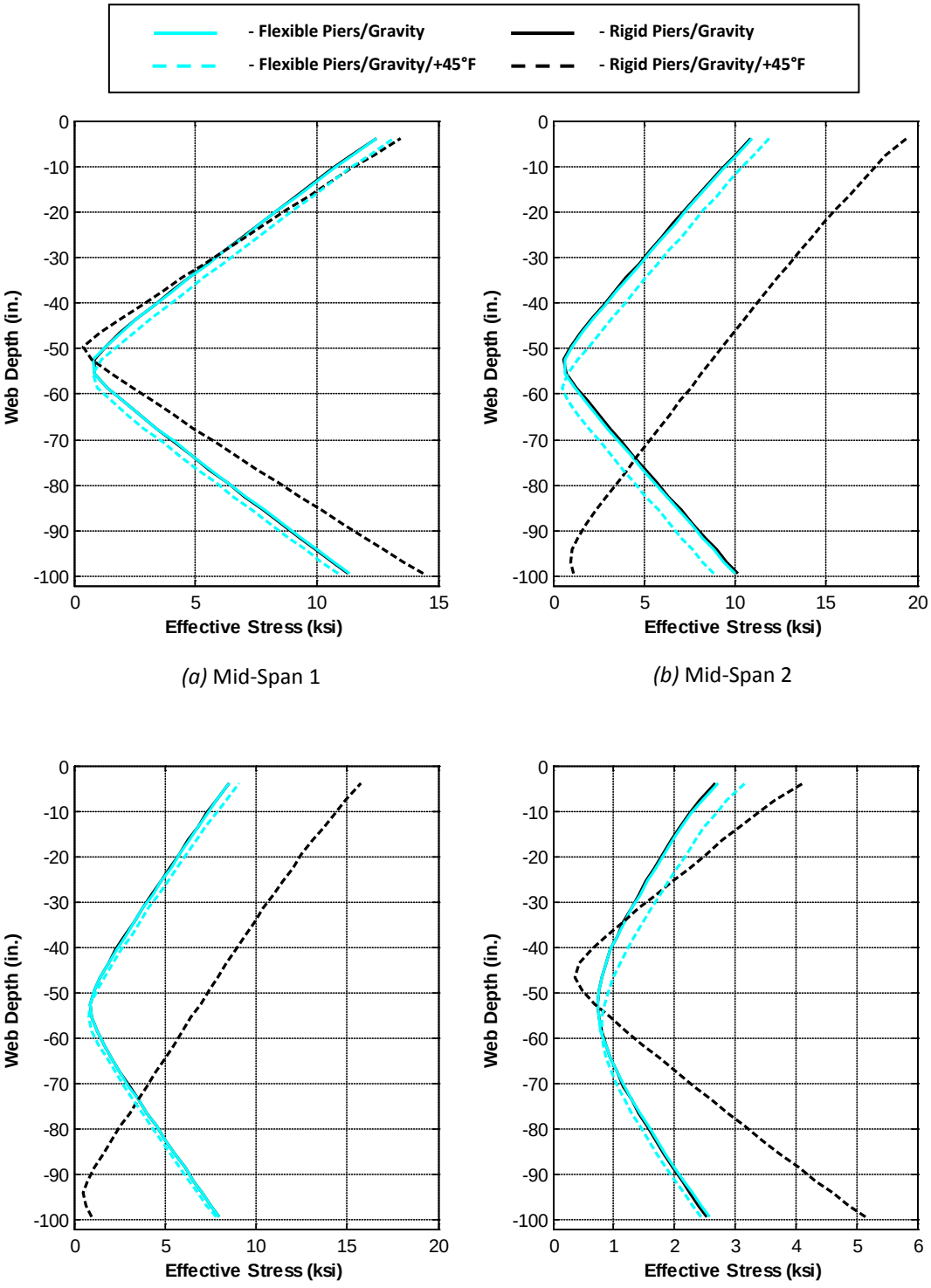


*(a)* Mid-Span 1

*(b)* Mid-Span 2

*(c)* Mid-Span 3

*(d)* Mid-Span 4

**Figure C.10. Girder 2 Mid-Span Web Effective Stress Profiles – Gravity and +45°F Loading**

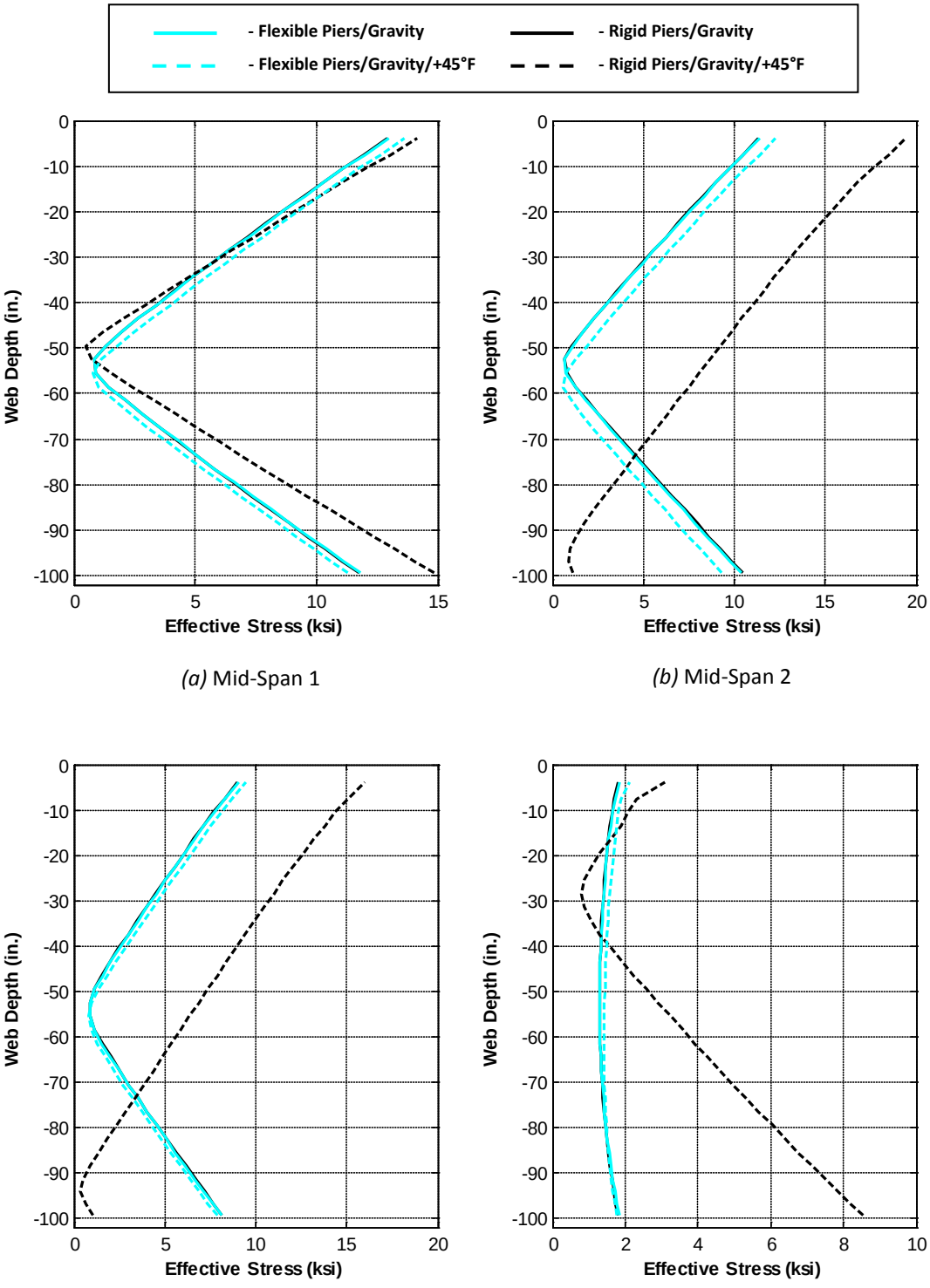


*(a)* Mid-Span 1

*(b)* Mid-Span 2

*(c)* Mid-Span 3

*(d)* Mid-Span 4

**Figure C.11. Girder 3 Mid-Span Web Effective Stress Profiles – Gravity and +45°F Loading**

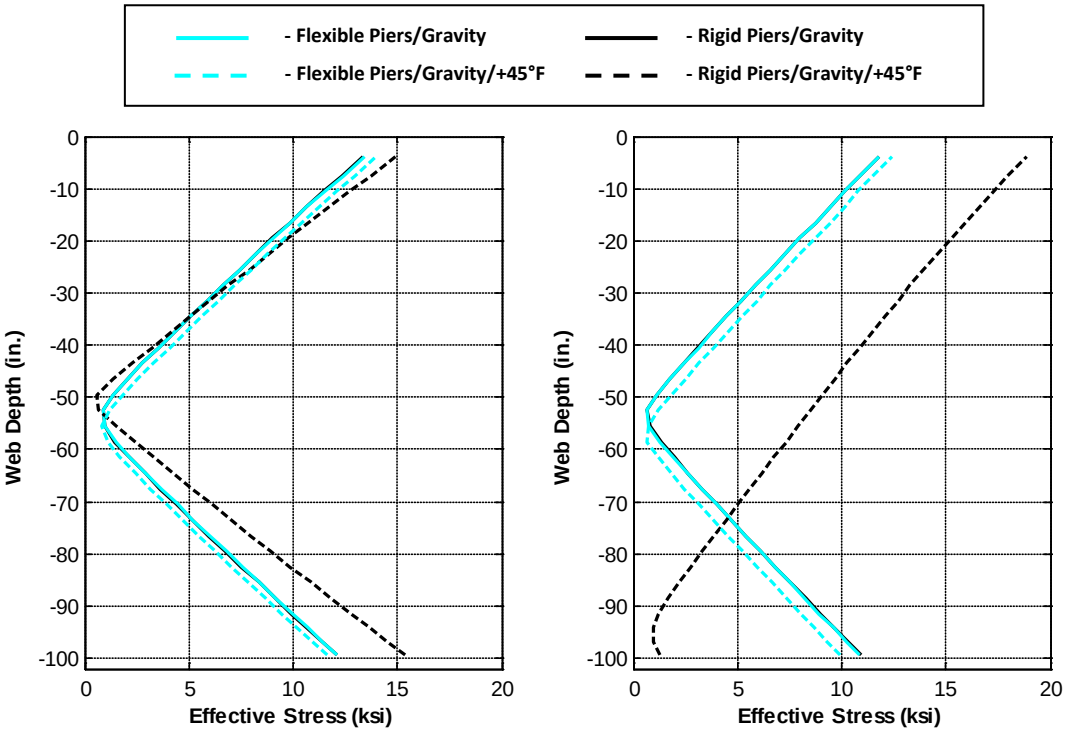


*(a)* Mid-Span 1

*(b)* Mid-Span 2

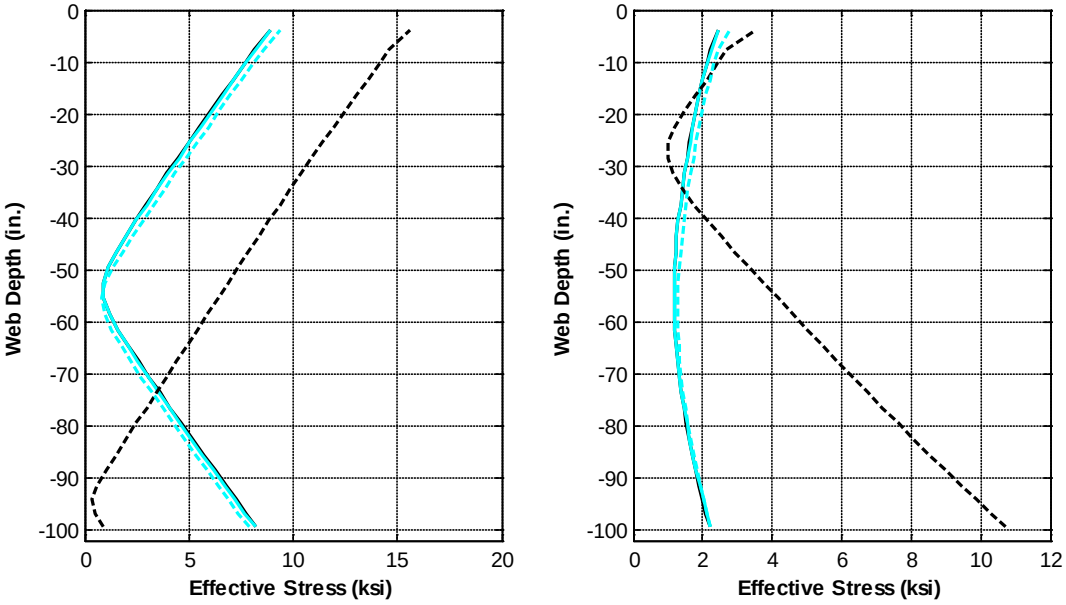


*(c)* Mid-Span 3

*(d)* Mid-Span 4

**Figure C.12. Girder 4 Mid-Span Web Effective Stress Profiles – Gravity and +45°F Loading**

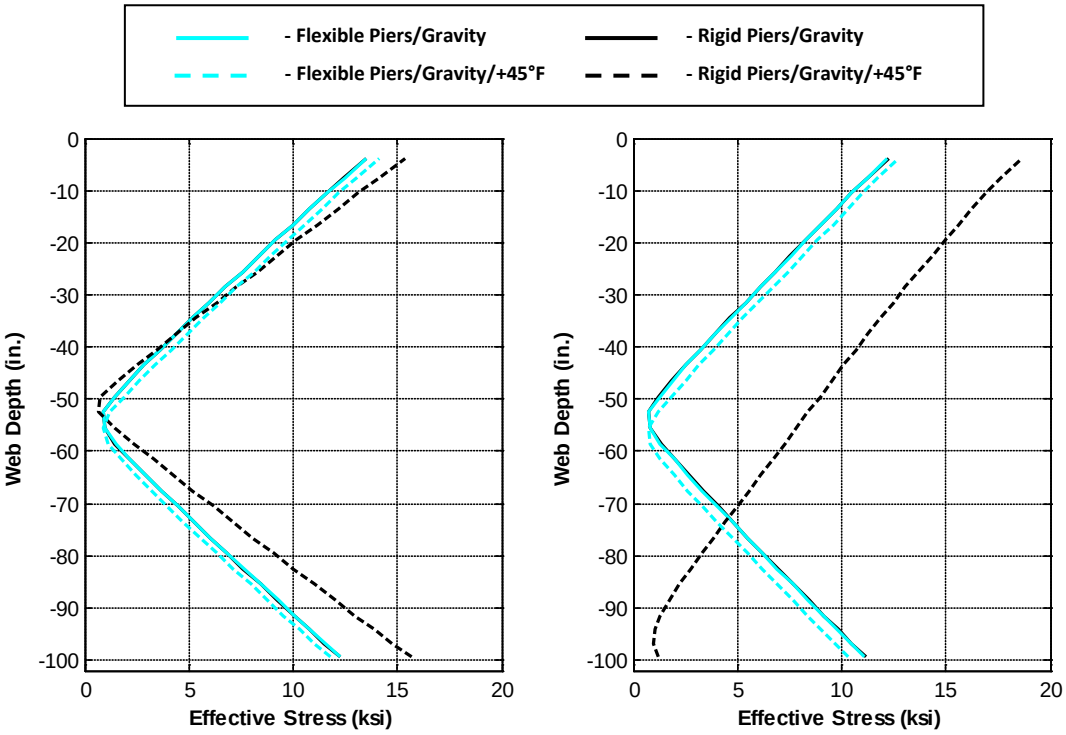


*(a)* Mid-Span 1

*(b)* Mid-Span 2

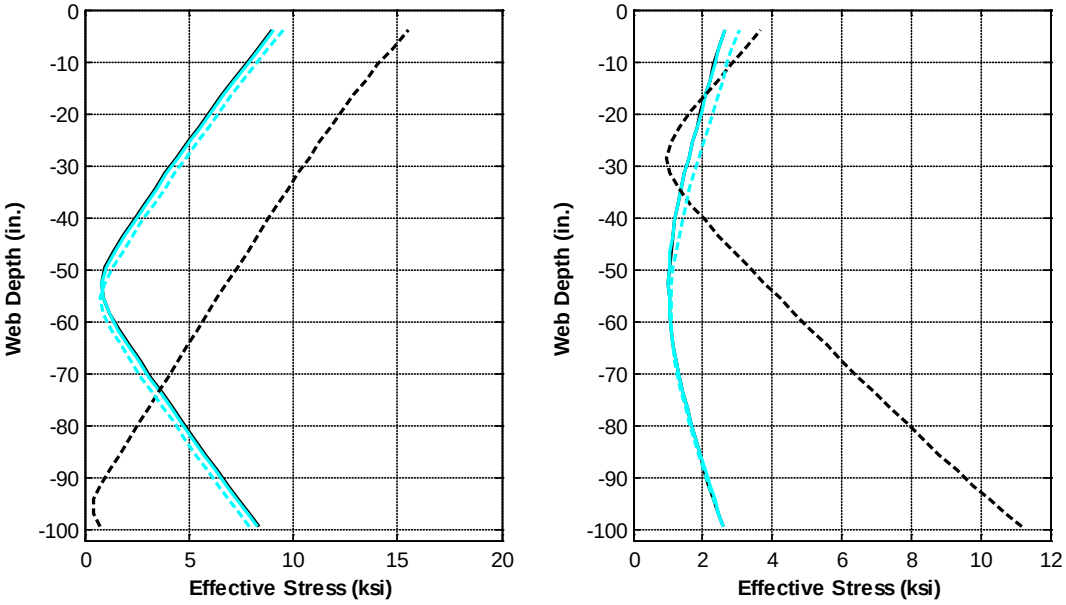


*(c)* Mid-Span 3

*(d)* Mid-Span 4

**Figure C.13. Girder 5 Mid-Span Web Effective Stress Profiles – Gravity and +45°F Loading**

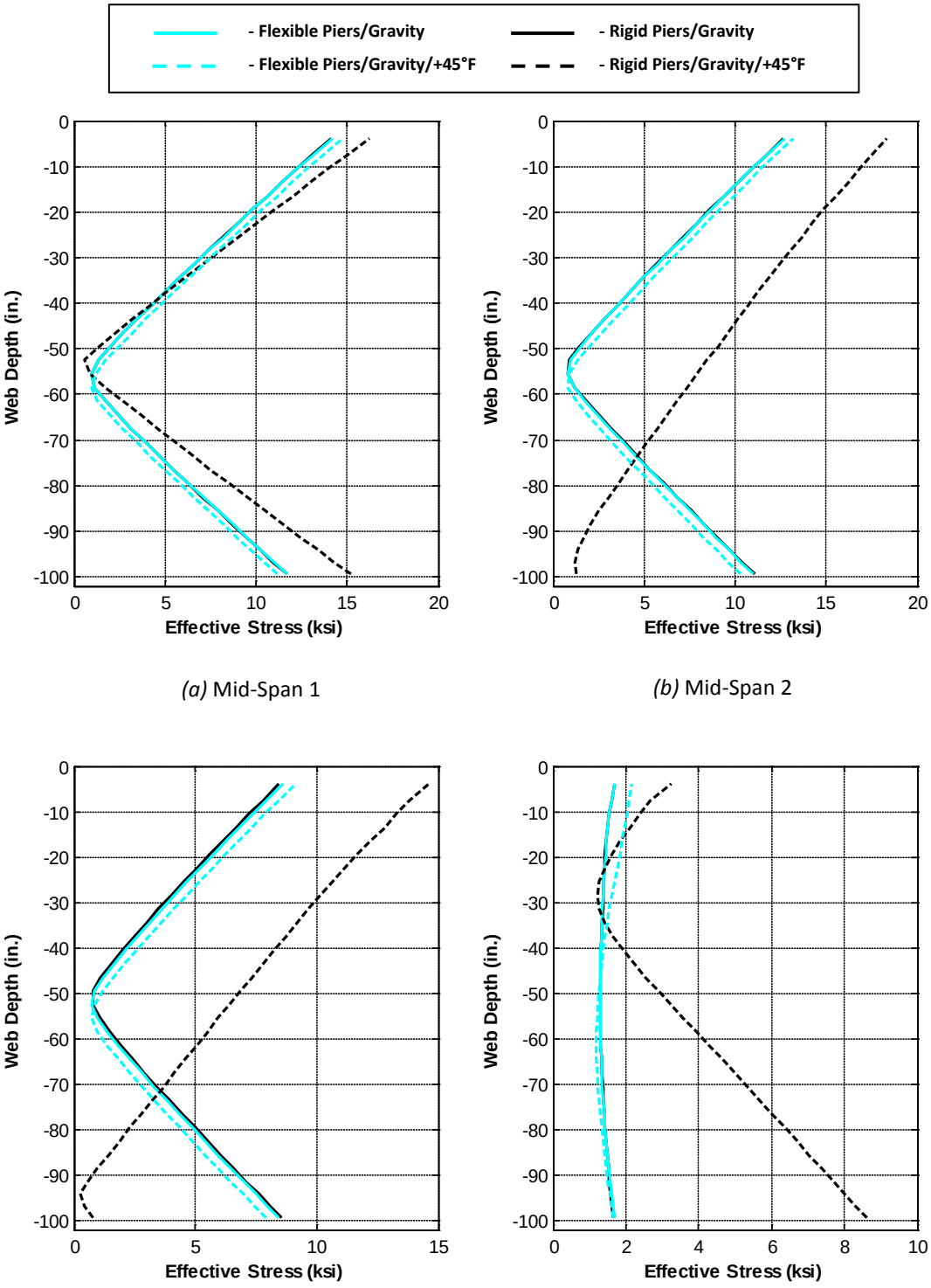


*(a)* Mid-Span 1

*(b)* Mid-Span 2

*(c)* Mid-Span 3

*(d)* Mid-Span 4

**Figure C.14. Girder 6 Mid-Span Web Effective Stress Profiles – Gravity and +45°F Loading**

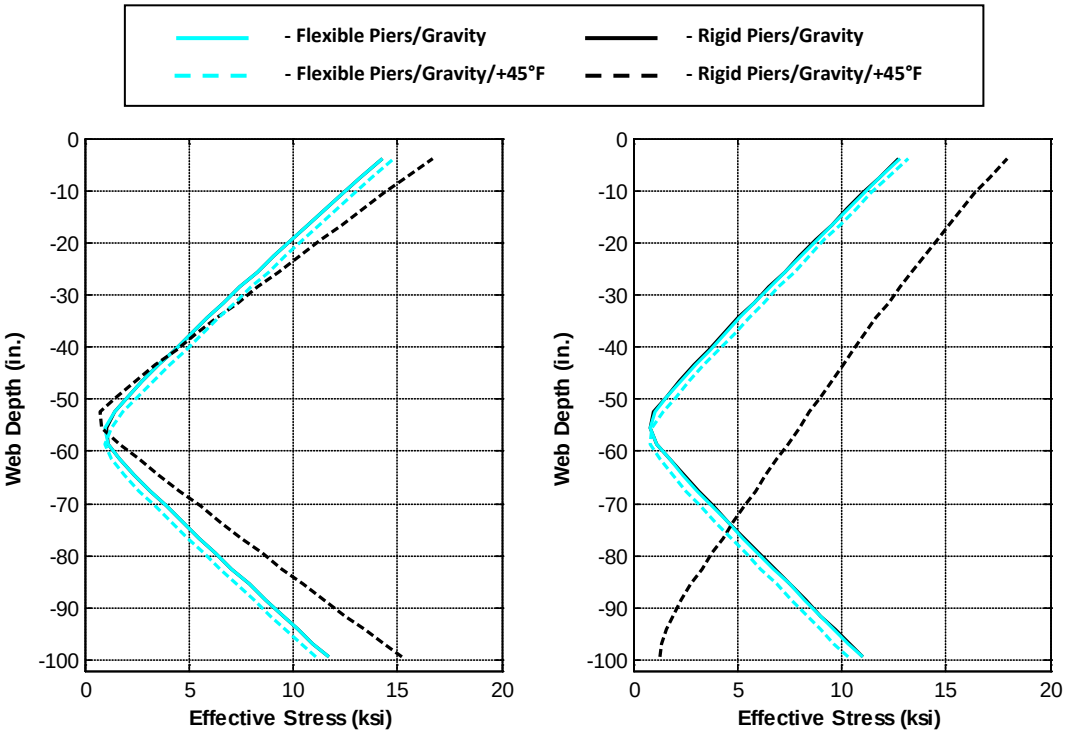


*(a)* Mid-Span 1

*(b)* Mid-Span 2

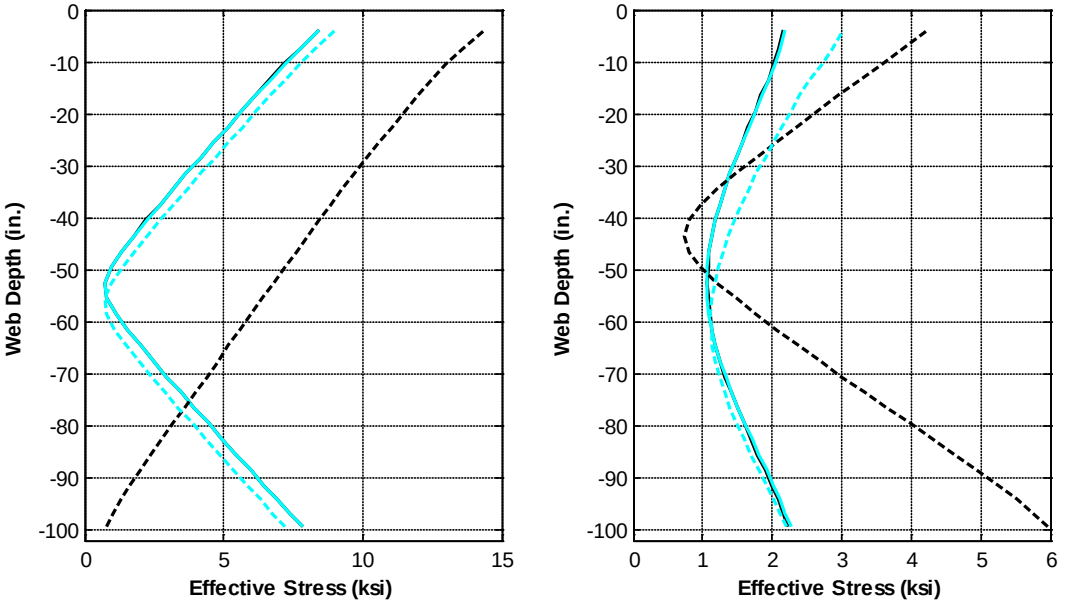


*(c)* Mid-Span 3

*(d)* Mid-Span 4

**Figure C.15. Girder 7 Mid-Span Web Effective Stress Profiles – Gravity and +45°F Loading**

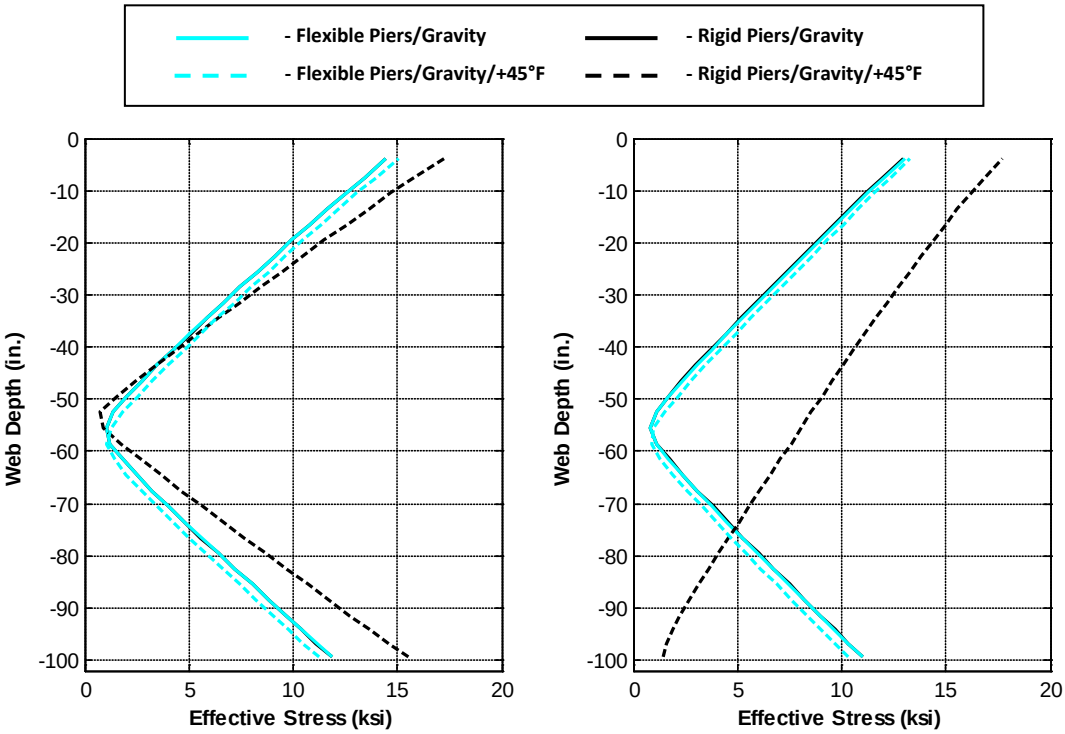


*(a)* Mid-Span 1

*(b)* Mid-Span 2

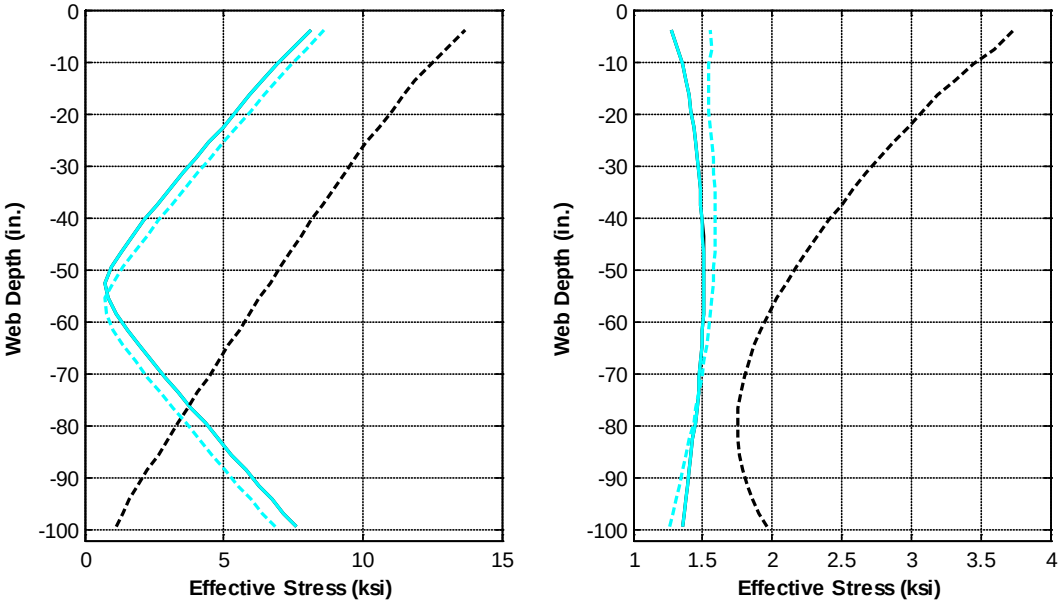


*(c)* Mid-Span 3

*(d)* Mid-Span 4

**Figure C.16. Girder 8 Mid-Span Web Effective Stress Profiles – Gravity and +45°F Loading**

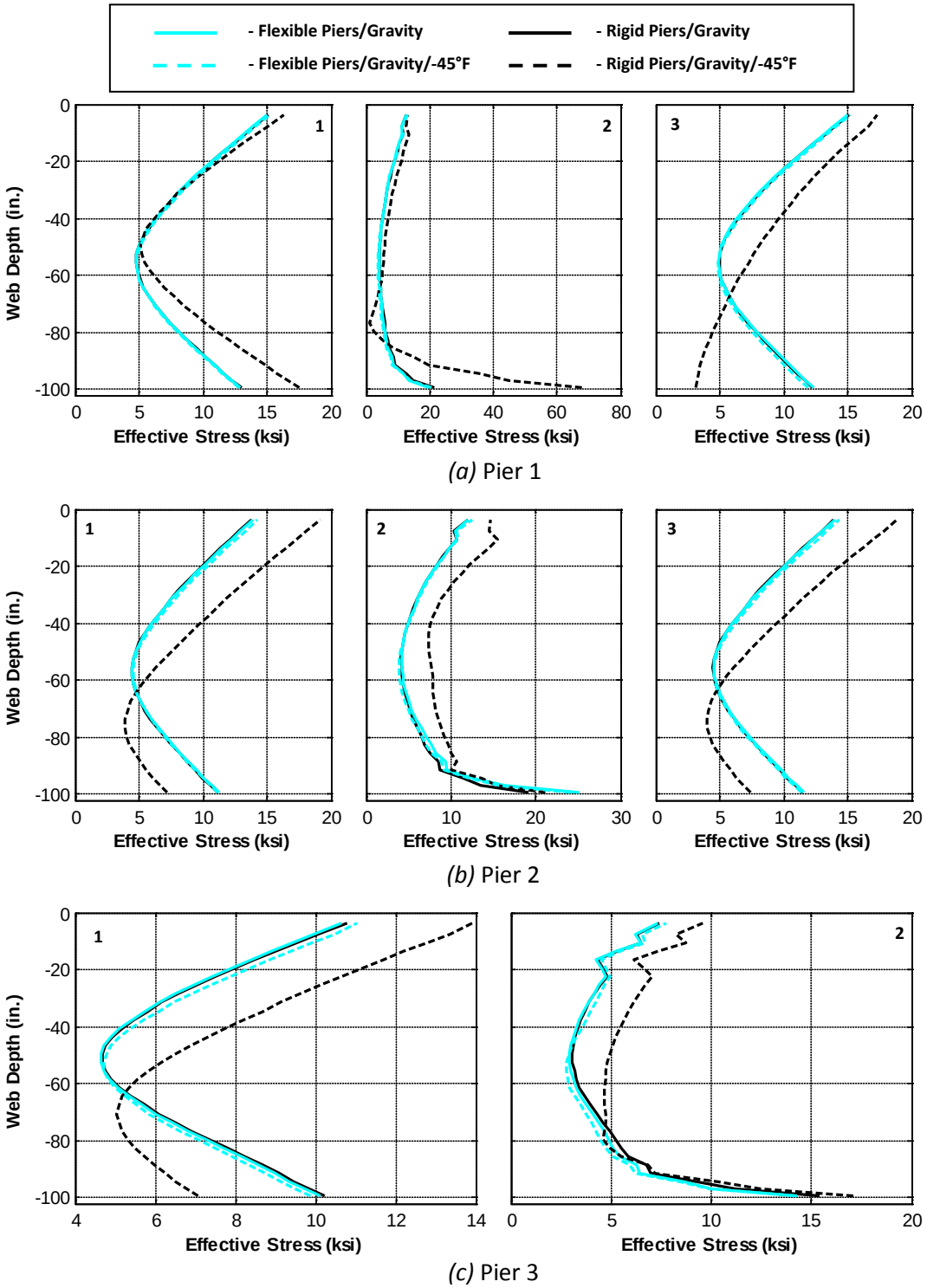


**Figure C.17. Girder 1 Pier Web Effective Stress Profiles – Gravity and -45°F Loading**

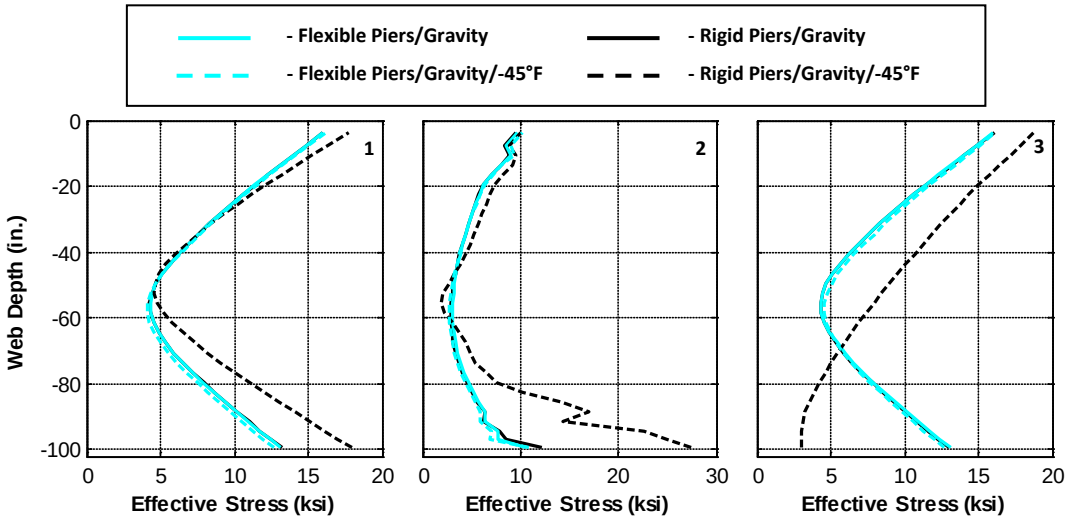


*(a)* Pier 1

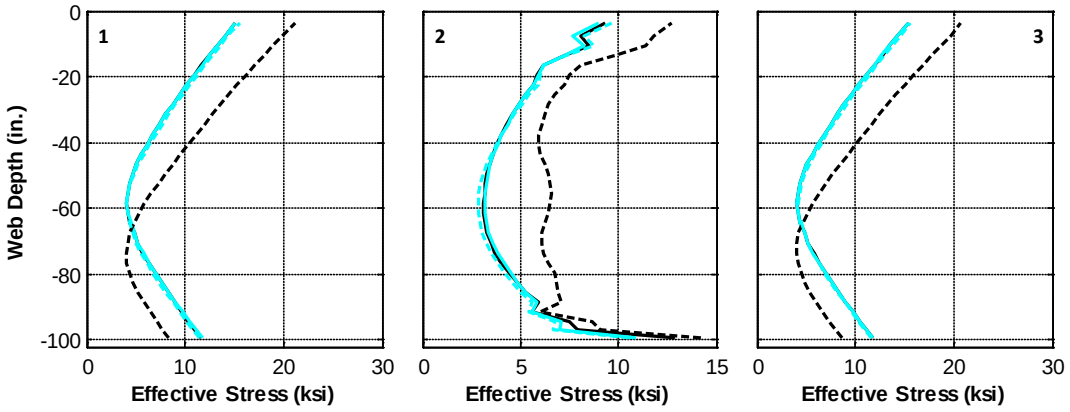


*(b)* Pier 2

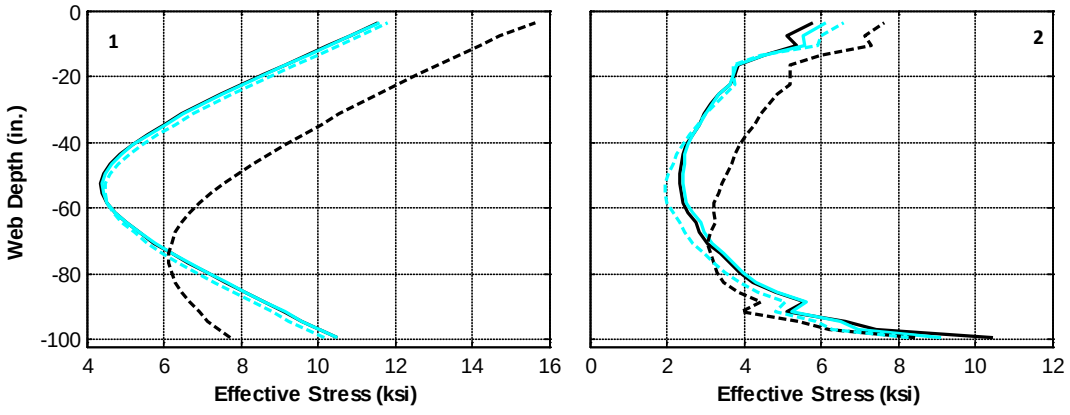


*(c)* Pier 3

**Figure C.18. Girder 2 Pier Web Effective Stress Profiles – Gravity and -45°F Loading**

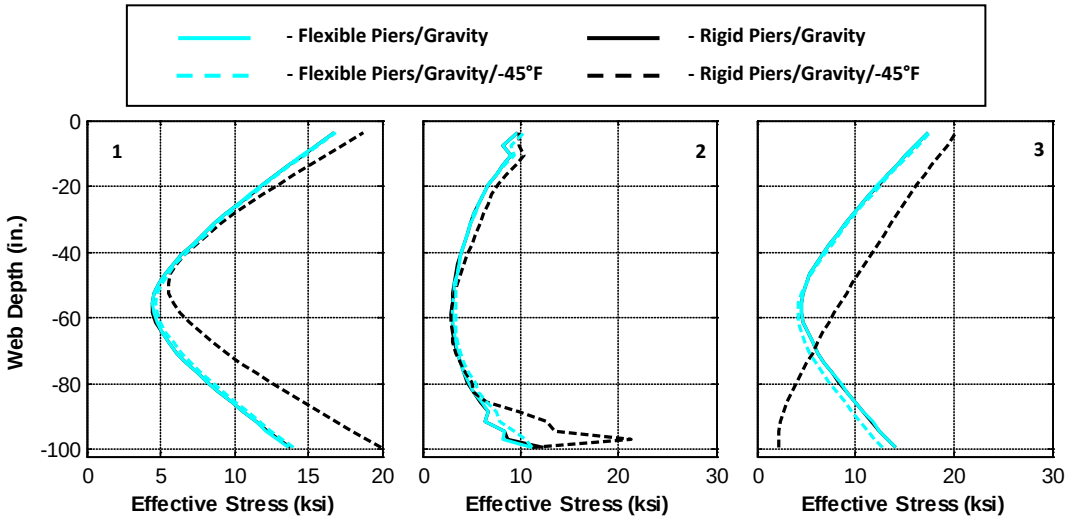


*(a)* Pier 1

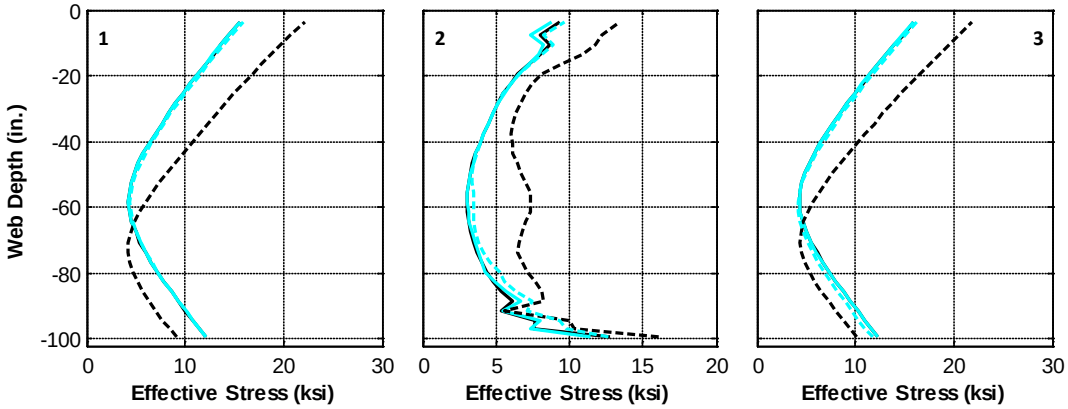


*(b)* Pier 2

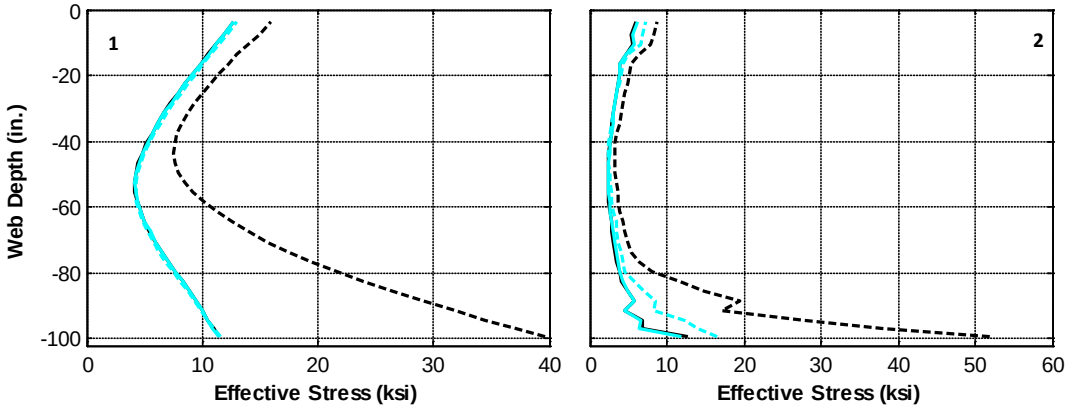


*(c)* Pier 3

**Figure C.19. Girder 3 Pier Web Effective Stress Profiles – Gravity and -45°F Loading**

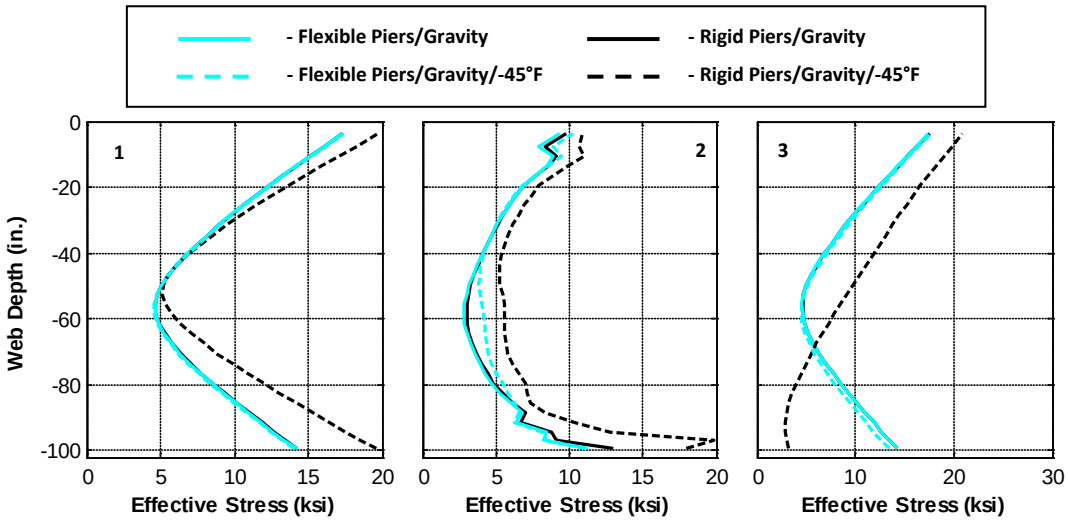


*(a)* Pier 1

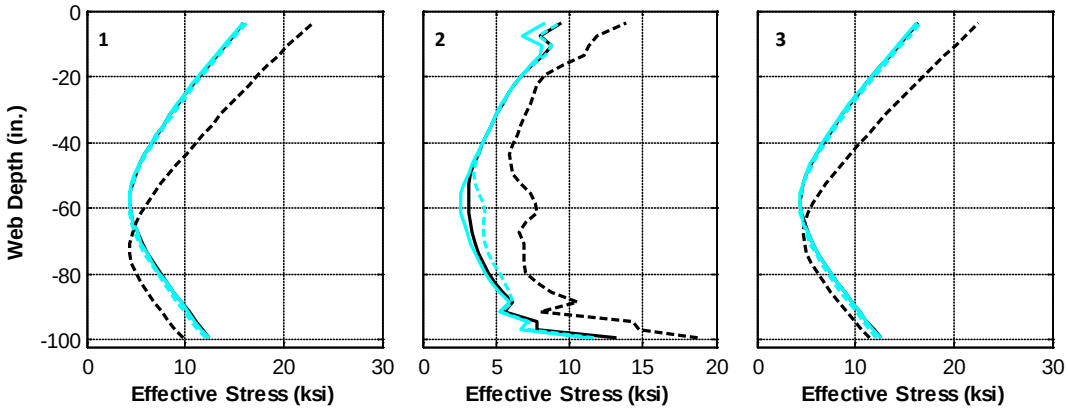


*(b)* Pier 2

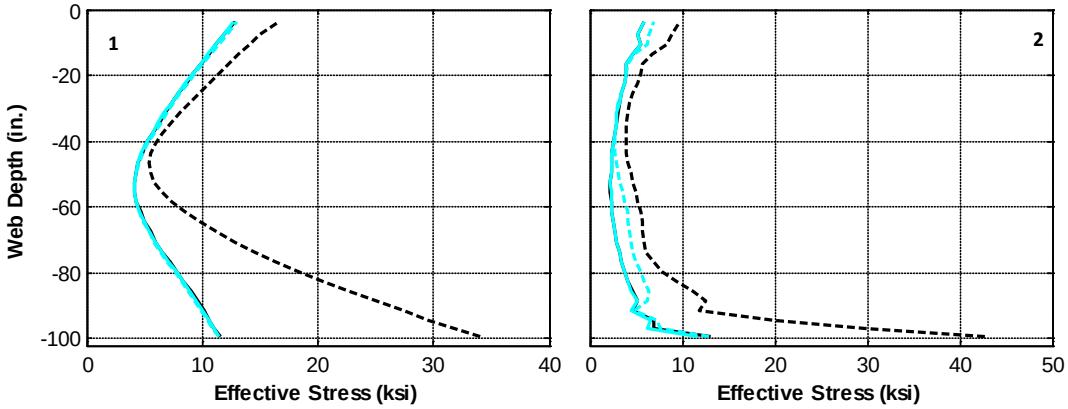


*(c)* Pier 3

**Figure C.20. Girder 4 Pier Web Effective Stress Profiles – Gravity and -45°F Loading**

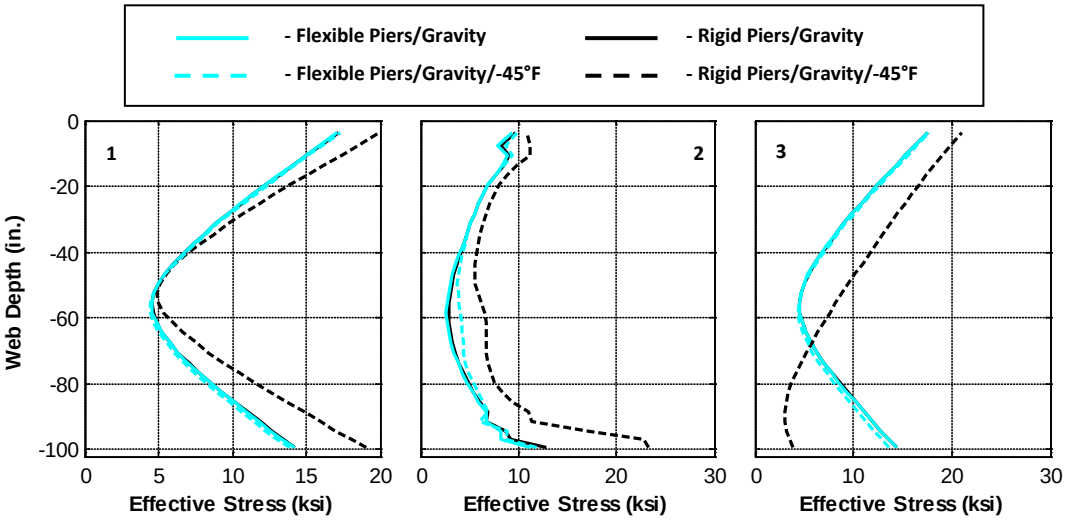


*(a)* Pier 1

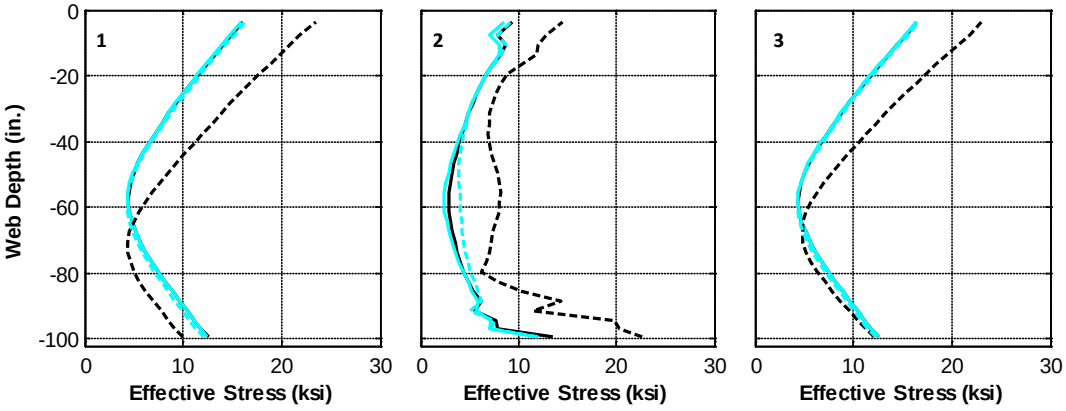


*(b)* Pier 2

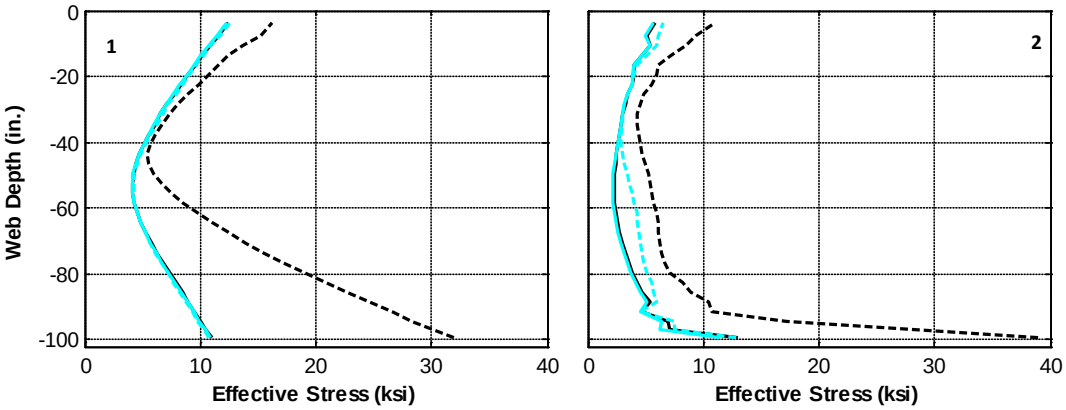


*(c)* Pier 3

**Figure C.21. Girder 5 Pier Web Effective Stress Profiles – Gravity and -45°F Loading**

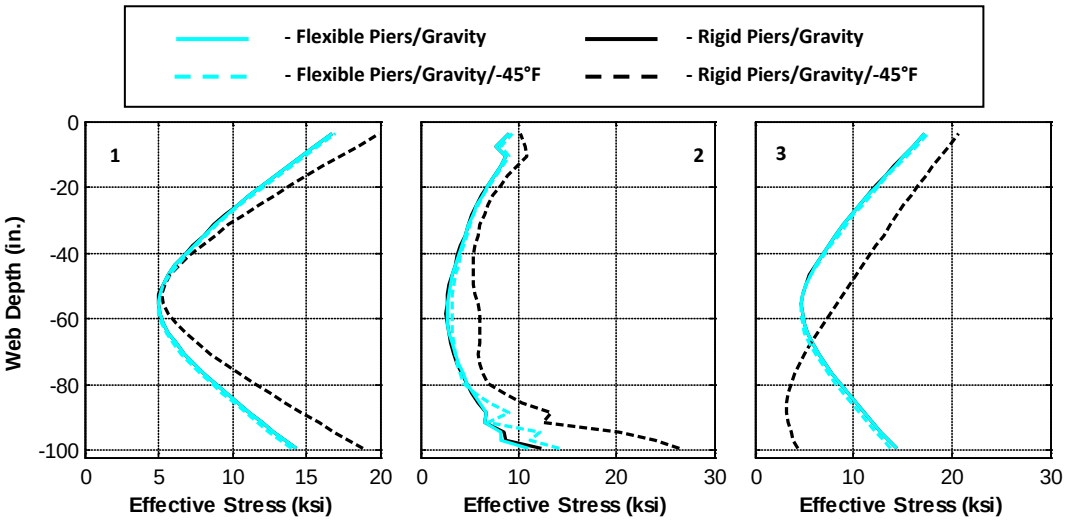


*(a)* Pier 1

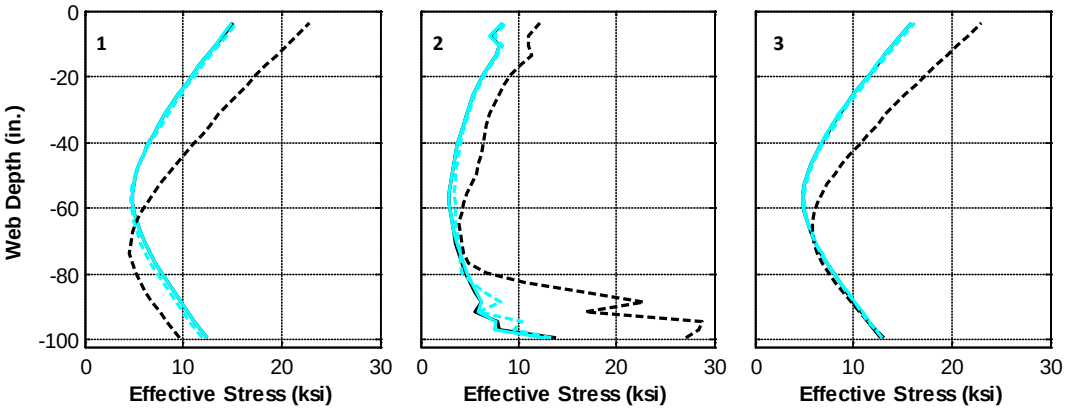


*(b)* Pier 2

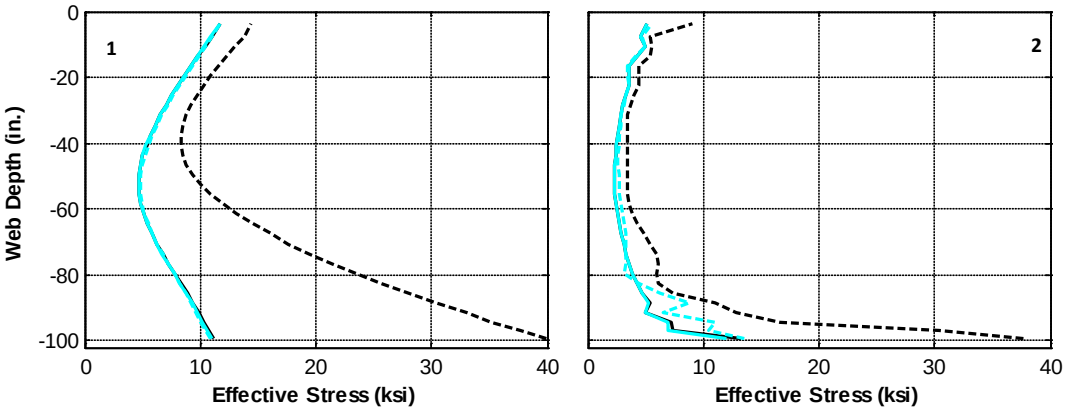


*(c)* Pier 3

**Figure C.22. Girder 6 Pier Web Effective Stress Profiles – Gravity and -45°F Loading**

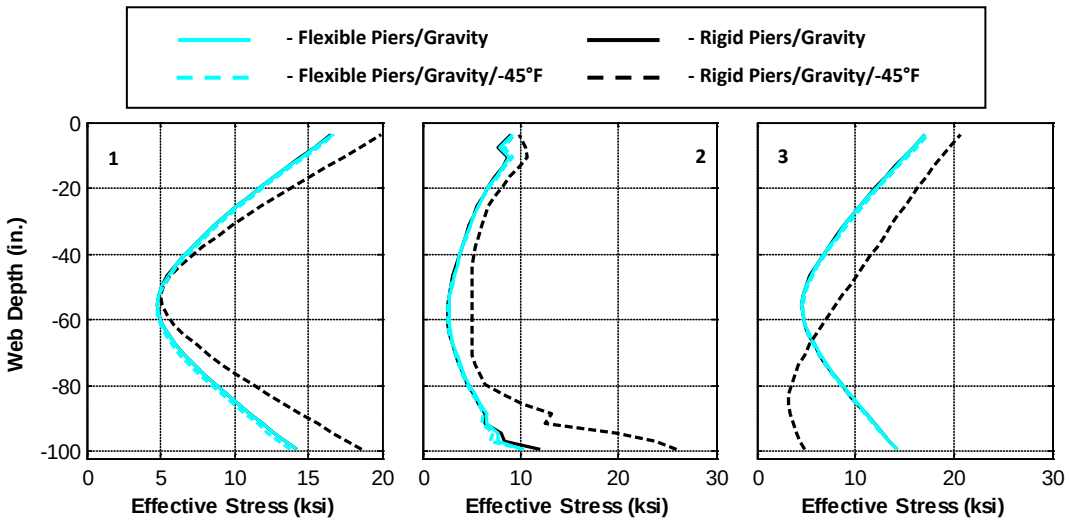


*(a)* Pier 1

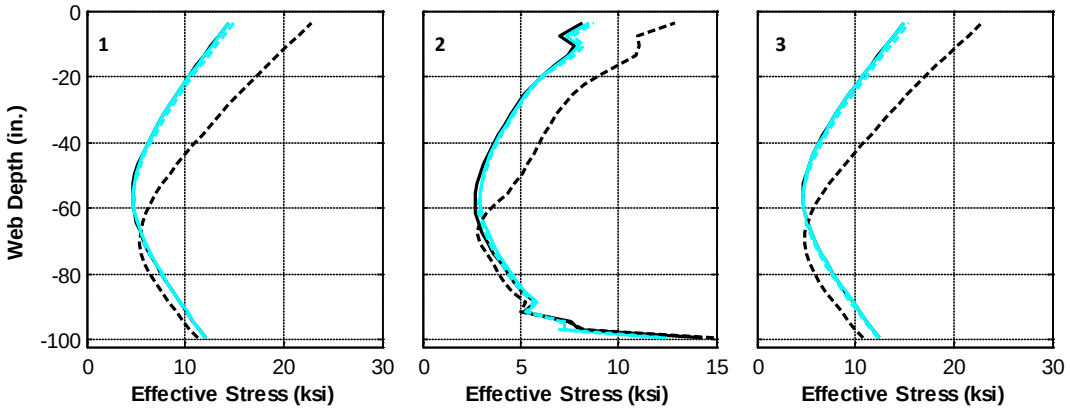


*(b)* Pier 2

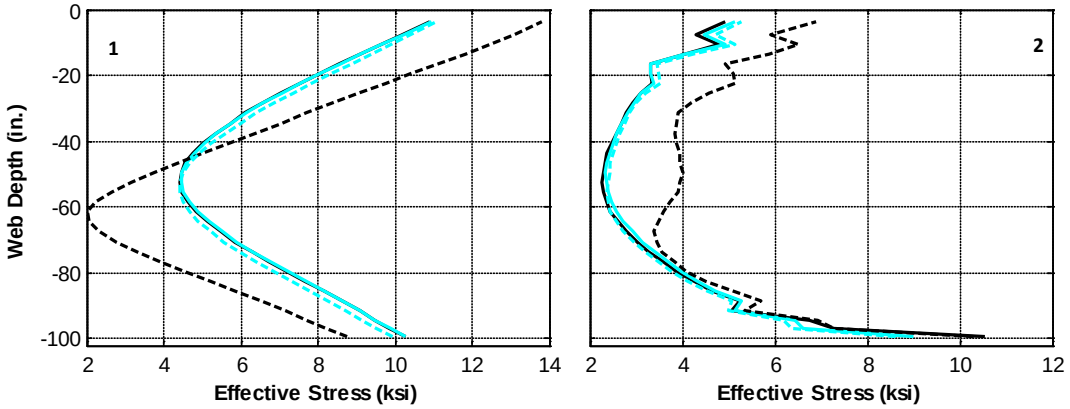


*(c)* Pier 3

**Figure C.23. Girder 7 Pier Web Effective Stress Profiles – Gravity and -45°F Loading**

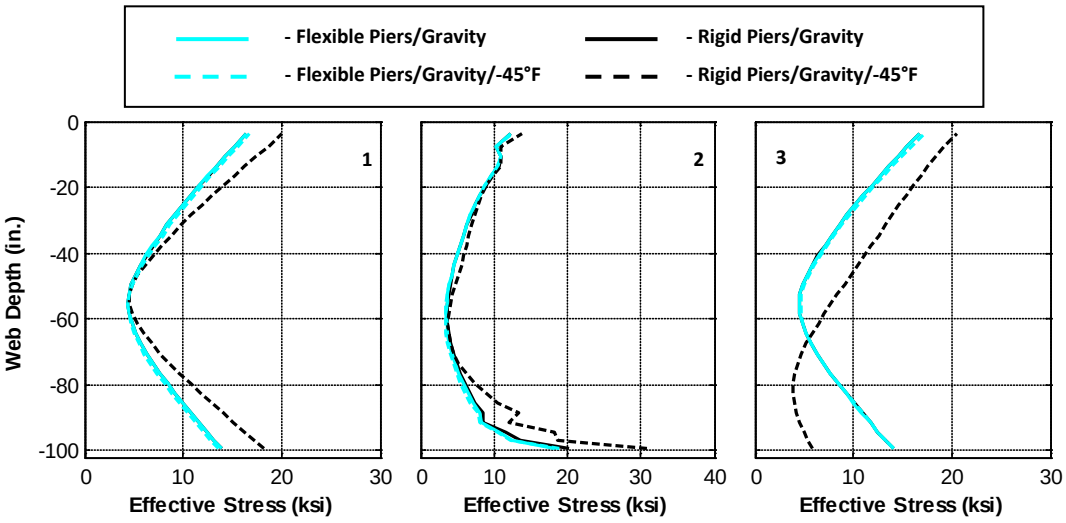


*(a)* Pier 1

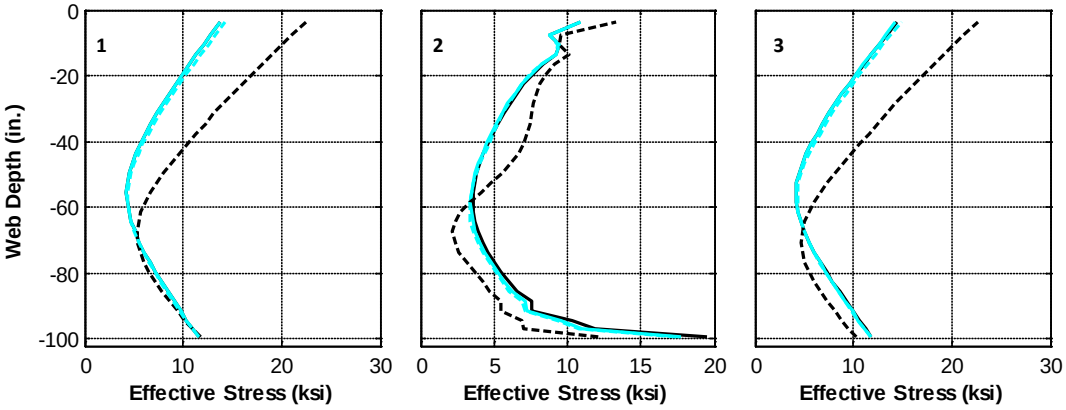


*(b)* Pier 2

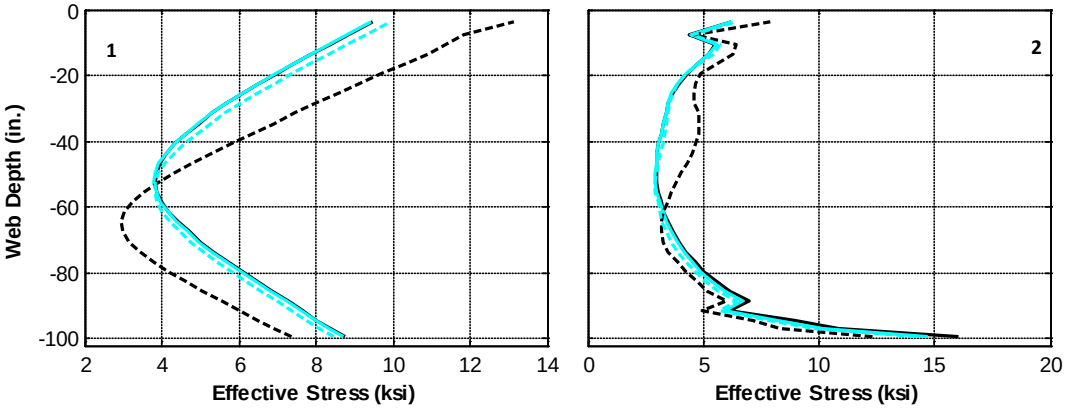


*(c)* Pier 3

**Figure C.24. Girder 8 Pier Web Effective Stress Profiles – Gravity and -45°F Loading**

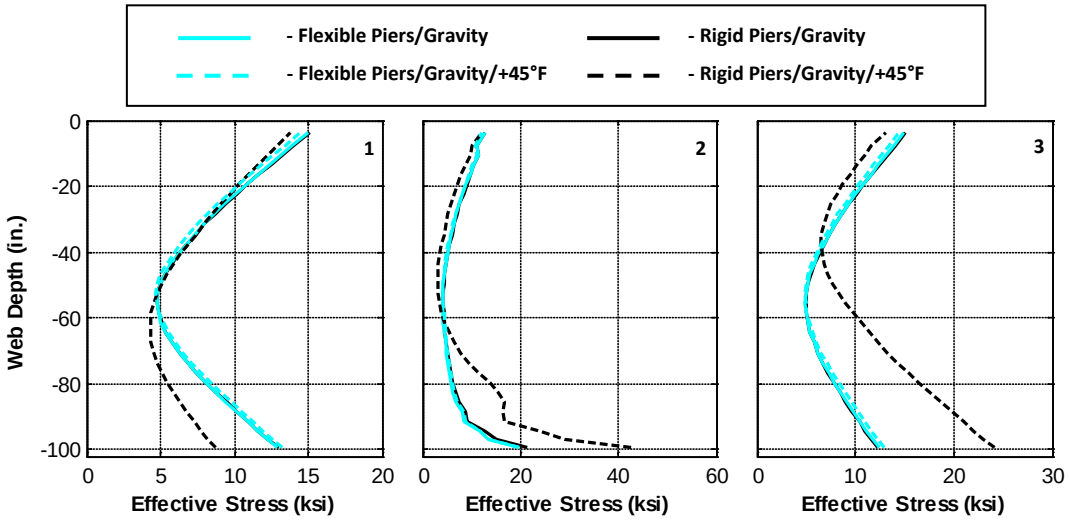


*(a)* Pier 1

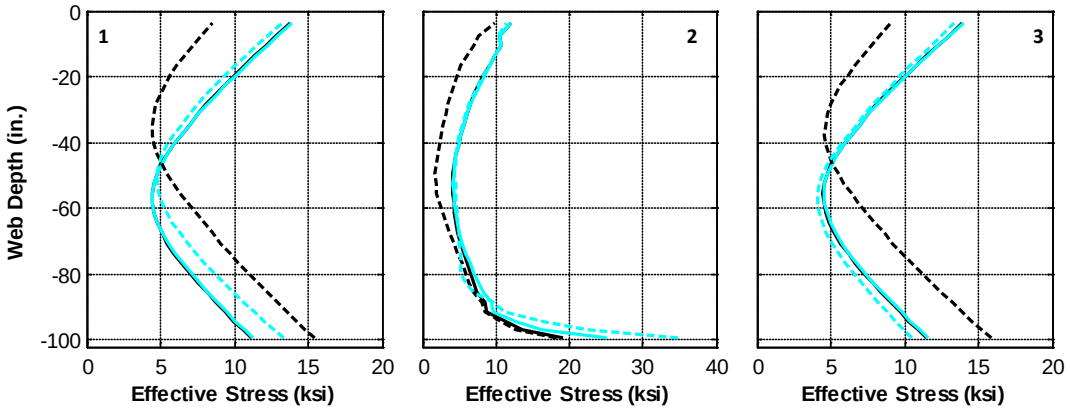


*(b)* Pier 2

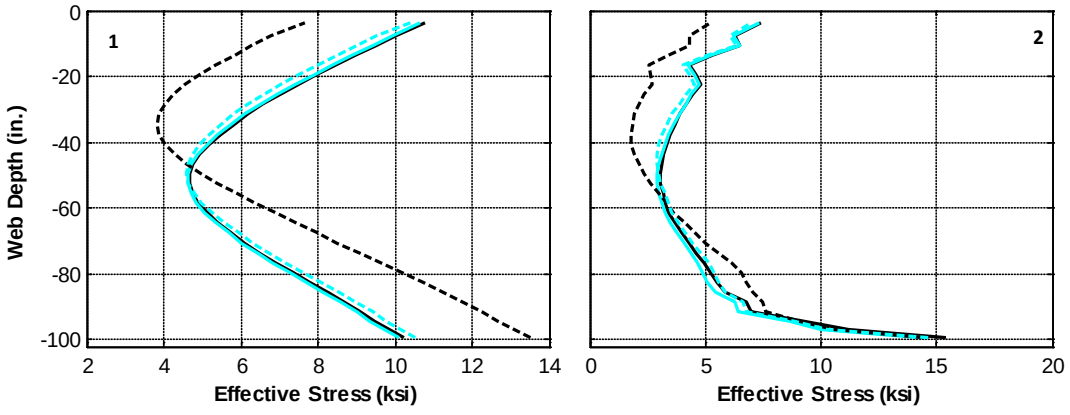


*(c)* Pier 3

**Figure C.25. Girder 1 Pier Web Effective Stress Profiles – Gravity and +45°F Loading**

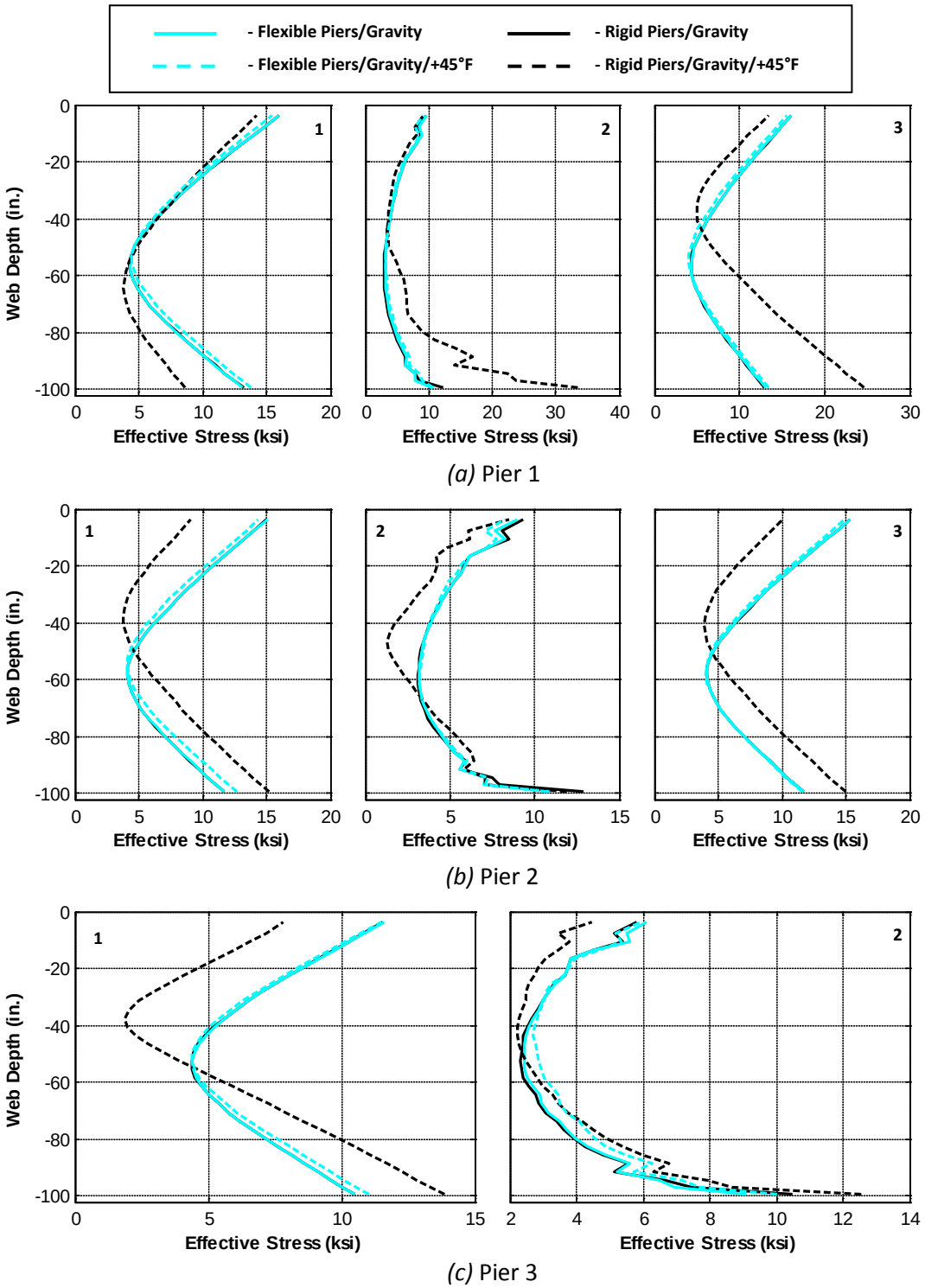


**Figure C.26. Girder 2 Pier Web Effective Stress Profiles – Gravity and +45°F Loading**

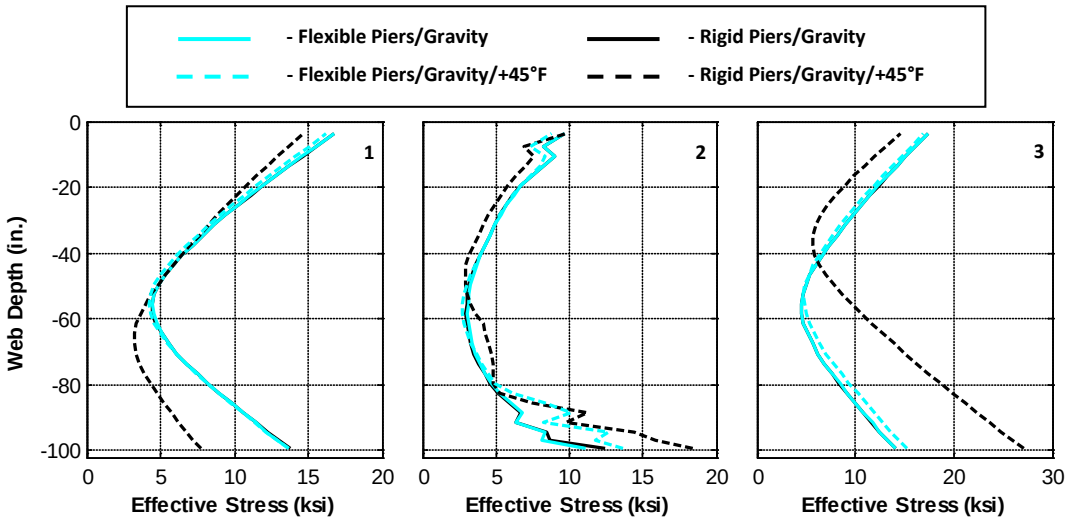


*(a)* Pier 1

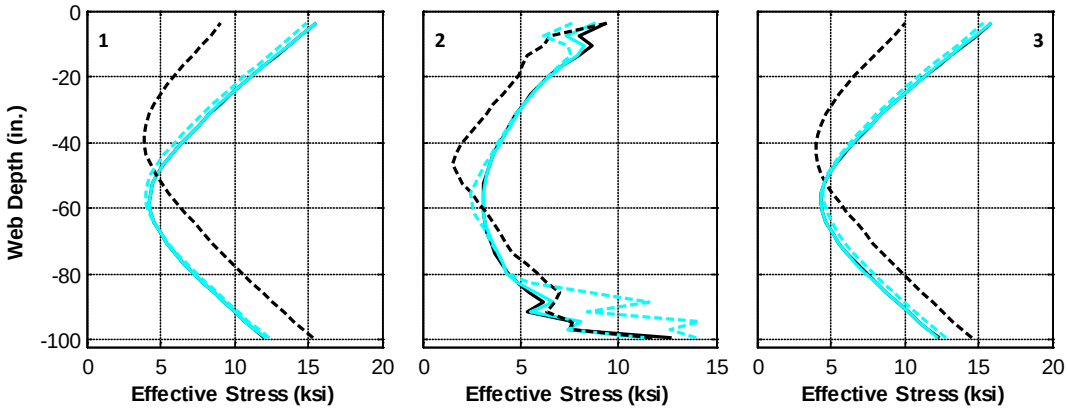


*(b)* Pier 2

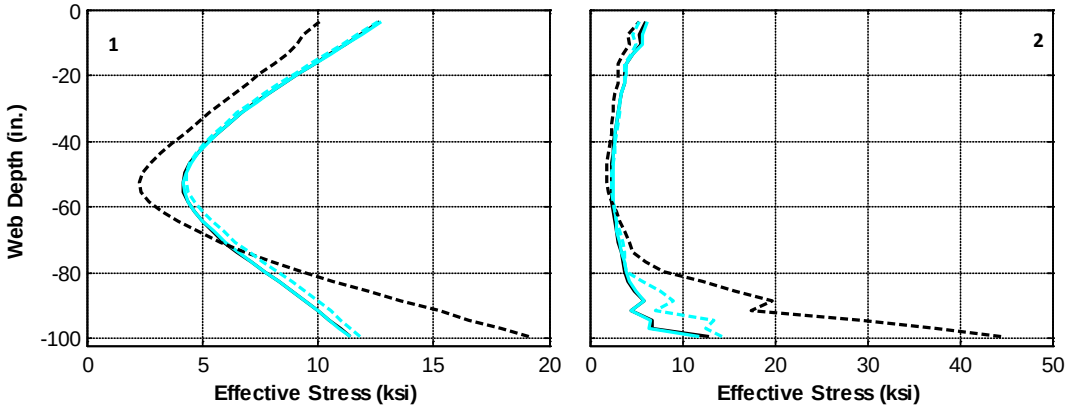


*(c)* Pier 3

**Figure C.27. Girder 3 Pier Web Effective Stress Profiles – Gravity and +45°F Loading**

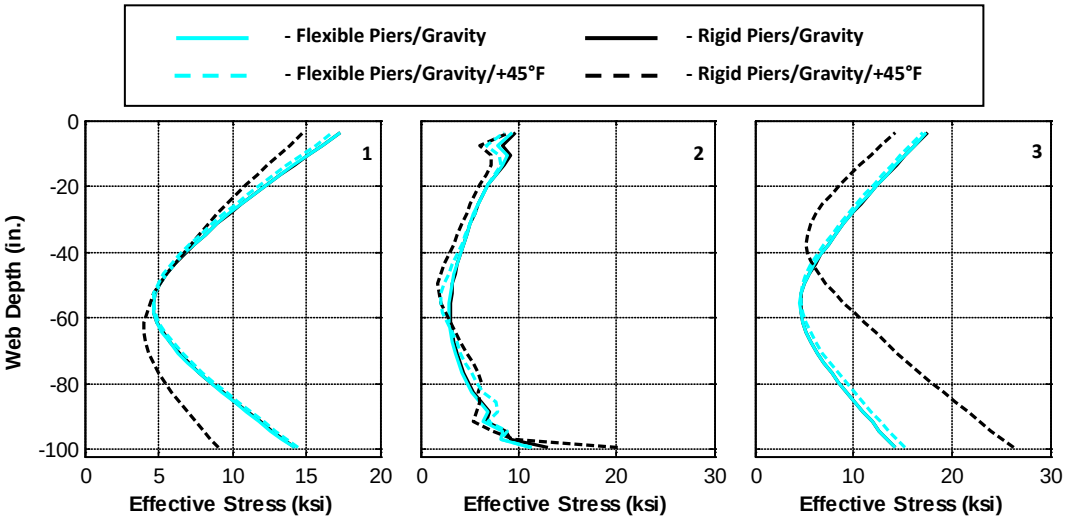


*(a)* Pier 1

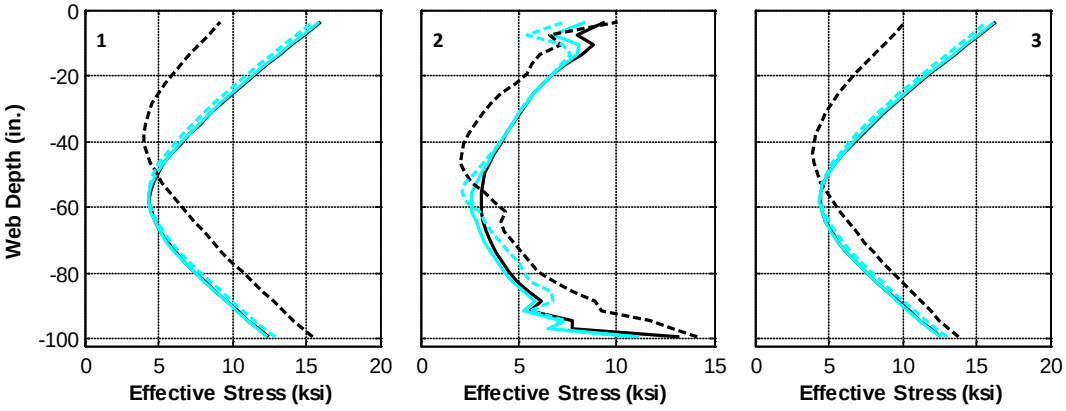


*(b)* Pier 2

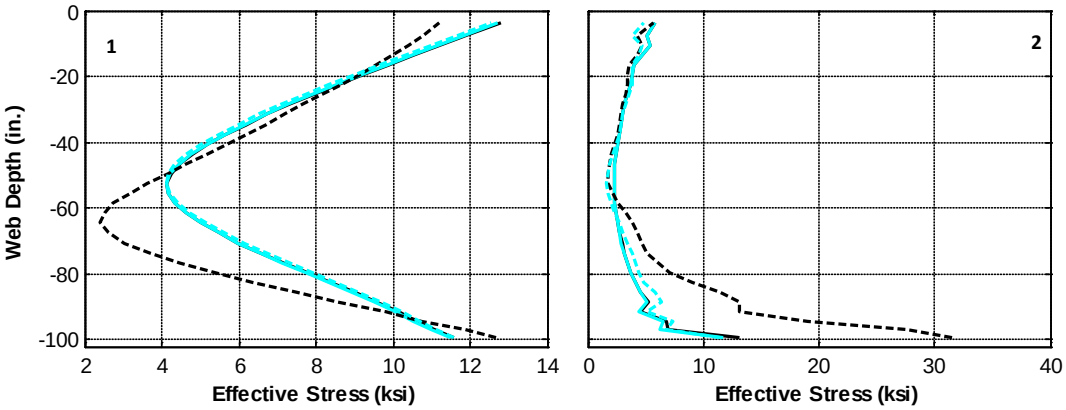


*(c)* Pier 3

**Figure C.28. Girder 4 Pier Web Effective Stress Profiles – Gravity and +45°F Loading**

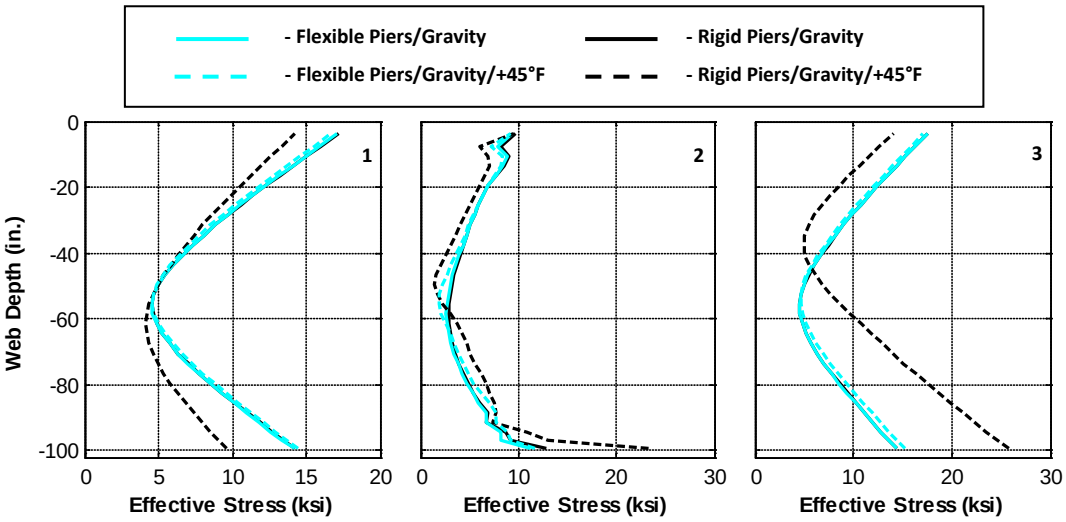


*(a)* Pier 1

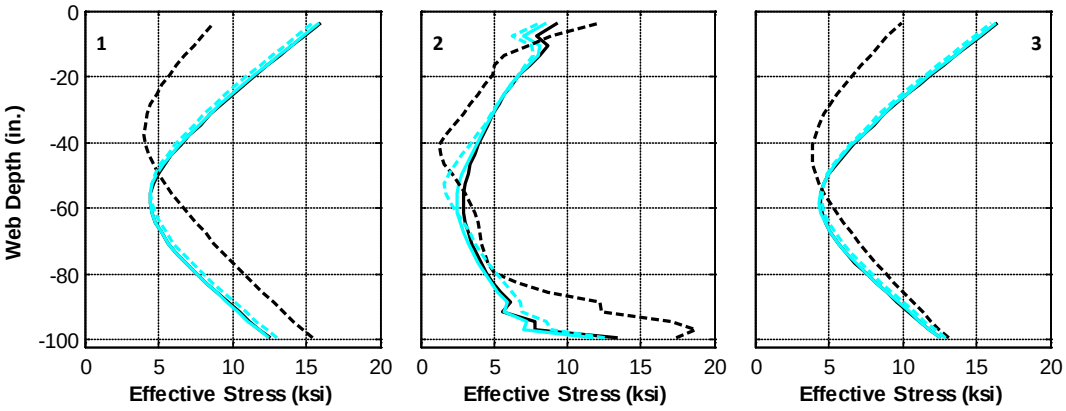


*(b)* Pier 2

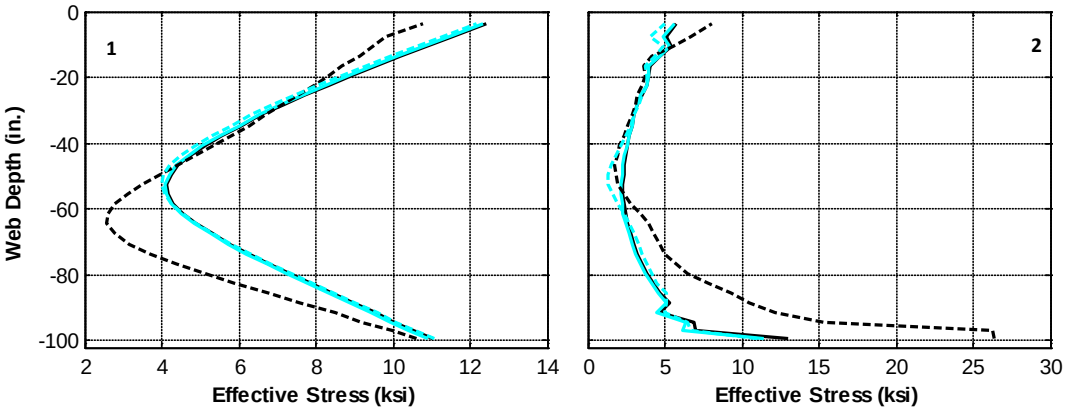


*(c)* Pier 3

**Figure C.29. Girder 5 Pier Web Effective Stress Profiles – Gravity and +45°F Loading**

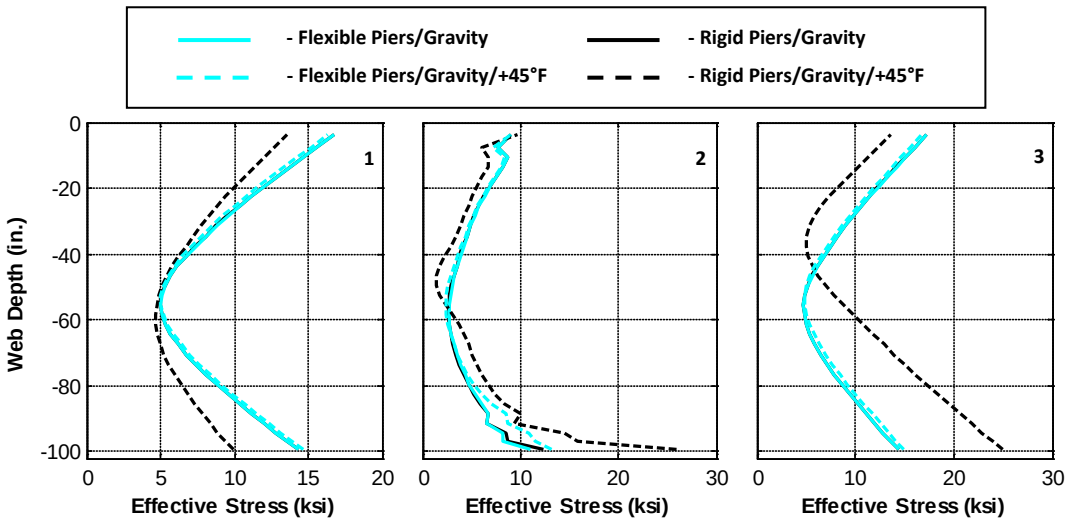


*(a)* Pier 1

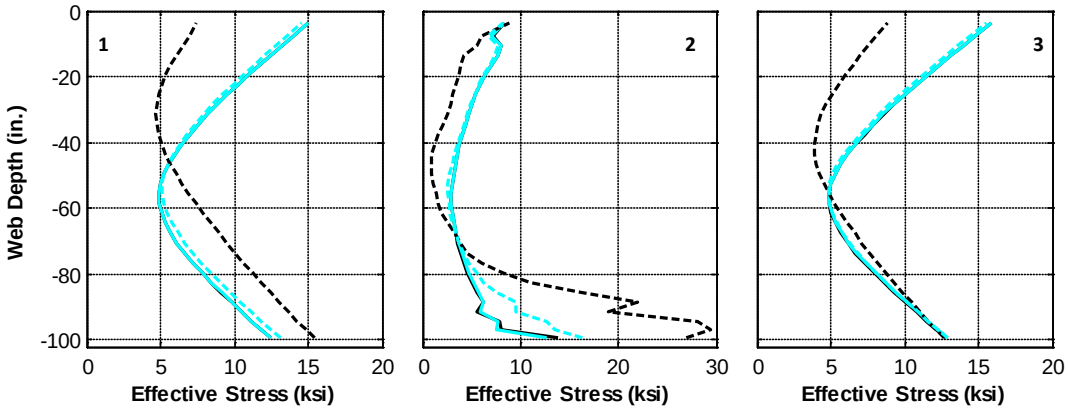


*(b)* Pier 2

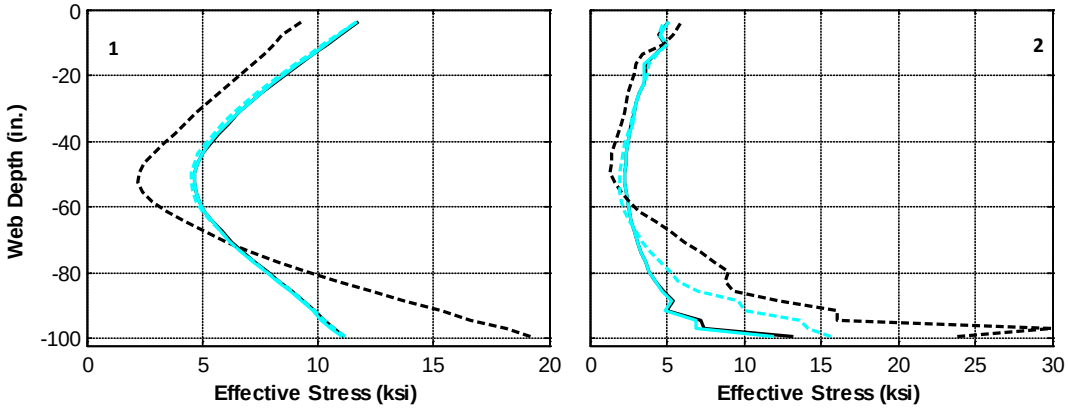


*(c)* Pier 3

**Figure C.30. Girder 6 Pier Web Effective Stress Profiles – Gravity and +45°F Loading**

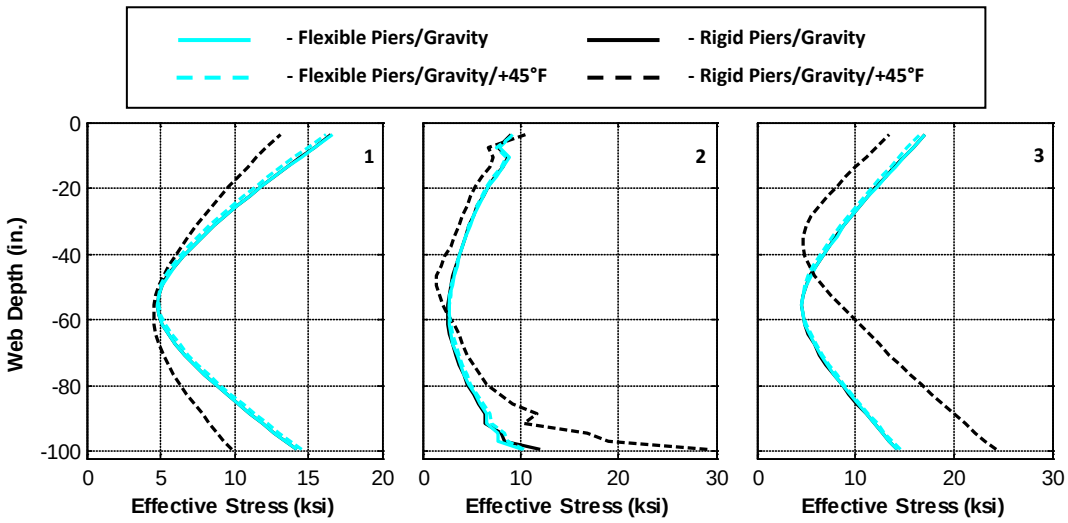


*(a)* Pier 1

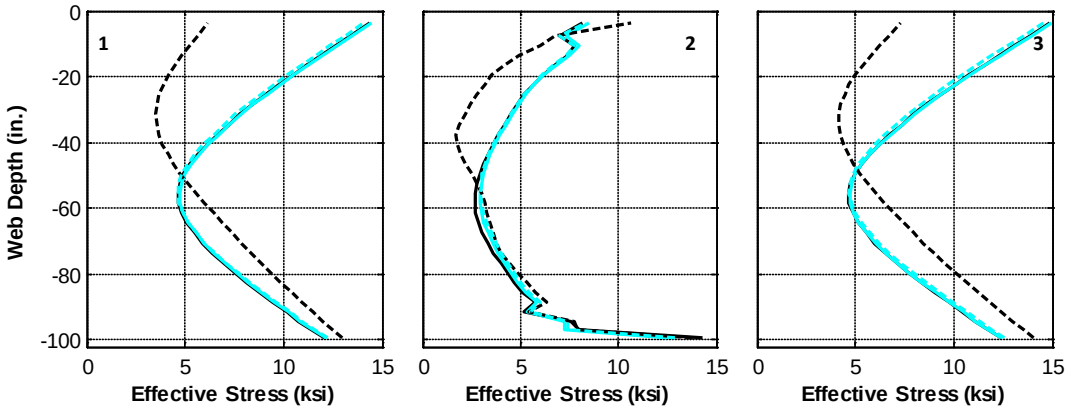


*(b)* Pier 2

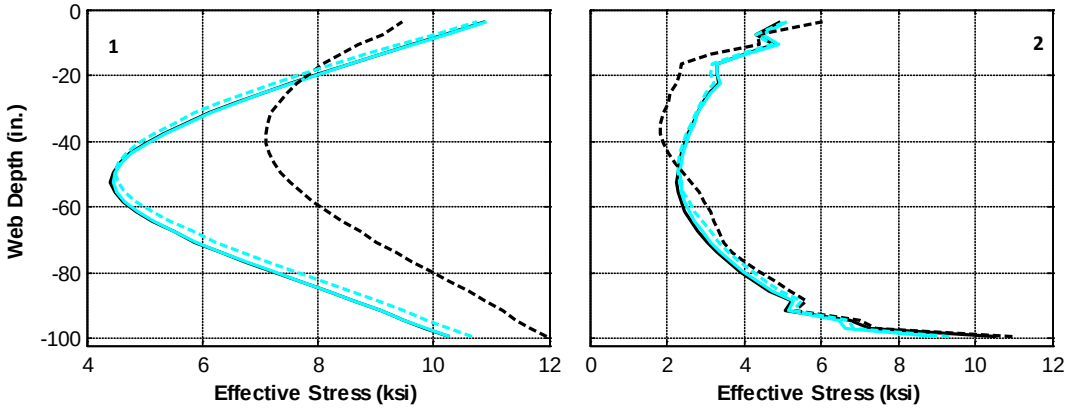


*(c)* Pier 3

**Figure C.31. Girder 7 Pier Web Effective Stress Profiles – Gravity and +45°F Loading**

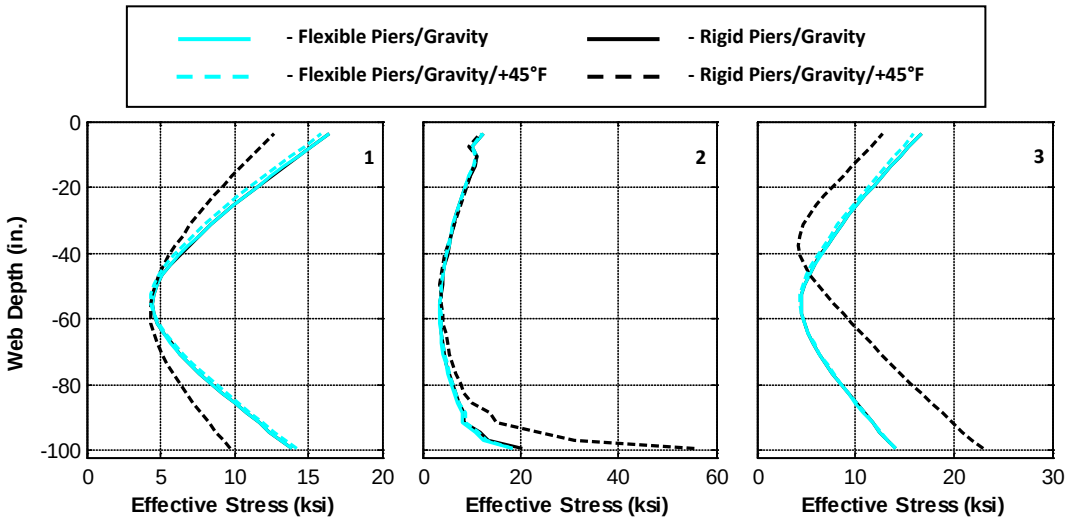


*(a)* Pier 1

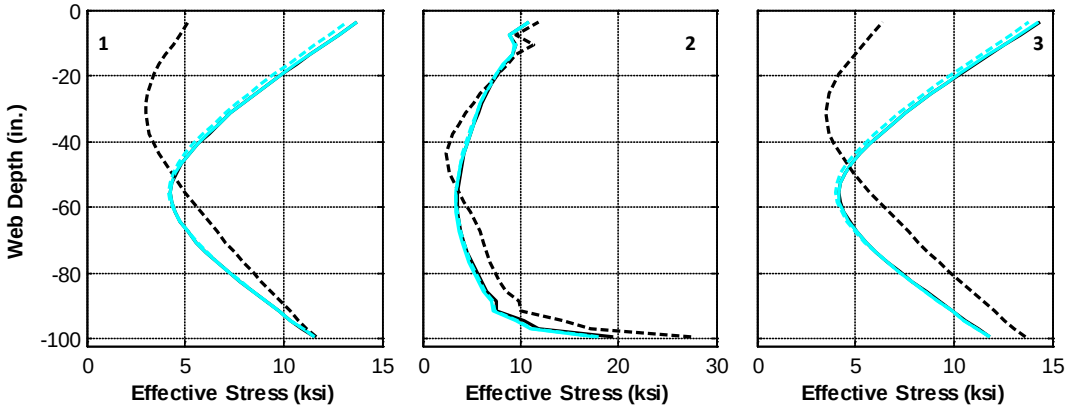


*(b)* Pier 2

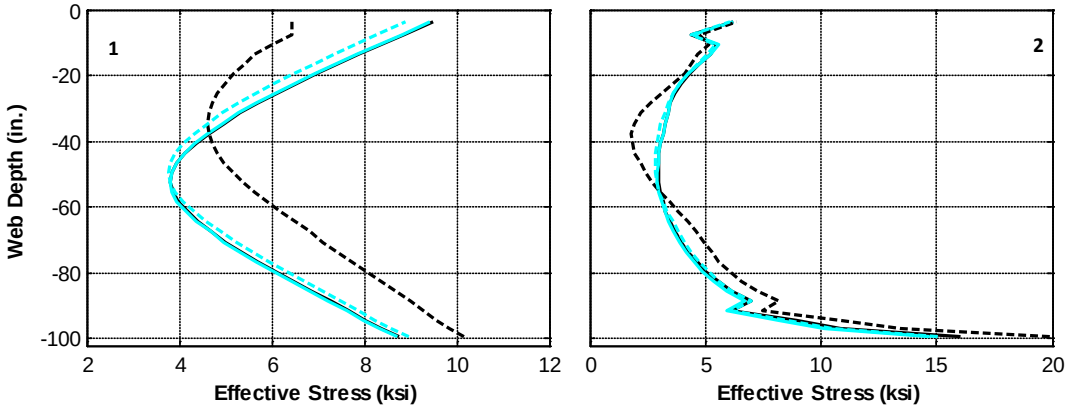


*(c)* Pier 3

**Figure C.32. Girder 8 Pier Web Effective Stress Profiles – Gravity and +45°F Loading**

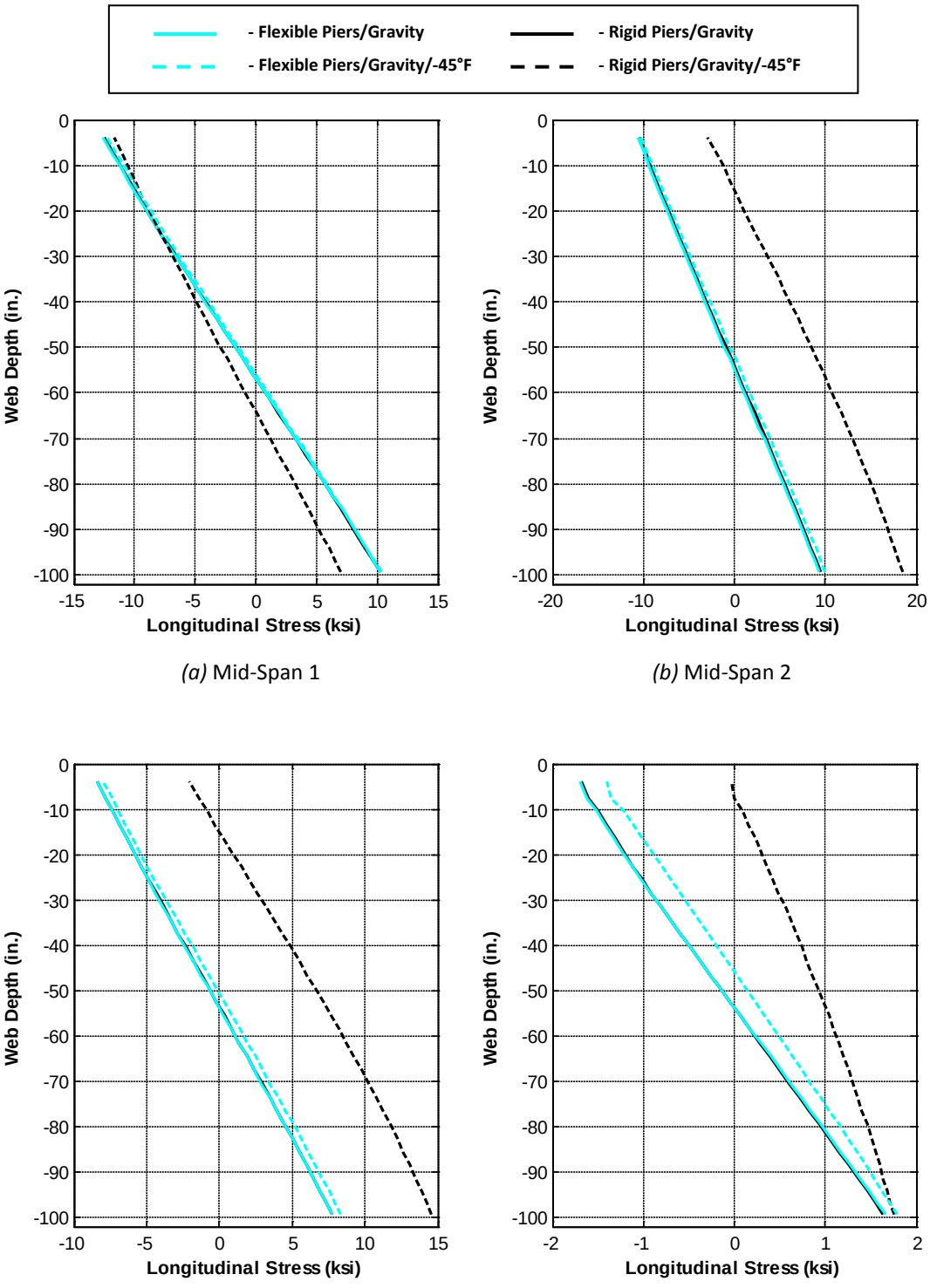


**Figure C.33. Girder 1 Mid-Span Web Longitudinal Stress Profiles – Gravity and -45°F Loading**

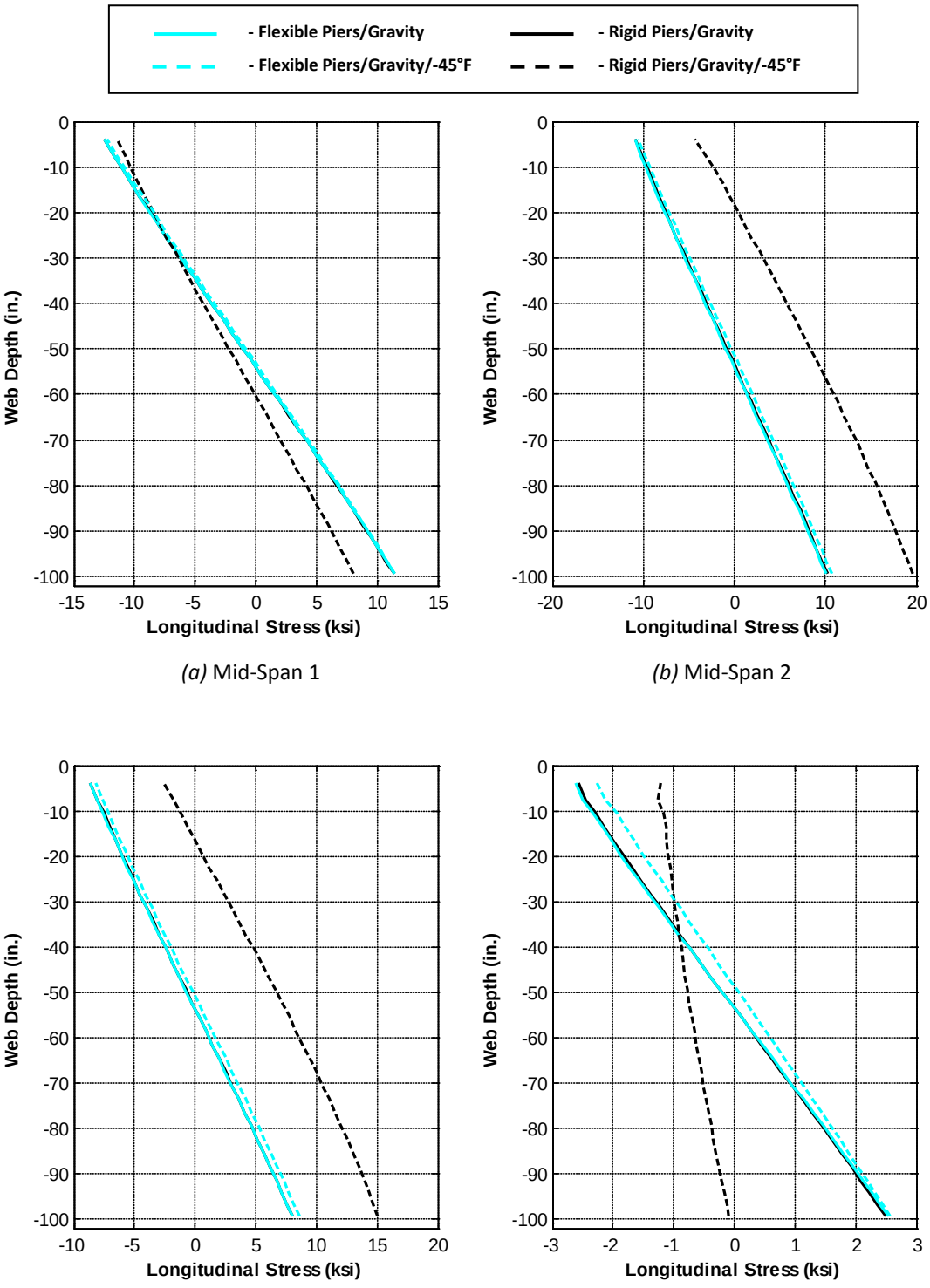


**Figure C.34. Girder 2 Mid-Span Web Longitudinal Stress Profiles – Gravity and -45°F Loading**

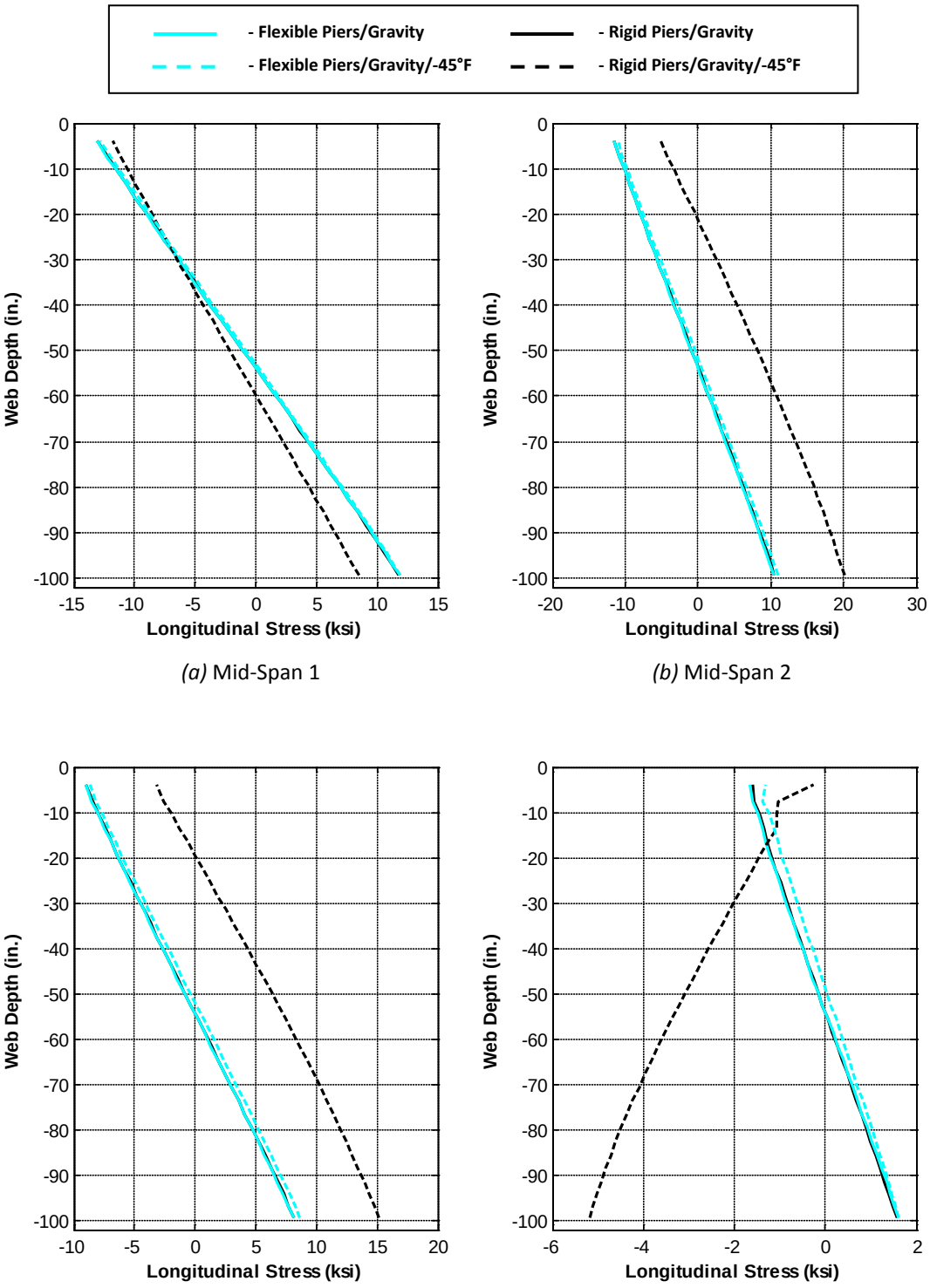


**Figure C.35. Girder 3 Mid-Span Web Longitudinal Stress Profiles – Gravity and -45°F Loading**

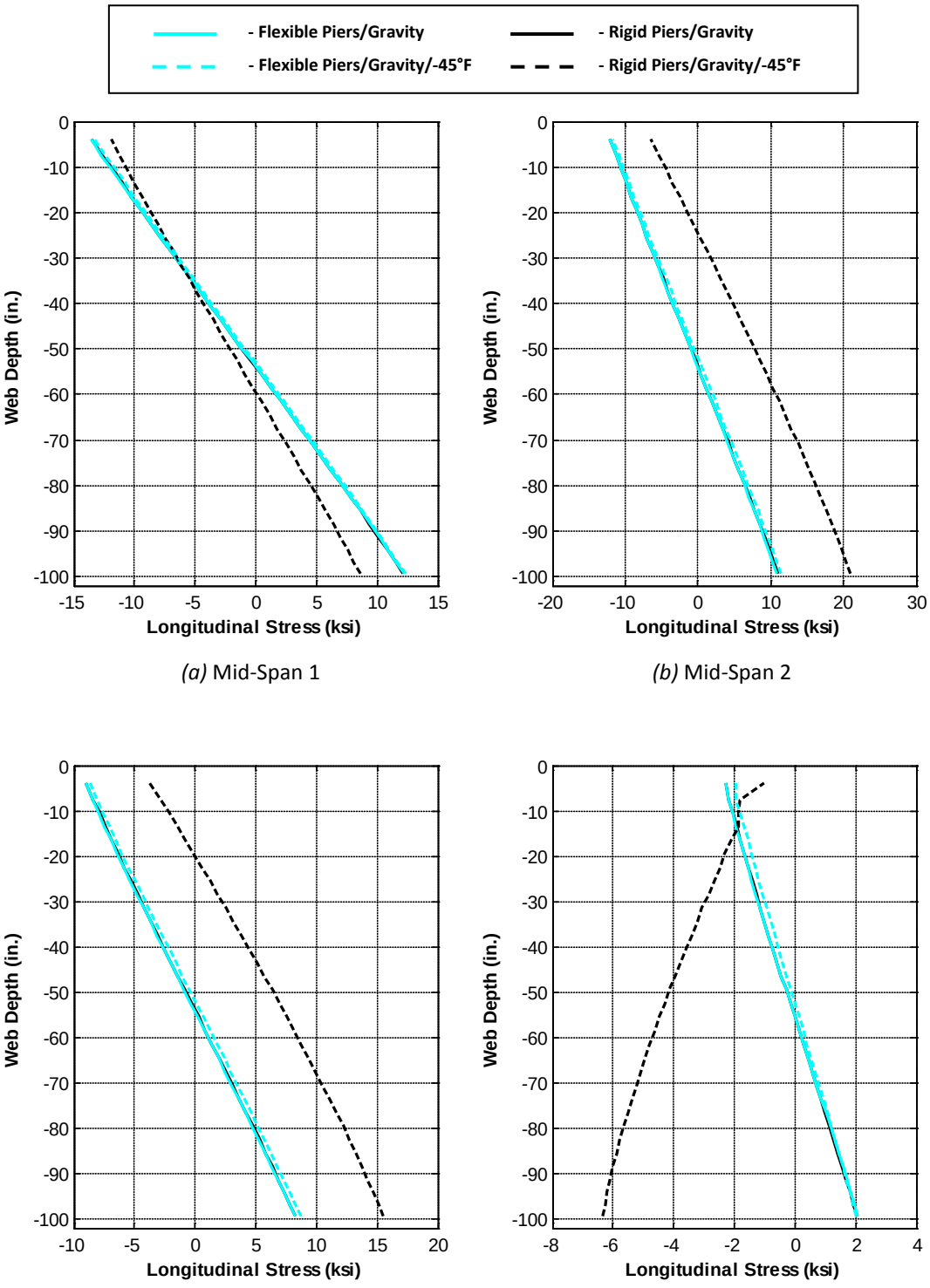


**Figure C.36. Girder 4 Mid-Span Web Longitudinal Stress Profiles – Gravity and -45°F Loading**

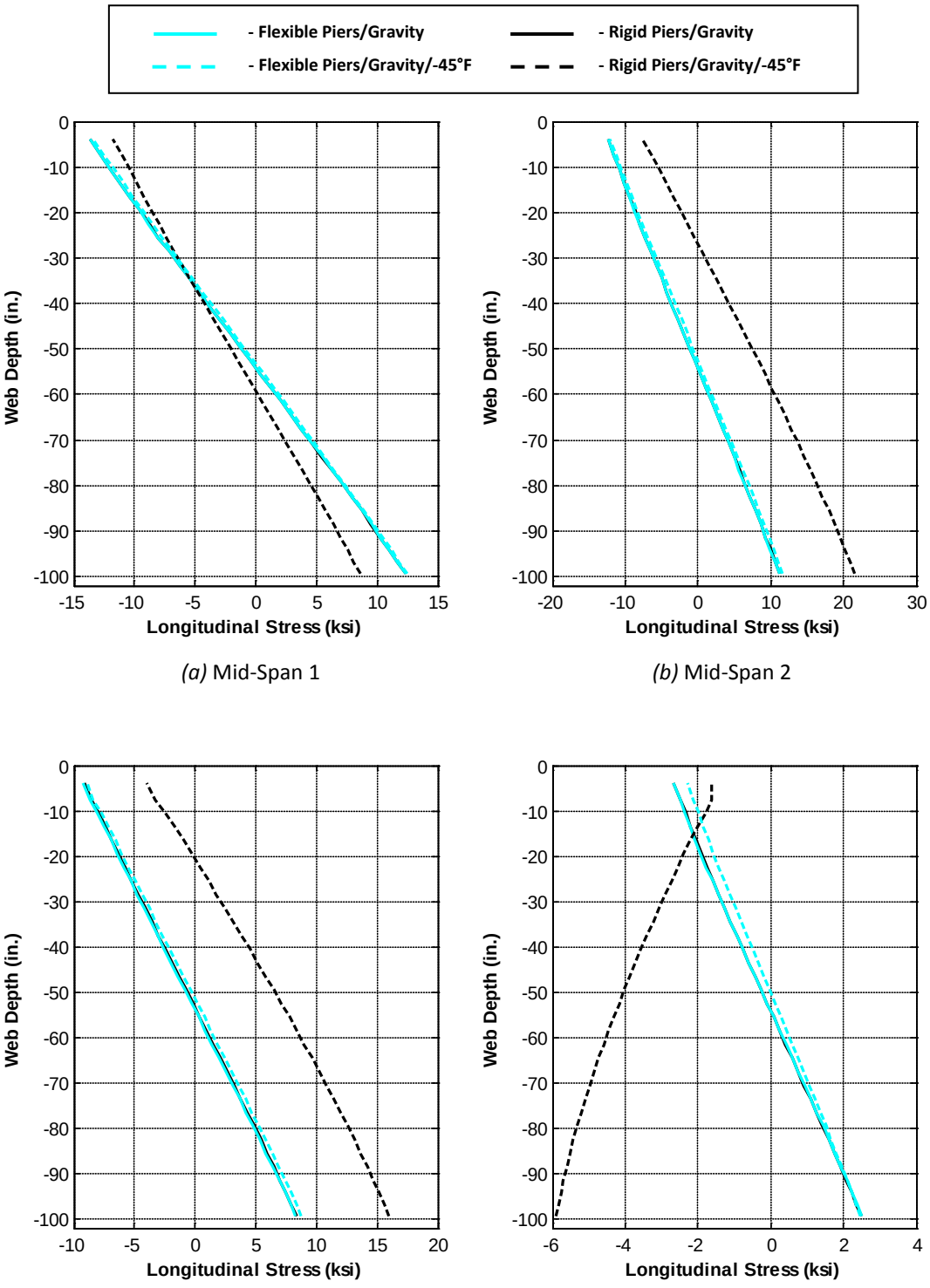


*(a)* Mid-Span 1

*(b)* Mid-Span 2

*(c)* Mid-Span 3

*(d)* Mid-Span 4

**Figure C.37. Girder 5 Mid-Span Web Longitudinal Stress Profiles – Gravity and -45°F Loading**

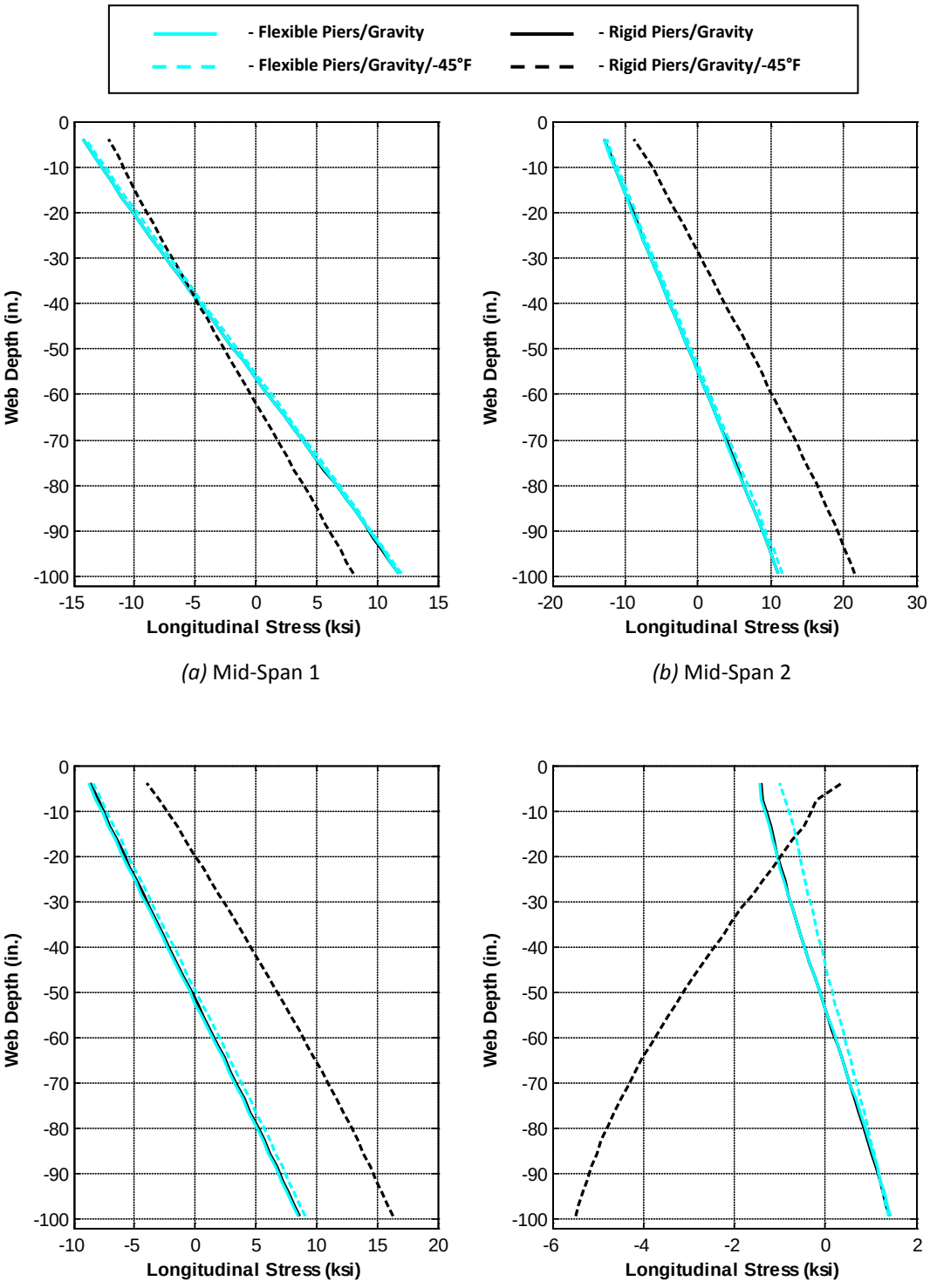


**Figure C.38. Girder 6 Mid-Span Web Longitudinal Stress Profiles – Gravity and -45°F Loading**

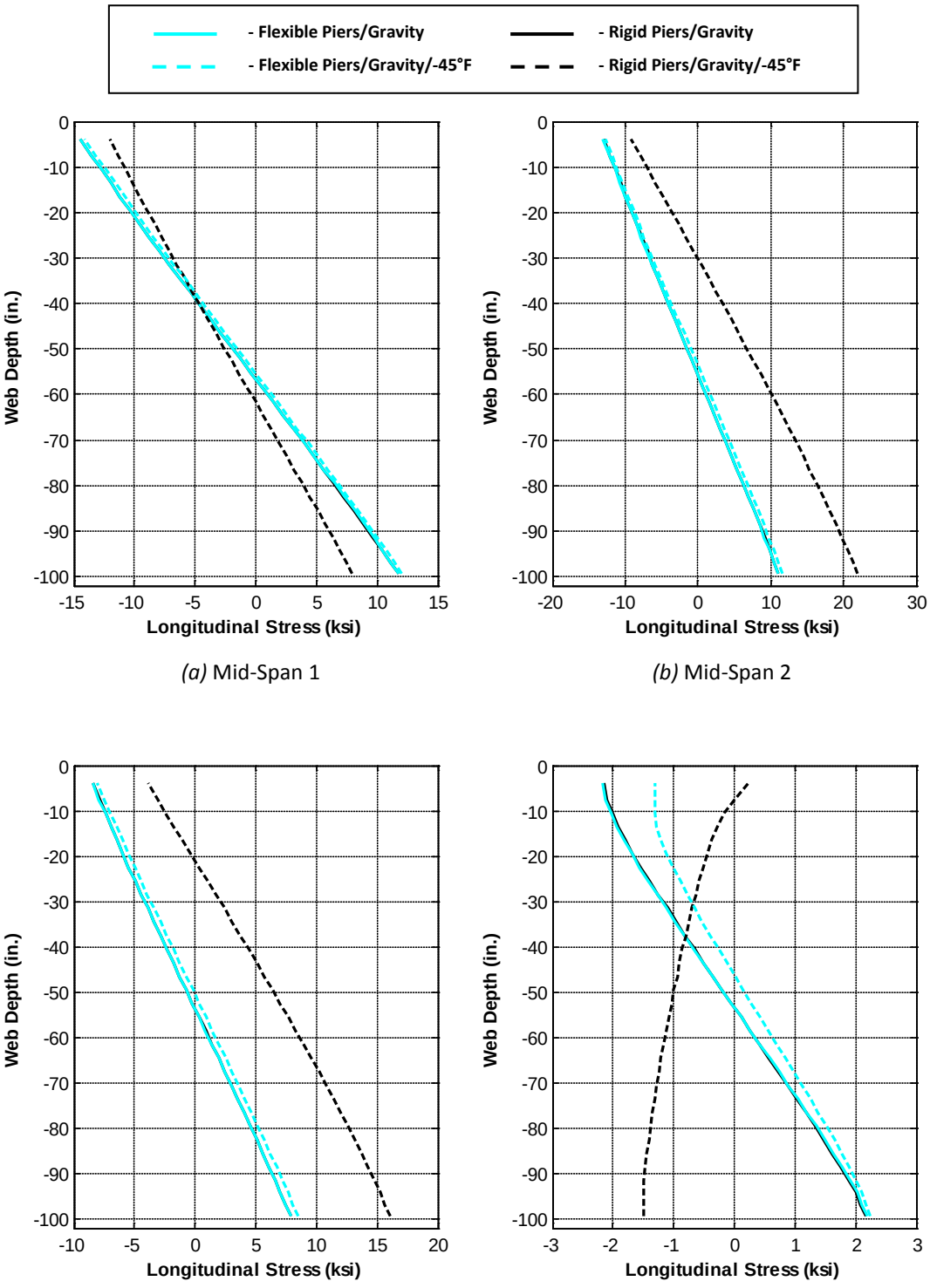


**Figure C.39. Girder 7 Mid-Span Web Longitudinal Stress Profiles – Gravity and -45°F Loading**

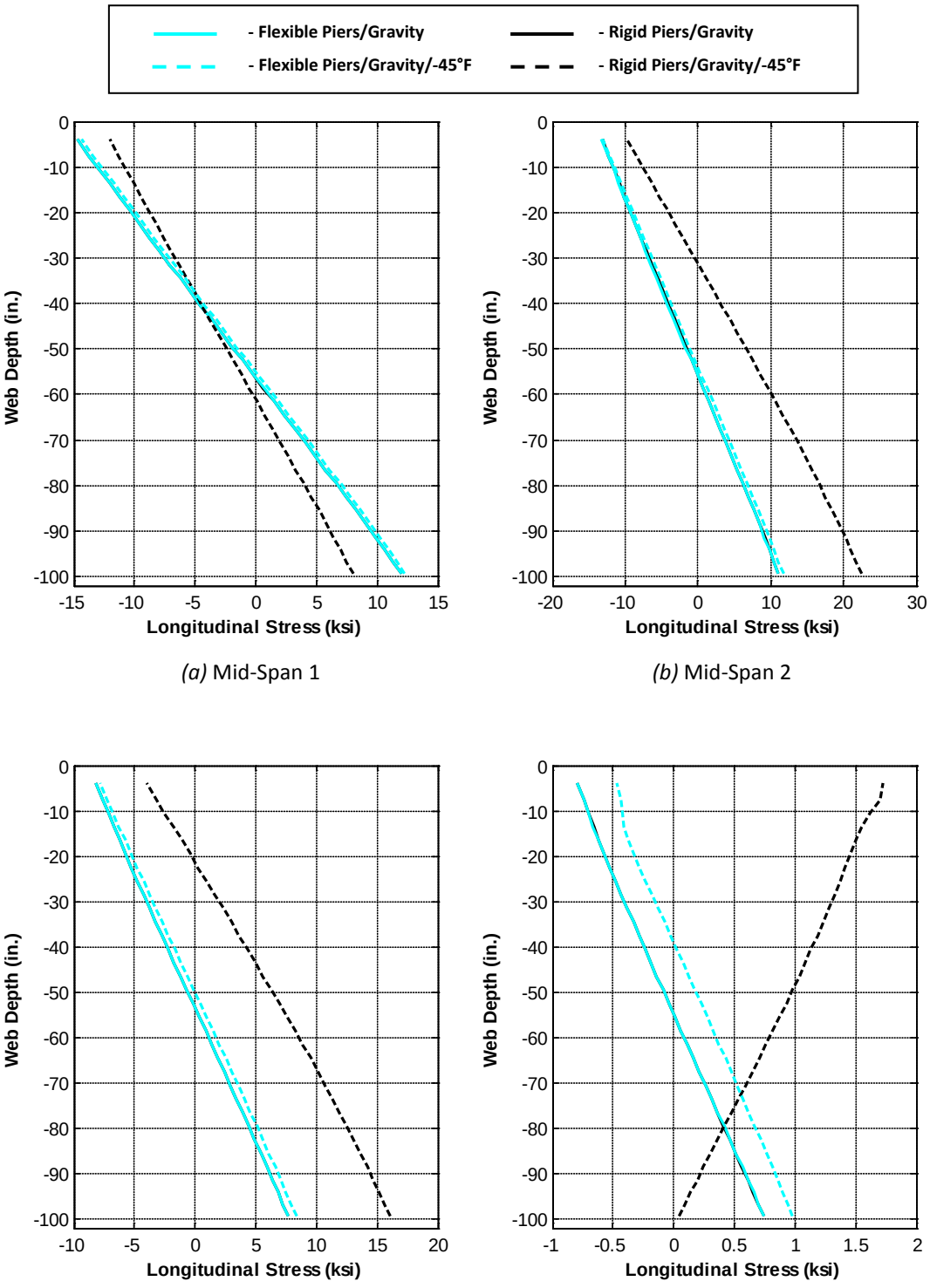


**Figure C.40. Girder 8 Mid-Span Web Longitudinal Stress Profiles – Gravity and -45°F Loading**

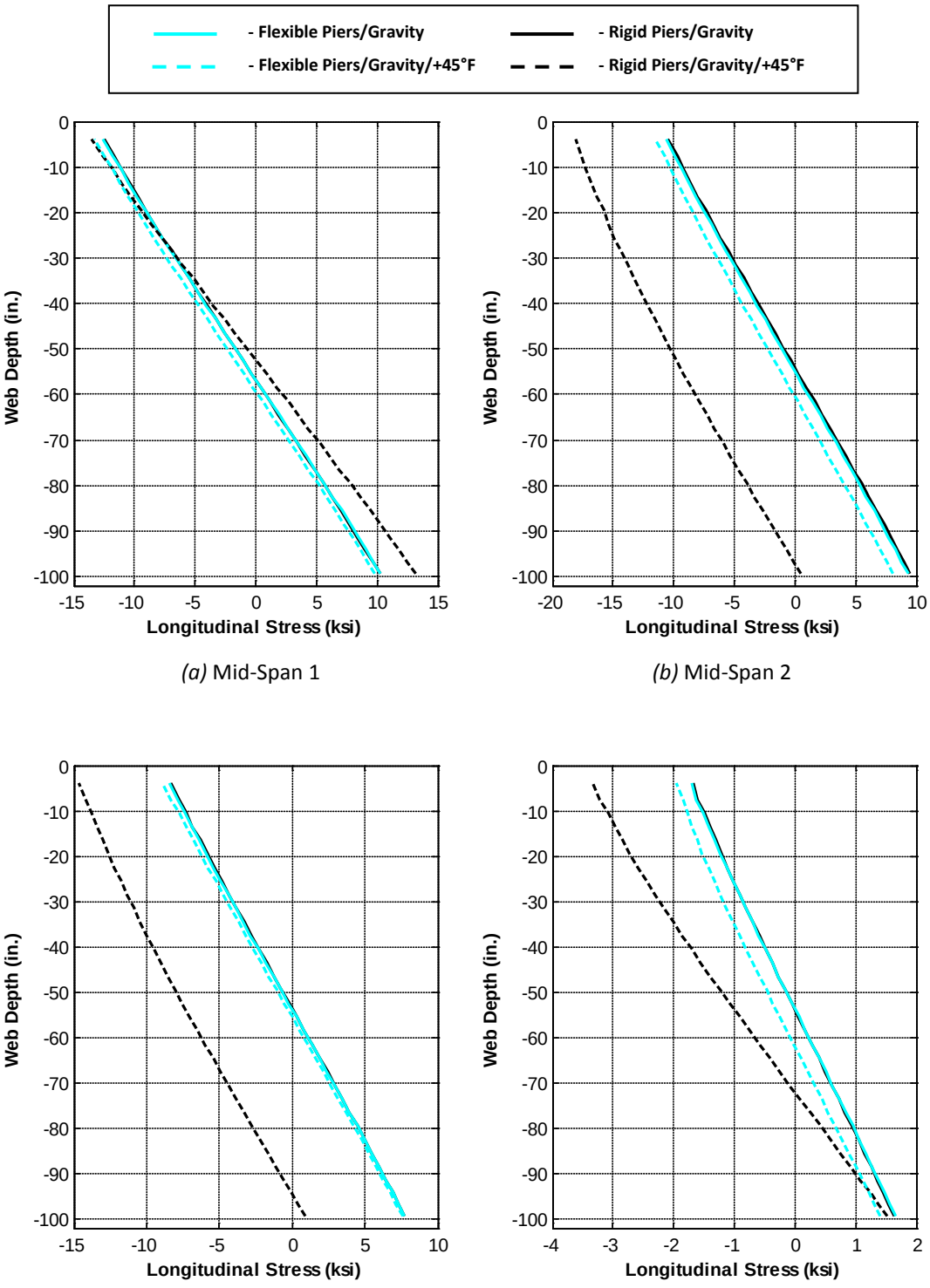


**Figure C.41. Girder 1 Mid-Span Web Longitudinal Stress Profiles – Gravity and +45°F Loading**

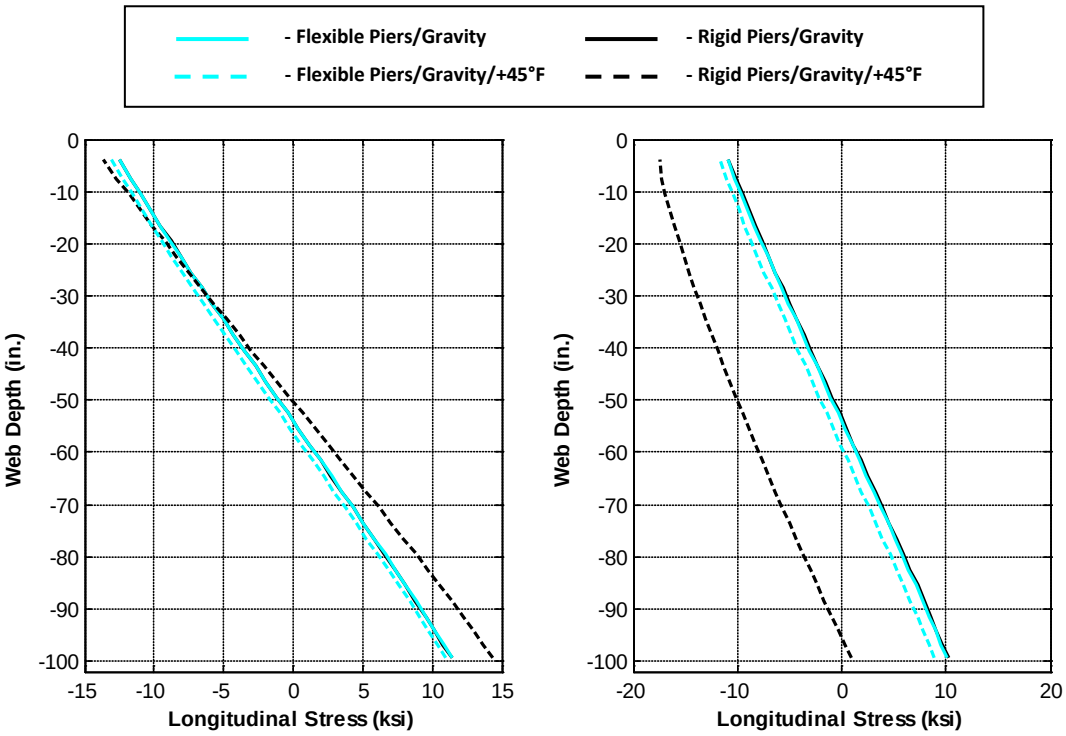


*(a)* Mid-Span 1

*(b)* Mid-Span 2

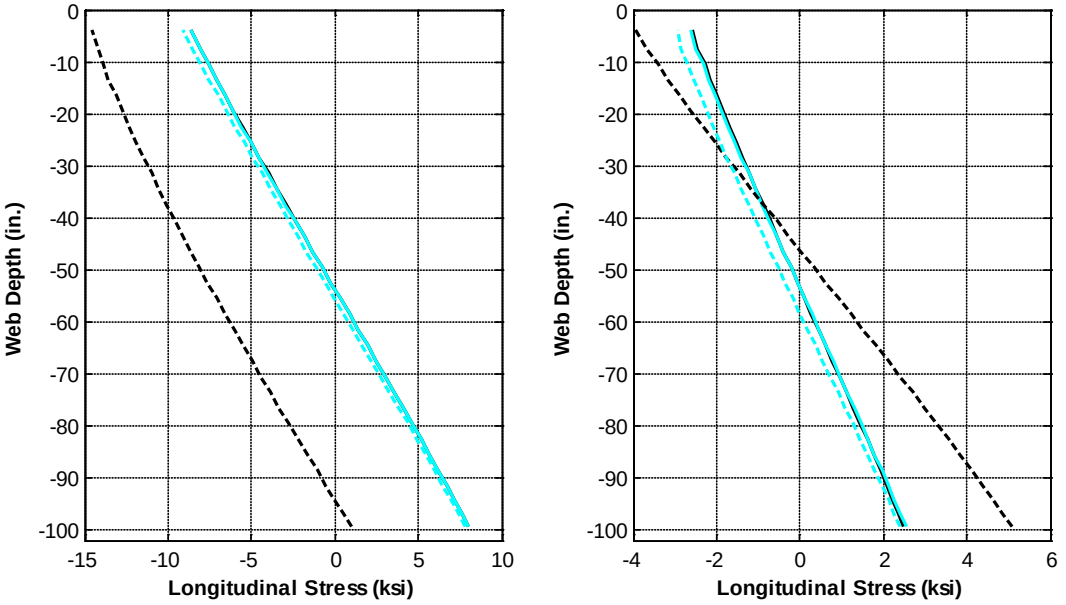


*(c)* Mid-Span 3

*(d)* Mid-Span 4

**Figure C.42. Girder 2 Mid-Span Web Longitudinal Stress Profiles – Gravity and +45°F Loading**

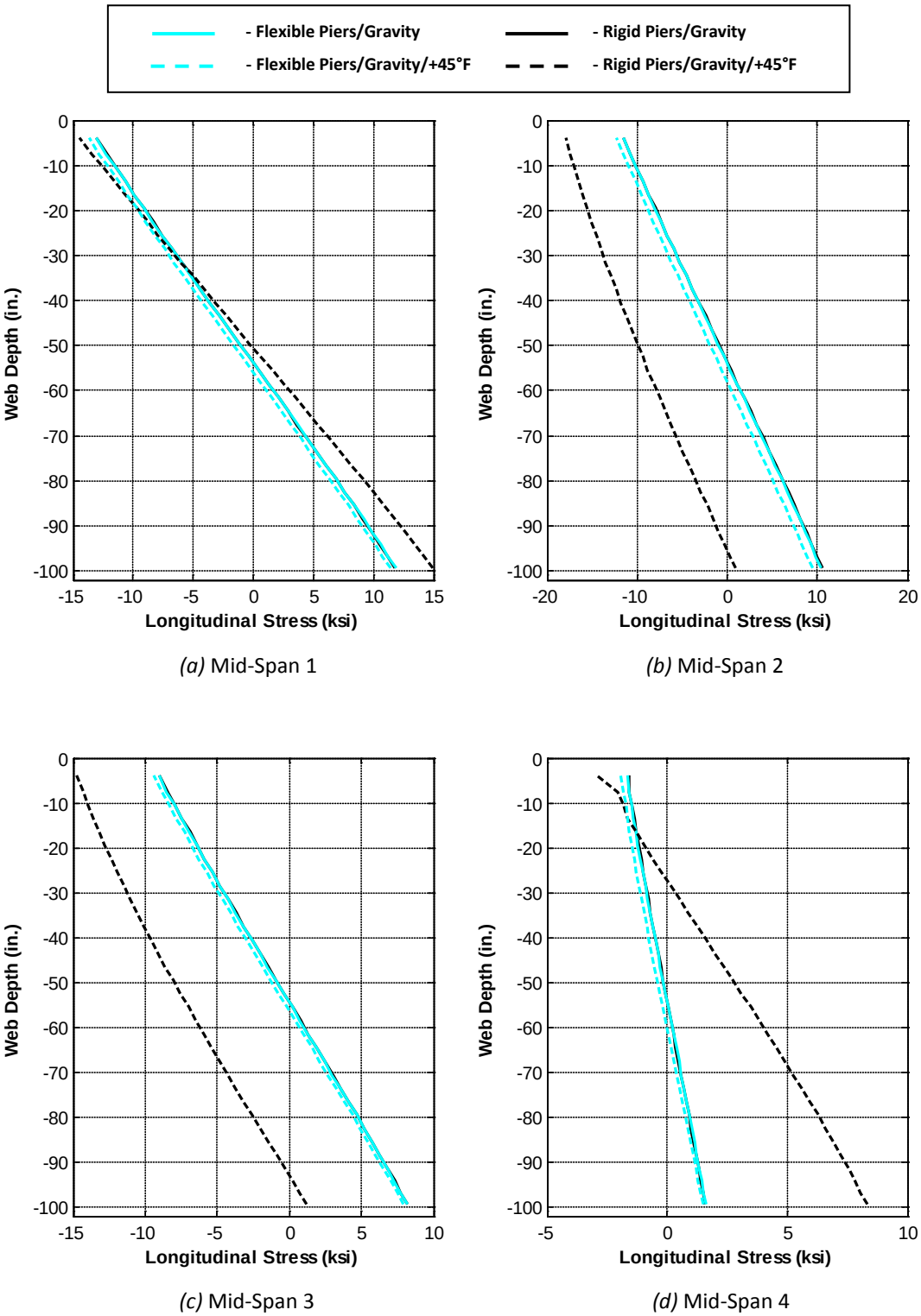


**Figure C.43. Girder 3 Mid-Span Web Longitudinal Stress Profiles – Gravity and +45°F Loading**

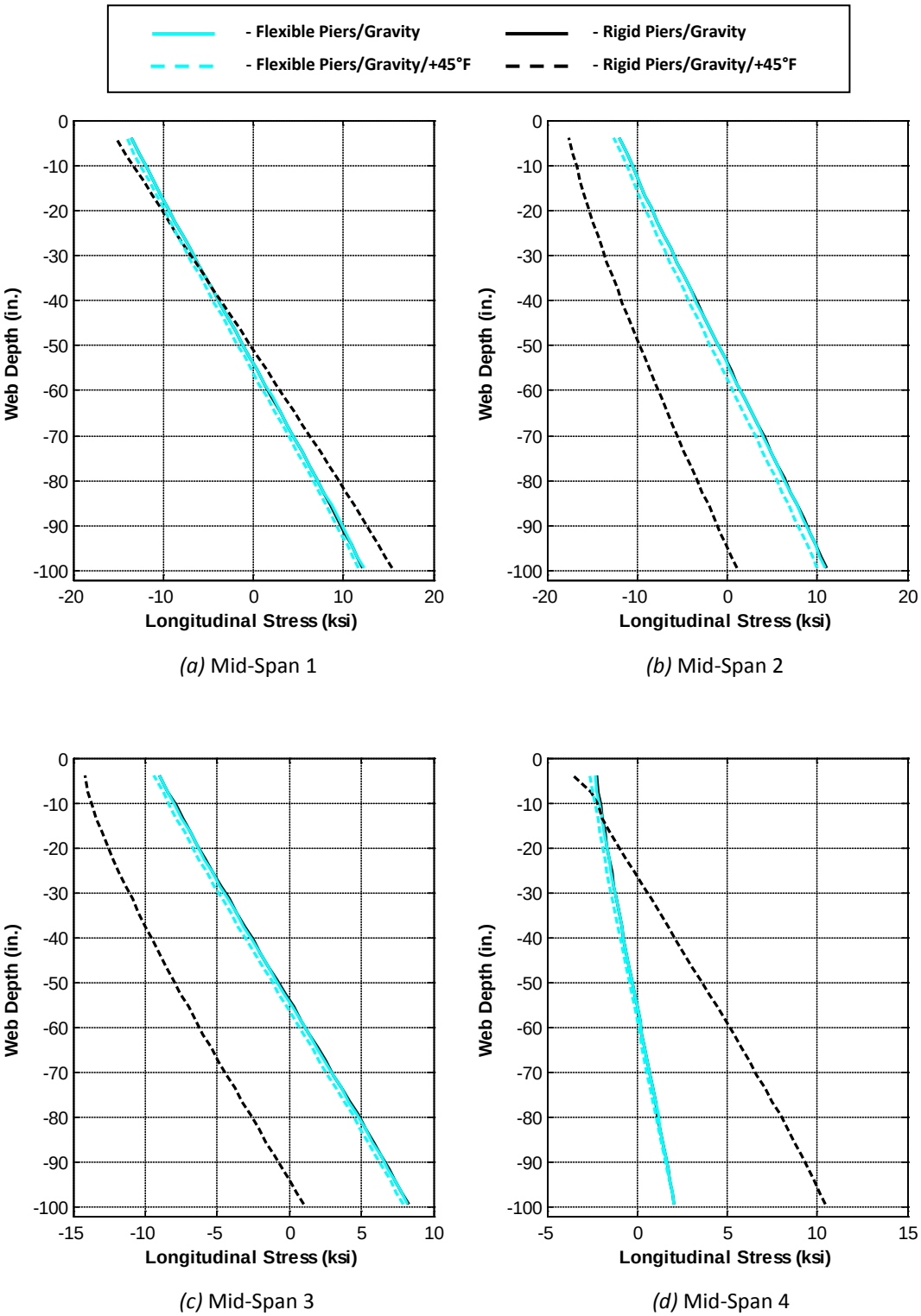


**Figure C.44. Girder 4 Mid-Span Web Longitudinal Stress Profiles – Gravity and +45°F Loading**

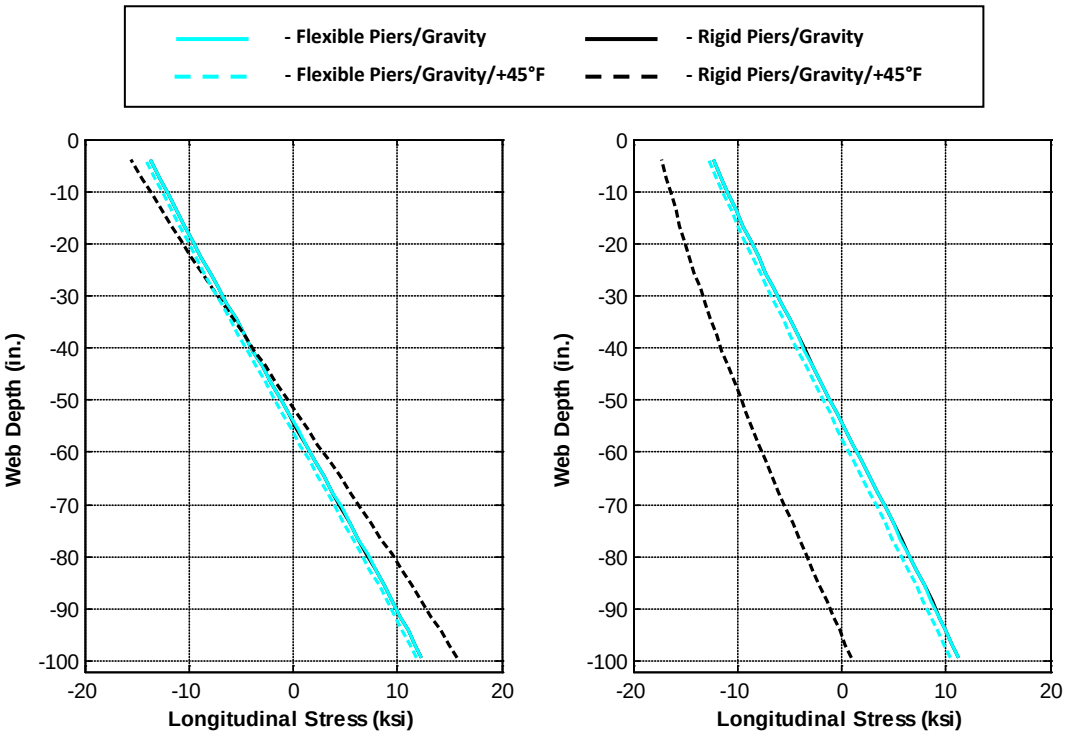


*(a)* Mid-Span 1

*(b)* Mid-Span 2

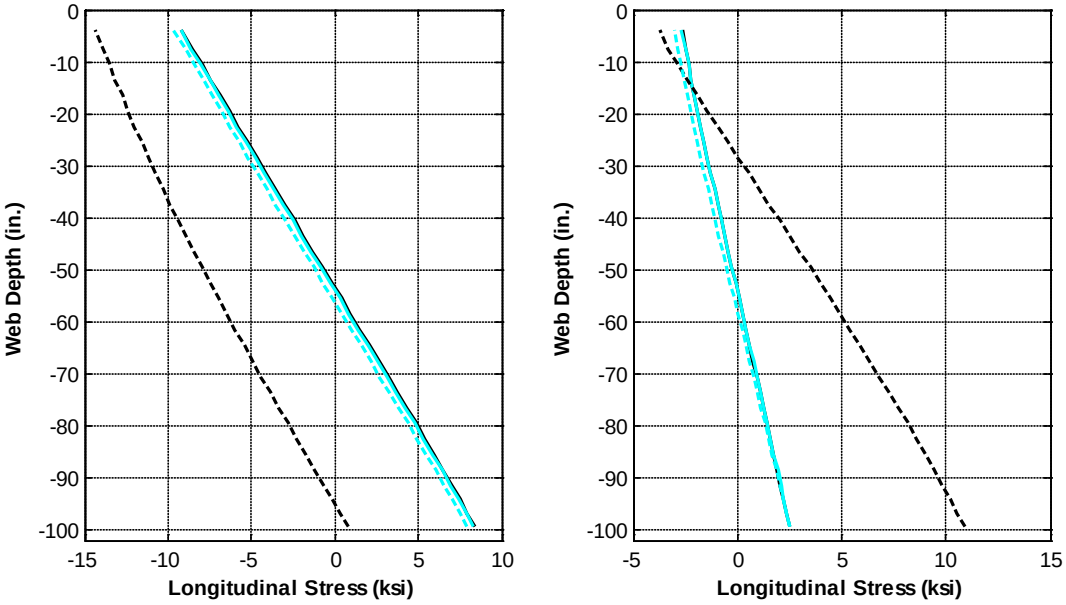


*(c)* Mid-Span 3

*(d)* Mid-Span 4

**Figure C.45. Girder 5 Mid-Span Web Longitudinal Stress Profiles – Gravity and +45°F Loading**

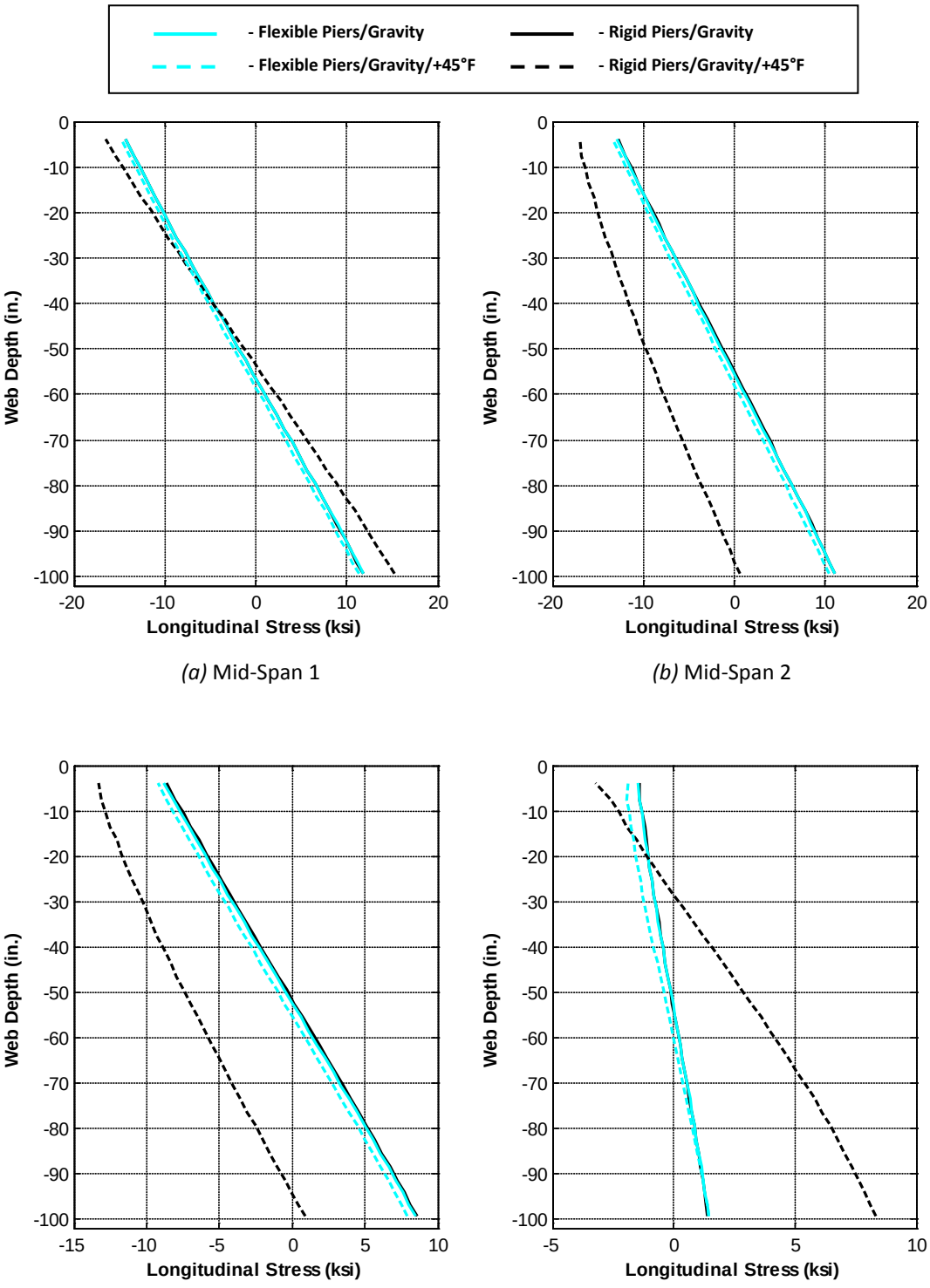


*(a)* Mid-Span 1

*(b)* Mid-Span 2

*(c)* Mid-Span 3

*(d)* Mid-Span 4

**Figure C.46. Girder 6 Mid-Span Web Longitudinal Stress Profiles – Gravity and +45°F Loading**

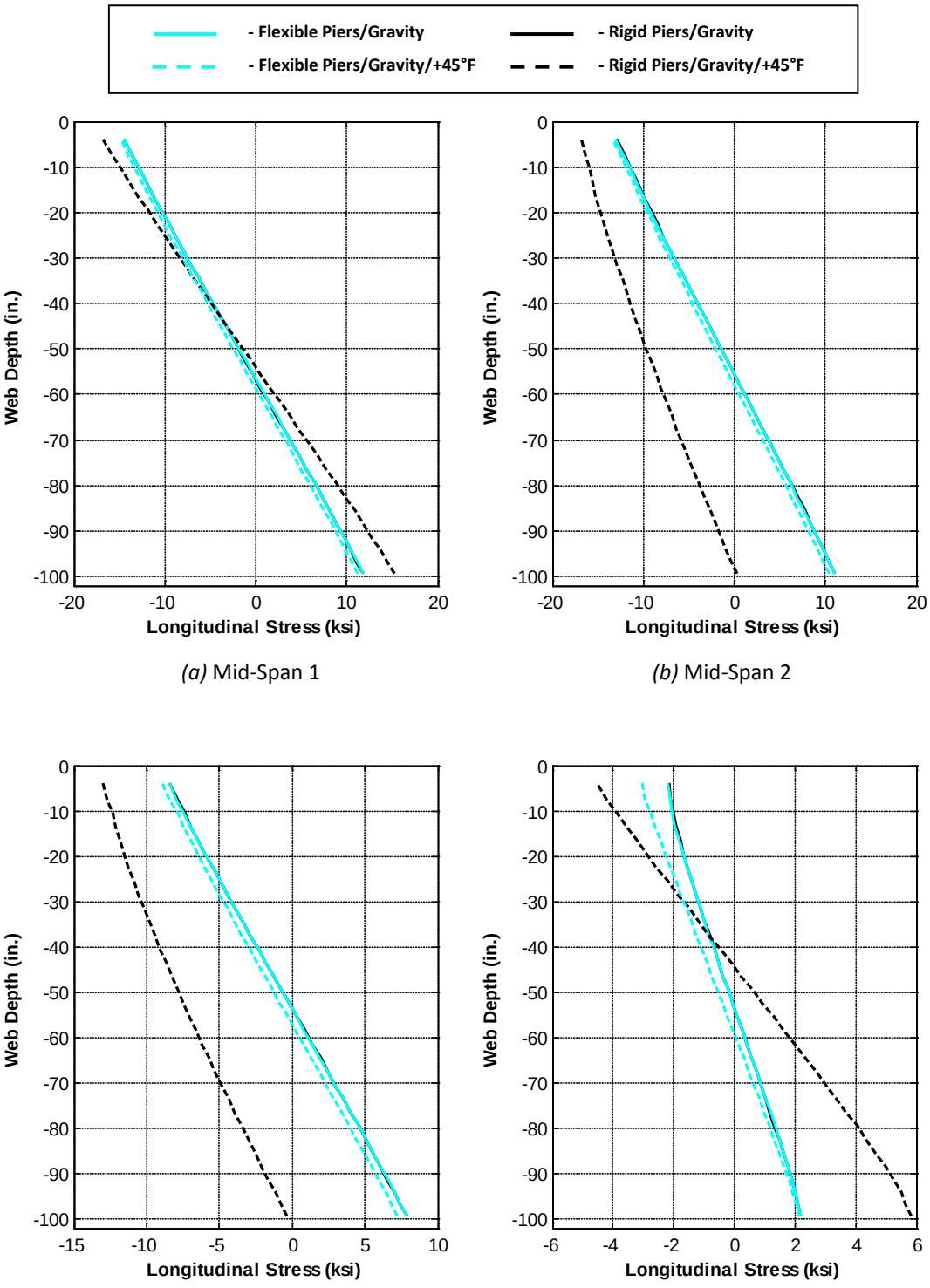


**Figure C.47. Girder 7 Mid-Span Web Longitudinal Stress Profiles – Gravity and +45°F Loading**

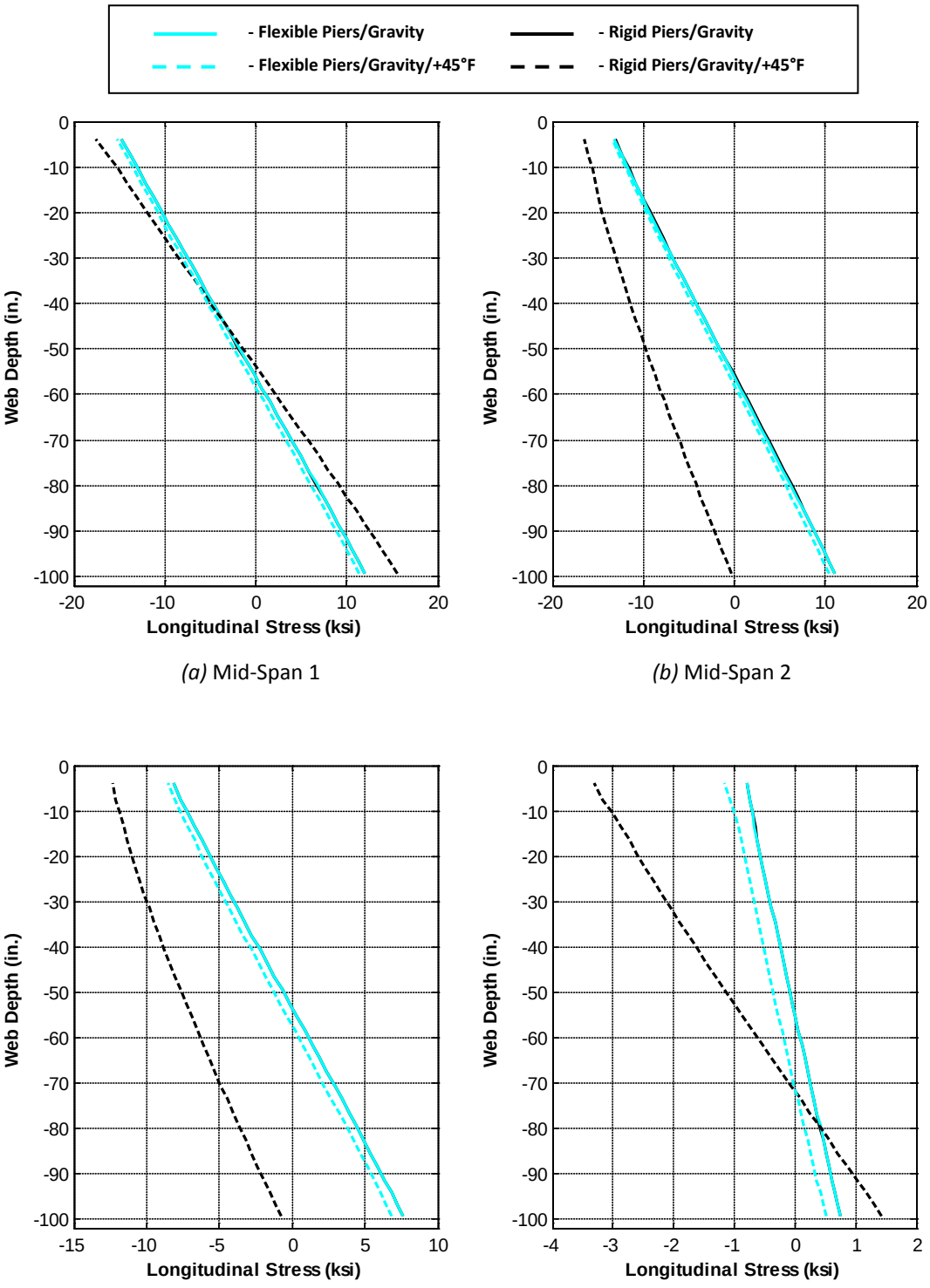


**Figure C.48. Girder 8 Mid-Span Web Longitudinal Stress Profiles – Gravity and +45°F Loading**

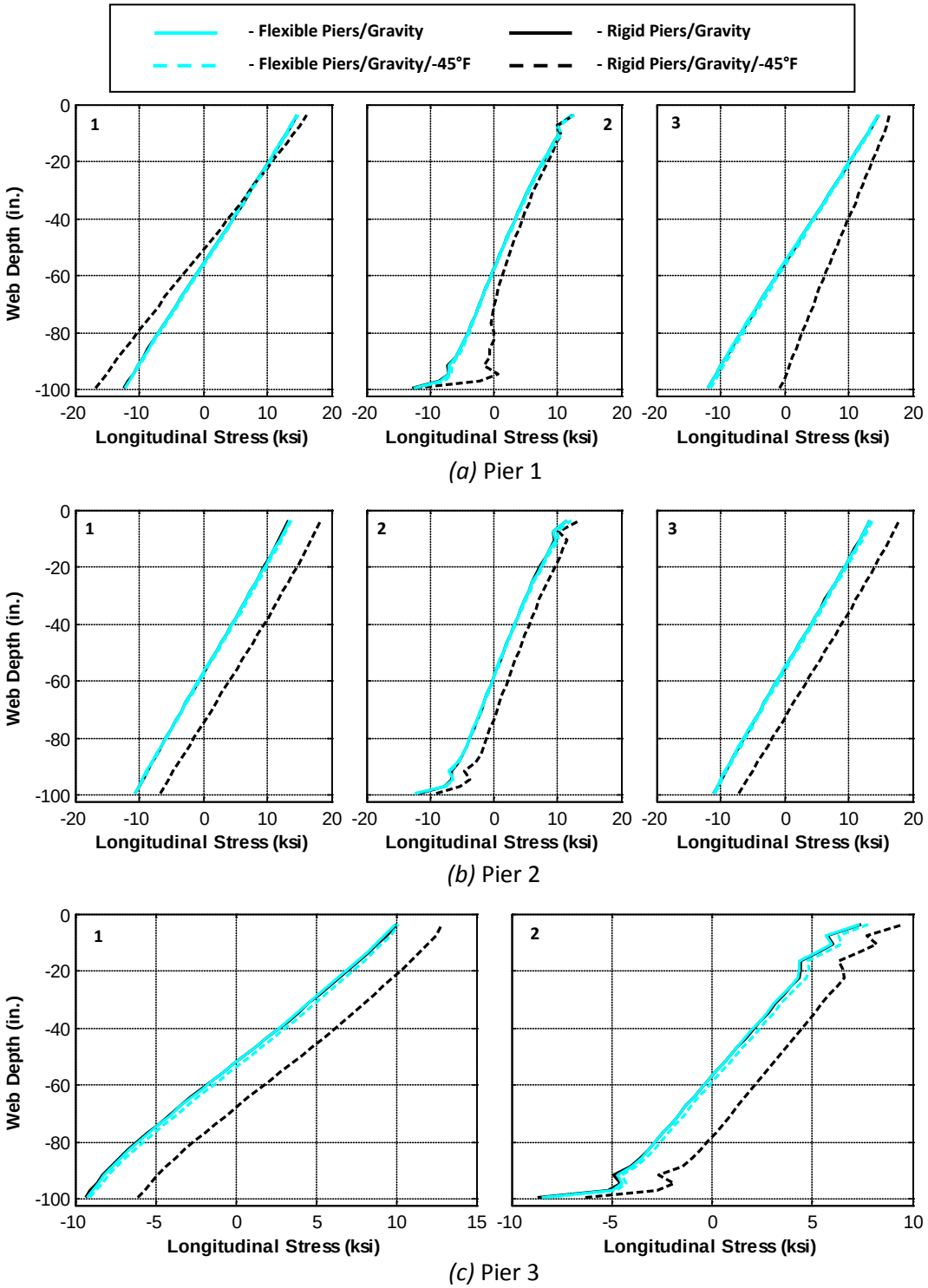


**Figure C.49. Girder 1 Pier Web Longitudinal Stress Profiles – Gravity and -45°F Loading**

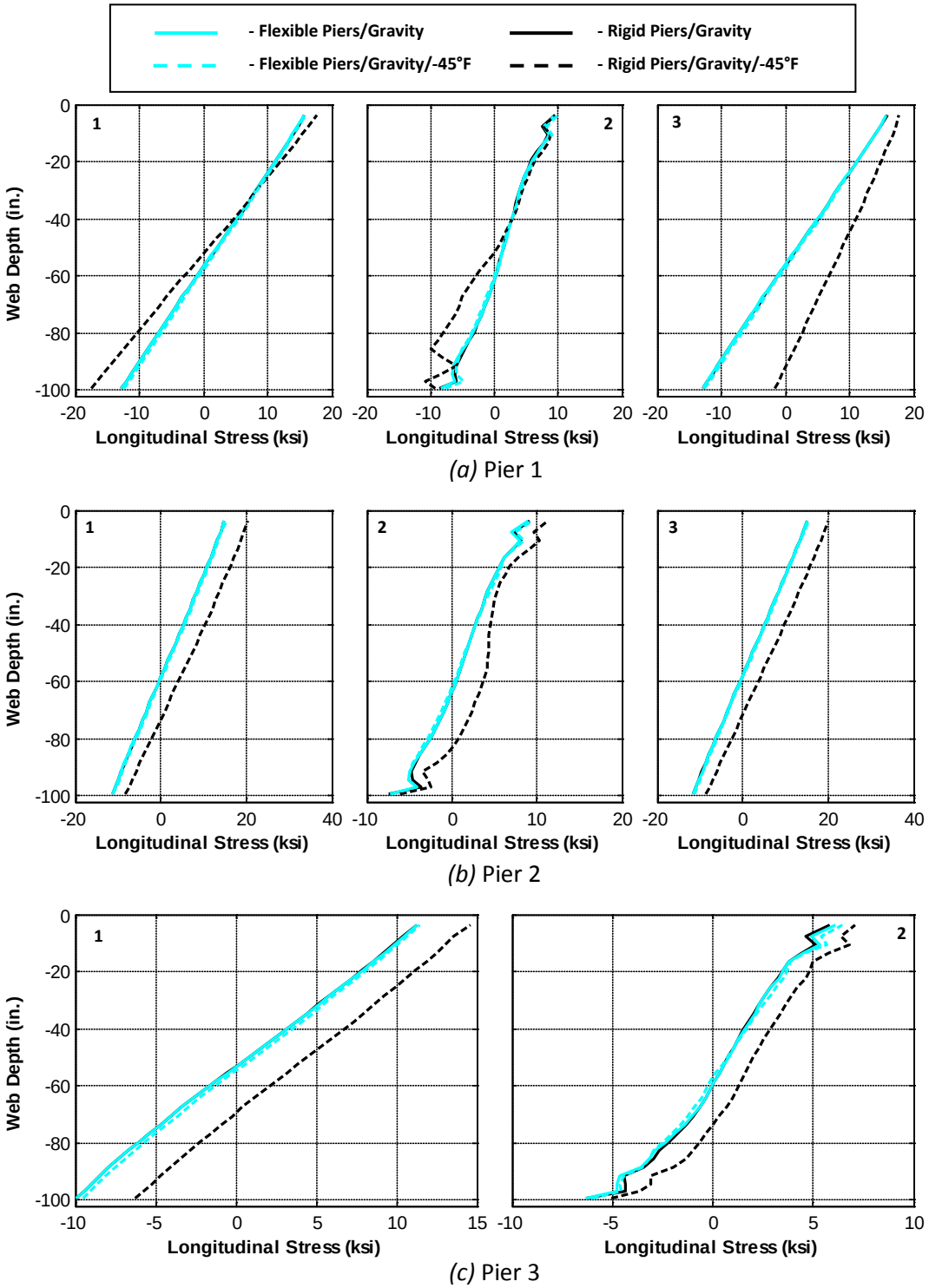


**Figure C.50. Girder 2 Pier Web Longitudinal Stress Profiles – Gravity and -45°F Loading**

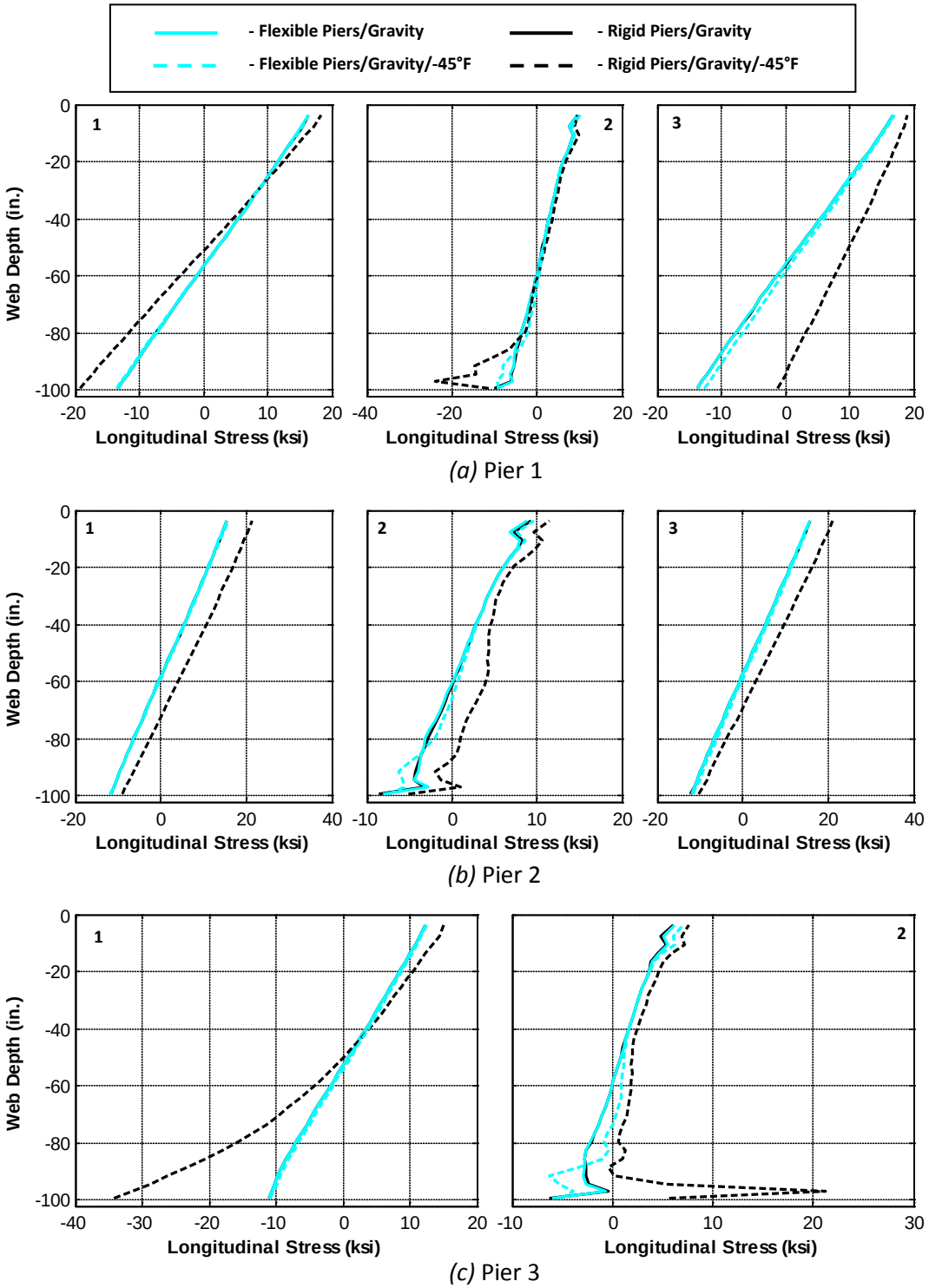


**Figure C.51. Girder 3 Pier Web Longitudinal Stress Profiles – Gravity and -45°F Loading**

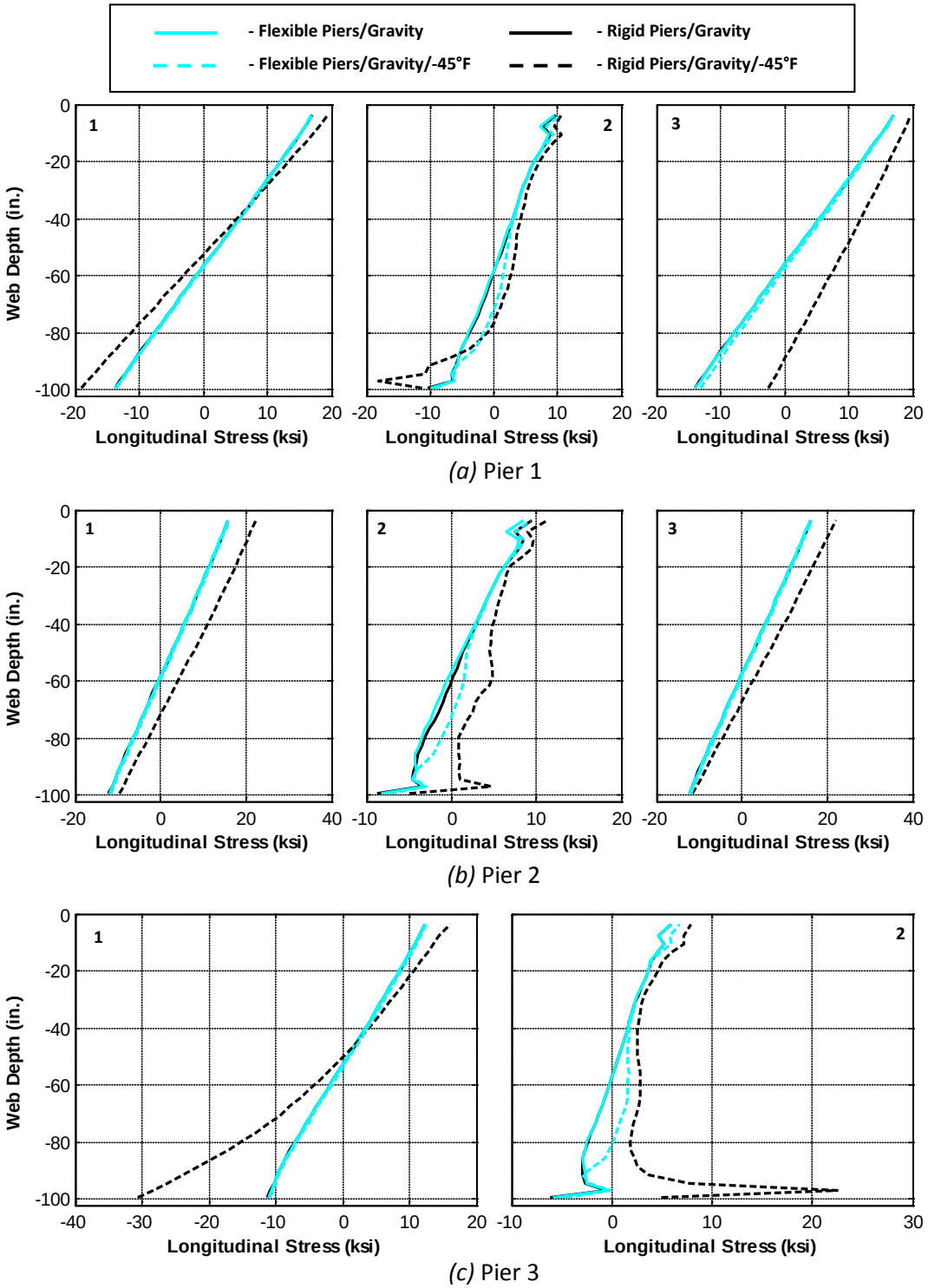


**Figure C.52. Girder 4 Pier Web Longitudinal Stress Profiles – Gravity and -45°F Loading**

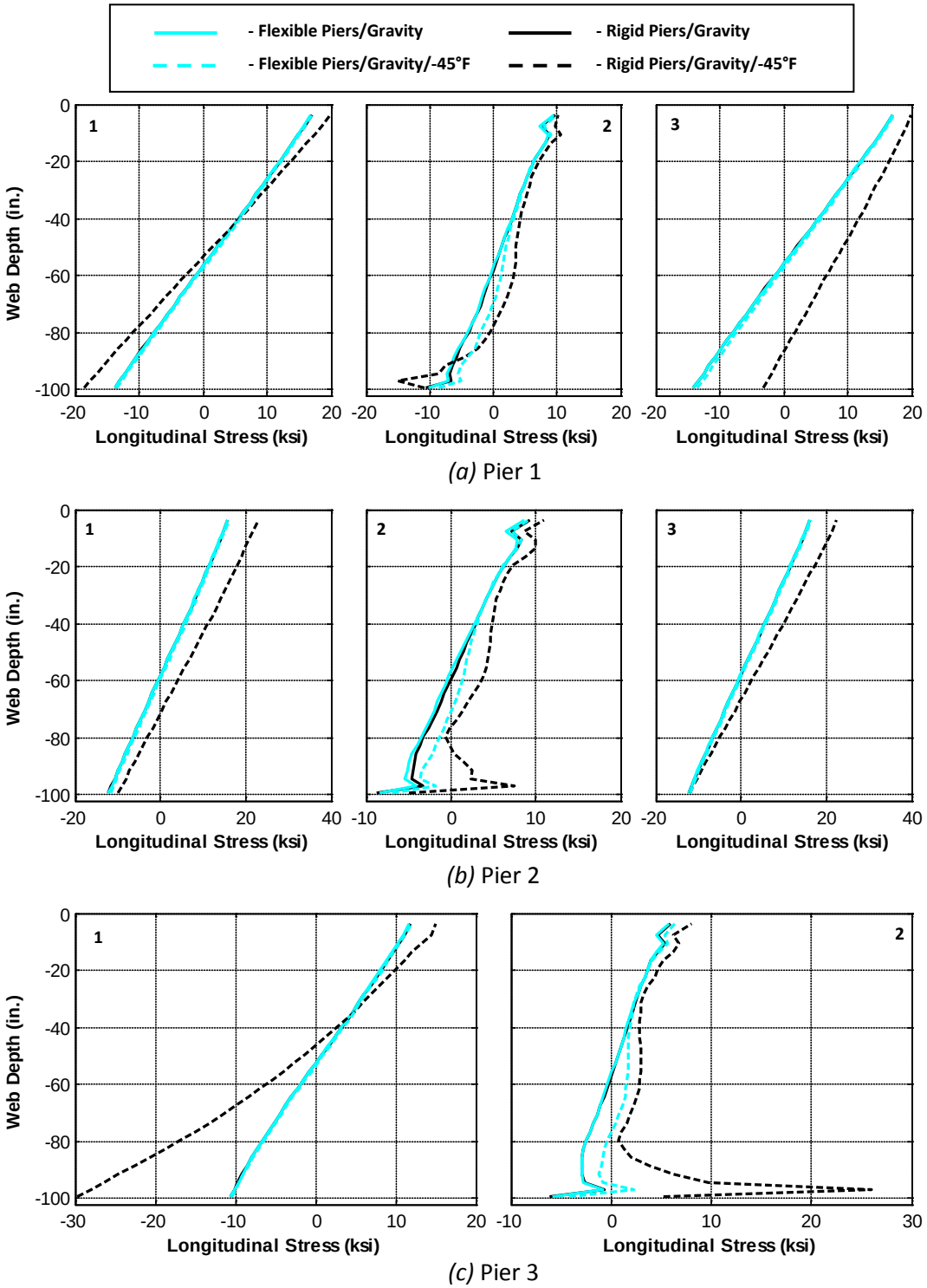


**Figure C.53. Girder 5 Pier Web Longitudinal Stress Profiles – Gravity and -45°F Loading**

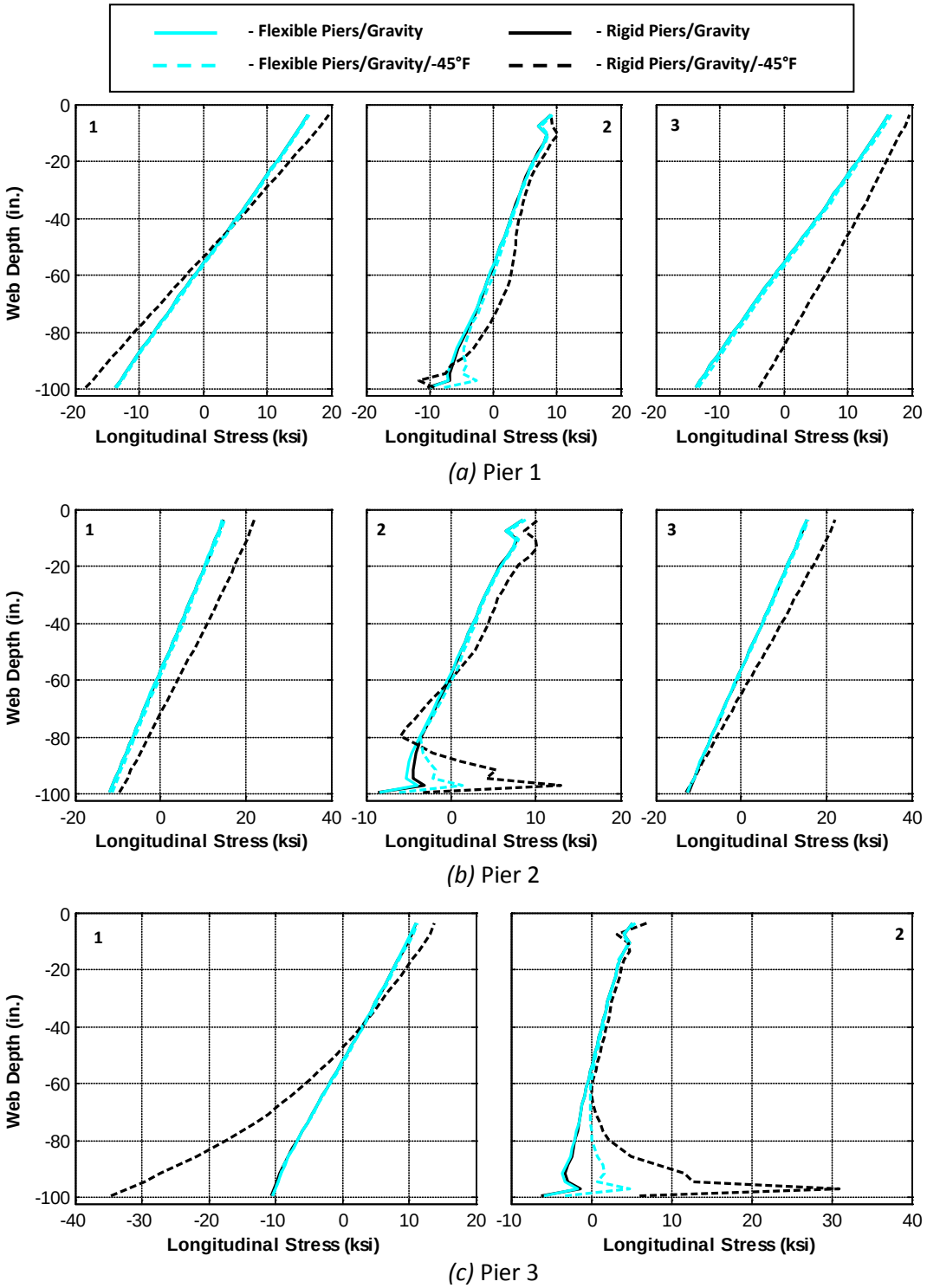


**Figure C.54. Girder 6 Pier Web Longitudinal Stress Profiles – Gravity and -45°F Loading**

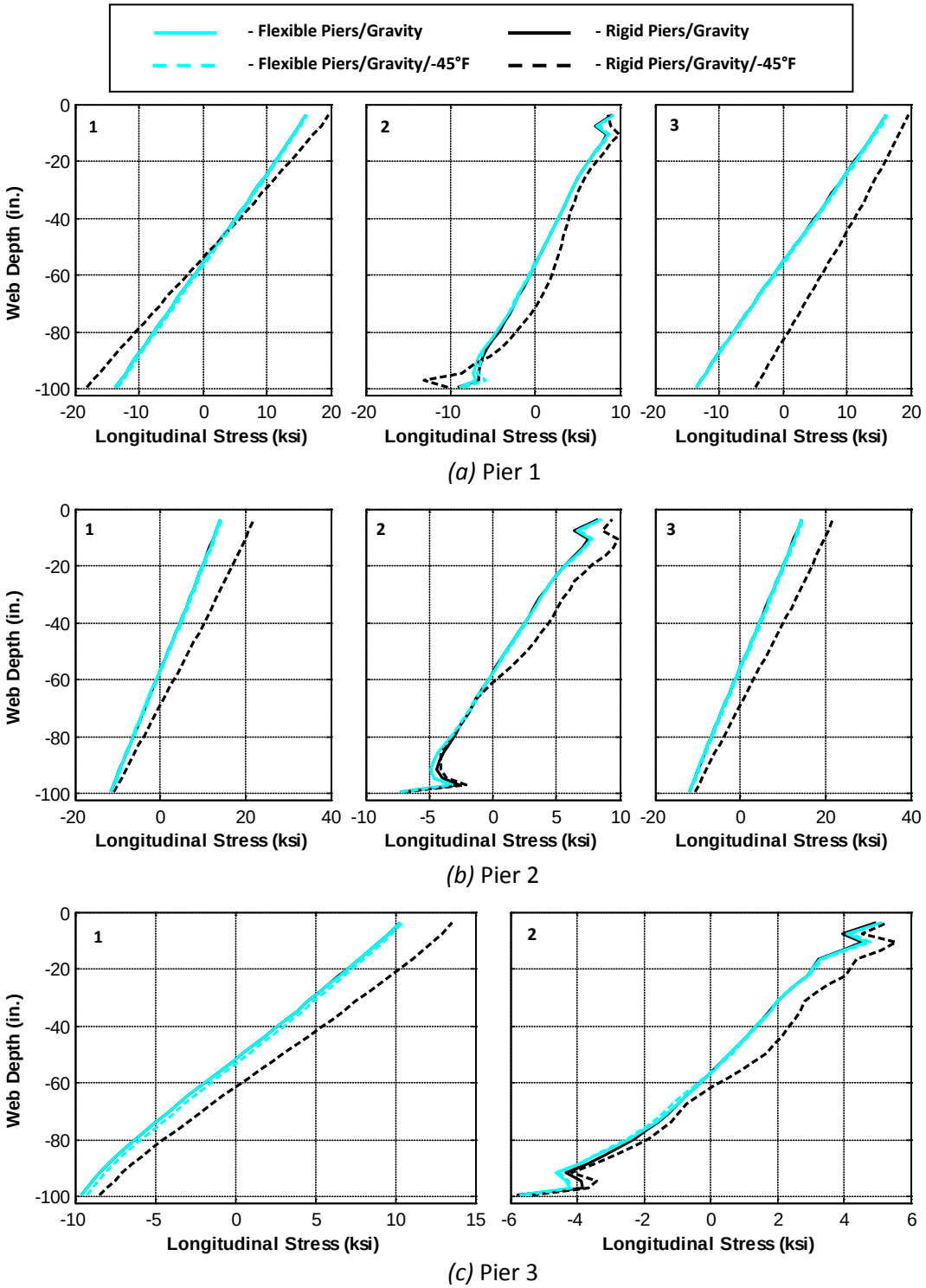


*(a)* Pier 1

*(b)* Pier 2

*(c)* Pier 3

**Figure C.55. Girder 7 Pier Web Longitudinal Stress Profiles – Gravity and -45°F Loading**

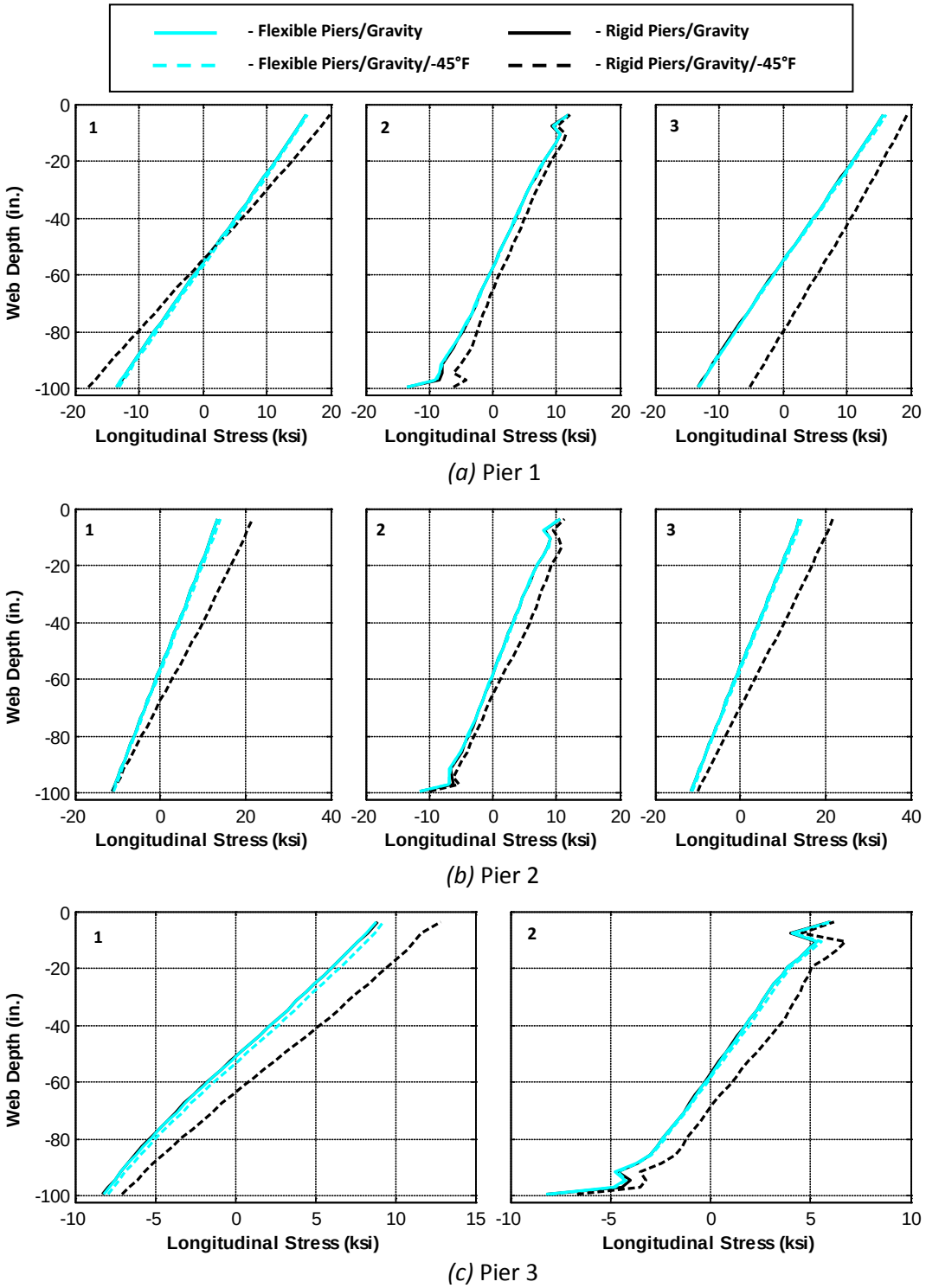


**Figure C.56. Girder 8 Pier Web Longitudinal Stress Profiles – Gravity and -45°F Loading**

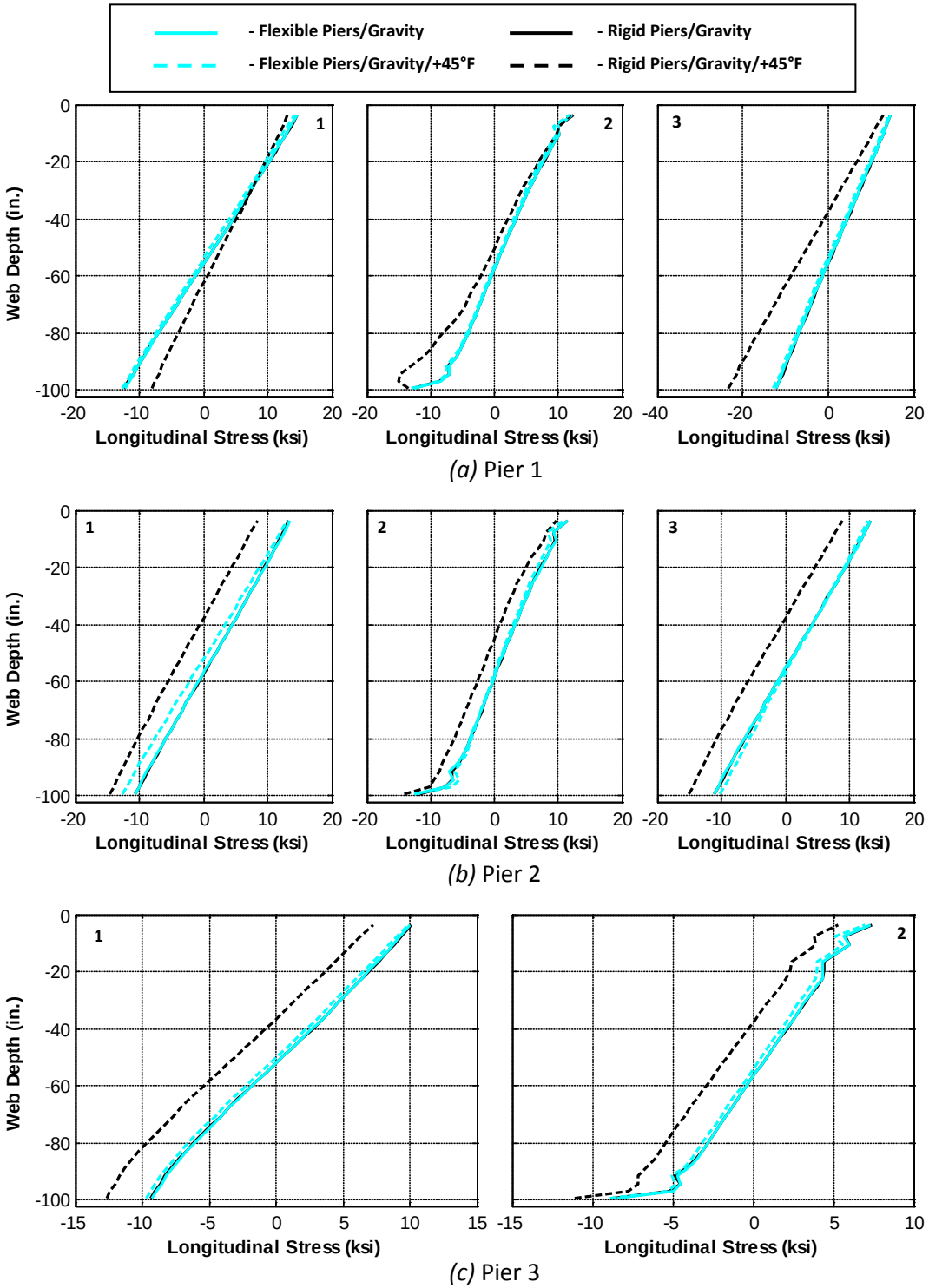


**Figure C.57. Girder 1 Pier Web Longitudinal Stress Profiles – Gravity and +45°F Loading**

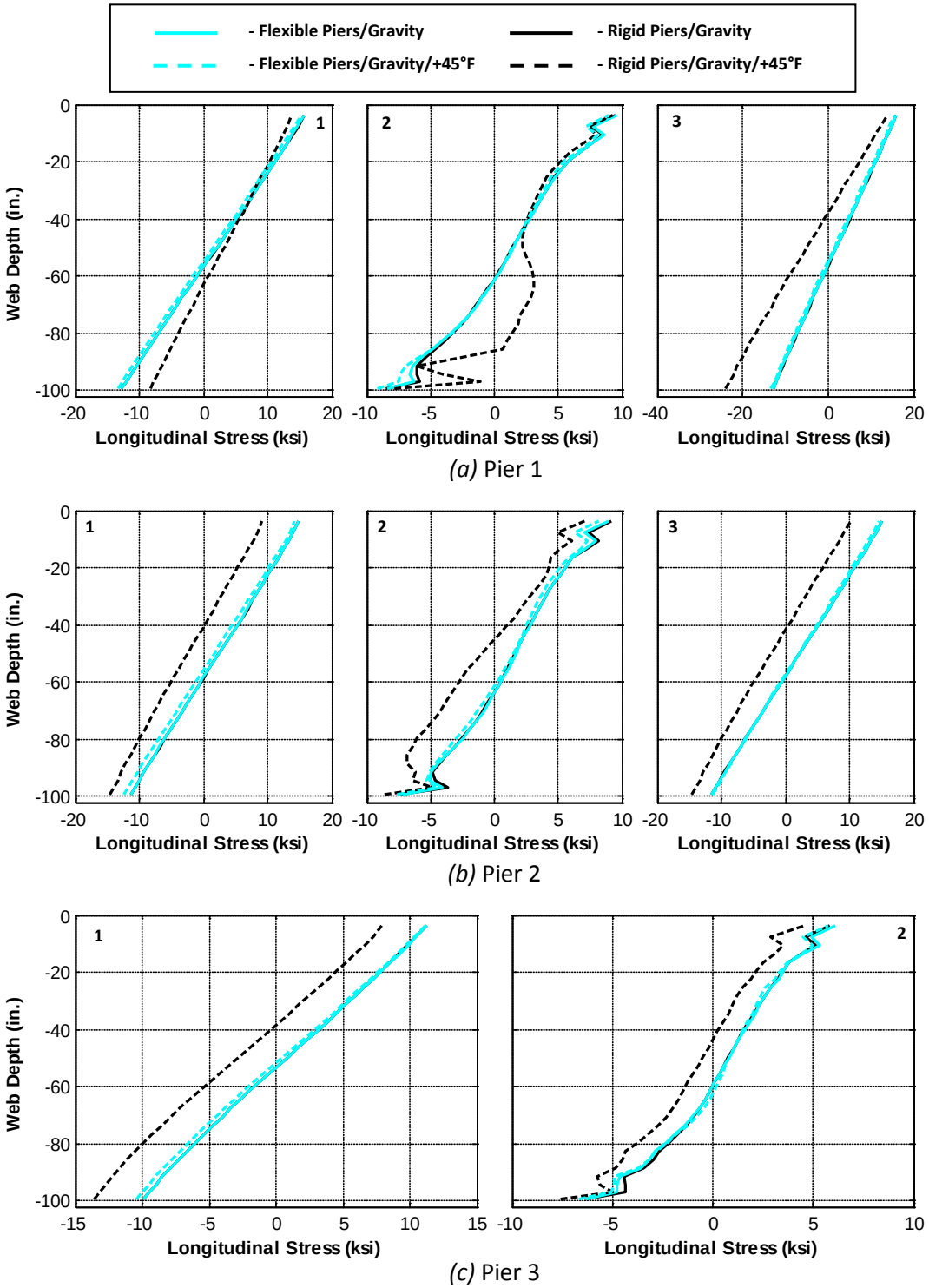


**Figure C.58. Girder 2 Pier Web Longitudinal Stress Profiles – Gravity and +45°F Loading**

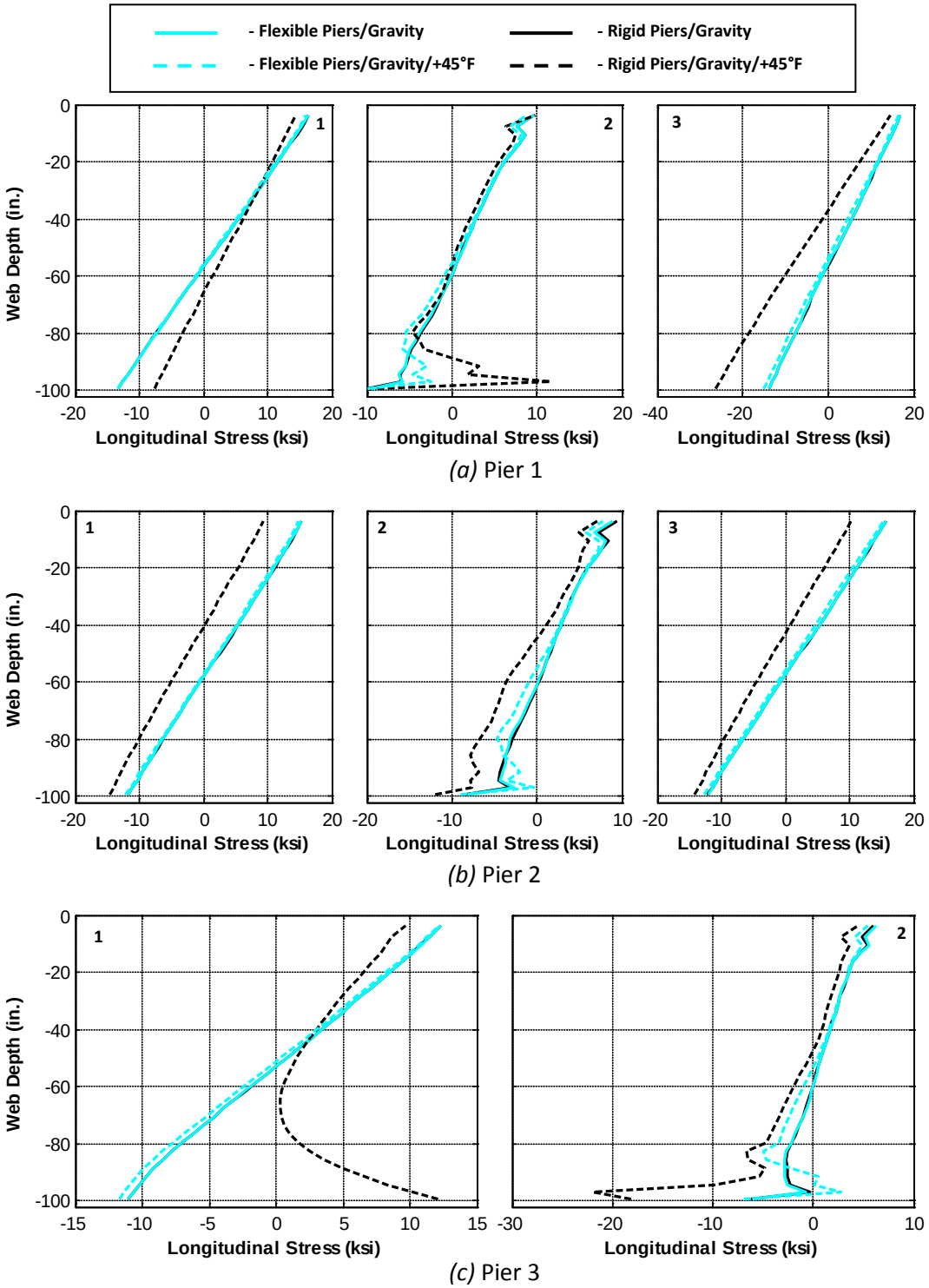


**Figure C.59. Girder 3 Pier Web Longitudinal Stress Profiles – Gravity and +45°F Loading**

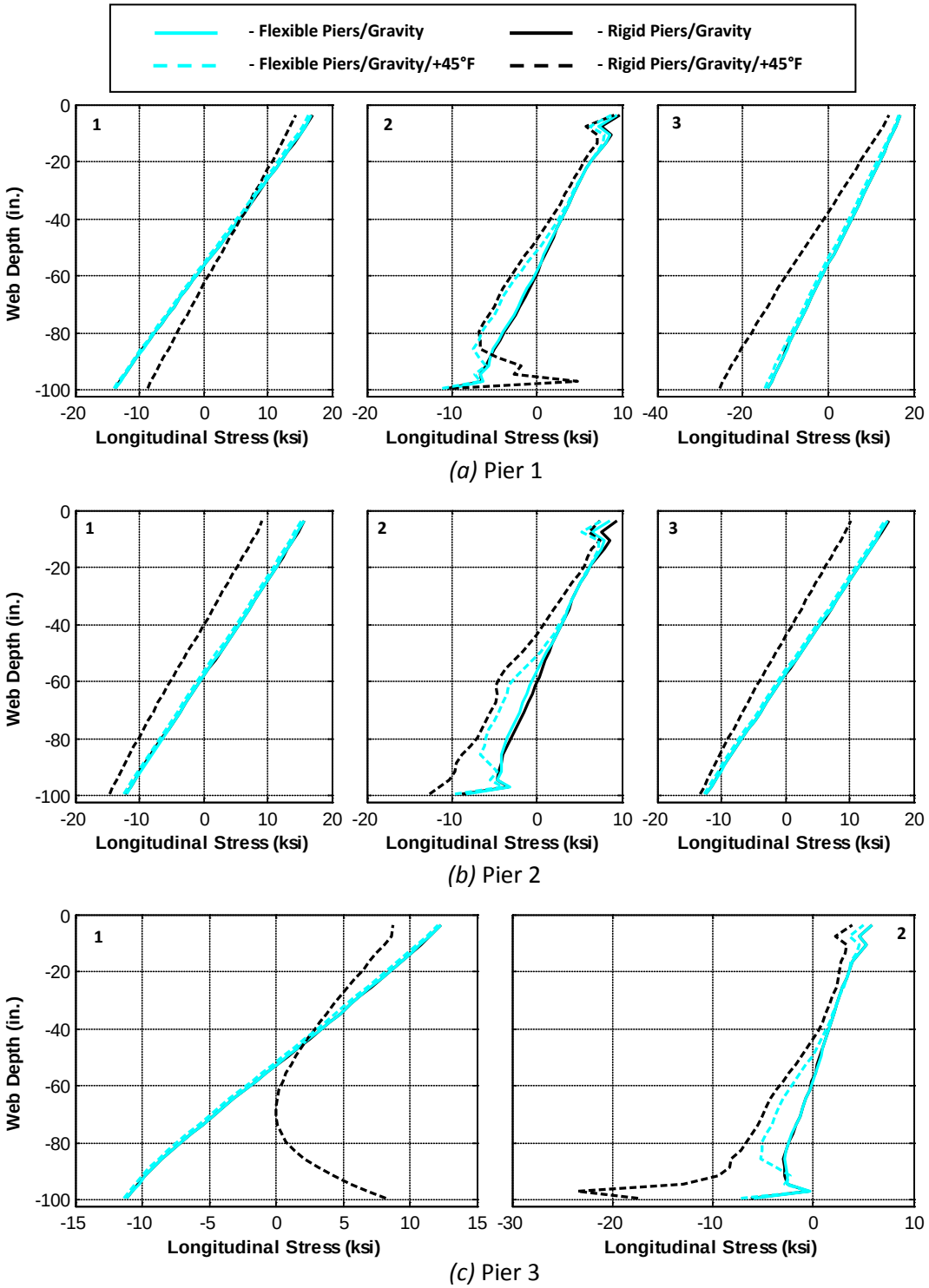


**Figure C.60. Girder 4 Pier Web Longitudinal Stress Profiles – Gravity and +45°F Loading**

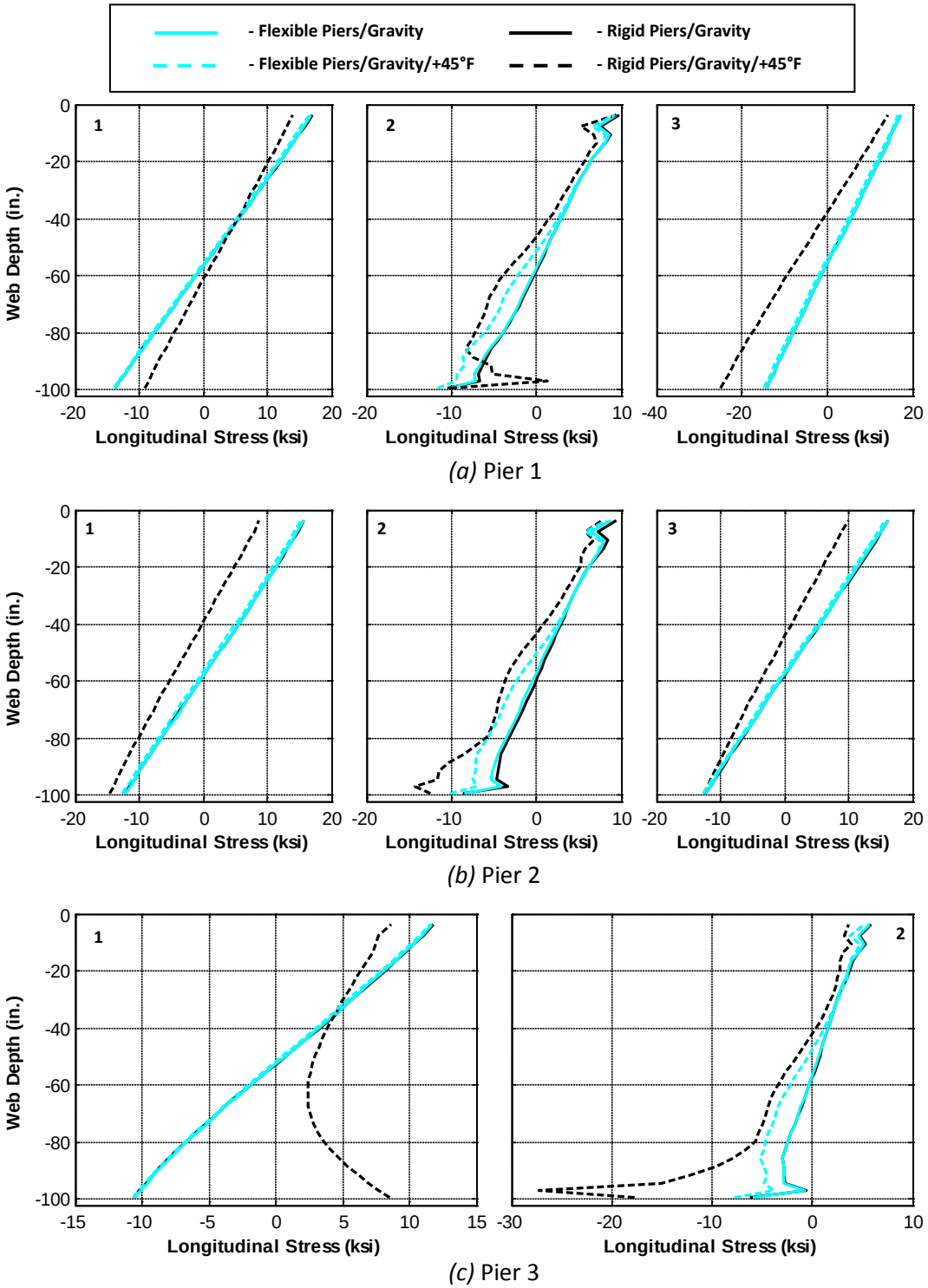


**Figure C.61. Girder 5 Pier Web Longitudinal Stress Profiles – Gravity and +45°F Loading**

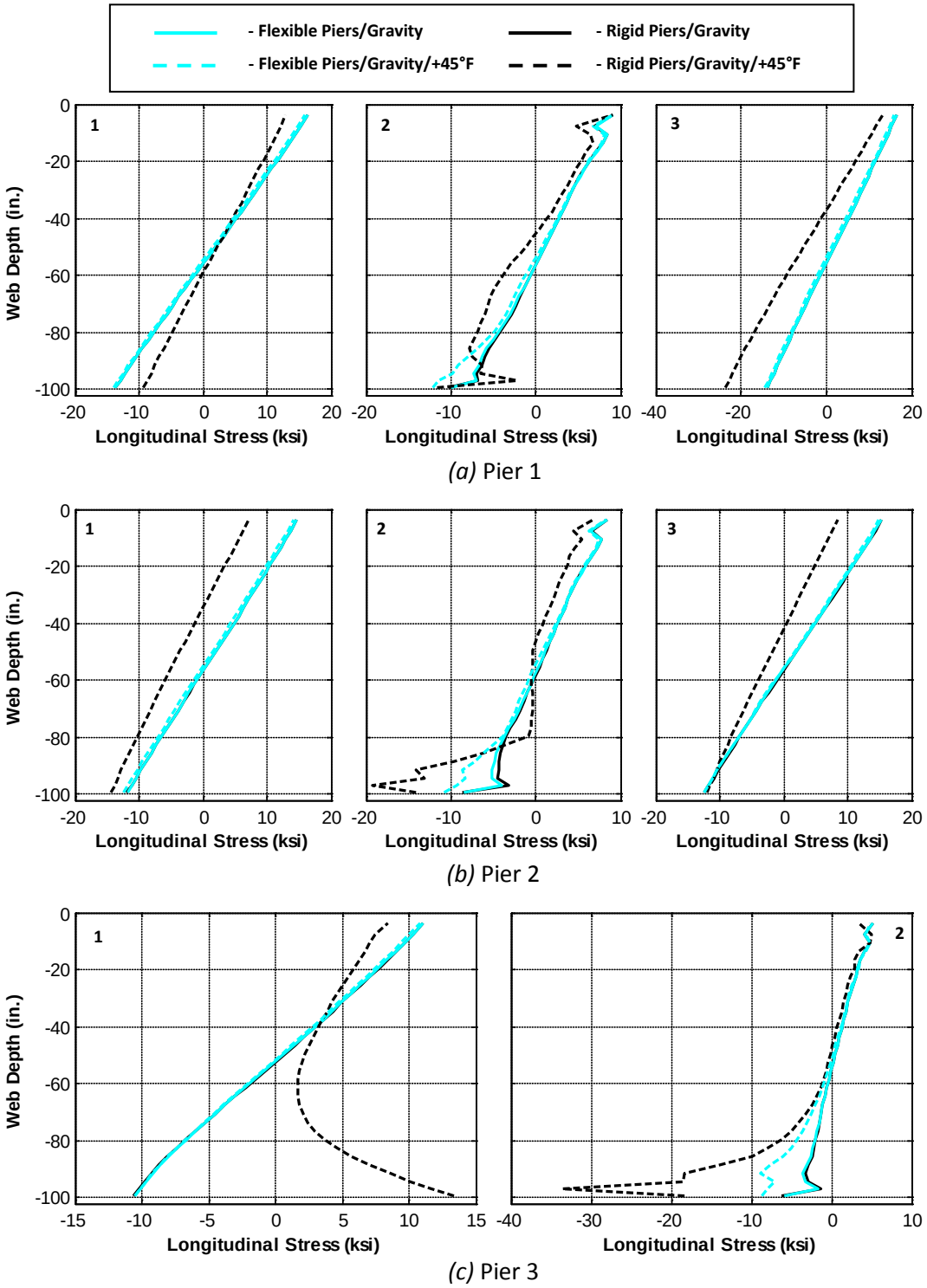


**Figure C.62. Girder 6 Pier Web Longitudinal Stress Profiles – Gravity and +45°F Loading**

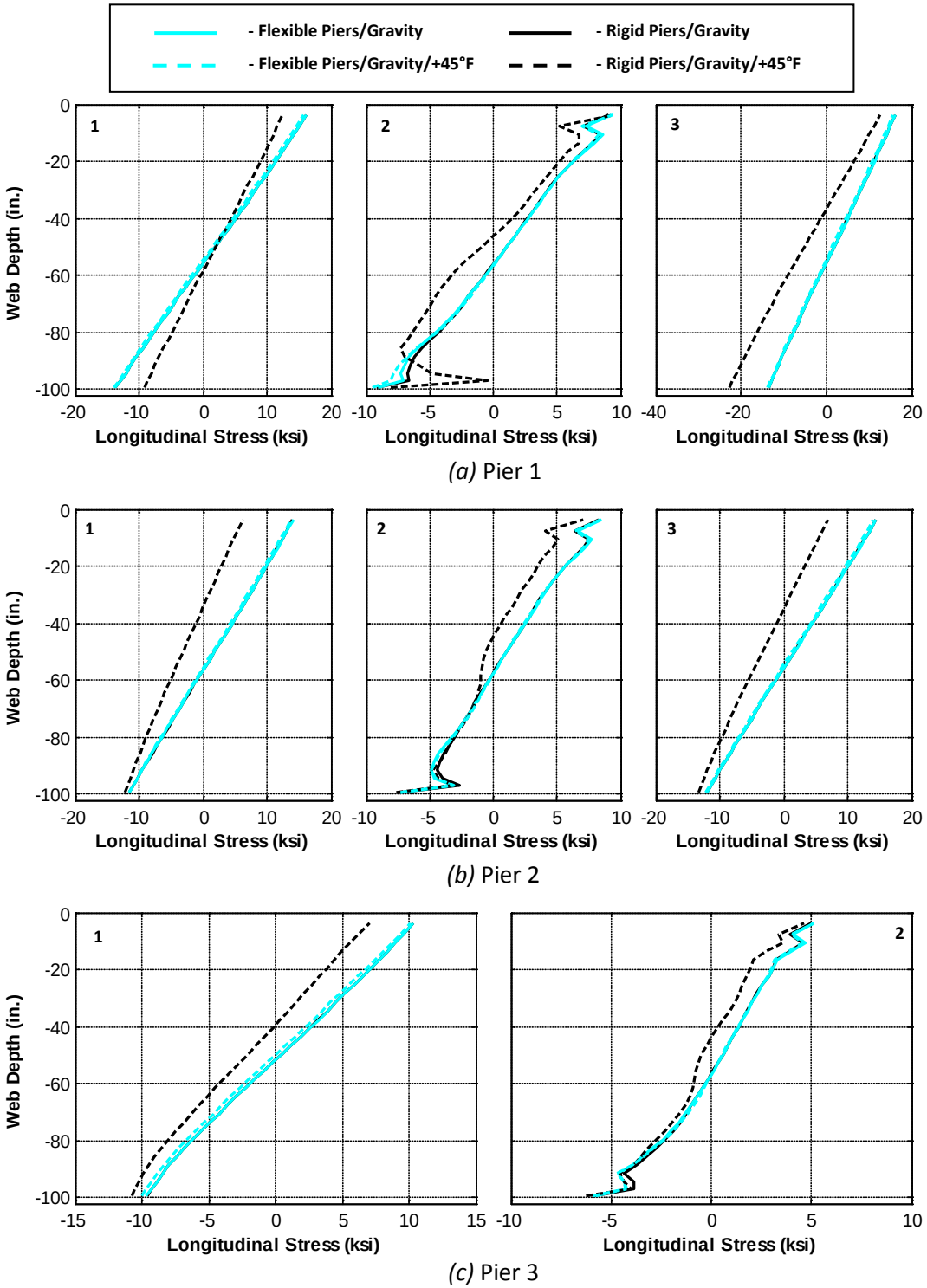


**Figure C.63. Girder 7 Pier Web Longitudinal Stress Profiles – Gravity and +45°F Loading**

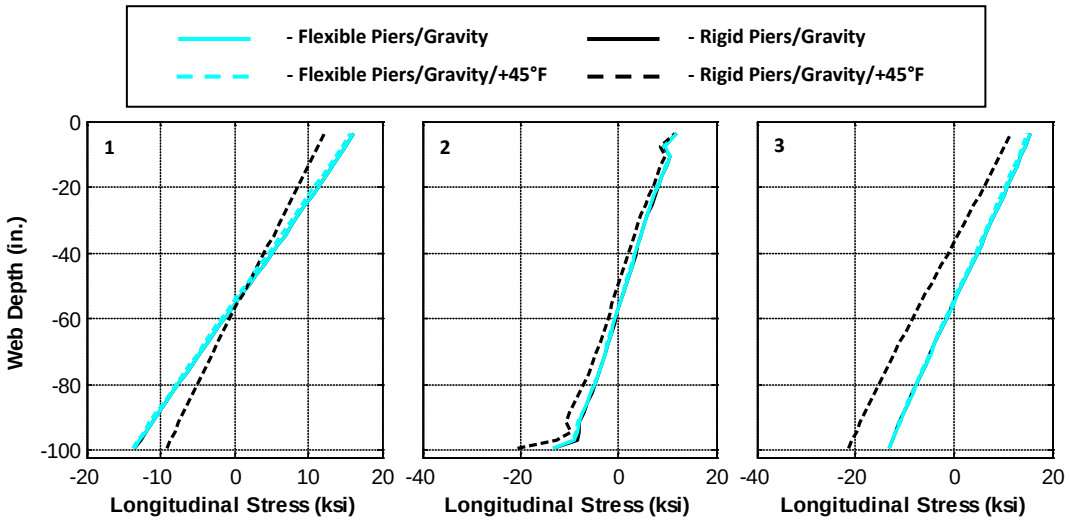


*(a)* Pier 1

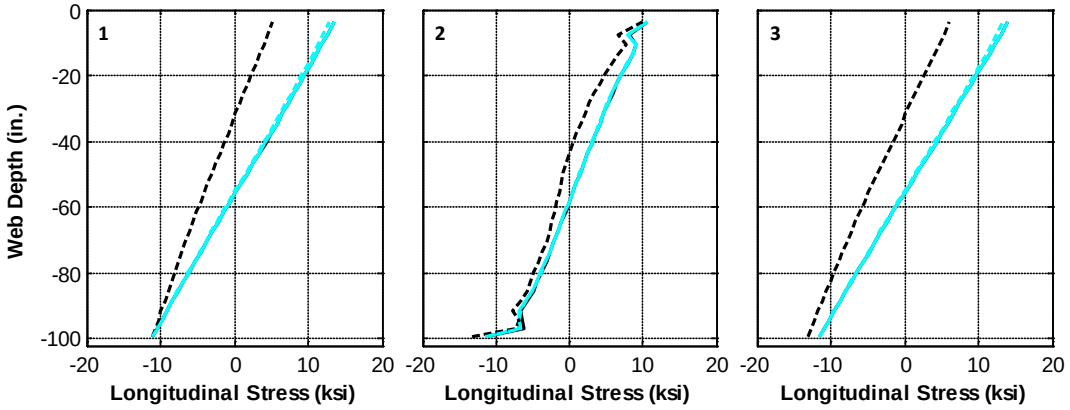


*(b)* Pier 2

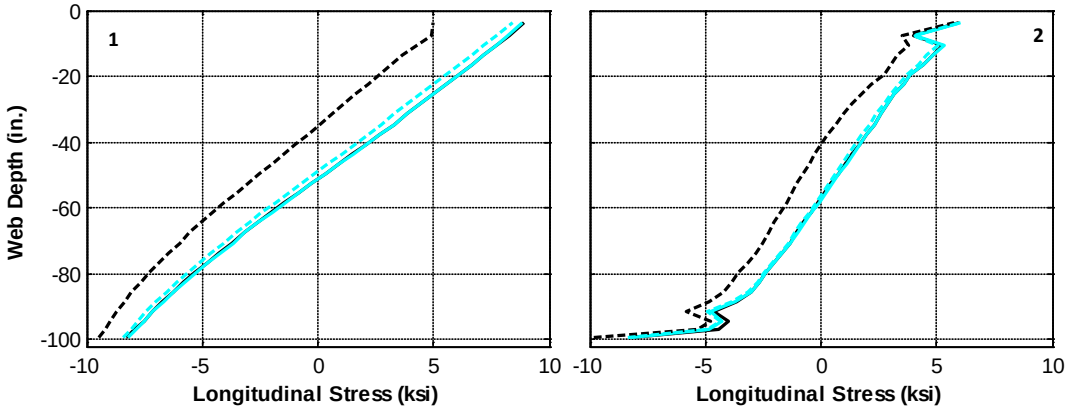


*(c)* Pier 3

**Figure C.64. Girder 8 Pier Web Longitudinal Stress Profiles – Gravity and +45°F Loading**